Investigating the role of a novel primase-polymerase, PrimPol, in DNA damage tolerance in vertebrate cells

A thesis submitted to the University of Sussex for the degree of Doctor of Philosophy

By

Julie Bianchi

March 2013

I hereby declare that this thesis has not been and will not be, submitted in whole or in part to another University for the award of any degree.

Julie Bianchi

University of Sussex

Julie Bianchi

Doctor of Philosophy Biochemistry

Investigating the role of PrimPol, a novel primase-polymerase, and its implication in DNA damage tolerance in vertebrate cells

Summary

Genome duplication is an essential task our cells have to achieve prior to cell division, and requires a highly specialized replication machinery to ensure it is performed in an accurate and complete manner. DNA primase and polymerases are essential components of the replisome. Primases initiate DNA replication by synthesising short RNA primers that are then elongated by faithful and processive replicative DNA polymerases. However, both exogenous and endogenous agents can damage DNA and hinder progression of the replicative machinery. Translesion synthesis DNA polymerases assist in bypassing these DNA lesions in a process called DNA damage tolerance that enables chromosomal replication to proceed in spite of damaged templates. This thesis details the characterisation of a novel eukaryotic DNA primase, coiled-coil domain containing protein (CCDC111), a member of the Archaeo Eukaryotic Primase (AEP) superfamily. Preliminary *in vitro* characterisation of CCDC111 demonstrated that the recombinant protein is capable of both DNA-dependent priming and polymerase activities, which is unprecedented for a eukaryotic polymerase, and it was therefore renamed Primase-Polymerase (PrimPol). The aim of this thesis was to provide one of the first cellular characterisations of PrimPol by generating a knockout of the gene in avian DT40 cells and also depleting the protein in human cells using RNAi. *In vivo* evidence supports the involvement of this novel polymerase in replication fork progression following replicative stress, such as exposure to UV light, but also during unperturbed DNA replication. Work in this thesis also indicates a role for PrimPol in mitochondrial DNA maintenance. Together, the data presented here establish a role for PrimPol in DNA damage tolerance in avian and human cells.

Acknowledgements

I would like to first thank my supervisor Aidan Doherty for giving me the opportunity to do this phD in his laboratory on this exciting new project. Secondly, I would like to thank Dr Helfrid Hochegger for his help with designing the DT40 KO targeting strategy, Dr Hégarat Nadia for all her help, patience and wisdom regarding DT40 cells, and for being such a great friend too! I'd also like to thank Dr Sabbioneda Simone for his advice regarding UV irradiation and PRR assay. More generally, I really would like to thank all the people from the Genome Centre for their time, patience and support who make this place such a nice environment to work, particularly to Gee, Bernie, Stuart, Queti, Tom and so many others. Then, I'd like to thank all the member of the Doherty lab, past and present, where this journey all started, with Andy, Alex, Nigel and Pierre, for their patience, especially when I arrived and couldn't really speak English! I'm also very grateful to Robbie who supervised me at first and showed me how to be efficient! I also would like to thank Laura, Stan, Ben, Ed, and Helen with their help on the project or in the lab; I don't forget Tamsyn, Dana and Angela, who showed me the way and looked after me when I started, and who became true friends.

Finally, I'd like to thank my family and Sean, which without this whole thesis would not have been possible.

Table of Contents

Abbreviations i

List of Figures vii

List of Tables x

CHAPTER I

Introduction 1

1.1. Structure of deoxyribonucleic acid 2

1.2. Nuclear DNA replication 2

1.2.1. Origin licensing and firing 3

1.2.2. Initiation of replication: DNA polymerase α-primase 4

1.2.3. DNA replication elongation 5

1.2.3.1. The clamp loader RFC and the DNA polymerase clamp PCNA 5

1.2.3.2. Polymerase delta and lagging strand synthesis 5

1.2.3.3. Polymerase epsilon and leading strand synthesis 6

1.3. Mitochondrial DNA 7

1.3.1. Mitochondrial genome 8

1.3.2. Mitochondrial DNA replication 9

1.3.3. The mitochondrial replisome 10

1.4. Overview of DNA damage and repair 11

1.4.1. UV light damage and genetic disorders associated with NER deficiency 12

1.5. Intra-S checkpoint 13

1.5.1. Cell cycle checkpoints: several points of control 13

1.5.2. Activation of ATR and the intra-S checkpoint 14

1.5.3. ATR/Chk1 pathway regulates both cell cycle and S-phase progression 15

1.5.3.1. Cell cycle progression: control of mitotic entry and origin firing 15

1.5.3.2. Intra-S checkpoint response following S-phase impediments 16

1.5.3.3. Involvement of ATR and Chk1 in replication fork maintenance 16

1.5.3.4. Regulation of ATR activation: replication fork protection complex 17

1.6. DNA damage tolerance 18

1.6.1. The Y-family Polymerases – uniquely adapted for TLS 19

1.6.2. DNA polymerase eta 20

1.6.3. DNA polymerases kappa and iota 20

1.6.4. Rev1, a recruitment platform with dCMP transferase activity 22

1.6.5. Polymerase zeta, “à mi-chemin” between replicative and TLS polymerase 23

1.6.6. PCNA ubiquitylation, choice between TLS Pol and template switch mechanisms 25

1.7. DNA Primases 27

1.7.1. Prokaryotic DnaG and archaeo-eukaryotic primases 27
1.7.2. Mechanisms of DNA primer synthesis, the five-step model 29
1.7.3. Evolutionary progression of AEP roles: towards the discovery of a novel eukaryotic primase 30

CHAPTER II

Materials and Methods 33

2.1. Material 34

2.2. Molecular Biology Methods 34

2.2.1. PCR 34
2.2.1.1. Mutagenesis and inverted PCR 35
2.2.1.2. RNA extraction and RT-PCR 36
2.2.1.3. Quantitative PCR for copy number variation analysis 36
2.2.2. Agarose gel electrophoresis 37
2.2.3. Enzymatic restriction digestion 38
2.2.4. DNA Ligation 38
2.2.5. Competent cells and transformation of DH5α 39
2.2.6. DNA preparation 40
2.2.7. DNA sequencing analysis 40
2.2.8. Standard cloning and sub-cloning technique 40
2.2.8.1. Cloning Gateway system 41
2.2.9. Genomic DNA extraction 42
2.2.9.1. DNA extraction from avian DT40 cells 42
2.2.9.2. DNA extraction from human cells 43
2.2.10. Southern blotting analysis 43
2.2.11. Probe labelling and hybridisation 44
2.2.12. Two dimensional agarose gel electrophoresis 45

2.3. Cellular Biology Methods 45

2.3.1. Cell culture 45
2.3.2. Transfection protocols 46
2.3.2.1. DT40 cells transfection and clones collection for gene targeting process 46
2.3.2.2. Human cells 47
2.3.2.2.1. RNAi transfection 47
2.3.2.2.2. DNA plasmid transfection 48
2.3.3. DNA damaging treatments 49
2.3.4. Flow cytometry analysis 49
2.3.5. Cellular fractionation 50
2.3.6. Microscopy analyses 51

2.3.6.1. Immunodetection of protein 51
2.3.6.2. Detection of S-phase cells in DT40 51
2.3.7. DNA fiber assay 52
2.3.7.1. Samples preparation and tilting process 52
2.3.7.2. Immunostaining 52
2.3.8. Post-replication repair assay 53
2.3.9. Tritium thymidine incorporation 54
2.3.10. Cell survival assays 54
2.3.10.1. Clonogenic survival on methylcellulose 54
2.3.10.2. CellTiter-Blue viability assay 55
2.3.11. Manual cell counting with haemocytometer 55
2.4. Biochemistry Methods 56
2.4.1. Preparation proteins extracts 56
2.4.2. SDS- Polyacrylamide Gel Electrophoresis (SDS-PAGE) 56
2.4.3. Western blot analysis 57
2.4.4. Antibody production and purification 57
2.4.4.1. Immunoblotting purification 58
2.4.4.2. Purification by crosslink column 58
2.4.4.2.1. Preparation column 58
2.4.4.2.2. Serum purification 59
2.4.5. Recombinant protein expression systems 59
2.4.5.1. Sf9 cells infection with baculovirus 59
2.4.5.2. *E. coli* SHuffle cells 59
2.4.5.2.1. Competent cells 59
2.4.5.2.2. Cells transformation 60
2.4.5.2.3. Protein expression in SHuffle cells 60
2.4.6. Purification of recombinant His tagged proteins 61
2.4.6.1. Affinity purification 61
2.4.6.1.1. Small scale purification (baculovirus system) 61
2.4.6.1.2. Immobilised Metal Affinity Chromatography (IMAC) 62
2.4.6.1.3. Heparin affinity 62
2.4.6.2. Ion exchange chromatography 63
2.4.6.3. Size exclusion chromatography 63
2.4.7. Preparation samples for mass spectrometry 63
2.4.8. Primer extension assay 64
2.5. Bioinformatic tools 64

CHAPTER III

Role of PrimPol in mitochondrial DNA maintenance 66

3.1. Introduction 67

3.2. Sub-cellular localisation of overexpressed human PrimPol 67

3.3. Involvement of PrimPol in mitochondrial DNA maintenance 69

3.3.1. Effect of PrimPol RNAi depletion on mtDNA copy number in human cells 70

3.3.1.1. Principle of quantitative PCR analysis and validation of the primer sets 70

3.3.1.2. Q-PCR analysis of mtDNA copy number in PrimPol depleted U2OS cells..... 71

3.3.1.3. Southern blot analysis of mtDNA copy number in PrimPol depleted U2OS cells 72

3.3.1.4. Q-PCR analysis of mtDNA copy number in several PrimPol depleted cell lines 73

3.3.2. Effect of PrimPol deletion on mtDNA maintenance in avian DT40 cells..... 74

3.3.2.1. Q-PCR and Southern blot analysis of mtDNA copy number in *PrimPol* $^{-/-}$ DT40 cells 74

3.3.2.2. 2D-gel analysis of mtDNA replication intermediates in *PrimPol* $^{-/-}$ DT40 cells . 75

3.3.2.3. Analysis of mtDNA mutations in *PrimPol*$^{-/-}$ DT40 cells..... 76

3.4. Effects of PrimPol RNAi depletion on cell proliferation 76

3.5. Re-localisation of PrimPol following DNA damage treatments 77

3.6. Discussion 79

3.6.1. PrimPol is not the "missing" mtDNA primase 79

3.6.2. Roles of PrimPol in mtDNA maintenance..... 80

3.6.2.1. Does PrimPol influence mtDNA turnover via DNA damage tolerance or repair? 80

3.6.2.2. Other factors causing mtDNA copy number to increase in PrimPol depleted cells 82

3.6.3. Data variability between different laboratories 83

3.6.4. Post-translational modification of PrimPol 85

CHAPTER IV

Generation of *PrimPol* knockout gene in avian DT40 cells 86

4.1. Introduction to gene disruption in avian DT40 cell line 87

4.2. First knockout strategy to disrupt *PrimPol* gene in DT40 cells 87

4.2.1. Strategy and design of *G. gallus PrimPol* targeted arms..... 87

4.2.2. Gateway cloning strategy for generation of the DT40 gene targeting constructs... 88

4.2.3. Generation of *PrimPol* heterozygotes (+/-) DT40 cell lines..... 89

4.2.4. Expression of human PrimPol in DT40 cells for complementation studies 90

4.3. Second knockout strategy to disrupt *PrimPol* gene in DT40 cells 91

4.3.1. Redesign of *G. gallus PrimPol* targeted arms..... 91

4.3.2. Generation of *G. gallus PrimPol* KO cells conditionally expressing human PrimPol 92

4.3.2.1. Preliminary characterisation of overexpressed human PrimPol in *G. gallus* KO cells 93
4.3.3. Generation of *G. gallus PrimPol* knockout clones 94
4.4. Preliminary characterisation of *PrimPol* knockout DT40 cell lines 95
4.4.1. Proliferation and cell cycle analysis in *PrimPol* $^{-/-}$ DT40 cells 95
4.4.2. Analysis of DNA replication in *PrimPol* $^{-/-}$ DT40 cells 96
4.5. Summary and discussion 98
4.5.1. Disruption of the *PrimPol* gene in avian DT40 cells 98
4.5.2. Study of human PrimPol in DT40 KO cells 99
4.5.3. Putative roles for PrimPol in nuclear DNA replication during unperturbed S-phase 100
4.5.4. Natural impediments potentially causing the recruitment of PrimPol in late S-phase 103
CHAPTER V
Exploring the role of *PrimPol* $^{-/-}$ DT40 cell lines following DNA damaging treatments 106
5.1. Introduction 107
5.2. Analysis of DNA damage sensitivity of *PrimPol* $^{-/-}$ DT40 cells 108
5.2.1. Clonogenic survival experiments on methylcellulose 108
5.2.2. Manual counting of UV-C cytotoxicity in avian *PrimPol* $^{-/-}$ cells 109
5.3. Analysis of *PrimPol* $^{-/-}$ cell viability following DNA damage treatments 110
5.3.1. Cell viability analysis with CellTiter-Blue assay 110
5.3.2. Cell viability analysis with CellTiter-Blue assay following UV-C irradiation 110
5.3.3. Cell viability analysis with CellTiter-Blue assay following 4NQO treatments 112
5.3.4. Cell viability analysis with CellTiter-Blue assay following X-ray irradiation 113
5.4. Role of PrimPol in chromosomal replication of UV damaged DNA 113
5.2.1. Involvement of PrimPol in DNA damage tolerance mechanisms 114
5.2.1.1. PrimPol requirement for replication fork progression 114
5.2.1.2. Sufficient post-replication repair in *PrimPol* $^{-/-}$ DT40 cells 115
5.2.2. Analysis of cell cycle progression in *PrimPol* $^{-/-}$ cells following UV-C irradiation 116
5.2.3. Analysis of apoptosis in *PrimPol* $^{-/-}$ cells following UV irradiation 118
5.2.4. Analysis of γH2AX foci formation in *PrimPol* $^{-/-}$ cells following UV irradiation 119
5.2.5. Analysis of human PrimPol cellular localisation following UV-C irradiation in DT40 *PrimPol* $^{-/-}$ cells 120
5.3. Influence of Chk1 inhibition in *PrimPol* $^{-/-}$ cells 122
5.3.1. Absence of PrimPol protects from UV-C cytotoxicity when Chk1 is inhibited 122
5.3.1.1. Cell viability assessment in *PrimPol* $^{-/-}$ cells following UV-C irradiation and Chk1 inhibition by UCN-01 123

5.3.1.2. Apoptosis response in *PrimPol* $^{-/-}$ cells following UV-C irradiation and Chk1 inhibition by UCN-01 124
5.3.2. Absence of PrimPol reduces aberrant DNA synthesis caused by Chk1 activity inhibition 125
5.3.3. Absence of PrimPol partially prevents the premature mitosis entry caused by Chk1 inhibition 126
5.3.4. Chk1 phosphorylation status in *PrimPol* $^{-/-}$ cells 127
5.4. Discussion 129
5.4.1. Summary 129
5.4.2. PrimPol's involvement in DNA damage tolerance mechanisms 129
5.4.3. Counterintuitive apoptosis response in the absence of PrimPol 132
5.4.3.1. Sensitivity of *PrimPol* $^{-/-}$ cells towards low doses UV-C irradiation 132
5.4.3.2. Replication-dependent apoptosis phenomenon - PrimPol pro-apoptotic role following high UV-C doses exposure 134
5.4.4. DNA damage tolerance, p53 status and apoptosis, study in XPV cells 135
5.4.5. Correlation of apoptosis response in *PrimPol* $^{-/-}$ cells and tc-NER deficient cells 135
5.4.6. Damage tolerance and intra-S checkpoint response, an intricate relationship 136
CHAPTER VI
Purification of recombinant human PrimPol protein 139
6.1. Expression of human PrimPol using a baculovirus insect cell system 140
6.1.1. Overview of expression studies of recombinant human PrimPol 140
6.1.2. Expression of human PrimPol using baculovirus expression system 140
6.1.3. Purification of PrimPol expressed in insect cells using a baculovirus system 141
6.1.4. PrimPol phosphorylation sites identified in recombinant PrimPol 142
6.2. Expression of human PrimPol using *E. coli* SHuffle system 143
6.2.1. Overview of *E. coli* SHuffle protein expression system 143
6.2.2. Optimisation of purification protocols in *E. coli* SHuffle cells 143
6.2.3. Human PrimPol recombinant protein is an active DNA polymerase 146
6.2.4. Purification of truncated forms of human PrimPol protein 147
6.3. Generation and purification of PrimPol polyclonal antibody 148
6.4. Summary and discussion 150
CHAPTER VII
Conclusions and future studies 151
References 157
Appendix 185

Abbreviations

2D-AGE	Two dimensional agarose gel electrophoresis
6-4PP	pyrimidine-pyrimidone photoproduct
8-oxo-G	8-oxo-7, 8-dihydroguanine
9-1-1	RAD9–HUS1–RAD1
A	Adenine
AEP	Archaeo-Eukaryotic Primase
APS	Ammonium persulphate
ATM	Ataxia telangiectasia mutated
ATP	Adenosine-5'-triphosphate
ATR	ATM and Rad3-related protein
ATRIP	ATR-interacting partner
bp	Base-pair
BPDE	Benzo(a)pyrene [B(a)P] diolepoxide
Bq	Becquerel
BSA	Bovine serum albumin
BER	Base excision repair
BrdU	Bromodeoxyuridine
C	Cytosine
^{14}C	Carbon 14
CDC	Cell division cycle
CDT1	Chromatin licensing and DNA replication factor 1
Ci	Curie
Cl	Chlorodeoxyuridine
CCDC111	Coiled-coil domain containing protein 111
cDNA	Complementary DNA
CDK1/2	Cyclin-dependent kinases 1 or 2

Chk1/2	Checkpoint kinase 1 or 2
Ct	Threshold cycle
DAPI	4',6-diamidino-2-phenylindole
Din (gene)	DNA damage-inducible (gene)
D-loop	Displacement loop
DOX	Doxycycline
DNA	Deoxyribonucleic acid
dRP	5‘-deoxyribose phosphate
DSB	DNA double-strand break
dsDNA	Double-stranded DNA
EdU	5-ethynyl-2'-deoxyuridine
ETC	Electron transfer chain
FCS	Foetal calf serum
FEN1	Flap endonuclease
FT	Flow through
^{3}H	Tritium
G	Guanine
GINS complex	(Go-Ichi-Ni-San, 5,1,2,3 in Japanese)
Gy	Gray
H-strand	Heavy strand mtDNA
H2AX	Histone H2A variant X
γH2AX	Histone H2A variant X phosphorylated on S139
HA	Hemagglutinin
Hek	Human embryonic kidney
His	Histidine
HIS	Histidinol (resistance-gene)
HLTF	Helicase-like transcription factor

HR	Homologous recombination
HRP	Horseradish peroxidase
HSP	Heavy strand promoter
IdU	Iododeoxyuridine
Ig	Immunoglobulin
IMS	Industrial methylated sprits
IMAC	Immobilized metal ion affinity chromatography
IPTG	Isopropyl β-D-1-thiogalactopyranoside
Kb	Kilobase
kDa	Kilodalton
KO	Knockout
LB	Luria-Bertani
LSP	Light strand promoter
Mec1	Mitosis entry checkpoint kinase
MMR	Mismatch repair
mtDNA	Mitochondrial DNA
mtSSB	Mitochondrial single stranded binding protein
MCM	Minichromosome maintenance
MMS	Methyl methanesulfonate
MRN	Mre11-Rad50-Nbs1
MTS	Mitochondrial targeting sequence
MW	Molecular weight
NCLDV	Nucleo-cytoplasmic large DNA viruses
NER	Nucleotide excision repair
NHEJ	Non-homologous end joining
Ni-NTA	Nickel-nitrilotriacetic acid resin
NCR	Non-coding region

NTP	Nucleoside triphosphate
OH	Origin of heavy strand DNA replication
OL	Origin of light strand DNA replication
ORC	Origin recognition complex
ORF	Open reading frame
OXPHOS	Oxidative phosphorylation
PAGE	Polyacrylamide gel electrophoresis
PBS	Phosphate buffered saline
PCR	Polymerase chain reaction
PCNA	Proliferating cell nuclear antigen
PI	Propidium iodide
PIKK	Phosphatidylinositol-3-kinase related kinase
PIP	PCNA interacting peptide
PMSF	Phenylmethylsulfonyl fluoride
Pol	Polymerase
PolDom	Polymerase domain of ligase D
POLRMT	Mitochondrial RNA polymerase
PPi	Pyrophosphate
Pre-RC	Pre-replication complex
Prim	DNA primase
Prim-Pol	DNA dependent primase-polymerase
PRR	Post-replicative repair
PURO	Puromycin (resistance-gene)
PVDF	Polyvinylidene difluoride
Q-PCR	Quantitative PCR
Rad (gene)	Radiation
Red-ox	Reduction-oxidation

rev (gene)	Reversionless (gene)
RIR	Rev1 Interaction Region
RF	Replication fork
RFC	Replication factor C
RFPC	Replication fork protection complex
RI	Replication intermediates
RITOLs	Ribonucleotide incorporation throughout the lagging strand
ROS	Reactive oxygen species
RPA	Replication protein A
RNA	Ribonucleic acid
RNAi	RNA interference
RRM	RNA Recognition Motif
rRNA	Ribosomal RNA
RT-PCR	Reverse transcription PCR
SDM	Strand displacement model
SDS	Sodium dodecyl sulphate
SHPRH	SNF2 histone-linker PHD and RING finger domain-containing helicase
SSB	Single-strand breaks
ssDNA	Single-stranded DNA
SUMO	Small Ubiquitin-like Modifier
SV40	Simian virus 40
S	Serine
S-phase	Synthesis phase
SOB	Super optimal broth
ssDNA	Single-stranded DNA
T	Thymine
TT	Thymidine-thymidine dimer

TAS	Termination-associated sequence
Tc-NER	Transcription-coupled NER
Tet	Tetracycline
TFAM	Mitochondrial transcription factor A
Tim	Timeless
Tipin	Timeless interacting protein
TLS	Trans-lesion synthesis
TopBP1	DNA topoisomerase II-binding protein 1
Toprim	Topoisomerase-primase
tRNA	Transfer RNA
TWINKLE	T7 gp4-like protein with intramitochondrial nucleoid localisation
Ub	Ubiquitin
UBM	Ubiquitin binding motif
UBZ	Ubiquitin binding zinc finger
U2OS	U2-osteosarcoma
USP	Ubiquitin specific protease
UV	Ultraviolet
WT	Wild type
XP	Xeroderma pigmentosum
XP-V	Xeroderma pigmentosum variant
XRCC	X-ray cross-complementing protein

List of Figures

Figure 1.1	Structure of DNA molecule and base pairing system	2
Figure 1.2	Origin of DNA replication	3
Figure 1.3	Pol α-prim complex	4
Figure 1.4	Lagging strand synthesis and replication fork	4
Figure 1.5	Mitochondrial respiratory chain and mtDNA molecule	7
Figure 1.6	Models of mtDNA replication by the mitochondrial replisome	9
Figure 1.7	DNA damages and repair mechanisms	11
Figure 1.8	Formation of UV photoproducts in DNA	12
Figure 1.9	Cell cycle checkpoints	13
Figure 1.10	ATR activation and Chk1 pathways	13
Figure 1.11	PCNA modifications and DNA damage tolerance	18
Figure 1.12	DNA polymerase families	19
Figure 1.13	Collaborative TLS mechanisms past UV photoproducts	20
Figure 1.14	Prokaryotic and eukaryotic primases	27
Figure 1.15	Two metal ions mechanism of nucleotidyl-transfer reaction	27
Figure 1.16	Five steps of DNA priming mechanism	28
Figure 1.17	Archaeo-eukaryotic primase family members	30
Figure 1.18	Archaeo-eukaryotic primases family clades	31
Figure 1.19	Multiple alignment of eukaryotic PrimPol homologues	31
Figure 3.1	Transient HA-PrimPol transfection for cellular localisation	68
Figure 3.2	Transient over-expression of PrimPol and sub-cellular fractionation analyses	68
Figure 3.3	Comparison Taqman and SYBR green Q-PCR technologies	70
Figure 3.4	Q-PCR primers validation for SYBR green technology: template titration assay	71
Figure 3.5	Analysis of PrimPol RNAi knockdown on mtDNA copy number	71
Figure 3.6	PrimPol RNAi knockdown optimisation and mtDNA copy number analysis	72
Figure 3.7	Time course Q-PCR analysis of mtDNA copy number in U2OS cells	72
Figure 3.8	Southern blot analysis of mtDNA copy number in U2OS cells	73
Figure 3.9	Q-PCR analysis of mtDNA copy number in various human cell lines	73
Figure 3.10	Q-PCR analysis of mtDNA copy number in DT40 cell lines	74
Figure 3.11	Southern blot analysis of mtDNA copy number in DT40 cell lines	74

Figure 3.12	2D-AGE analysis of mtDNA in *PrimPol* $^{-/-}$ DT40 cell lines	75
Figure 3.13	Chloramphenicol resistance assay	76
Figure 3.14	Cell proliferation analysis of PrimPol RNAi depleted osteosarcoma cell lines	76
Figure 3.15	Detergent resistant foci formation following DNA damage treatments in PrimPol stable Hek293 cell lines	77
Figure 4.1	First targeting strategy of *PrimPol* gene disruption in DT40 cells	87
Figure 4.2	Gateway cloning system of *G. gallus* PrimPol KO constructs	88
Figure 4.3	Clones obtained following the transfection of histidinol then puromycin constructs	89
Figure 4.4	Clones obtained following the transfection of puromycin then histidinol constructs	89
Figure 4.5	Human PrimPol conditional DT40 heterozygote (WT/HIS) clones	90
Figure 4.6	Second allele targeting in WT/HIS heterozygote clones expressing human PrimPol conditionally	91
Figure 4.7	Second targeting strategy of *PrimPol* gene disruption in DT40 cells	91
Figure 4.8	Allele targeting strategy 2, generating two human conditional KO clones	92
Figure 4.9	Characterisation of human conditional KO	92
Figure 4.10	Characterisation of human PrimPol conditional KO clones following doxycycline repression	92
Figure 4.11	Optimisation of doxycycline treatments in human conditional KO clones	93
Figure 4.12	Human PrimPol localisation in DT40 cells	93
Figure 4.13	Human PrimPol cellular localisation in relation to cell cycle analysis	94
Figure 4.14	Second allele targeting strategy generating two *G. gallus PrimPol* KO clones	94
Figure 4.15	Confirmation of two *PrimPol* DT40 knockout clones by Southern blot and RT-PCR analyses	94
Figure 4.16	Proliferation of *PrimPol* knockout clones	95
Figure 4.17	Cell cycle analysis of *PrimPol* knockout clones	95
Figure 4.18	DNA replication in unperturbed S phase	96
Figure 5.1	Abnormal colonies on methylcellulose of *PrimPol*$^{-/-}$ cells under unperturbed conditions	108
Figure 5.2	Abnormal colonies on methylcellulose after DNA damaging treatments	108
Figure 5.3	Effect of UV-C irradiation on cell morphology and cell survival	109

Figure 5.4	Cell viability assay using CellTiter-Blue technology	110
Figure 5.5	CellTiter-Blue viability assay after UV-C irradiation	111
Figure 5.6	CellTiter-Blue viability assay after 4NQO chronic treatment	112
Figure 5.7	CellTiter-Blue viability assay after X-ray irradiation	113
Figure 5.8	Analysis of DNA replication rate following UV-C irradiation	114
Figure 5.9	Replication fork progression after UV-C irradiation	114
Figure 5.10	Post-replication repair after UV-C irradiation	116
Figure 5.11	Analysis of cell cycle progression following UV-C irradiation	116
Figure 5.12	Cell cycle progression of BrdU pulse-labelled cells	117
Figure 5.13	Apoptosis assessment following UV-C irradiation	119
Figure 5.14	γH2AX immunolabelling following UV-C irradiation	119
Figure 5.15	Human PrimPol cellular localisation following UV-C irradiation	121
Figure 5.16	Human PrimPol foci formation following 5 J/m^2 UV-C irradiation	121
Figure 5.17	Influence of ChK1 inhibitor on cell viability	122
Figure 5.18	Influence of ChK1 inhibitor on cell survival after UV-C irradiation	124
Figure 5.19	Influence of ChK1 inhibitor on apoptosis after UV-C irradiation	124
Figure 5.20	Influence of ChK1 inhibition on DNA synthesis rate in *PrimPol* $^{-/-}$ cells	125
Figure 5.21	Influence of ChK1 inhibition on mitosis entry following UV-C irradiation	127
Figure 5.22	ChK1 phosphorylation status in *PrimPol* $^{-/-}$ cells following UV-C irradiation	128
Figure 5.23	Model of PrimPol's involvement in DNA damage tolerance mechanisms	130
Figure 5.24	Relationship between UV damage response and apoptosis mechanisms	135
Figure 6.1	Overview of baculovirus expression system	140
Figure 6.2	Small scale purification of PrimPol recombinant protein in Sf-9 cells using baculovirus system	141
Figure 6.3	PrimPol protein purification in Sf-9 cells using baculovirus system	141
Figure 6.4	Human PrimPol phosphorylated sites in Sf-9 and human cells	142
Figure 6.5	Modification of the redox state in *E. coli* SHuffle cells	143
Figure 6.6	Small scale expression of human PrimPol in *E. coli* SHuffle cells	143
Figure 6.7	Human PrimPol protein purification using in E. *coli* SHuffle cells	144
Figure 6.8	Human PrimPol protein elution profile on size exclusion column	145
Figure 6.9	Primer extension assay	146
Figure 6.10	PrimPol truncation purifications in *E. coli* SHuffle cells	147
Figure 6.11	Different purification methods of human PrimPol antibodies	148

List of Tables

Table 2.1	Commonly used solutions	34
Table 2.2	Mutagenesis primers	35
Table 2.3	RT-PCR primers	36
Table 2.4	Q-PCR primers	37
Table 2.5	Sequencing primers	40
Table 2.6	Primers used for Gateway cloning	42
Table 2.7	Plasmid constructs	42
Table 2.8	Primers used for generating Southern blot probes	44
Table 2.9	RNAi primer duplexes	48
Table 2.10	DNA damaging drugs	49
Table 2.11	Primary antibodies	50
Table 2.12	Secondary antibodies	50
Table 2.13	Oligonucleotides for primer extension assay	64

CHAPTER I

Introduction

1.1. Structure of deoxyribonucleic acid

The double-helical structure of deoxyribonucleic acid (DNA) was first published by Watson and Crick in 1953, based on unpublished X-ray data from Wilkins and Franklin (Watson and Crick, 1953; Wilkins *et al*., 1953; Franklin and Gosling, 1953). Each DNA strand is assembled into a long polymer of deoxyribonucleotides attached together by phosphodiester bound, where a phosphate group is covalently attached to two deoxyribose sugars, both linked to a nitrogenous base (figure 1.1A). Both strands are coiled together into a double-helix induced by the complementary hydrogen bond pairing of purine (adenine, guanine) and pyrimidine (thymine, cytosine) bases from each strand (Watson and Crick, 1953). Adenine and thymidine are paired together with two hydrogen bonds while cytosine and guanine form three (figure 1.1B). Each DNA strand is anti-parallel, containing its complementary sequence in the reverse order running in opposite directions (from 5' or 3') (figure 1.1C). In cells, DNA is largely maintained in a B-form conformation, where the helix is right-handed and one turn is completed every 10.5 base pairs (bp) in solution (Levitt, 1978). Rotation of the DNA helix around its axis can generate different contortion states of the molecule (positive or negative supercoiling) needing for protecting and packaging the genetic material (Rampakakis *et al.*, 2010). In eukaryotic cells, DNA is located in the cell nucleus and in the mitochondrion. Nuclear DNA molecules are compacted around histone proteins to form chromatin, allowing both physical protection of the genetic material and a way of regulating DNA metabolic processes. The human nuclear genome contains approximately 3 billion base pairs packaged in 23 chromosome pairs, containing the vast majority of protein-coding genes, whilst the mitochondrial genome is a circular plasmid of just 16,569 bp and is predominantly dedicated to the aerobic production of adenosine-5'-triphosphate (ATP) (see section 1.3).

1.2. Nuclear DNA replication

Faithful and complete duplication of the genetic material prior to cell division is key to maintaining genome stability. A sophisticated molecular machinery, composed of various specialised enzymes, is thus required to orchestrate this complex task occurring during a discrete replication phase of the cell cycle termed DNA synthesis or S-phase.

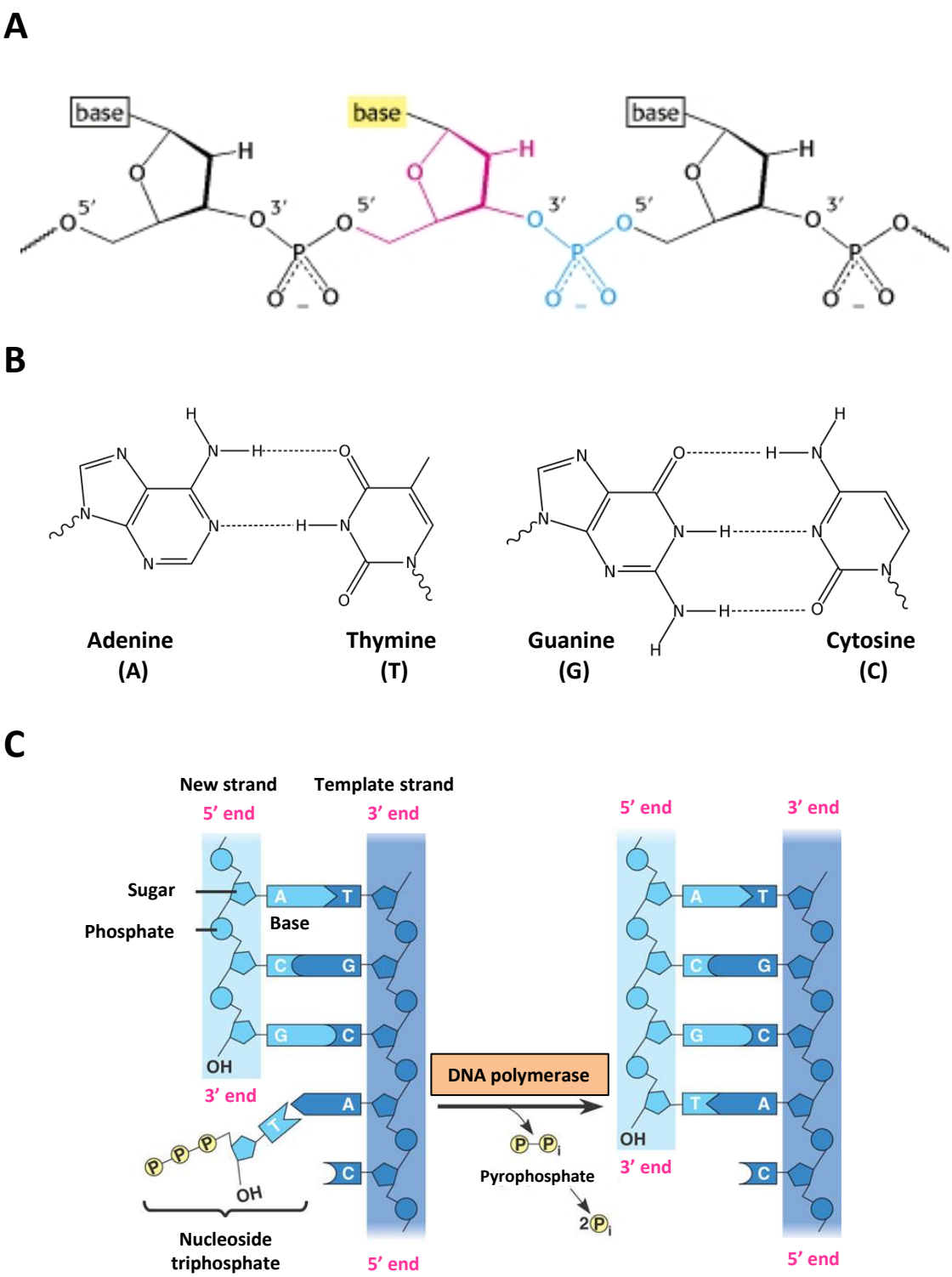

Figure 1.1: Structure of DNA molecule and base pairing system.

(**A**) Schematic of one strand of the DNA backbone molecule showing the phosphodiester bond between each nucleotides, which are composed of a deoxyribose sugar (pink), a phosphate group (blue) and a nitrogenous base (yellow). (**B**) Base pair system of the four nitrogenous bases, showing the hydrogen bonds (dashed lines) created between purine (adenine or guanine) and pyrimidine (thymidine and cytosine) pairs. (**C**) Schematic of the DNA double-stranded molecule showing the incorporation of a nucleoside triphosphate and the creation of a phosphodiester bond between the 3'OH end of the new strand and the 5' carbon of the incoming deoxyribose. A pyrophosphate molecule is then released. Images were taken from Biochemistry book, 5th edition (Berg *et al.*, 2002).

1.2.1. Origin licensing and firing

Initiation of DNA replication in eukaryotes occurs at specific sites of the genome named origins, which often contain a high proportion of A-T base pairs facilitating the dissociation of both DNA strands (Lodish *et al.*, 2000). However, in contrast with prokaryotes, no consensus sequences exist in eukaryotes to delineate origins, but instead chromatin structure and epigenetic markers are thought to play a role in determining origin position (Mechali, 2010). Prior to S-phase, during gap 1 (G1) period, the origin recognition complex (ORC), composed of 6 subunits (ORC1–ORC6), binds to a large number of origins (Bell and Stillman, 1992; Ohta *et al.*, 2003). ORC binding allows the recruitment of the pre-replication (pre-RC) complex, CDC6 (cell division cycle 6) then CDT1 (chromatin licensing and DNA replication factor 1) which permits the loading of the mini-chromosome maintenance (MCM) 2–7 helicase complex onto the DNA at the origin (Remus *et al.*, 2009) (figure 1.2A). This last step triggers origin licensing which is tightly regulated by CDT1 and Geminin to prevent multiple licensing of the same origin per cell cycle (Lutzmann *et al.*, 2006). However in multicellular organisms, MCM9 binding to CDT1 enables origin licensing by preventing Geminin regulation (Lutzmann and Mechali, 2008). Moreover, loading of the MCM2-7 complex stimulates the release of ORC and CDC6 (Tsakraklides and Bell, 2010) (figure 1.2A). At the beginning of S-phase, the MCM complex is phosphorylated by CDC7-Dbf4 and CDK2 allowing the binding of the GINS complex (Go-Ichi-Ni-San, 5,1,2,3 in Japanese) and CDC45, forming the CMG complex (CDC45-MCM2-7-GINS). This activates the helicase function and fires the licensed origin (figure 1.2B), allowing unwinding of the duplex DNA at the origin (Lei *et al.*, 1997; Krude *et al.*, 1997; Pacek *et al.*, 2004; Moyer *et al.*, 2006). Origins are organised into clusters, which are activated at different times during S-phase (Jackson and Pombo, 1998) in a stochastic manner (Patel *et al.*, 2006). The importance of CDKs (cyclin-dependent kinase) in regulating the firing of these clusters and overall DNA replication timing seems to be accepted, even if these complex mechanisms are not fully understood (Thomson *et al.*, 2010). Studies from yeast and Xenopus demonstrated the importance of DNA topoisomerase II-binding protein 1 or TopBP1 (Dpb11 in *Saccharomyces* (*S.*) *cerevisiae* or Cut5 in *S. pombe*) interaction with Treslin and polymerase epsilon (Pol ε) for the loading of CDC45 (Kumagai *et al.*, 2010; Masumoto *et al.*, 2000). The pre-RC is therefore converted into a replication fork (RF) complex (figure 1.2C) with the assembling of the replisome components (Masai *et al.*, 2010).

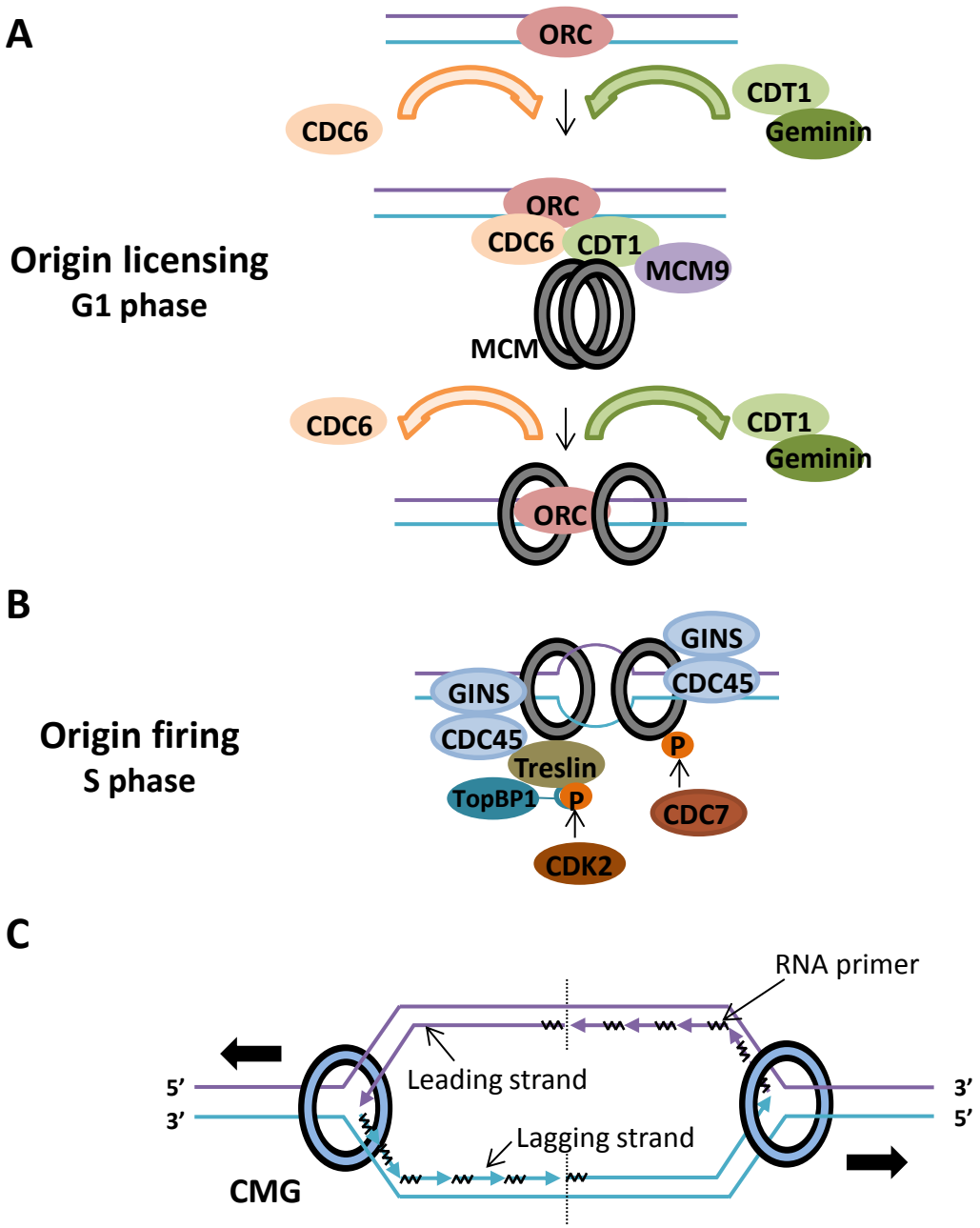

Figure 1.2: Origin of DNA replication.

(**A**) Origin recognition complex (ORC) binds to origin allowing recruitment of the pre-replication (pre-RC) complex, CDC6 (cell division cycle 6) then CDT1 (chromatin licensing and DNA replication factor 1) which permits the loading of the mini-chromosome maintenance (MCM) 2–7 helicase complex. Binding of CDT1 to Geminin allows regulation of origin licensing. (**B**) MCM complex gets phosphorylated by CDC7-Dbf4 and CDK2 allowing the binding of the GINS (Go-Ichi-Ni-San, 5,1,2,3 in Japanese) complex and CDC45, forming the CMG complex (CDC45-MCM2-7-GINS). Helicase function of MCM is thus activating allowing firing of the origin. TopBP1 and Treslin are also needed for the binding of CDC45 and thus regulate origin firing. (**C**) The pre-RC complex is then converted into a replication fork complex with the assembling of the replisome components to allow the continuous replication of the leading strand (5' to 3') and discontinuous synthesis of the lagging (3' to 5') strand, due to the anti-parallel nature to the duplex DNA.

1.2.2. Initiation of replication: DNA polymerase α-primase

Once the double-helix is unwound at the origin by the MCM 2-7 helicase complex, replication protein A (RPA), a heterotrimeric complex (70, 34 and 11 kDa subunits in human cells), coats the single-stranded (ss) DNA stimulating both the recruitment of polymerase α-primase (Pol α-prim) (Wold MS, 1997; Walter and Newport, 2000) and the helicase activity of the MCM 2-7 complex (Brill and Stillman, 1989). RPA also binds directly Pol α-prim (Dornreiter *et al.*, 1992; Vaithiyalingam *et al.*, 2010). Pol α-prim has the sole responsibility in the eukaryotic nucleus of initiating DNA synthesis *de novo* (Foiani *et al.*, 1997). Structural and mechanistic features of DNA polymerases and primases will be described further in section 1.7. The Pol α-prim complex is composed of four subunits in eukaryotes (figure 1.3), the smallest (50 kDa) is Prim1 (DNA primase 1) the catalytic subunit with a DNA-dependant RNA polymerase activity, responsible for the synthesis of RNA primers along with its accessory or large subunit (59 kDa) Prim2 (Santocanale *et al.*, 1993; Muzi-Falconi *et al*., 2003). The largest polypeptide (165 kDa) is the DNA polymerase catalytic subunit, Pol α (Plevani *et al.*, 1985), which has an accessory B subunit (77 kDa). A recent paper showed that Pol α contains a conserved C-terminal (C-ter) domain, which is important for the binding of Pol α with Prim2, and thus for the tethering of the primase activity at the replisome (Kilkenny *et al.*, 2012). Pol α B subunit has been shown to be essential for the initiation of replication and is believed to play a role in protein interactions and distinction between initiation of replication and lagging strand replication elongation (Foiani *et al.*, 1994; Muzi-Falconi *et al.,* 2003; Nasheuer *et al.*, 1991). Indeed, as replicative DNA polymerases can only synthesise DNA from 5' to 3', Pol α-prim complex is also needed for the lagging strand replication by initiating synthesis of each Okazaki fragment (Sakabe and Okazaki, 1966; Ogawa and Okazaki, 1980; Muzi-Falconi *et al.*, 2003). Initiation of DNA replication therefore starts with the synthesis of a short RNA primer (between 6 to 15 oligonucleotides) catalysed by Prim1 (Garg *et al.*, 2005) (figure 1.4A). The Pol α subunit extends this RNA primer with an approximately 30 nucleotides DNA chain (Waga and Stillman, 1998; Nethanel *et al.*, 1988) (figure 1.4A). Recognition of this RNA-DNA primer by replication factor C (RFC) leads to the displacement of Pol α by the sequential loading of proliferating cell nuclear antigen (PCNA) and the replicative polymerases (Tsurimoto and Stillman, 1991) (figure 1.4A).

A

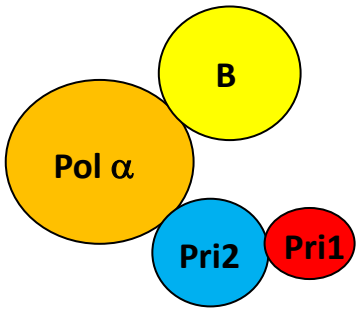

B

	Eukaryotes		Archaea	
	Human	***S. cerevisiae***	**Sulfolobus**	**Pyrococcus**
Pol α	**Polα** (165 kDa)	**Pol1** (180 kDa)	–	–
B subunit	B (77 kDa)	Pol12 (79 kDa)	–	–
Primase small	**PRIM1** (50 kDa)	**Pri1** (48 kDa)	**PriS** (38 kDa)	**Pfup41** (41 kDa)
Primase large	PRIM2 (59 kDa)	Pri2 (58 kDa)	PriL (36 kDa)	Pfup46 (46 kDa)

Figure 1.3: Pol α-prim complex.

(**A**) Cartoon depicting the 4 sub-units of the Pol α-prim complex in eukaryotes. Primase catalytic sub-unit Pri1 (red), and its accessory sub-unit Pri2 (blue), are responsible for synthesising a short RNA primer. Pol α polymerase (orange) requires its non-catalytic B sub-unit (yellow) to initiate DNA synthesis and elongate the RNA primer. (**B**) Nomenclature of representative eukaryotic Polα-prim complexes and primases sub-units in archaea. Molecular size are indicated in parentheses and the catalytic sub-units in bold. (Table was adapted from Lao-Sirieix *et al.*, 2005a).

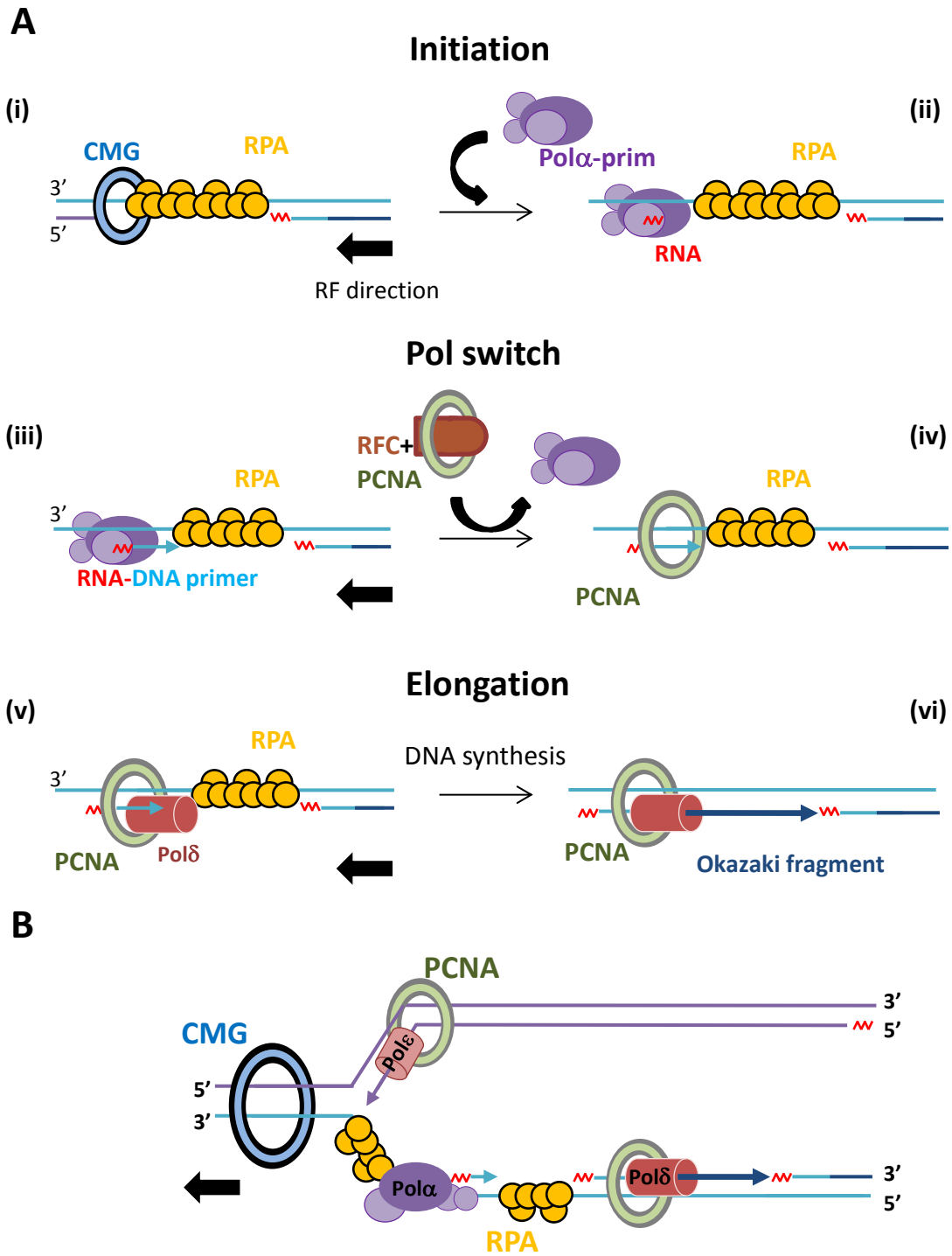

Figure 1.4: Lagging strand synthesis and replication fork.

(**A**) Helicase unwinding activity of the CMG complex (CDC45-MCM2-7-GINS) generates ssDNA rapidly coated by RPA protein (**i**). Polα-prim complex is then recruited and initiates replication by synthesising a short RNA primer (red) thanks to its primase subunit PRIM1 (**ii**). Polymerase activity of Polα can then extends the RNA primer from 5' to 3' and initiates DNA replication of the lagging strand (**iii**). Replication factor C (RFC)-PCNA complex triggers the polymerase switch by inhibiting Polα-prim activity and inducing its dissociation (**iv**). PCNA allows then the loading of the replicative polymerase Pol δ on the lagging strand (**v**) which can elongate the Okazaki fragment (**vi**). (**B**) Cartoon of a replication fork showing the lagging strand synthesis as described above and also the leading strand synthesis by Pol ε, also initiated by Polα-prim.

1.2.3. DNA replication elongation

1.2.3.1. The clamp loader RFC and the DNA polymerase clamp PCNA

RFC is a hetero-pentameric complex, which binds to the 3' end of primed DNA leading to the displacement of Pol α and the recruitment of PCNA (figure 1.4A). ATP binding of RFC stabilises the loading of PCNA whereas hydrolysis of the molecule causes dissociation of the clamp complex from DNA (Majka *et al.*, 2004). PCNA is composed of three identical monomers forming a ring shape, encircling the DNA helix (Krishna *et al.*, 1994). First described as polymerase delta (Pol δ) auxiliary protein (Prelich *et al.*, 1987), PCNA has been shown to stimulate the processivity of the polymerase by increasing its binding to the DNA substrate (Majka and Burger, 2004; Mozzherin *et al.*, 1999). Even if direct interaction between PCNA and the catalytic domain of Pol δ remains a source of controversy, strong interaction with the C subunit of the polymerase, containing a PCNA binding (PIP) motif, has been reported (Zhou *et al.*, 1997; Hughes *et al.*, 1999). In addition to its role during unperturbed chromosomal replication (in recruiting and stimulating polymerases activity), PCNA has also a central function in many other metabolic pathways (DNA repair, translesion synthesis, chromatin remodelling) via various post-translational modifications (reviewed by Moldovan *et al.*, 2007); more details will be provided in section 1.6.6.

1.2.3.2. Polymerase delta and lagging strand synthesis

To ensure high fidelity DNA synthesis, replicative polymerases contain a 3' to 5' exonuclease activity allowing proofreading mechanisms, increasing replication accuracy (Echols and Goodman, 1991). Due to the anti-parallel double-helical structure of the DNA molecule and the polymerase synthesis orientation (5' to 3'), replication of the lagging strand is discontinuous (figure 1.4). As mentioned previously, Pol α-prim initiates DNA synthesis by generating a primer which is then extended by Pol δ into a ~200 nucleotides Okazaki fragment (Nick McElhinny *et al.*, 2008). Our understanding of lagging strand synthesis stems from work in *Escherichia* (*E.*) *coli*, with polymerase III (Pol III) being responsible for highly processive DNA synthesis on both leading and lagging strands (Stillman, 1994). Footprinting experiments performed by Stukenberg and co-workers on the interaction between Pol III and its β clamp subunit (PCNA homologous) have shed the light on the polymerase "hopping model". They describe how Pol III dissociates from the β clamp when encountering a DNA duplex (corresponding to the following Okazaki fragment), and relocates onto the next primer-

template junction with the help of another β clamp unit (Stukenberg *et al.*, 1994). These studies highlighted then the importance of the polymerase clamp in orchestrating the switch between replicative polymerases (Moldovan *et al.*, 2007). Also, these experiments already suggested the implication of Pol δ in the maturation process of Okazaki fragments. Progression of the DNA polymerase induces a strand displacement of the RNA primer until Pol δ reaches the DNA duplex (primer-template), creating a nucleotide flap cleaved by the flap endonuclease FEN1 (Garg *et al.*, 2004; Maga *et al.*, 2001). Two other models, involving RNaseH2 or DNa2 have also been proposed in addition to a Pol δ idling model (Kao and Bambara, 2003), and once again, PCNA is involved in the coordination of the recruitment of the different factors (Beattie and Bell, 2011).

1.2.3.3. Polymerase epsilon and leading strand synthesis

Implication of a third essential replicative polymerase, Pol ε, came from studies in yeast (Morrison *et al.*, 1990). However, experiments performed using the simian virus (SV40) system described Pol δ as the replicative polymerase required for the synthesis of both the leading and lagging strand (Li *et al.*, 1984; Waga and Stillman, 1994). Elegant studies in yeast resolved this issue and demonstrated that Pol ε was involved in leading strand DNA synthesis (Pursell *et al.*, 2007). Pol ε is a heterotetramer composed of a large catalytic subunit (p261 in human), a smaller subunit with a 3' exonuclease activity (p59) and two small accessory subunits, p17 and p12, respectively dpb3 and 4 in yeast. Surprisingly dpb3 gene is only essential in *S. pombe* (not in *S. cerevisiae*) and depletion studies indicate the implication of the gene during initiation, elongation and late stages of DNA replication but also during cell division (Spiga and D'Urso, 2004). However, mutational studies reported the catalytic domain of Pol ε was dispensable for both yeast survivals (Dua *et al.*, 1999; Feng and D'Urso, 2001). Therefore two distinct models are still currently under debate in yeast: is Pol ε the sole replicative leading strand polymerase, as supported by Morrison and Sugino, or is Pol δ responsible for the elongation of both leading and lagging strands? Nonetheless, Pol ε has been shown to bind replication origins in an early stage of DNA replication (transition G1/S) following the formation of the pre-RC complex. Indeed temporal immunoprecipitation studies performed in *S. cerevisiae* revealed the binding of Pol ε during the initiation step of replication, following the formation of the pre-RC complex, in a hydroxyurea (HU) independent manner (Aparicio *et al.*, 1997). These findings were confirmed later on with the demonstration that a Polε-Dpb11 (TopBP1) complex was needed for the loading of the Pol α-prim complex and the initiation of DNA replication (Masumoto *et*

al., 2000). Moreover, mutations of Pol ε active site reducing its fidelity generated more DNA replication errors preferably on the leading strand (Pursell *et al.*, 2007). Shcherbakova and co-workers proposed therefore an intermediate model, where Pol ε is only needed at the beginning of replication, for initiation step and then extension of the short DNA primers synthesised by Pol α on the leading strand. Polε would thus only be needed at proximity of origins before Pol δ would take over and extend both lagging and leading strands simultaneously (Pavlov and Shcherbakova, 2010). According to the resemblance between yeast and human Pol ε complex, similar questions are legitimately asked regarding the contribution of this polymerase during the leading strand synthesis. Further *in vitro* studies with human cell extracts are attempted to address this question (Kang *et al.*, 2012) but whether this is the case *in vivo* remains to be determined.

Replication elongation terminates when two RFs converge. This event was believed to occur randomly in eukaryotic cells (Santamaria *et al.*, 2000), until this recent report showing the presence of replication termination sites in yeast chromosomes (Fachinetti *et al.*, 2010). In yeast and SV40 system, DNA strands intertwine or catetane at the end of replication and topoisomerase II is needed to resolve those structures (DiNardo *et al.*, 1984; Sundin and Varshavsky, 1981).

1.3. Mitochondrial DNA

Cellular DNA is also contained within the mitochondrion, first observed following electron microscopy in the 1960s (Nass and Nass, 1963). Mitochondria are small organelles responsible for cellular respiration which provides the main source of energy to the cell in the form of ATP by coupling an Electron Transfer Chain (ETC) to an ATP synthase pump (figure 1.5A). These reduction-oxidation (redox) reactions allow the transfer of electrons to a series of donor / acceptor molecules until the final reduction of an oxygen molecule to water (Larsson, 2010). However, redox reactions of the oxidative phosphorylation (OXPHOS) system also generate reactive oxygen species (ROS), which can damage the mitochondrial (mt) DNA molecule (Larsen *et al.*, 2005); see section 1.4.

A

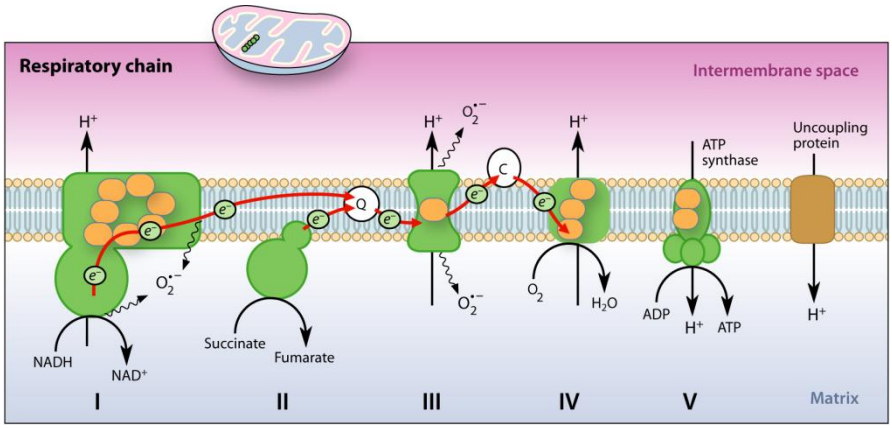

B

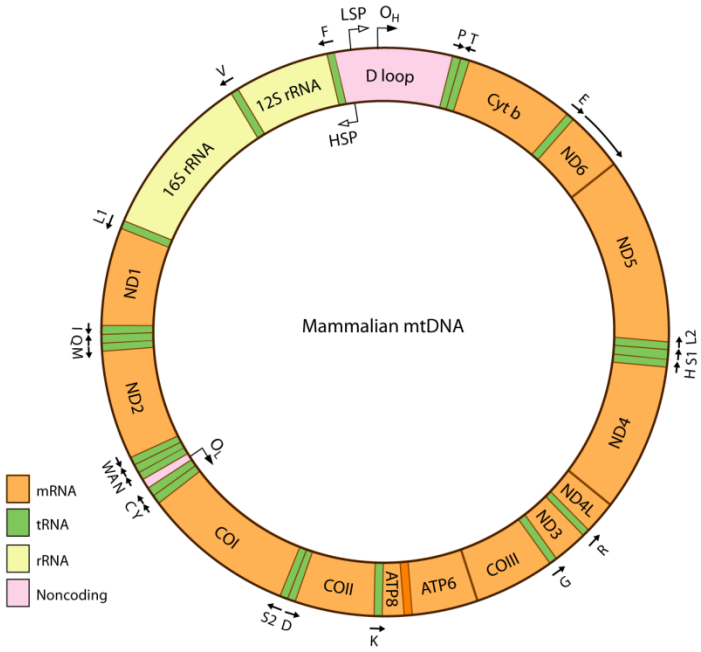

Figure 1.5: Mitochondrial respiratory chain and mtDNA molecule.

(**A**) Schematic of the inner mitochondrial membrane composed of five enzymes complexes (I to V), where I to IV carry the electrons transport chain (ETC) and complex V is the ATP synthase. Coenzyme Q and cytochrome *c* (Q and C white circles) help the transfer of electrons (e^-) along the ETC which is coupled with a proton (H^+) gradient across the membrane, essential for ATP synthesis. (**B**) Representation of mitochondrial DNA (mtDNA), a circular DNA molecule composed of two strands, heavy (outside circle) and light (inside circle) with their respective origins of replication (O_H and O_L) and transcription promoters (HSP and LSP). 14 tRNAs are transcribed from the H strand (right arrows below the green blocks) and 8 from the L strand (left arrows below the green blocks). All mRNAs (except ND6) are expressed from the H strand (orange blocks) as well as the 2 rRNAs (yellow blocks). Cartoons taken from (Larsson, 2010).

1.3.1. Mitochondrial genome

The mitochondrial genome is a 16 kb plasmid encoding 13 essential proteins of the ETC (out of ~90), 2 ribosomal (r) and 22 transfer (t) RNAs. Its two DNA strands can be discriminated by their densities due to a difference in their G/C content, the leading strand being richer in guanine and so is called the heavy (H) strand by opposition to the light (L) lagging strand (Falkenberg *et al.*, 2007). This small genome is very compact, containing no introns and only one significant non-coding region (NCR) of 1.1 kb. This area contains the promoters for transcription of both heavy and light strands (HSP and LSP respectively) and the origin of replication of the leading strand O_H (figure 1.5B), but also 650 bp downstream, a termination-associated sequence (TAS). Thereby replication of the H strand can be stopped after recognition of TAS sequences, creating a third strand which can stay stably hybridized to the H strand template, generating a displacement loop conformation (D-loop strand) (Clayton, 1982; Falkenberg *et al.*, 2007). Little is known about D-loop formation and its biological functions, and several hypotheses have been made, suggesting a role in nucleoids organisation (Holt *et al.*, 2007) or in mtDNA replication regulation (Wanrooij and Falkenberg, 2010).

An interesting characteristic of mtDNA is its maternal inheritance (Giles *et al.*, 1980); the sperm mitochondria are ubiquitylated inside the oocyte leading to the degradation of the paternal mtDNA (Sutovsky *et al.*, 1999). Apart from this specific case, a somatic mammalian cell contains thousands of copies of this circular genome, with ~6-10 copies per mitochondrion. This polyploidy aspect introduces the term of homoplasmy, when all the copies are the same, in opposition to heteroplasmy, corresponding to a mixture of wild type (WT) and mutant genomes within the same cell (Clay Montier *et al.*, 2009). In this case, it is important to consider the ratio of WT copy / mutant DNA to allocate a threshold level determining the appearance of biochemical defects in the OXPHOS pathway (Tuppen *et al.*, 2010).

The reason why mitochondria have their own genome separated from the nucleus is still not entirely known. The endosymbiont hypothesis suggests that mtDNA is only a vestige of an aerobic bacteria's genome that was engulfed to create the first eukaryotic cell (Kutik *et al.*, 2009). With the process of evolution, only a small number of genes have remained inside this organelle probably to keep the control of the synthesis of those key elements of the OXPHOS pathway separately from the nucleus division. This has a double advantage for the cell: the hydrophobic proteins do not have to cross the double membrane of the mitochondrion and the expression of those genes can be regulated by the respiratory pathway itself (Falkenberg *et al.*, 2007). Indeed, a correlation between mtDNA copy number and bioenergetic function

has been recently observed in esophageal squamous cell carcinoma (Lin *et al.*, 2012a). However, the system is not completely autonomous as nuclear encoded proteins are required for many mitochondrial metabolic processes.

1.3.2. Mitochondrial DNA replication

Unlike nuclear DNA, replication of the mitochondrial genome is not coordinated with cell division and occurs constitutively throughout the cell cycle (Bogenhagen and Clayton, 1977). The mechanisms that ensure the faithful replication of mtDNA are still under debate (Bogenhagen, *et al.*, 2003a and b; Holt, *et al.,* 2003). The first model suggests both strands are replicated continuously in an asynchronous manner (Clayton, 1982), whereas the second model proposes a coupled replication of both strands at the same time, as in the nucleus (Holt, 2000). The original model or strand displacement model (SDM), was based on electron microscopy observations and states the leading strand is replicated first by using the light strand as template creating a displacement of the parental H strand (figure 1.6A). After two third of the synthesis of the new H strand, the mitochondrial replisome reaches the origin of replication of the L strand (O_L), and the replication of the lagging strand can start in the opposite direction, using the displaced heavy strand as template (figure 1.6A). This way, both strands can be replicated continuously (from 5' to 3') but not at the same time, thus leaving the displaced parental H strand as ssDNA for a certain amount of time. Nearly 20 years after the SDM was first proposed, utilisation of two dimensional agarose gel electrophoresis (2D-AGE) brought another view of the mechanism of mtDNA replication. This technique separates DNA molecules by their size and shape, allowing visualization of replication intermediates (RI) (Friedman and Brewer, 1995). After treatment with single-strand nuclease of mtDNA extracts, some Y arc shaped RI remain suggesting the presence of double-strand replication fork conformation similar to nuclear replication; this evidence supports the idea that the replication of leading and lagging strands are coupled in mitochondria too (figure 1.6B). Further, 2D-gel analysis brought new evidence regarding SDM, as it was noticed the displaced parental H strand was coated with RNA and not mitochondrial ssDNA binding protein (mtSSB) (figure 1.6B). The name RITOLS was then suggested for Ribonucleotide Incorporation ThroughOut the Lagging Strand (Yasukawa *et al.*, 2006; Pohjoismaki *et al.*, 2010). As two separate models have been proposed to take place during mtDNA replication, further studies need to be done to understand how both replication systems can operate inside the organelle and whether

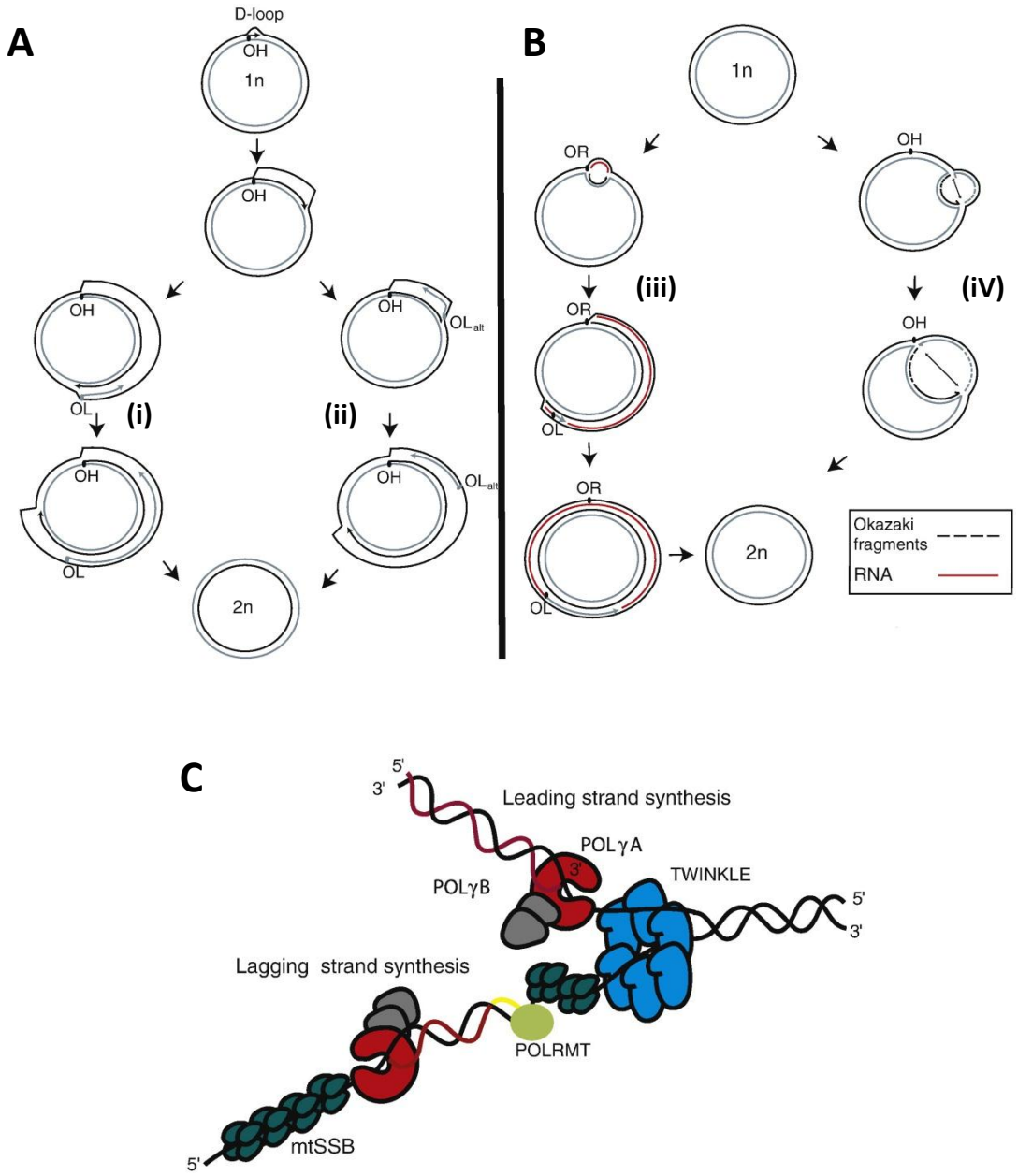

Figure 1.6: Models of mtDNA replication by the mitochondrial replisome.

Strand displacement model (SDM), depicted in (**A**), describes how mtDNA replication starts at the origin of replication OH and the synthesis of the leading strand displaces the heavy strand; replication of the lagging strand is then initiated when the OL is exposed (**i**) or at alternative (OL_{ALT}) lagging strand origin (**ii**). (**B**) SDM model (**i**) is depicted with the presence of RNA (red) protecting the displaced H strand during mtDNA replication process (RITOLS) (**iii**). The final model presents a discontinuous replication of the lagging strand (with Okazaki fragment) in a similar manner than nuclear DNA replication (**iv**). (**C**) Cartoon depicts the mtDNA replisome, with TWINKLE helicase (blue) unwinding the double helix and mtSSB (green) stabilizing ssDNA molecule. Polymerase γ subunits A (red) and B (grey) incorporate nucleotides to the new strand of DNA following RNA primer (yellow) synthesis by POLRMT(light green). (Cartoons were adapted from Wanrooij and Falkenberg, 2010).

specific mechanisms trigger the use of one or the other mode of replication (Holt and Reyes, 2012).

1.3.3. The mitochondrial replisome

As mentioned previously, all the proteins involved in mtDNA replication are encoded by nuclear genes and transcribed on cytosolic ribosomes. The minimal replisome reconstituted *in vitro* is composed of the mitochondrial DNA polymerase gamma (Pol γ), the helicase TWINKLE (T7 gp4-like protein with intramitochondrial nucleoid localisation), and mtSSB (Korhonen *et al.*, 2004) (figure 1.6C). Pol γ is composed of one catalytic subunit (γA) and one accessory subunit (γB) which binds DNA and increases the processivity of the polymerase activity; altogether they form a heterotrimer where two Pol γB subunits are needed for one Pol γA (Carrodeguas *et al.*, 2001; reviewed in Kaguni, 2004). Pol γ is part of the A family polymerase and like replicative polymerases the enzyme possesses a 3'-5' exonuclease activity but also 5'-deoxyribose phosphate (dRP) lyase activities, required for base excision repair (BER) (Kunkel and Mosbaugh, 1989; Pinz and Bogenhagen, 2000). TWINKLE is similar to the T7 primase-helicase required for bacteriophage replication, but does not possess a primase activity in human cells. Nevertheless, this enzyme is essential for mitochondrial genome maintenance (Milenkovic *et al.*, 2013) and several pathologies can be directly related to mutations in TWINKLE gene affecting the enzyme activity, thus creating OXPHOS dysfunction and energy defect particularly in muscle tissue (Spelbrink *et al.*, 2001). As TWINKLE and Pol γ cannot initiate DNA synthesis on their own, the search for a mitochondrial primase has begun nearly 30 years ago when priming activity was observed for the first time within the organelle (Wong and Clayton, 1985 and 1986). Previously it was determined Pol γ was the only polymerase present in the organelle (Hübscher *et al.*, 1979), and later studies confirmed Pol α was not responsible for priming mtDNA replication as aphidicolin treatments did not inhibited the duplication of the genome in the organelle (Zimmerman *et al.*, 1980; Geuskens *et al.*, 1981). Only recently, mitochondrial RNA polymerase (POLRMT) has been described to be responsible for synthesizing RNA primers required for the initiation of both leading and lagging strands replication (Wanrooij *et al.*, 2008; Fusté *et al.*, 2010).

1.4. Overview of DNA damage and repair

Despite being bound in a chromatin structure, DNA is constantly subject to damage. Environmental assaults, like ultra violet (UV) light, ionising radiation (gamma, X-ray) and genotoxic agents, can result in DNA strand breaks, modification of the nitrogenous bases, and distortion of the overall structure of the double-helix (reviewed in Friedberg, 2003). Endogenous metabolisms can be indirectly responsible for damaging the DNA molecule, the most common by-product being ROS. These free radicals are capable of oxidising the DNA molecule and frequently generate the highly mutagenic 8-oxo-7,8-dihydroguanine (8-oxo-G) (Cadet *et al.*, 2003), which can lead to a mis-incorporation of adenine opposite the damaged nucleotide during DNA replication (Avkin and Livneh, 2002). As previously mentioned, mtDNA being in close proximity to the OXPHOS pathway, the organelle genome is particularly exposed to ROS (section 1.3.1). DNA damage can also occur spontaneously, such as hydrolysis, oxidation and non-enzymatic methylation, leading to the decay of the DNA molecule (Lindahl, 1993). All these sources of damage could be mutagenic or cytotoxic if left unrepaired, and so cells have evolved several ways to overcome these problems, with a number of distinct versatile DNA repair and DNA damage tolerance machineries. Depending of the type of damage and the cell cycle stage in which the damages occur, different mechanisms will be employed to prevent the loss or modification of genetic information (figure 1.7). For example, the mechanism used to repair DNA double-strand breaks (DSBs) directly depends on the presence or not of the sister chromatid. Homologous Recombination (HR) can only occur during S or G2 phases when the sister chromatid is present, whereas Non-Homologous End Joining (NHEJ) occurs in G1 when no sister chromatid DNA can be used to repair the broken strand. In this case, heterodimer Ku70/ Ku80 brings each end of the broken strand in close proximity to allow the ligation by the complex X-ray cross-complementing protein (XRCC) 4 /ligase 4 (figure 1.7, bottom panels). When the DNA is damaged only on a single strand, depending of the type of lesion (single-strand breaks (SSBs), bulky and non-bulky base modifications, mismatch), three main repair pathways can be activated (Caldecott, 2008). All three follow a common mechanism: recognition of the damage, excision of the lesion or processing of the break, filling and subsequent sealing of the gap. Indeed, base excision repair (BER), nucleotide excision repair (NER) and mismatch repair (MMR) pathways contain proteins specialised in recognition and excision of the faulty material, and then employ specific enzymes or the replicative machinery to close the gap (figure 1.7, top panels). MMR is a post-replicative process which mainly corrects errors made by polymerases during replication (at nucleotides repeat or DNA loops for example) or as a result of non-repaired modified bases (8-

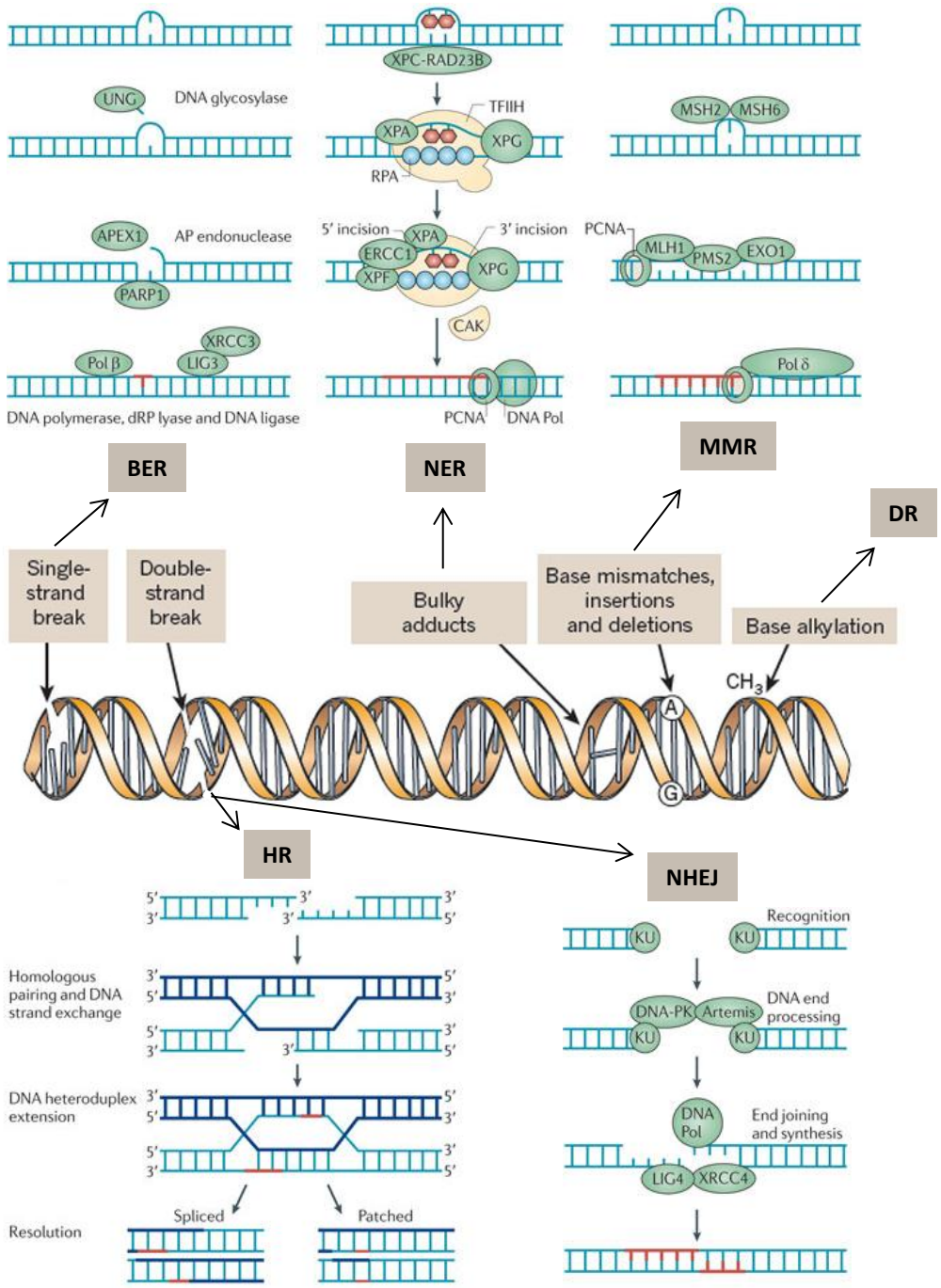

Figure 1.7: DNA damages and repair mechanisms.

Cartoon depicting the different ways the DNA molecule can be damaged. (Image was taken from Lord and Ashworth, 2012). Five major DNA repair pathways are depicted to explain how each type of damage can be fixed in eukaryotic cells. Base excision repair (BER) describes the removal of a single base by a glycosylase, leaving an abasic site being processed then filled and sealed by specialised enzymes. During Nucleotide excision repair (NER) incisions at several bases apart from the damaged DNA allow the removal of a several nucleotides which are then replaced by the replicative machinery. Mismatch repair (MMR) proteins can detect mis-pairing within the DNA molecule inducing endonuclease cleavage and gap filling by Pol δ. DSB can be faithfully repaired by homologous recombination (HR) when the sister chromatids are present (late S and G2 phases) whereas non homologous end joining (NHEJ) operates in G1 with Ku protein bringing the two ends to close proximity before being processed and re-ligated together. (Schematic was adapted from Lange *et al.*, 2011).

oxo-G leading a G:C to a T:A transition). BER deals mainly with small chemical alterations of the bases while NER intervenes with more complex injuries that induce helix distortion, which can block the replication and transcription machineries (Hoeijmakers, 2001). NER can be divided into two sub-pathways, global and transcription-coupled (tc) NER; with the latter process being initiated following RNA polymerase stalling during transcription (reviewed in Tornaletti, 2009). If DNA lesions are not repaired by BER and NER prior to S-phase and the passage of the RF, damage tolerance processes are required to prevent DNA replication from stalling (see section 1.6).

1.4.1. UV light damage and genetic disorders associated with NER deficiency

DNA damaged caused by exposure to UV light is particularly relevant for this thesis and is thus further described here. Exposure to solar UV radiation and atmospheric pollutant polycyclic aromatic hydrocarbons (PAH), which could be found in cigarette smoke, and fuel burning for example, can produce bulky adducts in our DNA. In laboratories, UV-C light and Benzo(a)pyrene [B(a)P] diolepoxide (BPDE), a metabolite of benzopyrene (byproduct of PAH), can be used to mimic the effect of those carcinogens (Thakker *et al.*, 1976). Exposure to UV-C (wavelength 100 to 295 nm) generates two main photoproducts within the DNA double helix, cyclobutane pyrimidine dimers (CPDs) and (6-4) pyrimidine-pyrimidone photoproducts [(6-4)PPs] (figure 1.8). Notably, UV-A and UV-B (320-400 nm and 295-320 nm wavelengths respectively) radiations, which terrestrial organisms are exposed to (ozone layer absorbing UV radiations < 310 nm), can also induce the formation of CPDs and 6-4 PPs (Drouin *et al.*, 1997; Mouret *et al.*, 2006). CPDs correspond to covalent bonds created between C_5 and C_6 atoms of adjacent pyrimidines, producing minor distortions of the double helix, whereas the linkage between carbons C_4 and C_6 of two adjacent pyrimidines in (6-4)PPs generates a more severe helix distortion (Rastogi *et al.*, 2010) (figure 1.8). Other damages can also arise from exposure to UV light (e.g Dewar isomers, free radicals, purine photoproducts) but to a lesser extent (figure 1.8). UV photoproducts in DNA can prove lethal to cells as they disrupt DNA replication and transcription processes (reviewed in Batista *et al.*, 2009), and so cells use NER to remove these lesions. Consequently, deficiency in NER pathways is associated with the development of genetic disorders (reviewed in Lehmann, 2003; Lehmann *et al.*, 2011). Three clinically distinct disorders have been identified to date, Xeroderma pigmentosum (XP), Cockayne syndrome (CS) and trichothiodystrophy (TTD), each corresponding to a deficiency in a specific category of NER factors. XP cells present defects in global NER factors (XPA to XPG) with XPC and XPE

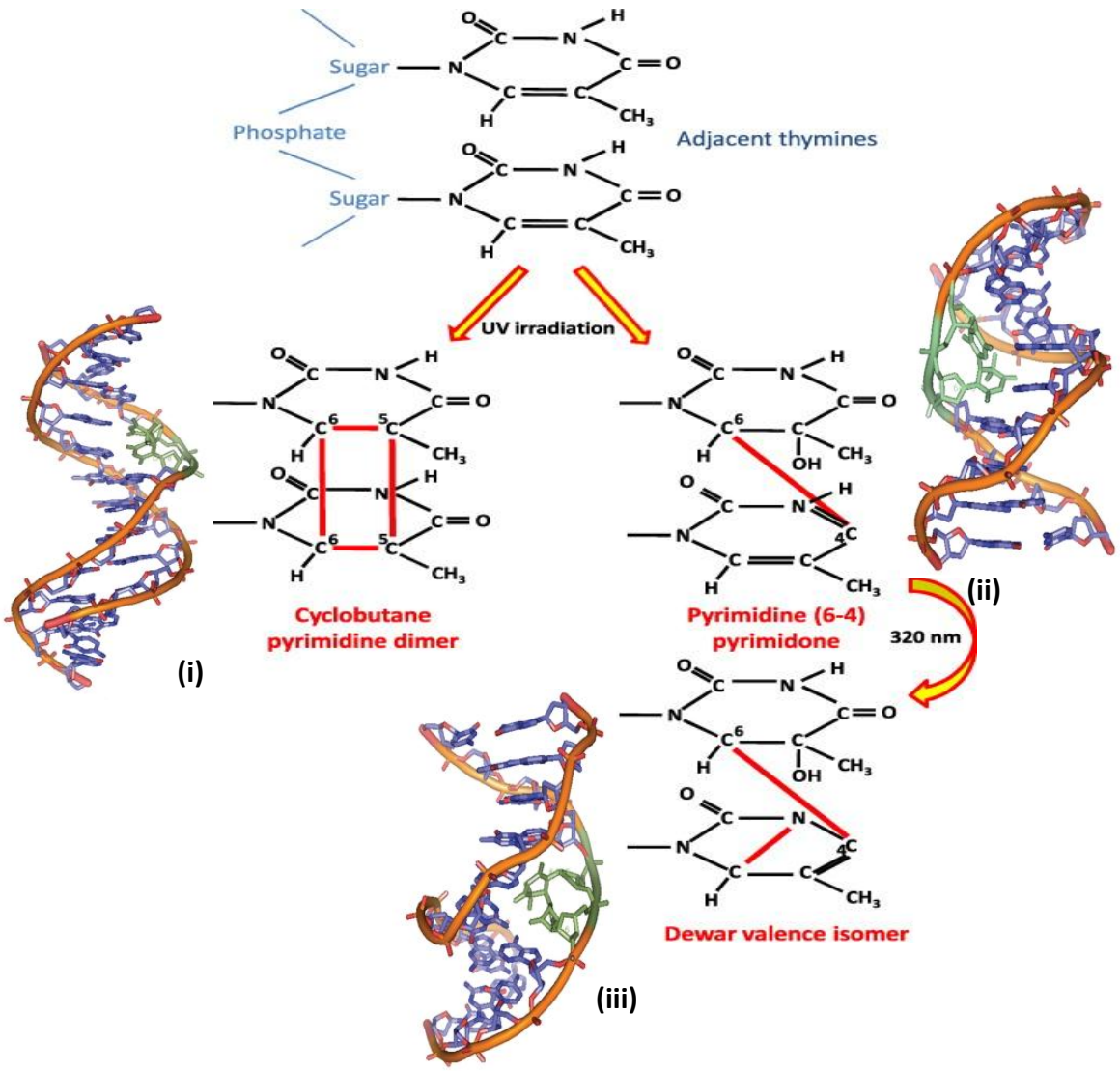

Figure 1.8: Formation of UV photoproducts in DNA.

Following UV exposure, covalent liaisons can be formed between carbon atoms (C^{number}) from adjacent pyrimidine, creating cyclobutane pyrimidine dimers (liaison between C^5 and C^6) (**i**) or pyrimidine (6-4) pyrimidone photoproducts (liaison between C^6 and C^4) (**ii**). Following UV-B or UV-A radiations (320nm), 6-4PPs can be converted into Dewar valence isomer (**iii**). The PPs are depicted in green in the 3D DNA cartoons (Schematic was taken from Batista *et al*., 2008 and the DNA cartoons taken from Rastogi *et al*., 2010)

acting specifically for the recognition of the photoproducts not involved in tc-NER; CS cells are deficient in tc-NER factors CSA and CSB, which are needed to assist RNA polymerase II (RNA pol II) progression when transcription blockages are encountered. CSB has also been shown to be involved in recruiting NER factors to stalled RNA pol II (Fousteri *et al*., 2006). Most TTD cells are deficient in transcription factor IIH (TFIIH), a ten-subunit complex needed for DNA unwinding activity involved in both global and tc-NER. Indeed patient cells with mutations in XPB, XPD and TTDA genes, all encoding different subunits of TFIIH, present characteristic TTD symptoms. There is a non-photosensitive form of the disease. Some patients with this form are mutated in TTDN1, but the functions of the gene involved are still unknown (Stefanini *et al*., 2010).

1.5. Intra-S checkpoint

Genome duplication is an essential and complex task our cells have to perform every cell cycle. Thus, a specific regulatory mechanism, called the intra-S checkpoint, monitors this process to ensure the efficient completion of this task before mitosis.

1.5.1. Cell cycle checkpoints: several points of control

Cell cycle checkpoints are control mechanisms assuring the passage from one cell cycle phase to another can be achieved safely. Cyclin-dependent kinases (CDK) 1 and 2 are two key factors of cell cycle regulation (Hochegger *et al.*, 2008). G1/S checkpoint, controlled by CDK2, determines whether the cells can replicate their genome and enter into another cycling phase (S-phase) or remain in a non-cycling (G0) stage (figure 1.9A). The G2/M checkpoint, controlled by CDK1, assures all chromosomes have been correctly duplicated before authorizing the entry into mitosis and cell division (cytokinesis) (figure 1.9A). Moreover, two internal checkpoints can be activated during S and M phases to ensure replication and mitosis processes are fully completed (figure 1.9A). Indeed, the mitotic spindle checkpoints intervenes at the end of metaphase to verify all the chromosomes are correctly aligned onto the metaphase plate before proceeding into chromosome segregation (Sullivan and Morgan, 2007) (figure 1.9A). The intra-S checkpoint on the other hand, monitors the progression of RFs and regulates origin firing (see section 1.5.2) (figure 1.9B and 1.10A). In order to approve the passage to the next phase of the cell cycle, checkpoint mechanisms also monitor the presence of DNA damage. CDK1 and 2 are both tightly controlled by DNA damage checkpoint mechanisms (Johnson and

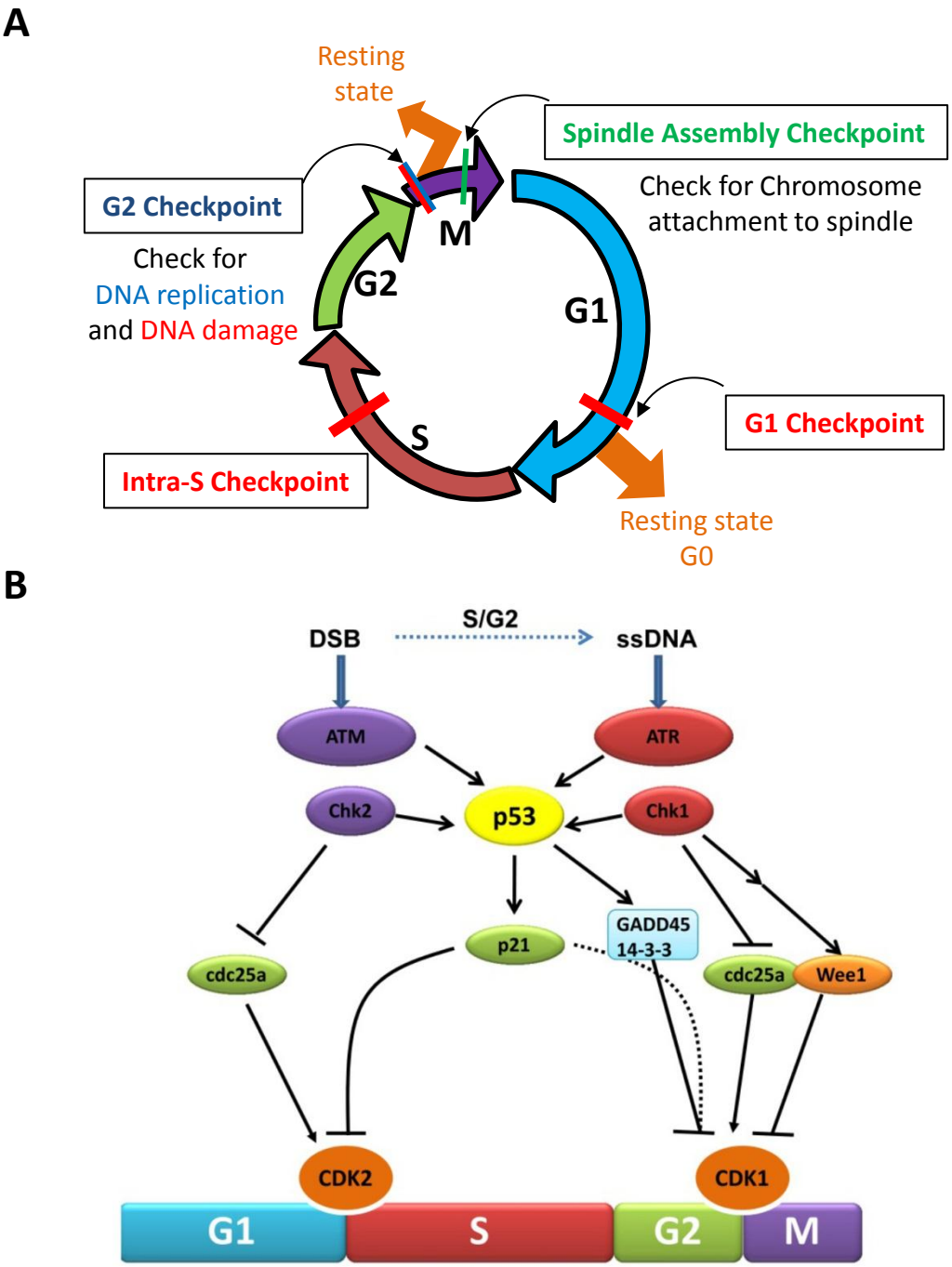

Figure 1.9: Cell cycle checkpoints.

(**A**) Cartoon depicting the cell cycle progression with the presence of different checkpoints controlling the completion of genome integrity (blue), chromosomes assembly (green) and the absence of DNA damage (red). Cells can thus arrest for a prolonged time in G0 or G2 state when problems are encountered (orange). (**B**) Control of the damage response checkpoint by ATM and ATR kinases following DSBs and ssDNA formation respectively. Downstream kinase effectors Chk1 and Chk2 regulate in a p53 independent manner CDK1 and 2 phosphorylation status, via inhibition of CDC25A phosphatase and activation of Wee1 kinase. A p53 dependent path, also inhibit G1/S and G2/M transitions via transcriptional targets p21, GADD45 and 14-3-3. (Cartoon was taken from Lopez-Contreras and Fernandez-Capetillo, 2012).

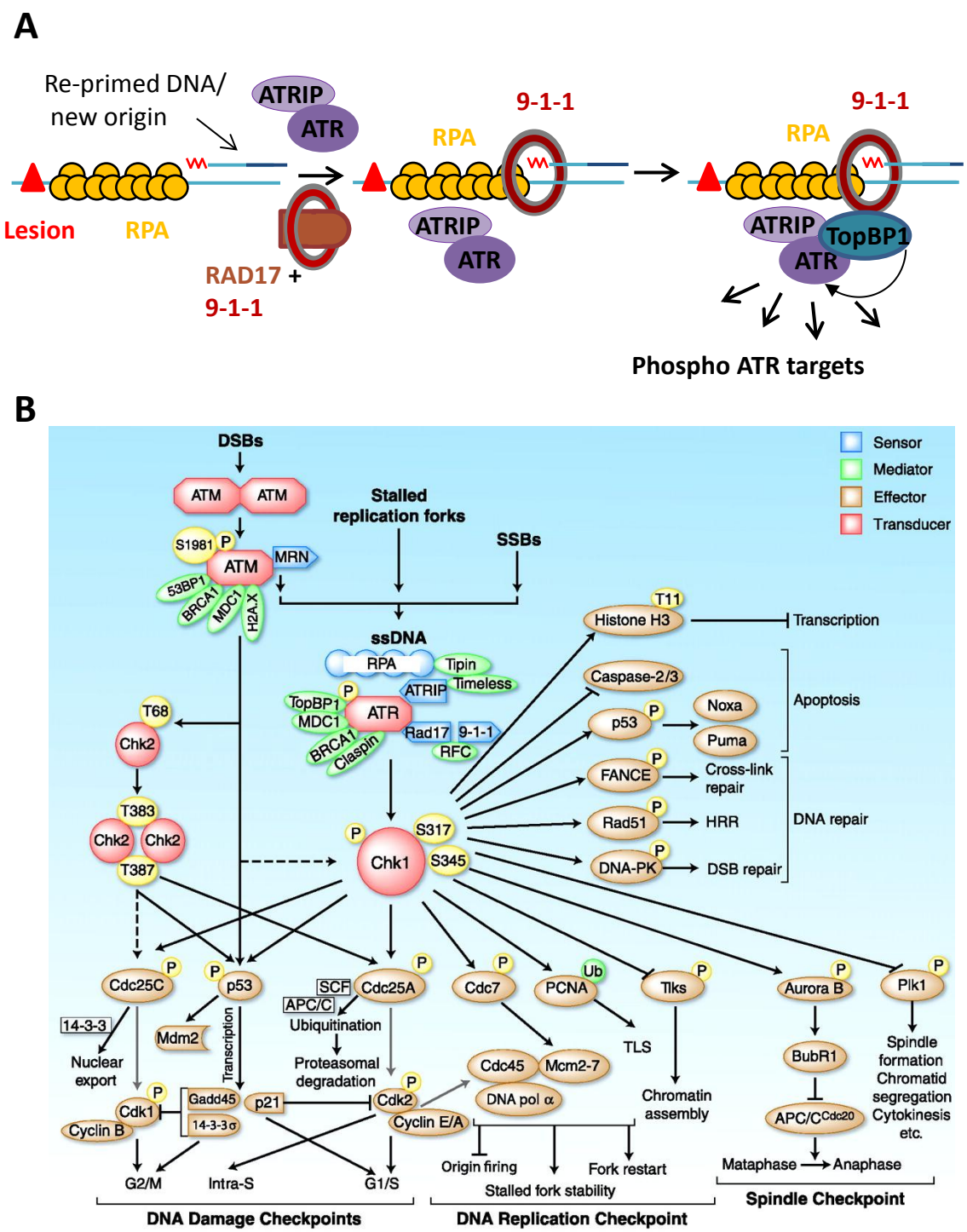

Figure 1.10: ATR activation and Chk1 pathways.

(**A**) Following replicative stress, DNA lesion (red triangle) induce uncoupling of helicase and polymerase activity leading to RPA (yellow) coating ssDNA, which induces the recruitment of ATR–ATRIP (purple) complex. RAD17 clamp loader brings then Rad9-Rad1-Hus1 (9-1-1) sliding clamp complex to the 5' end of the newly synthesised primer, which allows then the loading of TopBP1. 9-1-1 can also be loaded onto a 5' end of DNA initiated at a new origin. ATR gets fully activated once it interacts with TopBP1, and can then phosphorylate its targets. (**B**) Chk1 get phosphorylated by ATR on serine 345 and 317, allowing then phosphorylation of its downstream effectors involved in cell cycle checkpoint, DNA repair, apoptosis, and transcription mechanisms. Crosstalk between Chk1 and ATM/Chk2 activation are also described concerning the DNA damage checkpoint. (Cartoon was taken from Dai and Grant, 2010).

Shapiro, 2010) (figure 1.9B). Two main DNA damage sensing kinases, part of the PIKK (phosphatidylinositol-3-kinase related kinase) family, are responsible for triggering the DNA damage checkpoint and amplifying the DNA repair response, being ATM (Ataxia telangiectasia mutated) and ATR (ATM and Rad3-related protein) (figure 1.9B). ATM is activated following DSBs formation whereas the ATR response is induced during S-phase following RF stalling (Zhou *et al.*, 2003) (figure 1.9B and 1.10B). Following DSB, the MRN complex composed of Mre11-Rad50-Nbs1, recruits ATM to the break and triggers its activation resulting in the phosphorylation of checkpoint kinase 2 (Chk2) (Lee and Paull, 2004) (figure 1.10B). Following RF stalling, ATR is recruited to the stalled fork and activates its main effector Chk1, discussed in detail in the following section. One of the main goals of DNA damage checkpoints is thus to allocate more time for the cell to repair its damaged DNA by inducing a cell cycle arrest (Weinert and Hartwell, 1989) by inhibiting CDK 1 or 2 activities (figure 1.9B); otherwise the apoptosis response can be triggered by the presence of excess DNA damage (figure 1.10B).

1.5.2. Activation of ATR and the intra-S checkpoint

ATR becomes activated following RF stalling, when the MCM 2-7 helicase complex and the DNA polymerase activities are uncoupled, which results in extensive stretches of ssDNA coated by RPA downstream of the fork (Byun *et al.*, 2005) (figure 1.10A). Others factors, for example processing of UV damaged DNA by NER, or resection of a DSB, can produce ssDNA activating the intra-S checkpoint (Cimprich and Cortez, 2008). The production of RPA-coated ssDNA triggers the recruitment of ATR via ATRIP (ATR-interacting partner) and the RAD9–HUS1–RAD1 (9-1-1) and topoisomerase-binding protein 1 (TOPBP1) complexes (Byun *et al.*, 2005; Yang and Zou, 2006). TOPBP1 can then activate ATR, which in turn phosphorylates its targets (Mordes and Cortez, 2008). Further, studies from the Cimprich laboratory have highlighted the importance of primed RPA ssDNA for the checkpoint response, and notably for the loading of the 9-1-1 complex (Byun *et al.*, 2005) (figure 1.10A). Indeed, the authors demonstrated the uncoupling of the MCM helicase and DNA polymerase was not sufficient to activate the ATR effector Chk1 when Pol α and the replicative Pols were inhibited by aphidicolin treatments (Byun *et al.*, 2005). In line with this, loss of PCNA, Pol δ or Pol ε also reduces the phosphorylation of Chk1 (Van *et al.*, 2010), thus DNA synthesis at a stalled fork is needed to activate the checkpoint response. The current understanding of ATR activation involves a two-part mechanism; first, RPA coated ssDNA recruits ATR-ATRIP complex, and second, the 9-1-1 complex is recruited via the RFC-like clamp loader RAD17 (Bermudez *et al.*, 2003) onto a ss-ds

DNA junction on the 5' end of a downstream DNA strand, provided by a newly synthesised primer or an adjacent origin (figure 1.10A). Recently, the 9-1-1 complex has also been described to be needed for the amplification of the activation of ATR by TOPBP1 (Nam and Cortez, 2011; Lin *et al*., 2012b). Once activated, ATR can phosphorylate many targets (several hundreds), including its main effector Chk1, and also itself, in order to initiate the signalling cascade needed for regulating the cell cycle checkpoint, RF stability and origin firing.

1.5.3. ATR/Chk1 pathway regulates both cell cycle and S-phase progression

1.5.3.1. Cell cycle progression: control of mitotic entry and origin firing

Chk1, first characterized in fission yeast *S. pombe* (Walworth *et al.*, 1993), has since then been shown to contribute to the regulation of all cell cycle checkpoints defined to date (review in Dai and Grant, 2010) (figure 1.10B). Like ATR, both kinases are essential genes in higher eukaryotes, reflecting their roles in the DNA damage response (DDR) but also in unperturbed cell-cycle progression (Brown and Baltimore, 2000; Takai *et al.*, 2000). Following ATR activation, Chk1 is phosphorylated on serine residues 317 and 345 (Zhao and Piwnica-Worms, 2001) activating the kinase to phosphorylate in turn its own substrates (figure 1.10B). Claspin has been described as the main Chk1 regulator and also to be essential for ATR phosphorylation of Chk1 (Kumagai and Dunphy, 2000; Kumagai *et al.*, 2004). Once activated, Chk1 is released from chromatin to allow the diffusion of the signal through the nucleus (Smits *et al.*, 2006). As previously mentioned, ATR/Chk1 pathway controls the two major cell cycle checkpoint mechanisms, mitotic entry and origin firing, via the regulation of CDK1 and CDK2 respectively (figure 1.9B). Indeed, Chk1 activates the kinase Wee1, which inhibits the entry in mitosis by phosphorylating CDK1, and Chk1 also inhibits the phosphatase CDC25A responsible for removing the inhibitory phosphorylation of CDK (Furnari *et al.*, 1997; Beck *et al.*, 2010) (figure 1.9B). CDC25A also stimulates CDK2 activity (Sampath *et al.*, 2002) (figure 1.9B) and by consequence the loading of CDC45 onto the MCM complex at licensed origins (figure 1.2B). In the presence of activated Chk1, origin firing is then prevented via inhibition of CDK2. Moreover Chk1 induces phosphorylation of CDC7 which is also implicated in origin firing via its activation of the MCM complex (figure 1.2B) (Heffernan *et al.*, 2007). In line with this, Chk1 basal activity during unperturbed S-phase (not in response to damaging treatments) is also involved in replication progression by controlling origin activity (Maya-Mendoza *et al.*, 2007; Petermann *et al.*, 2010).

1.5.3.2. Intra-S checkpoint response following S-phase impediments

Bulky DNA lesions pose a substantial problem during DNA replication as they can physically block the replisome. The intra-S checkpoint has therefore a primordial role in response to this type of damage by triggering a cell cycle arrest and managing the damage repair machinery as described previously. However, it has been noticed that the checkpoint response varies according to the amount of damage encountered. Pulse-chase velocity-sedimentation experiments performed by Kaufmann and Cleaver allowed discrimination between low doses of UV-C, which inhibits only the initiation of replication, and higher doses exposure where both initiation and elongation steps are inhibited (Kaufmann and Cleaver, 1981; Cleaver *et al.*, 1983). Latter experiments, using DNA combing analysis, confirmed these data and the role of the intra-S checkpoint kinases ATR and Chk1 in the regulation of DNA initiation following UV treatments (Chastain *et al.*, 2006). However, a study performed by Heffernan and co-workers ruled out the involvement of the CDC25A-CDK2 pathway and proposed instead the CDC7-Dfb4 complex as a target of Chk1 following UV irradiation (Heffernan *et al.*, 2007). Using BPDE compound and chromatin immunoprecipitation (ChIP) experiments, Liu and co-workers found CDC45 chromatin association was reduced in a Chk1 dependent manner, but on the other hand, CDC25A, CDK2 and CDC7 were unlikely to be Chk1 targets following BPDE treatment (Liu *et al.*, 2006). Therefore different checkpoint responses could occur depending on the type and the intensity of damage perceived by the cell during S-phase.

1.5.3.3. Involvement of ATR and Chk1 in replication fork maintenance

Increasing evidence has also shown the importance of ATR and Chk1 in maintaining replication fork stability. Firstly, it was demonstrated in yeast that following methyl methanesulfonate (MMS) treatment, mitosis entry checkpoint kinase or Mec1 (ATR ortholog) deficient cells presented an increased number of collapsed RFs (Tercero and Diffley, 2001). To date, it is still not known exactly which mechanism(s) permit the maintenance of RFs. Several hypotheses suggest ATR signaling could prevent DSB formation during HR repair via endonuclease Mus81 (Lopez and Fernandez-Capetillo, 2010), or be involved in RF restart (Friedel *et al.*, 2009). Nonetheless, ChIP experiments performed in yeast revealed a direct interaction between Mec1 (ATR) and Pol α and ε following HU treatment (Cobb *et al.*, 2003). Moreover, following a study in Xenopus under replication stress, ATR signalling has been involved in promoting new origin firing (via MCM helicase activity and polo-like kinase Plk1) in proximity of stalled RF

(Trenz *et al.*, 2008). This mechanism, in apparent contradiction with the previously described path Chk1-CDC25A-CDK2 which inhibits global origin firing, ensures completion of DNA replication by activating dormant origins during replication stress (Ge *et al.*, 2007).

A role of Chk1 has also been demonstrated to be independent of ATR activation. First following UV-C irradiation, a recent study from the Gottifredi laboratory has highlighted the role of Chk1 during RF progression independently of its kinase activity (Speroni *et al.*, 2012). According to the authors, Chk1 was necessary for the recruitment of TLS polymerases Pol eta (η) and iota (ι) at the stalled RF, in an ATR independent mechanism. The authors suggested this recruitment was via Chk1 PIP motif, which is needed for Chk1 to release from chromatin following UV irradiation (Scorah *et al.*, 2008). A previous study also reported Chk1 was involved in PCNA ubiquitylation following UV-C in a kinase independent manner via Claspin and Timeless (Tim) (Yang *et al.*, 2008). A second role of Chk1 independent of ATR activation has been observed during normal S-phase. Indeed, Chk1 has been shown to have a direct influence on RF progression in unperturbed conditions. Following the protein depletion by RNAi, or in DT40 knockout (KO) cells, DNA combing analysis revealed a severe decrease of RF speed (Petermann *et al.*, 2006). An increased number of active origins were also observed, but not sufficiently to compensate the decrease of RF speed. The authors concluded Chk1 was needed to maintain the stability of individual RFs. Claspin depletion also produces similar phenotypes, with a decrease of RF rate, and a double deletion Claspin/Chk1 has an additive effect on RF speed (Petermann *et al.*, 2008).

1.5.3.4. Regulation of ATR activation: replication fork protection complex

Experiments performed with UV-C exposure have unravelled three novels factors implicated within the intra-S checkpoint signalling, Claspin, Tim and Timeless interacting protein (Tipin), which together form the replication fork protection complex (RFPC) (Noguchi *et al.*, 2004). Depletion of Claspin and Tim was reported to diminish significantly Chk1 activation by ATR in response to UV-C irradiation (Kemp *et al.*, 2010). Moreover depletion of Tim and Tipin can reverse the effect of the checkpoint activation following UV treatment and release inhibition of replication initiation (Unsal-Kacmaz *et al.*, 2007). In the same study, Tipin was also shown to be responsible for the decrease of DNA chain elongation in active replicons, as a response of the intra-S checkpoint activation. On the other hand, during unperturbed conditions, Tim was shown to have a direct impact on RF progression during normal replication, as its deletion was followed with a 50% decrease of DNA chain elongation (Unsal-Kacmaz *et al.*, 2007). Tim-Tipin

complex seems therefore to have a role within the replisome of coupling DNA unwinding with DNA synthesis (helicase-polymerase coupling function) in order to prevent ssDNA accumulation and over activation of ATR-Chk1 pathway (Smith *et al.*, 2009). Studies in Xenopus by the Costanzo group have identified And1 as a Tipin binding partner and together they promote and stabilize loading of Pol α on chromatin (Errico *et al.*, 2009) thus influencing ATR activation.

1.6. DNA damage tolerance

During S-phase when a RF encounters a lesion, NER can no longer repair the damaged DNA. Thus, cells use damage tolerance to allow completion of genome duplication and to return the lesion back in double-stranded (ds) DNA, where it can be subsequently repaired. PCNA ubiquitylation (figure 1.11A) is believed to be involved in controlling damage tolerance mechanisms, the two most common processes being translesion synthesis (TLS) and template switching (figure 1.11B). In the first case, a switch between replicative and TLS polymerases occurs to allow the bypass of the lesion and complete DNA replication (figure 1.11B). In the second case, a strand invasion mechanism occurs to utilise the undamaged sister chromatid as a new template to allow DNA replication to bypass the lesion (figure 1.11B). A third process, called fork reversal, which produces a so-called “chicken foot” structure (figure 1.11B), has also been described in prokaryotes (Courcelle *et al.*, 2003), however little evidence of this process exists in eukaryotic cells (Lopes *et al.*, 2006). Ubiquitylation of the polymerase sliding clamp PCNA (figure 1.11A) is crucial for the coordination of damage tolerance, however a number of studies also elevated the Y-family polymerase Rev1 to a central position in this process (reviewed in Sale, 2012).

Evidence of DNA damage tolerance mechanisms has first been described in NER deficient *E. coli* cells with Rupp and Howard-Flanders work showing following UV irradiation ssDNA gaps are created then subsequently sealed by HR mechanisms (Rupp and Howard-Flanders, 1968; Rupp *et al.*, 1971). In mammalian cells, a similar experiment has been adapted to allow the author to visualise the filling of these gaps with *de novo* DNA synthesis and not recombination events (Lehmann, 1972). Later on, this technique was re-used to demonstrate XP variant (XP-V) cells were deficient in post-replication repair or PRR (Lehmann *et al.*, 1975). It took nearly 20 years to discover the gene defective in these cells was encoding for a translesion synthesis polymerase, Pol η, which can efficiently bypass the most common UV photoproducts, CPDs (Masutani *et al.*, 1999; Johnson *et al.*, 1999b). The damage tolerance

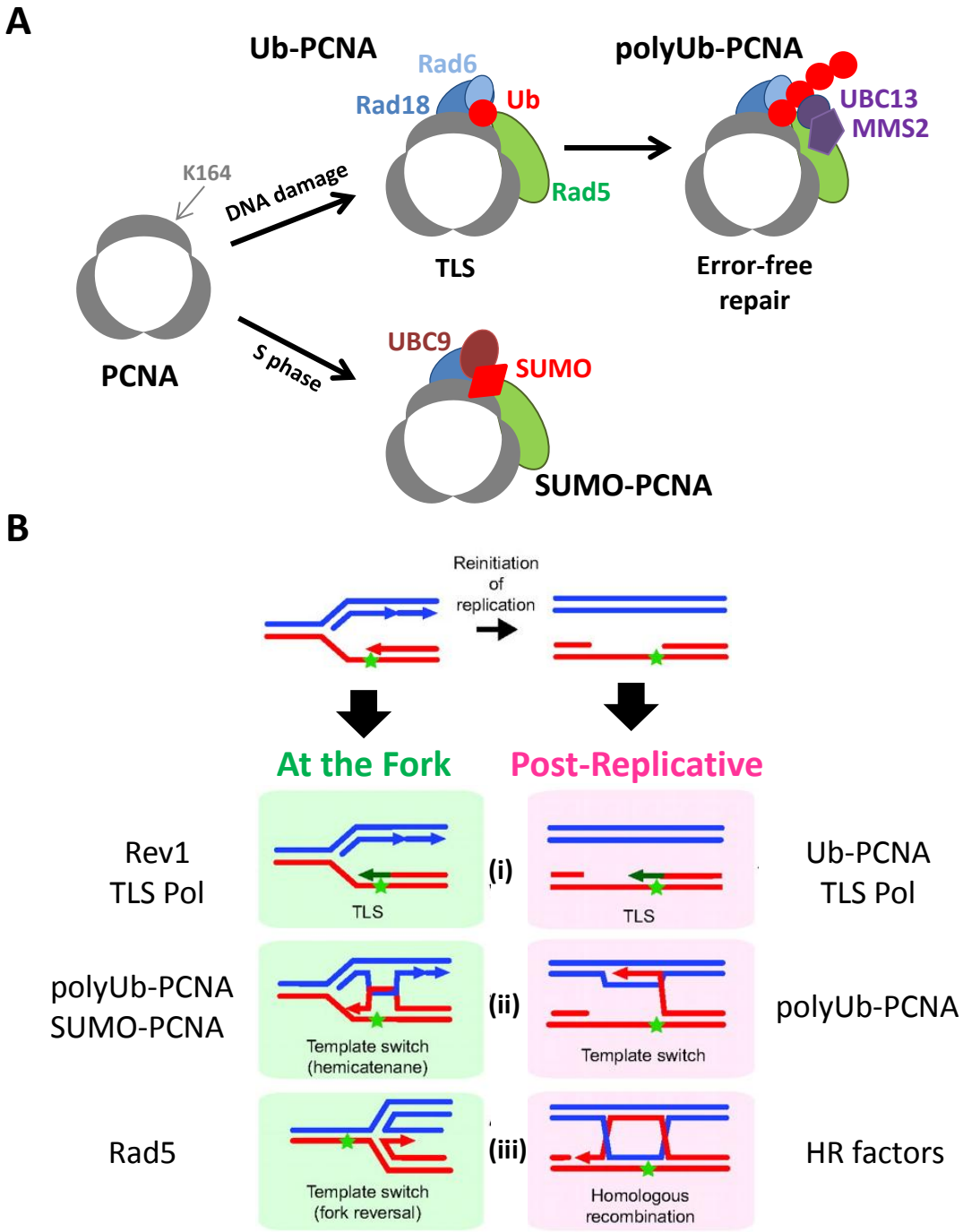

Figure 1.11: PCNA modifications and DNA damage tolerance.

(**A**) In response to DNA damage, PCNA can get mono-ubiquitylated (Ub-PCNA) on K164 by RAD6 and RAD18, E2 and E3 Ub ligases. Poly-ubiquitylation of PCNA (polyUb-PCNA) can then occur thanks to UBC13 and MMS2, both recruited to chromatin by RAD5, linking ubiquitin molecules together on their lysine K63. PCNA can also get SUMOylated (SUMO-PCNA) by UBC9, which binds to RAD18 and RAD5, and SUMO ligase. (Cartoon was adapted from Hoege *et al.*, 2002) (**B**). Damage tolerance can occur during replication (green) or post-replicatively (pink). In both cases, 3 alternative ways can be used to overcome the damaged DNA; (**i**) TLS Pol are recruited to the damage by Rev1 or Ub-PCNA. (**ii**) Template switch mechanisms can occur following polyUb or SUMO-PCNA. (**iii**) PCNA independent mechanisms involving Homologous Recombination (HR) factors or RF reversal mechanisms can also happen. (Cartoon was adapted from Sale, 2012).

field expanded then quickly after that with a plethora of new TLS polymerases being discovered and regrouped in a new sub-category, the Y-family polymerases (Ohmori *et al.*, 2001).

1.6.1. The Y-family Polymerases – uniquely adapted for TLS

TLS polymerases are composed of the Y-family polymerases eta (η), iota (ι), kappa (κ) and Rev1 and B family polymerase zeta (ζ). Although numerous DNA polymerases can catalyse TLS, it is the Y-family polymerases that are uniquely adapted for this process, and this is reflected in the structure of their catalytic site. The active site of all DNA polymerases conforms to a "right hand" topology forming a "U" shaped cleft, in which the catalytic residues sit in the "palm" subdomain, whilst the "fingers" and "thumb" subdomains grasp the DNA molecule (Ollis *et al.*, 1985; Rothwell and Maksman, 2005) (figure 1.12A). However, Y-family polymerases also possess a "little finger" which appears to be a key feature discriminating the specificity of each Y-family polymerase towards their DNA lesion of choice (Boudsocq *et al.*, 2004) (figure 1.12A). Moreover, in comparison to the replicative family B-polymerases, Y-family polymerases have a more spacious catalytic site with shorter fingers and thumb subdomains, thus diminishing the contacts towards DNA template and nucleotides. These features facilitate TLS but result in decreased processivity and fidelity on an undamaged DNA template (Sale *et al.*, 2012) (figure 1.12A). Pol η for example can only incorporate few nucleotides before its dissociation from the DNA template (Washington *et al.*, 1999), whereas Pol δ can extend up to 7 kb in a single DNA template binding event (Burgers, 1991). A recent study has demonstrated the crucial role of a polypeptide linker in tethering the catalytic domain and the C-ter DNA binding domain of Y-family polymerases (Wilson *et al.*, 2012). Modification of this internal domain of the enzyme influences the fidelity of the polymerase by changing the orientation of the catalytic site and the binding with its substrate. In addition to these structural differences between Y-family and replicative (A and B families) DNA polymerases, another key feature that distinguishes both types of enzymes is the presence of a 3' to 5' exonuclease activity (figure 1.12B). Indeed, Pol γ, δ and ε all possess this intrinsic proofreading capability of removing nucleotides introduced by mistake during the elongation phase of DNA synthesis. However, TLS polymerases lack this activity reinforcing their low fidelity on undamaged DNA and facilitating (mis)incorporation opposite damaged DNA templates (Sale *et al.*, 2012).

A

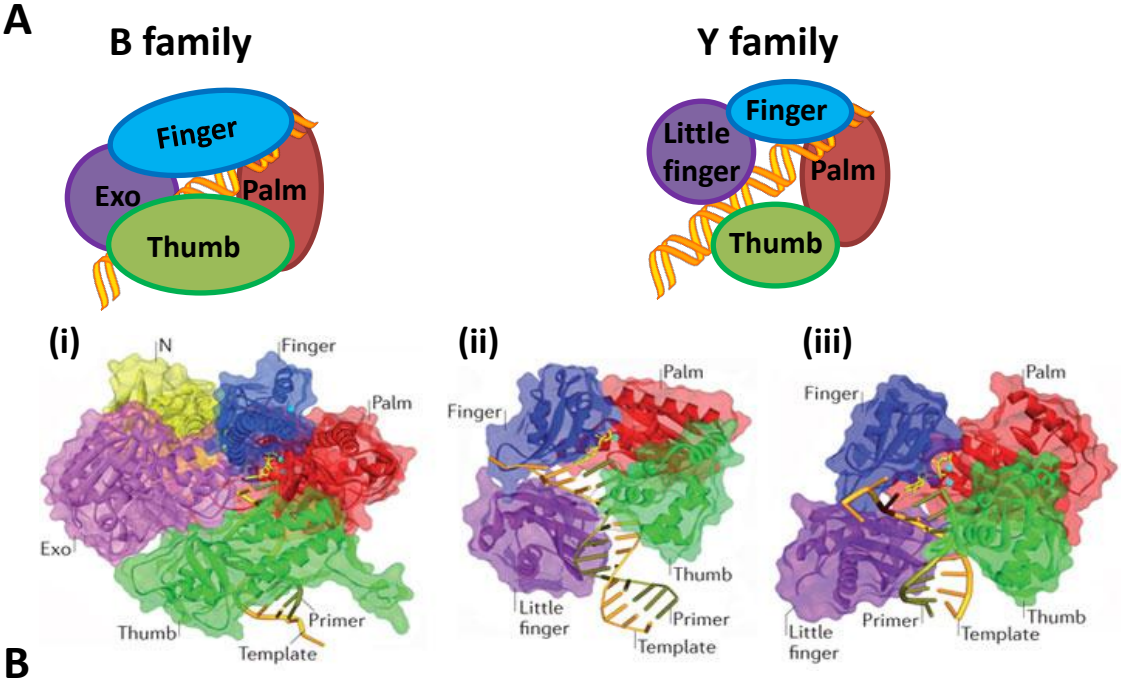

B

Family (phylogeny)	members	main activities	additional domains
A (*E.coli* Pol I)	Pol γ	mtDNA replication and repair (BER)	3'-5' exo, dRP-lyase
	Pol θ	Defence against IR? TLS? BER?	dRP-lyase, helicase-like
	Pol ν	ICL repair? TLS?	no
B (*E.coli* Pol II)	Pol α	DNA replication priming	no
	Pol δ	DNA replication (Okazaki fragment), NER, MMR	3'-5' exo
	Pol ε	DNA replication NER, MMR	3'-5' exo
	Pol ζ	TLS, mutagenesis	no
X (*H.sapien* Pol β)	Pol β	BER, meiotic recombination	dRP-lyase
	Pol λ	VDJ, end joining ? BER?	dRP-lyase
	Pol μ	VDJ, end joining?	no
	TDT	Immunoglobulin diversity, end joining?	no
Y (*E.coli* DinB)	Pol η	TLS (bypass CPDs)	no
	Pol ι	TLS, BER	dRP-lyase
	Pol κ	TLS, (bulky lesions), NER	no
	Rev1	TLS, platform to anchor TLS pol	no

Figure 1.12: DNA polymerase families.

(**A**) Right hand structure of B and Y family polymerases. Both types of polymerases have a palm (red), thumb (green), and finger (blue) like motifs forming a U shaped cleft where DNA molecule can fit. Thumb and finger from Y family Pol are shorter reducing the contact with the DNA template. B family polymerases (**i**) also have an exonuclease domain whereas Y family Pol (**ii** and **iii**) have a little finger domain (purple). Crystal structures of B family bacteriophage RB69 Pol (**i**), Y family archaeal (Sulfolobus solfataricus) Dpo4 (**ii**) and human Pol η (**iii**), with DNA molecules. (Cartoon was adapted from Sale *et al.*, 2012). (**B**) Table summarising eukaryotic DNA polymerases regrouped in 4 main families according to their phylogenetic resemblance (in parentheses, name of the protein of reference). Uncertain activities are followed by a question mark. Additional domain providing 3'-5' exonuclease (3'-5' exo), deoxyribose 5-phosphate (dRP) lyase and helicase activities are also indicated. (Table was adapted from Lange *et al.*, 2011).

1.6.2. DNA polymerase eta

Pol η (or RAD30A in yeast) is the only TLS polymerase directly associated with a genetic disorder, XP-V, thus explaining why it has been studied extensively (Masutani *et al.*, 1999; Johnson *et al.*, 1999b). XP is characterised by sensitivity to sunlight and a predisposition to skin cancers, but whilst the majority of XP diseases are caused by a defect within the NER pathway (Lehmann *et al.*, 2011) (section 1.4.1), XP-V patients, lacking functional Pol η, are defective in DNA synthesis following UV irradiation (Lehmann *et al.*, 1975). This is due to the principal role of Pol η in bypassing the most frequent UV photoproduct CPDs, which is achieved in an error free manner as two adenines are inserted opposite a thymidine-thymidine (TT) dimer (Johnson *et al.*, 1999a) (figure 1.13A). Moreover, the polymerase can remodel the distorted DNA helix into a stable B-form conformation (referred as a "molecular splint") to prevent any slippage or frameshift mutations occurring downstream of the lesion (Biertümpfel *et al.*, 2010). In Pol η deficient XP-V cells, Pol ι has been reported to take over this responsibility with the collaboration of Pol κ and ζ in an error-prone mechanism (Dumstorf *et al.*, 2006; Ziv *et al.*, 2009) (figure 1.13A). This could then explain why XP-V cells present higher mutations rate following UV light exposure (Maher *et al.*, 1976; reviewed in Cordonnier and Fuchs, 1999).

A role of Pol η during unchallenged S-phase has also been demonstrated by the Hoffmann group. Their research attributed the recruitment of Pol η at chromosome fragile sites and the involvement of both Pol η and κ at naturally occurring non-B DNA structures, like G-quadruplexes (G4) (Rey *et al.*, 2009; Bétous *et al.*, 2009). Pol η, like Rev1, seems to also participate in another important DNA metabolic process with the generation of somatic mutations during immunoglobulin (Ig) gene hypermutation (Kano *et al.*, 2012). Following the deamination of a cytosine to uracil, initiated by AID (activation-induced by deaminase), DNA replication or repair mechanisms generate mutations depending on the polymerase involved in the process. Pol η was shown to be mutagenic opposite A and T predominantly (Zeng *et al.*, 2001). In addition to this role in single-base substitution during Ig diversification, Pol η has also been shown to participate in HR mediated gene conversion and DSB repair (Kawamoto *et al.*, 2005).

1.6.3. DNA polymerases kappa and iota

According to phylogenetic analysis of the Y-family polymerases, Pol κ is the closest member to *E. coli* Pol IV (encoded by DNA damage-inducible DinB gene) and is the most conserved of all Y-

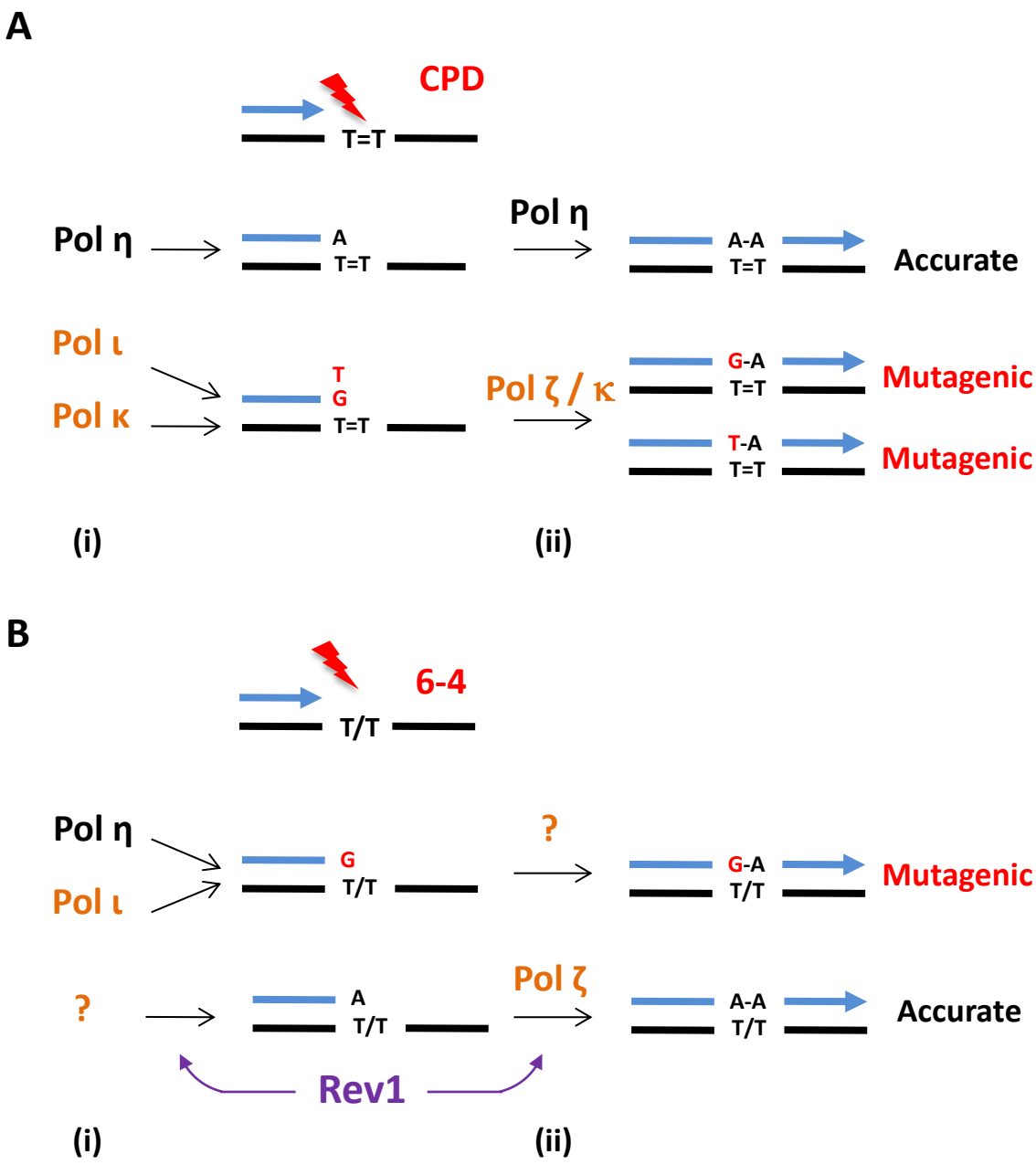

Figure 1.13: Collaborative TLS mechanisms past UV photoproducts.

Involvement of TLS polymerases in the bypass of UV photoproducts across CPDs (**A**) or 6-4PPs (**B**). Collaborative polymerase mechanism is described in XP-V cells (orange) or Pol η proficient cells (black). Inserter polymerase (**i**) incorporates the first nucleotide opposite the 3' end of the lesion, whereas extender polymerase (**ii**) adds a nucleotide opposite the 5' end of the lesion and beyond (blue arrow). Non-catalytic function of Rev1 (or platform function), assisting both insertion and extension steps, is also indicated (purple). Mutagenic (red) or error-free (accurate) TLS processes are indicated on the right. Both models are adapted from *in vivo* data provided by (Ziv *et al.*, 2009) for CPDs and by (Yoon *et al.*, 2010; Szüts *et al.*, 2008) for 6-4PPs.

family polymerases as it is present in all domains of life, but is lacking in *S. cerevisiae* (Ohmori *et al.*, 2001). Pol κ, originally called Pol theta (θ), has been described as the most accurate Y-family polymerase on undamaged DNA with an error rate of 10^{-3} (Johnson *et al.*, 2000; Burgers *et al.*, 2001). Pol κ has been demonstrated *in vitro* to have little ability to incorporate opposite UV photoproducts, and has been described as an extender of mismatched termini (Haracska *et al.*, 2002; Washington *et al.*, 2002). This has been supported by an *in vivo* study in XP-V cells in which Pol κ played a minor role in CPD bypass (Ziv *et al.*, 2009) (figure 1.13A). These properties of Pol κ can be explained by the relatively constricted catalytic site and the presence of an additional subdomain, the N-terminal (N-ter) clasp, which allows Pol κ to encircle the DNA molecule (Lone *et al.*, 2007). However, these features are also responsible for increasing the tendency of Pol κ to skip one nucleotide leading to a -1 frameshift, which was previously observed in other DinB prokaryotic homologues (Lone *et al.*, 2007). Another similarity with Pol κ homologues is the capacity of the human enzyme to bypass B[a]P adducts *in vitro* (Ohashi *et al.*, 2000), in line with this, it has been observed that Pol κ KO (*Pol* $\kappa^{-/-}$) mice cells are more sensitive to the killing and mutagenesis effect of this drug (Ogi *et al.*, 2002).

Pol κ has also been implicated in the DNA synthetic step of NER (Ogi and Lehmann, 2006). The Y-family polymerase is recruited by PCNA and XRCC1 to sites of NER (Ogi *et al.*, 2010), and is suggested to be required during conditions of low dNTP concentrations (following HU treatment for example) or when the template for repair is abnormal (Lehmann, 2011). Sensitivity of *Pol* $\kappa^{-/-}$ mice cells toward UV exposure could then be due to role of the enzyme in NER or TLS (Ogi *et al.*, 2002).

Pol ι, also referred as *RAD30B*, is a paralogue of Pol η. Pol ι has also been shown *in vitro* to incorporate nucleotides opposite the 3'T of CPDs and (6-4)PPs (Tissier *et al.*, 2000), and to contribute *in vivo*, in collaboration with Pol ζ, to error-prone TLS bypass of CPDs (Ziv *et al.*, 2009) (figure 1.13). One characteristic feature of Pol ι concerns its fidelity towards different non-damaged template; Pol ι incorporates a correct dT opposite an dA with a high percentage of success, while generally fails to incorporate a dA opposite a dT template and instead places a dG (3 to 10 times more often than dA). This distinction comes from a particularity of the active site of the enzyme, to restrain the positioning of the template nucleotide in a specific orientation (*syn* or *anti*) (Johnson *et al.*, 2006). One direct consequence concerns the replication of 8-oxo-G as Pol ι restricts the oxidised base in a *syn* position and thus allows the correct Watson-Crick pairing of a dC (Kirouac and Ling, 2011). Pol ι has also been shown to be involved in BER; the enzyme possesses dRP lyase activity, and can perform BER *in vitro*

(Bebenek *et al.*, 2001). Also, Pol ι down-regulated cells are more sensitive to oxidative stress and present a reduced BER activity (Petta *et al.*, 2008).

1.6.4. Rev1, a recruitment platform with dCMP transferase activity

Characterisation of *rev1* gene, part of the *reversionless* mutants family, was first described due to the loss of mutations obtained after depletion of the gene in budding yeast following UV treatments (Lemontt, 1971). It was thought originally that the protein was an accessory factor inducing a reduction of the fidelity of replicative polymerases. However, it was found that the *rev1* gene actually encodes a deoxycytidyl transferase, capable of incorporating dC opposite a templated G or abasic site (Nelson *et al.*, 1996). Rev1 can also correctly incorporate dC opposite bulky G adducts (N^2-dG) adducts (Zhang *et al.*, 2002). Rev1's specialisation to bypass these lesions was highlighted in the crystal structure of this Y-family polymerase (Nair *et al.*, 2005). When Rev1 encounters a guanine on the DNA template, the base is flipped out of the helix through interaction with the little finger domain; the templated guanine is replaced by an arginine residue (part of Rev1 little finger sub-domain), which hydrogen bonds specifically with the incoming dCTP. This mechanism, preventing the need for hydrogen bonding with the templated base, ensures the correct incorporation of dC opposite adducted guanines and abasic site (Nair *et al.*, 2005).

In addition to its catalytic activity, Rev1 is also needed for recruitment of other TLS polymerases to sites of UV damage. Indeed, Rev1 cannot incorporate opposite TT dimers *in vitro* but is required for their bypass *in vivo* (Nelson *et al.*, 2000; Szüts *et al.*, 2008), and several reports have built up a two or three steps model requiring the non-catalytic part of Rev1 (Ross *et al.*, 2005; Wojtaszek *et al.*, 2012a and b). Indeed, a Rev1 Interaction Region (RIR) has been characterised in several TLS polymerases, recognising the C-ter domain of Rev1 (Guo *et al.*, 2003; Kosarek *et al.*, 2008). Complementation studies of *rev1* KO DT40 cells with different human Rev1 polypeptides (hRev1) have confirmed this by the rescue of WT phenotypes following UV-C or 4NQO treatments with full length, N-ter deletion and catalytic null hRev1, but not with C-ter truncation mutants (Edmunds *et al.*, 2008). A direct collaboration between Rev1 and Pol ζ has also been characterised for the bypass of (6-4)PPs *in vivo*, where Rev1 is involved in the recruitment of Pol ζ and also the maintenance of its frame fidelity past the lesion (Szüts *et al.*, 2008) (figure 1.13B). Crystal structure of a quaternary TLS polymerase complex has confirmed this model showing that the Rev1 C-ter domain acts as a platform,

binding simultaneously to the RIR of Pol κ and Rev7 subunit of Pol ζ (Wojtaszek *et al.*, 2012a and b). This configuration has been proposed to explain the two steps model in which a first polymerase (Pol κ) acts as an inserter (incorporating the nucleotide opposite the lesion) and a second one (Pol ζ) as an extender (prolonging the synthesis until the replicative polymerase takes over) (figure 1.13B).

Rev1 also participates in the replication of naturally occurring impediments arising during unperturbed DNA synthesis, such as nucleotide repeats and G4 quadruplex structures. The first case was demonstrated in budding yeast where the presence of Rev1 BRCT domain reduces the mutability at CAG.CTG tracks, without the need of the catalytic activity of the enzyme (Collins *et al.*, 2007). Also, like Pol η and κ (but not Pol ι), Rev1 has been implicated in the bypass of G4 DNA structures and more specifically, for their replication on the leading strand (Bétous *et al.*, 2009; Sarkies *et al.*, 2010). In this case, Rev1 deoxycytidyl transferase activity seems to be an active part of the process possibly by generating dC tracks destabilising the dG rich template. The same study also analysed how the absence of Rev1 impacts on epigenetics by forcing the cells to use another damage tolerance pathway to replicate past G4 structures. Loss of dimethylated histones and increase of newly synthesized histones was observed in those cells following ChIP, resulting in up-regulation of the transcription of the genes containing G4 structures (Sarkies *et al.*, 2010). As mentioned previously, Rev1 also participates to Ig gene hypermutation (Kano *et al.*, 2012), with a G-C mutation signature (Ross and Sale, 2006; Jansen *et al*., 2006).

1.6.5. Polymerase zeta, “à mi-chemin” between replicative and TLS polymerase

Pol ζ is a member of the B-family DNA polymerases and shares features of both replicative and Y-family polymerases. First, the enzyme, composed of two subunits, a catalytic Rev3 and an accessory Rev7, also binds to Pol δ B and C accessory subunits, respectively called Pol 31 and Pol 32 in yeast (Johnson *et al.*, 2012) and called p50 and p66 in humans (Baranovskiy *et al.*, 2012). Indeed, epistatic studies performed in yeast have shown both Rev3 and Pol32 to be implicated in the same pathway, and the deletion of Pol32 increased UV-induced mutagenesis (Hanna *et al.*, 2007). Subsequently, the Prakash group co-purified the whole complex and defined the residues in Rev3 essential for the binding with Pol δ subunits, and confirmed the importance of these interactions for cell survival following UV irradiation (Johnson *et al.*, 2012). These characteristics, also conserved in human cells, led to an alternative polymerase

switch model, where accessory subunits p50 and p66 of Pol δ stay anchored to PCNA to allow a switch between Pol δ and Pol ζ catalytic domain when the replisome encounters a DNA impediment (Baranovskiy *et al.*, 2012). As previously mentioned, Rev1 also participates in Pol ζ recruitment after UV exposure and especially at the site of (6-4)PPs (Szüts *et al.*, 2008; Wojtaszek *et al.*, 2012a). In line with this, Pol ζ has been shown to contribute to an error-free bypass of UV lesion (6-4)PPs *in vivo* (Yoon *et al.*, 2010) (figure 1.13B).

Another similarity between Pol ζ and other B family members concerns Pol ζ enzymatic fidelity which is comparable to replicative polymerase Pol α, and is thus between the highly accurate family-B polymerases (δ, ε) and the low fidelity Y-family polymerases. Indeed, Pol ζ's error rate is ~10^{-4} and so about two orders of magnitude better than Pol η (~10^{-2}) but much lower than Pol δ or Pol ε presenting an error rate between 10^{-6} and 10^{-7} (Thomas *et al.*, 1991). Despite this relatively high fidelity, Pol ζ contributes to mutagenesis via its enhanced capability of extending primer termini generated by other TLS polymerases opposite DNA lesions (Prakash *et al.*, 2005). Pol ζ has therefore been described as an extender polymerase in TLS (figure 1.13), the enzyme been shown to bypass various DNA lesions, including a non-DNA hydrocarbon chain template (Maor-Shoshani *et al.*, 2003; reviewed in Livneh *et al.*, 2010). A prime example of the cooperation between two TLS polymerases has been exposed in DT40 studies performed by Takeda's laboratory, with the generation of a double KO Pol η/ Pol ζ strain being less sensitive to UV-C irradiation than a single Pol ζ deficient cell line (Hirota *et al.*, 2010). Another study analysed Pol ζ's collaboration with Pol η or Pol κ in the bypass of cisplatin-GG (cisPt-GG) adducts, and found the process mutagenic when involving Pol κ but not Pol η (Shachar *et al.*, 2009).

Pol ζ (*REV3L*) is the only TLS polymerase to date reported to be embryonic lethal in mice, showing the importance of the enzyme during unperturbed DNA replication (Bemark *et al.*, 2000; Esposito *et al.*, 2000; Wittschieben *et al.*, 2000). However, unlike Pol δ and ε, Pol ζ is not essential in yeast. An elegant study performed by Lange et al. (2012), using inducible KO primary mouse fibroblasts, determined Pol ζ is needed for the completion of every cell cycle otherwise cells accumulate replication-dependant DSBs leading to senescence or apoptosis. The authors suggested Pol ζ has an essential role in the bypass of naturally occurring DNA lesions, such as those caused by oxidative stress. Other studies in yeast demonstrated the requirement of Pol ζ in the post-replicative bypass of ribonucleotides mis-incorporated during normal DNA replication (Lazzaro *et al.*, 2012). In line with this, it has been demonstrated in yeast and mammalian cells that replicative polymerases can incorporate ribonucleotides

during normal S-phase, leading to genomic instability (Nick McElhinny *et al.*, 2010; Reijns *et al.*, 2012).

1.6.6. PCNA ubiquitylation, choice between TLS Pol and template switch mechanisms

As discussed briefly previously, TLS is only one DNA damage tolerance mechanism that is available during genome duplication, the second mechanism being template switching, a HR-driven error-free bypass process (reviewed in Li and Heyer, 2008). This mechanism utilizes the undamaged newly synthesised sister chromatid as a DNA template to complete the duplication of the strand containing the DNA lesion, and uses the HR machinery. The post-translational modification of the polymerase clamp PCNA is crucial in the choice between these two damage tolerance pathways, and was first characterised in yeast. PCNA gets first mono-ubiquitylated on a conserved lysine (K164) residue by Rad6 and Rad18, respectively E2 and E3 ubiquitin ligases (figure 1.11A). Subsequently, a poly-ubiquitin chain can be formed (linking together each ubiquitin molecules on their lysine 63) catalysed by the successive actions of a heterodimeric E2 ligase Ubc13-Msm2 and E3 ligase Rad5 (Hoege *et al.*, 2002) (figure 1.11A). Mono-ubiquitylation is the trigger for TLS-mediated damage tolerance, whilst poly-ubiquitylation triggers error-free template switching (Hoege *et al.*, 2002; Stelter and Ulrich, 2003). PCNA can also be SUMOylated on lysine 164 or 127 (figure 1.11A), potentially regulating PCNA ubiquitylation as both post-translational modifications occur on the same residue of the protein (Hoege *et al.*, 2002). It has also been suggested the SUMOylation can prevent unnecessary recombination during S-phase as this modification allows PCNA to displace Rad51 from DNA via Srs2 anti-recombinase protein (Papouli *et al.*, 2005; Pfander *et al.*, 2005). PCNA can also be deubiquitylated by ubiquitin specific protease 1 (USP1), which is inactivated by auto-cleavage following UV irradiation, and thus contributes to genomic stability by preventing excessive TLS (Huang *et al.*, 2006).

Like activation of the intra-S checkpoint (section 1.5.2), primed RPA-coated ssDNA produced after replication fork stalling, is the trigger for mono-ubiquitylation of PCNA (Chang *et al.*, 2006), mediated by RPA recruitment of Rad18 (Davies *et al.*, 2008). Template switch mechanism involves the formation of Rad51 filaments leading to strand invasion and the creation of a Holiday junction or X-shape like DNA structure similar to HR repair (Li and Heyer, 2008). This error-free pathway seems to be used more often in yeast than in human cells as depletion of the Rad5 human homologues HLTF (helicase-like transcription factor) and SHPRH

(SNF2, histone-linker, PHD and RING finger domain-containing helicase) generate only minor defects (Hendel *et al.*, 2011; Krijger *et al.*, 2011). Despite poly-ubiquitylation of PCNA being shown to occur in mammalian cells (Chiu *et al.*, 2006; Brun *et al.*, 2010) mono-ubiquitylation of PCNA remains the predominant event (Kannouche *et al.*, 2004; Lehmann, 2011). Moreover, Rad5 mammalian homologues have been shown to be involved in the recruitment of the correct Y-family polymerase to prevent mutagenicity during damage bypass (Lin *et al.*, 2011). Indeed, in this study the HLTF pathway is activated following UV irradiation whilst SHPRH in response to MMS treatments. Both E3 ligases compete for the binding with Rad18, thus SHPRH recruitment is accompanied with HLTF degradation, and activation of PCNA poly-ubiquitylation, leading to Pol κ recruitment (Lin *et al.*, 2011). On the other hand, following UV irradiation, Rad18-SHPRH interaction is suppressed, allowing the binding of HLTF to Rad18 and PCNA mono-ubiquitylation, thus the recruitment of Pol η; by this way, mutagenic Pol κ cannot operate (Lin *et al.*, 2011). PCNA ubiquitylation state, mono or poly-ubiquitylated appears then to be more complicated than originally anticipated with yeast genetics for the determination of the appropriate damage tolerance pathway.

Nonetheless, mono-ubiquitylation of PCNA seems to be a trigger for the loading of Y-family polymerases onto the stalled primer terminus via an interaction between the polymerases C-ter ubiquitin binding motif (UBM or UBZ when contains a zinc-finger domain) and the ubiquitin moiety of the DNA clamp PCNA (Kannouche *et al.*, 2004; Bienko *et al.*, 2005; Yoon *et al.*, 2012). Also, Pol η, ι, and κ, contain PIP boxes allowing further contacts with the polymerase sliding clamp (Haracska *et al.*, 2001a, 2001b, 2002a). This simple model of PCNA ubiquitylation triggering the recruitment of TLS polymerases to bypass the lesion, originally described in yeast, has been greatly complicated in recent years with apparent contradicting data provided in mice, chicken, and human cells. Briefly, it has been reported that TLS can occur independently of PCNA ubiquitylation, in both DT40 (Edmunds *et al.*, 2008) and with human cell extracts (Nikolaishvili-Feinberg *et al.*, 2008; Schmutz *et al.*, 2010). However, other studies state that Rad18 is indispensable for TLS function in both mice and human cells (Yoon *et al.*, 2012), and similarly PCNA ubiquitylation was said to be also critical for TLS (Temviriyanukul *et al.*, 2012). An elegant study from the Livneh laboratory attempted to solve this matter by demonstrating in mammals PCNA ubiquitylation is an important mechanism and is required for a maximal TLS response, but is not an essential process (Hendel *et al.*, 2011). Participation of Rev1 or direct interaction with PCNA via the PIP box motif or other interaction with unknown ubiquitylated protein (Gohler *et al.*, 2011) can also contribute to the recruitment of TLS polymerases to the damage site. Crosstalk between the different pathways

of damage tolerance and repair (TLS, template switch, HR, intra-S checkpoint) have led to the conclusion that collaborative mechanisms can take place depending on the type of lesions endorsed and the intensity of the damage received (e.g: cluster of damage) (Sale, 2012).

1.7. DNA Primases

A universal feature of DNA polymerases is their inability to initiate DNA synthesis *de novo*. All known cellular replication systems employ a specialised DNA-dependant RNA polymerase called a primase, to synthesise short RNA molecules that are subsequently extended by DNA polymerases. However, many viruses and phages can also use tRNAs (retroelements), amino acid side chains (adenoviruses and bacteriophages) or a processed nick in a DNA strand (rolling circle replication model) to allow DNA polymerases (or reverse transcriptases in the case of retroviruses) to begin DNA synthesis (Iyer *et al.*, 2005).

1.7.1. Prokaryotic DnaG and archaeo-eukaryotic primases

DNA Primases can be categorised into two superfamilies: the Archaeo-Eukaryotic Primases (AEPs) and the bacterial DnaG primases (figure 1.14A). Prim1 is the representative member of AEP for eukaryotes and PriS for archaea. In contrast with monomeric DnaG, archaea and eukaryotic replicative primases function in a complex of either two (archaea) or four (eukaryotic) subunits (figure 1.14A). Despite being functionally related, these two superfamilies are evolutionarily unrelated and structurally distinct. DnaG primases have a Toprim (Topoisomerase-primase)-fold domain within their catalytic core whereas AEPs contain a highly derived RNA Recognition Motif (RRM) (Aravind *et al.*, 1998; Augustin *et al.*, 2001) (figure 1.14A). Only a limited number of primase crystal structures have been solved but confirmed both DnaG and AEP primases are structurally distinct from DNA polymerases and also from one another (figure 1.14B). No DNA polymerase finger or thumb-like subdomains were observed, but instead AEPs adopt a two-domain fold (a catalytic or prim domain and an unknown motif) and DnaG a cashew-shaped core domain (Keck and Berger, 2001) (figure 1.14B). However, despite this tertiary structural disparity, DNA polymerases and AEP primases utilise the same mechanism to incorporate dNTPs or NTPs during respective elongation step of DNA synthesis (figure 1.15). Briefly, as originally described in the seminal studies of Arthur Kornberg and colleagues, a nucleophilic attack occurs between the 3’ hydroxyl group (OH) of

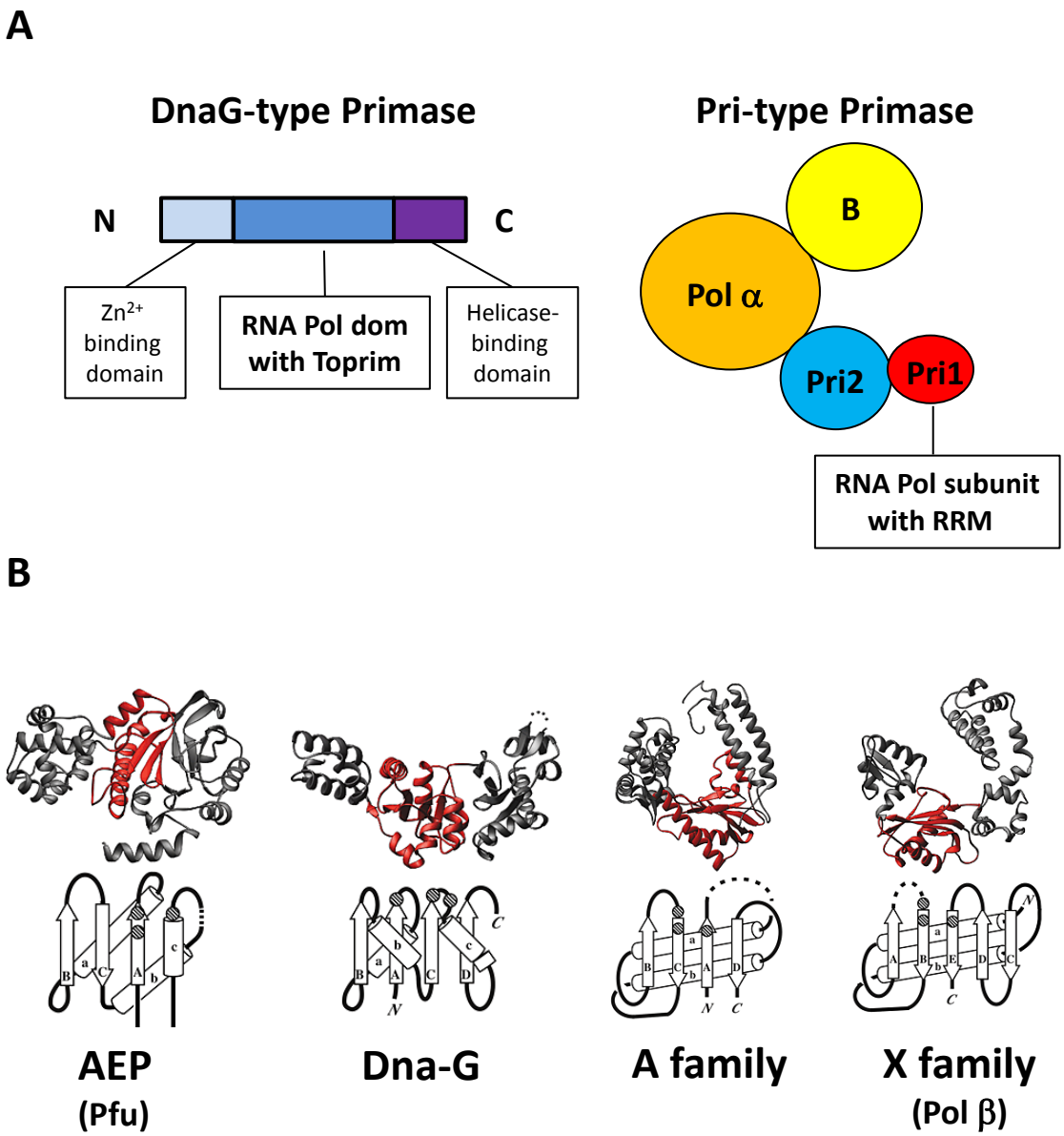

Figure 1.14: Prokaryotic and eukaryotic primases.

(**A**) Cartoon of Dna-G type primase (left side), composed of a zinc binding domain (light blue), RNA polymerase domain with a topoisomerase-primase (Toprim) motif (dark blue) and helicase binding domain (purple). Eukaryotic primases (right side) are composed of 4 subunits, 2 large ones (orange and yellow) with DNA polymerase activity and 2 smaller ones (blue and red), with the smallest subunit containing the catalytic RNA recognition motif (RRM). Archaeal primases are only composed of the 2 smallest subunits (p58 and p48). (Cartoon was adapted from Keck and Berger, 2001). (**B**) Crystal structures of 2 primases, AEP(*Pyrococcus furiosus*) and Dna-G (*E. coli*), and 2 DNA polymerases from A and X families, respectively Pol I and Pol β. The catalytic core of these enzymes (red) are represented by topology diagrams bellow the ribbon diagrams. Conserved acidic residues involved in the catalysis, or triad catalytic, are represented as hatched circles. AEP, A and X family polymerases have superimposable catalytic triad, but not Dna-G like primases. (Cartoon was taken from Augustin *et al*., 2001).

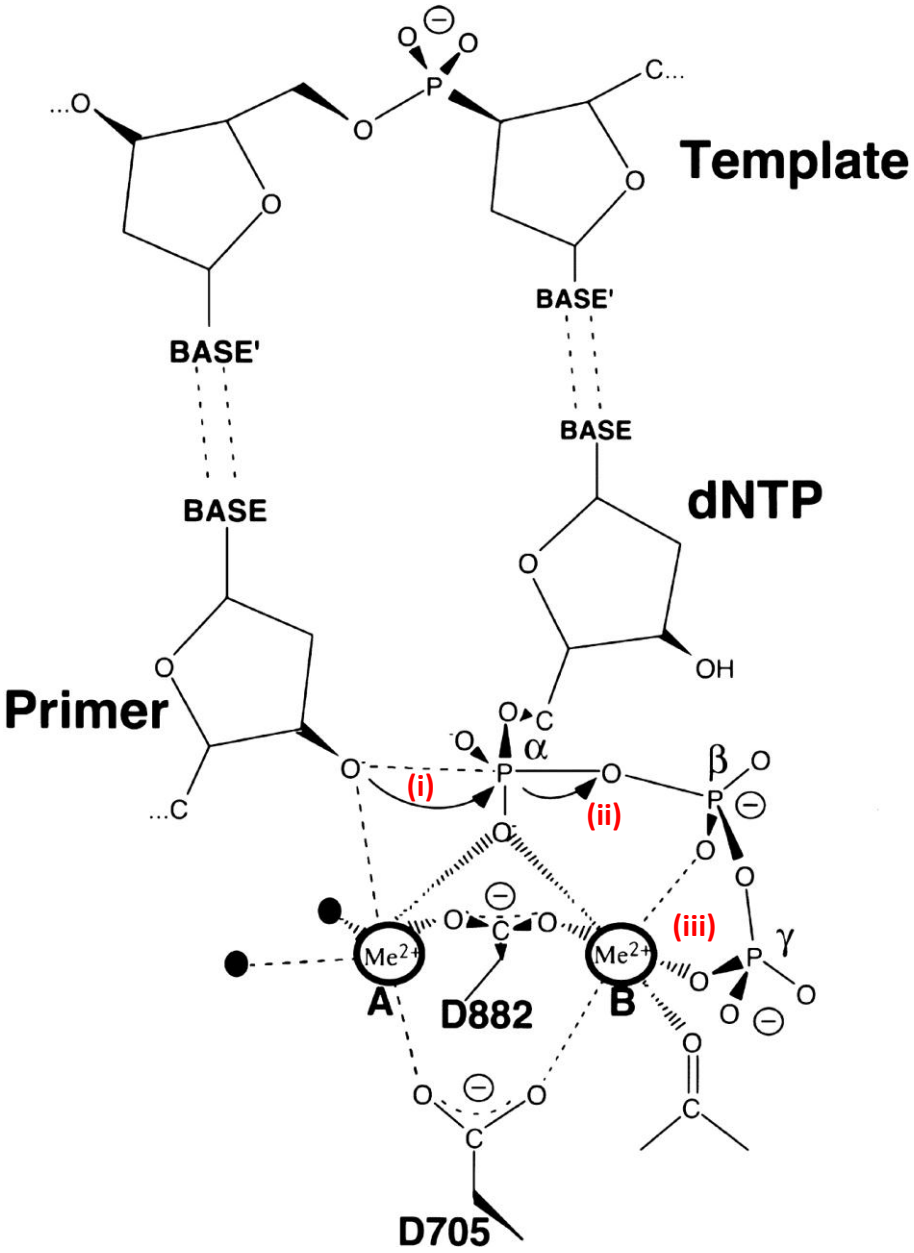

Figure 1.15: Two metal ions mechanism of nucleotidyl-transfer reaction.

Catalytic residues of *E.coli* DNA Pol I (aspartate D705 and D882) stabilize two metal ions A and B (black circles). Metal ion A triggers the nucleophilic attack of the 3'-OH group of the primer onto the α-phosphate of the dNTP resulting in the creation of a new phospho-diester bond (**i**) and the breakage of the bond between α and β phosphate (**ii**). Metal ion B stabilizes β and γ phosphates for the release of the pyrophosphate (PPi) (**iii**). (Cartoon was adapted from Steitz *et al*., 1999).

the primer terminus and the α-phosphate group of the incoming complementary dNTP (or NTP) to create a phosphodiester bond (Bessman *et al.*, 1956; Rothwell and Waksman, 2005) (figure 1.15). The reaction generates the release of a pyrophosphate (PPi) product providing the energy required by the polymerase for the catalysis of the reaction. Two aspartate residues from the catalytic site of the DNA or RNA polymerase allow the binding two metal ions, typically magnesium, which stabilise a transition state during the phosphoryl transfer reaction (figure 1.15). Crystal structure analysis of *Pyrococcus horikoshii* DNA primase in a complex with UTP strongly suggested the acidic residues of the catalytic triad of the primase are essential for the binding of the divalent metal ions (Ito *et al.*, 2003), in a similar manner than in DNA polymerases. This has now been observed in the structures of a divergent AEP-like polymerase, bacterial NHEJ primase (PolDom or LigDPol), that contained two metals ions in its catalytic centre, which readied the enzyme for phosphoryl transfer (Pitcher *et al*., 2007a; Brissett *et al.*, 2011). Indeed, it has been shown that acidic residues forming the catalytic triad of both AEP and DNA polymerases are superimposable (Augustin *et al.*, 2001) (figure 1.14B). Another similarity between AEPs and Pol-X family member Pol beta (β) has been observed with the presence of a "Pol β like" domain (closely related to the 8 kDa domain of Pol β) in the centre part of the large subunit of human primase p58 (Kirk and Kuchta, 1999a). A convergent evolutionary mechanism can possibly explain the similarity between primases and DNA polymerases as *in silico* analysis demonstrate both AEP and DNA polymerases (from A, B, and Y families) share a highly derived RRM (Iyer *et al.*, 2005).

Prokaryotic DnaG and AEP primases have both a zinc-binding motif, positioned either in close proximity to the primase catalytic site (AEP) or further apart (DnaG) (Lao-Sirieix *et al.*, 2005a). Studies on DnaG primases from bacteriophage T7 suggest a role for this zinc-binding motif in template sequence recognition (Mendelman *et al.*, 1994). More recently, crystallographic studies performed with archaeal heterodimeric primase subunits (PriS and PriL) from *Sulfolobus solfataricus* also implicated the zinc-binding domain in DNA template binding (Lao-Sirieix *et al.*, 2005b). Surprisingly the authors reported an increased primase activity in a zinc-finger null mutant, and also a reduced size of the RNA primers produced (Lao-Sirieix *et al.*, 2005b).

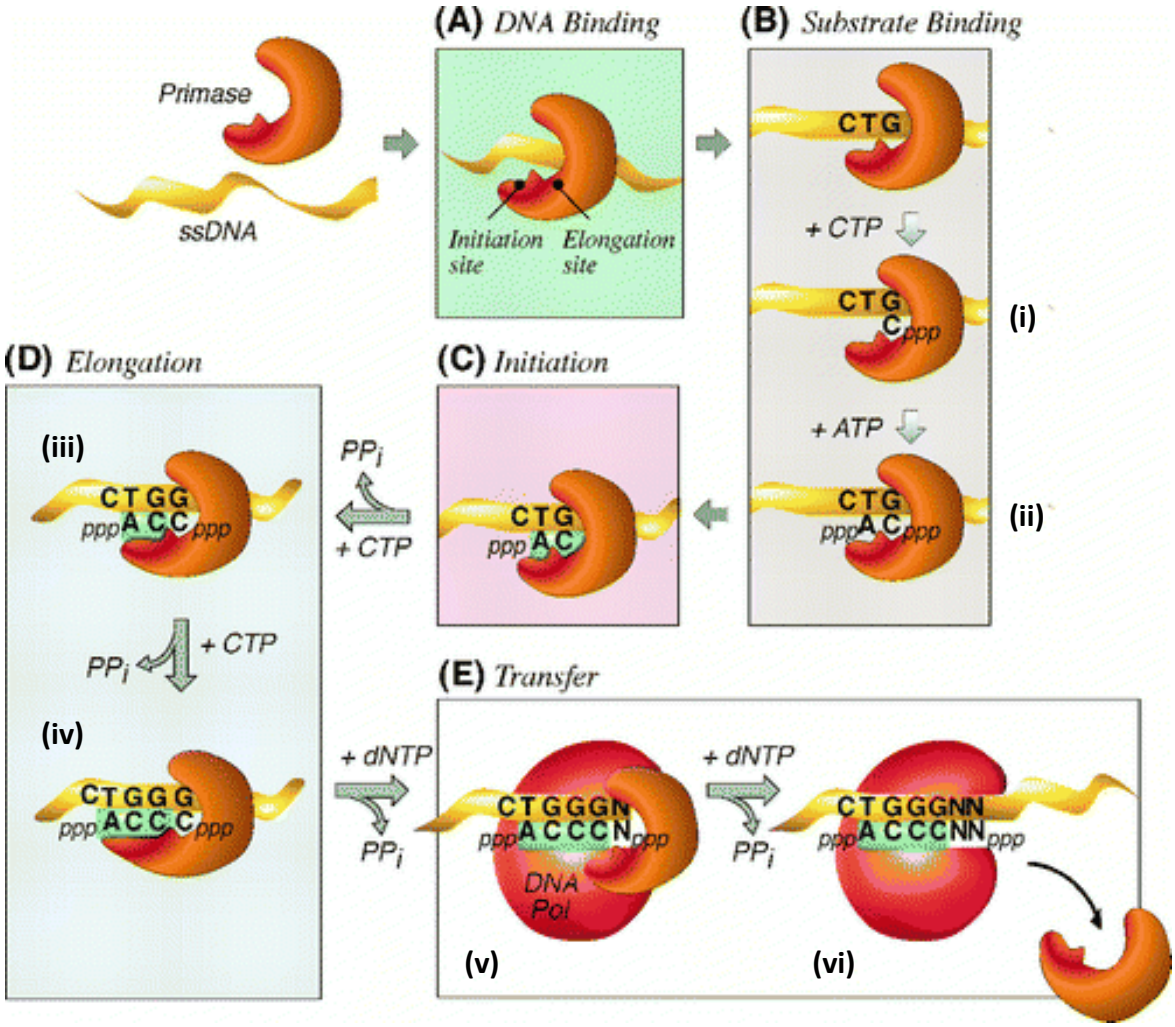

Figure 1.16: Five steps of DNA priming mechanism.

Following the binding of DNA primase (orange) to ssDNA (yellow) (**A**), the first NTP (CTP here) binds to the elongation site of the enzyme (**i**) then the second NTP (ATP here) binds to the initiation site (**ii**) according to the base pairing with the DNA template (**B**). Initiation step (**C**) corresponds then to the creation of a phospho-diester bond binding both NTPs together and releasing of a pyrophosphate group (PPi). The second bound nucleotide (ATP), keeping its 3 phosphate groups, marks in fact the 5' end of this novel oligonucleotide, and the subsequent nucleotides are then incorporated after the first bound NTP (CTP here). Thus this first step allows an apparent 3' to 5' NTP addition. A novel NTP binds to the primase elongation site, and the previous di-nucleotide (AC) is moved to the initiation site of the enzyme (**iii**), allowing elongation of the nascent primer by nucleotidyl transfer step and creation of a novel phospho-diester bond (**iv**) (**D**). DNA Pol (red) can then bind to this RNA primer (green) (**v**) and remove the primase (**vi**) to allow dNTP incorporation on the 3' end (**E**). (Cartoon was adapted from Frick and Richardson, 2001).

1.7.2. Mechanisms of DNA primer synthesis, the five-step model

Richardson and co-workers have proposed a mechanism explaining the general mode of action of primases, independently of their origin (AEP or DnaG), and is summarized in figure 1.16 (Frick *et al.*, 1999; Arezi and Kuchta, 2000). Following DNA binding (step 1), when the primase encounters the appropriate DNA sequence, binding of the NTP substrate occurs (step 2). This step is variable between AEP or DnaG primases. Prokaryotic and viral enzymes need to bind to a specific tri-nucleotides sequence also called template recognition site to trigger NTP binding, whereas eukaryotic primases only need the presence of pyrimidines within the DNA template (reviewed in Frick and Richardson, 2001). Indeed, studies in simian cells infected with SV40 virus showed that primer initiation sites always begin with purine NTPs (Yamaguchi *et al.*, 1985). More particularly, eukaryotic primases initiate RNA primer synthesis at the 3' end of a pyrimidine cluster (Suzuki *et al.*, 1993). Modifications of this 3' region of the template, as well as using manganese ions (Mn^{2+}), or increasing NTP concentrations can reduce the primase specificity for its substrate binding (Kirk and Kuchta, 1999b). One peculiarity of the second step of the primer synthesis mechanism resides in the formation of a 3'-5' dinucleotide at the beginning of the reaction (figure 1.16). The first NTP bound by the enzyme corresponds in fact to the second nucleotide in the primer (figure 1.16). The second NTP bound by the primase is indeed positioned on the 5' end of the primer (Sheaff and Kuchta, 1993). In contrast with a conventional phosphoryl transfer reaction (depicted figure 1.14), the nucleophilic attack is then triggered by the 3'OH group of the incoming NTP (secondly bound to the primase) onto the alpha phosphate of the first nucleotide bound by the primase. This dinucleotide formation step (or initiation step) appears also to be the limiting rate of primer synthesis (Sheaff and Kuchta, 1993). Observation of this quaternary complex (primase, ssDNA, two NTPS) led to the conclusion primases have two separate nucleotide binding sites, termed initiation and elongation sites, the last one corresponding to the actual active site of the enzyme, where catalysis occurs (Frick and Richardson, 2001) (figure 1.16). The primase can then incorporate further nucleotides in a conventional 5' to 3' by moving its active site towards this direction during the elongation step (step 4) (figure 1.16). The final step of the mechanism consists then in the transfer of the oligonucleotide to a replicative DNA polymerase, which can extend the primer with dNTPs (reviewed in Frick and Richardson, 2001) (figure 1.16).

The length of the final RNA primer is variable among species but on average primers are ~10 nucleotides long, apart from certain bacteriophages generating 2-5 nucleotides long primers (Frick and Richardson, 2001). It has been reported that a minimum primer size of ~7

nucleotides long is required for DNA polymerases, otherwise a shorter oligonucleotide could slip and interfere with the catalytic site of the enzyme (Kornberg and Baker, 1992). It appears most primases, except archaeal AEPs, have the ability to count primer length (Liu *et al.*, 2001; Frick and Richardson, 2001). This intrinsic feature is still not fully understood but it has been speculated that the zinc-binding domain of a DnaG primase could regulate the activity of a neighbour primase in a trans-interaction regulation mechanism (Qimron *et al.*, 2006). For eukaryotic primases a "hinge-closing" model has also been proposed where the accessory subunit of human primase, p58, is needed for the counting process (review in Kuchta and Stengel, 2010). This model is based on a mutagenesis analysis performed on the "Pol β like" domain of p58, demonstrating the importance of this accessory subunit in the nucleotides counting process (Zerbe and Kuchta, 2002). The large subunit (Pri L) has also been implicated in RNA counting in an archaeal AEP complex from *S. solfataricus* (Lao-Sirieix *et al.*, 2005).

1.7.3. Evolutionary progression of AEP roles: towards the discovery of a novel eukaryotic primase

For a long time, AEPs have been considered to be enzymes that are only required for initiating DNA replication by providing short RNA primers to be elongated by replicative polymerases. However, this was first challenged with identification of AEP domain in prokaryotes which use DnaG enzyme as replicative primase. Moreover, this prokaryotic AEP domain was often found in a multi-domain protein (ligase D) co-operonic with homologues of the eukaryotic NHEJ component Ku (Koonin *et al*., 2000; Aravind and Koonin, 2001; Doherty *et al.*, 2001; Weller and Doherty, 2001). This suggested the existence of prokaryotic NHEJ, which was subsequently, demonstrated *in vitro* and *in vivo* (Weller *et al*., 2002; Della *et al*., 2004). Work performed in Aidan Doherty's lab has then focused on characterising the AEP domain contained in this prokaryotic NHEJ component ligase D. *Mycobacterium tuberculosis* (*Mt*) or *smegmatis* (*Ms*) ligase D (*Mt* or *Ms* LigD) is a multifunctional enzyme possessing DNA ligase, nuclease and polymerase (PolDom/LigDPol) activities on the same polypeptide but residing in distinct catalytic domains (Pitcher *et al*., 2005). Indeed, in many organisms, these activities are encoded by distinct genes all arranged in the same operon. PolDom is a member of the AEP family of primases (Aravind and Koonin, 2001; Doherty *et al.*, 2001; Pitcher *et al.*, 2007a). Notably, PolDom is a versatile nucleotidyl-transferase capable of primase and DNA polymerase (gap-filling with DNA/RNA) and terminal transferase activities (Della *et al.*, 2004; Pitcher *et al.,* 2005; Pitcher *et al.*, 2007a). Analysis of the structural database confirmed the homology of

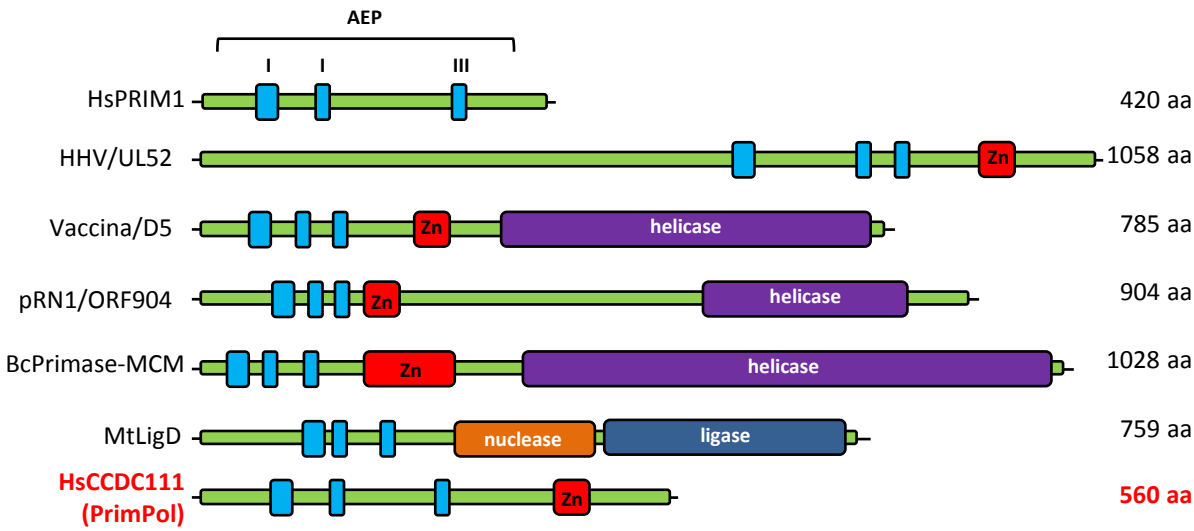

Figure 1.17: Archaeo-eukaryotic primase family members.

Cartoon depicting the domain organisation of various AEP members. Three conserved motifs responsible for the catalysis of AEP enzymes are depicted (light blue), along with zinc finger UL52 like motif (red), absent from PRIM1 and MtLigD, being in different AEP clades. AEP enzymes possessing supplemental enzymatic activities are also depicted, with helicase (purple), ligase (dark blue) and nuclease (orange) domains. Size of the respective proteins are added to the right of the cartoon. Human (Hs PRIM1) is the reference member of the AEP superfamily and together with the novel AEP coiled-coil domain containing protein (CCDC111), are the only AEPs identified to date in the human genome. Two viral AEPS are represented here, the human herpesviral (HHV) UL52 primase and vaccina D5 primase. ORF904 is encoded on the pRN1 plasmid of the archaeon *Sulfolobus*. Two prokaryotic AEPs contain multiple domains, *Bacillus cereus* primase with AEP-MCM helicase fusion, and *Mycobacterium tuberculosis* NHEJ primase Ligase D (LigD). Domain organisation was deduced from Iyer *et al*., 2005.

bacterial PolDom with the catalytic core of AEPs and the distinction from its prokaryotic counterpart DnaG primase (figure 1.17). Studies from our group have shown that PolDom is a *bona fida* member of the AEP structural superfamily (Pitcher *et al.*, 2007a) that has evolved specifically to operate as DNA polymerase, and not as primase, to mediate NHEJ DNA break repair processes in prokaryotes (Brissett *et al.*, 2007 and 2011). Indeed, crystallographic studies have identified that PolDom contains extra motif allowing the formation of a deeper cleft on the surface, presumably needed for specific DNA binding requirements (Zhu *et al*., 2006; Pitcher *et al.*, 2007a). This work was the first study to establish that AEPs can have more diverse roles in other cellular pathways. Moreover, archaeal replicative primases PriS (in *Pyrococcus furiosus* and *Sulfolobus solfataricus*) have also been shown to be capable of DNA polymerase and terminal transferase activities (Bocquier *et al.*, 2001; Lao Sirieix and Bell, 2004). These findings thus extend the link between AEP and Pol X family polymerases, as bacterial AEPs are the bacterial NHEJ polymerases whilst Pol X family members (Pol μ, λ and TDT) are NHEJ polymerases in eukaryotes (Pitcher *et al.*, 2007b). Work performed in the Doherty and Blanco laboratories on bacterial AEP and eukaryotic Pol X family members respectively has thus led to the search for novel eukaryotic AEP enzymes and the subsequent investigation of possible involvement of these orthologues in novel DNA repair mechanisms. Using a Psi-BLAST (position-specific iterated basic local alignment search tool) and consensus AEP sequence search models, coiled-coil domain containing (CCDC)111 gene has been identified as a novel eukaryotic AEP member. *In silico* analysis performed by Iyer and co-workers also supported the presence of another novel eukaryotic primase in human cells, referred as Eukprim2 (Iyer *et al.*, 2005), providing an opportunity to confirm this evolutionary role of AEPs predicted by Doherty and co-workers. This phylogenetic study, describing 13 distinct families of AEP, placed Eukprim2 or *CCDC111* gene (also called *FLJ33167*) in herpes-viruses and nucleo-cytoplasmic large DNA viruses (NCLDV) clade of AEPs (Iyer *et al.*, 2005) (figure 1.18). The gene is present in a broad range of organisms, in plants, protists, animals, but is absent from prokaryotes and archaea. Further, *CCDC111* is not represented in all eukaryotes, as the gene is also absent in yeast, *Caenorhabditis elegans* and *Drosophila.*

Preliminary characterisation of human *CCDC111* gene, located on chromosome 4 (4q35.1), and the purification of the human recombinant protein, demonstrated that CCDC111 possesses both DNA-dependent RNA primase and DNA polymerase activities *in vitro*, leading to the renaming of the polypeptide: PrimPol. Alignment of PrimPol homologues from a diverse range of eukaryotes, allowed the identification of two conserved domains with the polypeptide, a catalytic AEP domain, essential for primase/ polymerase activities, and a

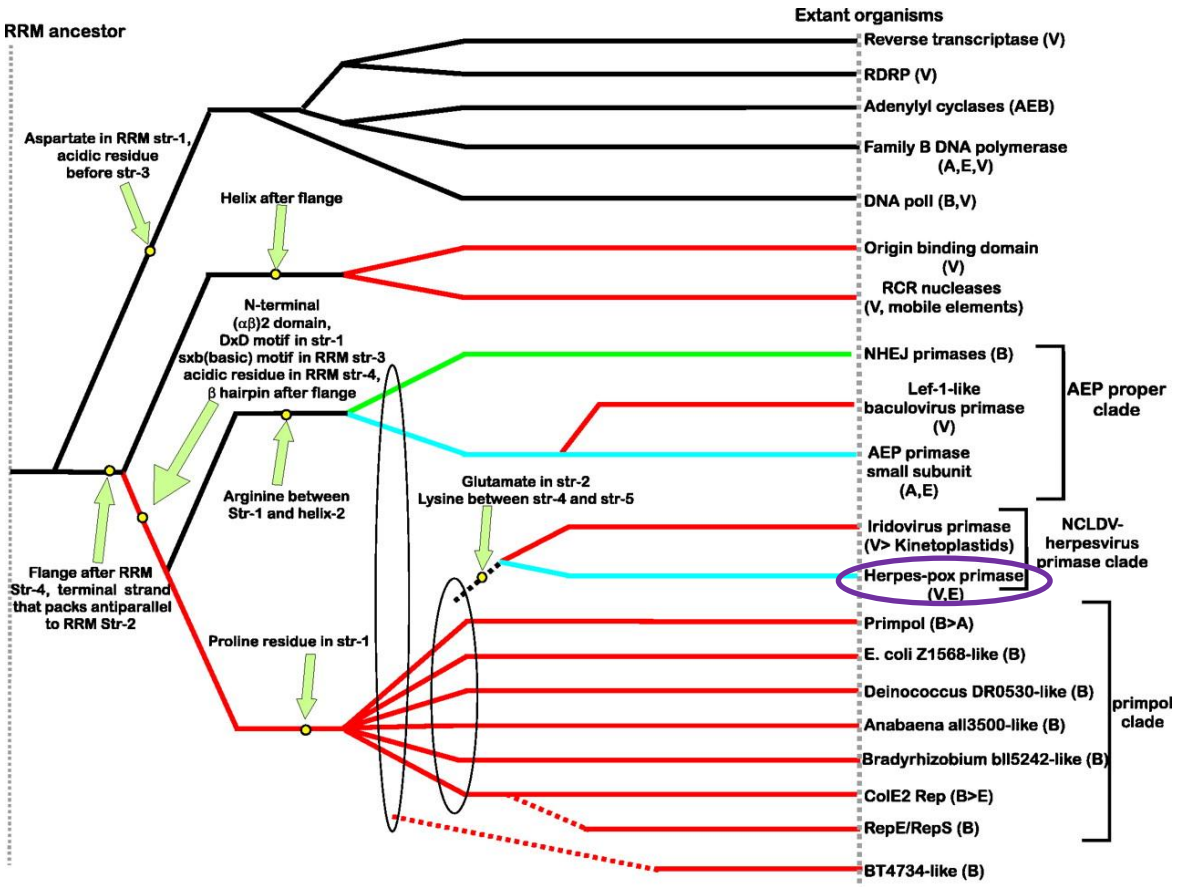

Figure 1.18: Archaeo-eukaryotic primase family clades.

Phylogenetic organisation of the 13 AEPs clades issue from a common RNA recognition motif (RRM) ancestor are regrouped under 3 main categories, AEP proper clade containing replicative primase enzymes (blue), herpes-viruses and nucleo-cytoplasmic large DNA viruses (NCLDV), and a primpol clade with enzymes capable of primase and polymerase activitties. A novel eukaryotic AEP (CCDC111 like enzyme) study in this thesis is circled in purple. Archaeal and eukaryotic branches (blue), bacterial branches (green), branches that include predominantly proteins from plasmids, phages and mobile elements (red) are distinguished. Ancestral branches and branches outside the AEP superfamily are in black. The different species contained in each clade are written in brackets, Bacteria (B), Archaea (A), Eukaryotes (E), Viruses (V). symbol > represents a proposed lateral transfer. Green arrows depict the residues within the designated motif (Str, for strand) determining the phylogenetic separation. (Schematic was taken from Iyer *et al*., 2005).

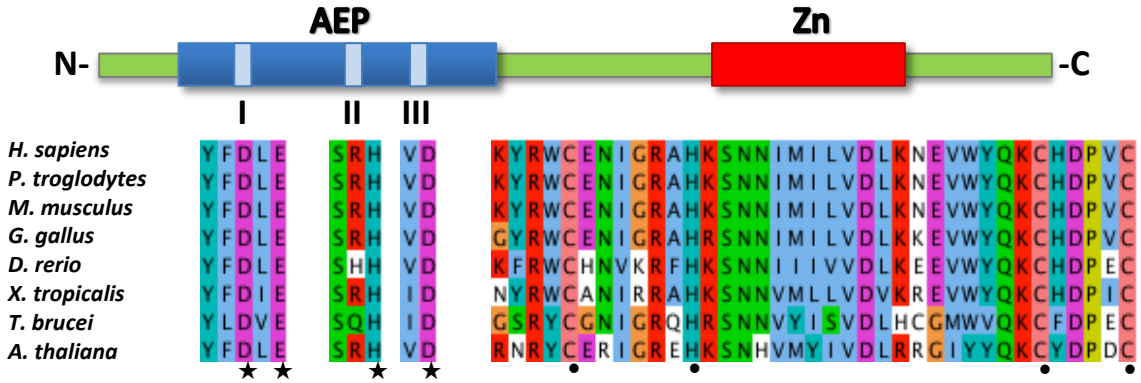

Figure 1.19: Multiple alignment of eukaryotic PrimPol homologs.

Cartoon depicting human PrimPol protein with the two conserved domains, AEP domain (blue) and zinc finger domain (red). AEP domain is composed of three motifs (light blue) corresponding to consensus sequences identifying the catalytic triad residues (motifs I and III) and NTP binding residue (motif II). Multiple alignment of eight PrimPol homologs is provided to visualise the conserved residues important for the catalysis DED (stars), or for the zinc chelating CHC2 (black dots).

putative UL52-like zinc-finger binding motif (figure 1.19). The catalytic core (or AEP domain) contains the three consensus motifs (I, II, III), previously described to be essential for the primase activity of AEPs (Iyer *et al.*, 2005); residues within motifs I and III are believed to be responsible for the catalysis, and those within motif II, needed for nucleotides binding (figure 1.19). However, in PrimPol's case, motif I is composed of the consensus residues DxE (aspartate, x, glutamate) whereas previous studies on AEP enzymes described the consensus residues of motif I as DxD (Iyer *et al.*, 2005). Thus PrimPol uses a different combination of acidic metal-chelating residues for the catalysis reaction (figure 1.19). This feature (DxE) is also shared with pRN1 archaeon replicase enzyme possessing both primase and polymerase activities (Lipps *et al.*, 2003 and 2004). The second conserved domain among PrimPol homologues is a C-ter CHC_2 (Cys-His-Cys-Cys) zinc-finger domain, which is similar to the zinc ribbon found in UL52 primase-helicase of herpes simplex viruses. Studies in herpesviridae showed that this domain is important for primase, helicase, ATPase and DNA binding activities of herpes virus helicase-primase complex (Chen *et al.*, 2005). The zinc-binding domain of prokaryotic DnaG primases also functions in template sequence recognition (Mendelman *et al.*, 1994) as discussed previously (section 1.7.2).

The aim of this thesis was to provide one of the first cellular characterisations of PrimPol in human and DT40 avian cells. In the first chapter, I describe how fluorescence microscopy and cellular fractionation procedures were used to determine the cellular localisation of tagged over-expressed human PrimPol. Subsequently, a thorough analysis of mtDNA copy number variation was performed by quantitavie (Q) PCR method in several cell lines depleted of the human or avian PrimPol protein. The second chapter describes the strategy used to disrupt *PrimPol* gene in avian DT40 cells and provides a preliminary characterisation of two *PrimPol* $^{-/-}$ DT40 cell lines grown in unperturbed conditions. The third results chapter shows the phenotypes obtained following treatments of both PrimPol KO cell lines with DNA damaging agents and the identification of a role of this novel primase-polymerase in damage tolerance mechanisms is discussed. Finally, the last results chapter describes the optimisation of expression and chromatography purification protocols for the production of recombinant human PrimPol. Production and purification of human PrimPol-specific antibodies raised against this antigen is also described.

CHAPTER II

Materials and Methods

Reagents were purchased from Sigma or Fisher unless otherwise stated.

2.1. Material

	Final concentrations (1X buffer)
PBS	137 mM NaCl, 2.7 mM KCl, 10 mM Na2HPO4, 2 mM KH2PO4 (pH 7.4).
PBS,T	1X PBS, 0.1% (v/v) Tween 20.
TAE	40 mM Tris-Acetate, 1 mM EDTA, pH 8.3
TBE	89 mM Tris, 2 mM EDTA, 0.89 M Boric Acid, pH 8.3
TBS	20 mM Tris, 280 mM NaCl, pH 7.5
TBS,T	1X TBS, 0.05% (v/v) Tween 20
TE	10 mM Tris-HCl (pH 8.0), 1 mM EDTA (pH 8.0).

	Final concentrations (sterile media)
LB	1% tryptone, 1% NaCl, 0.5% yeast extract
SOB	2% bactotryptone, 0.5% yeast extract , 10 mM NaCl, 2.5 mM KCl
SOC	SOB supplemented with 10 mM $MgCl_2$

Table 2.1 Commonly used solutions are prepared internally by support staff and shared through the whole Centre. They are provided following autoclaving sterilisation.

2.2. Molecular Biology Methods

2.2.1. PCR

Polymerase Chain Reaction (PCR) was performed using Phusion® High fidelity DNA polymerase kit (Thermo scientific) following manufacturer's instructions. DNA polymerase used in the kit has been engineered to improve accuracy, speed and performance of the reaction, allowing elongation of long and potentially difficult fragments to be replicated in a reasonable time. The use between one of the two buffers provided in the kit depended on the GC content on the DNA templates. Others parameters needing to be adjust for each reaction were the annealing temperature of the primers, the time of the DNA extension step, considering the polymerase elongation rate being 15-30 seconds per kilobase (s/kb), and the total number of cycles. A typical PCR reaction mixture of 50 µl contained 100 ng of DNA template, 1X reaction buffer, 200 µM of dNTP mix (EB), 0.5 µM of each primer, 1U of Phusion enzyme and most of the time, especially with GC rich template, 4% DMSO was added to disrupt potential secondary structures within DNA template and primers. A typical PCR program consisted of a denaturation step at 98°C for 45s (seconds) followed by 25-30 cycles of denaturation (98°C for 10s), annealing (55-65°C for 15s), and elongation (72°C for 30-60s) steps. An extra 10 minutes at 72°C was performed before the temperature was dropped to 4°C.

Genomic DT40 DNA was a gift from the Hocchegger's laboratory and was used with GC buffer. The primers utilised for amplifying homologous sequences ARMS are described in table 2.6. PrimPol human cDNA was purchased (I.M.A.G.E clone) and was cloned in pEt28a by a previous colleague. Truncation studies and catalytic null mutants were obtained after directed mutagenesis PCR using the primers described in table 2.2. PCR purification kit QIAquick® (Qiagen) was used according to manufacturer's instruction to purify PCR products previously checked by agarose gel electrophoresis.

2.2.1.1. Mutagenesis and inverted PCR

Mutagenesis PCR were performed on plasmid DNA following the standard PCR procedure described previously, with a pair of complementary primers containing the mutations desired (table 2.2). At the end of the reaction, 1 μl of *DpnI* enzyme (New England Biolabs) was added to the 50 μl of the PCR reaction and placed at 37°C for 1 hour to digest methylated DNA (corresponding to the plasmid used as PCR template). In specific occasions, when a substantial amount of DNA needed to be removed at the beginning or the middle of the open reading frame (e.g. N-ter truncation constructs), a protocol adapted from the inverted PCR method (Ochman *et al.*, 1988) was used. Primers, orientated in the reverse direction than usually used in a conventional PCR, were designed to flank the region which needed to be removed (table 2.2). Primers were synthesised with a 5' phosphate in order to perform the ligation of the PCR product and complete the deletion. Therefore, after *DpnI* treatment, ligation step was performed using T4 DNA ligase (New England Biolabs) before transforming DH5α competent *E. coli* cells.

PrimPol mutants	Primer	Sequences 5' to 3'
$A_{114}xA_{116}$	FOR	GGTTTGTTAAAT**g**CCAAA**g**CAAAATAAAGCT
	REV	AGCTTTATTTTG**c**TTTGG**c**ATTTAACAAACC
ΔNter 60	FOR	**P**-GACGTTCATGTATTTGCTTTGG
	REV	**P**-CATATGGCTGCCGCG
C-ter 464 stop	FOR	GTTTCCCATTACCT**taa**GAAGTATGTCTC
	REV	GAGACATACTTCttaAGGTAATGGGAAAC

Table 2.2 Mutagenesis primers forward (FOR) and reverse (REV) were used for generating different PrimPol recombinant mutant proteins. Residues 114 and 116 were mutated to alanines (A_{114} and A_{116}) to generate a catalytic null mutant. N-terminus truncation of the first 60 amino acids (ΔNter 60) was done by inverting PCR using 5' phosphorylated primers (P). Insertion of a stop codon TAA interrupted the polypeptide at the amino acid 464 (C-ter 464 stop).

2.2.1.2. RNA extraction and RT-PCR

DT40 cell pellets (corresponding to $5x10^6$ cells roughly) were lysed using RLT buffer (Qiagen) followed by a centrifugation step onto QIAshredder columns (Qiagen). RNA was then extracted using RNeasy® kit (Qiagen) according to manufacturer's instructions. After elution in RNase free water, RNA yield was measured using NanoDrop technology (Thermo scientific), and the quality of the preparation was checked by agarose gel electrophoresis.

SuperScript™ One-Step PCR kit (Invitrogen) was used with 1 μg of total RNA, 0.2 μM final of each primers, 1 μl of enzyme mix (reverse transcriptase and Platinum Taq polymerase being mixed together) and 2X reaction buffer (containing 0.4 mM of each dNTP and 2.4 mM MgSO4). Typical PCR program consisted in one cycle for the cDNA synthesis at 55°C for 25 minutes follow by a denaturation step at 94°C for 2 minutes, followed by 40 cycles corresponding to normal PCR amplification (denaturation at 94°C for 15s, annealing at 55-60°C for 30s and elongation at 68-72°C at 1 kb/min). A final extension step at 68°C for 5 minutes ended the process. Primers used for RT-PCR analysis are described in table 2.3.

	Primer sequences 5' to 3'	**Region *G. gallus* PrimPol cDNA**
PrimPol_FOR	ATGAAGAGAAAATGGGAAGAAAGAGTGAAGAAAGTTG	1-730 bp
PrimPol_REV	AGCCTTTGGAAGCATCTTCGACT	
Bora_FOR	ATGGGCGATACAGAAGAAGCCCAAATGCAG	absent
Bora_REV	CTCGAGAGGAGAAGGAACTATGAGACTCTTTGTGAAAACTCC	

Table 2.3 RT-PCR primers used to confirm *PrimPol* DT40 KO, recognising PrimPol cDNA or another *G. gallus* protein, Bora, to confirm the quality of the RNA preparation.

2.2.1.3. Quantitative PCR for copy number variation analysis

Cell pellets were washed in PBS (table 2.1) then resuspended directly in the well in lysis buffer (75 mM NaCl, 50 mM EDTA, 0.2% SDS, and 0.4 mg/ml proteinase K (NEB) followed by 2 hours incubation at 50°C. DNA was then precipitated in 1 volume isopropanol at 4°C overnight. After centrifugation at 8500g for 30 minutes at 4°C, pellet was washed with 70% ethanol, air dried and re-suspended in 50-400 μl TE (table 2.1) depending on the amount of cells originally in the well. Genomic DNA concentration, assessed by NanoDrop technology was then diluted to 5 ng/μl in TE. Q-PCR reaction mixture was composed of 5 μl of DNA template, 4 μl of primers mix (reverse and forward primers at 3.5 μM each), 3.5 μl of water and 12.5 μl of SYBR® (Synergy

Brands, Inc.) Green reagent (Thermofisher). DNA template was carefully distributed in each well of a 96 wells plate (Agilent Technologies) before a master mix primers-SYBR green was added. The plate was then sealed (Agilent Technologies) and all the content collected in the bottom of the well by centrifugation before to be placed on the thermocycler (Stratagene). Typical Q-PCR program consisted of a denaturation step at 95°C for 10 minutes (min) followed by 40 cycles of denaturation (95°C for 30s), annealing (60°C for 1 min), and elongation (72°C for 1 min) steps. A dissociation cycle was then performed for 1 minute at 95°C, 30s at 65°C and 30s at 95°C to check the specificity of the primers binding. Primers were designed (table 2.4) using Primer3 software (http://frodo.wi.mit.edu/) according to specific criteria such as GC content (40-60%), Tm (59-60°C), and length of amplicon (80-120 bp).

			Primer sequences 5' to 3'
Human	GAPDH	FOR	CATCAATGGAAATCCCATCA
		REV	GGAGCCACACCATCCTAGTT
	COXII	FOR	ACGGCGGACTAATCTTCAAC
		REV	CGATTGTCAACGTCAAGGAG
	β actin	FOR	TCCTCCCTGGAGAAGAGCTA
		REV	GAAGGAAGGCTGGAAGAGTG
	Cytochrome b	FOR	CATCGGACGAGGCCTATATT
		REV	AGCCTATGAAGGCTGTTGCT
G. gallus	APP	FOR	CCAATGTTGTCGAAGCCAACC
		REV	ACCATTGCACTGCTTCCATCC
	COXII	FOR	AATCTGAACCATCCTACCGC
		REV	GGGTGAGATCAGGTTCGTCG

Table 2.4 Q-PCR primers used to determine mtDNA copy number in human and DT40 (*G. gallus*) cells. Primers were either specific of mtDNA sequences (cytochrome c oxydase subunit 2, COXII, and cytochrome b), or nuclear housekeeping genes (Glyceraldehyde 3-phosphate dehydrogenase, GAPDH, β-actin and amyloid-β precursor protein, APP).

2.2.2. Agarose gel electrophoresis

Agarose poured gel were utilised for several purposes, checking DNA/RNA size and quality, for Southern blotting and 2D-gel analyses. Therefore various amount of agarose powder were dissolved in 1X TAE or TBE (table 2.1) to obtain the percentage wanted (from 0.4% w/v for 2D-gel to 2% for low size DNA fragments analysis). TBE was used instead of TAE for Southern and 2D-gel analyses, where higher resolution was required. Addition of ethidium bromide (Sigma) at ~0.3 µg/ml, when needed, allowed the visualisation of double stranded DNA. Voltages and

timing of the electrophoresis depended on the application, typically 100 V were applied for 20 minutes for common DNA analysis, whereas low voltages for longer time increased the sharpness of the signal (Southern blotting and 2D-gel analyses). DNA was loaded into the gel with NEB 6X dye, containing bromophenol blue, ficoll and SDS, to allow visualisation, sinking and denaturation of the DNA molecules. Molecular ladder (1 kb or 100 bp, NEB) was also used to determine the size of the fragments to analyse after visualisation under UV light with a UV illuminator (Syngene InGenius Gel Documentation System). Images were taken using GeneSnap (Syngene).

2.2.3. Enzymatic restriction digestion

Varyious amounts of DNA (2 to 30 μg) were digested with restriction enzymes depending on the type of application required, whether analytical or preparative. Accordingly, amount of enzymes, DNA material and digestion buffers (NEB) were adjusted in an appropriate volume of reaction in order to maintain a percentage of glycerol below 10% to prevent star activity. In theory 1 unit of enzyme can digest 1 μg of DNA in 1 hour (at the appropriate temperature) in 50 μl, however generally a 5 to 10 times excess of enzyme was recommended to prevent any eventual difficulties (quality of the DNA preparation mainly). Time of the reaction could also be increased when large amount of DNA was needed to be digested (up to overnight digestion if the enzyme allowed it). At the end of the reaction, analysis of the efficiency of the digest was appreciated on agarose gel electrophoresis if the size of the DNA was sufficiently modified (analytical digestion). Otherwise, digested DNA was purified using QIAquick® Spin kit (Qiagen) or gel extraction method, like GENECLEAN® II kit (Qbiogene Inc.) according to manufacturer's instructions.

2.2.4. DNA Ligation

Ligation assays were performed mainly during cloning procedures to ligate a PCR product into the desired vector, both being digested with two different enzymes (generating cohesive ends preferentially) to ensure the insertion of the PCR fragment in the correct orientation. Reactions were performed with an excess of insert molecules in relation to the vector (3:1 or 6:1 ratios). The size and the amount of both insert and vector were assessed by electrophoresis and NanoDrop quantification. Typically 50 ng of vector was used with a 3 to 6

time molecular excess of insert, and 1 μl of T4 DNA ligase (NEB) was added into diluted T4 ligase reaction buffer (NEB) and the final volume adjusted to 20 μl with water. Reactions were performed either for 1 hour at room temperature or at 16°C overnight before 3 to 5 μl of the reaction was used for transforming competent *E. coli* DH5α. Ligation control reactions were performed with either no insert or no ligase enzyme to test the amount of uncut vector (or vector cut with only one enzyme) present and determine the level of background.

2.2.5. Competent cells and transformation of DH5α

Overnight culture of single colony picked *E. coli* DH5α was performed at 37°C under agitation (185 rpm) in 3 ml of Luria-Bertani or LB medium (table 2.1). This saturated culture was then diluted into a larger volume of SOC medium (table 2.1) into baffled flask with the appropriate amount of aeration, and placed onto a shaker at 18°C until the optical density at 600 nm (OD_{600}) reached ~0.4. Bacterial growth was then stopped on ice for 10 minutes before collecting the cells by centrifugation at 4000 rpm at 4°C. In the following steps of the protocol, cells were kept on ice as much as possible. After removal of the supernatant, cell pellet was gently resuspended into ice cold TB buffer (10 mM PIPES pH 6.7, 15 mM $CaCl_2$, 55 mM $MnCl_2$, 250 mM KCl) then left on ice for 10 minutes. The same operation was repeated (centrifugation followed by resuspension in TB buffer) and 0.7% dimethyl sulfoxide (DMSO, VWR) added. Competent cells were then aliquoted and snapped frozen in liquid nitrogen before to be kept at -80°C. Cells efficiency (between 1 x 10^6 to 1 x 10^7 cells μg^{-1}) was verified by transforming serial dilution of pUC18 plasmid and counting the amount of colonies obtained in relation to the amount of DNA incorporated.

Depending on the efficiency on the previous step, the appropriate amount of cell was transformed with the DNA material to be amplified. Typically, 1 μl of 100 ng miniprep plasmid (section 2.2.6) or 5 μl of ligation reaction were added to 50 μl of competent cells and left on ice for 10 minutes. Heat shock at 42°C for 40 seconds followed by 5 minutes on ice allowed the penetration of the DNA through the chemically permeabilised bacterial cell walls. Incubation at 37°C in LB medium for approximately 40 minutes allowed multiplication of the cells before plating them onto solidified agar and incubated them overnight into 37°C incubator. Agar plates also contained the appropriate antibiotic (ampicillin at 100 μg/ml or kanamycin at 30 μg/ml, depending on the vector been transformed) to select only the DH5α cells containing the recombinant plasmid.

2.2.6. DNA preparation

During cloning process, or for amplification of small amount of plasmid stock, QIAprep Miniprep kit (Qiagen) was utilised according to manufacturer's instructions. Briefly, 3 ml culture (in LB medium containing the appropriate antibiotic) was inoculated with a single colony of DH5α and grown overnight at 37°C under agitation (185 rpm). DNA was extracted following cells lysis, and purified using QIAprep columns and buffers contained in the kit. During cloning procedure, the amount of colonies tested depended on the efficiency of the ligation process (and the amount of background obtained with uncut vectors).

Larger DNA preparations were achieved by using QIAfilter plasmid preparation (following Qiagen manual instructions), midi or maxiprep kit being used depending on the amount of DNA required. Therefore accordingly, between 50 ml to 250 ml cultures were started in LB medium (containing antibiotic needed) by diluting a 3 ml pre-culture (grown for 8 hours at 37°C) and placed at 37°C overnight under agitation (185 rpm).

2.2.7. DNA sequencing analysis

A small amount of DNA preparation (~500 ng) was sent to GATC Company with appropriate amount of primers if necessary (described in table 2.5) otherwise universal primers were used (e.g. T7). Results were analysed using Chromas (Technelysium Pty. Ltd.) and SeqBuilder (lasergene) software.

	Primer sequences 5' to 3'	Human PrimPol cDNA position
primer 1_FOR	GAAGGTTTTCAGTGTTCTCCC	1108
primer 2_FOR	GGCTACAGAGGAAAGCTGG	711
primer 3_REV	TGAAAGGTCAGGACTGCTTTGCTC	769
primer 4_REV	TCCTGGGTTGGCAGGTTTGTTA	351

Table 2.5 Sequencing primers were designed at different positions of human PrimPol cDNA in either forward (FOR) or reverse (REV) orientation to be able to cover the whole cDNA sequence.

2.2.8. Standard cloning and sub-cloning technique

Standard cloning procedures consisted in the succession of PCR reaction followed by agarose electrophoresis and PCR cleaning of the amplified DNA sequence of interest, before digesting

insert and vector overnight with appropriate restriction enzymes. The following day, ligation and DH5α transformation were performed. DNA was then extracted (with miniprep kit) and checked by restriction digestion followed by electrophoresis analysis to visualise the presence of both vector and insert. Final plasmids were also checked by DNA sequences analysis (GATC Company). However when the DNA sequence of interest was taken from one vector and cloned into another vector by only using restriction digestion (and no PCR step), a sub-cloning procedure was then undertaken. Ligation step followed by DH5α transformation, plasmid preparation and sequencing were similar to previously described. All the plasmids used during this thesis are summarised in table 2.7.

2.2.8.1. Cloning Gateway system

All the vectors used in the MultiSite Gateway® system (Invitrogen) have been kindly donated by Dr Hochegger, and the cloning method described previously (Iiizumi *et al.*, 2006). Gateway system allowed rapid cloning by the use of recombination process instead of classical DNA ligation. Briefly, 5' ARM and 3'ARM, corresponding to the beginning and the end of the gene respectively, were amplify by PCR using primers containing recombination sequences specific of each entry vector (table 2.6). After PCR purification step and NanoDrop quantification, recombination step was performed for several hours at room temperature with 75 ng of donor plasmid, 50 ng of purified PCR and 1 µl of BP Clonase® II (Invitrogen). A proteinase K treatment for 10 minutes at 37°C was used to deactivate the enzyme. *E. coli* transformation followed by QIAprep Miniprep kit allowed the amplification and the preparation of each DNA construct. A last recombination event with both entry vectors (5' and 3' ARM) and a donor vector containing an antibiotic resistance marker (puromycin or histidinol) was then performed to obtain the final construct. 75 ng of each plasmid were mixed with 1 µl of LR Clonase® II (Invitrogen) enzyme and left overnight at room temperature. Proteinase K treatment, *E. coli* transformation and plasmid preparation (QIAprep Miniprep kit) were repeated as before. Constructs were checked by PCR, using forward primer of the upstream ARM and reverse primer of the downstream ARM (table 2.6). The size of the amplicon corresponded to the length of 5'ARM, antibiotic marker and 3'ARM added together. Sequencing analysis (GATC company) was also used to confirm no mutations were introduced during the PCR process. A list of all the plasmids generated during this thesis are summarised in table 2.7.

		Primer sequences 5' to 3'	Region *G. gallus PrimPol* gene
1st strategy	upstream ARM primer FOR	5'-**GGGGACAACTTTGTATAGAAAAGTTGG** GCGGCAGCGCGCGGGCCGCGGAGAGG-3'	1-3025bp
	upstream ARM primer REV	5'-**GGGGACTGCTTTTTTGTACAAACT** TGTATACATTTAAATATCTTTGTGGATC-3'	
	downstream ARM primer FOR	5'-**GGGGACAGCTTTCTTGTACAAAGTGG** TGAGAGGGGAGCTGAAAGCAGTTT-3'	12250-14243bp
	downstream ARM primer REV	5'-**GGGGACAACTTTGTATAATAAAGTTG** CCATGGGCTCTGTTTAAACAAACAAGC-3'	
2nd strategy (Puromycin construct)	upstream ARM primer FOR	5'-**GGGGACAACTTTGTATAGAAAAGTTG** TTAAAGGTTTGAGTGATTCTGAATATAGCC-3'	3050-5051bp
	upstream ARM primer REV	5'-**GGGGACTGCTTTTTTGTACAAACTTG** TTACTCCTTGCAGGTTTTCACAAATC-3'	
	downstream ARM primer FOR	5'-**GGGGACAGCTTTCTTGTACAAAGTGG** AACCAAATACAGTCCATGCTGAAAC-3'	11061 – 12240bp
	downstream ARM primer REV	5'-**GGGGACAACTTTGTATAATAAAGTTGG** TGGCCAACTAAGACTATGCAAAC-3'	

Table 2.6 Primers used to generate DT40 targeting ARMs with Gateway cloning. Recombination sequences, *att* B4, B1, B2 and B3, corresponding to upstream ARM primer FOR, REV, downstream ARM primer FOR, and REV respectively, are represented in bold, and allowed recombination with both entry vectors (pDONRP4-P1R for upstream ARM and pDONRP2R-P3 for downstream ARM). Position of each ARM within the genomic area of *G. gallus PrimPol* gene was indicated on the right column of the table.

2.2.9. Genomic DNA extraction

2.2.9.1. DNA extraction from avian DT40 cells

Large amount of cells (5 x 10^6 to 1 x 10^7 or a very confluent well of a 6 wells plate) was collected and lysed into a buffer containing 200 mM NaCl, 20 mM EDTA, 40 mM Tris pH 8.0, 0.5% SDS, supplemented with 0.5% β-mercaptoethanol and 200 μg/ml proteinase K, before to be placed in water bath at 55°C overnight. The following day, proteins were precipitated into saturated NaCl (6 M) and the pellet removed after centrifugation (13000 rpm for 30-45 minutes at 4°C). DNA was then precipitated into 100% ethanol (on ice for 5 minutes), pelleted by centrifugation (6000 rpm for 15 minutes at 4°C) then washed into 70% ethanol. After centrifugation and complete removal of ethanol, air-dried DNA pellet was re-suspended into 10-20 μl of water and kept at 4°C until restriction digestion.

Constructs	vector (origin)	length cDNA (bp)/ genomic DNA position	cloning sites	predicted MW (kDa)		Origin
Human PrimPol						
Tet-luc-hPrimPol	pTRE/loxP/luc (Takeda lab)	1683 (FL, WT)	BamHI-MluI	65	-	this thesis
His-PrimPol_Nter60del	pEt28a (Novagen)	1503	NdeI-BamHI	60	N-ter tag	this thesis
His-PrimPol_Cter464stop	pEt28a	1392	NdeI-BamHI	58.7	N-ter tag	this thesis
His-PrimPol_AxA	pEt28a	1683	NdeI-BamHI	65	N-ter tag	this thesis
His-PrimPol	pEt28a	1683 (FL, WT)	NdeI-BamHI	65	N-ter tag	Doherty lab
Nter-GFP-PrimPol	pEGFP-C1 (Clontech)	1683 (FL, WT)	XhoI-BamHI	95	N-ter tag	Doherty lab
Cter-GFP-PrimPol	pEGFP-N1 (Clontech)	1683 (FL, WT)	XbaI-BamHI	95	C-ter tag	Doherty lab
HA-PrimPol	pCI-Neo (Promega)	1683 (FL, WT)	XhoI-MluI	66	C-ter tag	Doherty lab
		HA tag	XbaI-NotI			
***G. gallus* PrimPol**						
pDONR-5'ARM	pDONR-P4R-P1 (Invitrogen)	1-3025	**Gateway system**			this thesis
pDONR-3'ARM	pDONR-P2R-P3 (Invitrogen)	12250-14243				this thesis
pDONR-5'ARM2	pDONR-P4R-P1	3050-5051				this thesis
pDONR-3'ARM2	pDONR-P2R-P3	11061-12240				this thesis
pDEST-PURO-KO	pDEST R4-R3 (Invitrogen)	1-3025 & 12250-14243				this thesis
pDEST-HIS-KO	pDEST R4-R3	1-3025 & 12250-14243				this thesis
pDEST-PURO-KO2	pDEST R4-R3	3050-5051& 11061-12240				this thesis

Table 2.7 Plasmid constructs were either generated during this thesis or previously engineered in the Doherty lab (origin). Backbone vectors, used for each construct are indicated with their origin in parentheses. Length in base pair (bp) of human cDNA or the position of *G. gallus* genomic DNA are shown, when appropriate, the mention full length wild type (FL, WT) is indicated. Human PrimPol cDNA (and the *Hemagglutinin* (*HA) Tag*) were introduced into the vectors in between the restriction enzymatic sites indicated. Molecular weight (MW) and the final position of the tag (N or C-terminal) are shown when necessary.

2.2.9.2. DNA extraction from human cells

Large amount of cells (5 x 10^6 to 1 x 10^7 or two semi-confluent 10cm dishes) was collected and washed into PBS before adding the lysis buffer (75 mM NaCl, 50 mM EDTA, 20 mM Hepes-NaOH pH 7.8, 0.5%SDS, 0.2 mg/ml proteinase K). Once lysed, phenol/chloroform extraction was performed to extract the DNA and remove proteins and cell debris. DNA was precipitated with 100 mM NaCl and isopropanol (v/v), washed with 70% ethanol and left overnight at 4°C in TE. The following day, the same steps of the protocol were repeated, lysis, phenol/chloroform extraction and salt/ isopropanol precipitation. DNA was resuspended in TE, quantified with NanoDrop technology and kept at 4°C until restriction digestion.

2.2.10. Southern blotting analysis

Overnight digested genomic DNA (30 μg for DT40 analysis, 5 μg for human samples) was loaded onto 1% agarose gel containing ethidium bromide and electrophoresis was performed at low voltages for few hours. Picture of the gel under UV light with a ruler positioned next to the molecular ladder were taken to allow future determination of the size of the bands obtained after radioactivity probing. DNA within the agarose gel was then depurinated in 0.25 M HCl for 15 minutes to facilitate transfer operation. A denaturation step (in 1.5 M NaCl, 0.5 M NaOH buffer) was then performed for 30 minutes to allow future hybridisation of the radiolabelled probe. Finally the gel was neutralised in 2 consecutives bath (with 1.5 M NaCl, 0.5 M Tris pH 7.5 buffer) for 30 minutes each. DNA was then transferred onto a positively charged nylon membrane (Hybond N, GE Healthcare) by capillary blotting. Whatman 3MM paper soaked into 20X SSC buffer (3 M NaCl, 0.3 M citric acid pH 7.0) was used to form a bridge between the gel and the 20X SSC buffer reservoir. DNA gel, placed in top of the bridge, was then covered by the nylon membrane (pre-soaked in water) and 3 sheets of 3MM paper (soaked in 20X SSC) in top of it. A large amount of absorbent paper was added on top and heavy weight maintained the whole montage in place, applying pressure to help the capillarity process. After overnight transfer, the membrane was rinsed in 2X SSC then the DNA cross-linked with UV light using Stratalinker 2400 (Stratagene).

2.2.11. Probe labelling and hybridisation

Southern blot probes were generated by PCR using primers (described in table 2.8). 50 ng of purified PCR product (diluted in water) were denatured for 5 minutes at 95°C followed by 5 minutes on ice. Ready-To-Go™ dCTP DNA labelling beads (GE Healthcare) were resuspended with the diluted probe and 20-50 μCi [α-^{32}P] dCTP added for 15 minutes at 37°C in order to radio-labelled the probe. DyeEx™ (Qiagen) purification columns were used to remove excess of non-incorporated labelled nucleotides. Radio-labelled probe was then heat denatured and cooled on ice, ready to be used for hybridisation with Southern blot membrane.

Cross-linked Southern membrane was first pre-hybridised for 30 minutes in hybridisation buffer (ExpressHyb, Clontech) then incubated over-night in the same buffer containing the radio-labelled probe. Hybridisation temperatures were adjusted depending on the DNA templates, 58°C for DT40 samples and 65°C for human samples. Membrane was then washed with 2X SSC for 15 minutes, then twice in 2X SSC, 0.1% SDS for 30 minutes each time, and then, depending on the level of radioactive back-ground, a further wash in 0.1X SSC, 0.1% SDS for 15 minutes was performed to increase the stringency of the lavage. All washes were done at the same temperature than hybridisation step to improve efficiency of removal of unspecific bound probes. Autoradiography detection was applied using phosphor screen (Raytek) and Fujifilm imager.

			Primer sequences 5' to 3'	Primers positions
H1	**Human** mtDNA	FOR	TTACAGTCAAATCCCTTCTCGTCC	16341-151
		REV	GGATGAGGCAGGAATCAAAGACAG	
18S	**Human** 18S DNA	FOR	GTTGGTGGAG**C**GATTTGTCT	110422-110832
		REV	GGCCTCACTAAACCATCCAA	
OH	***gallus*** mtDNA OH area	FOR	TCAGCAACCCCTGCTTGT	432-853
		REV	GCATTTGGTTATGGTTCTTCCACC	
18S	***gallus*** 18S DNA	FOR	GCAGCCGCGGTAATTCCAGCTCC	537-1027
		REV	CGCCGCCGGATCGCGAGTCGGCATC	
probe 2	***gallus*** PrimPol gene	FOR	ACGGAGTGCAAGGAGGTAAC	14333-14890
		REV	GACTGGATCGTGGCACTTC	

Table 2.8 Primers used for generating Southern blot probes of human or *G. gallus* (bold) mtDNA, rDNA or PrimPol genes are indicated. Position of the area of the genomic DNA being amplified is indicated (primers position) as well as the orientation of each primer, forward (FOR) or reverse (REV).

2.2.12. Two dimensional agarose gel electrophoresis

Genomic DNA, ~10 μg prepared as described in (section 2.2.9), was digested with appropriate restriction enzyme. Precipitation step, performed in 2 volumes ethanol 100%, 0.1 volume 3 M sodium acetate and 50 μg glycogen for 1 hour at -80°C, was followed by centrifugation at 13000 rpm for 20 minutes, allowing reduction of the final volume and further purification of the DNA preparation. After 70% ethanol wash and air-drying step, DNA was re-suspended in 20 μl TE, 5 μl of loading buffer was added and the samples loaded onto a 0.4% TBE agarose gel without any ethidium bromide. First dimension electrophoresis, to separate DNA fragments by their sizes (about 4 kb with this agarose percentage), was performed overnight at 30 V in TBE buffer in the dark, at room temperature. Slices of agarose containing the migrated DNA samples were cut, rotated to 90° and poured into 1% TBE agarose gel containing 500 ng/ml ethidium bromide. Second dimension electrophoresis, separating DNA molecules by their shapes, were run at 4°C at 90 V with a pumping system allowing the recycling of ethidium bromide in the TBE buffer (at 10 ng/ml) back in the top of the gel. Standard Southern blot analysis was then performed to visualise and quantify the DNA.

2.3. Cellular Biology Methods

2.3.1. Cell culture

DT40 cells (Clone 653) were maintained in suspension at 39°C with 5% CO_2 in RPMI 1640 (Invitrogen) medium supplemented with 10% (v/v) foetal calf serum (FCS), 1% (v/v) chicken serum (Sigma), 1% (v/v) penicillin-streptomycin (Pen-strep), 2 mM L-glutamine (L-glu) and 10^{-5}M β-mercaptoethanol to prevent cells for clumping together. Cells were diluted every day or every other day to keep them in exponential growth (concentration between 0.5 to 2 x 10^6 cells ml^{-1}).

Adherent human cells were cultured at 37°C (with 5% CO_2) either in DMEM (Invitrogen) with 10% FCS for osteosarcoma U2 (U2OS) and 143B cells, and Human embryonic kidney (Hek293) cell lines, whereas MRC5 were grown in MEM (Invitrogen) supplemented with 15% FCS. In both cases, 1% (v/v) Pen-strep, and 1% (v/v) L-glu were also added to the media. Cells were maintained in culture until 80% confluency was reached and then were transferred into a new flask by trypsinisation protocol. Briefly, cells were washed with warmed PBS buffer, and incubated for approximately 5 minutes at 37°C with a small volume of trypsin, enough to just

cover their surface. Vigorous resuspension of the cells with warm medium containing FCS allowed inactivation of the trypsin and detachment of the cells from the plastic at the same time. Centrifugation and resuspension of the pellet in fresh complete medium into the appropriate volume allowed dilution of the cellular suspension to the amount needed.

When cells needed to be kept for long storage in liquid nitrogen container, following trypsinisation (or only centrifugation step with DT40), cell pellet was resuspended in small volume of medium containing 10% sterile DMSO. Aliquots into cryotubes were made and cooled slowly into a cryobomb at -80°C for 2-3 days before to be placed at -180°C. By opposition, thawing cells was quickly performed by immersing the cryotube into a 37°C water bath before resuspended them into warmed complete medium. A centrifugation step allowed removal of DMSO containing medium and a quick recovery for the cells.

2.3.2. Transfection protocols

2.3.2.1. DT40 cells transfection and clones collection for gene targeting process

Targeted vectors, generated via Gateway® cloning system, were introduced by electroporation following manufacturer instructions (Bio-Rad Gene Pulser® apparatus). Briefly 20 μg of linearized, ethanol-precipitated DNA (resuspended in water under sterile conditions) were added into ice-cold 0.4 cm Gene Pulser cuvette (BioRad) containing 1 x 10^7 cells (resuspended into 500 μl of chilled PBS). After 10 minutes incubation on ice, electroporation was performed at 550 V and 25 μF at infinite resistance. Following the pulse, cells were incubated on ice for a further 10 minutes before to be resuspended into 20 ml of warm medium and incubated at 39°C. The next day, cells were diluted into a final volume of 80 ml medium containing appropriate antibiotic selection, histidinol (1 mg/ml) or puromycin (0.5 μg/ml) and distributed into four 96 wells plate using a multi-channel pipette. Cells were let to grow at 39°C until colonies became visible in the bottom of the well. Clones were then re-amplify in a larger volume, the 200 μl transfered into 5 ml of fresh warmed media, without any antibiotic selection, and let grown at 39°C until the well became confluent. A small aliquot (1 ml) was then frozen in 10% DMSO and kept at -80°C while the rest of the well was collected for genomic DNA extraction and Southern blot analysis (section 2.2.9.1).

Similar protocol was used for the generation of conditional human PrimPol (hPrimPol), where Tet-off vector and pTRE-LoxP-luc-hPrimPol plasmids (table 2.7) were electroporated

together. Different ratios of the amount of each vector were used to optimise the transfection conditions, and 2 mg/ml of selection marker Geneticin® (or G418, Invitrogen) was added the following day. The rest of the protocol was identic. Luciferase assay (Steady-Glo®, Promega) was performed according to manufacturer's instructions to screen the clones containing pTRE-lox-luc vector. Briefly, 2 ml of saturated culture was collected by centrifugation and the cells were resuspended into 50 µl 1X lysis buffer (Promega kit) diluted into PBS before taking out 5 µl of lysate and adding it to 20 µl of luciferase substrate. Luminescence was read using GloMax® fluorometer (Promega).

2.3.2.2. Human cells

PrimPol RNA interference (RNAi) was designed following Invitrogen stealth software instructions, where PrimPol open reading frame (ORF) was inserted and the oligonucleotides sequences were selected to have a GC content comprised between 35 and 55%. Algorithms used in the software allowed design of RNAi duplex with reduced off-target and non-specific effects (table 2.9).

2.3.2.2.1. RNAi transfection

Protocols were adapted and optimised depending on the cell line and the application performed following the gene silencing step. Hiperfect® reagent (Qiagen) was first utilised with U2OS cells following manufacturer's recommendations on the fast forward protocol where the cells were transfected during the seeding process. Cell confluency and the amount of RNAi and transfection reagent were optimised to improve the efficiency of the transfection. Cells were seeded at 12 x 10^4 cells ml^{-1} in 2 ml of complete medium and homogenously spread into a well of 6 wells plate. For each reaction, RNAi duplexes (table 2.9) were diluted to 10 nM final concentration with 6 µl of Hiperfect reagent into 100 µl of OptiMEM® (Invitrogen) minimal medium. The mix was left for 5–10 min at room temperature (15–25°C) to allow the formation of transfection complexes and then distributed drop-wise onto the cells before to place them back in the 37°C incubator. A second round of transfection was performed if necessary at either 24 or 48 hours following the first one. In this case, the same proportions of RNAi, Hiperfect and OptiMEM were mixed together and added to the cells already in culture. Cells were collected at different time points depending on the experiment.

A second RNAi protocol was also used to follow Holt's laboratory procedures, where Lipofectamine® (Invitrogen) reagent was used. Cells were plated the day before the transfection at 10-15% confluency (~4 x 10^4 cells ml^{-1}) in 6 well plates in medium containing FCS but no antibiotics. The following day, RNAi (10 nM final) and Lipofectamine (3.6 μl per reaction) were both diluted separately into 300 μl OptiMEM. Both mix were then combined together and left for 20 minutes at room temperature. Cells were washed with warmed PBS and 600 μl of mix were distributed drop-wise directly on top of the cells (without any medium in the well). Following 4 hours incubation period at 37°C (5% CO_2), 600 μl of DMEM medium supplemented with 30% FCS (but no antibiotics) was added. The next day, medium was replaced with complete medium (10% FCS and antibiotics).

	primer sequences 5' to 3'	cDNA	Protein
PrimPol RNAi	GAGGAAACCGUUGUCCUCAGUGUAU AUACACUGAGGACAACGGUUUCCUC	59-84	20-28
TWINKLE RNAi	GCAAAGCAUCAGGACUGUAAUAGAU AUCUAUUACAGUCCUGAUGCUUUGC	1476-1500	492-500
Control RNAi	GCUAGCCGUCGAUUCUCAAUCGUAU AUACGAUUGAGAAUCGACGGCUAGC	-	-

Table 2.9 RNAi primer duplexes were either designed according to Invitrogen algorithm stealth software (PrimPol and control RNAi) or the sequence determined in a previous publication (TWINKLE RNAi, Tyynismaa *et al.*, 2004). RNAi duplexes were ordered from Invitrogen website.

2.3.2.2.2. DNA plasmid transfection

Cells were transiently transfected with GFP or HA tagged PrimPol plasmids (table 2.7) using FuGENE® (Promega) reagent according to manufacturer's instructions. For immunofluorescence studies, cells were seeded onto sterilised cover slips (Fisher) covering the bottom of the well (24 wells plate) at approximately 50% confluency (~3 x 10^4 cells) in 500 μl complete medium. The following day, 3 μl FuGENE reagent was diluted into 100 μl OptiMEM and left for 5 minutes at room temperature before adding 1 μg DNA and incubated for a further 30 minutes at room temperature. The mix was then distributed drop-wise onto cells maintained in media without antibiotics and the media changed the following day. For Western blot analysis, protocol was similar but the cells were seeded into 6 well plates, at 1 x 10^5 cells.

2.3.3. DNA damaging treatments

Drugs powder, purchased from Sigma, were resuspended with the appropriate diluent and aliquots were stored at -20°C, at the exception of MMS which was already in suspension, and kept at room temperature under a chemical hood before to be diluted just before used in PBS (table 2.10).

For irradiation treatments, a UV-C germicidal lamp (made at the Sussex University) containing a 6W bulb (254 nm, Phillips) was used and calibrated before every use with a radiometer (International light technologies). X ray treatments were performed at 250 kV, 12 mA with a dose of 0.5 Gy/min and a ^{137}Cs gamma-source was used at 8.3 Gy/s.

	Storage before dilution	Stock solutions (diluent)	Storage after dilution
Chloramphenicol	4°C	34 mg/ml (ethanol)	-20°C
4-Nitroquinoline 1-oxide, **4NQO**	-20°C	1.9 mg/ml (DMSO)	-20°C
Methyl methanesulfonate, **MMS**	RT°C	1.3 g/ml (PBS)	-
Cisplatin, **CDDP**	-20°C	5 mM (DMSO)	-
Camptothecin, **CPT**	4°C	10 mM (DMSO)	-

Table 2.10 DNA damaging drugs were kept at the appropriate temperature before resuspension within a specific diluent (in brackets) to the concentrations indicated; these stock solutions were then either used immediately (-) and further diluted if necessary, or stored at -20°C for future usage.

2.3.4. Flow cytometry analysis

Cell cycle distribution and S-phase progression analyses were performed in DT40 cells following protocols adapted from (Hégarat *et al.*, 2012). DT40 cells were spun down, washed with ice-cold PBS, and then fixed by adding 70% ethanol (pre-chilled at -20°C) drop-wise while vortexing the cellular suspension. Cells could then be kept at -20°C until further analyses. Otherwise, cells were pelleted by centrifugation (1500 rpm for 3 minutes), rinsed in PBS containing 3% BSA (PBS/BSA)preventing cells from sticking to the eppendorf walls, and finally resuspended in PBS/BSA (BSA fraction V, Sigma) supplemented with 150 µg/ml RNase A and 5 µg/ml propidium iodide (PI) and kept at 4°C overnight in the dark. Following strong vortexing step, labelled cells were transferred into round bottom tubes (Becton Dickinson, BD) through their filter cap in order to remove eventual large particles, and samples were analysed with FACSCanto™ flow cytometer (BD) and FACSDiva™ software (BD) according to manufacturer's instructions.

Analyses of actively replicating cells were performed following a 20 minutes pulse with 25 μM bromodeoxyuridine (BrdU, Sigma-Aldrich) and then collecting and fixing the cells as previously described. Denaturation step with 2M HCl, 0.5% triton X100 for 30 minutes was performed following ethanol removal and PBS/BSA washes. Cells were then washed 2 times with PBS/BSA before proceeding to the antibody incubation (mouse monoclonal anti-BrdU (BD) at 1/100, table 2.11) for 1 hour at room temperature. A further two washes in PBS/BSA allowed removal of any unbound antibody before 1 hour incubation at room temperature was performed with Alexa fluor-488 anti-mouse (Invitrogen) antibody (table 2.12). PI staining was performed as previously described. BrdU staining intensity (FITC) was plotted against PI staining to allow accurate characterisation of cell cycle distribution and the proportion of S-phase cells.

2.3.5. Cellular fractionation

Large amount of cells (1 to 1.5 x 10^6) were harvested (by trypsinisation), PBS washed and lysed in cold hypotonic buffer (10 mM HEPES (pH 7.9), 1.5 mM MgCl2, 10 mM KCl) supplemented with 1 mM dithiothreitol (DTT), protease inhibitors cocktail (Sigma), 17 μg/ml phenylmethylsulfonyl fluoride (PMSF), and 34 μg/ml benzamidine. An approximate estimation of the cell pellet allowed the determination of the volume of lysis buffer to use (~10x cell pellet volume), called V1. Following 10 minutes incubation on ice, the cellular suspension was passed several times through a 1ml syringe with 27 gauge needle to physically disrupt the cell walls. Nuclear and cytoplasmic crude fractions were separated by centrifugation at 10,000-11,000g for 20 minutes at 4°C. Supernatant, corresponding to the cytoplasmic fraction, was collected and kept aside on ice. Pellet was first washed with lysis buffer and then resuspended in half the volume V1, and left for 45 minutes on ice in extraction buffer (20 mM HEPES (pH 7.9), 1.5 mM MgCl, 0.42M NaCl, 0.2 mM EDTA, 25% (v/v) glycerol) supplemented with DTT, protease inhibitors cocktail, PMSF, and benzamidine as before. Nuclei were then disrupted with repeated passages through a 27 gauge needle as before and placed at 4°C under rocking for 30 minutes. A final centrifugation at 20-21,000g for 5 minutes at 4°C allowed the collection of nuclear protein extract (supernatant). Total proteins concentration of each fraction was determined by Lowry assay and extracts were snapped frozen in liquid nitrogen before storage at -20°C.

Epitope	Source	Clones	Species	Dilution		Application
HA	Abcam	HA.C5	mouse	1/500	PBS, 2% BSA	IF
PrimPol	Doherty lab/ Blanco lab		rabbit	1/200	PBS, 2% BSA	IF
PrimPol	Doherty lab		rabbit	1/1000	5% milk PBS,T	WB
BrdU	BD	B44	mouse	1/100	PBS, 3% BSA	FACS/IF
BrdU	BD	B44	mouse	1/500	1%BSA, PBS,T	fiber
BrdU	Abcam	ICR1	rat	1/1000	1%BSA, PBS,T	fiber
γH2AX	Abcam	9F3	mouse	1/800	PBS, 3% BSA	IF
Rad51	Santa Cruz	H92	rabbit	1/100	PBS, 3% BSA	IF
Tubulin	Sigma	B-5-1-2	mouse	1/2000	5% milk PBS,T	WB
XRCC1	Caldecott	33-2-5	mouse	1/100	5% milk PBS,T	WB
P-Chk1	Cell signaling	133D3	rabbit	1/500	PBS, 3% BSA	WB
ChK1	Cell signaling	2G1D5	mouse	1/500	5% milk PBS,T	WB
PCNA	Abcam	PC10	mouse	1/2000	5% milk PBS,T	WB
β-Actin	Sigma	AC74	mouse	1/7500	5% milk PBS,T	WB
His-HRP	Abcam	AB1187	rabbit	1/5000	5% milk PBS,T	WB

Table 2.11 Primary antibodies were either purchased from commercial companies (clones number is indicated) or homemade (source). Antibodies were raised in different species, as indicated. Appropriate dilutions and buffer to use are described for each applications, immunofluorescence (IF), Western blot (WB), flow cytometry (FACS), and DNA spreading (fiber) analyses. Antibody P-Chk1 recognises phosphorylated Chk1 on serine 345. Antibody recognising histidine was coupled to horseradish peroxidase (HIS-HRP) preventing use of a secondary antibody.

Antibody	Source	Types	Dilution		Application
rabbit	Invitrogen	Alexa fluor-488	1/2000	PBS, 2% BSA	IF
mouse	Invitrogen	(green)/ 594 (red)	1/2000	PBS, 2% BSA	IF
mouse	Invitrogen	Alexa fluor-594	1/500	1%BSA, PBS,T	DNA fibers
rat	Invitrogen	Alexa fluor-488	1/500	1%BSA, PBS,T	DNA fibers
mouse	Abcam	HRP	1/5000	5% milk, PBS,T	WB
rabbit	Abcam	HRP	1/5000	5% milk, PBS,T	WB

Table 2.12 Secondary antibodies were used to recognise the primary antibodies described above, thus were directed towards different species immunoglobulin. These commercial antibodies (source) were either fluorescently conjugated with green (Alexa fluor-488) or red (Alexa fluor-594) dyes, or coupled to horseradish peroxidase (HRP). Appropriate dilutions and buffers to use are described for each applications, immunofluorescence (IF), Western blot (WB), and DNA spreading (DNA fibers) analyses.

2.3.6. Microscopy analyses

2.3.6.1. Immunodetection of protein

Adherent human cells were seeded directly onto sterilised cover slips (Fisher), coated with poly_L_lysine (Invitrogen) if necessary (Hek293), whereas DT40 cells were collected onto a slide by cytospinning process. Typically 150 µl of DT40 cells at 50 x 10^4 cells ml^{-1} were collected in order to obtain a decent coverage of the surface of the slide. In specific occasions, MitoTracker® deep red (Invitrogen) at 250 nM was added to the cell growth medium for 30 minutes to allow visualisation of mitochondria. Human or chicken cells were then fixed with 3% (v/v) paraformaldehyde (PAF, Science Services Gmbh) in PBS for 10 minutes. A triton extraction treatment was sometime performed (when indicated) in human cells to remove soluble proteins before fixation. In this case, 0.5% triton was added onto the cover slip for 30 seconds and quickly removed with PBS before adding 3% PAF. Following fixation treatment, slides and cover slips were washed 3 times in PBS and could stay for several days at 4°C immerged in this buffer if necessary. Before proceeding to immunostaining step, human cells were permeabilised with 0.2% triton and DT40 cells with 0.1% NP40 for 10 minutes, then washed with PBS. A blocking step with 2% (human cells) or 3% (DT40 cells) BSA for 20 minutes was then performed. Primary antibodies (table 2.11) were diluted in blocking buffer and incubated for 1 hour at room temperature (or 30 minutes at 37°C if necessary). Following PBS washes, secondary antibodies (Alexa Fluor, Invitrogen, table 2.12) were added at 1/2000 in blocking buffer in the same conditions than primary antibodies. After PBS washes, ProLong® Gold anti-fade 4',6-diamidino-2-phenylindole (DAPI, Invitrogen) was added to allow the mounting cover slip over the slide (cells and DAPI comprise inbetween). Nail varnish was then used to seal the montage and to prevent the cell for drying out.

2.3.6.2. Detection of S-phase cells in DT40

Two different methods have been used, classical BrdU (5-Bromo-2'-deoxyuridine) incorporation and more recent Click-iT® EdU (5-ethynyl-2'-deoxyuridine, Invitrogen) technology, where no denaturation step was required. Both thymidine analogue compounds were first added to the growth medium of the cell at 25 µM final concentration for 20 minutes. Following cytospinning and 3% PAF fixation, cells pulsed with BrdU were denatured with 4N HCl (30 minutes at room temperature), washed with PBS then blocked in PBS, 0.1% Tween, 3% BSA (1 hour at room temperature) before following standard primary (anti-BrdU, BD) and

secondary antibodies (tables 2.11 and 2.12) incubations and washes as previously described. According to Invitrogen's instructions, 100 µl Click-iT® EdU cocktail was added onto the cells between permeabilisation and blocking steps (described previously), and left for 30 minutes in the dark at room temperature. Because no denaturation was performed, standard immunoblotting protocols (described previously) could be applied to detect proteins localisation in actively replicating cells. DAPI staining and mounting processes were performed as previously described.

2.3.7. DNA fiber assay

2.3.7.1. Samples preparation and tilting process

DNA fiber spreading assays were performed as previously described (Edmunds *et al*., 2008). Briefly, 25 µM chlorodeoxyuridine (CldU, Sigma) was pulsed for 20 minutes in exponential growing DT40 cells (5 x 10^6 cells) before adding 250 nM iododeoxyuridine (IdU, Sigma). UV-C treatments were performed (when needed) inbetween both labelling periods, keeping the cells in 1% serum medium in this case. By this way, no centrifugation steps were required allowing continuity and minimising cellular stress during the labelling process. Cells were then washed and resuspended at 1 x 10^6 cells ml^{-1} in chilled PBS, then diluted in half with non-labelled DT40 cells to reduce DNA fibers density and facilitate immunostaining detection. Small volume of cells (2.5 µl) was then spotted onto a glass slide into 7.5 µl of spreading lysis buffer (0.5% SDS, 200 mM Tris pH 7.5, 50 mM EDTA). The mixture was left for ~6 minutes at room temperature horizontally before tilting the slide at 15° to allow the spreading of the DNA fibers. The angle was adjusted if necessary to allow a slow descent (3-4 minutes to reach the bottom of the slide). Slides were first air dried then fixed into (3:1) methanol/acetic acid for 10 minutes, air dried again and kept at 4°C until immunostaining.

2.3.7.2. Immunostaining

Due to the similarity of CldU and IdU epitopes, DNA fiber staining protocol was done sequentially, where first a rat anti-BrdU antibody (Abcam, table 2.11) was used to detect CldU then a BrdU antibody raised in mice (BD, table 2.11) was employed for IdU recognition. After rehydration of the slides, DNA fibers were acid treated with 2.5M HCl for 1 hour at room temperature. Following PBS washes, a blocking step in PBS, 0.1% tween, 1% BSA (PBS^+) was

proceed for 1 hour at ~20°C. Incubation with rat anti-BrdU (1/1000 in PBS^+, table 2.11) was performed for 1 hour at 37°C, then the slides were washed 3 times in PBS before fixing them with 4% PAF for 10 minutes. After 3 washes in PBS and 3 in PBS^+, slides were incubated overnight at 4°C with mouse anti-BrdU antibody (1/500 in PBS^+, table 2.11). The next day, slides were incubated for 6 minutes in 20mM Tris pH 8.0, 0.5M Nacl, 0.5% tween, then washed (3 times in PBS, 3 times in PBS^+) before both secondary antibodies (anti-rat Alexa Fluor 488 and anti-mouse Alexa Fluor 594, Invitrogen, table 2.12) diluted at 1/250 each were added for 1 hour at 37°C. Slides were finally washed 3 times in PBS, 3 times in PBS^+ and a further 3 times in PBS before mounting a long cover slip using Fluoromount™ (Sigma). Slides could be kept at -20°C once nail varnished was applied.

2.3.8. Post-replication repair assay

This pulse-chase assay, performed in DT40 cells, was adapted from (Edmunds *et al*., 2008) and (Lehmann *et al.*, 1975). Briefly 6 x 10^5 cells, resuspended in 500 µl of PBS were seeded into 3cm dishes and irradiated (if necessary) with 4 J/m^2 UV-C light (254nm). PBS was then removed very gently, irradiated DT40 cells being attached to the bottom of the dish, before proceeding to the tritium (^3H) thymidine 20 minutes pulse (500 µl of media added with 0.93 MBq/ml [methyl- ^3H] thymidine). PBS wash was then performed very gently, and 1 ml of fresh media, containing 10 µM unlabelled thymidine, was added. Following the 90 minutes chase period, cells were lysed in 150 µl of 0.2M NaOH, 20 mM EDTA and irradiated on ice with 20 Gy (^{137}Cs gamma-source) to fractionate the DNA molecules. DNA was then separated onto a 4 ml 5%-20% (w/v) sucrose gradient prepared with 0.2M NaOH, 0.5M NaCl, by centrifugation at 14000 rpm for 15 hours at 20°C (Beckman XL90, ultracentrifugation). Fractions, collected onto Whatman paper (grade 17 chromatography), were fixed to this support by successive treatments (5 minutes each) in 5% trichloroacetic acid followed by 2 bathes in industrial methylated sprits (IMS). The filter papers were then dried overnight, incubated in 1 ml Ecoscint™ A (National Diagnostics) and radioactivity levels measured with a liquid scintillator (Beckman Coulter).

2.3.9. Tritium thymidine incorporation

This assay was used to allow determination of DNA synthesis rate following or not DNA damaging treatments in DT40 cells. Conditions for tritium thymidine chase were adapted from PRR assay. A carbon-14 (^{14}C) thymidine pre-labelling was performed for ~2 doubling times prior to the tritium pulse to allow normalisation of total amount of DNA. Typically, 2 x 10^6 cells were resuspended in 11 ml of media containing 0.02 μCi/ml of ^{14}C-thymidine and incubated for 16 hours at 39°C. Cells were washed in PBS twice, resuspended at 6 x 10^5 cells ml^{-1} in PBS and distributed in 3 cm dishes before UV-C irradiation treatments were applied, if necessary. PBS was then very gently removed before proceeding to the ^3H-thymidine 20 minutes pulse (500 μl of media added with 0.93 MBq/ml ^3H-thymidine). Cells were washed with PBS, lysed into 150 μl of 0.2M NaOH, 20 mM EDTA and 50 μl was spotted twice onto Whatman paper. Readings of acid-insoluble decays were performed using liquid scintillator (Beckman Coulter).

2.3.10. Cell survival assays

2.3.10.1. Clonogenic survival on methylcellulose

As DT40 cells grow in suspension, conventional clonogenic survival assays have to be adapted to be performed onto a methylcellulose containing medium. Preparation of this support was made as described (Simpson and Sale, 2006), where briefly 7.5g of methylcellulose 4000 centipoise (Across) was diluted and autoclaved into 216 ml distilled water. Good resuspension of the powder was a critical step to obtain a homogenous material at the end. One vial of DMEM F12 (Invitrogen) powder supplemented with 1.125g of NaHCO3 was dissolved into 500 ml of water and filtered sterilised (0.22 μm filter) before to be added to the methylcellulose (cooled at room temperature). Medium was then stirred overnight at 4°C, and the next day, complemented with 10% FCS, 1% chicken serum, pen-strep antibiotics and stirred all day at 4°C before to be aliquoted and kept at 4°C. Before use, methylcellulose was warmed up in 37°C water bath, or for chronic treatments, pre-stirred with the DNA damaging agent for ~30 minutes, in a 37°C heated room. 5 ml of methylcellulose was poured per well of a 6 wells plate and 50 μl of diluted cells were spread and well distributed all over the well. Plates were placed at 39°C and the colonies left to grow for ~7-10 days.

2.3.10.2. CellTiter-Blue viability assay

CellTiter-Blue® technology (Promega) was used to determine DT40 cell viability following DNA damaging treatments, according to manufacturer's instructions. For irradiation treatments, depending of the dose of irradiation, ~3 x 10^5 cells (between 1 to 6 x 10^5) were either resuspended in PBS (UV-C) or in complete medium (X-ray) in the appropriate size dish (3 to 10 cm) before to be irradiated with germicidal lamp or X-ray. Following UV-C irradiation, complete medium was added into the plates, the volume depending on the size of the dish and thus on the strength of the irradiation. Chronic treatment with 4NQO (Sigma) were performed into 12 wells plates with ~1.5 x 10^4 cells (between 0.75 to 3 x 10^4) diluted into 1 ml of media containing the drug. Cells were cultured at 39°C for various amount of time. When necessary, cells were diluted into fresh complete media (with no drug) to assess the cell viability following different recovery times. 100 µl of cells were aliquoted in triplicate wells of a 96 wells plate and 20 µl of CellTiter-Blue reagent was added. If necessary, cells were diluted in fresh medium before addition of the reagent to ensure the linearity of the reading. Plates were incubated at 39°C for ~3 hours before the fluorescence was measured with GloMax® plate reader.

2.3.11. Manual cell counting with haemocytometer

This basic technique was used to assess the number of viable cells in cellular suspension, following human cell trypsinisation or cells growing in suspension. It was therefore used in many protocols, to address the volume of cellular suspension to dispense before transfection and infection protocols, to monitor growth proliferation, and in specific occasions for cells survival experiments. Dilution of the cells with 0.08% Trypan Blue (exclusion dye, Invitrogen) allowed accurate determination of the amount of dead (blue) cells and viable (unstained) cells. Haemocytometer chamber was filled by capillary action, and the cells manually counted under microscopic observations. For accurate assessment, dilutions and scoring were repeated 2 or 3 times.

2.4. Biochemistry Methods

2.4.1. Preparation proteins extracts

Protein samples from human and DT40 cells were extracted using radioimmunoprecipitation assay (RIPA) buffer (20 mM Tris pH 8.0, 150 mM NaCl, 1% NP40, 0.5 mM EDTA, 10% glycerol, 0.1% SDS, 1% Na-deoxycholate) supplemented with protease inhibitor cocktail (Roche). Typically 5 x 10^6 DT40 cells pellet, washed in PBS, was lysed with 50 μl of buffer and one well of a 6 wells plate (80% confluent) of human cells was lysed with 25 μl of RIPA buffer following trypsinisation. Lysis was performed for 1 hour on ice, with regular vortexing pulses, before pelleting cell debris by centrifugation at 14000 rpm for 5 minutes at 4°C. Supernatant was collected, kept on ice and 2 μl used for Lowry assay (Biorad) to assess the protein concentration of the sample. In general, 40 μg of total protein extracts were loaded onto polyacrylamide gel for Western blot analysis.

2.4.2. SDS- Polyacrylamide Gel Electrophoresis (SDS-PAGE)

This electrophoresis in denaturing conditions allowed separation of proteins according to their molecular weight. Sizes of the proteins to be separated onto the gel determined the percentage of polyacrylamide to use. High molecular weight (MW) proteins were resolved on low percentage and *vice versa*. Generally 8-15% polyacrylamide gel were used, and prepared as described in (Sambrook and Russell, 2006). Briefly a master mix composed of 30% acrylamide/bisacylamide (37.5:1) mix (National Diagnostics), 375 mM Tris pH 8.8, 0.1% SDS was prepared before adding at the last minute 0.1% ammonium persulphate and 0.04% (v/v) tetramethylethylenediamine (TEMED, Fisher) to initiate the polymerisation process. Gel was poured into 1 or 1.5 mm Novex® Gel Cassettes (Invitrogen) and water added on the top to help keeping a straight line. Once the gel was set, water was removed and a stacking gel mix (5% acylamide mix, 125 mM Tris pH 6.7, 0.1% SDS, 0.1% ammonium persulphate, 0.1% (v/v) TEMED) poured on top. Combs were added before the stacking gel started polymerising. Gels could be kept are 4°C in humidified saran paper for 1-2 weeks but were recommended to be used fresh.

Protein samples, supplemented with Laemmli buffer (50 mM Tris-Cl pH 6.8, 2% SDS, 0.1% bromophenol blue, 10% glycerol and 2% β-mercaptoethanol added prior to use) were denatured for 5 minutes at 95°C before to be loaded onto the gel. MW ladder, Precision Plus

Protein™ (BioRad) was also loaded to evaluate the proteins sizes. Depending on the detection method to be used, ladder was either unstained (Coomassie staining) or dual coloured (immunodetection). Electrophoresis was then performed in SDS running buffer (25 mM Tris, 250 mM glycine, 0.01% w/v SDS) at 150V for ~1 hour until the loading dye reached the bottom of the gel. Gels were then either stained in Coomassie solution (50% methanol, 10% acetic acid, 0.5% (w/v) Coomassie blue) or processed for Western blot analysis (see below). In the first case, following 10 minutes staining period on a rocking platform, gels were destained into 10% methanol, 10% acetic acid until distinct individual bands were visible. Gels were washed in water and dried.

2.4.3. Western blot analysis

This technique allows transfer of proteins samples into polyvinylidene difluoride (PVDF) membrane (Millipore) to permit immunoblotting detection and visualisation of the protein of interest. Following SDS-PAGE, pre-soaked gel and membrane in transfer buffer (20 mM Tris, 50 mM glycine, 10% methanol) were layered next to each other into 3 MM Whatman paper (Fisher) and sponges (pre-soaked) stack. The montage, placed into XCell II™ Blot Module (Invitrogen), was submitted to 25V for ~70 minutes allowing proteins migration from the gel towards the positive electrode, into the membrane. A blocking step, into TBS,T (table 2.1) containing 5% (w/v) non-fat dried milk (Marvel) was performed on a rocker for 1 hour at room temperature, to saturate the membrane and prevent non-specific binding of antibodies. Incubation with primary antibody (table 2.11) diluted into TBS,T and 5% milk (of 3% BSA for phosphor-specific antibodies) was performed either at 4°C overnight or for 1-2 hours at room temperature under agitation. Membrane was then washed 3 times in TBS,T before secondary antibodies (table 2.12), conjugated with horseradish peroxidase (HRP) and diluted in TBS,T and 5% milk were added for 1 hour at room temperature under agitation. Final washes in TBS,T were performed before enhanced chemiluminescence (ECL, GE Healthcare) detection was applied according to manufacturer's instructions.

2.4.4. Antibody production and purification

Antibody generated toward the protein of interest was produced by Eurogentec following a 28 days immunisation program, where 2 rabbits were injected with the purified protein of

interest and animal blood serum collected at different times. 1 mg of recombinant protein purified from *E. coli* SHuffle system was sent to the company to perform immunisation process.

2.4.4.1. Immunoblotting purification

Purified recombinant proteins, from baculovirus or *E. coli* SHuffle expression systems, were resolved onto 10% SDS-PAGE where 5 μg of protein was loaded into 4 individual wells. Following electrophoresis, proteins were transfer into PVDF membrane which was then blocked into TBS,T 5% milk as described previously (section 2.4.3). Each portion of the membrane containing the recombinant protein was then excised and these small blots were washed twice in TBS,T for 5 minutes each time, before to be incubated overnight at 4°C with 500 μl of serum. The next day, serum was removed and kept aside on ice, and the bands washed 4 times with 500 μl of TBS,T (5 minutes for each wash). Purified immunoglobulins, which specifically bound to the recombinant protein, were eluted with 150 μl of glycine buffer (500 mM NaCl, 50 mM glycine, 0.5% Tween 20, 0.1% BSA, pH 2-3) and the blot submitted to a 20 seconds vortex pulse before adding 25 μl of 1M Tris pH 8.8. Four consecutive elutions were performed for each 4 blots and all first elutions were pooled together (E1), all 2nd elutions together (E2), etc… Thimerosal at 0.01% was added to prevent any contaminations and the purified antibody elutions were kept at 4°C for short term storage otherwise aliquoted and kept at -20°C.

2.4.4.2. Purification by crosslink column

2.4.4.2.1. Preparation column

Recombinant protein used to raise the antibody (expressed in *E. coli* SHuffle cells) was cross-linked onto a column using AminoLink Immobilization kit (Pierce) according to manufacturer's instructions. Briefly, 1 mg of protein prepared in coupling buffer pH 7.2 (0.1M NaP, 0.15M NaCl) via buffer exchange (Biorad micro-spin column), was added to 1 ml of resin 50% slurry. Following 4 hours incubation at room temperature under agitation, unbound proteins were collected and the resin incubated with reducing agent cyanoborohydride (20 mM) overnight on a wheel at 4°C. Two washes with quenching buffer (1M Tris pH 7.4) were performed before blocking the remaining active sites of the resin with quenching buffer supplemented with

cyanoborohydride (100 mM). Following 30 minutes incubation at room temperature under agitation, the column was washed with 1M NaCl (10 column volumes, CV) then with PBS and finally kept in PBS, 0.05% sodium azide at 4°C.

2.4.4.2.2. Serum purification

Column was first rinsed with PBS (10 CV) before the serum, supplemented with 1X PBS, was added. Following overnight binding at 4°C, flow through was collected (unbound serum), and the column washed 4 times with PBS, once with PBS supplemented with 500 mM NaCl and finally with PBS only. Elution of immunoglobulins recognising the protein of interest was performed with 200 mM glycine buffer (pH 2.3). 1 ml fractions (2 volumes of resin) were collected in tubes containing 100 µl of 1.5 mM Tris pH 8.8. Resin was then kept at 4°C in PBS, 0.05% sodium azide. Purified sera were then tested by Western blot analyses using serial dilutions of the different elutions obtained, on membranes blotted with recombinant overexpressed or endogenous PrimPol proteins.

2.4.5. Recombinant protein expression systems

2.4.5.1. Sf9 cells infection with baculovirus

All baculovirus procedures followed the guidance of Bac to Bac (Invitrogen) manual. Briefly, Sf9 insect cells (cultured in Sf-900 II SFM, containing 50 units ml^{-1} penicillin and 50 µg/ml streptomycin final concentrations) were infected at 2 x 10^6 cells ml^{-1} with the appropriate amount of pre-amplified virus. For a small scale assay, typically 15 ml of cells were infected with 200 µl of virus P IV (~10^7 pfu ml^{-1}) for 96 hours. For larger scale purifications, appropriate amount of cells were infected with proportional amount of virus. Cells were then pelleted at 1500 rpm for 5 minutes, freeze in liquid nitrogen and stored at -80°C until protein purification.

2.4.5.2. *E. coli* SHuffle cells

2.4.5.2.1. Competent cells

Overnight culture of single colony picked *E. coli* SHuffle cells (NEB) was performed at 30°C under agitation (185 rpm) in 3 ml of LB medium. This saturated culture was then diluted into a

larger volume of super optimal broth (SOB) medium (table 2.1) supplemented with 10 mM $MgCl_2$ into baffled flask with the appropriate amount of aeration, and placed onto a shaker at 18°C until the optical density at 600 nm (OD_{600}) reached ~0.4. Bacterial growth was then stopped on ice for 10 minutes before collecting the cells by centrifugation at 4000 rpm at 4°C. In the following steps of the protocol, cells were kept on ice as much as possible. After removal of the supernatant, cell pellet was gently resuspended into ice cold 0.1M $CaCl_2$, then left on ice for 20 minutes. Following centrifugation (4000 rpm, 10 minutes at 4°C), pellet was resuspended gently in 0.1M $CaCl_2$, 15% glycerol and small aliquots were snap frozen in liquid nitrogen then kept at -80°C.

2.4.5.2.2. Cells transformation

E. coli SHuffle cells were transformed with plasmid of interest according to NEB's guide line. Briefly, cells were kept on ice for 10 minutes before introducing the DNA, and then were kept for a further 30 minutes on ice before performing the heat shock at 42°C for 30 seconds. Following another 5 minutes period on ice, LB was added to the cells and the culture placed at 30°C for 1 hour under agitation (185 rpm). Cells were then plated onto agar plates containing appropriate antibiotic selection and placed at 30°C overnight.

2.4.5.2.3. Protein expression in SHuffle cells

Overnight culture of single colony picked of transformed *E. coli* SHuffle cells was performed at 30°C under agitation (185 rpm) in 3 ml of LB medium supplemented with appropriate antibiotic. Next day, a large culture was seeded by diluting the overnight pre-culture into baffled flasks (providing sufficient aeration) containing LB supplemented with same antibiotic and 100 µM zinc sulphate (for zinc-finger protein) then placed at 30°C under agitation (185 rpm) until OD_{600} reached ~0.5. At this stage, growing cultures were stopped on ice for 10 minutes and isopropyl β-D-1-thiogalactopyranoside (IPTG, Melford laboratories) was added to switch on the promoter regulating the expression of the protein of interest. Typically 0.4 mM IPTG was added and cultures were placed back into the incubator under agitation (185 rpm). Temperature and time of induction were variable and protein dependent, generally optimised first in a small scale assay. Cells were then recovered by centrifugation at 5000 rpm for 10

minutes at 4°C (Sorvall, SL-6000 rotor) and cell pellets frozen in liquid nitrogen and placed at -80°C.

Small scale assays were generally performed with 10 ml of IPTG-induced cultures incubated for 2-3 hours at 25-30°C or 16 hours at 18-20°C, before collecting the cells by centrifugation and freezing the pellets. Proteins were extracted on ice using lysis buffer containing generally 50 mM Tris, 300 mM NaCl, 10% glycerol. Lysates were sonicated briefly and soluble proteins recovered by centrifugation at 14000 rpm for 30 minutes at 4°C. Western blot analyses were performed with antibody raised against histidine (His) or the protein of interest to evaluate optimum expression conditions.

2.4.6. Purification of recombinant His tagged proteins

2.4.6.1. Affinity purification

All the protocols described in this section are recommended to be proceeded at 4°C to prevent protein degradation. Protein samples were then kept on ice before and after the passage onto the chromatographic columns.

2.4.6.1.1. Small scale purification (baculovirus system)

Cell pellet was lysed on ice in buffer containing 25 mM Tris, 300 mM NaCl, 0.5% Triton, 1 mM DTT, 1 mM imidazole (VWR), pH 7.5, supplemented with protease inhibitors EDTA free cocktail (Sigma). Cell debris were pelleted by centrifugation (13000 rpm for 15 minutes, 4°C) and the soluble proteins loaded onto nickel-nitrilotriacetic acid resin (Ni-NTA resin, Qiagen) corresponding to metal-chelate beads poured into a disposable column (BioRad). The resin (500 µl at 50% slurry) was rinsed and pre-equilibrated in lysis buffer at 4°C for 10 minutes before loading of the protein sample. His-tagged proteins were left to bind onto the resin for 1 hour at 4°C on a rolling wheel. After collection of the flow through, the resin was washed with lysis buffer containing increasing amount of imidazole (10 to 30 mM). Successive elution steps were performed using 500 µl of buffer containing 300 mM imidazole. Glycerol at 10% final was added before snap freezing the proteins samples and storage at -80°C.

2.4.6.1.2. Immobilised Metal Affinity Chromatography (IMAC)

Large volume of culture, previously pelleted and frozen at -80°C, were lysed on ice for 30-60 minutes under stirring in lysis or A buffer (50 mM Tris pH 7.5, 500 mM NaCl, 30 mM imidazole, 10% glycerol, 5 mM β-mercaptoethanol, 17 µg/ml PMSF, 34 µg/ml benzamidine) supplemented with 1% NP40 and 1 mg/ml lysozyme. Samples were then sonicated (Vibracell sonicator) on ice (amplitude 25%) for ~10 minutes with 30 seconds pulses (10 seconds ON/OFF intervals) until lysates were no longer viscous. Soluble proteins were recovered by centrifugation at 18000 rpm for 1 hour at 4°C (Sorvall, RC26 Plus, SS-34 rotor) and insoluble proteins (pellet) were kept separately for analytical purposes (SDS-PAGE and Coomassie staining). Ni-NTA column (~5 ml volume), connected to an automatic pumping system (ÄKTAprime, Amersham pharmacia) was rinsed with water then equilibrated with A buffer before loading the protein sample at 3 ml/min flow rate. Unbound proteins were collected with the flow through and the resin washed with ~50-100 column volumes of A buffer until protein absorbance (UV light at 280 nm) measured at the exit of the column, decreased to the background level. More thorough washes were performed (when indicated) with increasing concentration of B buffer (50 mM Tris pH 7.5, 300 mM NaCl, 300 mM imidazole, 10% glycerol, 17 µg/ml PMSF, 34 µg/ml benzamidine), until final elution of all the proteins was performed with 100% B. Level of expression and purity of the preparation was assessed by SDS-PAGE and Coomassie staining. Samples were concentrated if necessary using Vivaspin™ concentrator (GE Healthcare) and protein concentration measured with NanoDrop technology. Samples were either snap frozen in small aliquots in liquid nitrogen before to be stored at -80°C or kept at 4°C until the next purification step.

2.4.6.1.3. Heparin affinity

Generally, proteins binding DNA also bind to heparin resin therefore providing an efficient way to further purify the sample following IMAC or ion exchange columns. Protein sample was then diluted in A buffer with no salt (50 mM Tris pH 7.5, 2 mM DTT, 10% glycerol) and loaded onto Hi-trap heparin column (GE Healthcare) previously equilibrated in A buffer. Column was then washed in A before a step elution in B buffer (A supplemented with 1M NaCl) was performed.

2.4.6.2. Ion exchange chromatography

Ion exchange chromatography allows separation of proteins according to their isoelectric point. Anion exchange mono-Q column (GE Healthcare) was used either with standard ÄKTAprime system or with fast protein liquid chromatography (FPLC) technology on ÄKTA™ Purifier (Amersham pharmacia) according to manufacturer's instructions. Protein samples were diluted and eluted in similar buffers than used with Heparin column (section 2.4.6.1), with either gradient (0 to 1M NaCl) or a step elution (once the salt concentration for elution of the contaminants was determined).

2.4.6.3. Size exclusion chromatography

Size exclusion chromatography allows separation of proteins by their MW and conformational features (multimerization status mainly). It is usually used as a final step of the purification process to generate fine separation and collect individual species fractions (suitable for crystallographic studies). This chromatography could also be used to buffer exchange the sample when necessary. Running buffer typically contained 50 mM Tris pH 7.5, 300 mM NaCl, 10% glycerol, was filtered (0.22 μm) before to be used to equilibrate the Superdex column (S200, GE Healthcare). Samples were concentrated to a small volume (<5 ml), and centrifugated (14000 rpm, 5 minutes, 4°C) before being injected carefully through a loop (1 or 5 ml) without inducing any air bubbles. Small proteins were kept longer inside the support of the column therefore collected last. Column was previously calibrated using standard size markers (GE Healthcare) to allow accurate determination of the size of the protein of interest according to its volume of elution. Following Coomassie analysis and NanoDrop measurements, protein samples were aliquoted and snap frozen before storage at -80°C.

2.4.7. Preparation samples for mass spectrometry

Purified protein samples were buffer exchanged using Micro Bio-Spin® column (Biorad) to replace Tris, salt and glycerol with 50 mM Hepes, according to manufacturer's instructions. Electrophoresis on 8% polyacrylamide gel followed by Coomassie staining treatment (with filtered staining solution) was performed with 1 μg of the protein of interest before excision of the bands. Analysis was performed by Mark Skehel (Clare hall) laboratory.

2.4.8. Primer extension assay

Protocols were adapted from Jozwiakowski and Connolly, 2010. Primers used for this assay were HPLC purified and generated by ATDbio (see table 2.13). A small (20 mer) 5' fluorescently labelled (hexachlorofluorescein) primer was annealed with a template-primer (50 mer) in buffer (50 mM Tris pH 8.0, 50 mM NaCl, 1 mM EDTA). Reaction was performed at 95°C for 3 minutes then the temperature was decreased slowly to ~20°C. 20 nM of annealed primers were incubated for 30 minutes at 37°C with 100 nM enzyme, 1X NEB buffer 1 and 200 μM dNTP (Roche). Reaction was then quenched with an equal volume of 2X stop buffer (95% formamide, 40 mM EDTA, 200 nM competitor oligonucleotide, with bromophenol blue and xylene cyanol). An excess of non-labelled oligonucleotide competitor, corresponding to the complementary sequence of the template, was used to prevent fluorescent products re-annealing with the template, therefore preventing smearing. Quenching was performed for 5 minutes at 95°C before loading the samples (10 nM fluorescent products) onto a denaturing urea-PAGE. Gel (15% polyacrylamide bis-acrylamide (19:1) solution (National Diagnostics), 7M urea, TBE, 0.1% ammonium persulphate (APS), 0.03% TEMED) was pre-run at a constant wattage of 15 watts for 30 minutes in TBE. Following 3-4 hours electrophoresis at 15-17W, fluorescence was detected by scanning the gel using a FLA-1500 scanner (FUJI).

		Sequences 5' to 3'
Primer Extension	Labelled primer	**5'-Hex**-TGTCGTCTGTTCGGTCGTTC
	Template	CGCGCAGGGCGCACAACAGCCTTGAAGACCGAACGACCGAACAGACGACA
	Competitor	TGTCGTCTGTTCGGTCGTTCGGTCTTCAAGGCTGTTGTGCGCCCTGCGCG

Table 2.13 Oligonucleotides for primer extension assay, 5' labelled primer with hexachlorofluorescein (Hex) was designed to anneal opposite the template-primer (template) in order to provide a 5' overhanging end to allow primer extension by a DNA dependent polymerase. Competitor primer was designed complementarily of the template primer sequence. All primers are written 5' to 3'orientation.

2.5. Bioinformatic tools

DNA sequences and map data of genomes were retrieved via the National Centre for Biotechnology Information (NCBI) (Sayers *et al*., 2011) and the UCSC genome browser (Kent *et al*., 2002) was specifically used to consult the chicken genome database. Expasy tools (Gasteiger *et al*., 2005) were used for prediction of polypeptide MW and isoelectric point (ProtParam). MultAlin (Corpet, 1988) allowed protein alignment and ClustalW2 (Larkin *et al*., 2007) DNA sequences alignments studies. Mitoprot website (Claros *et al.*, 1996) was used to

predict the probability of amino acids sequence to contain a MLS. Prediction of secondary structures were obtained using PSIPRED server (Jones *et al*., 1999). Quantification of Southern blot and Western blot signals were achieved thanks to AIDA image analyser (raytest) and Image J software.

CHAPTER III

Role of PrimPol in mitochondrial DNA maintenance

3.1. Introduction

DNA primases are specialised DNA-dependent RNA polymerases essential for the initiation of DNA replication. Indeed, they synthesise short RNA oligomers *de novo*, providing a free 3' OH required by replicative polymerases to prime DNA synthesis. Primases can be divided in two groups, Archaeo-Eukaryotic Primases (AEP) and bacterial DnaG superfamily, depending on the structure of their catalytic site, which are evolutionarily unrelated and structurally distinct. Recently, a novel member of the AEP superfamily has been discovered in human cells, *CCDC111* also called *FLJ 33167* gene (Iyer *et al*., 2005). To date, only one primase has been characterised in human cells, the Prim1 subunit of the Pol α complex, which is essential for the initiation of DNA replication at origins and each Okazaki fragments for the lagging strand synthesis. Preliminary studies in the Doherty lab and in collaboration with Luis Blanco (Center of Molecular Biology `Severo Ochoa` or CBMSO, Madrid), confirmed that recombinant human CCDC111 was capable of both primase and polymerase activities *in vitro*, therefore the protein was renamed PrimPol. This enzyme is part of the UL52-like primase and contains a C-ter zinc-finger domain characteristic of the herpes-pox family (Iyer *et al.*, 2005). *PrimPol* gene is present on chromosome 4 of human cells.

In order to provide an initial characterisation of this novel eukaryotic primase-polymerase, the first aim of this chapter was to determine the sub-cellular localisation of the protein in human cells. The second goal was to explore PrimPol knockdown phenotypes by using predominantly RNAi depletion and then confirmed in avian *PrimPol* $^{-/-}$ KO cell lines; description of the generation of the KO DT40 cell lines will be provided in the following chapter (Chapter 4).

3.2. Sub-cellular localisation of overexpressed human PrimPol

Having identified a novel protein, one of the first priorities was to determine its cellular localisation. Given the protein *in vitro* polymerase activity, it was expected PrimPol to localise within the nucleus or the mitochondrion, as both compartments contain DNA molecules. PrimPol cDNA was cloned into different backbone plasmid vectors (e.g pUC, pET) for the different purposes of the project (Andrew Green and Aidan Doherty, unpublished data). Here, haemagglutin (HA) and enhanced green fluorescent protein (eGFP) tagged PrimPol constructs (table 2.7) were used to perform fluorescent microscopy and visualise if the overexpressed ectopic protein accumulated specifically in one compartment of the cell. Initial experiments

with eGFP tagged PrimPol, which is a relatively quick method as it removes the need for immunostaining, produced images of poor quality, often with saturated fluorescent signals throughout the cell (data not shown). Constructs containing a C-ter HA tag proved more suitable for immunofluoresence analysis and determination of PrimPol sub-cellular localisation (figure 3.1). U2OS cells were transiently transfected using FuGENE® HD reagent and subjected to immunofluorescence staining 48 or 72 hours later. These cells are flat and contain a large area of cytoplasm making them ideal for fluorescence microscopy, especially for mitochondrial studies (Duxin *et al.*, 2009). Indeed, as we observed a cytoplasmic localisation of PrimPol, we wanted to check if the protein was also located within the mitochondrion. To this purpose, MitoTracker® dye was used due to its ability to specifically stain mitochondria. It was therefore possible to visualise co-localisation of ectopic HA-PrimPol predominantly with mitochondria (figure 3.1A). Nuclear signal was also visible, but not in every cell (figure 3.1A), suggesting PrimPol may also be present in the nucleus. However comparison of fluorescent signals obtained with the empty HA vector, which appeared to localise in a similar manner (figure 3.1B), prevented firm conclusions regarding PrimPol's sub-cellular localisation to be made.

To further investigate the localisation of PrimPol, sub-cellular fractionation experiments were then performed. First, a PrimPol antibody, generated by Luis Blanco's laboratory against insoluble recombinant protein produced in *E. coli*, was tested against recombinant PrimPol over-expressed in Hek293 cells, to check its specificity (figure 3.2A). The predicted MW of PrimPol polypeptide is 65 kDa, thus with the addition of the eGFP epitope, PrimPol recombinant proteins were predicted to be 94.9 kDa and 92 kDa for the C-ter and N-ter versions respectively of the tagged proteins (ExPASy tool). In line with this, a band of approximately 100 kDa was observed by Western blot analysis only in samples containing eGFP-PrimPol and no signal was detected in samples transfected with empty vectors, confirming the specificity of the antibody (figure 3.2A). Moreover, this analysis confirmed the very strong eGFP signal previously seen by microscopy, and also suggests that eGFP tagged PrimPol is subject to degradation, as a lot of lower MW species were detected by Western blot analysis (figure 3.2A, lanes 1 and 2). A major degradation product of around 50 kDa was observed (figure 3.2A, short exposure blot on the right, lane 2), in every overexpressed recombinant PrimPol protein samples, independently of the backbone vector used and absent from empty vector preparations (figure 3.2). Having the tag in the C-ter part of the protein (figure 3.2A, lane 2 and 4) seemed to enhance this process. Nonetheless, the PrimPol antibody specifically recognised the overexpressed protein and was thus suitable to analyse protein localisation.

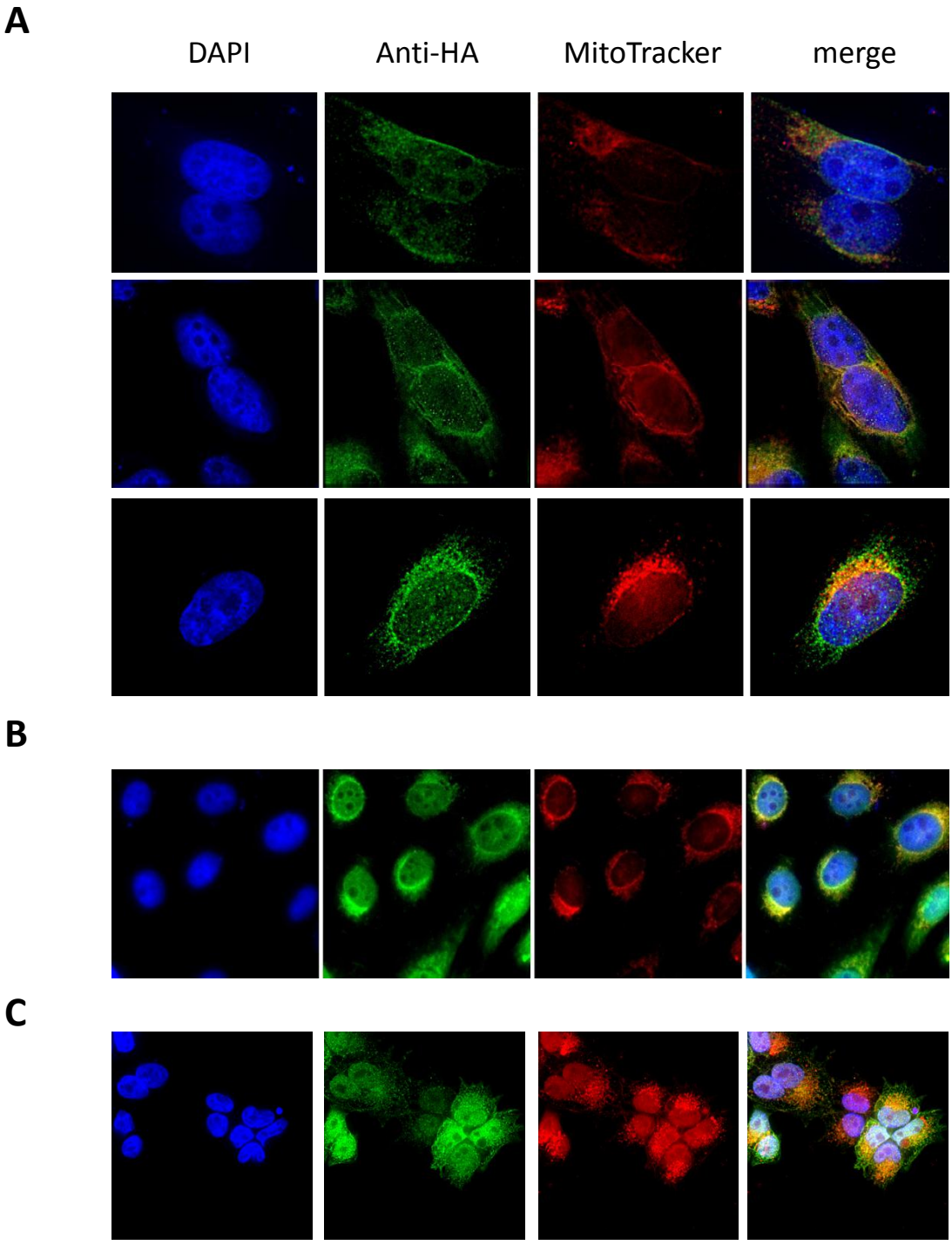

Figure 3.1: Overexpression of HA-PrimPol in human cells for cellular localisation studies.

(**A**) Immunofluorescent detection of HA-PrimPol (green) construct transiently transfected in U2OS cells. Counterstaining with MitoTracker (red) allowed visualisation of mitochondria, and DAPI staining (blue) delimitated the nucleus of each cell. (**B**) Images obtained with U2OS cells transfected with HA tagged empty vector and subjected to similar immunodetection as in (**A**). Images were taken 72 hours after transfection using DeltaVision microscopy and deconvolution technology. (**C**) Stable Hek293 cells induced for HA-PrimPol expression by addition of doxycycline (10 ng/ml, 18 hours) were subjected to immunofluorescent analysis as in (**A**). Cell line and images were generated by Sean Rudd.

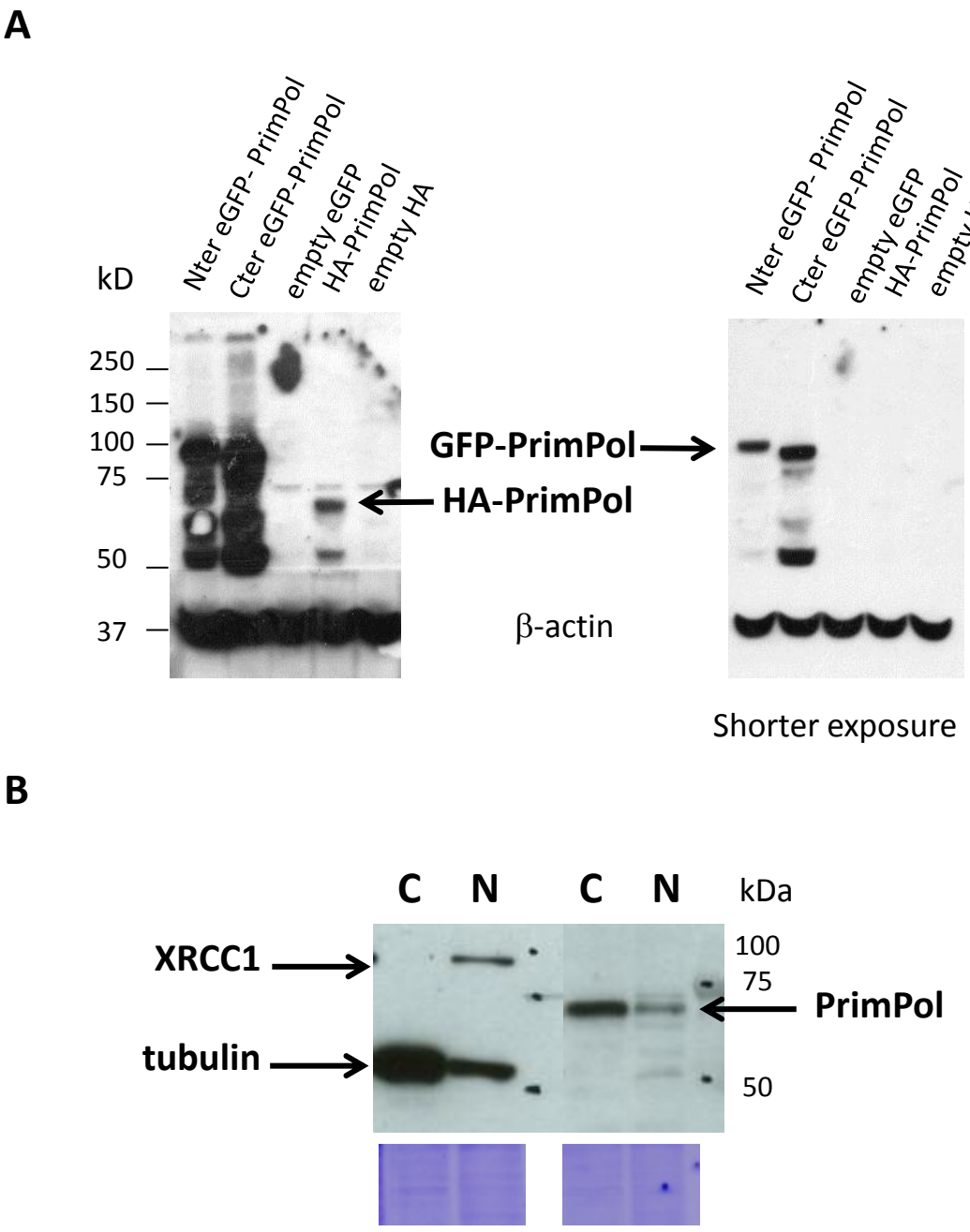

Figure 3.2: Transient over-expression of PrimPol and sub-cellular fractionation analyses.

(**A**) Western blot analysis of transient over-expressed eGFP or HA tagged PrimPol were performed in Hek293 cells using PrimPol antibody and β-actin as loading control. Blot on the right side corresponded to a shorter exposure of the left side membrane. (**B**) Nuclear (N) and cytoplasmic (C) fractions of U2OS cells were subjected to Western blot analysis using XRCC1 as a nuclear marker and tubulin as a cytoplasmic one. The same fractions were also submitted to immuno-detection with a PrimPol antibody to determine the level of expression of endogenous protein in each compartment. Coomassie staining of SDS-PAGE allowed evaluation of the loading of the Western blot above.

To confirm PrimPol's cellular localisation, U2OS cells were lysed using hypotonic buffer and separated into nuclear and cytoplasmic fractions (figure 3.2B). Purity of each fraction was confirmed by Western blot analysis using XRCC1 and tubulin antibodies, which are nuclear and cytoplasmic proteins respectively. A small proportion of cytoplasmic protein was still present in the nuclear fraction as indicated by the presence of tubulin in the nuclear sample (figure 3.2B). However, this crude fractionation method confirmed PrimPol was mainly located in the cytoplasm of these U2OS cells (figure 3.2B). The presence of PrimPol within the nucleus could not be confirmed with this method as a proportion of PrimPol detected in the nuclear fraction (figure 3.2B) could reflect the cytoplasmic contamination of this sample with unlysed whole cells (Cooper and Spelbrink, 2008).

Using these preliminary observations, detailed above, further localisation studies have been undertaken in the Doherty lab. Immunofluorescence and sub-cellular fractionation studies were performed with both endogenous PrimPol and using a Hek293 cell line stably over-expressing HA-tagged PrimPol under an inducible promoter (figure 3.1C, Sean Rudd). These studies confirmed that PrimPol is present throughout the cell, with a portion inside the nucleus and the mitochondrion of human cells.

3.3. Involvement of PrimPol in mitochondrial DNA maintenance

The propagation of mtDNA is very different from nuclear DNA, as only one DNA polymerase, Pol γ, is needed to maintain this small genome (~16 kb) (Hance *et al*., 2005), and DNA replication is constitutive throughout the cell cycle (Bogenhagen and Clayton, 1977; Clayton, 1982). Moreover, multiple copies of this circular genome are present in each mitochondrion, therefore thousands per somatic cell, as first shown in *Drosophila* (Solignac *et al.*, 1983), and later in mouse (Jenuth *et al.*, 1997) and human cells (Jazin *et al.*, 1996). To date Pol γ is the only DNA-dependent DNA polymerase present within the mitochondrion, and several studies have shown its importance in regulating the steady state of mtDNA copy number (Kelly *et al.*, 2012; Chu *et al.*, 2007). The mechanisms underlying mtDNA replication are still under debate with two modes of replications being proposed (Bogenhagen, *et al.*, 2003a and b; Holt, *et al.,* 2003). Originally it was thought this small genome was replicated continuously but in an asynchronous manner, starting with the leading strand synthesis and generating a displacement of the lagging strand. Once the replisome reaches the origin of replication O_L synthesis of the second strand began (Clayton *et al.*, 1982). An alternative model was then

suggested following 2D-AGE analysis, where both mtDNA strands would be replicated at the same time in a coupled and symmetrical manner, as in the nucleus (Holt *et al.,* 2000). Moreover, no sole mtDNA primase has been characterised to initiate DNA replication in the organelle, although the activity has been reported (Wong and Clayton, 1985). Instead, the transcripts synthesised by POLRMT are used as primers by Pol γ to initiate mtDNA replication (Xu and Clayton, 1996; Wanrooij *et al.*, 2008; Fusté *et al.*, 2010).

Therefore, having discovered the presence of the uncharacterised primase-polymerase PrimPol within the mitochondrion (figure 3.1A; appendix A), we first wanted to verify if PrimPol was required for mtDNA replication or maintenance, by studying mtDNA copy number variations following PrimPol depletion. Two approaches were used, an RNAi transient depletion in various human cell lines, and a homologous disruption of the gene in avian DT40 cells.

3.3.1. Effect of PrimPol RNAi depletion on mtDNA copy number in human cells

3.3.1.1. Principle of quantitative PCR analysis and validation of the primer sets

SYBR green Q-PCR technology (depicted in figure 3.3), was first used to analyse mtDNA copy number. Real time PCR allows the amount of newly replicated amplicons synthesised during the PCR reaction to be followed. Indeed, SYBR green dye only emits a strong fluorescent signal upon binding to dsDNA, so an exponential increase of the fluorescence signal can be measured after each cycle of the PCR reaction. To process the data, the comparative threshold method was utilised (Bookout and Mangelsdorf, 2003). The level of mtDNA copy number was compared between cells treated with mock RNAi and RNAi targeting the protein of interest. Instead of using titration curves of the samples, an internal control was utilised, corresponding to a probe recognising a nuclear housekeeping gene. By this way, every sample were normalised for the amount of DNA initially present at the beginning of the reaction.

The relative DNA copy number was then calculated by using these formulae:

$$2^{-\Delta\Delta Ct}$$

where $\Delta\Delta Ct = \Delta Ct_{\ RNAi} - \Delta Ct_{\ mock\ treated}$

and $\Delta Ct = Ct_{\ mtDNA} - Ct_{\ nDNA2}$ or $\Delta Ct = Ct_{\ nDNA1} - Ct_{\ nDNA2}$

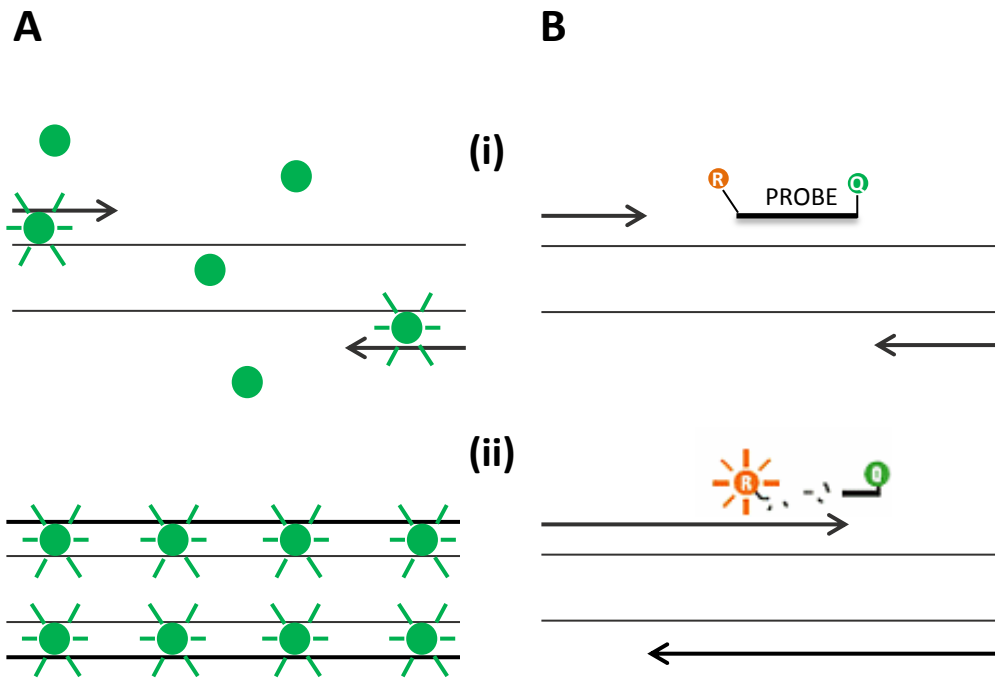

Figure 3.3: Comparison Taqman and SYBR green Q-PCR technologies.

(**A**) Schematic explaining SYBR green technology during Q-PCR reaction, where the reagent dye (green circles) fluoresces only when bound to double-stranded DNA arising during the PCR reaction (green circles surrounded with green blocks). Black arrow represent the nascent DNA strand created during the Q-PCR reaction. (**i**) Representation of the beginning of the Q-PCR reactions, where most of the dye are still free between the denatured DNA template (black lines). (**ii**) Schematic of the end product of the Q-PCR where all the SYBR green molecules are bound to double-strand DNA. (**B**) Cartoon describing Taqman technology where a fluorescent reporter dye (letter R in orange circle) and a quencher (letter Q in green circle) are maintained to close proximity on a probe at the beginning of the reaction (**i**). Following the progression of the PCR reaction, the probe get cleaved releasing the fluorescent dye (R circles surrounded with orange blocks) (**ii**). Cartoon was adapted from Life technologies web site.

Ct value, standing for threshold cycle, corresponds to the PCR cycle where the fluorescence level starts to increase in an exponential way. Therefore a low Ct value means a large amount of templated DNA (sequence recognised by the primers) was present at the beginning of the reaction resulting in an early increase of the fluorescence (early PCR cycle).

Primers were designed in order to amplify a short area (maximum 200 bp) of the mitochondrial genes *COXII* and *CYT-B* and nuclear housekeeping genes *β-actin* and *GAPDH*. Several sets of primers were tested in a template titration assay before selecting a pair suitable for further analyses (figure 3.4). To this purpose, a range of genomic DNA dilutions was used as template for the Q-PCR reaction and a standard curve plot was selected on the analysis setting mode of the thermocycler. Correlation coefficients R^2 were calculated by the machine and needed to be above 0.95 for the primer set to be validated (figure 3.4). Appropriate dissociation curves profiles were also taken into account (data not shown). Preliminary experiments were performed using both COXII and CYT-B primers and gave similar results (data not shown). It was then decided to procede using COXII primers only. GAPDH was used as internal control in every Q-PCR analyses (housekeeping gene data needed for delta Ct calculation), whereas β-actin primers were employed as gene of interest to follow nuclear copy number variations.

3.3.1.2. Q-PCR analysis of mtDNA copy number in PrimPol depleted U2OS cells

In order to explore the role of PrimPol in mtDNA maintenance, RNAi mediated depletion of PrimPol needed to be first optimised. The methodology is based on the principle that the exogenous RNA duplex (RNAi) can activate an RNA-induced silencing complex (RISC) to target the corresponding mRNA sequence. A cut is then introduced at a specific site, resulting in the degradation of this mRNA (Filipowicz, 2005). Experiments were first performed to determine the choice of cell type and transfection reagent to successfully deplete PrimPol protein, and then the ratio of RNAi and transfection reagent per reaction were adjusted to improve the depletion (data not shown). Initially, U2OS cells were chosen, using 10 nM PrimPol RNAi duplex introduced into these cells using Hiperfect (Qiagen) cationic lipid transfection reagent, allowing the formation of a liposome able to fuse through the membrane of the cell.

To determine if PrimPol depletion affects mtDNA copy number, U2OS cells were RNAi treated and at different time points following transfection, protein and genomic DNA samples were extracted and submitted to Western blot (figures 3.5A and 3.6A) and Q-PCR (figures 3.5B

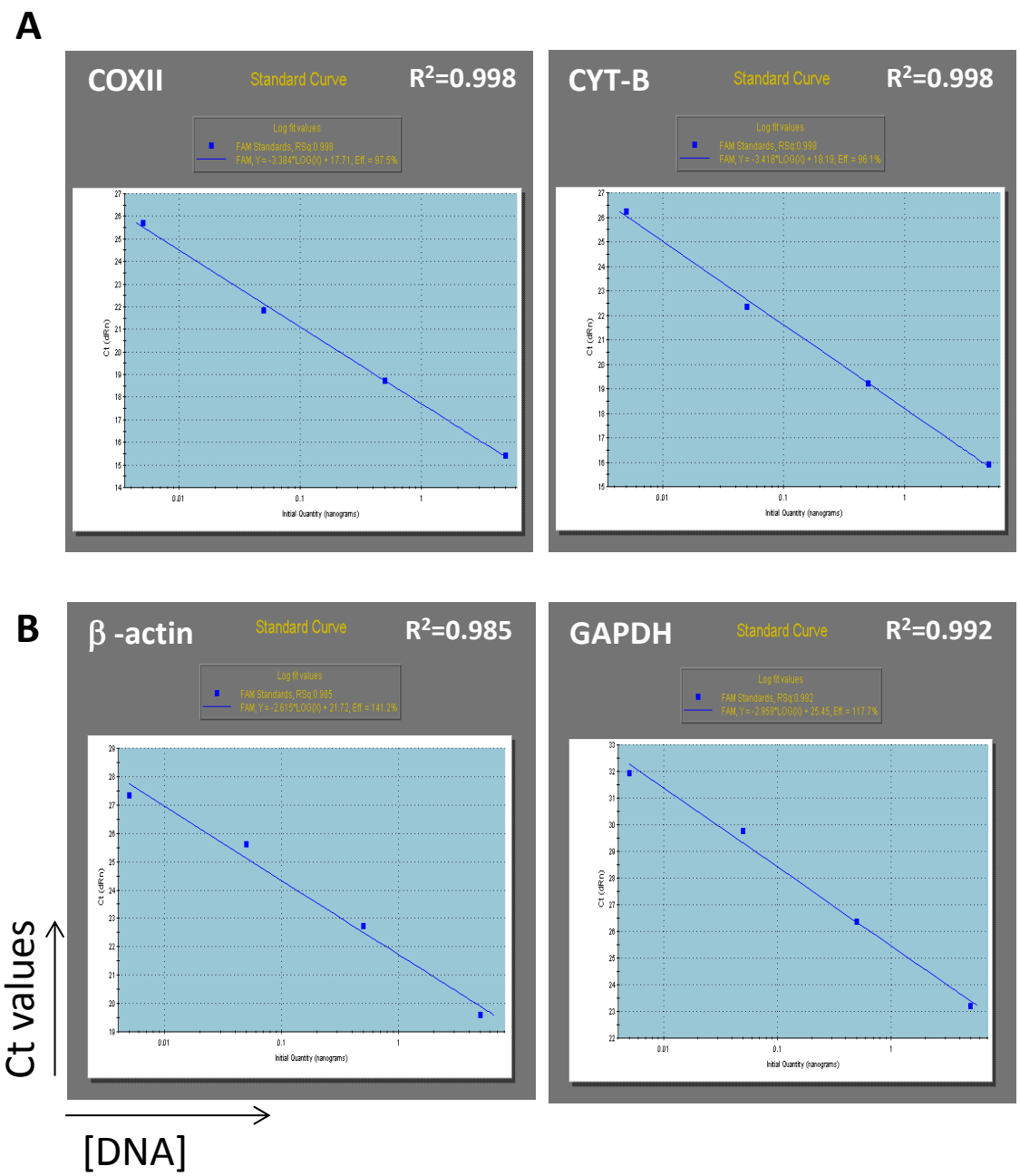

Figure 3.4: Q-PCR primers validation for SYBR green technology: template titration assay.

(**A**) Standard curve plots of Q-PCR primers specific of mitochondrial DNA genes, cytochrome c oxydase subunit 2 (COXII) and cytochrome b (CYT-B). Correlation coefficient R^2 value (right corner) should be above 0.95 to validate the set of primer. (**B)** Housekeeping genes β-actin and glyceraldehyde 3-phosphate dehydrogenase (GAPDH) are used as internal control due to their constant expression levels. Ct values are inversely proportional of the amount of DNA (range from 0.005 to 5 ng/µl).

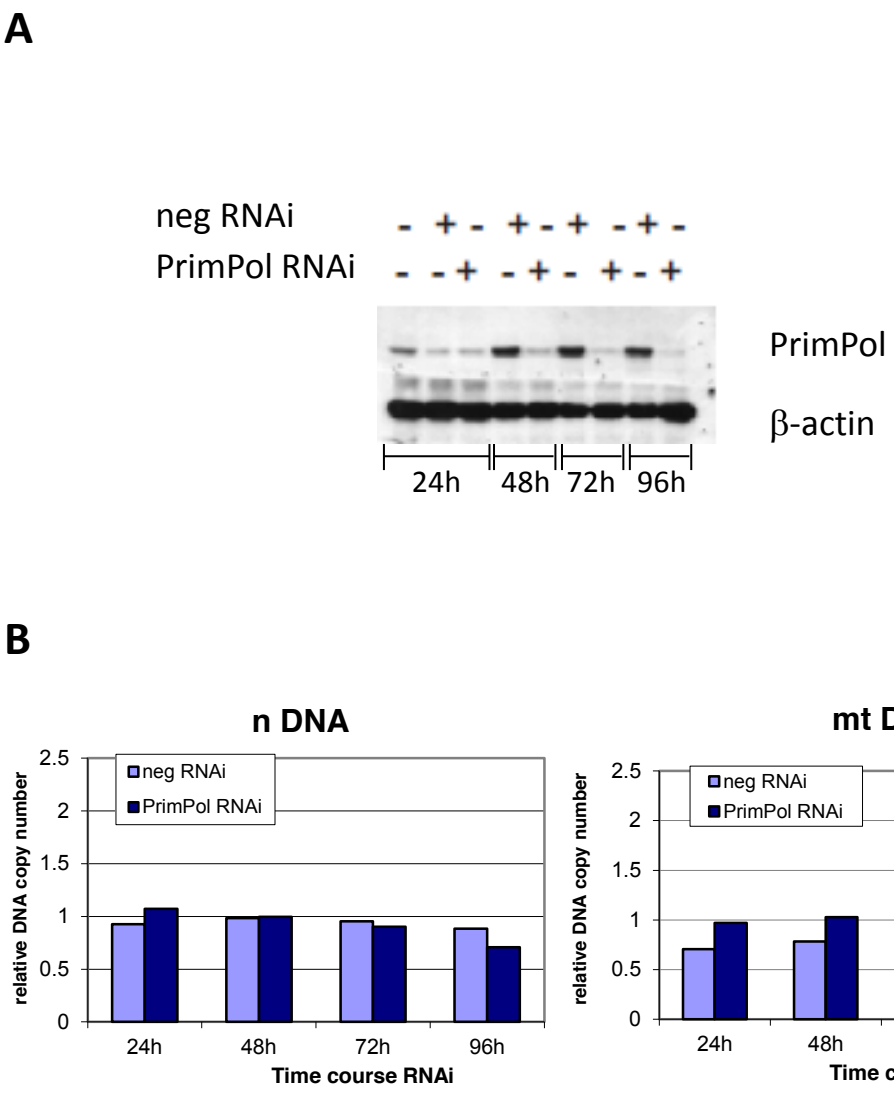

Figure 3.5: Analysis of PrimPol RNAi knockdown on mtDNA copy number.

(**A**) Western blot analysis of PrimPol RNAi knock-down in U2OS cells. Samples were collected at different time points (hours indicated under the blot) after a single round of transfection with Hiperfect reagent and analysed using PrimPol antibody and β-actin as loading control. Non targeted RNAi (neg RNAi) was used as a transfection control. (**B**) Q-PCR data obtained from the same samples than in (**A**); Nuclear DNA (n DNA) copy number was obtained using β-actin primer set, while mitochondrial DNA (mtDNA) with cytochrome c oxydase subunit 2 (COXII) primers. Glyceraldehyde 3-phosphate dehydrogenase (GAPDH) level was use as internal control for both analyses.

and 3.6B) analyses. Samples treated with PrimPol RNAi presented a specific depletion of the PrimPol protein when compared to samples transfected with the non-targeted RNAi, which had no significant sequence similarity towards any human genes and is therefore used as a negative control (figures 3.5A and 3.6A). In both experiments, optimum knockdown of PrimPol protein was observed at 72 and 96 hours post transfection (figures 3.5A and 3.6A). At these time points, a substantial increase in mtDNA copy number was also observed by Q-PCR analysis using the comparative threshold method described in section 3.3.1.1 (figures 3.5B and 3.6B). Indeed, no great variations were observed with nuclear DNA (figure 3.5B and 3.6B, charts on the left) but a 1.5 fold increase of mtDNA copy number was observed on average following PrimPol RNAi transfection 72 and 96 hours post treatment (figures 3.5B and 3.6B). At 24 and 48 hour time points, when PrimPol protein depletion was only partial (figures 3.5A and 3.6A), no significant variation of mtDNA copy number was observed (figures 3.5B and 3.6B). Moreover, performing two rounds of RNAi treatments did not improve the efficiency of the knockdown (figure 3.6A) or the variation of mtDNA copy number (figure 3.6B). It was also noticed that the use of the non-targeted RNAi induced mild variations of DNA copy number (figures 3.5B and 3.6B, light blue bars). Therefore, reliability of this control was questioned and the following Q-PCR analyses were performed using only mock transfected cells as a negative control, setting the copy number arbitrarily as 1 (figures 3.7 and 3.9). Time course experiments were then repeated several times in U2OS cells and on average mtDNA copy number was increased by 1.2 to 1.3 fold following 48, 72 or 96 hours PrimPol RNAi transfection (figure 3.7). No significant differences were observed between the different time points analysed, therefore following experiments were performed at the intermediate time point 72 hours post RNAi depletion. Taken together, these data indicate that PrimPol depletion by RNAi in U2OS cells induces an increase in mtDNA copy number, and therefore implicate PrimPol in the maintenance of mtDNA.

3.3.1.3. Southern blot analysis of mtDNA copy number in PrimPol depleted U2OS cells

In order to confirm the data obtained by Q-PCR analysis with another method, Southern blot experiments were undertaken to analyse mtDNA copy number following PrimPol RNAi. Moreover, RNAi depletion of the mitochondrial replicative helicase TWINKLE was also performed to provide a positive control, as this protein is essential for mtDNA replication (Tyynismaa *et al.*, 2004). Genomic DNA was prepared from RNAi treated cells, digested with *NdeI* and resolved by gel electrophoresis. A transfer onto a nylon membrane allowed

A

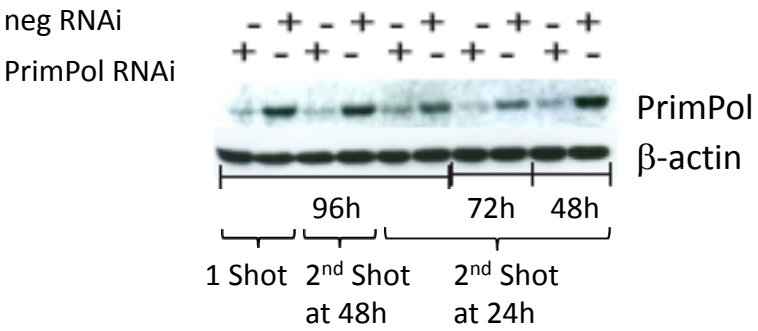

B

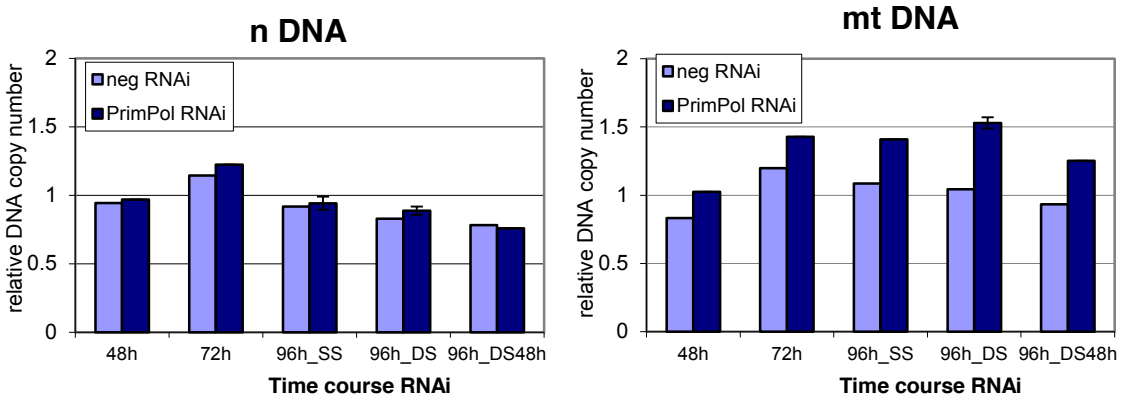

Figure 3.6: PrimPol RNAi knockdown optimisation and mtDNA copy number analysis.

(**A**) U2OS cells were transfected with PrimPol or non-targeted (neg) RNAi, either once (1 shot) or twice; the second round of transfection was either at 24 hours or 48 hours after seeding, as indicated under the blot (2nd shot). Western blot analysis was performed using PrimPol antibody and β-actin as loading control. (**B**) DNA was extracted for Q-PCR analysis at the same time points than the Western blot samples and with the same transfection treatments (single shot, SS; double shot, DS; double shot at 48 hours, DS48h); Nuclear DNA (n DNA) copy number was obtained using β-actin primer set, while mitochondrial DNA (mt DNA) with cytochrome c oxydase subunit 2 (COXII) primers. Glyceraldehyde 3-phosphate dehydrogenase (GAPDH) level was use as internal control for both analyses.

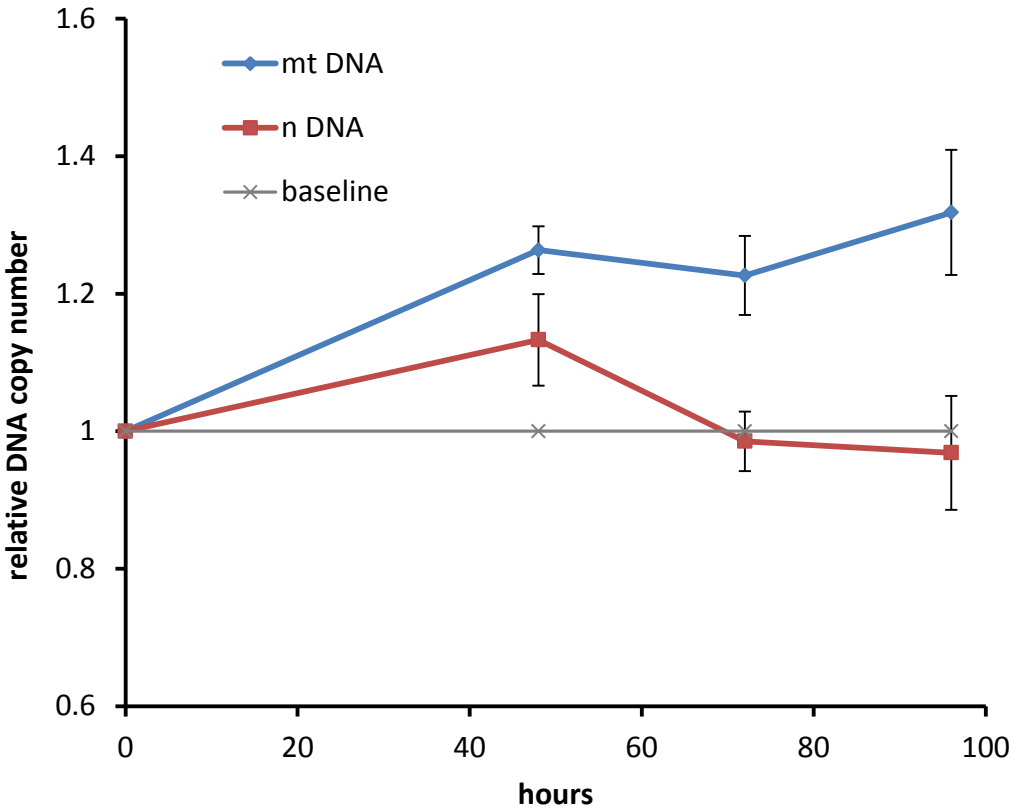

Figure 3.7: Time course Q-PCR analysis of mtDNA copy number in U2OS cells.

Summary of Q-PCR data obtained in U2OS cells transiently depleted with PrimPol RNAi and samples collected at different time points after RNAi transfection. Variation of mitochondrial DNA (blue line) and nuclear DNA (red line) copy number was assessed by comparison with the baseline level (grey line) corresponding to mock treated cells. Error bars denote standard deviation of at least 3 independent experiments (6 experiments for 72 hour time point), all obtained using SYBR green technology.

hybridization with radiolabelled probes specific for mitochondrial or nuclear DNA and auto-radioagraphy detection (figures 3.8A and B). A band at approximately 8 kb, instead of the expected 16 kb, was obtained with mitochondrial H1 probe due to the presence of an extra *NheI* site present in these cells. Indeed it has been previously reported a single nucleotide polymorphism occurring at position 11 347 of mtDNA can be found in 3 out of 2704 mtDNA sequences (Ingman and Gyllensten, 2006). Nonetheless, signal intensities were measured using Image J software and the ratio mitochondrial/ nuclear DNA (mtDNA/nDNA) calculated (figure 3.8C). As expected, TWINKLE depleted samples presented a 35% decrease in mtDNA copy number (figure 3.8C). However treatments with PrimPol RNAi did not cause a significant difference in mtDNA copy number (figure 3.8C). PrimPol protein levels were checked by Western blot analysis and confirmed the efficiency of the protein knockdown following RNAi transfection (figure 3.8D).

This experiment was only performed once and further experiments were attempted but gave inconsistent results due to technical difficulties (data not shown). Furthermore, a more robust system was obtained in the meantime with the generation of stable KO cell lines produced in avian DT40 cells (see section 3.3.2).

3.3.1.4. Q-PCR analysis of mtDNA copy number in several PrimPol depleted cell lines

To confirm that the increase of mtDNA copy number observed previously in U2OS cells following PrimPol RNAi was not a cell type specific phenotype, Q-PCR analyses were undertaken in various cultured human cell lines. In addition to U2OS cells, osteosarcoma 143B cells, embryonic kidney Hek293 cells, and non-diseased MRC5 fibroblasts, were transfected with 10 nM PrimPol RNAi and analysed 72 hours after. TWINKLE RNAi was again used as a positive control and a ~50% decrease in mtDNA copy number was repeatedly observed in all cell lines tested, as reported previously (Tyynismaa *et al.*, 2004), thus validating the robustness of the assay (figure 3.9A, grey bars). In contrast, PrimPol protein depletion was accompanied with a ~20% increase in mtDNA copy number in all cell lines tested (figure 3.9A). Efficient PrimPol protein depletion was confirmed in all cell lines by Western blot analysis which showed an approximately 70% decrease in protein level on average (figure 3.9B). This confirms the initial result, that RNAi depletion of PrimPol in cultured human cells results in an increase in mtDNA copy number, and supports the involvement of PrimPol in the maintenance of the mitochondrial genome.

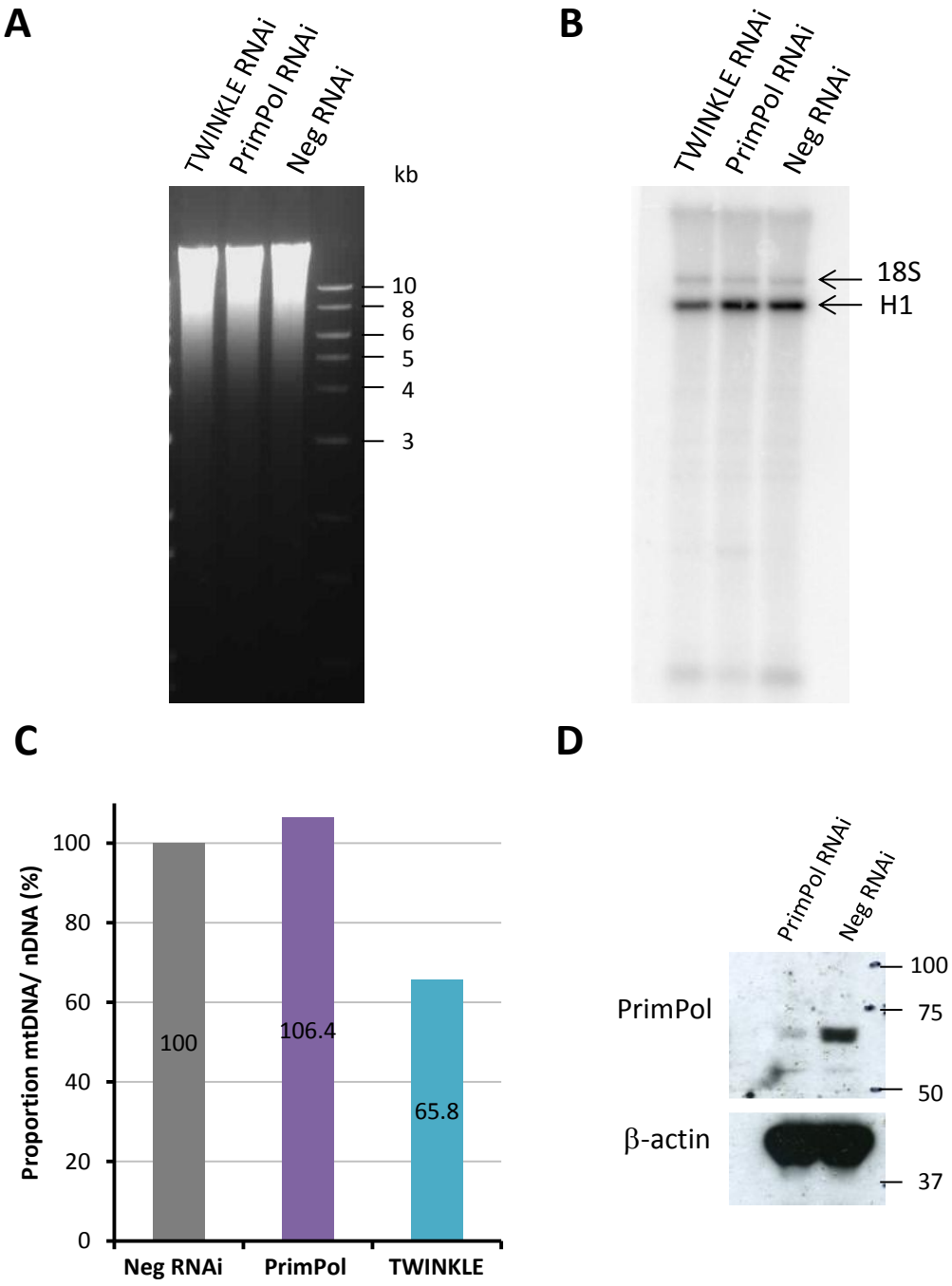

Figure 3.8: Southern blot analysis of mtDNA copy number in U2OS cells.

(**A**) DNA was extracted from U2OS cells 72 hours after transfection with TWINKLE, PrimPol or non-targeted RNAi (neg RNAi). Five microgram was digested with *NdeI* enzyme and loaded onto 1% agarose gel containing ethidium bromide in order to visualise the total amount of DNA. (**B**) Southern blot analysis with radiolabelled probes H1 and 18S (specific of mitochondrial DNA and nuclear-encoded rDNA respectively) allowed visualisation of each DNA species. (**C**) Quantification of Southern blot bands was performed with Image J software to determine the relative amount of mtDNA following depletion of PrimPol or TWINKLE in those cells. (**D**) Samples used for Southern blot experiment were submitted to Western blot analysis to evaluate PrimPol protein expression levels. Experiment performed only one time.

A

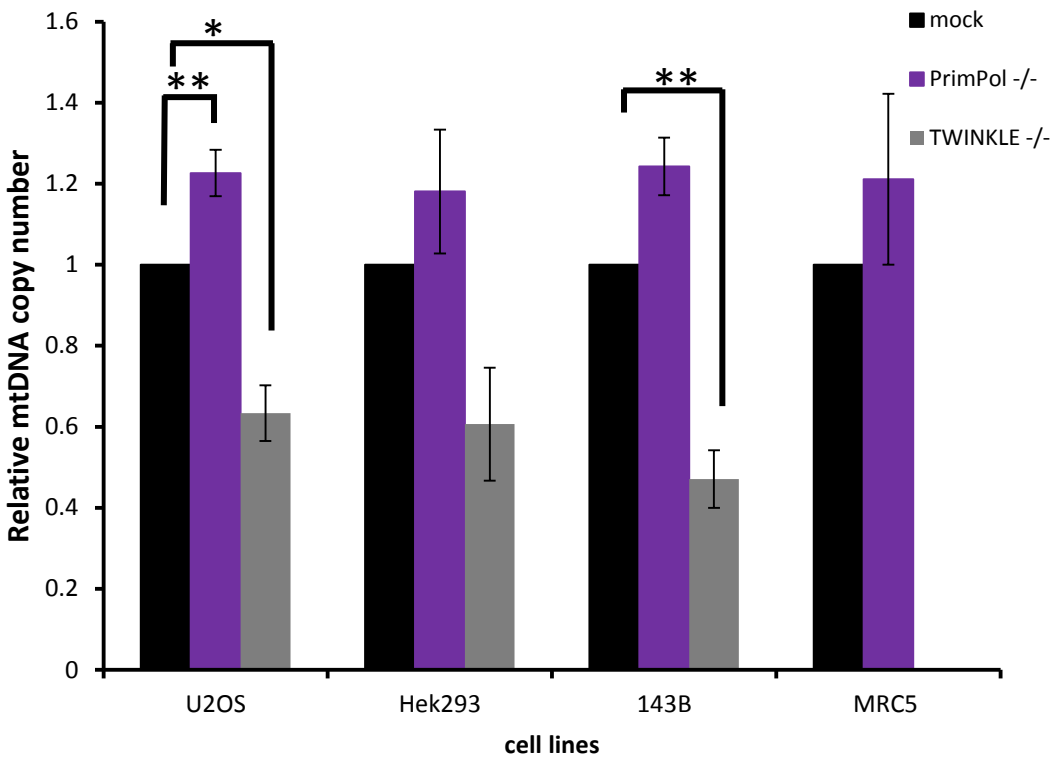

B

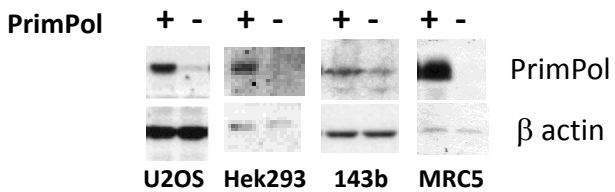

Figure 3.9: Q-PCR analysis of mtDNA copy number in various human cell lines.

(**A**) Osteosarcoma (U2OS and 143b), embryonic kidney (Hek293) and lung fibroblast (MRC5) cells were either mock transfected (black), or transfected with PrimPol RNAi (purple) or TWINKLE RNAi (grey). DNA was extracted at 72 hours and mtDNA copy number was analysed by Q-PCR. Error bars denoted standard deviation of at least 2 experiments (U2OS: n=7; Hek293: n=3; 143B: n=4; MRC5: n=2) and significance was assessed by t-test with two tails moments (* corresponds to *p<0.01* and ** for *p<0.001*). (**B**) Western blot analyses of PrimPol RNAi depletion in several cell lines. β-actin was used as loading control. Representative analysis of the RNAi knockdown efficiency at 72 hours after transfection is shown here.

Fluorescent microscopy using PicoGreen® technology was also tested, but analyses were inconclusive. This fluorescent nucleic acid dye has been described to be suitable for quantification of the variation of mtDNA content (Ashley *et al.*, 2005). However mtDNA staining by PicoGreen has to be performed in living cells complicating the analysis. Moreover the assay was not sensitive enough to detect the small variation expected (below 1.5 fold), as even following TWINKLE depletion, no obvious differences were observed (data not shown).

3.3.2. Effect of PrimPol deletion on mtDNA maintenance in avian DT40 cells

3.3.2.1. Q-PCR and Southern blot analysis of mtDNA copy number in *PrimPol* $^{-/-}$ DT40 cells

To produce a robust system in which to analyse the effects of PrimPol's absence, I generated two *PrimPol* KO cell lines in avian B lymphocytes DT40 cells. The generation and detailed characterisation of these KO cell lines will be described in Chapters 4 and 5. Briefly, bi-allelic expression of the *G. gallus PrimPol* (*CCDC111*) gene was disrupted with puromycin and histidinol antibiotic selection markers. A complementary cell line with inducible expression of human PrimPol was also made employing the Tet-off system in a *G. gallus PrimPol* null background. The advantage of having both RNAi studies in human cells and avian KO system was to gain a more complete understanding of PrimPol's role, and to verify if this role was conserved within other vertebrates.

The mtDNA copy number of the two PrimPol KO clones (clones 1 and 2) and the human conditional cell line, which constitutively expresses human PrimPol in the absence of doxycycline in the media, was determined by Q-PCR using both SYBR green and Taqman methodologies (as described in figure 3.3). A significant increase of mtDNA copy number was observed in KO clone 1 compared to WT DT40 cells, increasing up to 1.3 fold (figure 3.10) similar to what was previously observed in human cells treated with PrimPol RNAi. However, no significant difference was observed in KO clone 2 with a 1.06 fold increase, and a similar result was observed with the complementation cell line (figure 3.10).

The mtDNA copy number in the PrimPol KO cell lines was further analysed using Southern blot technique (figure 3.11). Genomic DNA was first digested with *XbaI* restriction enzyme to linearize mtDNA molecules which can then be visualised with a radiolabelled probe specific of the replication origin O_H area (figure 3.11A). By this way, two separated fragments can be analysed at the same time, a 16 kb molecule corresponding to full length mtDNA and a

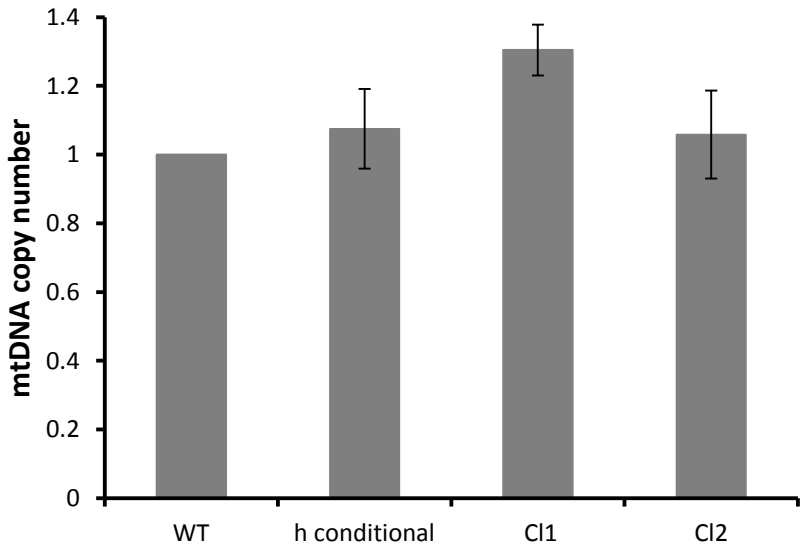

Figure 3.10: Q-PCR analysis of mtDNA copy number in DT40 cell lines.

Genomic DNA of WT DT40 cells, both *PrimPol* $^{-/-}$ clones (Cl1 and Cl2) and *PrimPol* $^{-/-}$ cells complemented with human PrimPol (h conditional) was subjected to Q-PCR analysis using SYBR green and Taqman technologies. Cytochrome c oxydase subunit 2 (COXII) and amyloid-β precursor protein (APP) primers were used for amplifying mtDNA and nuclear DNA respectively. Error bars represent standard deviation of two experiments.

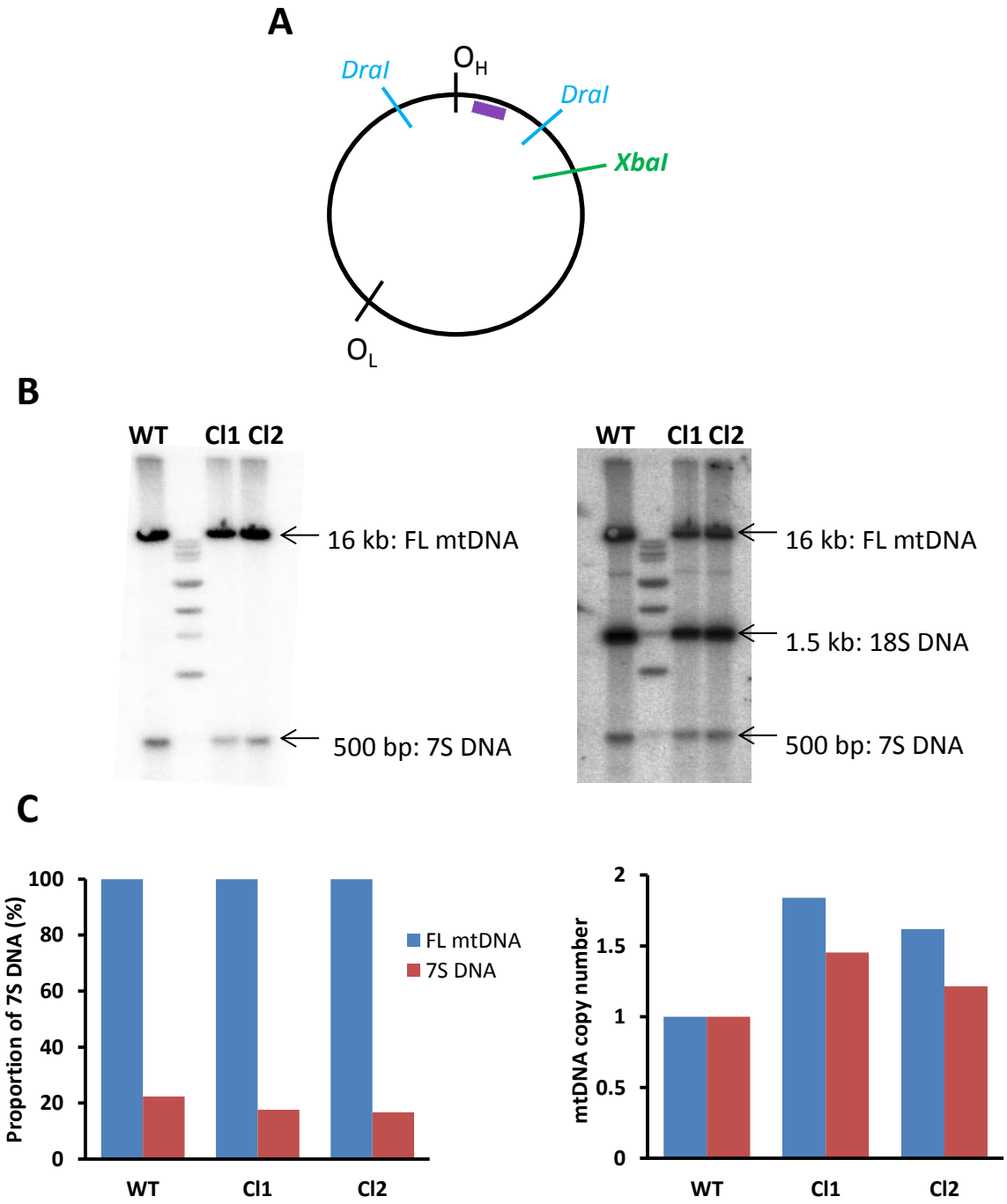

Figure 3.11: Southern blot analysis of mtDNA copy number in DT40 cell lines.

(**A**) Cartoon representing mtDNA molecule with both origins of replication O_H and O_L and the position of *DraI* and *XbaI* restriction sites (blue and green bars respectively), and OH probe (purple square). (**B**) Genomic DNA (4 μg) of WT DT40 cells and both *PrimPol* $^{-/-}$ clones (Cl1 and Cl2) was linearised by *XbaI* restriction digestion, loaded onto 1% TBE agarose gel and visualised using a radiolabelled OH probe (specific of mtDNA at O_H site) by Southern blot analysis. The same membrane was re-hybridised with radiolabelled probe specific of 18S rDNA for normalisation purposes (right panel, middle band 1.5kb). (**C**) Quantification of Southern blot signals obtained in (**B**) were normalised with either full length (FL) mtDNA (left bar chart) or 18S rDNA (right bar chart) signals. Blue bars correspond to total mtDNA molecules and red bars to mtDNA molecules containing 7S DNA.

500 bp fragment corresponding to 7S DNA (figure 3.11B). 7S DNA molecule corresponds to a short third strand found within the non-coding region (NCR) of some mtDNA molecules, and is believed to be a product of an aborted replication of the H strand, thus creating a displacement (or D-loop) of this H strand (Kasamatsu *et al.*, 1971). The proportion of mtDNA molecules containing this third strand of DNA was then calculated by normalising the intensity of the signal of the 500 bp band with the 16 kb signal for each DT40 clone using AIDA image analyser software. In both PrimPol KO clones, fewer mtDNA molecules containing the 7S DNA strand were observed, on average 16% of the total mtDNA molecules compared to 22% within the WT DT40 population (figure 3.11C, left chart). The same membrane was then re-hybridised with a probe specific to 18S rDNA to normalise the loading between the different samples and then allow the quantification of mtDNA copy number for each cell line (figure 3.11B, right gel). Both KO clones contained more copies of their mitochondrial DNA as the relative signal (full length mtDNA/ 18S) was increased on average by 1.7 fold compared to WT cells (figure 3.11C, right chart, blue bars). As a result, the relative amount of mtDNA molecules containing a third strand (7S DNA) was increased by 1.3 fold on average in both KO cell lines compared to WT DT40 cells (figure 3.11C, right chart, red bars). Taken together, Q-PCR data and Southern blot analysis performed in chicken KO cells reinforce the previous conclusions drawn in human cells, indicating the absence of PrimPol results in an increase in mtDNA copy number.

3.3.2.2. 2D-gel analysis of mtDNA replication intermediates in *PrimPol* $^{-/-}$ DT40 cells

Having confirmed in two different vertebrate organisms (four human cell lines and avian B lymphocytes) that the absence of PrimPol correlates with an increase of mtDNA copy number, analysis of mtDNA RI were next undertaken. Two dimensional agarose gel electrophoresis (2D-AGE) analysis was performed in the *PrimPol* $^{-/-}$ DT40 cells to determine if a prolonged absence of PrimPol directly affects mtDNA replication mechanisms. This method allows the examination of DNA RI by combining two successive electrophoresis steps and Southern blot analysis (Friedman and Brewer, 1995). DNA molecules were first separated by their mass in a low percentage agarose gel ran at a low voltage. In the second dimension, the gel slice was rotated through ninety degrees and cast within a higher percentage agarose gel containing ethidium bromide and this second dimension electrophoresis was performed at a higher voltage to allow separation of DNA molecules by their mass and shape (figure 3.12A). The Southern blot strategy adopted required a *DraI* digestion of mtDNA in order to visualise a 3.6 kb fragment centred on the O_H (depicted in figure 3.11A). The presence of RI, such as

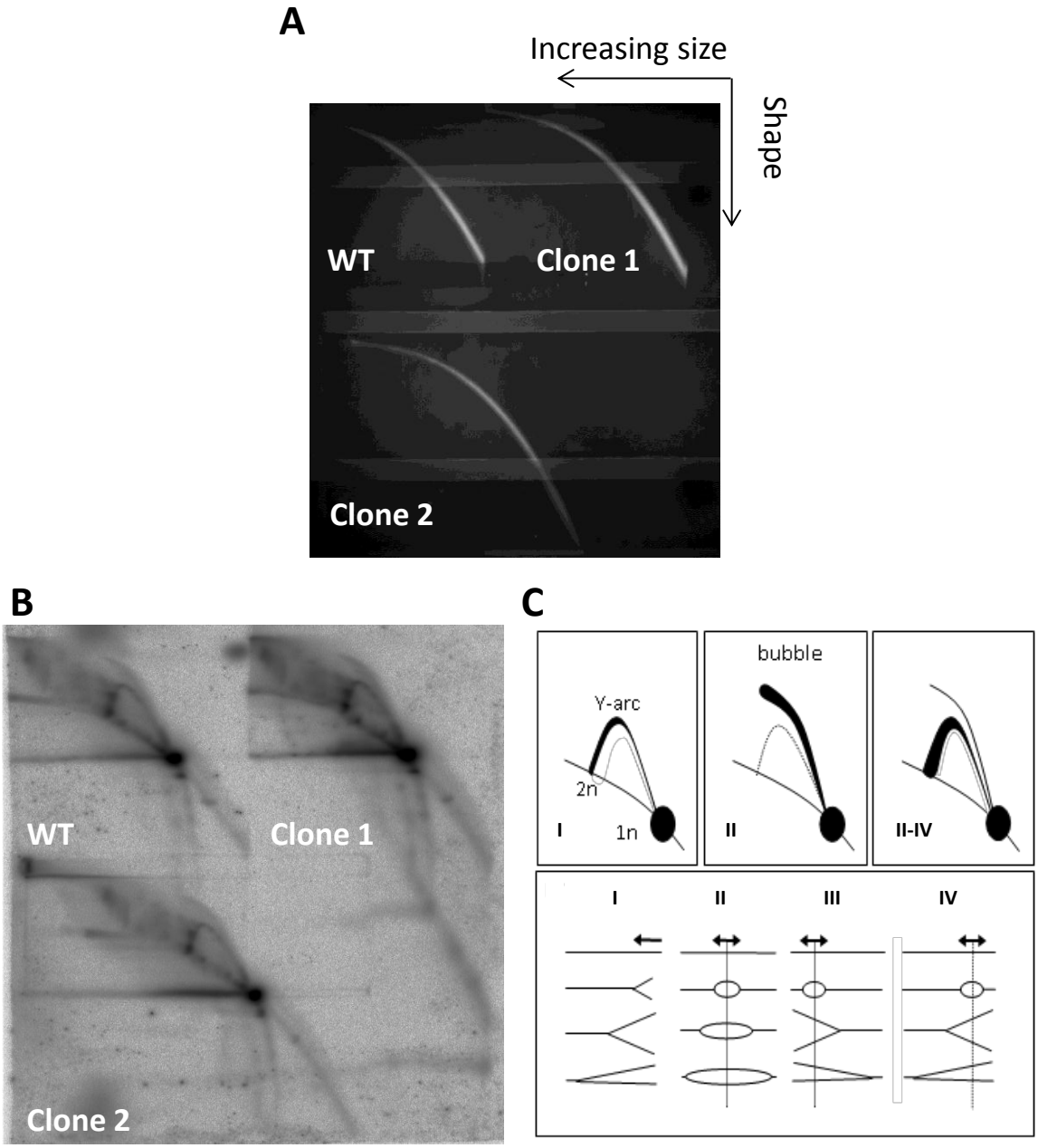

Figure 3.12: 2D-AGE analysis of mtDNA in *PrimPol* $^{-/-}$ DT40 cell lines.

(**A**) Genomic DNA (10 μg) of WT DT40 cells (upper left corner), *PrimPol* $^{-/-}$ clone 1 (upper right corner) and *PrimPol* $^{-/-}$ clone 2 (bottom left corner) was digested by *DraI* (to linearize a 3.6 kb mtDNA fragment), and loaded onto 0.4% TBE agarose gel (with no ethidium bromide) for electrophoretic separation based on the size of DNA fragments (30V for 16 hours). To separate the DNA molecules by their shape, a 2nd dimension electrophoresis was performed with 1% TBE agarose gel (+ ethidium bromide) at 90V for 16 hours at 4°C. (**B**) 2D-gel was analysed by Southern blotting using radiolabelled probe OH to visualise replication intermediates described in (**C**) (cartoon adapted from Reyes *et al.*, 2007). (**I**) Progression of replication fork generating a Y-arc shape; 2n annotation corresponded to the fully replicated fragment. 1n spot symbolised unreplicated linearized mtDNA fragment. (**II**) Progression of replication bubble initiated at an origin of replication. (**II-IV**) Multiple initiation sites (initiated from both origin and on-going replication) within the mtDNA fragment analysed.

replication forks and bubbles, which are visualised as arcs and spots (figure 3.12B and C), indicate the initiation of DNA replication from this origin. Genomic DNA samples from both PrimPol KO clones were analysed using this technique in comparison to samples taken from WT DT40 cells. No obvious differences were observed in terms of pattern and amount of RI, indicating no specific replication pausing or any major defects caused by the lack of PrimPol (figure 3.12B). Thus, the absence of PrimPol does not directly affect the mode of mitochondrial DNA replication in avian cells.

3.3.2.3. Analysis of mtDNA mutations in *PrimPol*$^{-/-}$ DT40 cells

Having established PrimPol's involvement in mtDNA maintenance, a chloramphenicol resistance assay was used to determine if the absence of PrimPol affects the mutation rate of mtDNA. Chloramphenicol binds to rRNAs which prevents mitochondrial protein production and therefore decrease cell viability (Kroon *et al.*, 1965). This feature of mitochondrial ribosomes is similar to bacterial ribosomes reflecting the evolutionary conservation between mitochondria and bacteria (Benne and Sloof, 1987), reinforcing the endosymbiotic theory (Kutik *et al.*, 2009). However, cells can become resistant to this antibiotic by gaining a single point mutation in the rRNA genes encoded within mtDNA (Coon *et al.*, 1977). *PrimPol* $^{-/-}$ DT40 cells were more sensitive to chronic chloramphenicol treatments (24 and 48 hours) than WT cells (figure 3.13), suggesting a diminished mtDNA mutation rate. Indeed, if more point mutations were present within mtDNA genome a better survival of the cells would be expected as they would have more chances to become resistant to the antibiotic. However this preliminary data needs to be repeated with several clonal expansions and the mutation rates to be assessed specifically before confirming PrimPol involvement within mitochondrial error-prone DNA synthesis.

3.4. Effects of PrimPol RNAi depletion on cell proliferation

During the initial process of PrimPol cellular characterisation, it was decided to monitor cell proliferation following RNAi depletion in human cells. Growth curves were assessed in U2OS cells by manually counting the population doubling every 24 hours following RNAi transfection (figure 3.14A). Transfection with TWINKLE RNAi delayed the cell growth by approximately 24 hours, but the cells were still able to double exponentially after that (figure 3.14A, turquoise

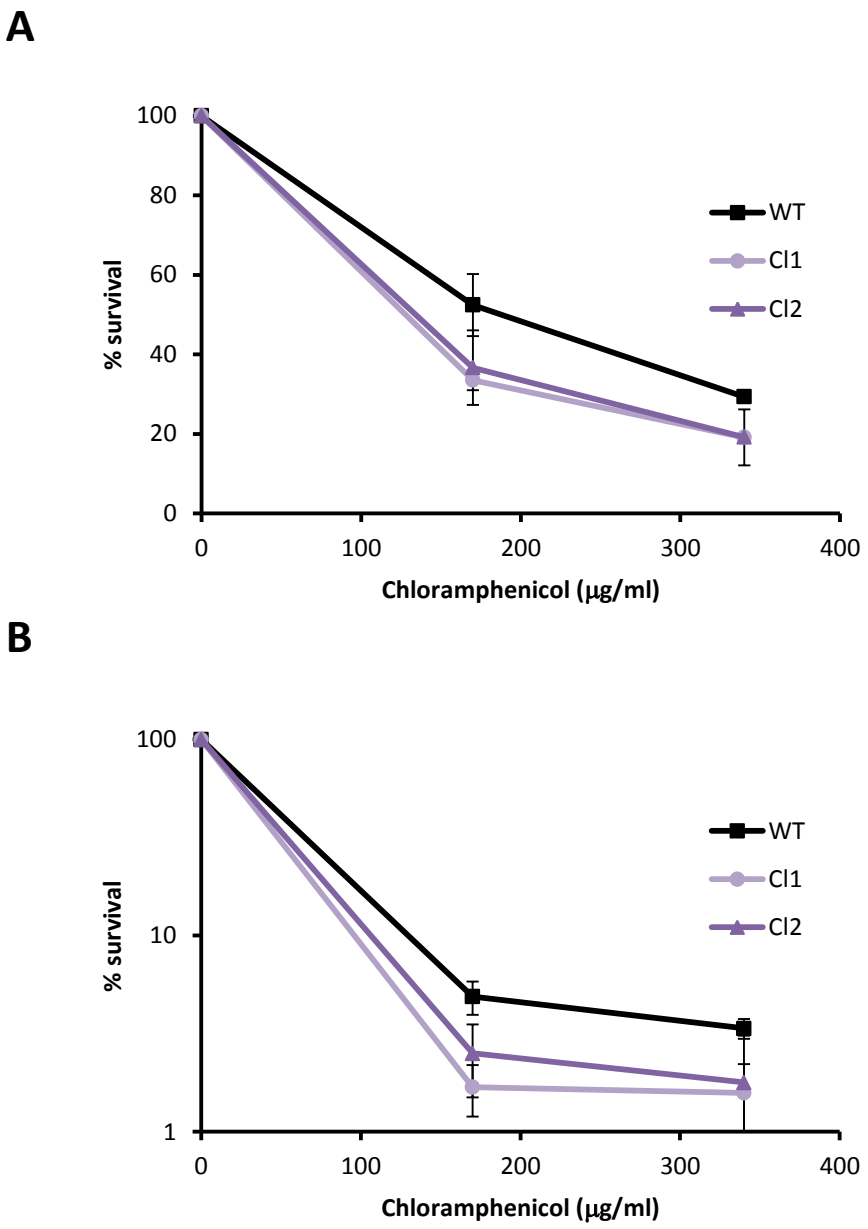

Figure 3.13: Chloramphenicol resistance assay.

(**A**) Cell survival of WT DT40 cells (black) or both *PrimPol* $^{-/-}$ clones (light and dark purple) was assessed by manual counting using a haemocytometer and cells stained with Trypan Blue exclusion dye, following 24 hours of chronic treatment with chloramphenicol drug in the liquid cultures. (**B**) Cell survival assessed the same way but 48h following chronic treatment with chloramphenicol.

A

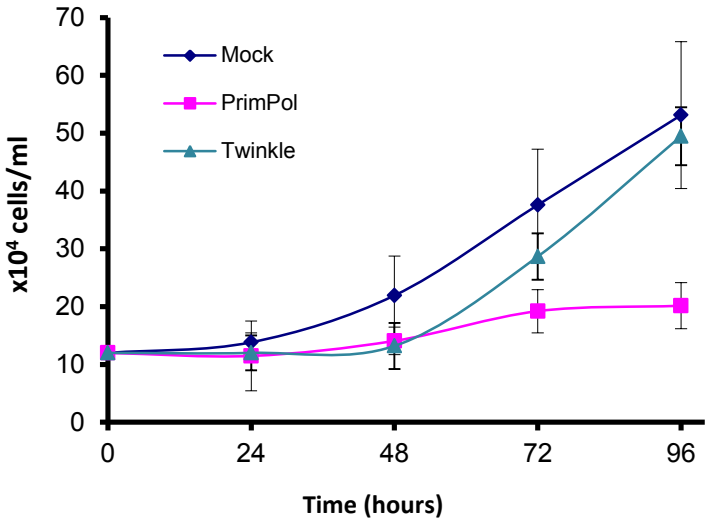

B

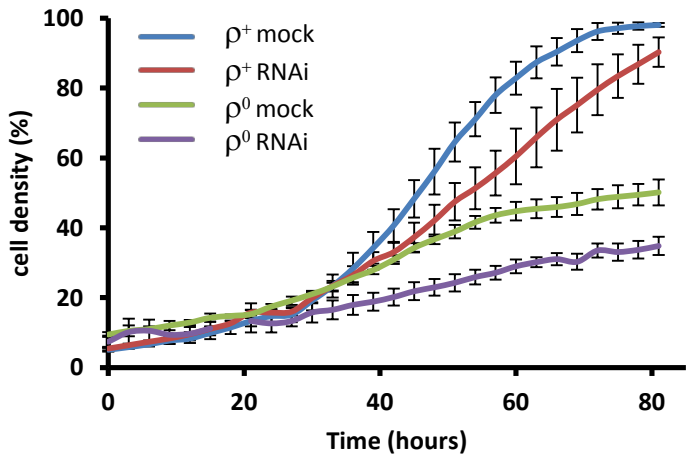

Figure 3.14: Cell proliferation analysis of PrimPol RNAi depleted osteosarcoma cell lines.

(**A**) U2OS cells were either mock transfected (blue), or transfected with PrimPol RNAi (purple) or TWINKLE RNAi (green). Cell number was assessed every 24 hours by manual counting using an haemocytometer and Trypan Blue exclusion dye staining. Error bars denoted standard deviation of 4 independent experiments. (**B**) Wild type 143B cells (ρ^+ blue and red lines) and cells lacking mtDNA (ρ^0 green and purple lines) were either mock (blue and green) or PrimPol RNAi (red and purple) transfected, and cell density monitored using an Incucyte phase contrast microscope at 3 hourly intervals over 80 hours. Data are representative of 3 independent experiments, and error bars denote standard deviation of triplicate wells in which 9 regions were analysed per sample. (Experiment with Incucyte was performed by Laura Bailey).

line). However, PrimPol RNAi treated cells experienced a significant growth delay resulting in a reduction of more than 50% of cell numbers compared to mock sample, 96 hours post transfection (figure 3.14A, pink line). Nonetheless, no further cytotoxicity was observed following this treatment, suggesting the difference of cell numbers was not a result of an increase of apoptosis, but a decrease in growth rate instead. In DT40 PrimPol KO cells a small but reproducible proliferative defect was also observed (see section 4.3.1). To determine if this phenomenon was related to a potential mtDNA maintenance defect, cell proliferation was assessed in both 143B proficient (WT) or mtDNA deficient (ρ^0) cells (figure 3.14B). This experiment was performed using Incucyte microscopy technology to assess the cell confluency overtime. Indeed, this live-cell imaging system allows taking pictures at different places of each transfected wells every 3 hours over several days. A growth delay was also observed after PrimPol RNAi treatment in WT 143B cells but was less pronounced than in U2OS cells (figure 3.14B, red and blue lines, Laura Bailey). However, ρ^0 cells lacking mtDNA (and surviving on glycolysis), presented a similar proliferation defect (~20 hours delay), indicating this growth delay was independent of PrimPol's role towards mitochondrial genome (figure 3.14B, green and purple lines). This suggests PrimPol has other implications outside this organelle, most likely within the nucleus.

3.5. Re-localisation of PrimPol following DNA damage treatments

In order to study PrimPol's involvement within nuclear DNA metabolism, and following preliminary observations made in KO DT40 cells (Chapters 4 and 5), DNA damage treatments were performed in human cells stably expressing inducible epitope-tagged PrimPol (figures 3.15). As previously discussed at the beginning of this chapter, PrimPol cellular localisation studies were greatly facilitated by using human cell line which stably over-express Flag-strep or HA tagged PrimPol under an inducible tetracycline promoter (figure 3.1C). In unperturbed cells, stably over-expressed PrimPol protein was evenly distributed throughout the cell nucleus and cytoplasmic compartments in these cells, showing partial co-localisation with mitochondria (figure 3.1C). Detergent (triton) extraction of these cells, which removes soluble proteins and leaving only proteins bound to cellular sub-structures (e.g chromatin), greatly reduced immunofluorescent detection of PrimPol (figure 3.15A). This indicates that in an asynchronous population, PrimPol protein is mainly soluble, and therefore not bound to any cellular structures. In contrast, after treatment with UV mimetic 4NQO or alkylating drug MMS, PrimPol assembles into triton-resistant sub-nuclear foci in cells (figure 3.15B and C). Both

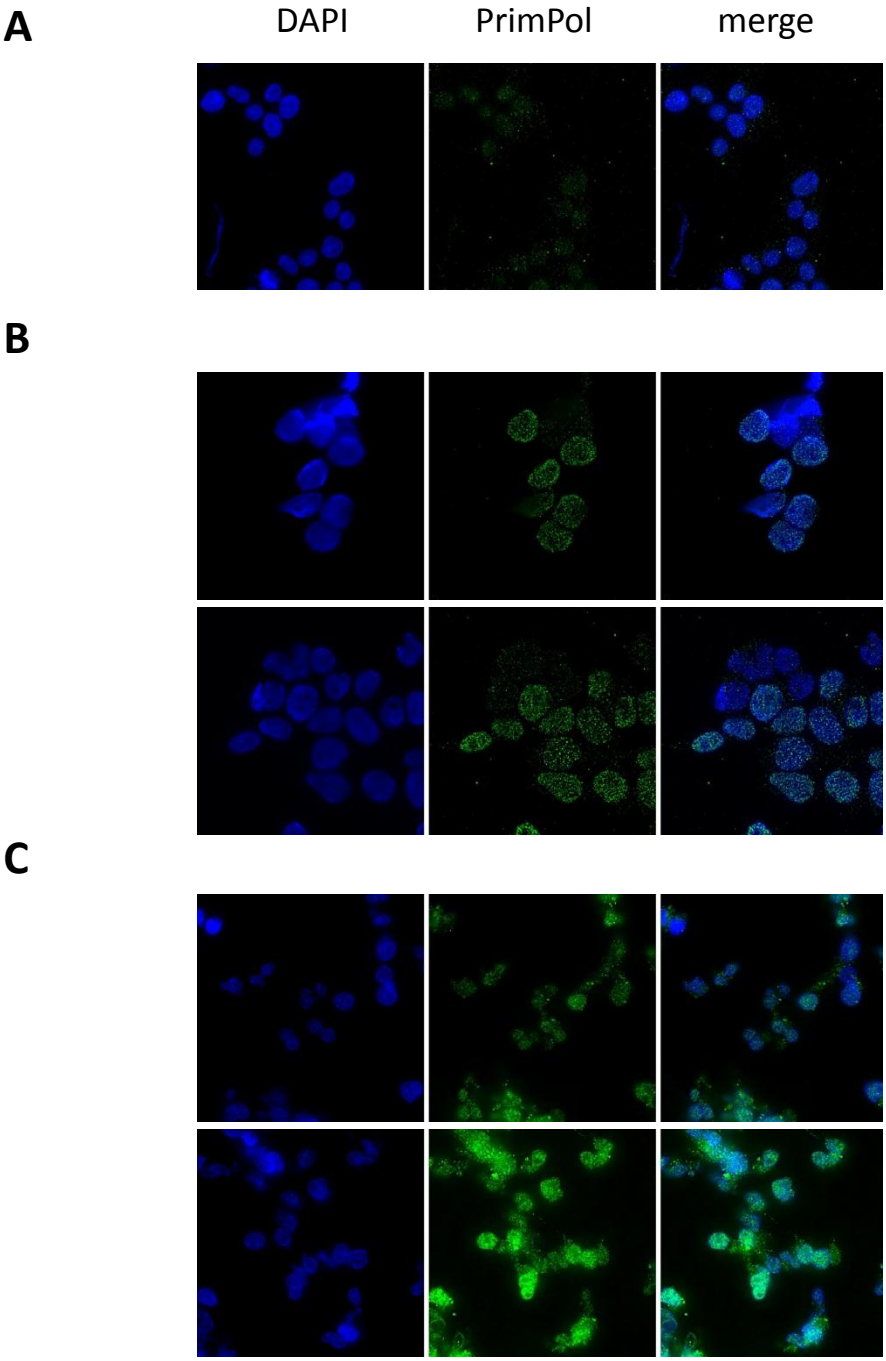

Figure 3.15: Detergent resistant signal following DNA damage treatments in PrimPol stable Hek293 cell lines .

HEK293-T stable cell line expressing Flag-Strep PrimPol after induction with doxycycline for 16 hours, were either mock treated (**A**), or damaged for 7 hours with 1 μg/ml 4-nitroquinoline-1-oxide (4NQO) (**B**) or with 0.01% methyl methanesulfonate (MMS) (**C**). A triton extraction step (0.5% for 30 seconds) was performed before paraformaldehyde fixation in order to remove soluble proteins before immunostaining with PrimPol antibody (green) and counterstaining with DAPI (blue).

compounds have been previously described to induce RF stalling (Minca and Kowalski, 2011; Sánchez *et al.*, 2012). Moreover, in MMS treated cells, triton-resistant PrimPol foci appeared in the cytoplasm (figure 3.15C), possibly reflecting PrimPol's role in mitochondria. These data indicate that following induction of DNA damage, PrimPol re-localises from the detergent-soluble compartments of the cell, and becomes tightly associated with a cellular substructure, most likely chromatin in the nucleus. This indicates a role for PrimPol in the cellular response to DNA damage.

Moreover, following these experiments, over-expressed PrimPol was demonstrated to be chromatin-bound after UV-C treatment, as it was present in the detergent insoluble fraction, and could be subsequently solubilised by DNase treatment (Sean Rudd, Aidan Doherty personal communication; appendix A). Absence of triton-resistant PrimPol foci following ionising radiation suggested a specific recruitment of PrimPol to the chromatin following replication stress (Sean Rudd, Aidan Doherty, personal communication; appendix A).

3.6. Discussion

Preliminary characterisation of a novel eukaryotic DNA primase-polymerase, PrimPol, was undertaken to first determine the localisation of this protein in human cells. Immunofluorescence detection, using a HA-tagged version of the protein and cellular fractionation experiments, revealed a predominantly cytoplasmic localisation of PrimPol. This initial work was pursued and established the mitochondrial localisation of PrimPol (Sean Rudd, Aidan Doherty, personal communication; appendix A). It was thus decided to examine mtDNA maintenance following PrimPol depletion by RNAi in human cells and also in DT40 KO cell lines. A Q-PCR approach revealed an unexpected increase in mtDNA copy number, also confirmed in avian cells by Southern blot analysis. However, mtDNA RI were unperturbed in the absence of PrimPol when analysed by 2D-gel electrophoresis. Interestingly, a preliminary chloramphenicol assay suggested PrimPol might also participate in the generation of mtDNA mutations possibly via error-prone DNA synthesis within the organelle, but this assay needs to be confirmed. Involvement of PrimPol in nuclear processes was also suspected as cell proliferation was significantly affected following PrimPol RNAi depletion. Moreover, a recruitment of this novel primase-polymerase to chromatin following DNA damage treatments was also visualised by immunofluorescence studies performed with stably tagged PrimPol cell line. Given PrimPol *in vitro* TLS capability (appendix A), it can be hypothesised the protein is recruited to the nucleus to bypass specific DNA lesions encountered by the replication machinery.

Together, these data strongly suggest both mitochondrial and nuclear roles for PrimPol in maintaining the cell's genomic material, possibly by TLS or re-priming activities in both compartments.

3.6.1. PrimPol is not the "missing" mtDNA primase

Despite the relative simplicity of this small plasmid genome (~16 kb), mechanisms underlying mtDNA replication are still under debate (Bogenhagen and Clayton, 2003a and b; Holt and Jacobs, 2003). Moreover, the first study describing a DNA primase activity within the mitochondrion did not identify the protein responsible for this activity (Wong and Clayton, 1985). Therefore, it was tempting at first to attribute this role to this novel eukaryotic primase which appeared to be located within this organelle, solving the mystery of the "missing replicative DNA primase". However, evidence provided here, following PrimPol RNAi depletion or its complete absence (DT40 KO cells), demonstrate that this novel primase is not essential

for the replication of mtDNA molecules, as without this enzyme the number of mtDNA copies was increased (figures 3.5 to 3.11). Moreover, no significant RIs variation was observed by 2D-AGE analysis in both systems (figure 3.12 for DT40 analysis and Reis, Bianchi and Holt, unpublished data, for human PrimPol RNAi cells). Furthermore, in the early studies describing the primase activity isolated in mitochondria extracts, the authors discovered the enzyme needed to be associated with structural RNA to be active (Wong and Clayton, 1986). However, this specific feature is not required for PrimPol activity (Aidan Doherty and Luis Blanco, personal communication), confirming another enzyme is responsible for mtDNA initiation. Consistent with this, shortly after the beginning of our investigations on PrimPol, RNA polymerase POLRMT has been described to be responsible for initiating mtDNA replication (Wanrooij *et al.*, 2008) and has since been shown to prime both leading and lagging strands synthesis in mitochondria (Fusté *et al.*, 2010).

3.6.2. Roles of PrimPol in mtDNA maintenance

3.6.2.1. Does PrimPol influence mtDNA turnover via DNA damage tolerance or repair?

Even though PrimPol is present within the mitochondrion, its depletion did not interfere with mtDNA RIs as no differences were observed by 2D-AGE analysis, as mentioned in the previous section. Additionally, PrimPol depletion did not generate a decrease of mtDNA copy number like depletion of mitochondrial core replisome components such as Pol γ (Hance *et al.*, 2005; Di Re *et al.*, 2009) or TWINKLE (Tyynismaa *et al.*, 2004). Instead, an increase of mtDNA copy number was observed following PrimPol RNAi depletion in human (figures 3.5 to 3.9) and in DT40 *PrimPol* $^{-/-}$ cells (figures 3.10 and 3.11). These data are consistent with PrimPol not being required for the duplication of every mtDNA molecule, and therefore, a role for PrimPol in the repair and/or tolerance of mtDNA damage could be suspected. Indeed, as mtDNA resides in close proximity to the OXPHOS pathway generating ROS and mtDNA molecules are not protected by histone proteins, the mitochondrial genome is at substantial risk of being endogenously damaged (Xu *et al.*, 2009; Cline SD, 2012). Although it is counterintuitive to see an increase of mtDNA copy number in the presence of more mtDNA damaged molecules, it is not unprecedented. Indeed, Malakhova and co-workers also observed an increase of mtDNA copy number in rat tissues exposed to ionising radiation (Malakhova *et al.*, 2005). The authors suggested cells encountered an energy deficiency due to the incapacity of the OXPHOS pathway to generate ATP as a result of damaged or mutated mtDNA following irradiation. As a

result, an increase of newly synthesised mtDNA would allow compensation of the genomic information loss. These conclusions follow two recent models explaining how mitochondrial heteroplasmy can be regulated by the organelle to tolerate a proportion of mutated mtDNA molecules. Indeed, respiratory functions have been reported to become impaired when more than 60% of mtDNA copies become mutated (Hayashi *et al.*, 1991). The first model suggests ATP requirement or nucleotides availability could be responsible for the fluctuations of mtDNA copy numbers (Tang *et al*., 2000). The second model provides a global answer by depicting mtDNA regulation as a giant scale, ordering new synthesis or degradation of mtDNA molecules when either lower or higher threshold levels are reached (Clay Montier *et al.*, 2010). The authors proposed low mtDNA copy number level can be detected by the organelle to trigger synthesis of new mtDNA molecules and *vice versa*, above a higher threshold, mtDNA molecules are targeted for degradation. According to this model, if too many mtDNA molecules are degraded in response to DNA damage treatments or deficiency in repair mechanisms, an increase of newly synthesised mtDNA would take place in a compensatory manner. Due to mtDNA heteroplasmy and the limited availability of DNA repair pathways within the organelle (reviewed by Cline SD, 2012), it can be envisaged that mitochondria increase the synthesis of their undamaged genome instead of repairing the faulty copies, to sustain the proportion of mutated mtDNA copy number below the 60% threshold mentioned previously. The question of whether mtDNA faulty copies are degraded or not, is still not clear, especially with the apparent scarcity of a mitochondrial checkpoint (Holt, 2010). However, recent studies have proven irreparably damaged mtDNA molecules are specifically targeted for degradation (Alexeyev *et al.*, 2008; Liu *et al.*, 2010), preventing replication of these defective copies and therefore mutagenesis within the organelle. Also, stalling of POLRMT RNA transcripts has been shown to trigger mitophagy events (Youle and Narendra, 2011). To sum up, new mtDNA synthesis can be employed by the organelle in response to DNA damaging treatments or deficient repair mechanisms.

Work in this chapter has also demonstrated that PrimPol contributes to error-prone DNA synthesis in mitochondria (figure 3.13). Indeed in the absence of PrimPol, mtDNA appeared to have fewer mutations, meaning fewer cells were able to survive chloramphenicol antibiotic treatment. In the nucleus, TLS polymerases carry out unfaithful replication leading to mutagenesis. Consistent with this, *in vitro* data from the Doherty lab using recombinant human PrimPol protein (Chapter 6, figure 6.5) has shown this novel polymerase to be capable of TLS (appendix A). It can therefore be envisaged, in unchallenged conditions, PrimPol to be recruited to mitochondria to bypass DNA lesions caused by high levels of endogenous ROS and

therefore contributes to maintain mtDNA replication of the damaged molecules. Otherwise DSBs could arise after stalling of DNA or RNA polymerases during mitochondrial replication or transcription, leading to irreparable damage within these mtDNA molecules and their targeting for degradation (Liu *et al.*, 2010). Indeed, Pol γ has been reported to frequently stall during the bypass of the main oxidative product 8-oxo-G (Graziewicz *et al.*, 2007). Moreover, Pol γ has a poor ability to bypass helix distorting bulky lesions due to its 3'-5' exonuclease activity (Kasiviswanathan *et al.*, 2012), reinforcing the idea another enzyme could be needed in the organelle to assist the replicative polymerase in its task.

Following this initial report on mtDNA mutagenesis and copy number variations, further experiments could be undertaken to investigate the involvement of PrimPol in mitochondrial TLS mechanisms. Following UV irradiations, more in depth mutagenesis analysis and copy number variations could be recorded in the absence of the novel primase-polymerase. One specific approach could also mirror the study performed by Duxin and co-workers, who followed maintenance protein DNa2 foci accumulation within nucleoids after mtDNA replication stalling in cells overexpressing TWINKLE mutants (Duxin *et al.*, 2009; Wanrooij *et al.*, 2007). Another approach looking at variation of TFAM expression levels should also be monitored to identify a potential PrimPol influence on this nucleoid component. Indeed, several studies have demonstrated TFAM levels correlate with mtDNA copy number (Ekstrand *et al.*, 2004; Pohjoismäki *et al.*, 2006; Xu *et al.*, 2009) but Yoshida and co-workers have also shown TFAM as a damage recognition factor potentially involved in targeting defective mtDNA molecules for degradation (Yoshida *et al.*, 2002 and 2003). Further investigations of TFAM expression levels in PrimPol null-background could provide new evidences to improve our understanding of PrimPol's involvement on mtDNA maintenance.

3.6.2.2. Other factors causing mtDNA copy number to increase in PrimPol depleted cells

To understand if increase in mtDNA copy number could result from mechanisms not directly involved in mtDNA replication, reports from the literature were analysed.

First, a technical artefact has been previously described to be responsible for an increase of mtDNA copy number analysed by Q-PCR (Chen *et al.*, 2007). The authors showed the importance of pre-heated treatments to denature efficiently mtDNA molecules otherwise variations of the ratio supercoiled to relaxed DNA molecules can occur and interfere with the Q-PCR analysis. It is then possible to speculate the absence of PrimPol could lead to an

increase level of relaxed mtDNA molecules (with higher proportion of broken DNA molecules for example), allowing an early amplification of the fluorescent signal by Q-PCR. One way to test this hypothesis would be by using long PCR technology, which specifically measures the presence of DNA damage (Santos *et al.*, 2006; Hunter *et al.*, 2010), within WT and *PrimPol* $^{-/-}$ samples. Also adding a pre-heated treatment (for example 20 minutes at 95°C) before performing the Q-PCR analysis (which already starts with a 10 minutes treatment at 95°C) would be a way to prevent any kind of artefact like this to occur.

Another indirect explanation for this increase mtDNA copy number could be linked to the growth defect observed after PrimPol RNAi treatments (figure 3.14). It has been shown previously that arrested cells in G0/G1 following mimosine or high-dose hydrogen peroxide treatments did not affect mitochondria expansion resulting therefore in an increase of mtDNA content per cell (Lee *et al.*, 2000). Other studies also observed this "concentration effect" where G2/M arrested cells by tyrosine kinase inhibitor or genistein treatments contained more mtDNA than dividing cells, unable to separate their mtDNA content into their daughter cells (Mancini *et al.*, 1997; Pagliacci *et al.*, 1993). Following PrimPol RNAi depletion, it is then difficult to determine if the protein is directly involved in mtDNA maintenance or if the phenotype observed in the organelle is only a secondary effect of the cell cycle arrest. However, having confirmed the increased of mtDNA copy number in two independent PrimPol KO cell lines, in chicken (figures 3.10 and 3.11) and more recently in human normal fibroblasts (MRC5) cells (Laura Bailey, Aidan Doherty, personal communication), where the cells proliferate normally, it seems more likely that PrimPol is directly involved in mtDNA maintenance processes.

3.6.3. Data variability between different laboratories

Q-PCR analyses of mtDNA copy number have also been undertaken in collaborator's Ian Holt laboratory (MRC-Mitochondrial Biology Unit, Cambridge) and contradicting results were obtained. Using RNAi depletion of PrimPol in osteosarcoma cell line 143B, a decrease in mtDNA copy number was observed. Experiments were repeated several times in our laboratory to ensure the reproducibility of the analyses. Our data were obtained using SYBR green Q-PCR technology, whilst Holt and co-workers used Taqman technology, thus it was thought originally using two different methods could explain the divergent results. We then repeated the experiment using the Taqman method following identical protocols (same cell

line (143B), same RNAi duplexes, same Q-PCR primers and probes), but the results were still opposite (data not shown). However, one parameter remained subject to variability: cell confluency at the time of the transfection, as it was based on personal evaluation of the cell density coverage of the well. Also, an even spreading of the cells could improve the transfection efficiency. Moreover, the poor sensitivity of Western blot analysis could not allow the appreciation of small variation of RNAi depletion efficiency. Therefore, even if both laboratories obtained PrimPol protein knockdown, it was not possible to evaluate accurately this parameter. Reverse transcriptase quantitative-PCR (RT-qPCR) experiments should thus be undertaken to determine a potential distinction between both laboratories RNAi depletion. Moreover, an increase of mtDNA copy was observed in Holt's laboratory at early time points following RNAi treatment (48 hours) and also in cells transfected at higher density (data not shown). From this point of view, it appears mtDNA copy number would first increase when PrimPol protein is partially depleted and then decrease when depletion is optimum. This would imply PrimPol's knockdowns performed in our laboratory were not as efficient as in Holt's laboratory. However, using TWINKLE RNAi as a positive control, transfection conditions employed here were sufficient to visualise a decrease of the mtDNA copy number after depletion of this mtDNA replisome factor. Nevertheless, it is still possible to speculate that because Holt's laboratory transfection conditions were performed at lower cell confluency, they resulted in a stronger and possibly more harmful treatment for the cells. As a result, a different cellular response could be generated (e.g. trigger apoptosis, mitophagy) and the depletion of PrimPol protein, associated with a strong cellular stress, would lead to a decrease of mtDNA copy number. On the other hand, a more transient/progressive depletion (RNAi performed at higher confluency) or a KO of the gene, would result in the compensatory effect discussed earlier, where the cells synthesise more copies of WT mtDNA to compensate the potentially aberrant mtDNA induced by the loss of PrimPol. Further, following this analysis, mtDNA copy number variation was also undertaken in other organisms where *PrimPol* gene was stably disrupted (chicken, human and mouse cells, Julie Bianchi, Laura Bailey, Travis Stracker, unpublished data) and an increase mtDNA copy number was also observed in all cases.

Study of mtDNA copy number variation was intended as a quick and easy way to investigate PrimPol's involvement within the mtDNA maintenance. Analyses performed in both laboratories agreed on a mitochondrial role of PrimPol, but further investigations are now needed to understand more in-depth mechanisms of this involvement and how the organelle

survive in its absence (e.g seahorse technology to follow ATP production, markers of mitophagy).

3.6.4. Post-translational modification of PrimPol

Early investigations regarding PrimPol's localisation using GFP constructs showed the overexpressed protein was highly unstable (figure 3.2A). The use of a smaller tag allowed confirmation of PrimPol's localisation within the mitochondria, and thus it was possible to suspect the protein may be processed in order to gain entry to the organelle. However, no mitochondrial targeting sequence (MTS) was found within the polypeptide sequence and mitochondrial fractions purified from Hek293 stably expressing PrimPol contained the C-ter epitope-tagged version of the protein (Sean Rudd, Aidan Doherty, personal communication). Further experiments using proteasome inhibitors could inform us more specifically on PrimPol's degradation processes. Indeed, recent investigations in the laboratory have shown PrimPol could be SUMOylated and ubiquitylated *in vitro* (Violetta Soura, Aidan Doherty, personal communication). Moreover, mass spectrometry analyses have identified potential phosphorylation sites (chapter 6) and localisation studies have now been undertaken with phospho-mutated versions of the protein (Laura Bailey, Aidan Doherty, personal communication). All these post-translational modifications may be important features for the cellular localisation of PrimPol and potentially regulate the shuttle of the protein from one compartment to another, and also could play a role in the recruitment of the protein in response to DNA damages. To support this idea, some truncation and mutagenesis studies should be undertaken to see the influence of these different post-translational modifications on PrimPol localisation following DNA damaging treatments.

CHAPTER IV

Generation of *PrimPol* knockout gene in avian DT40 cells

4.1. Introduction to gene disruption in avian DT40 cell line

In order to provide a robust cell system in which to characterise PrimPol, and limit the variability linked with RNAi transfection protocols, it was decided to generate a *PrimPol* KO cell line using the avian DT40 system. Human KO can also be achieved but are generally more time consuming and present lower probability of success. DT40 cells are chicken B-lymphocytes that are immortalized by an avian leucosis virus, and exhibit a targeted integration frequency similar to that of random integration (Buerstedde and Takeda, 1991). Thus, DT40 cells provide an ideal model system for reverse genetic studies in vertebrate somatic cells. HR mechanism can permit the incorporation of an exogenous vector specifically between targeted loci of the gene, thereby disrupting its expression. Positive clones can then be selected by antibiotic selection, owing to expression of the resistant marker contained inside the vector. This approach is similar to the one used with murine embryonic stem cells but can potentially be achieved much faster, and can allow characterisation of genes that are difficult to study in mammalian cells. Indeed, in the case of *Atm* gene, for example, DT40 KO cells can grow normally while fibroblasts from *Atm*-deficient mice present strong growth defects (Xu *et al.*, 1996; Takao *et al*., 1999). In another example, KO of the catalytic subunit Rev3 of Pol ζ is embryonic lethal in mice but viable in DT40 cells (Bemark *et al*., 2000; Sonoda *et al*., 2003). Moreover, the tedious process of gene deletion in mammalian cells is facilitated by the rapid division time of DT40 cells (~8 hours) and their growth in suspension. Another advantage of DT40 cells is the possibility to rapidly disrupt multiple genes within a single cell line, allowing epistasis analysis to understand the pathway(s) in which PrimPol operates.

The aim of this Chapter was then to disrupt the *PrimPol* gene in DT40 cells, to determine if the gene was essential for the cell viability and, finally, to characterise the KO cell's behaviour and phenotypes in the absence of PrimPol expression.

4.2. First knockout strategy to disrupt *PrimPol* gene in DT40 cells

4.2.1. Strategy and design of *G. gallus PrimPol* targeted arms

The *PrimPol G. gallus* gene composed of 16005 bp with 11 exons is located on chromosome 4 (position 38,931,716 to 38,947,734; appendix B), therefore resulting in bi-allelic expression, and is depicted on figure 4.1A according to information available on public database (University of California Santa Cruz (UCSC) genome browser). The design of the targeting

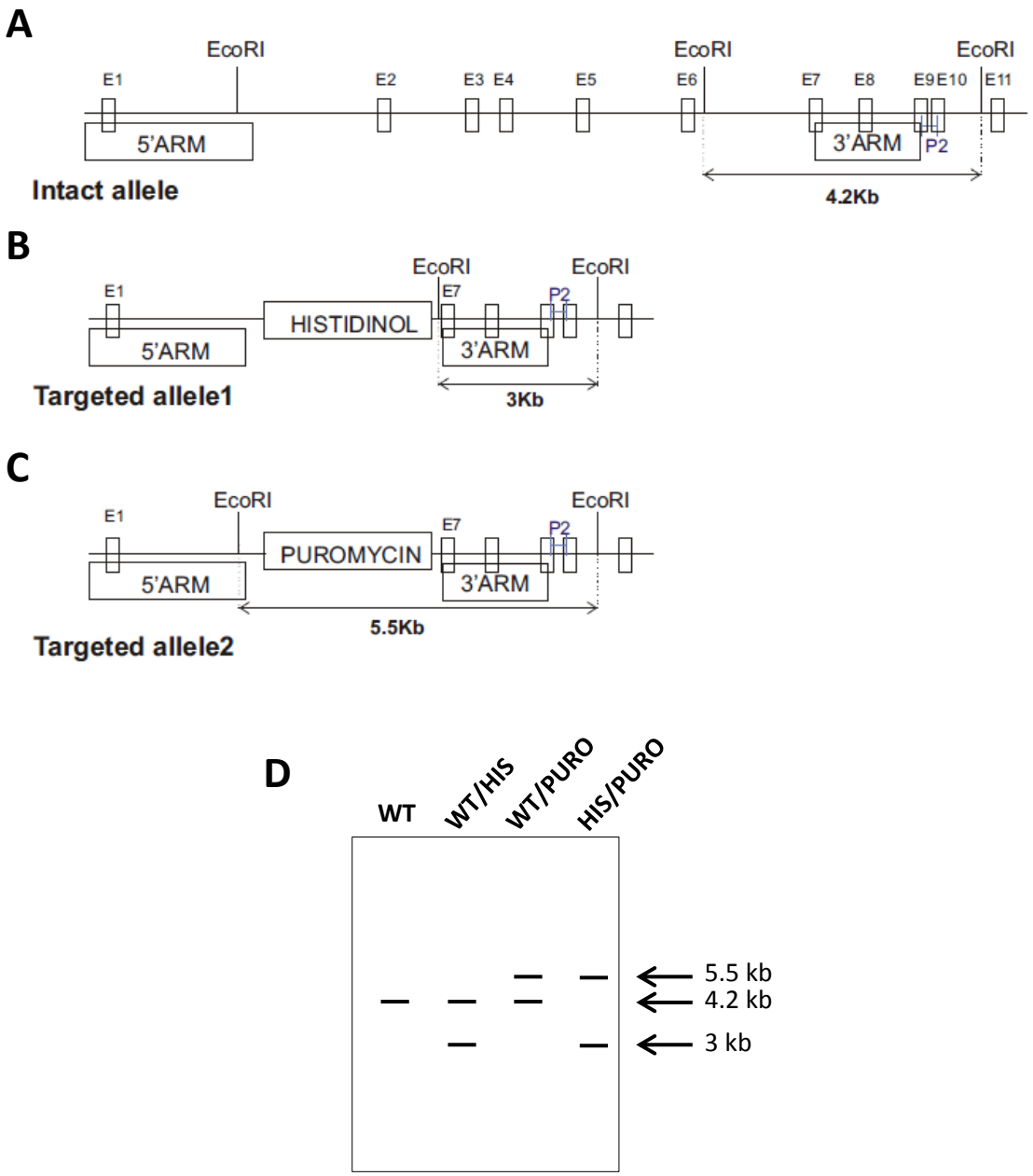

Figure 4.1: First targeting strategy of *PrimPol* gene disruption in DT40 cells.

(**A**) Illustration of the wild type allele of the *G. Gallus PrimPol* gene, with its 11 exons (square boxes) and *EcoRI* restriction sites. Targeted 5' and 3' arms are depicted to visualize where the recombination events take place, and P2 symbolizes the localisation of the Southern blot probe on the gene. (**B**) Schematic of the mutant allele after recombination with histidinol or (**C**) puromycin vectors. (**D**) Cartoon of the theoretical Southern blot patterns illustrating the different allelic disruption profiles, obtained after hybridisation of the probe P2 and *EcoRI* digestion. First lane shows wild type pattern (WT) with a 4.2 kb band as explained in (**A**). The second lane presents WT/HIS pattern with both 3 kb band specific of histidinol disruption (as in **B**) and the WT 4.2 kb species. The third lane indicates the WT/PURO profile with the 5.5 kb band corresponding of the integration of the puromycin cassette (as in **C**) and the WT 4.2 kb species. The last lane depicts HIS/PURO KO profile with the absence of the WT 4.2 kb band.

vectors containing the homologous sequence of the gene was a crucial step of the KO process and was performed with the help of Dr Helfrid Hochegger. The 5' arm was designed to recognize the first 3025 bp of the gene within the 1st exon, and the 3' arm designed to be homologous of the genomic area included between 12250 bp and 14243 bp thus regrouping exons 7, 8 and 9 (figure 4.1A). Therefore, once the targeted recombination event occurred, 9225 bp of the gene (containing exons 2 to 6) will be replaced by either a histidinol (HIS) or puromycin (PURO) antibiotic resistance cassettes. The deletion of the complete coding sequence of the gene would be better to avoid any risk of interference of remaining protein expression, however it has been reported that a wide distance between both target arms decreases the targeting frequency (Arakawa and Buerstedde, 2006). The size of the target arms was also a critical point as longer arms are believed to increase the efficiency but are more difficult to handle (Arakawa and Buerstedde, 2006). A general consensus suggested each arm should be longer than 1 kb and combined together, between 3 and 12 kb. The delineation of the targeted arms also took into consideration the position of enzymatic restriction sites within the genomic DNA. Indeed, Southern blot analysis is used to discriminate targeted clones from the ones where random integration of the antibiotic resistance cassette occurred. The strategy adopted here is summarised in figure 4.1, which also shows the different patterns obtained following Southern blot analysis using *EcoRI* enzymatic digestion and radiolabelled probe P2 (table 2.8). Histidinol and puromycin constructs contained both an internal *EcoRI* site, respectively downstream and upstream of the resistance cassette, in the loxP flanking sites (Iiizumi *et al.*, 2006). Once targeted recombination occurred, the genomic *EcoRI* restriction site upstream the P2 probe was removed by the exogenous cassette introducing its own *EcoRI* site, therefore changing the Southern blot analysis banding pattern. A cartoon was drawn in figure 4.1D to visualise the characteristic bands specific of each configuration, 4.2 kb for WT alleles, 3 kb for HIS disrupted allele and 5.5 kb following integration of PURO construct.

4.2.2. Gateway cloning strategy for generation of the DT40 gene targeting constructs

Following the genomic PCR of both targeted arms, the Gateway® cloning system was used to integrate these sequences into the final vectors along with the antibiotic resistance cassettes (PURO or HIS). The method was previously described by Iiizumi and co-workers (Iiizumi *et al.*, 2006). Briefly, a succession of two recombination events, each using specific recombination sequences (attX), allowed the rapid, efficient and orientated, cloning of the gene fragments (figure 4.2). First, a BP recombination reaction occurred between PCR products (targeted

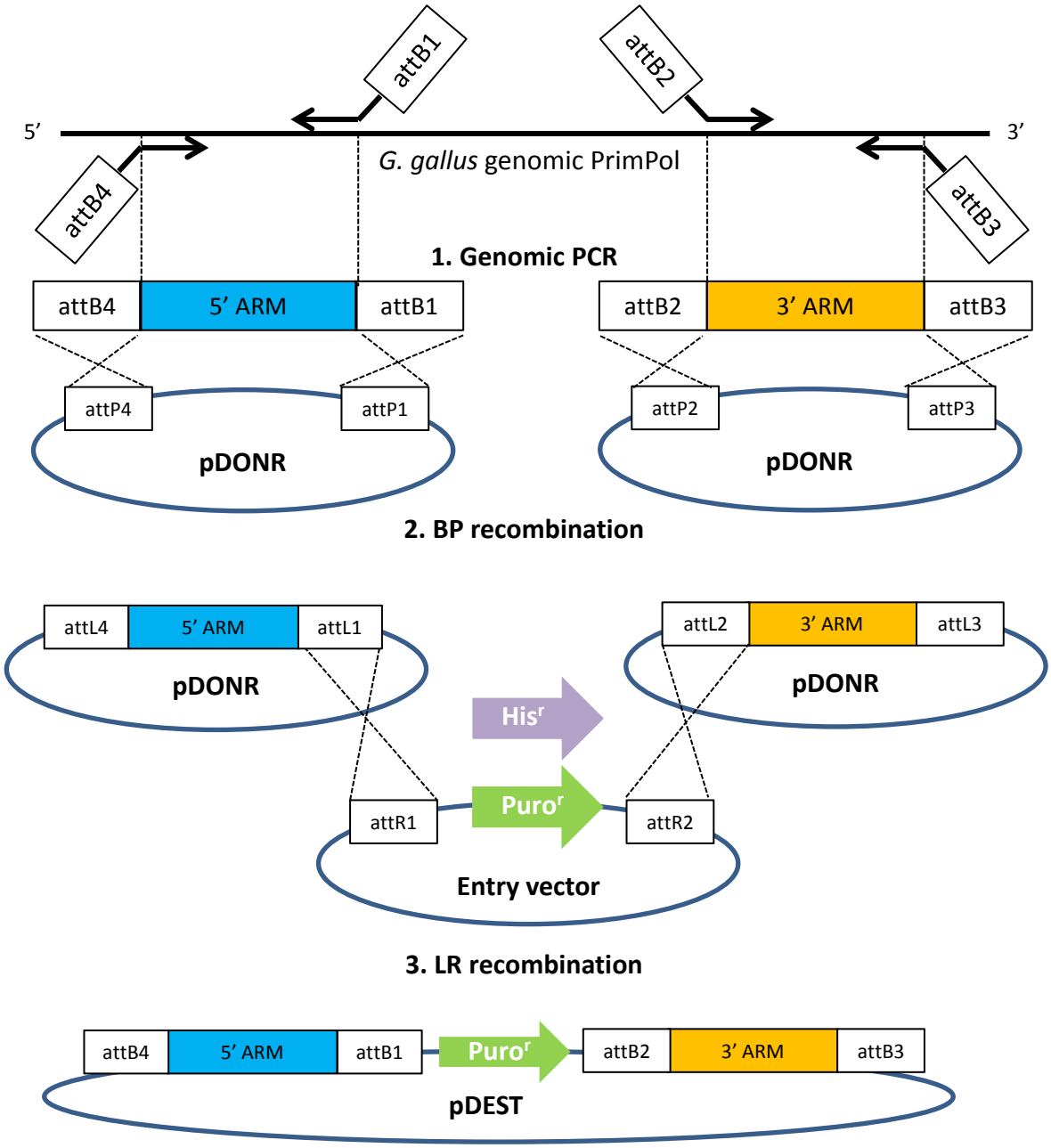

Figure 4.2: Gateway cloning system of *G. gallus* PrimPol KO constructs.

Illustration of the *G. gallus PrimPol* gene (black line) to visualise the position of the PCR primers (black arrows) containing recombination sequences (attB) and delineating target arms (5' and 3' ARMs). Following genomic PCR (**1**) both arms were inserted into pDONR vectors (containing attP recombination sequences) by BP recombination (**2**). This reaction resulted in the creation of attL recombination sequences flanking each targeted arms. Entry vectors, containing histidinol (His^r) or puromycin ($Puro^r$) resistance markers , along with pDONR constructs were integrated together to one pDEST plasmid (containing attR sequences) by LR recombination (**3**). This reaction resulted in a final plasmid containing both targeted arms flanked by attB sites and the appropriate resistance marker. (Cartoon adapted from Iiizumi *et al*., 2006).

genomic arms) flanked by attB sequences and a pDONR vector containing attP sequences (figure 4.2). A LR recombination reaction was then only possible between pDONR vectors containing attL sites (produced after recombination of attB and attP together) and therefore the targeted arm, and a pDEST vector containing attR sites (figure 4.2). By this way, the presence of original pDONR vectors (non-recombined vectors) would not affect the final reaction. Moreover, the system contained another level of control, with the use of ccdB sequences present in original vectors flanked by attP (in pDONR) or attR (in pDEST). Expression of this gene prevented *E. coli* cells from growing, therefore only cells transformed with recombined vectors could be amplified following BP and LR recombination reactions. All plasmids generated with the Gateway system are summarized in table 2.7.

4.2.3. Generation of *PrimPol* heterozygotes (+/-) DT40 cell lines

To disrupt the first *PrimPol* allele, WT DT40 cells were electroporated with the final pDEST-HIS construct (table 2.7) and HIS resistant clones were collected 7 to 10 days later. Genomic DNA was extracted and Southern blot analysis was performed as described previously (section 4.2.1.1). Disruption of the first allele generated 54 resistant clones but in only one case (clone 3) the recombination was targeted to *PrimPol* gene, giving rise to one heterozygote clone WT/HIS (figure 4.3A). This clone was then re-amplified and transfected with pDEST-PURO construct in order to disrupt the second allele. However, following two independent transfections, no *PrimPol* $^{-/-}$ clones presented the HIS/PURO pattern (figure 4.3B). In 79 clones collected, 7 presented a targeted insertion of the PURO cassette but on the allele previously disrupted by the HIS cassette, generating a WT/PURO pattern on the Southern blot analysis (figure 4.3B, black arrows). It was then decided to reverse the process and transfect WT DT40 clones with the pDEST-PURO construct first (figure 4.4A) followed by pDEST-HIS construct, in order to obtain a *PrimPol* KO. Two heterozygote clones WT/PURO (named 16 and 19) were then obtained (figure 4.4A, black arrows) and then transfected in turn with the pDEST-HIS construct (figure 4.4B). Transfection of the clone 16 gave rise to 40 clones with 9 corresponding to a targeted insertion of the antibiotic resistance cassette (figure 4.4B, top gel, black arrows), and transfection of the clone 19 generated 86 clones (figure 4.4B, bottom two gels), with 25 targeted insertions (figure 4.4B, black arrows). All these 34 clones, resulting of a *PrimPol* targeted insertion of the HIS cassette, presented a Southern blot analysis WT/HIS pattern indicating the second resistance cassette was permuted with the previous one already disrupting the *PrimPol* allele, leaving the WT allele unaffected.

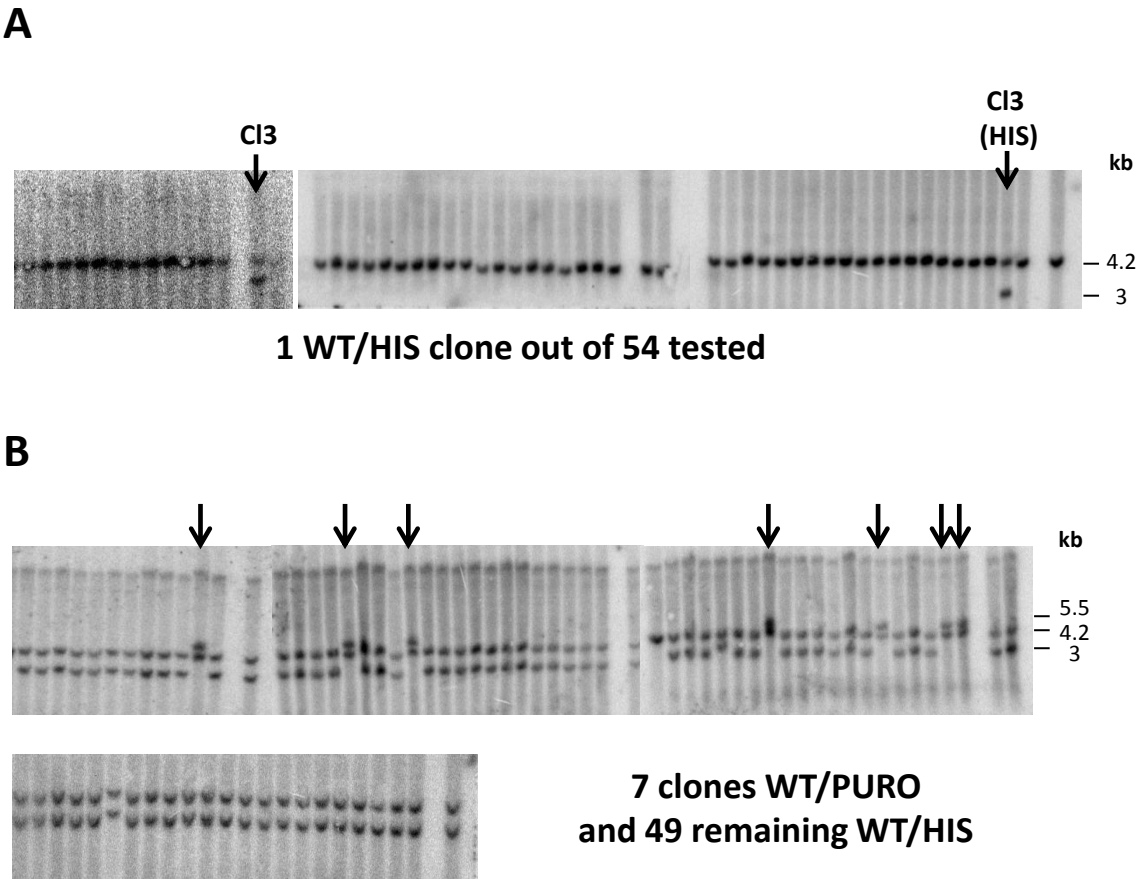

Figure 4.3: Clones obtained following the transfection of histidinol then puromycin constructs.

(**A**) Southern blot analysis of 54 clones obtained after transfection of WT cells with histidinol pDEST plasmid, using radiolabelled probe P2 and *EcoRI* enzymatic digestion. Clone number 3 (below arrow) was the only one presenting the 3 kb band indicating the disruption of *PrimPol* gene. (**B**) 79 clones were obtained following two independent transfections (top and bottom gels) of heterozygote clone 3 (WT/HIS) with puromycin pDEST plasmid. 7 clones (arrows) presented the 5.5 kb band specific of the disruption of WT *PrimPol* allele with Puro^r cassette, but also contain the WT 4.2 kb band, giving rise to WT/PURO clones.

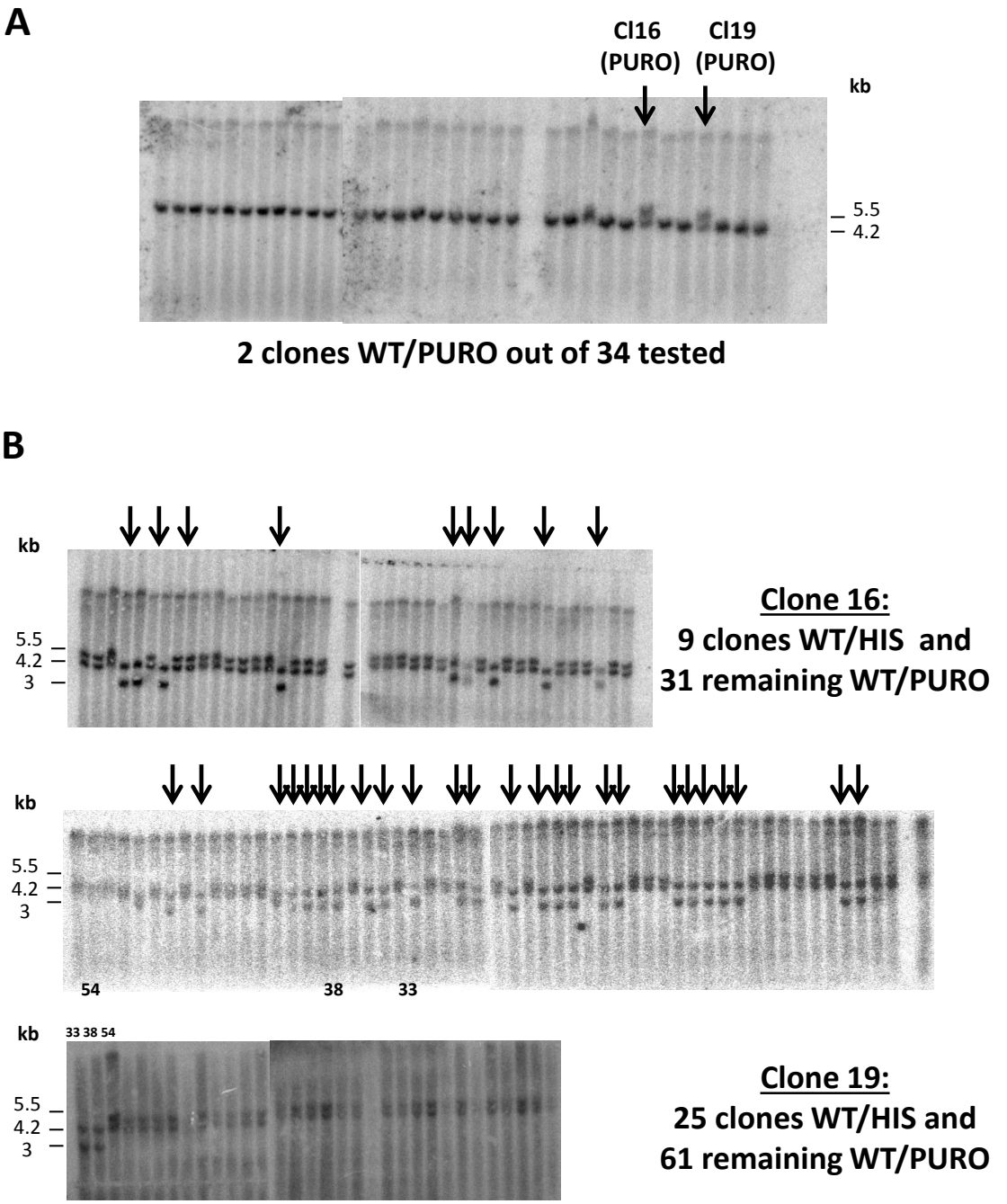

Figure 4.4: Clones obtained following the transfection of puromycin then histidinol constructs.

(**A**) Southern blot analysis of 34 clones obtained after transfection of WT cells with puromycin pDEST plasmid, using P2 probe and *EcoRI* enzymatic digestion. Clones 16 and 19 (below arrows) both presented the 5.5 kb band indicating the disruption of *PrimPol* gene. (**B**) 126 clones were collected following transfection of heterozygote (WT/PURO) clone 16 (top gel) and clone 19 (bottom two gels) with histidinol pDEST plasmid. 34 clones presenting the pattern WT/HIS (4.2 kb and 3 kb signals respectively) are indicated with black arrows. Clones 33, 38 and 54 were re-loaded for confirmation purposes onto the bottom gel.

To summarise, in both attempts, transfection of heterozygotes WT/HIS or WT/PURO clones with the second appropriate antibiotic resistance cassette only conferred a switch between both selection markers, preventing a homozygote disruption of *PrimPol* gene. The probability of this phenomenon occurring 100% of the time could be explained by two reasons; the recombination event was facilitating by the fact the 5' and 3' targeted arms were already in close proximity in the first mutated allele (separated only by the antibiotic cassette, roughly 2 kb) by comparison to the WT allele (9 kb). The second explanation could be that *PrimPol* gene is essential for the cell survival. Therefore, when HR occurred and disrupted the second WT allele, these cells could not survive without expressing the *PrimPol* gene, hence no *PrimPol* $^{-/-}$ clones were obtained.

4.2.4. Expression of human PrimPol in DT40 cells for complementation studies

To determine whether *G. gallus PrimPol* is an essential gene, a conditional KO strategy was employed where recombinant human PrimPol cDNA was constitutively expressed on an exogenous vector randomly integrated in the *G. gallus* genome. Human PrimPol protein is shorter than its avian homologue (560 versus 605 amino acids) and shares ~50% identical residues, with all the characteristic motifs within the AEP and UL52 zinc-binding domains being highly conserved (appendix B). In the eventuality that *G. gallus PrimPol* is an essential gene, and its role is evolutionary conserved throughout vertebrates, chicken cells should still be able to grow after disruption of both *PrimPol* alleles due to the expression of ectopic human PrimPol protein. A strategy using an inducible tetracycline (Tet) repressible promoter was adopted to allow phenotypic studies by specifically switching-off the expression of the protein when needed (figure 4.5A). Human PrimPol cDNA was therefore sub-cloned into a rescue plasmid containing a Tet-off inducible promoter and a luciferase reporter gene (figure 4.5A; table 2.7), which enables monitoring of the transgene expression level and also the selection of positive clones by measuring luciferase activity (Yamazoe *et al.*, 2004). *PrimPol* heterozygote (WT/HIS) clone 3 was chosen and co-transfected with pTRE-LoxP-hPrimPol-luc rescue plasmid (table 2.7) and a Tet-off vector (Clontech) containing a neomycin resistance marker. Eleven clones were able to grow in the presence of the selection marker geneticin (G418), and the luciferase screen revealed two clones (clone 7 and 10) responded to the expression of the reporter gene in an inducible manner (figure 4.5B and C). Indeed, addition of doxycycline (DOX) at 1 μg/ml for 48 hours in the growth media resulted in a significant reduction of the

A

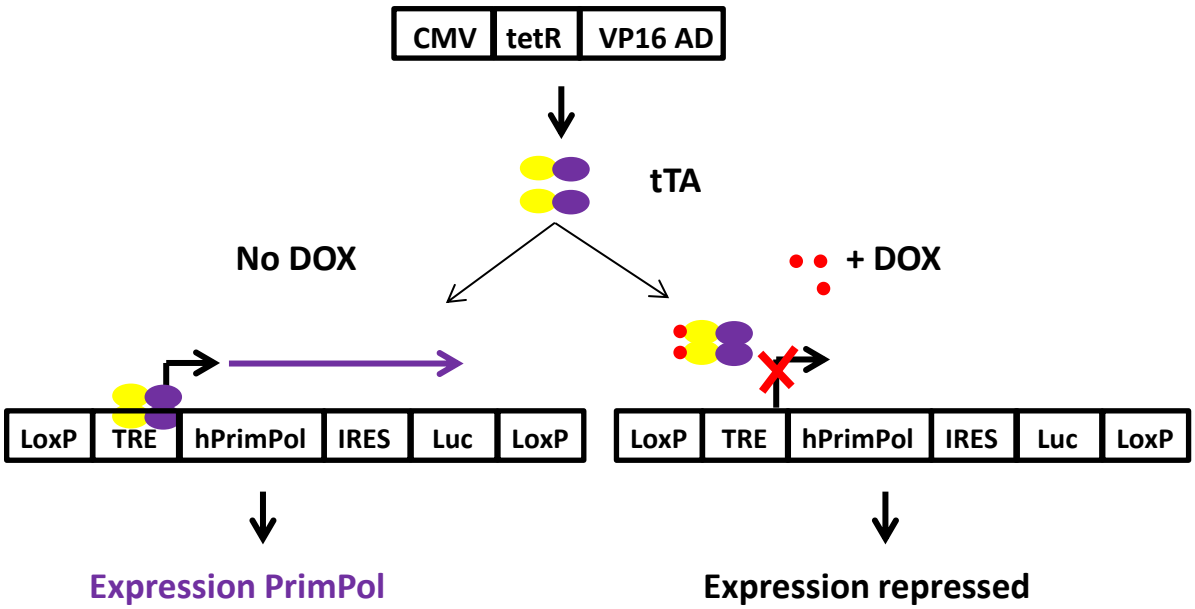

B

	-DOX	+DOX
PBS	218	
CTR+ 1-24	31869640	2718
Clone 1	189	201
Clone 2	215	339
Clone 3	141	126
Clone 4	188	130
Clone 5	183	83
Clone 6	640	79
Clone 7	869853	1762
Clone 8	232	
Clone 10	669112	2719
Clone 11	120	100

C

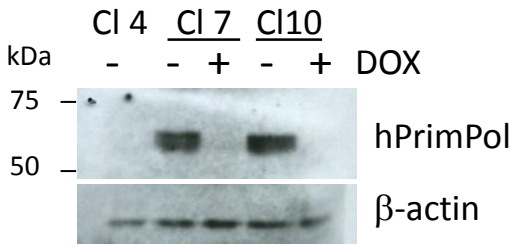

Figure 4.5: Human PrimPol conditional DT40 heterozygote (WT/HIS) clones.

(**A**) Cartoon illustrating the Tet-off system used for doxycycline (DOX) inducible switch-off expression of human PrimPol (hPrimPol) (Adapted from Zhu, 2002). Tetracycline transactivator (tTA) created by fusion of tetracycline repressor (TetR) and VP16 (produced by Herpes Simplex Virus), can bind in the absence of DOX onto a Tet response element (TRE) activating the promoter thus the transcription of the genes downstream. Internal ribosome entry site (IRES) allows the distinct translation of luciferase (Luc) mRNA downstream of hPrimPol. (**B**) Luciferase assay performed on 10 clones obtained following transfection of heterozygote clone 3 WT/HIS with Tet-off system plasmids depicted in (**A**). A control cell line (CTR+ 1-24) was used to validate the system (Hégarat *et al.*, 2011), and PBS to estimate background levels. Treatment with doxycycline (+DOX) were performed for 48 hours. (**C**) Western blot analysis using human PrimPol antibody (hPrimPol) and β-actin levels for loading control, was performed with clones (Cl) analysed in (**B**). Absence or addition of DOX (1 μg/ml for 120 hours) was indicated by – and + symbols respectively.

luminescence signal (figure 4.5B) and human PrimPol protein expression, visible by Western blot analysis (figure 4.5C).

Having successfully disrupted the first allele of the *G. gallus PrimPol* gene and introduced an ectopic vector constitutively expressing the human protein, I then repeated the targeting of the second WT allele using pDEST-PURO construct in both heterozygote WT/HIS conditional clones 7 and 10. Unfortunately, in both cases the WT allele remained unaffected as 23 non-targeted events occurred after transfection of clone 7, and for clone 10, a further 39 random integrations conferred puromycin resistance to the cells (figure 4.6A and B). In 7 other cases, the PURO cassette was inserted on the allele already disrupted with the HIS marker, generated WT/PURO Southern blot pattern (figure 4.6B).

To conclude, the presence of ectopic human PrimPol in the cells did not prevent the switch between both antibiotic resistance cassettes, suggesting either an inefficient complementation of the human homologue or an intrinsic problem with the KO strategy. Given the high degree of conservation between both human and chicken PrimPol proteins, the initial targeting strategy was thus reconsidered.

4.3. Second knockout strategy to disrupt *PrimPol* gene in DT40 cells

4.3.1. Redesign of *G. gallus PrimPol* targeted arms

As mentioned previously, by using the same set of recombination sequences for both histidinol and puromycin pDEST constructs, recombination events between both cassettes can be facilitated by the close proximity of both targeted arms. On the other hand, on the WT allele, 9 kb of genomic DNA separate the recombination sequences, increasing the difficulty of the targeting event from occurring. To verify whether this could explain the failure of the KO strategy, I decided to generate another pDEST-PURO construct with 5' and 3' arms designed in the genomic DNA area already replaced by the HIS cassette on the first mutated allele. In this case, heterozygote clone WT/HIS could only be targeted on the WT allele by this new PURO construct (pDEST-PURO2, table 2.7), as depicted in figure 4.7A and 4.7C. Preventing the switch between both disruptive cassettes, by having different recombination sequences, should increase the probability of targeting specifically the WT allele. The new 5' arm, called 5'ARM2, was designed to be homologous to the genomic DNA area included between 3050 and 5051 bp (as previous recombination arm stopped at the position 3025 bp) therefore containing exon 2

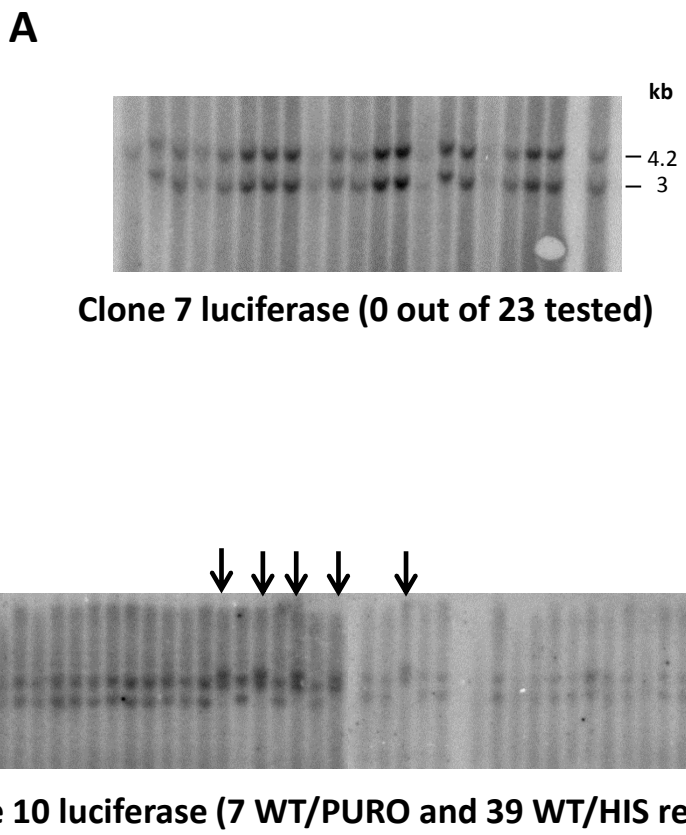

Figure 4.6: Second allele targeting in WT/HIS heterozygote clones expressing human PrimPol conditionally.

Transfection of heterozygote clone WT/HIS expressing human PrimPol with pDEST plasmid containing puromycin disruption cassette to target the second allele. (**A**) Southern blot analysis of 23 puromycin resistant clones obtained after transfection of luciferase positive clone 7; number of clones presenting a targeted integration within *Gallus PrimPol* gene is written inside parentheses. (**B**) Southern blot analysis of 46 clones issue of transfection of luciferase clone 10, presenting 7 clones (arrows) where both disruption cassettes have been switched, leaving the WT allele in position.

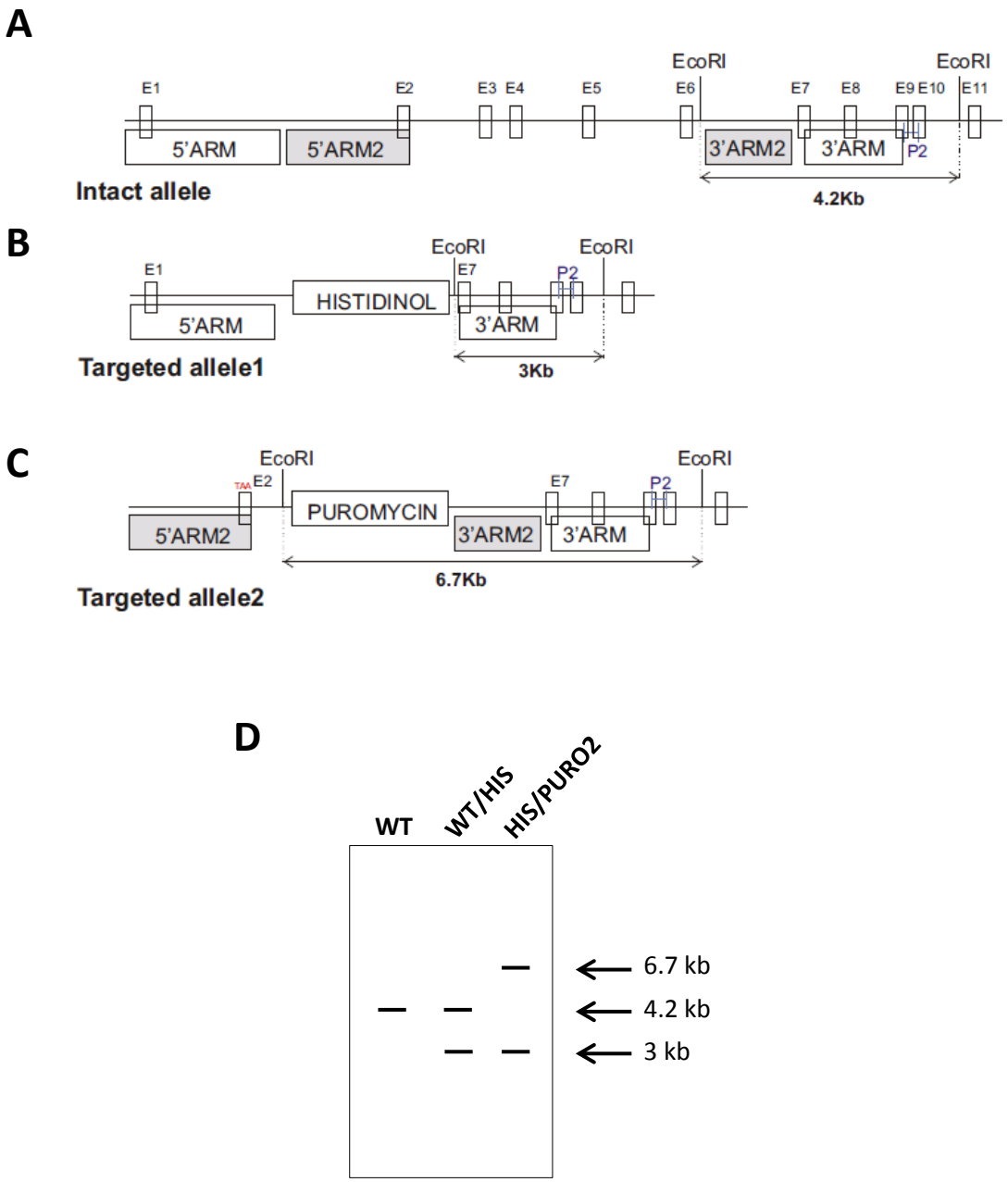

Figure 4.7: Second targeting strategy of *PrimPol* gene disruption in DT40 cells.

(**A**) Illustration of the genomic position of the new targeted arms (grey boxes) designed downstream of the 5'ARM (5'ARM2) and upstream of the 3'ARM (3'ARM2), in order to specifically target the WT allele of heterozygotes clones (WT/HIS). (**B**) The first allele, targeted by histidinol (HIS) construct, was the same than in the previous strategy, whereas the second allele (**C**) targeted by puromycin (PURO) construct contained the new recombination arms (5' and 3' ARM2). (**D**) Cartoon depicting the different Southern blot profiles which can be obtained after using this new strategy. Transfection of the heterozygote clone WT/HIS (as in figure 4.1), with the new PURO2 construct should only give rise to KO clones HIS/PURO2 (with bands at 3 and 6.7 kb corresponding to HIS and PURO2 allele disrupted respectively) or non targeting integration of the puromycin marker in WT/HIS clones.

with the start codon of the ORF (figure 4.7A and C). A stop codon (TAA) was then added at the end of the reverse primer used to amplify this genomic DNA to ensure a premature interruption of any protein expression. In this case, even if unexpected splicing events resulting, for example, in the removal of the antibiotic cassette, *G. gallus* PrimPol protein would be aborted with this early termination modification. In order to be able to keep the same Southern blot strategy, 3'ARM2 boundaries were delimited just after the *EcoRI* site (11017 bp) and before the start of 3'ARM construct, targeting the sequences 11061-12240 bp of the genomic DNA. As a result, the signal obtained after Southern blot analysis (with *EcoRI* restriction digestion and radiolabelled probe P2) was 1.2 kb bigger (6.7 kb instead of 5.5 kb) than following disruption with the first pDEST-PURO vector (figure 4.7C and D). The Gateway cloning system was employed as described previously (section 4.2.2) using new sets of PCR primers (table 2.6, 2nd strategy) to generate this pDEST-PURO2 vector (table 2.7).

4.3.2. Generation of *G. gallus PrimPol* KO cells conditionally expressing human PrimPol

To increase the chance of obtaining a KO clone, I first decided to try this new strategy onto the conditional heterozygotes clones expressing human PrimPol cDNA. Heterozygote WT/HIS, conditional clone 7 (from the luciferase assay, section 4.2.4), was transfected with pDEST-PURO2 construct and the first attempt proved successful as two clones (out of 37) presented the Southern blot pattern HIS/PURO2 (figure 4.8A). Following this initial screening, positive clones 4 and 8 were thawed and amplified in order to prepare fresh genomic DNA and another Southern blot analysis was performed (figure 4.8B), confirming the loss of both WT *PrimPol* alleles by the disappearance of the 4.2 kb band. These *G. gallus PrimPol* $^{-/-}$ cells, expressing human PrimPol protein constituvely (-DOX), doubled every ~8 hours (figure 4.9A, blue line). Following addition of DOX to the media for four days, and thus repressing the expression of ectopic human PrimPol protein, no significant growth defect were observed (figure 4.9A, red line). In line with the lack of proliferative defect, addition of DOX did not affect the cell cycle distribution of these cells either (figure 4.9B, right panel). A more thorough analysis of ectopic human PrimPol protein expression was then investigated to rule out any fault within the Tet-off system. Addition of 1 μg/ml DOX for 24 hours switched-off the luciferase reporter gene efficiently (figure 4.10A), but Western blot analysis of cell lysates revealed the persistence of human PrimPol protein expression (figure 4.10B). Increasing DOX concentration up to 4-fold (dilution 1/250, figure 4.10C) did not improve the efficiency of the repression of the TRE promoter in clone 8. Time course analysis of DOX treatments also proved unfruitful for these

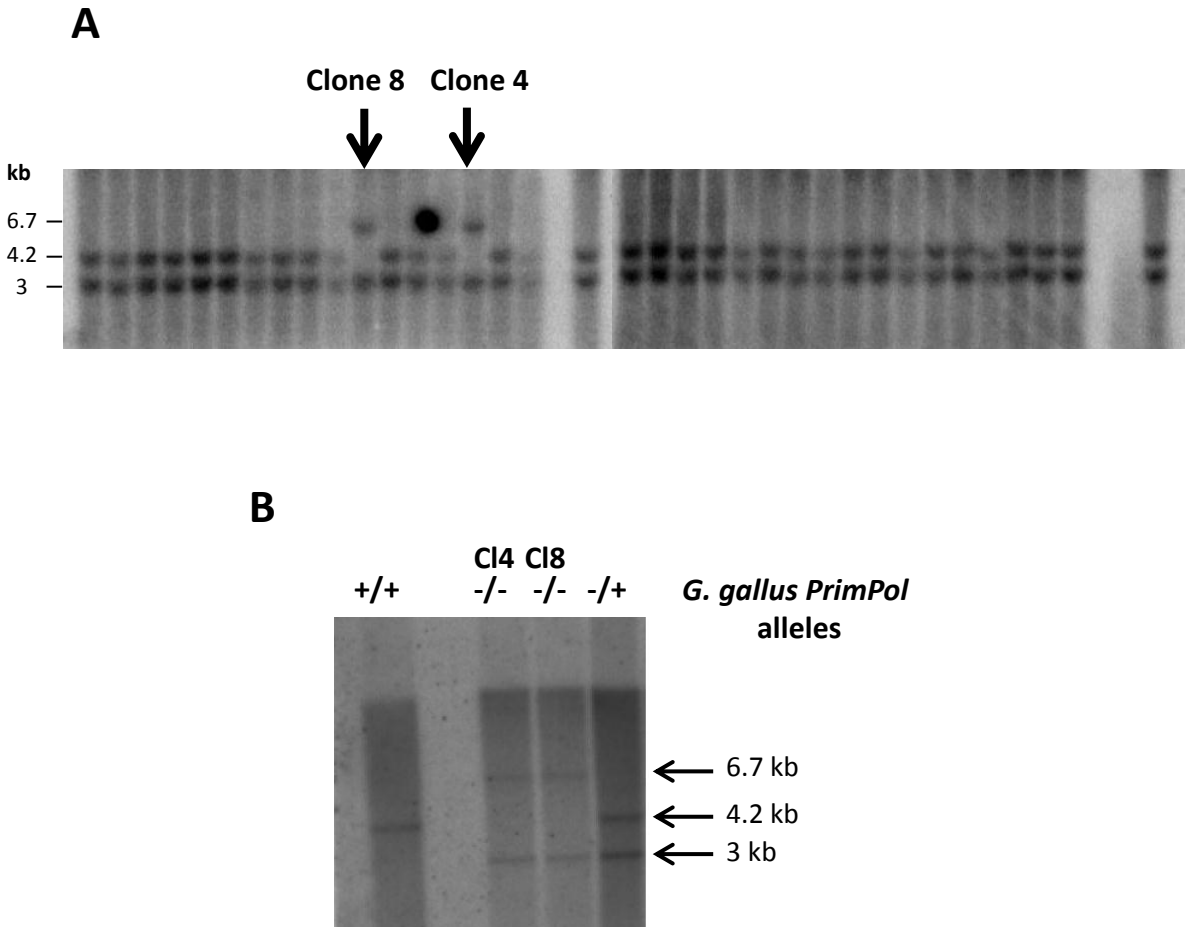

Figure 4.8: Allele targeting strategy 2, generating two human conditional KO clones.

(**A**) Southern blot analysis of 37 puromycin resistant clones obtained after transfection of luciferase positive clone 7 (WT/HIS) expressing ectopic human PrimPol protein. Clones 4 and 8 presented targeted integration of Puro^r cassette (6.7 kb band) without affecting the previous disrupted allele with histidinol (3 kb band). (**B**) Confirmation of the absence of the WT alleles in those KO clones was performed by another Southern blot analysis with newly prepared genomic DNA from fresh cultures of clones 4 and 8.

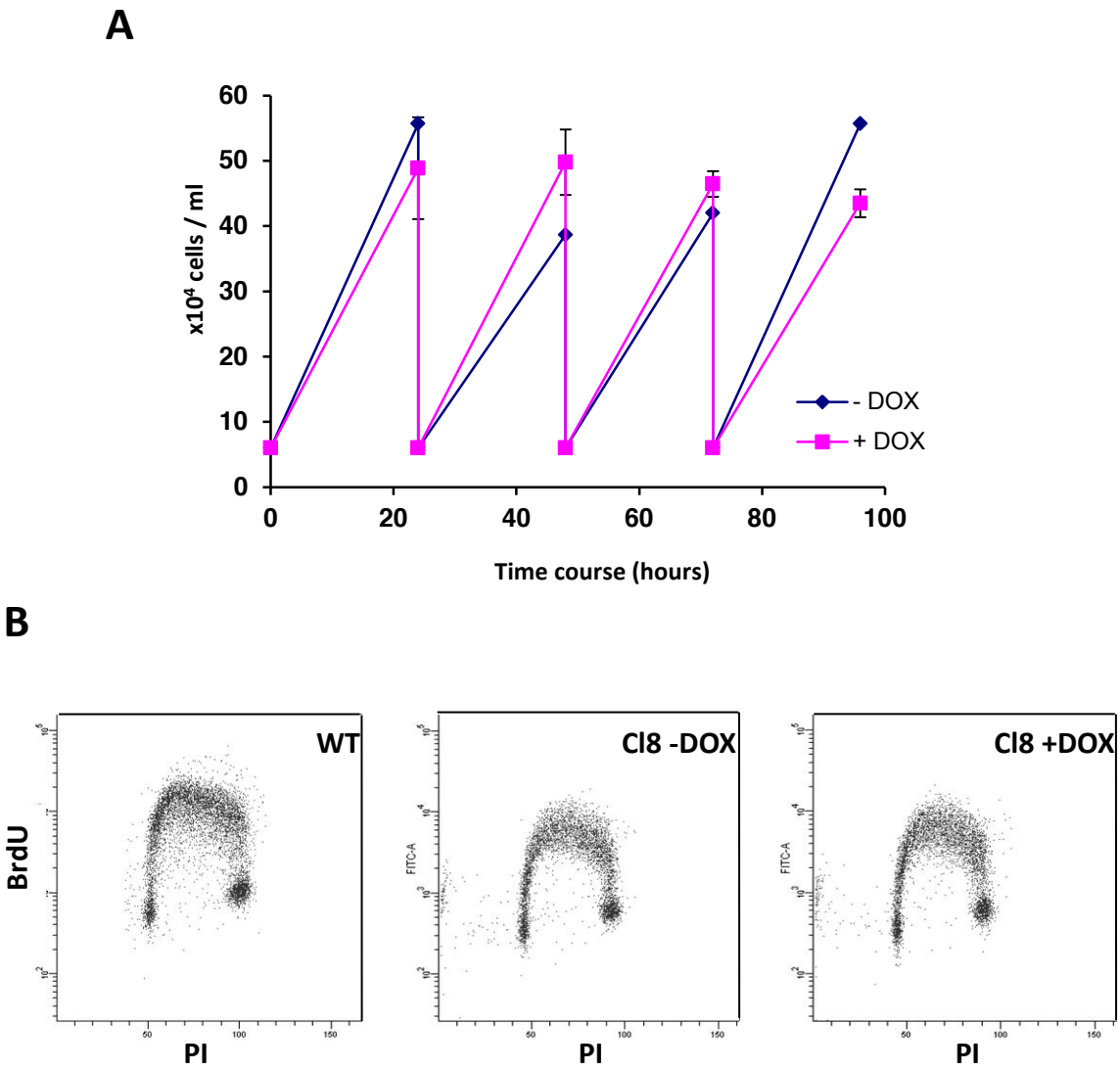

Figure 4.9: Characterisation of human conditional KO.

(**A**) Influence of human PrimPol protein repression by 1 μg/ml doxycycline treatment (+DOX) over 96 hours. Cells were diluted to $6x10^4$ cells ml^{-1} every 24 hours and counted with haemocytometer using Trypan Blue exclusion dye; Error bars represent standard deviation of 3 independent cultures. (**B**) Following a 20 minutes BrdU pulse, cells were co-stained with BrdU-FITC antibodies and propidium iodide (PI) for flow cytometry analysis. Cells pre-treated for 24 hours with 1 μg/ml doxycycline (+DOX) before BrdU pulse did not present any obvious cell cycle defect.

A

	-DOX	+DOX
PBS	218	
Clone4	3,588,146	1,983
Clone8	1,568,123	7,144

B

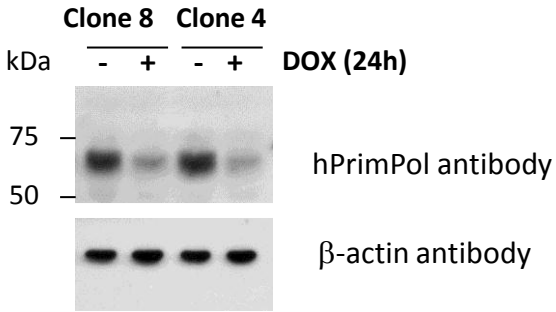

C

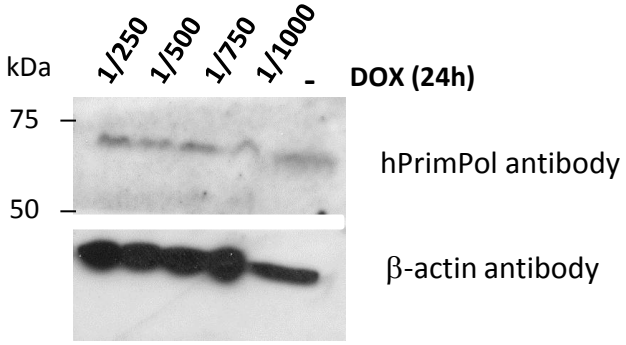

Clone 8

Figure 4.10: Characterisation of human PrimPol conditional KO clones following doxycycline repression.

(**A**) Luciferase activity assay was performed in the absence (-DOX) or after 24 hours treatment with 1 μg/ml doxycycline (+DOX) for both PrimPol KO clones 4 and 8. PBS was used to evaluate the background levels. (**B**) Western blot analysis with human PrimPol antibody confirmed the reduction of expression of ectopic protein after addition of doxycycline at 1 μg/ml (dilution 1/1000) for 24 hours in both KO clones; human β-actin antibody was used as loading control. (**C**) Western blot analysis after 24 hours of doxycycline treatment with increasing doses of the drug (1/1000 to 1/250 dilutions) in conditional KO clone 8 only. Remaining amount of ectopic PrimPol protein was evaluated with human antibody and β-actin was used as loading control.

clones as human PrimPol protein was still present follow 96 hours of drug treatment (figure 4.11).

4.3.2.1. Preliminary characterisation of overexpressed human PrimPol in *G. gallus* KO cells

To gain further understanding on human PrimPol and to see how the expression of the ectopic protein behaves in DT40 cells, a closer look at early time points following DOX addition allowed the following of human PrimPol protein degradation process (figure 4.11B). Interestingly, a major degradation product was visualised 8 hours following repression of protein expression but also in untreated sample collected at 24 hours (figure 4.11B, no DOX). This 50 kDa fragment has also been observed in human cells overexpressing PrimPol (figure 3.2), suggesting PrimPol polypeptide is subject to similar processing events in both DT40 and human cells. Following these observations, further experiments can investigate PrimPol protein stability and map domains by limited proteolysis to see eventual correlation with these degradations products. Another biochemical feature of PrimPol protein observed in human cells is its phosphorylation state and the appearance of a doublet at the full length size predicted to migrate on SDS-PAGE analysis (Chapter 6, figure 6.3). Here again, human PrimPol protein expressed in DT40 cells presented a similar doublet at ~60 kDa (figure 4.11B, middle panel). Interestingly, the upper band seemed to disappear 16 hours (and even more clearly at 24 hours) after addition of DOX, resulting on the visualisation of the non-phosphorylated species (lower band) only (figure 4.11B).

Following these biochemical observations, an immunofluorescence approach was also undertaken to further characterise ectopic expression of human PrimPol protein in avian *PrimPol* $^{-/-}$ cells and to see if the human protein has a similar sub-cellular localisation profile. Co-staining with human PrimPol antibody and DNA-intercalating dye DAPI, allowed visualisation of the cellular localisation of PrimPol and also an estimation of the protein overexpression levels. Immunofluorescence signal was specific to the human PrimPol protein expression as addition of DOX strongly reduced the visualisation of the protein (figure 4.12A, right panel). Ectopic expression of human PrimPol protein was visualised in both nucleus and cytoplasm of DT40 cells (figure 4.12A, left panel). However, some cells seemed to display a much stronger expression of human PrimPol protein, resulting in an intense fluorescence possibly masking the signal of neighbouring cells (figure 4.12A, bottom picture with saturated signal). To further characterise the cytoplasmic localisation of human PrimPol protein,

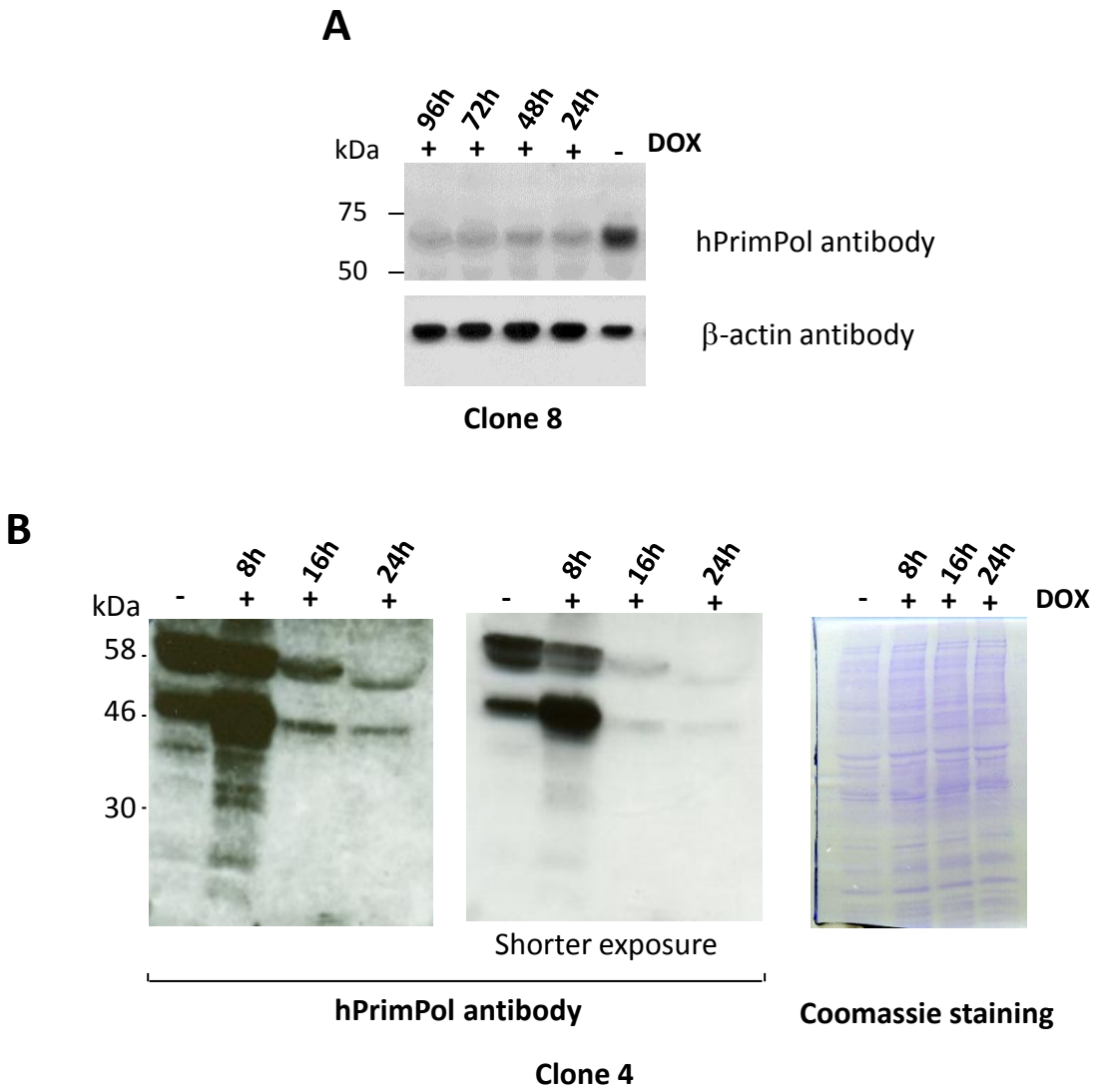

Figure 4.11: Optimisation of doxycycline treatments in human conditional KO clones.

(**A**) Human conditional KO clone 8 was cultured in media containing 1 μg/ml doxycycline (+DOX) for different amounts of time (h, hours above the blot) before samples were taken for Western blot analysis using human PrimPol antibody; β-actin was used as loading control. Expression levels of ectopic PrimPol protein were compared to untreated samples, collected at the later time point of each analysis (-DOX). (**B**) Early time course experiment (as in A) was performed in clone 4 only by Western blot analysis with human PrimPol antibody. Use of Coomassie stained gel as loading control (gel far right) instead of β-actin detection allowed to blot the integral membrane with hPrimPol antibody to visualise species smaller than the full length size. A shorter exposure of the same membrane (middle panel) is shown to help visualisation of individual bands.

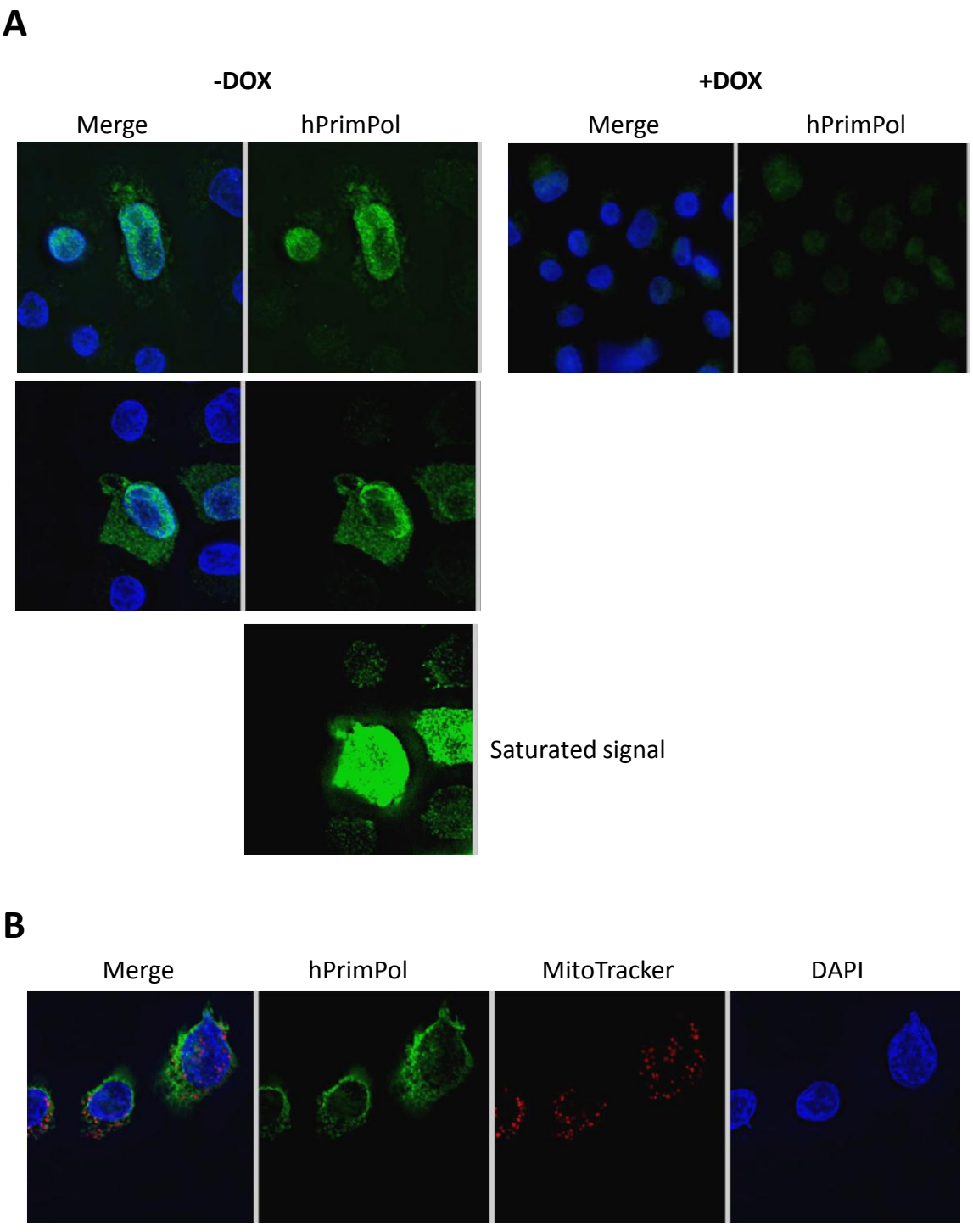

Figure 4.12: Human PrimPol localisation in DT40 cells.

(**A**) Immunofluorescence analysis using human PrimPol antibody (1:200) and DAPI staining (blue). Following 24 hours treatment with 1 μg/ml doxycycline (+DOX), human PrimPol signal (green) was strongly reduced (right panel). Difference of expression levels of hPrimPol appeared more clearly when FITC signal was saturated (bottom panel). (**B**) MitoTracker deep red (250 nM final concentration) was used to counterstain mitochondria and to visualise eventual human PrimPol colocalisation within the organelle.

MitoTracker dye was used to stain active mitochondria, but no human PrimPol protein was observed co-localising with this organelle (figure 4.12B, merged signals). Having noticed different patterns of cellular localisation (mainly nuclear or mainly cytoplasmic or equally in both compartments) and different expression levels of ectopic human PrimPol protein, this prompted the question whether the expression of this ectopic protein was cell cycle regulated. To address this, Click-iT® EdU technology permitted the co-staining of S-phase cells, which actively incorporate this modified nucleoside analogue, with human PrimPol immunofluorescent signal. By combining the EdU staining pattern and the different sizes of nuclei (visualised by DAPI staining), cell cycle phases of each cell could be determined easily: EdU negative cells with a small nucleus (nuclear radius bellow 4 μm) were G1 cells, while a large nucleus (nuclear radius above 5.2 μm) denoted G2 cells (Yabuki *et al*., 2009), and EdU positive cells were S-phase cells. No clear pattern was observed and an example of the different configurations observed is shown in figure 4.13. On the top panel, one cell was EdU negative with a large nucleus, therefore in G2 phase, and presented a similar human PrimPol protein localisation pattern (nuclear and peri-nuclear staining) than its neighbour S-phase cells. On the bottom panel of figure 4.13, two small nuclei cells with no EdU staining (G1 cells) also displayed human PrimPol protein signals in both cellular compartments. According to this experiment it was possible to conclude ectopic human PrimPol protein localisation was not cell cycle regulated.

4.3.3. Generation of *G. gallus PrimPol* knockout clones

Having successfully disrupted both WT alleles in cells conditionally expressing human PrimPol protein, but failed to completely deplete the expression of ectopic human PrimPol protein by addition of DOX (figures 4.10 and 4.11), disruption of the avian *PrimPol* gene was resumed in heterozygote DT40 cells (not expressing human PrimPol) using the second targeting strategy. Heterozygote WT/HIS clone 3 was transfected with the pDEST-PURO2 construct (table 2.7; figure 4.7C), and despite the first two unsuccessful attempts (figure 4.14A and B), the third try generated two *PrimPol* KO clones presenting the Southern blot pattern HIS/PURO2 (figure 4.14C, clone 1 and 2). Both clones were then re-amplified and fresh genomic DNA prepared to confirm the loss of both WT *PrimPol* alleles by a new Southern blot analysis (figure 4.15A). To further verify disruption of *G. gallus PrimPol* gene and therefore the lack of PrimPol protein expression in these cells, RNA samples were extracted (figure 4.15B) and RT-PCR assays performed (figure 4.15C). No amplicons were obtained when using primers specific of *G. gallus*

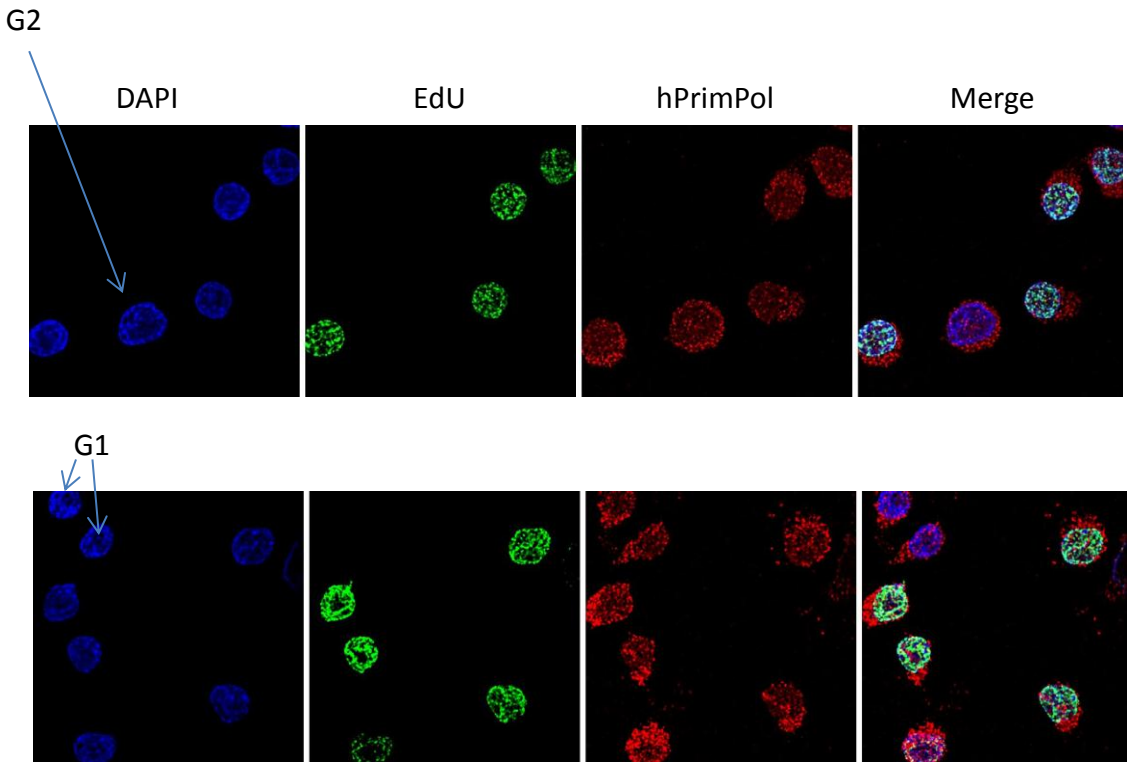

Figure 4.13: Human PrimPol cellular localisation in relation to cell cycle analysis.

Immunofluorescence analysis using human PrimPol antibody (red), DAPI staining (blue) and click-it EdU (green) technology (Invitrogen) to visualise actively replicating cells. Non denaturing conditions used with click-it EdU allowed co-staining with human PrimPol antibody (1:200); Size of DAPI stained nuclei in combination with EdU patterns, permitted distinction between G1, S and G2 cells (as indicated with arrows, S phase cells being EdU positive or green cells).

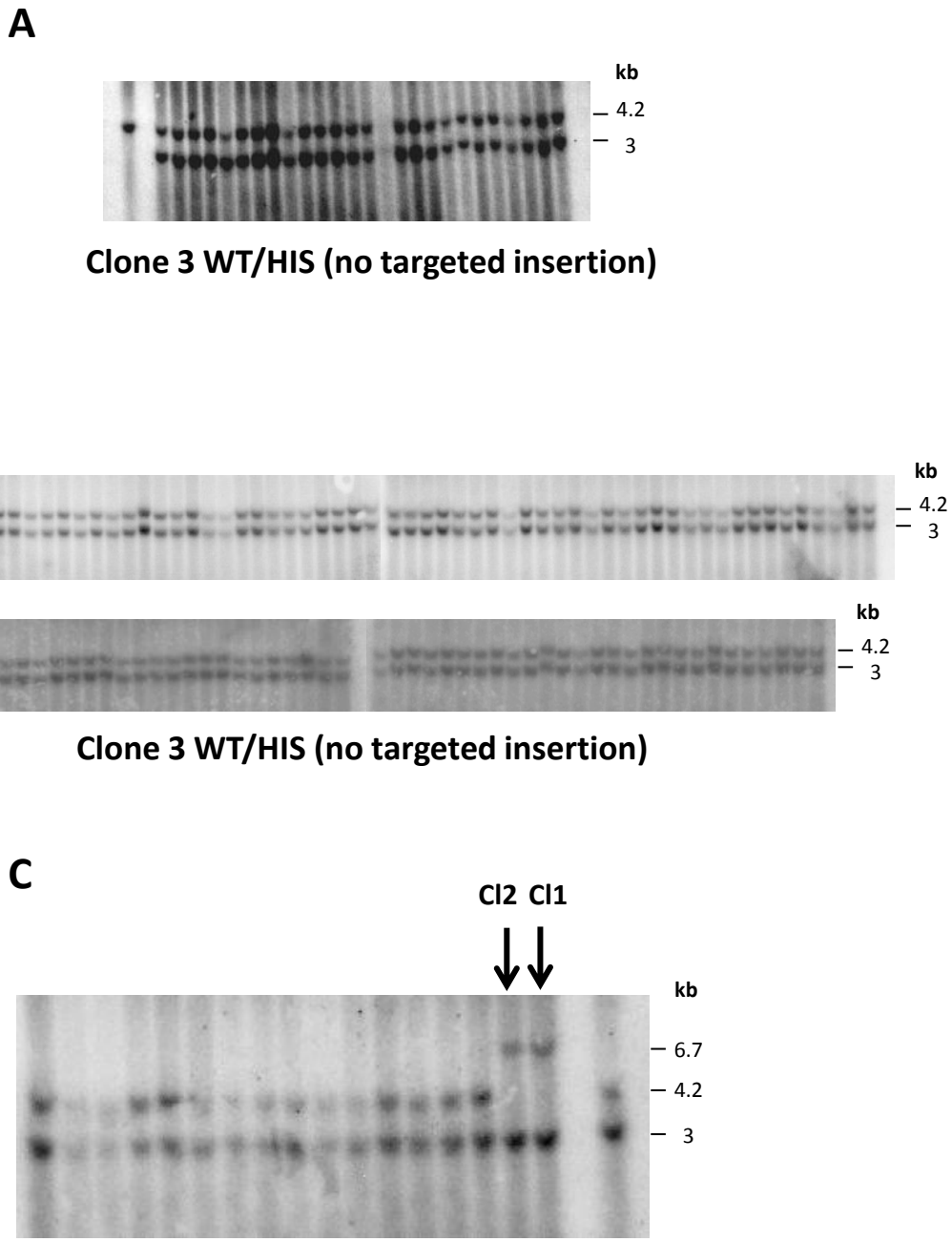

Figure 4.14: Second allele targeting strategy generating two *G. gallus PrimPol* KO clones.

Southern blot analysis of puromycin resistant clones obtained after transfection of heterozygote clone 3 (WT/HIS) with pDEST-PURO2 construct. (**A**) First transfection attempt presented only random integration of puromycin resistant (Puro^r) marker in every 26 clones collected. (**B**) Second transfection attempt was performed with media containing new synthetic serum Hyclone. All 113 clones also presented random integration of Puro^r cassette. (**C**) Clones 1 and 2 (Cl1 and 2) presented targeted integration of Puro^r marker without affecting previous HIS disrupted allele (3 kb band) generating the HIS/PURO2 pattern, and thus corresponding to two individual *G. gallus PrimPol* gene knockout cell lines.

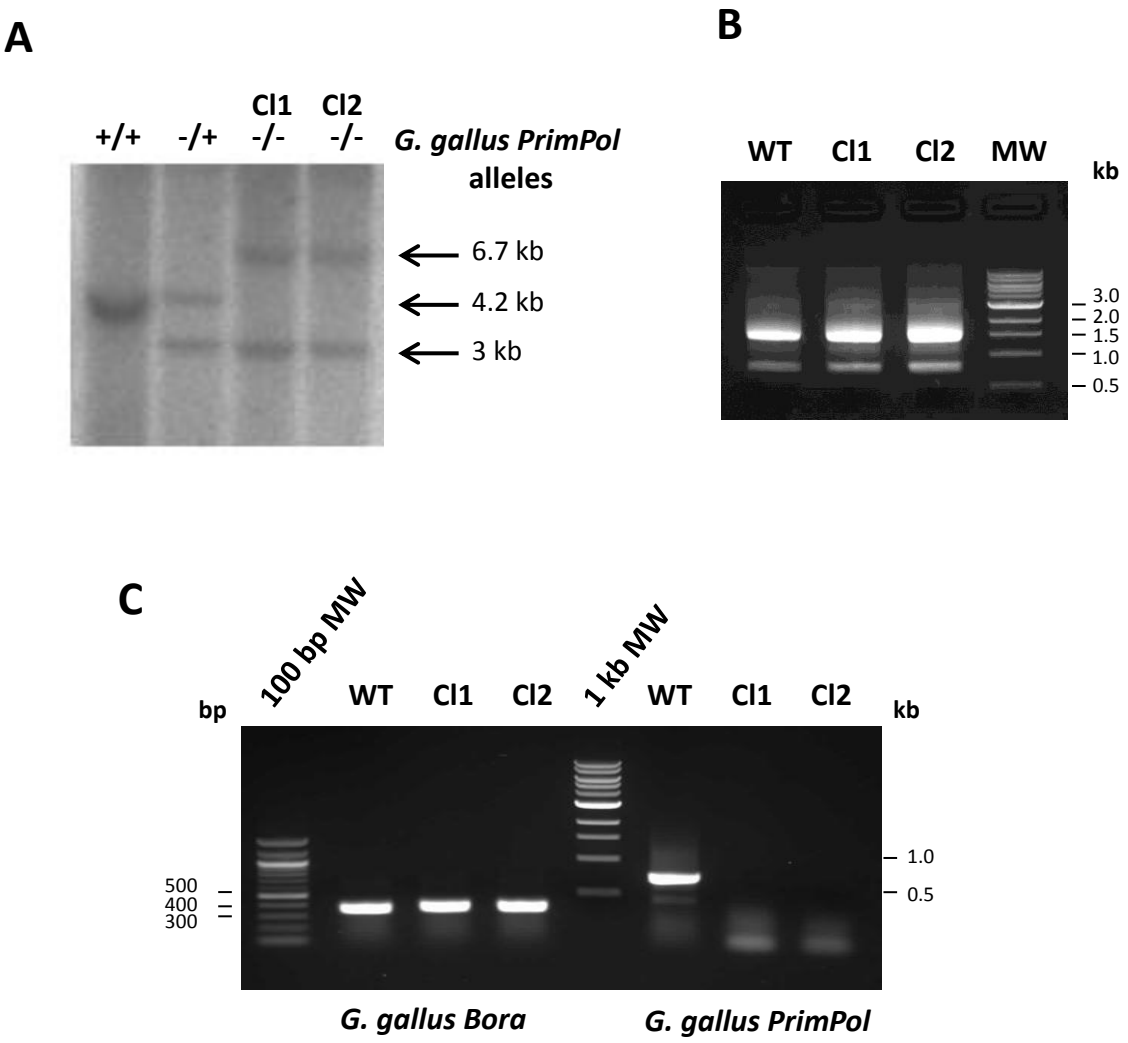

Figure 4.15: Confirmation of two *PrimPol* DT40 knockout clones by Southern blot and RT-PCR analyses.

(**A**) Genomic DNA of WT DT40 cells (+/+), heterozygotes (+/-) and knockout clones (-/-) 1 and 2 (Cl1 and Cl2), was digested with *EcoRI* enzyme and submitted to Southern blot analysis with radiolabelled probe P2 specific of *G. gallus PrimPol* gene. (**B**) RNA samples were extracted from both clones and WT cells and 1 μg of RNA was loaded onto 1% agarose gel to check the quality of the samples. In order to confirm the disruption of *PrimPol* gene in both KO clones, RT-PCR were performed (**C**) with primers specific of *G. gallus PrimPol* gene (right part of the gel) or non-specific (recognising *G. gallus Bora* cDNA) primers (left part of the gel).

PrimPol cDNA (table 2.3) with KO clones 1 and 2 samples, whereas samples prepared from WT cells generated a ~700 bp band following the same RT-PCR (figure 4.15C, right agarose gel). Quality of the RNA samples were verified by using primers specific of another *G. gallus* gene (table 2.3, *G. gallus* Bora primers) and similar RT-PCR signals were obtained in all three samples (figure 4.15C, left agarose gel) confirming the presence of total RNA in the KO clones. Taken together, these data indicate the successful disruption of *PrimPol* gene in avian DT40 cells, thus confirming *PrimPol* is not an essential gene.

4.4. Preliminary characterisation of *PrimPol* knockout DT40 cell lines

4.4.1. Proliferation and cell cycle analysis in *PrimPol* $^{-/-}$ DT40 cells

It was first investigated whether PrimPol was required for normal cell proliferation. Both *PrimPol* KO clones (*PrimPol* $^{-/-}$) and WT DT40 cells were grown in liquid culture and diluted every 24 hours (3 cell divisions) in order to keep the cultures at an optimal cell density of ~50 x 10^4 cells ml^{-1}. On average, all cultures doubled in a similar manner and no apparent proliferative defects were observed. However, when the cultures were diluted to a lower cell density, both *PrimPol* $^{-/-}$ clones took a longer time than WT DT40 cells to recover from the dilution. To quantify this, growth curves were assessed for each culture over a 56 hour period, with duplicate cultures diluted at 1 x 10^4 cells ml^{-1} and the number of cells measured on haemocytometer with Trypan Blue exclusion dye staining (figure 4.16A). Multiple experiments were performed and the doubling-time of each strain was calculated via an exponential regression algorithm online method (Roth, 2006) (figure 4.16B). A 40 minute and a 70 minute increase in doubling-time were observed in clone 1 and 2, compared to WT DT40 cells, resulting in a doubling-time increase of 8% and 15% respectively.

To further understand the cause of this proliferative defect observed in *PrimPol* $^{-/-}$ cells, the cell cycle distribution of these clones was analysed. WT DT40 cells spend on average 4 hours in S phase, 1 hour in G1, 2 hours in G2 and 30 to 60 minutes in mitosis (Helfrid Hochegger, Nadia Hégarat, personal communication), whereas the majority of asynchronous human cells in culture are in G1 phase. Thymidine analogue BrdU was incorporated and visualised by flow cytometry analysis to indicate the proportion of actively replicating cells within asynchronous population (figure 4.17A). Co-staining cells with DNA intercalating PI reagent, allowed determination of the DNA content of the cell population analysed. In this way, an accurate discrimination of each phase of the cell cycle was achieved, G1 cells

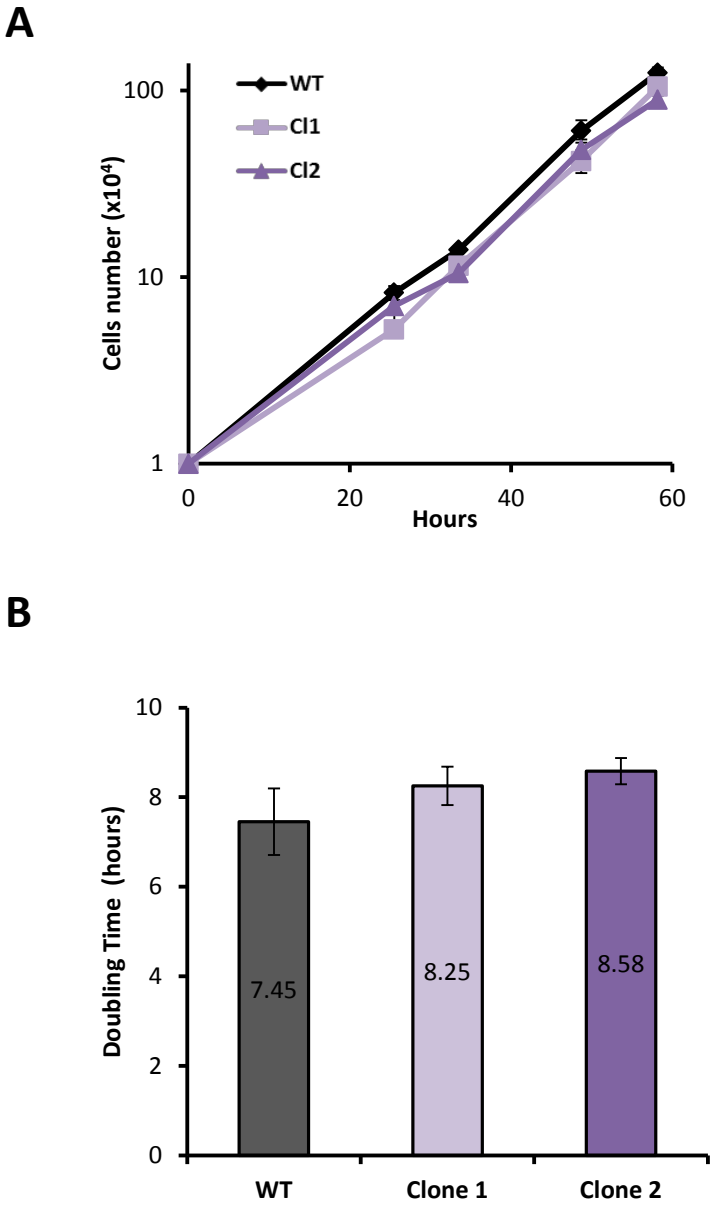

Figure 4.16: Proliferation of *PrimPol* knockout clones.

(**A**) Growth curves of DT40 WT (black line) and *PrimPol* $^{-/-}$ (light and dark purple for clone 1 and 2 respectively) cells were assessed by counting duplicate cultures of each population over 7 generations (56 hours), using a haemocytometer with Trypan Blue exclusion dye staining. (**B)** Doubling time for each population was determined using an online exponential regression algorithm (Roth, 2006); average of 3 independent experiments was indicated in the middle of each plot and the standard deviation represented by error bars.

A

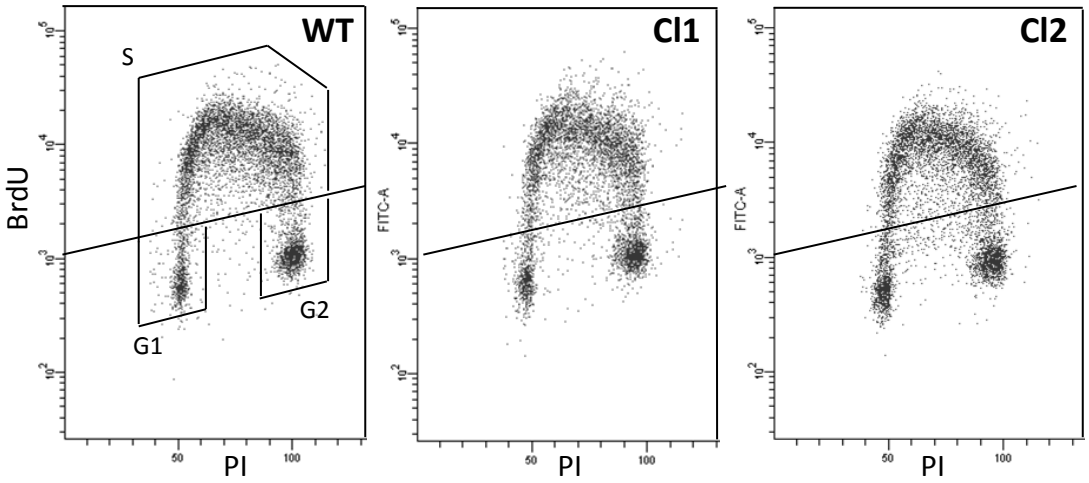

B

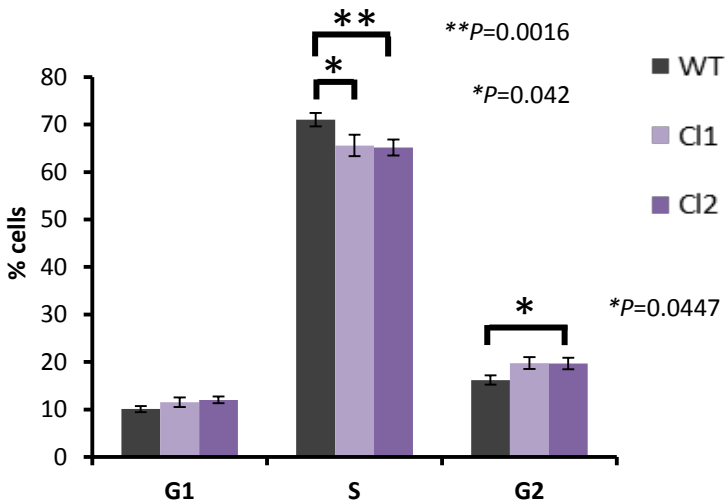

C

	% mitotic cells
WT	1.2
Clone 1	3.1
Clone 2	1.95

Figure 4.17: Cell cycle analysis of *PrimPol* knockout clones.

(**A**) Cell cycle profiles of WT DT40 (left panel) or both *PrimPol* $^{-/-}$ clones (clone 1, middle panel and clone 2, right panel) was determined using flow cytometry analysis following BrdU incorporation (20 minutes pulse). (**B**) Quantification of the proportion of cells present in each phase of the cell cycle for WT DT40 (grey) and both *PrimPol* $^{-/-}$ clones (clone 1 and 2, light and dark purple respectively) ; error bars denote standard deviation of 5 experiments, and the t-test was assessed with two tails moments to determine p values (**P*). (**C**) Percentage of mitotic cells for each asynchronous population was assessed by counting DAPI stained cells presenting condensed chromosomes (at least 300 cells were scored).

corresponding to BrdU negative diploid cells (2N, bottom left quadrant), S-phase cells to BrdU positive population, and G2/M cells to BrdU negative cells with a 4N ploidy (bottom right quadrant) (figure 4.17A). This flow cytometry analysis, repeated five times, indicated both *PrimPol* KO clones had a significantly lower proportion of cells actively incorporating BrdU than WT cell population (65% compared to 71% in WT cells) (figure 4.17B). Indeed, cells lacking PrimPol protein appeared to slightly accumulate in G2 phase instead (~20% compared to ~16% in WT cells), and they also had a higher proportion of mitotic cells (assessed by DAPI counting, figure 4.17C). However, the length of mitosis was similar in *PrimPol* $^{-/-}$ and WT DT40 cells, according to live cell imaging records. Following a transient transfection with histone H2B tagged with GFP, mitosis events were visualised and timed in KO and WT DT40 cells, and no significant differences were observed between both cell lines (Helfrid Hochegger, personal communication).

4.4.2. Analysis of DNA replication in *PrimPol* $^{-/-}$ DT40 cells

Having deleted a DNA primase-polymerase gene in avian cells and observed a delay in cell proliferation and changes within the cell cycle distribution, it was logical to next investigate overall DNA replication. A radioactive thymidine uptake experiment was performed by using ^{3}H and ^{14}C radiolabelled nucleotides. Overnight labelling (corresponding to approximately two doubling times) with ^{14}C thymidine was used as an internal control to normalise the amount of cells in each sample. A short 20 minutes pulse was performed with ^{3}H thymidine to determine the ability of cells to incorporate nucleotides during DNA replication. Radioactivity levels corresponding to each signal were measured individually using a dual program on a liquid scintillator (Beckman Coulter). After normalisation with ^{14}C signal, the percentage of ^{3}H thymidine uptake was calculated and compared to the WT cell population. A 15 to 20% decrease was observed on average in both *PrimPol* KO clones (figure 4.18A) indicating overall DNA replication was reduced in the absence of PrimPol.

To further investigate this phenotype, DNA fiber analysis was performed using DNA spreading methodology. This technique was first developed by Jackson and Pombo in 1998 to study replicon clusters and how nuclear organisation regulates S-phase progression (Jackson and Pombo, 1998). This assay allows visualisation of newly synthesised DNA by immunostaining of two thymidine analogues, CldU and IdU, added into the media sequentially (figure 4.18B). This dual labelling enables determination of RF direction and discrimination of

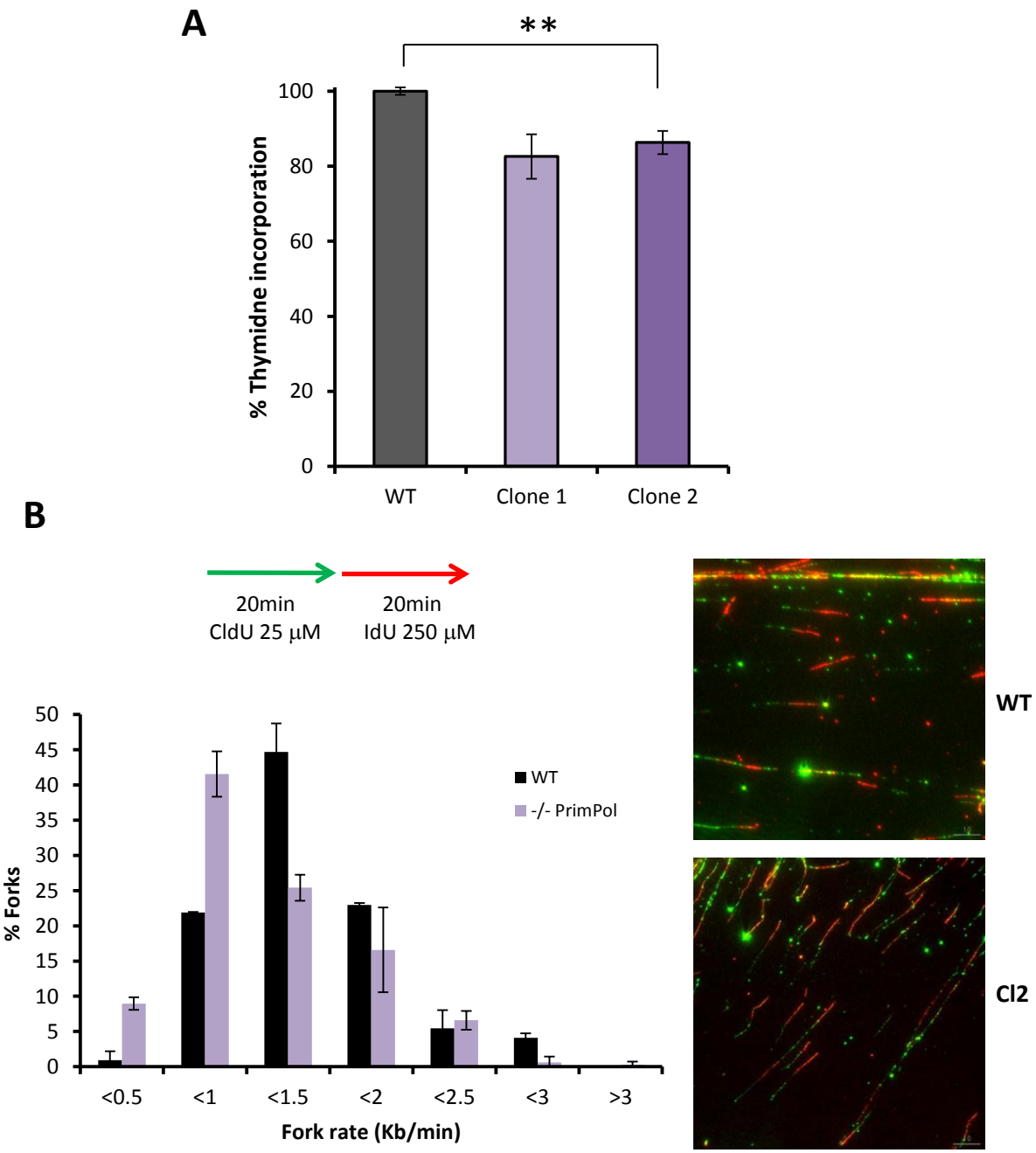

Figure 4.18: DNA replication in unperturbed S phase.

(**A**) WT (grey) and PrimPol KO (light and dark purple) cells were first labeled with Carbon-14 (^{14}C) thymidine for 16 hours and then pulse-labeled for 20 minutes with tritium thymidine. Incorporation rate was calculated after normalisation with ^{14}C signal for total DNA content. Error bars represent standard deviation of 3 independent experiments. (**B**) DNA spreading experiment. Cartoon depicting the labeling process (top left panel). Distribution of replication fork speed in WT (black) or PrimPol KO (purple) populations. Data represent the average of two independent experiments where at least 100 fibers were analysed each time. PrimPol KO data correspond to the average of both KO clones. Pictures representative of newly synthesised DNA fibers after immunostaining with CldU and IdU antibodies, in WT and *PrimPol*$^{-/-}$ clone 2 (Cl2) cells (right panel).

different replication structures (Schwab *et al.*, 2011). Here, only elongated RF were analysed by measuring the length of the red tracks (corresponding of IdU labelling) preceded by a green track (CldU labelling) on one side only (figure 4.18B). Structures containing single track or alternation of both colours (green-red-green or red-green-red) were ignored in order to discard new origin and termination events. By this way, RF rate was calculated for WT and *PrimPol* KO populations using OMERO software (Allan *et al.*, 2012) to measure the red tracks length and convert the pixels into micrometers. The conversion factor 1 μm= 2.59 kb was used to convert those measurements (Jackson and Pombo, 1998) and allow a calculation of the fork speed in kb/min (figure 4.18B). Both *PrimPol* KO clones presented a higher proportion of slower forks with an average speed of halogenated nucleotides incorporation of 1.1 kb/min compared to 1.4 kb/min in WT population (figure 4.18B). Taken together with the results of the previous radioactive thymidine uptake experiment, these data are consistent with a role for PrimPol in nuclear DNA replication during normal cell proliferation in DT40 cells.

4.5. Summary and discussion

This Chapter details the disruption of the *PrimPol* gene in avian DT40 cells and indicates that this novel primase-polymerase is not an essential protein in this vertebrate cell line. Minor proliferative and cell cycle defects were observed in *PrimPol* KO cells, and these cells had a decreased rate of DNA synthesis and slower RF speed. Together, these data are consistent with the involvement of PrimPol in some aspects of nuclear DNA replication during normal cell proliferation.

4.5.1. Disruption of the *PrimPol* gene in avian DT40 cells

This first half of this Chapter describes the gene targeting strategies used to disrupt the *PrimPol* gene in avian DT40 cells. Although this process was not as straight forward as originally anticipated (Iiizumi *et al.*, 2006), two *PrimPol* KO clones were obtained, as well as two KO strains constitutively expressing human PrimPol under an inducible (Tet-off) promoter.

The conventional gene targeting strategy for DT40 cells (Iiizumi *et al.*, 2006) (first strategy employed here) was unsuccessful for the disruption of the avian *PrimPol* gene. Several explanations can be envisaged. Natural selection pressure mechanisms (epigenetics factors or specific chromatin structures for example) linked to the genomic sequence context surrounding the *PrimPol* gene could have been responsible for the lack of success during the second allele targeting process. Notably, one particular feature of the *PrimPol* gene is its close proximity with caspase-3 (*CASP3*) gene in higher eukaryotic species (human, avian, mice, xenopus, etc…). This apoptosis-related cysteine peptidase is essential for normal brain development as KO mice dye at 3 weeks of age (Kuida *et al.*, 1996). It is therefore possible to speculate that the close proximity between *PrimPol* and *CASP3* genes was responsible for preventing a targeted HR of the second allele of the *Primpol* gene, as it could potentially disturb the expression of this neighbouring essential gene. However, the second targeting strategy, which used two different sets of targeting sequences (one for each allele to be disrupted), prevented the switch between both antibiotic selection markers, doubling the chance of targeting the remaining WT allele. By this way it was then possible to obtain the disruption of both *G. gallus PrimPol* alleles, and to conclude the failure of the first strategy was probably due to the long distance between both homologous arms (5' and 3' ARMS) on the WT allele and was not related to the genomic context. Therefore, the close proximity of both genomic targeted arms on the first disrupted allele, facilitated the second recombination event

to take place on the same allele and not on the WT allele, leading to this switch between both antibiotic markers observed in every targeted recombination event while using the first strategy. One way to verify this would be by using the first strategy and add both antibiotic selections (PURO and HIS) during the transfection of heterozygote clone while targeting the remaining WT allele. This should then prevent the growth of heterozygote clones where the switch between both antibiotic markers occurred, and increase the probability of selecting clones with both *PrimPol* alleles disrupted.

Nonetheless, use of the second targeting strategy overcame these problems by greatly increasing the probability of targeting the WT *PrimPol* allele of the heterozygote clone. However, re-design of the targeted 5' arm (5'ARM2), which enclosed homologous sequences containing exon 2 of the *PrimPol* gene, thus contained the start codon of the ORF. A truncated version of PrimPol protein consisting of 60 amino acids could then be expressed (stop codon introduced at position 61), potentially generating a polypeptide with a predicted MW of 7 kDa. Also, the genomic area remaining after integration of the disruption cassette, from exon 7 until the end of the ORF, could potentially encode for a predicted 30 kDa peptide containing the UL52 zinc-finger domain of PrimPol. The first methionine in frame being Met19, a 248 amino acids peptide could therefore be expressed but should not possess any polymerase activity due to the absence of the catalytic residues in the AEP domain (DxE encoded in exon 3). However, it is not clear whether this polypeptide would fold correctly and remain stable, or would be subject to degradation. To verify this, immunoprecipitation of endogenous PrimPol protein could provide an answer, but unfortunately no PrimPol antibody tested so far recognised the endogenous avian polypeptide. Also RT-PCR experiments with primers designed within this area of the gene should be performed to complete the previous analysis (figure 4.15) and verify if any mRNA transcripts are synthesised downstream of the antibiotic markers.

4.5.2. Study of human PrimPol in DT40 KO cells

Expression of human PrimPol cDNA in a Tet-off rescue vector, originally used for generating a conditional strain (in the event of PrimPol being essential for cell survival), was finally utilised for complementation and immunofluorescence localisation purposes. Indeed, using the human antibody allowed us to visualise the sub-cellular localisation of exogenous human PrimPol protein, however the expression level appeared quite variable from one cell to another (figure

4.12). Being expressed constitutively on a stably integrated plasmid, every cell should produce in theory the same amount of human PrimPol in the absence of DOX. However different levels of expression were visible (figure 4.12A), suggesting a possible variation in the amount of protein subjected to post-translational modifications such as degradation. Indeed, in the Western blot analysis (figure 4.11B) a strong band at 50 kDa was already visible in the lane without any DOX, indicating a high level of processing events (roughly a third of the total amount of full length protein) occurring endogenously. Another backbone expression vector containing a weaker promoter could be used to compare the level of expression (by immunofluorescence) and degradation (by Western blot analysis) of human PrimPol and exclude any artefact due to the overexpression system. Also, more clones could be selected by luciferase screening with lower expression level. In this case, it would be preferential to transfect both *PrimPol* $^{-/-}$ clones 1 and 2 with either human PrimPol tagged with GFP, or expressed in an inducible (Tet-on) promoter to perform precise complementation studies. Furthermore, this complementation system could be useful for in depth studies of rescue phenotypes and therefore address specific roles to the different parts and domains of the protein. Sub-cellular localisation studies of human PrimPol could be then re-analysed with different truncations or point mutations, affecting phosphorylation, ubiquitylation or SUMOylation status or the binding with partners for example, thus potentially influencing the transit of the protein within the cell. Moreover, this rescue system could also contribute to provide a better understanding of the role of the zinc-finger domain towards PrimPol polymerase and/or primase activities *in vivo*; potentially roles have been speculated for example in DNA template recognition and regulation of the enzymatic activity of PrimPol.

4.5.3. Putative roles for PrimPol in nuclear DNA replication during unperturbed S-phase

PrimPol KO cells were able to grow normally in liquid condition (figure 4.16A) and did not present any morphological abnormalities. However, it was noticed cell proliferation was roughly 10% slower than in the WT population (figure 4.16B). Cell cycle analysis indicated the proportion of KO cells in G2 phase was slightly increased and fewer cells were in S-phase (figure 4.17B). However, DNA replication assays, using either incorporation of radioactive thymidine (figure 4.18A) or DNA fibers analysis (figure 4.18B), revealed an S-phase defect with a reduced capacity of the KO cells to replicate their DNA. Several hypotheses can be suggested to explain these phenotypes.

The first hypothesis is the participation of PrimPol in the incorporation of modified nucleotides during normal DNA replication (like thymidine analogues BrdU, CldU, or IdU for example). Given PrimPol is part of the AEP superfamily, this enzyme would be predicted to have a flexible catalytic site that could accommodate a range of substrates. It is then possible to speculate that such an enzyme could be recruited during S-phase when an excess of thymidine analogue is present in the media to assist replicative polymerases to incorporate this non-physiological nucleotide. Even if the replicative polymerases can incorporate the modified nucleotide, their exonuclease activity (or some other control mechanisms) could subsequently remove the modified base, and PrimPol would be then needed to complete these gaps. Moreover, it has been previously shown *in vitro* incorporation of modified dNTPs can greatly vary depending on the polymerase employed and its exonuclease activity efficiency (Anderson *et al.*, 2005; Sobolewski *et al.*, 2011). In line with this, cell cycle analysis using BrdU measurements coupled with flow cytometry analysis would be perturbed in *PrimPol* $^{-/-}$ cells compared to WT DT40 samples. According to this hypothesis, during a short 20 minutes pulse, KO cells would then incorporate less BrdU compared to WT cells, resulting in an apparent decrease of the proportion of BrdU positive cells. Depending when PrimPol functions during nuclear S-phase, this could have distinct consequences on the cell cycle analysis. If the novel polymerase intervenes during the middle of S-phase, the proportion of BrdU negative cells (with DNA content comprise between 2N and 4N) should be increased and visible on the flow cytometry profiles (figure 4.17A). However, if PrimPol is only recruited at the end of S-phase (4N content cells), BrdU negative cells would then be merged with G2/M cells and both populations be indistinguishable on PI/BrdU double staining analysis. In this case, a decrease of BrdU positive (denoted S-phase cells in this analysis) would be associated with an increase of G2/M cells, as seen in figure 4.17B. To conclude, flow cytometry analysis suggests that PrimPol could be specifically recruited at the end of S-phase, once the bulk of the genome duplication is achieved, to help the completion of DNA replication in a post-replicative manner. The same conclusions could also be extrapolated to the analysis of DNA replication rate (figure 4.18). A replication defect occurring in late S-phase in the absence of PrimPol would still reduce the overall replication rate in KO cells compared to WT cells (figure 4.18A) and increase the proportion of slow RFs (figure 4.18B). On the other hand, the small decrease of replication rate observed in the absence of PrimPol (figure 4.18) cannot explain the reduction of the proportion of BrdU positive cells (figure 4.17B). Indeed, this assay is not quantitative in the same way ^{3}H thymidine incorporation is, as the flow cytometry analysis allows measurement of the proportion of cells actively replicating their DNA. Therefore, if only 10% less BrdU was

incorporated during replication due to a RF rate decrease, the percentage of S-phase cells would still stay the same. To verify this hypothesis, *in vitro* experiments looking at the ability of recombinant human PrimPol to incorporate modified nucleotides can be performed and compared to the ability of replicative polymerases to do the same.

The second hypothesis is based on the recruitment of PrimPol to facilitate replication of endogenously occurring DNA lesions, either by its primase or polymerase activity, to help the completion of the genome duplication in the appropriate amount of time. Therefore, the bulk of DNA synthesis could occur without PrimPol and only a small decrease of BrdU incorporation would be noticed in KO cells (figure 4.17A and B). Overall replication rate (figure 4.18A) and RF speed (figure 4.18B) would then also be perturbed in *PrimPol* $^{-/-}$ cells compared to WT DT40 cells. This damage tolerance feature of PrimPol could explain the fact the novel polymerase is not a key component of the replisome, otherwise the protein would have been discovered and characterised by now. According to this hypothesis, in the absence of PrimPol, when replicative polymerases encounter a lesion leading to the stalling of the RF machinery, a decrease of thymidine incorporation and a higher proportion of RF with a lower replication rate (figure 4.18) would occur. Nonetheless, RF restart or new origin firing (dormant origin) mechanisms could allow S-phase progression, and only a delay in the final stage of the completion of genomic duplication could be observed. The cell would then rely more on post-replication mechanisms to fill the gaps left behind the replication machinery, stalling at those natural impediments and restarting downstream in the absence of PrimPol. A delay in late S or G2 phases would then be recorded (figure 4.17B). In this model, PrimPol recruitment would be needed during S-phase to assist RF progression, but be noticeable only in a later time, in accordance to both flow cytometry and DNA fibers analysis.

In a final hypothesis, we speculate that PrimPol could be specifically recruited in late S-phase or early G2 to help the RF machinery to complete DNA synthesis processes in specific areas of the genome, which are specifically replicated at the end of S-phase. Indeed, in the divergent eukaryote *Trypanosoma brucei*, experiments performed with inducible PrimPol (TbPrimPol2) RNAi knockdown strains also highlighted the importance of PrimPol in G2 phase (Sean Rudd, Aidan Doherty, personal communication). These cells were able to duplicate the bulk of their genetic material (normal S-phase by flow cytometry analysis) but the data suggested PrimPol had an essential role during late or post-replicative phases. Further investigations regarding PrimPol's implication within post-replication mechanisms are also undertaken in the next Chapter of this thesis.

In summary, as PrimPol is a novel uncharacterised polymerase, we cannot exclude this enzyme could have a direct role in incorporating modified nucleotides, explaining these mild decrease in BrdU, ^{3}H thymidine and CldU/IdU incorporations observed in KO cells (figures 4.17 and 4.18). It is also possible to suspect a role for PrimPol in DNA damage tolerance mechanisms assisting replicative polymerases during normal S-phase, either all along the replication phase or specifically at its end. In any cases, the absence of PrimPol would be then accompanied with a delay in the completion of the duplication of the genome, and therefore an accumulation of cells in late S or G2 phase.

4.5.4. Natural impediments potentially causing the recruitment of PrimPol in late S-phase

In line with the last hypothesis mentioned above, several examples have been described in the literature where natural impediments specifically arise at the end of S-phase. When RF stalls at these types of lesions, PrimPol could then be recruited to overcome these obstacles or either restarts the replication machinery downstream. Studies from the Hoffmann laboratory (CRCT, Toulouse) have previously demonstrated the involvement of TLS polymerases during unperturbed S-phase to overcome non-B DNA structures naturally occurring during replication processes (Bétous *et al.*, 2009) and also at common fragile sites (Rey *et al.*, 2009). A very detailed review by Ekaterina and Sergei Mirkin documents natural impediments potentially responsible for RF stalling (Mirkin and Mirkin, 2007). Given PrimPol intrinsic features as a member of the AEP family, its malleable active site makes this enzyme a strong candidate for bypass of helix distorting templates (as observed in appendix A with DNA template containing UV photoproducts). A potential role in RF restart thanks to its primase activity remains also a possibility. Therefore, PrimPol could be recruited after collision between RF and transcription machinery, or at hairpins or G4 DNA structures arising at specific sequences area of the genome. Common and rare fragile sites, composed of nucleotide repeats potentially forming those secondary structures, are located in areas of the genome which have been reported to be replicated late in S-phase (Durkin *et al.*, 2007). It is therefore possible to speculate a specific recruitment of PrimPol during late S-phase to assist the replication machinery to overcome these difficult areas of the genome to be replicated. Distinction between a potential TLS role of PrimPol to overcome these DNA structures or a re-priming activity downstream of the G4 structures is a difficult matter to address experimentally. However, analysis of mutagenesis

profiles in DT40 cells transformed with a plasmid containing this type of structure can be performed (Sarkies *et al.*, 2010).

Replication dynamic and DNA structure seem therefore to be correlated, and recent studies have started to map the replication schedule of the genome (Chagin *et al.*, 2010). According to these analyses, actively transcribed genes would be replicated early due to the open chromatin structure (euchromatin area) allowing both machineries to perform their tasks (Takeda *et al.*, 2005). To determine if PrimPol intervenes at a specific time during nuclear replication, co-localisation studies between endogenous protein (or stably overexpressed PrimPol) and pulsed BrdU could provide the answer. However, in a very low percentage of human cells, overexpressed PrimPol assembled into detergent resistant foci during unperturbed S-phase following triton extraction (<0.5%; Sean Rudd, Aidan Doherty, personal communication). After aphidicolin treatments on asynchronised normal human fibroblasts, sub-cellular fractionation studies revealed PrimPol was chromatin associated when the cells were arrested in S-phase, but no more detectable in this fraction 3 hours after removal of the drug (Sean Rudd, Aidan Doherty, personal communication). Those data support the hypothesis PrimPol is needed only transiently during S-phase making immunofluorescence study difficult to achieve. A GFP knock-in DT40 strain could help to solve these issues by allowing live cell imaging during unperturbed S-phase. In the case triton extraction would be needed to visualise only chromatin bound PrimPol, elutriation experiments could be performed to accurately synchronise DT40 cells (via their size) before analysing PrimPol localisation during the cell cycle.

In order to understand whether PrimPol could be needed during normal S-phase, another factor of DNA replication dynamic to investigate concerned origin distribution and firing. Data obtained relative to this topic are issue from complicated computational studies of genome wide analysis which I'm going to summarize briefly. The timing of origin firing is believed to happen in a stochastic manner (Patel *et al.*, 2006), however, analysis of origin localisation (in a particular DNA structure), distribution (rich or poor origins areas), and efficiency of activation, were more instructive. Indeed, replication initiation rate has been calculated in various species (yeast, fruit fly, xenopus, and human) in relation to S-phase progression (Goldar *et al.,* 2009). A similar Gaussian distribution reported in every case allowed the authors to conclude initiation of replication was optimal during mid-S phase. Others publications confirmed early origins were less efficiently activated (Heichinger *et al.*, 2006) and also more dispersed than mid-S phase ones (Frum *et al.*, 2009). Chromatin structure,

recycling firing elements (heterochromatin represses MCM activity), checkpoint response (ATR/ Chk1 pathway repressing origin initiation in late S-phase) and probably other factors, are potentially responsible for the decrease of replication rate at the end of S-phase (Herrick, 2011). Moreover, recent studies on chromosomes fragile sites have established these particular sites of the genome (situated in dense heterochromatin areas) are replicated in late S-phase and surrounded by very few origins (Debatisse *et al.*, 2012). Therefore replication of these sites is believed to be more prone to pausing or delay generating un-complete replication leading to chromosomes breakage during mitosis. It is then possible to speculate PrimPol could be specifically involved at the end of S-phase in maintaining RF progression (possibly via its re-priming activity) on these long forks in areas of more dispersed origins. On the other hand, it would also be interesting to understand if the absence of PrimPol could trigger dormant origin firing to compensate the reduction of RF speed observed (figure 4.18), thus potentially explaining why the flow cytometry profile (figure 4.17) did not indicate an increase of S-phase cells. Indeed, a similar phenotype has been observed in *Chk1* $^{-/-}$ DT40 cells, where RF speed was decreased (~50%) and firing of dormant origins was increased but not sufficiently to compensate RF decrease (Petermann *et al*., 2006; Maya-Mendoza *et al*., 2007; Petermann *et al*., 2010). DNA combing technique should then be performed in order to study those mechanisms involving replication origin density in *PrimPol* KO cells.

CHAPTER V

Exploring the role of *PrimPol* $^{-/-}$ DT40 cell lines following DNA damaging treatments

5.1. Introduction

PrimPol is a novel eukaryotic primase-polymerase of the AEP superfamily, and like prokaryotic and archaeal AEPs, is capable of DNA-dependent RNA/DNA priming and DNA-dependant DNA synthesis (Aidan Doherty and Luis Blanco, unpublished data). Preliminary characterisation of PrimPol in human cells, following RNAi depletion (Chapter 3) or in *PrimPol* $^{-/-}$ chicken cells (Chapter 4), revealed a possible role for this protein in nuclear DNA replication. Given PrimPol's dual activities as a DNA primase and polymerase, a number of roles can be hypothesised. Other than initiation of DNA replication at origins and Okazaki fragments, primases have been implicated in DNA damage tolerance by re-priming downstream of replication blocking DNA lesions, thus facilitating progression of replication on damaged DNA. This has been demonstrated *in vitro* in *E. coli* (Heller and Marians, 2006; Yeeles and Marians, 2011) and also proposed to occur in eukaryotes (Lehmann, 1972; Lopes *et al.*, 2006; Elvers *et al.*, 2011) although this has not been mechanistically described. PrimPol is also a DNA polymerase and therefore could be required for a DNA synthetic process, given the inherent flexibility of the AEP fold (Lao-Sirieix *et al.*, 2005; Pitcher *et al.*, 2007a), PrimPol could be required to synthesise DNA on difficult to replicate templates to assist the replicative polymerases, a role currently ascribed to the TLS polymerases or HR machinery (Lehmann AR, 2006; Guo *et al.*, 2009 ; Ulrich, 2011).

Damage tolerance was first reported following UV light irradiation (Rupp and Howard-Flanders, 1968). Since UV-C irradiation has been widely used to study DNA repair and TLS mechanisms as it induces the formation of two major helix distorting lesions, CPDs and (6-4)PPs (Rastogi *et al.*, 2010). UV photoproducts in DNA can prove lethal to cells as they disrupt DNA replication and transcription processes (reviewed in Batista *et al*., 2009), and so cells use NER to remove these lesions. However, NER can only operate on dsDNA otherwise cytotoxic DSB could arise while the repair process takes place; thus re-enforcing the need for TLS to occur during DNA synthesis phase to prevent the stalling of replicative polymerase at the sites of blocking lesions. Collaborative recruitment of NER (upstream and downstream the RF) and TLS (at the fork) pathways operates then to maintain RF progression along damage template (Gilljam *et al.*, 2012). More specifically, in the case of tc-NER, removal of the damaged DNA is essential to prevent apoptosis events related to transcription impairments (Lagerwerf *et al.*, 2011).

In line with the previous characterisation of PrimPol within chromosomal replication, a role in DNA damage tolerance following replication stress was then speculated. The aim of this

Chapter was thus to study the DNA damage survival phenotypes and cellular consequences of treating *PrimPol* $^{-/-}$ avian cells with a variety of damaging agents, including UV-C irradiation and replication stress inducing genotoxins. Involvement of PrimPol within damage tolerance pathways was then investigated. Finally, disruption of the intra-S checkpoint response in *PrimPol* $^{-/-}$ avian cells was initiated to study the influence of the novel primase-polymerase onto Chk1 pathway.

5.2. Analysis of DNA damage sensitivity of *PrimPol*$^{-/-}$ DT40 cells

5.2.1. Clonogenic survival experiments on methylcellulose

DT40 cells have been widely used to study DNA repair pathways by clonogenic survival due to their rapid growth (three times quicker than human cells) and the gene targeting advantages described earlier in the previous Chapter facilitating epistatic studies. Because these cells grow normally in suspension in liquid media, they have to be immobilised in a viscous medium containing methylcellulose to be able to form individual colonies (Simpson and Sale, 2006). The number of colonies obtained after DNA damaging treatment has to be normalised according to the plating efficiency, which corresponds to the number of colonies obtained for 100 cells inoculated (without any DNA damaging treatment). However, both PrimPol KO clones presented two distinct types of colonies on methylcellulose media when no prior damage was inflicted (figure 5.1). The first type was similar to the colonies formed in WT cells, circular shape with a defined outline, whereas an abnormal shaped bigger colony with a diffused outline was also visible is both mutants (figure 5.1, red arrows). In proportion, this second type of colony (to be referred to from here on as an abnormal colony) represented 50 to 60% of the total amount of colonies obtained in non-damage conditions. The human PrimPol complementation strain also presented these abnormal colonies, but to a lesser extent (20 to 30%). *PrimPol* $^{-/-}$ cells were exposed to a variety of DNA insults (DNA strand breaks induced by X-ray irradiation, methylation of bases by MMS, DNA crosslinking with cisplatin, and topoisomerase inhibition by camptothecin) and colonies examined for survival and growth. Abnormal colonies were evident in *PrimPol* $^{-/-}$ compared to WT. However, aberrant colonies were also visible in WT DT40 population treated with UV mimetic 4NQO chemical (figure 5.2). Abnormal colonies were also observed occasionally with WT cells but to a much lesser extent, for example after CPT treatments (figure 5.2). Using a GelCount automaton (from Oxford Optronix laboratory), which scans the plates at high resolution, a dual colony counting strategy

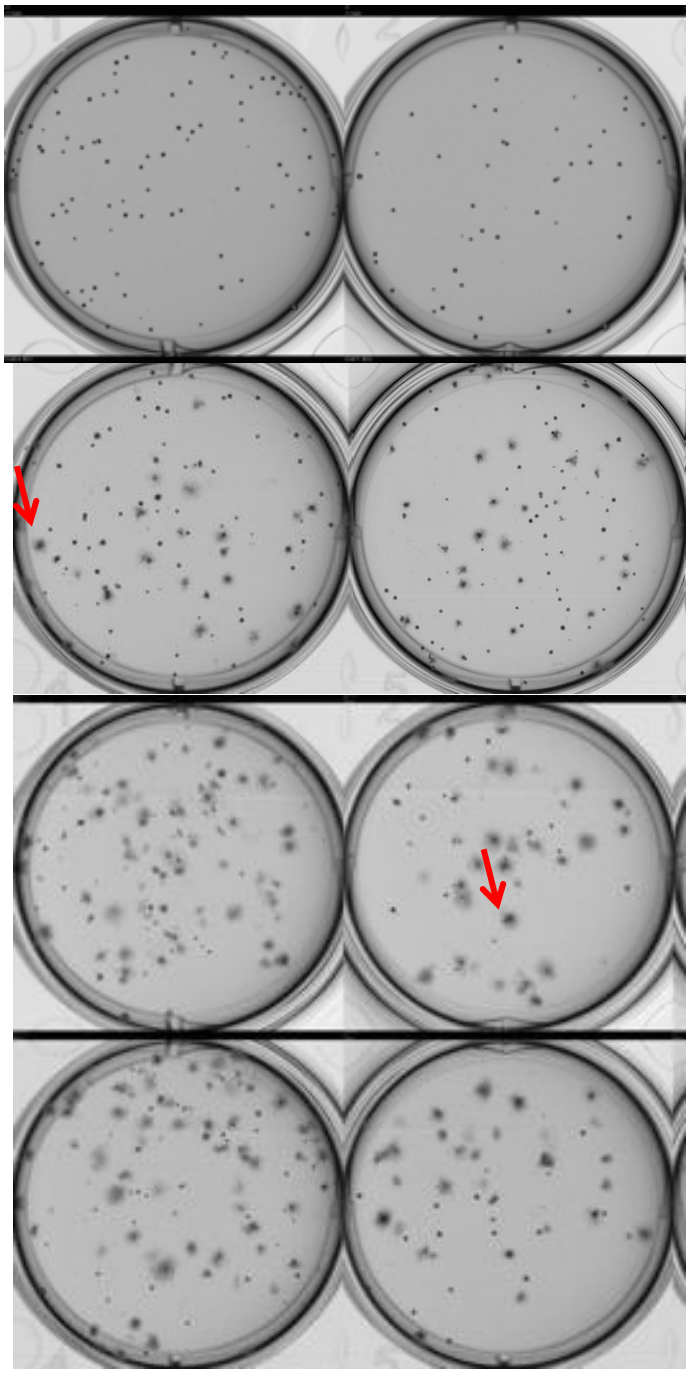

Figure 5.1: Abnormal colonies on methylcellulose of *PrimPol*$^{-/-}$ cells under unperturbed conditions.

WT, human conditional (hPrimPol protein expressed in *G. gallus PrimPol* $^{-/-}$) and both *PrimPol*$^{-/-}$ clones DT40 cultures were diluted and spread onto methylcellulose media and grown at 39°C for ~7 days until colonies start appearing. No DNA damaging treatments were induced before or after the spreading onto the cellulose. Images were taken with a GelCount automaton (Oxford Optronix laboratory). The red arrows correspond to examples of abnormal shaped colonies.

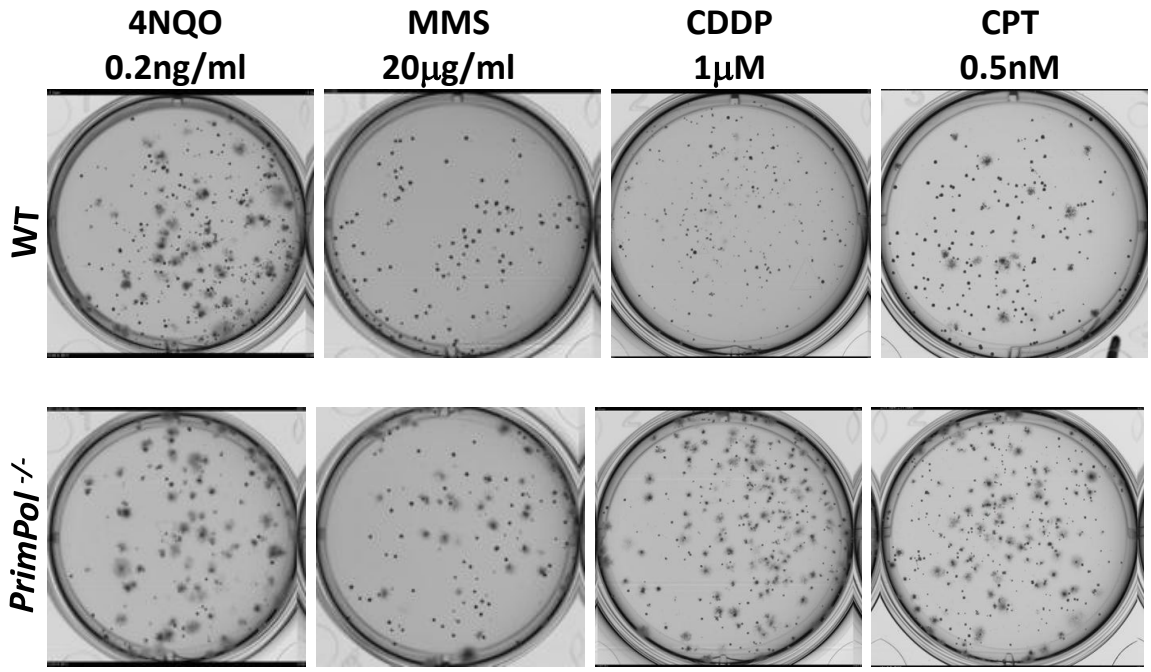

Figure 5.2: Abnormal colonies on methylcellulose after DNA damaging treatments.

WT cells (top row) or *PrimPol*$^{-/-}$ clone 2 (bottom row) were diluted and spread onto methylcellulose media containing 4-nitroquinoline-1-oxide (4NQO at 0.2 ng/ml), methyl methanesulfonate (MMS at 20 μg/ml), cisplatin (CDDP at 1 μM) or camptothecin (CPT at 0.5 nM) and were incubated at 39°C for seven days until colonies start formed. Pictures were taken with a GelCount automaton (Oxford Optronix laboratory).

was generated to automatize the counting process in order to increase the reproducibility of the assay. Unfortunately, results were still quite variable and time consuming (to correct the automatic distinction of both types of colony). In addition, the final analysis was too speculative (with the two types of colonies) and not well detailed in the literature, it was thus decided to look for an alternative solution.

5.2.2. Manual counting of UV-C cytotoxicity in avian *PrimPol* $^{-/-}$ cells

Whilst seeking an alternative method to analyse *PrimPol* $^{-/-}$ cells survival assays, an initial UV-C survival was performed by manual counting using a haemocytometer and Trypan Blue staining (figure 5.3A). This exclusion dye allows visualisation of blue dead cells unable to prevent absorption of the dye. Cells irradiated with different exposure times under 254 nm UV light were then left to recover for 48 hours at 39°C before being counted manually (figure 5.3A). WT DT40 cells were sensitive in a dose-dependent manner (figure 5.3A, black line). In contrast, both *PrimPol* $^{-/-}$ cell lines presented a stronger sensitivity to low doses of UV-C irradiation but an apparent resistance to higher UV fluences (figure 5.3A, purple lines). An inflection point was observed around 2 J/m^2 of UV-C irradiation, thus at 4 J/m^2 WT and KO cells showed similar UV-C cytotoxicity, and the absence of PrimPol appeared to even prevent the killing effect of higher fluences (figure 5.3A). Moreover, following 48 hours UV-C irradiation, DT40 cells were observed under differential interference contrast (DIC) microscopy and *PrimPol* $^{-/-}$ cells presented some surprisingly large cells compared to WT population (figure 5.3B). A recognized phenomenon in DT40 cells is its size expansion in G2 phase due to its large 4N nucleus (Yabuki *et al.*, 2009). Moreover, it has been reported in the literature that some DT40 cell lines presenting mitosis delay also have an expanded cell size (Um *et al.*, 2001; Swamynathan *et al.*, 2002). Furthermore, this phenomenon has been more frequently observed in yeast, with an increase in cell size observed in response to cell cycle perturbations (Turner *et al.*, 2012). We hypothesized then than DT40 cells lacking PrimPol are more affected by UV-C irradiation and stay arrested in G2 phase for a longer time than WT cells.

A

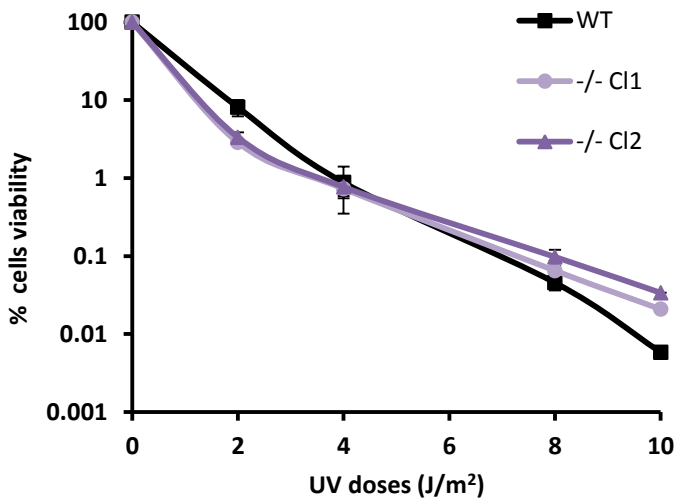

B

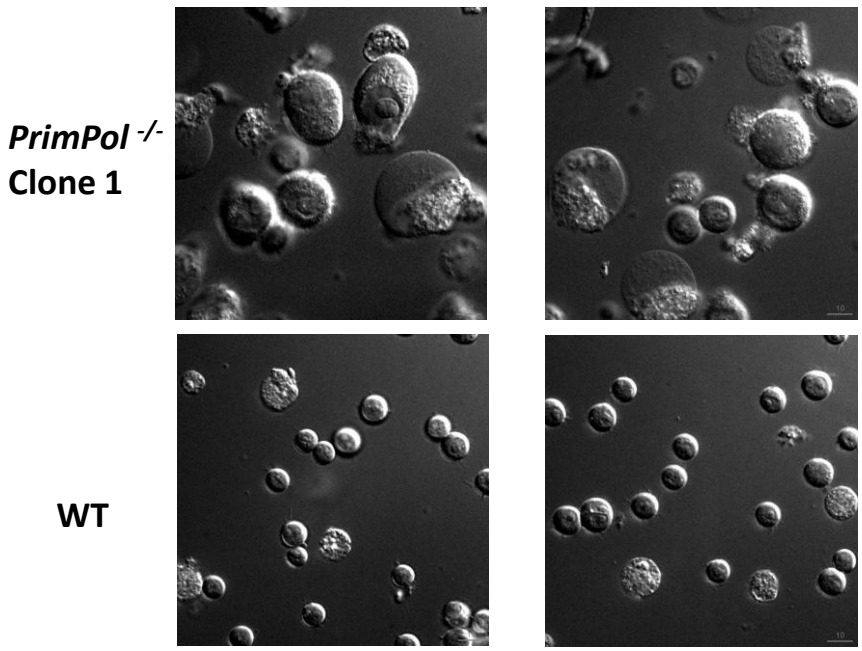

Figure 5.3: Effect of UV-C irradiation on cell morphology and cell survival.

(**A**) Cell viability was assessed in WT and *PrimPol* $^{-/-}$ cells (-/- Cl1 and Cl2) by manual counting (on haemocytometer) of Trypan Blue stained cells, 48 hours after UV-C irradiation. Error bars represent standard deviation of two independent experiments. (**B**) *PrimPol* $^{-/-}$ cells (clone 1) (top panel) and WT DT40 cells (bottom) were irradiated with 5 J/m^2 of UV-C light and allowed to recover for 48 hours in a 39°C incubator. Live cell imaging was processed using personal DV (DeltaVision) with DIC light (Differential interference contrast) microscopy. Both set of images (two different fields for each population) were taken using the same magnification lens (x 60). Scale bar in bottom right indicates 10 μm.

5.3. Analysis of *PrimPol* $^{-/-}$ cell viability following DNA damage treatments

5.3.1. Cell viability analysis with CellTiter-Blue assay

A recent publication from the Takeda group demonstrated a good correlation between cell viability assays performed 48 hours after DNA damaging treatment and clonogenic survivals in DT40 cells (Ji *et al.*, 2009). It has also been reported in the literature that other DNA repair DT40 mutants (CtIP$^{+/-/-}$BRCA1$^{-/-}$ clones) could not form colonies in semi-solid methylcellulose medium (Nakamura *et al.*, 2010). In these papers, the authors used an ATP based assay as the level of this metabolic marker correlate with the number of viable cells. Many different cell viability assays are commercially available notably CellTiter-Blue® which is based on efficient redox metabolic chain reactions to reduce resazurin reagent to the fluorescent compound resofurin (figure 5.4A). Although this fluorescent detection is less sensitive than in the ATP-based assay (CellTiter-Glo) used in the studies mentioned above, the detection sensitivity (390 cells in 96 well plate compared to 50 cells in CellTiter-Glo) should not be a problem here, as long as this assay is not used for high throughput screening. Cell number titration was then performed to assess the linearity of the reading and to confirm the proportionality between viable cells and fluorescence emission. Following an initial experiment to determinate the optimal incubation time of the CellTiter-Blue reagent with the cells, serial dilutions of WT and KO DT40 cells were performed (figure 5.4). Range of cells comprise between 10 000 to 80 000 cells ml^{-1} gave a linear fluorescent signal in both DT40 cell lines following 4 hours incubation at 39°C with CellTiter-Blue reagent (figure 5.4B). It was noticed a loss of the linearity of the signal could occur in the presence of too many cells (figure 5.4B, error bar at 80 x 10^3 cells with purple line). Nonetheless, *PrimPol* $^{-/-}$ cells behaving in a similar manner than WT DT40, CellTiter-Blue technology can then be used to determine cell viability following DNA damaging treatments, as long as the fluorescence readings are obtained within a linear range (with a cell concentration around 40 x 10^3 cells ml^{-1}). Cell number titration curves have thus to be performed for each experiment to determine the end of the linearity zone. Moreover, saturated signal samples can be easily discriminated by the pink coloration of the well containing too much resofurin.

5.3.2. Cell viability analysis with CellTiter-Blue assay following UV-C irradiation

Following preliminary analysis of the cell viability following UV-C irradiation by manual cell counting on haemocytometer with Trypan Blue staining (figure 5.3A), a more accurate

A

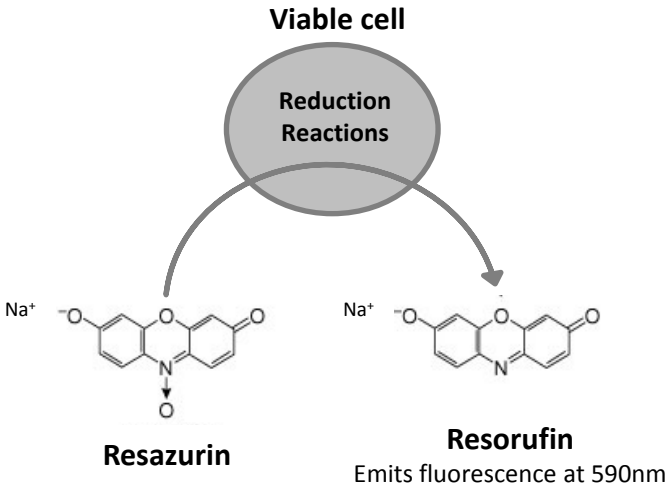

B

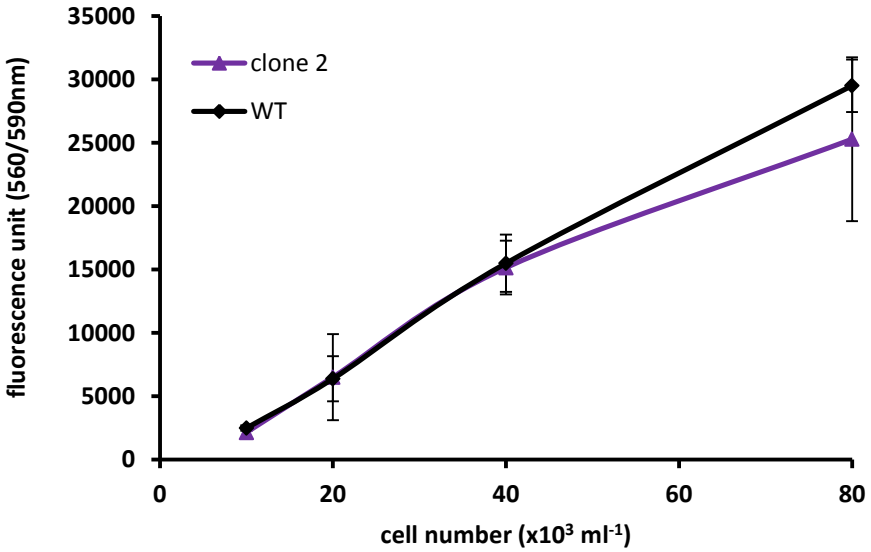

Figure 5.4: Cell viability assay using CellTiter-Blue technology.

(**A**) Cartoon depicting the conversion of CellTiter-Blue substrate Resazurin to the fluorescent molecule Resorufin by reduction reactions occurring in viable cells (picture taken from Promega online documentation). (**B**) Cultures of non treated WT and *PrimPol* $^{-/-}$ (clone 2) cells were manually counted (with an haemocytometer) and serial diluted into 96 well plate before CellTiter-Blue substrate was added and the plate incubated at 39°C for 4 hours. Fluorescence was read at 590 nm (resorufin excitation at 560 nm) using a GloMax plate reader. Error bars denote standard deviation of triplicate dilutions for each population.

assessment was performed by using CellTiter-Blue technology as described in section 5.3.1. The reagent was added at 48 hours following UV-C irradiation, and both *PrimPol* $^{-/-}$ cell lines were again more sensitive to UV-C doses below 4 J/m^2 only (figure 5.5A, top plot) as previously observed (figure 5.3A). Following 8 J/m^2 WT DT40 appeared more sensitive to the irradiation treatment than in the absence of PrimPol (figure 5.5A, top plot). The low doses sensitivity was confirmed as a 4-fold decrease of the fluorescence was recorded at 0.5 and 1 J/m^2 and the survival rate was reduced by half in *PrimPol* $^{-/-}$ cells compared to WT DT40 following 2 J/m^2 UV-C irradiation (figure 5.5A, bottom left plot). This small difference (2 times) was nonetheless reproducible, as indicated by the t-test performed at 2 J/m^2 corresponding to 6 independent experiments (figure 5.5A, bottom left plot). A Pol η KO DT40 cell line (kindly provided by Takeda and Sale laboratories) was used as a positive control of UV-C sensitivity (Kawamoto *et al.*, 2005) and also to compare *PrimPol* $^{-/-}$ phenotype to that of a well-characterised TLS polymerase. When cell viability was assessed 48 hours after irradiation, phenotypes observed in both polymerases (Pol η and PrimPol) deficient cells were very similar. However, it was quite surprising to see almost no sensitivity was recorded following irradiation with 4 and 8 J/m^2 in *Polη* $^{-/-}$ cells (figure 5.5A, top right plot) which does not correlate with clonogenic survival data from the literature (Kawamoto *et al.*, 2005; Hirota *et al.*, 2010). Taken together with the previous conclusions drawn from the morphologic observations of PrimPol irradiated cells (figure 5.3B), a G2 cell cycle arrest was suspected to explain this lack of apparent sensitivity at high UV-C fluences. To verify this hypothesis, cell viability was assessed following various recovery time points after irradiation to overcome this potential cell cycle arrest. CellTiter-Blue measurements performed 72 hours after irradiation gave similar survival patterns than the one obtained at 48 hours (data not shown), but at later times post-irradiation (96, 120 and 144 hours), *Polη* $^{-/-}$ cells sensitivity at high UV-C fluences became more obvious (figure 5.5B). However, loss of PrimPol only affects cell viability after low doses of UV-C irradiation (below 2 J/m^2) as the cells behaved in a similar manner than WT DT40 cells above this UV-C dose (figure 5.5B). To confirm the low dose sensitivity was specific of PrimPol's gene disruption, human PrimPol protein expressed in an avian *PrimPol* null background was also tested (figure 5.5, orange curve). Presence of the ectopic human PrimPol protein fully rescued the UV sensitivity of *PrimPol* $^{-/-}$ cells at 2 J/m^2, but only partially complemented the loss of endogenous PrimPol at 0.5 and 1 J/m^2, with 66% and 50% complementation observed respectively at these doses (figure 5.5, orange curve). Taken together, these data suggest PrimPol protects vertebrate cells from low doses UV-C induced cytotoxicity.

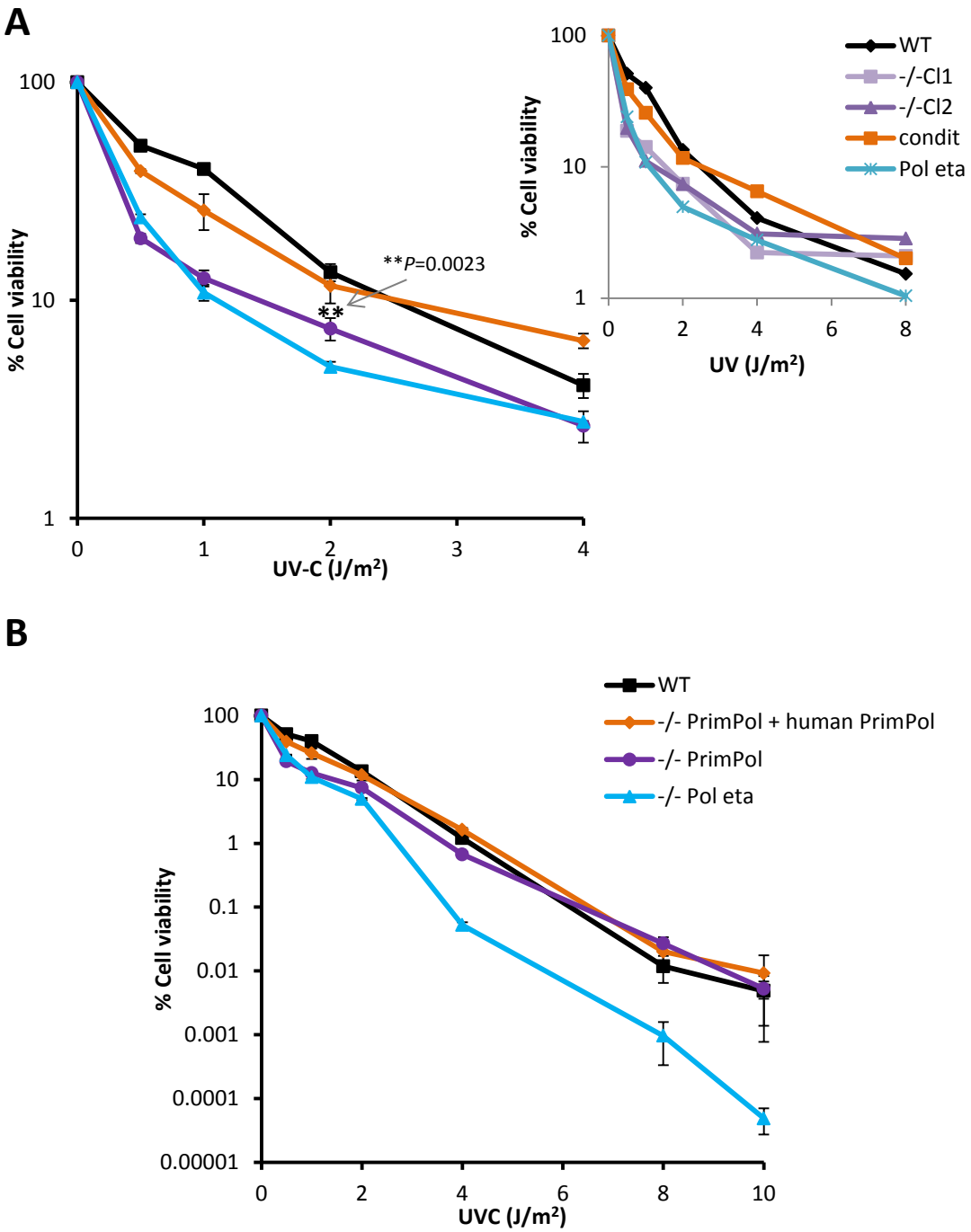

Figure 5.5: CellTiter-Blue viability assay after UV-C irradiation.

(**A**) Cells irradiated with UV-C in PBS were re-suspended in complete media and allow to recover for 48 hours before viability was assessed using CellTiter-Blue technology. Right Plot shows both *PrimPol* $^{-/-}$ clones (light and dark purple) and UV-C treatments up to 8 J/m^2, whereas left plot presents the average of both *PrimPol* $^{-/-}$ clones (purple) and UV-C doses up to 4 J/m^2. Error bars denote standard deviation of at least three independent experiments (*PrimPol* $^{-/-}$ at 2 J/m^2, t-test assessed with two tails moments). (**B**) Irradiated cells were left to recover for 144 hours or diluted in complete media if necessary (UV-C doses < 4 J/m^2 and non irradiated cells) before cell viability was measured to avoid cell cycle arrest masking UV sensitivity. Error bars represent standard deviation of 2 experiments.

5.3.3. Cell viability analysis with CellTiter-Blue assay following 4NQO treatments

To further characterise the phenotype observed after UV-C irradiation, the chemical reagent 4NQO was tested in a similar cell viability assay. Indeed, 4NQO is also referred to as a UV mimetic agent as it forms DNA adducts which are repair by NER (Snyderwine and Bohr, 1992) or otherwise, would lead to RF stalling. Three principal adducts are resulting from the attack of guanine and adenine bases by this drug, N-(guan-8-yl)-4-aminoquinoline 1-oxide (or dGuo-C8-AQO, modification of nitrenium anion in C8), dGuo-N2-AQO and dAdo-N6-AQO (resulting of the carbocation attack of guanine N2 and adenine N6 respectively) (Galiegue-Zouitina *et al.*, 1986). These bulky adducts, like CPDs and (6-4)PPs induced by UV light, pose a physical blockage for replicative polymerases. A chronic treatment with 4NQO for 48 hours was inflicted to the different DT40 cell lines before cell viability was assessed by CellTiter-Blue technology (figure 5.6A). In a similar way to what previously observed after UV-C irradiation, a low dose sensitivity was apparent for PrimPol and Pol η deficient cells (figure 5.6A). Also, after treatment with higher concentrations of this UV mimetic drug, *PrimPol* $^{-/-}$ cells exhibit an apparent resistance to this toxic agent. Indeed, a 3.5-fold increase of cell viability was observed after 3.2 ng/ml of 4NQO exposure in *PrimPol* $^{-/-}$ cells in comparison with WT DT40 cells (purple and black lines, figure 5.6A). Moreover, complementation with human PrimPol protein did not reverse this phenotype (orange line, figure 5.6A). To verify if this apparent resistance was due to a cell cycle arrest (as previously speculated after UV-C irradiation), a recovery time course experiment was performed after a 48 hours chronic treatment with 4NQO (figure 5.6B, C, D). After removal of the carcinogenic reagent, WT cells recover quicker than PrimPol and Pol η KO cells, allowing the visualisation of the cytotoxic effect of the drug. Following 48 hours recovery, a 10-fold decrease of cell viability was observed in *PrimPol* $^{-/-}$ cells, and at 72 hours after removal of the drug, a 50-fold difference was observed between WT and PrimPol deficient cells (figure 5.6B and C, respectively). However, following 96 hours recovery, *PrimPol* $^{-/-}$ cells were not arrested anymore as the difference in cell viability was less consequent as a 35-fold decrease was observed (figure 5.6D). In the three recovery time points tested, 48, 72 and 96 hours, *PrimPol* $^{-/-}$ cells exhibited a slightly stronger sensitivity than *Polη* $^{-/-}$ cells (figure 5.6, blue and purple lines). However, expression of ectopic human PrimPol protein appeared to rescue PrimPol deletion in a 4NQO dose dependent manner; a full rescue was observed at low doses (0.5 and 1 ng/ml 4NQO), and a ~70% rescue was observed at 1.6 ng/ml 4NQO, but a partial rescue was only achieved after exposure to 3.2 ng/ml 4NQO (figure 5.6). Taken together, these data suggest PrimPol protects cells against cytotoxicity induced by

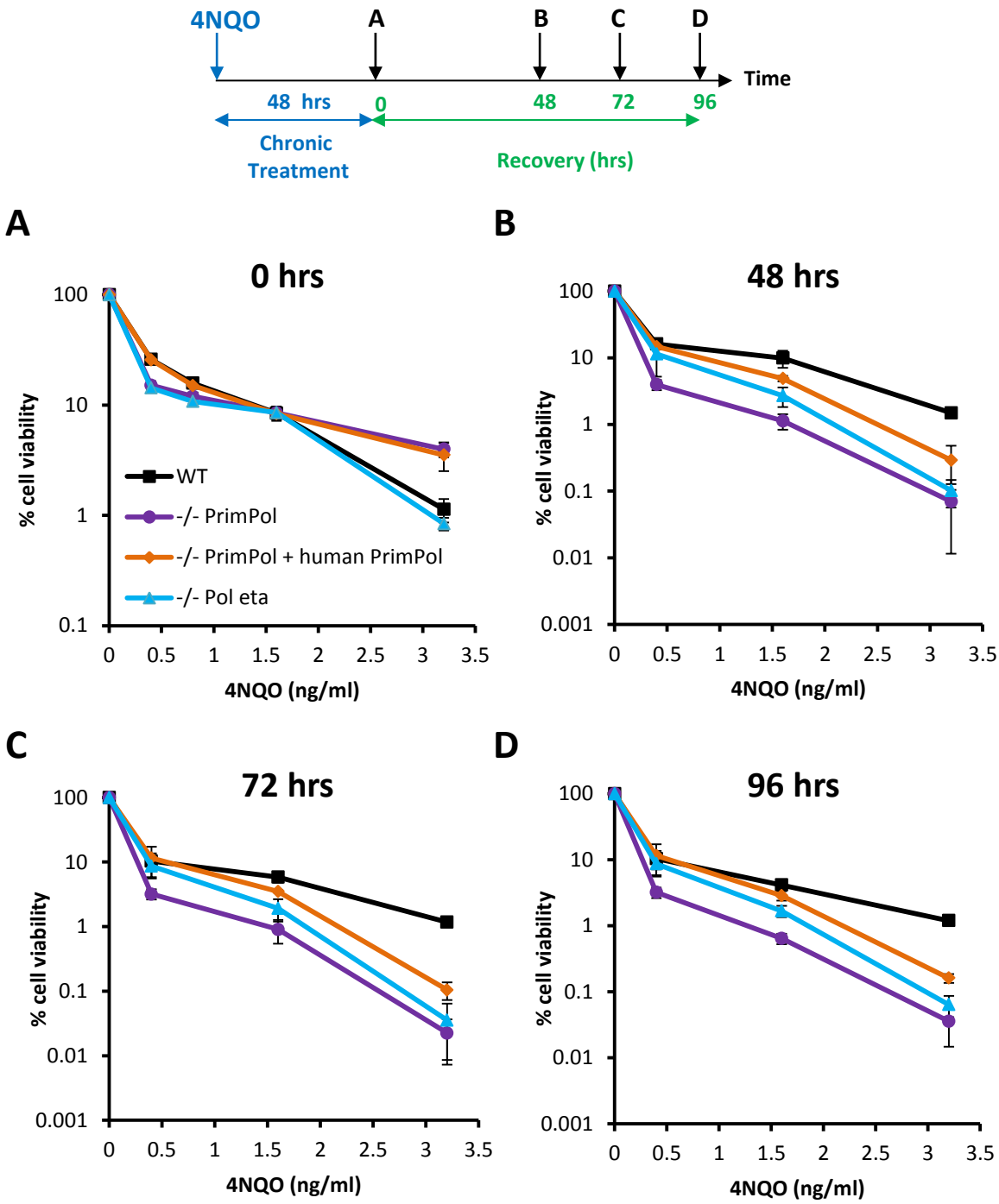

Figure 5.6: CellTiter-Blue viability assay after 4NQO chronic treatment.

Schematic explaining the time scale of the experiment; 4-nitroquinoline 1-oxide (4NQO) was diluted into the growth media and left with WT (black), *PrimPol* $^{-/-}$ (purple), human conditional (orange) and *Polη* $^{-/-}$ (blue) DT40 cells for 48 hours chronic treatment before the cell viability was assessed by CellTiter-Blue technology at different time point, 0 (**A**), 48 (**B**), 72 (**C**) and 96 hours (**D**). Cultures were diluted in complete media (without any drug) every 24 hours to assess **B**, **C** and **D** time points. Error bars represent standard deviation of three independent experiments (**A**) or two independent experiments (**B**, **C**, and **D**). *PrimPol* $^{-/-}$ (purple line) corresponds to the average of both KO clones.

the chemical drug 4NQO, and thus confirm an implication of this novel primase-polymerase in response to replicative stress.

5.3.4. Cell viability analysis with CellTiter-Blue assay following X-ray irradiation

To investigate further the implication of PrimPol following DNA damaging treatments and determine if this novel factor could also be involved in response to other type of damage than bulky lesions, cell viability of DT40 cells was assessed following X-ray irradiation. Ionizing radiation leads to the creation of SSB and DSB mainly, highly toxic for the cells (Hada and Georgakilas, 2008). Also, previous studies from the Doherty lab have shown the direct involvement of bacterial AEP primases (PolDom) in the NHEJ break repair pathway (Pitcher *et al.*, 2007b). Irradiation with a range of X-ray doses was performed on DT40 cells serial diluted on liquid media. Cells were allowed to grow for 48 hours at 39°C before CellTiter-Blue reagent was added and the fluorescence signals recorded. No significant differences were observed between WT, both *PrimPol* $^{-/-}$ cell lines and KO cells expressing the human PrimPol protein, with all cell lines surviving in a very similar manner to irradiation with 4 and 8 Gy (figure 5.7). According to this result it is possible to conclude PrimPol is not needed in response to any DNA damaging treatments, such as DSB, but is needed following bulky adducts formation. In line with this, no triton-resistant foci were observed following ionising radiation in Hek293 cells stably over-expressing Flag-strep or HA tagged PrimPol (Sean Rudd, Aidan Doherty, personal communication; appendix A) as previously mentioned in section 3.5. It is thus possible to conclude that eukaryotic and bacterial AEP members, PrimPol and PolDom respectively, have evolved with distinct roles, as an implication of human PrimPol within NHEJ pathway seems unlikely but still remains to be fully established.

5.4. Role of PrimPol in chromosomal replication of UV damaged DNA

Having confirmed *PrimPol* $^{-/-}$ cells were specifically sensitive to replication stress (UV-C, 4NQO) but not to DSB inducer (X-ray irradiation), we decided to focus first on characterising phenotypes associated with UV-C irradiation. Moreover, as discussed in the previous Chapter, the absence of PrimPol during unperturbed S-phase is accompanied with a decrease of RF speed, and a slight accumulation of cells in late S or G2 phase (figures 4.17 and 4.18). Therefore, a role for PrimPol in DNA damage tolerance was hypothesised. DNA damage

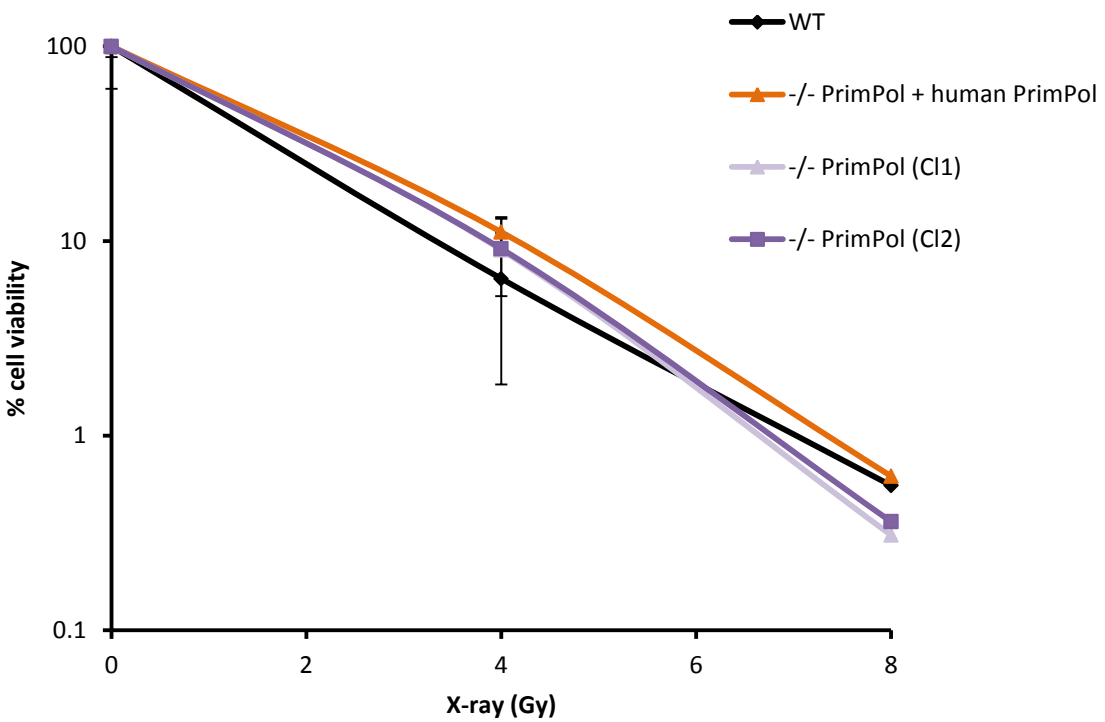

Figure 5.7: CellTiter-Blue viability assay after X-ray irradiation.

Cell viability of WT DT40 cells (black), human conditional or *PrimPol* $^{-/-}$ cell expressing human PrimPol protein (orange) and both *PrimPol* $^{-/-}$ clones (light and dark purple) was assessed by using CellTiter-Blue technology 48 hours after X-ray irradiation. Error bars denote standard deviation of two independent experiments.

tolerance can occur either during ongoing replication or in a post replicative manner (Ulrich, 2011), thus PrimPol's involvement in these two processes was investigated.

5.2.1. Involvement of PrimPol in DNA damage tolerance mechanisms

5.2.1.1. PrimPol requirement for replication fork progression

It was decided to test whether PrimPol was required for RF progression on UV-C damaged DNA (figure 5.8A). Following 2, 4 or 8 J/m^2 UV-C irradiation doses, a 20 minutes pulse with ^{3}H thymidine was performed and the uptake of radioactive nucleotide was normalised against ^{14}C thymidine pre-labelling (figure 5.8). The thymidine up-take was compared to mock irradiated cells for each population in order to compare only the influence of irradiation onto the replication rate between the different populations, and to discard the defect in thymidine incorporation observed previously in non-irradiated *PrimPol* $^{-/-}$ cells (figure 4.18). In both WT and PrimPol KO cells, a decrease in ^{3}H thymidine incorporation was observed following UV-C irradiation (figure 5.8), which is consistent with an activation of the intra-S checkpoint at the sites of UV-damaged DNA, physically blocking RF progression (reviewed Kaufmann, 2010). However, both PrimPol KO clones presented a further decrease in replication rate when compared to WT cells following UV-C exposure (figure 5.8B). A 1.2-fold decrease was observed following 2 and 4 J/m^2 UV-C irradiations, and a 1.4-fold decrease following 8 J/m^2 UV-C irradiation, with the replication rate being diminished from 57% to 41% in the absence of PrimPol (figure 5.8B). Notably, *PrimPol* $^{-/-}$ cells irradiated with 2 J/m^2 UV-C had a similar incorporation rate (66%) than WT cells irradiated with 4 J/m^2 UV-C; similarly, after 4 J/m^2 UV-C irradiation, absence of PrimPol generated a decrease of the replication rate to the same level than WT cells irradiated with 8 J/m^2 UV-C (56% ; figure 5.8B). This result implies PrimPol is required for efficient replication of UV-C damaged DNA *in vivo*.

To further characterise PrimPol's involvement in the replication of UV damaged DNA, analysis of RF progression following UV-C irradiation was undertaken in the *PrimPol* KO clones. As previously described in section 4.4.2, the DNA spreading method was adapted here to analyse newly synthesised DNA following UV-C irradiation, with the cells being exposed to 20 J/m^2 UV-C between the CldU and Idu labelling periods (figure 5.9A). Both halogenated nucleotide signals were visualised by immunofluorescence microscopy (figure 5.9B) and accurately measured using the software OMERO (Allan *et al.*, 2012) in order to calculate the ratio between the "incorporation rate" before and after UV-C irradiation, or CldU / IdU signals

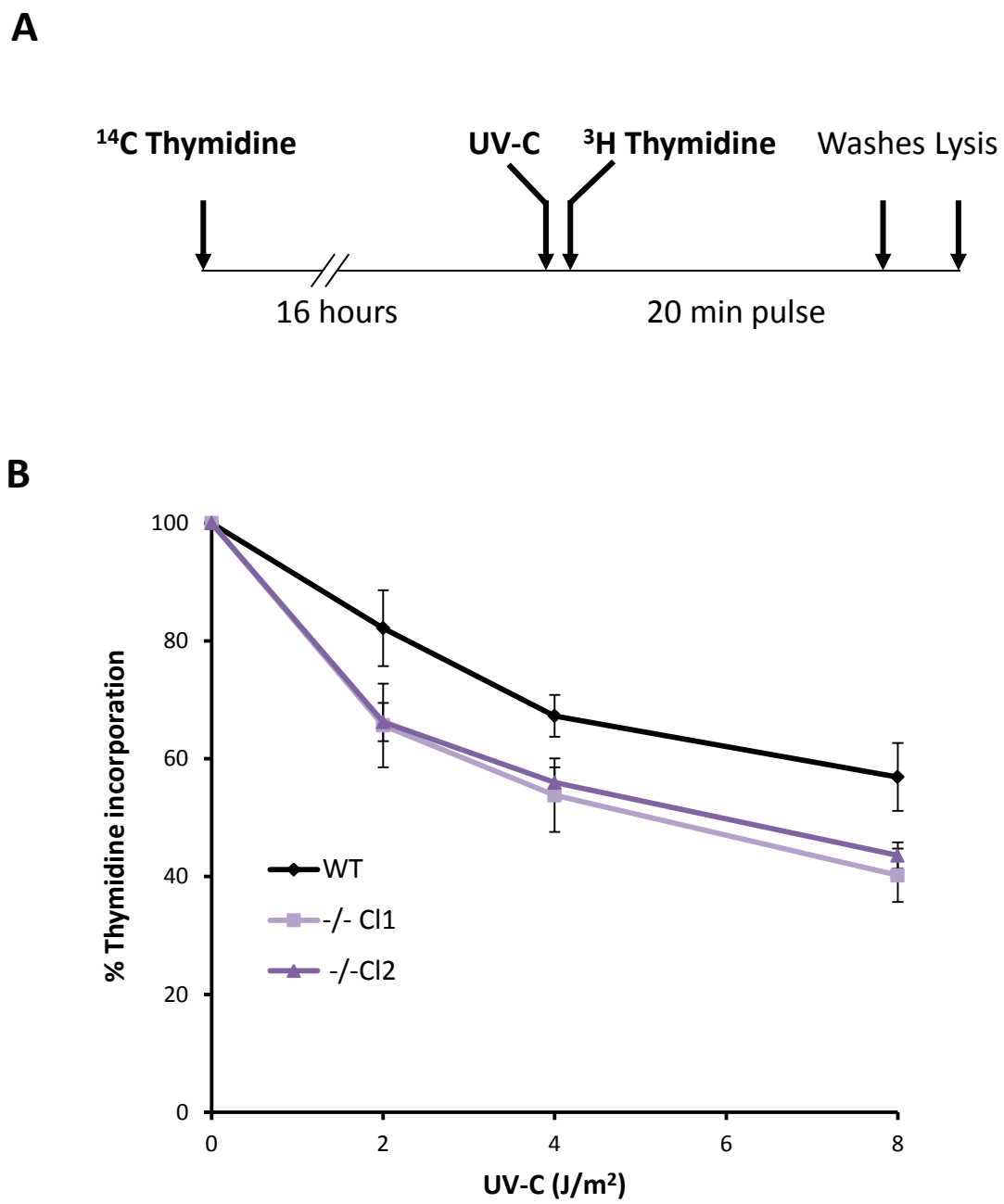

Figure 5.8: Analysis of DNA replication rate following UV-C irradiation.

(**A**) Schematic depicting the labelling process of the thymidine uptake experiment. (**B**) WT (black line) and both *PrimPol* $^{-/-}$ (light and dark purple lines) cells were pulse-labeled for 20 minutes with tritium (^{3}H) thymidine following UV-C irradiation. Incorporation rate was calculated and normalised against undamaged cells using ^{14}C thymidine overnight pre-labeling for total DNA normalisation. Error bars represent standard deviation of 3 independent experiments.

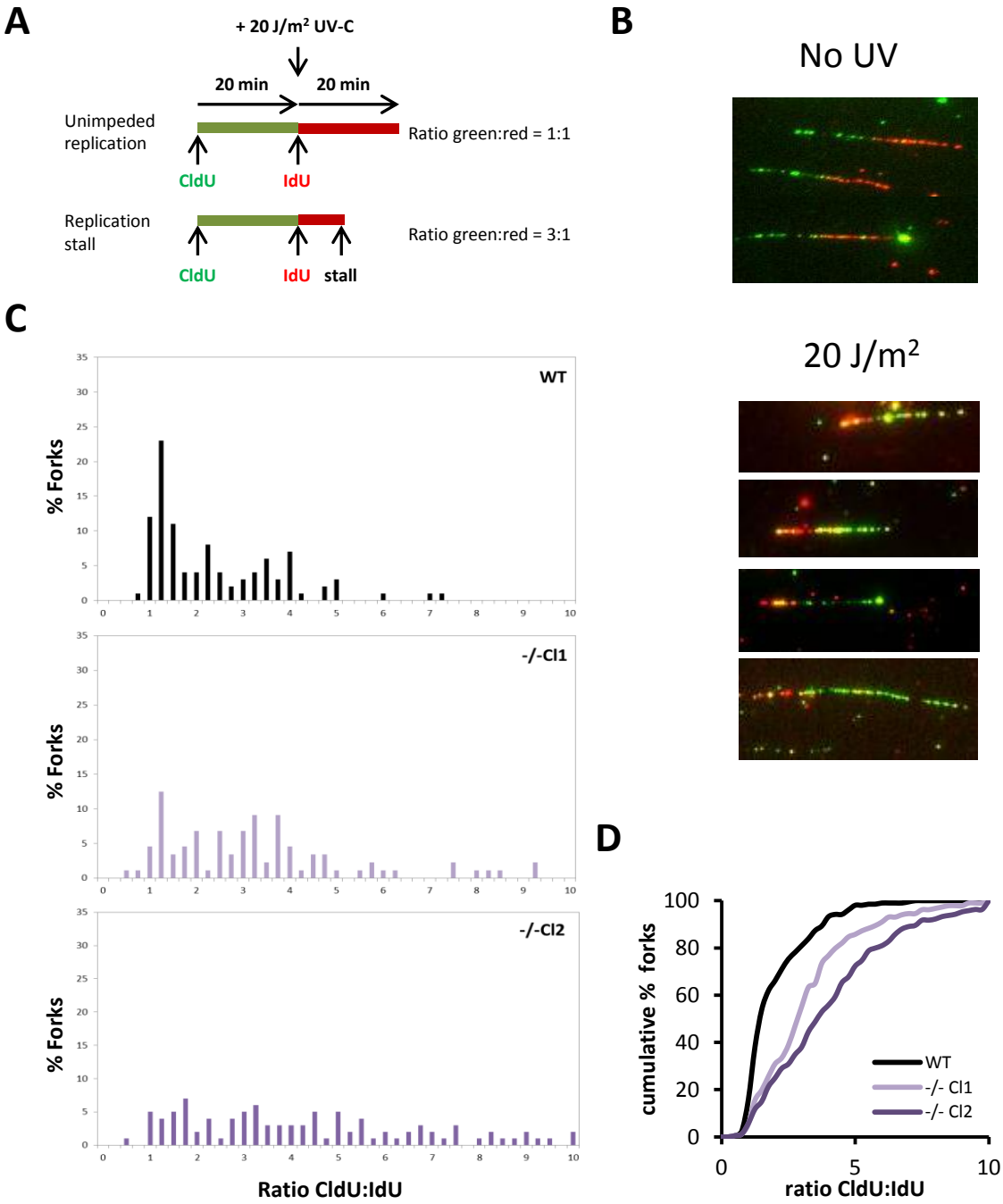

Figure 5.9: Replication fork progression after UV-C irradiation.

(**A**) Cartoon depicting the DNA fiber labeling process and order of incorporation of thymidine analogues CldU (before UV-C exposure) and IdU (after 20 J/m^2 UV-C irradiation). (**B**) Example of fibers images taken under normal replication condition (no UV, top panel) or after UV-C irradiation (20 J/m^2, bottom panels) following immunofluorescence staining. (**C**) CldU and IdU tracks visualised as in (**B**) were measured using OMERO software. CldU:IdU ratios distribution was assessed for WT DT40 cells (upper panel) and both *PrimPol* $^{-/-}$ clones (middle and lower panels). Data are representative of 2 sets of experiments with at least 100 fibers scored each time. (**D**) Average of both experiments mentioned in (**C**) are represented as a cumulative percentage of forks at each ratio following 20 J/m^2 UV-C irradiation.

Because both labelling periods were performed for 20 minutes, this ratio corresponded to the average length of green tracks divided by the average length of the red tracks. When RFs did not encounter any obstacles during those 40 minutes, this ratio was close to 1, whereas forks blocked or slowed down by UV-C damaged DNA induced a shortening of the second track (red tracks) resulting in an increase of this ratio (figure 5.9A). According to Edmunds and co-workers, following a 20 J/m^2 UV-C irradiation treatment in DT40 cells, RFs have a very high probability to encounter impediments (>85%) as pyrimidine dimers could be found every 11 kb along the genome (Edmunds *et al.*, 2008). In this study, the mean ratio obtained after this dose in WT DT40 cells was around 2.2 compared to 1.5 here (figure 5.9C and D), suggesting either a weaker irradiation treatment (variation of the UV source) or a difference inbetween the two WT DT40 strains used. Nonetheless, *PrimPol* $^{-/-}$ cells showed a substantial increase in the spread and mean of CldU:IdU ratios, with averages of 3 and 3.5 for clone 1 and 2 respectively (figure 5.9C and D), thus corresponding to a 2-fold increase of the WT ratio. In Edmunds' study, a 1.6-fold increase of the WT ratio was observed in the absence of Rev1 (Edmunds *et al.*, 2008). These data indicate that, in the absence of PrimPol, a marked increase in delay or blockage of RF progression is observed after UV-C irradiation, demonstrating that PrimPol is required for the efficient replication of UV-C damaged DNA, possibly implicating this protein in damage tolerance.

5.2.1.2. Analysis of post-replication repair capacity in *PrimPol* $^{-/-}$ DT40 cells

DNA damage tolerance can occur directly at stalled RF but also during later processes following the bulk of DNA synthesis (PRR) (reviewed in Ulrich, 2011). One particular pathway has been well studied in response of UV irradiation, the characterisation of the TLS polymerase Pol η, responsible for causing the skin disorder XP-V (Masutani *et al.*, 1999; Johnson *et al.*, 1999). Prior to the identification of the gene, XP-V cells had been first characterised as being impaired for DNA synthesis following UV irradiation (Lehmann *et al.*, 1975). The technique employed then used tritiated thymidine to label newly synthesized DNA following UV-C irradiation, and alkaline sucrose gradient centrifugation to separate the size of the DNA molecules, as first described by Rupp and Howard-Flanders in 1968. Indeed, they were the first to discover that DNA synthesis of UV irradiated NER-deficient *E. coli* cells was discontinuous, with the resulting gaps subsequently sealed (Rupp and Howard-Flanders, 1968). The term PRR was thus employed to refer the repair of these ssDNA gaps left encompassing bulky (6-4)PPs or CPDs lesions following RF progression. Therefore, to understand whether PrimPol is also involved in

filling these gaps or in re-priming the RF downstream these bulky lesions and thus creating the gaps, a PRR assay was performed in *PrimPol* $^{-/-}$ clones (figure 5.10). Pulse-chased samples from non-treated or UV-C irradiated DT40 cells were lysed, loaded onto sucrose gradient and separated by velocity sedimentation as described in figure 5.10A. In the control *Pol* $\eta^{-/-}$ cells, irradiated DNA had a smaller sedimentation rate on the sucrose gradient than non-irradiated sample (figure 5.10B, red arrow) characteristic of a PRR defect and the incapability to fully fill the gaps and complete DNA replication. However, UV-C irradiated *PrimPol* $^{-/-}$ cells molecular weight profile (figure 5.10, red line) was following the same pattern than non-damaged *PrimPol* $^{-/-}$ cells (figure 5.10, blue line), similar to WT DT40 cells (figure 5.10, middle and top panels respectively). These results suggest then that PrimPol is not required for post-replicative gap filling mechanism.

5.2.2. Analysis of cell cycle progression in *PrimPol* $^{-/-}$ cells following UV-C irradiation

Previous data support a role of PrimPol in assisting RF progression on UV damaged DNA but its participation in PRR mechanisms seems unlikely. To confirm these findings and to address the temporal recruitment of PrimPol following UV-C irradiation, a cell cycle analysis was performed. A BrdU and PI double staining protocol was used to follow the progression of UV-C irradiated cells through the different stages of the cell cycle in the absence of PrimPol (figure 5.11 and 5.12). Depending on when the BrdU pulse was performed (before or after UV-C irradiation) and the amount of time between the pulse and the fixation of the cells, two different analyses were achieved.

In the first analysis, the cells were irradiated first and then left to recover for various amounts of time (2 to 24 hours) before performing a 20 minutes BrdU pulse and immediate collection (figure 5.11A). Following 2 J/m^2 UV-C irradiation, both WT and *PrimPol* $^{-/-}$ cell cycle kinetics were similar and presented an enrichment of G2 cells at 16 hours post-irradiation, which was slightly more pronounced in *PrimPol* $^{-/-}$ cells (figure 5.11B). However, at 24 hours post UV-C irradiation, an important decrease of the proportion of S-phase *PrimPol* $^{-/-}$ cells was observed compared to WT DT40 cells, with only 18% of the KO population being in S-phase compared to 32% in WT cells (figure 5.11B). The proportion of G2 cells being only slightly higher, 32% instead of 27% in WT cells, and an equal proportion of G1 cells being recorded (9.5%), this difference of S-phase could be explained by an increase proportion of dead cells (figure 5.11B). Indeed, an increase in the sub-G1 population was recorded with 32% of *PrimPol*

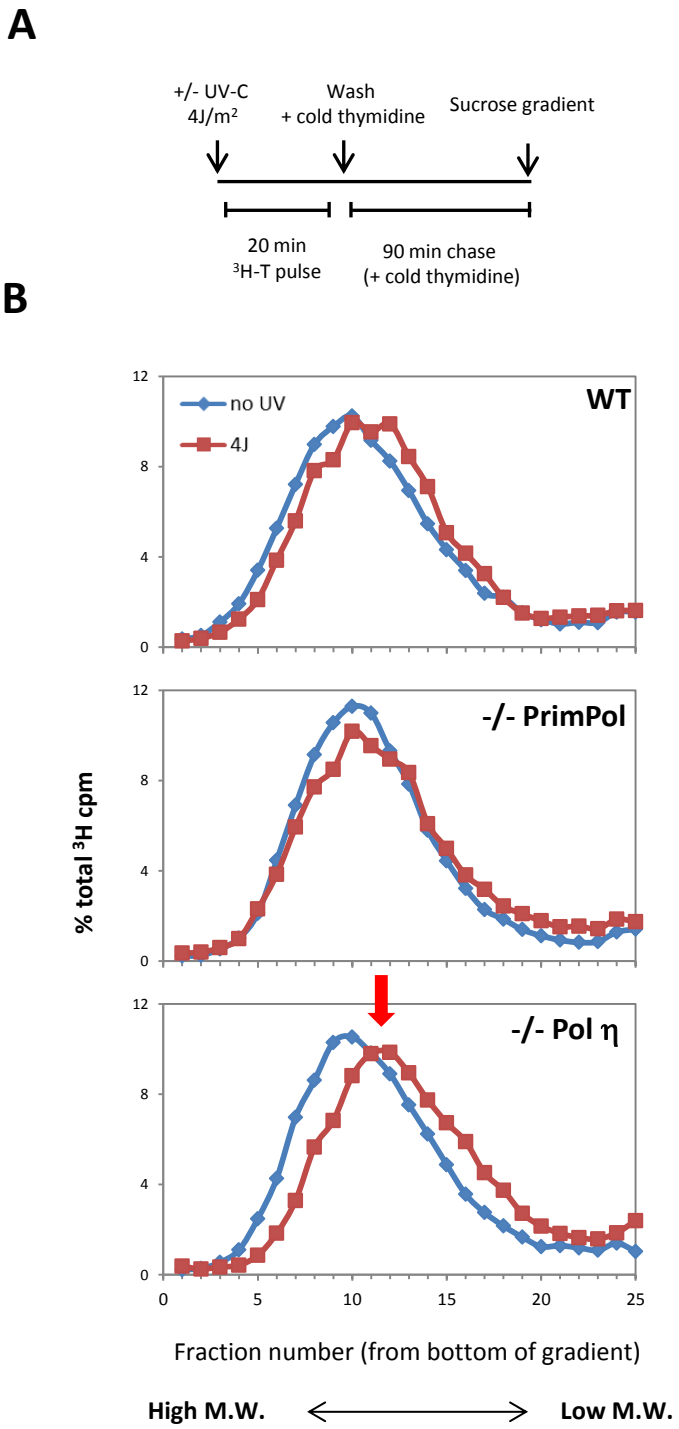

Figure 5.10: Post-replication repair after UV-C irradiation.

(**A**) Cartoon depicting velocity sedimentation analysis of radio-labeled nascent DNA following exposure of 4 J/m^2 UV-C. (**B**) Relative amount of radioactivity in each fraction of the gradient was plotted in order to visualize the cell capability to fill post-replicative single-stranded gaps left behind replication forks after exposure of 4 J/m^2 UV-C (red line). The red arrow indicates post-replicative repair defect observed in Pol η deficient cells (bottom panel). Data representative of two experiments for *Polη* $^{-/-}$ and at least three for *PrimPol* $^{-/-}$.

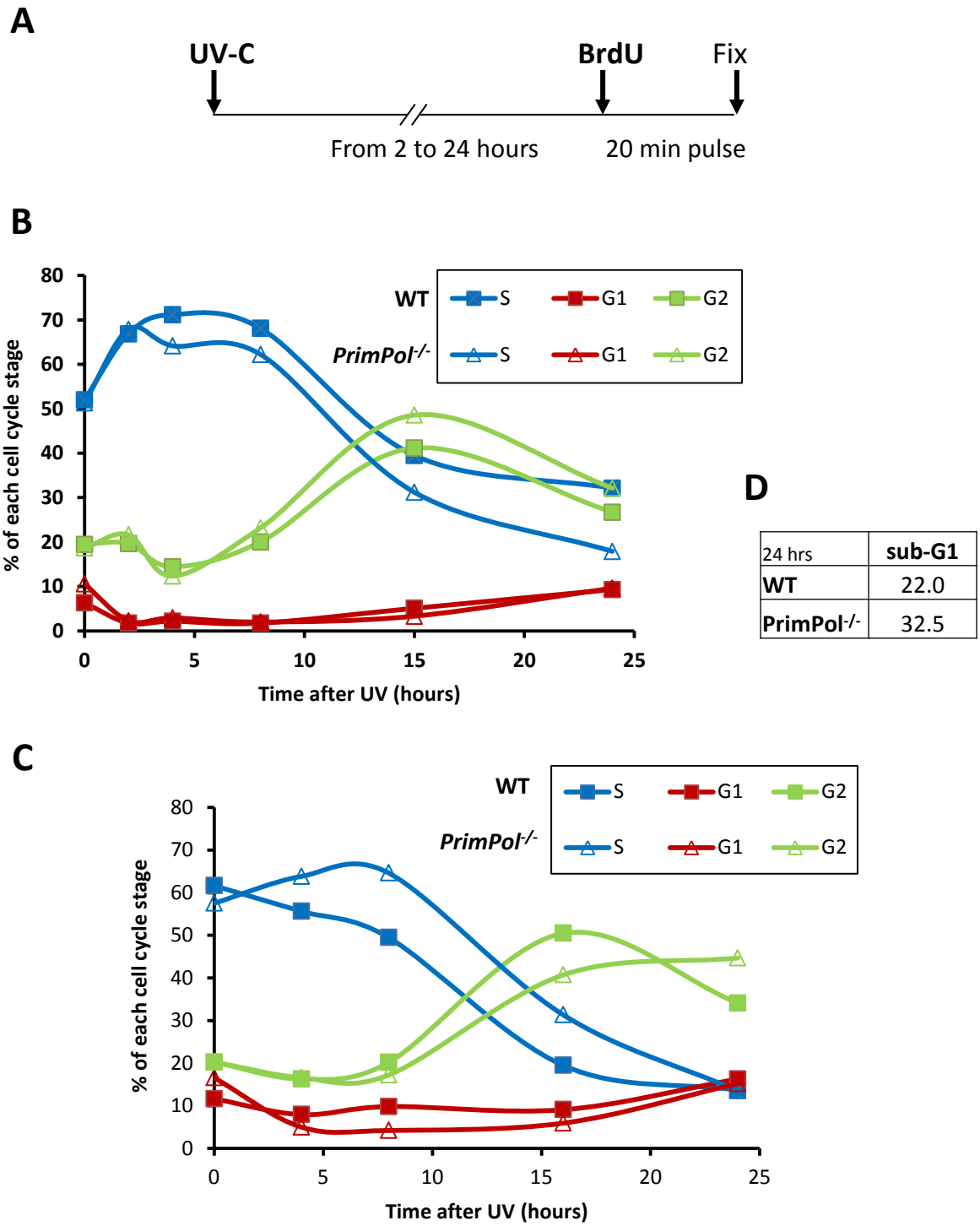

Figure 5.11: Analysis of cell cycle progression following UV-C irradiation.

(**A**) Schematic depicting the experimental procedure. Time course experiments performed after 2 J/m^2 (**B**) or 5 J/m^2 (**C**) UV-C irradiation. At different times after irradiation, cells were pulse-labelled with BrdU and stained with PI for flow cytometry analysis. Percentage of S-phase cells (BrdU positive) are represented in blue lines, G2 cells in green and G1 cells in red. Samples obtained from WT cells are indicated with a square, whereas *PrimPol* $^{-/-}$ samples with a triangle. (**D**) Proportion of sub-G1 cells population recorded at 24 hours following 2 J/m^2 UV-C irradiation. Data representative of two independent experiments.

$^{-/-}$ cells compared to 22% of WT cells contained less than 2N DNA content (figure 5.11D). On the other hand, following 5 J/m^2 irradiation, cell cycle progression of *PrimPol* $^{-/-}$ cells was more strongly affected than WT DT40 cells as the KO cells remained in S-phase for a longer time (figure 5.11C). Indeed, at 8 and 16 hour time points, 1.3 and 1.6-fold increases of the proportion of S-phase cells were observed respectively in the absence of PrimPol compared to WT DT40 cells (figure 5.11C, blue triangles and squares). Eventually, *PrimPol* $^{-/-}$ UV-C irradiated cells progressed through S to G2 phase with an approximately 8 hours delay, as the G2 peak was reached at 16 hours for WT cells and only at 24 hours for *PrimPol* $^{-/-}$ cells (figure 5.11C, green squares and triangles). To conclude, PrimPol is needed for efficient S-phase progression following 5 J/m^2 UV-C whereas following a lower exposure (2 J/m^2), cell cycle progression is not strongly altered but the absence of PrimPol lead to an increase of cell death.

The second analysis allowed a labelling of S-phase cells (BrdU positive cells) prior to UV-C irradiation, in order to follow specifically their progression through the cell cycle (from 2N to 4N thanks to PI staining) by collecting the cells at different time points following irradiation (figure 5.12A). It is important to remember in this analysis, because the BrdU pulse has been performed at the beginning of the experiment and different recovery times were allowed following UV-C irradiation, only the DNA content (PI staining) of the cells at the time of the collection can determine their cell cycle stage. Thus, BrdU positive cells only indicate these cells were in S-phase during the UV-C irradiation period. Mock-irradiated WT and *PrimPol* $^{-/-}$ cells progressed in a similar manner, despite the difference observed at 10 and 16 hours where a small proportion of *PrimPol* $^{-/-}$ cells accumulate in G2 (figure 5.12B, blue arrows), as previously observed in Chapter 4 (figure 4.17B). Nonetheless, three asynchronous patterns were observed at 8, 16 and 24 hours in the absence of irradiation in both cell lines (figure 5.12B). On the other hand, following 2 and 5 J/m^2 UV-C irradiations (figure 5.12C and D respectively), cell cycle kinetics were strongly impeded in comparison to the mock-irradiated profiles at the same time points (figure 5.12, compared C and D to B). Indeed, after 24 hours, UV-C irradiated cells did not progress through mitosis and instead accumulated in a 4N state (figure 5.12C and D, right profiles). In mock-irradiated cells (figure 5.12B), both WT and *PrimPol* $^{-/-}$ profiles looked very similar and progressed through the cycle in a similar manner. After 2 J/m^2 UV-C irradiation, the progression through S-phase was slowed down in both cell lines in a similar way, but the 4N peaks observed at 16 and 24 hours in *PrimPol* $^{-/-}$ cells were wider, indicating a DNA content disparity (figure 5.12C). After 5 J/m^2 UV-C irradiation, the delay in S-phase progression previously observed in figure 5.11C was also visible here (blue arrows), and could now be allocated to a delay in progression of both S-phase (top arrows) and G1 phase

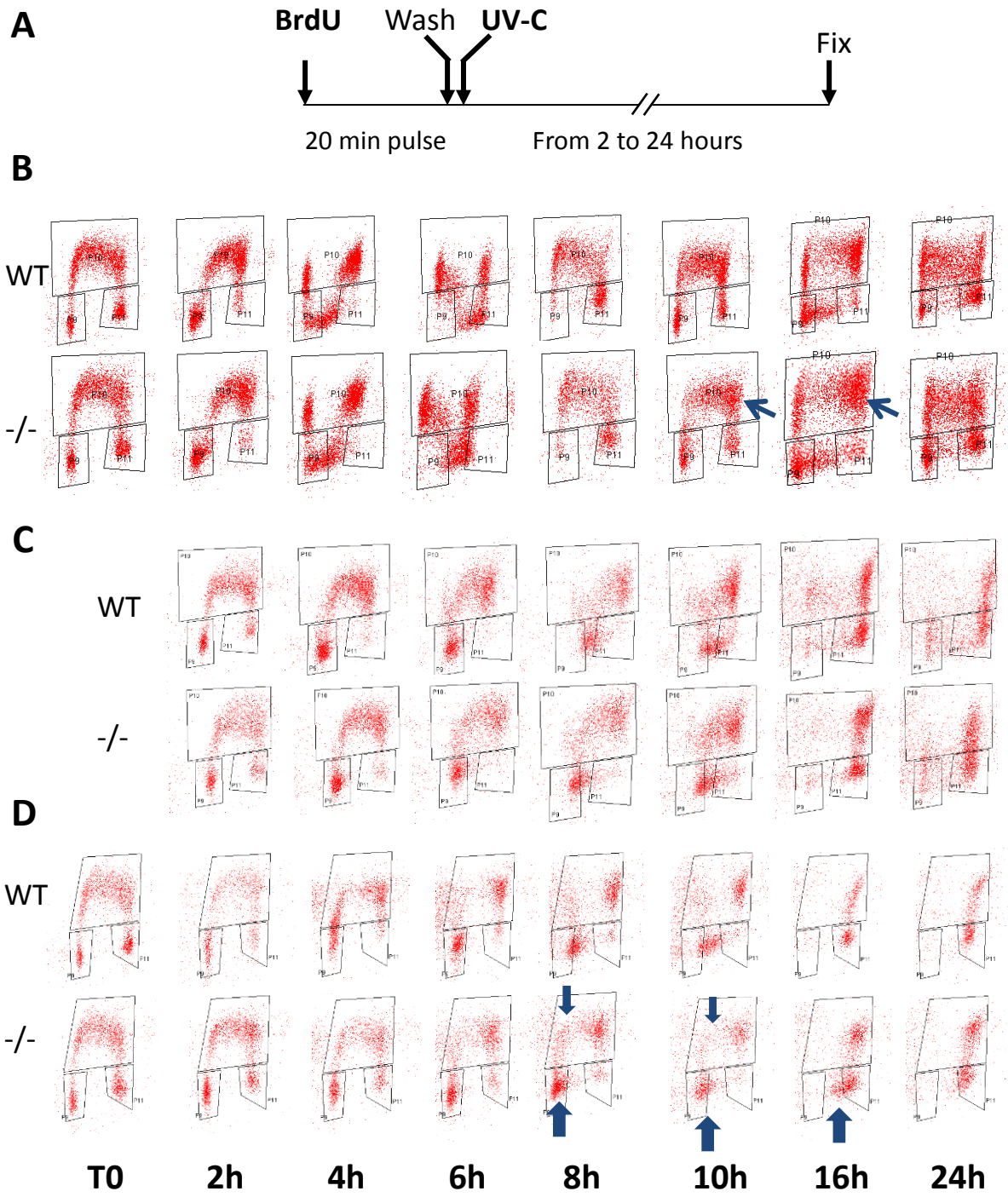

Figure 5.12: Cell cycle progression of BrdU pulse-labelled cells.

(**A**) Schematic describing the experimental procedure. Asynchronous populations of WT or *PrimPol* $^{-/-}$ DT40 cells were pulse labelled for 20 minutes with BrdU and then returned to the incubator (**B**) or were UV-C irradiated (**C** and **D**) immediately (T0) and collected at different time points (2 to 24 hours). PI and BrdU co-staining allow the following of the progression of the cell through the cell cycle via flow cytometry. (**B**) Cell cycle progression of mock-irradiated samples, whereas in (**C**) cells were irradiated with 2 J/m^2 and (**D**) with 5 J/m^2 of UV-C light. Blue arrows indicate the delayed *PrimPol* $^{-/-}$ cells by comparison with WT cells. Data representative of two independent experiments.

(bottom arrows) irradiated cells (figure 5.12D). The 30-60% increase in the proportion of *PrimPol* $^{-/-}$ S-phase cells (figure 5.11C, blue squares and triangles) can now be explained by first a delay of S-phase irradiated cells to progress through S-phase (figure 5.12D, 8 hour point, top arrow) while WT cells have already reached a 4N content. In a second time, G1 or G2 (BrdU negative) irradiated *PrimPol* $^{-/-}$ cells, were delayed in S-phase but not in the WT population (figure 5.12D, 16 hour time point, bottom arrow). Following 2 or 5 J/m^2 irradiation (figure 5.12C and D), WT and *PrimPol* $^{-/-}$ cell cycle flow cytometry profiles obtained at 24 hours post-irradiation were similar (cells blocked in 4N content). Later time point analysis (36 and 48 hours) were also collected but could not be analysed by flow cytometry due to the high levels of cytotoxicity generated by the irradiation process (data not shown).

To conclude, after 2 J/m^2 UV-C irradiation, where *PrimPol* $^{-/-}$ cells have been shown to be more sensitive than WT DT40 cells to this low dose exposure (figure 5.5), cell cycle progression was not impeded by the absence of the polymerase (figure 5.11B and 5.12C). However, following 5 J/m^2 UV-C irradiation, where *PrimPol* $^{-/-}$ cells were no longer sensitive compared to WT DT40 cells, a further delay in S-phase progression was observed (figures 5.11C and 5.12D). This absence of cell cycle regulation following low dose UV-C irradiation could be directly linked to the increase cytotoxicity observed in *PrimPol* $^{-/-}$ cells following UV-C irradiation < 2 J/m^2, thus prompted further investigations of the intra-S checkpoint response in the absence of PrimPol (section 5.3). Nonetheless, UV-C induced cytotoxicity observed at low dose and the delay in S-phase progression observed after high dose irradiation are both consistent with the fact PrimPol is required for RF progression on UV damaged DNA.

5.2.3. Analysis of apoptosis in *PrimPol* $^{-/-}$ cells following UV irradiation

Preliminary analysis of sub-G1 populations recorded by flow cytometry indicated a stronger apoptotic response in *PrimPol* $^{-/-}$ cells than WT DT40 cells following low dose of UV-C irradiation (figure 5.11D). No significant differences were observed following high fluence exposure (data not shown). It was then decided to investigate more thoroughly this apoptotic response following UV-C irradiation by using DAPI staining and fluorescence microscopy. Indeed, apoptotic cells present characteristic fragmented nuclei, and are easily recognisable compared to mitotic cells, with condensed chromosomes, or plain nuclei cycling cells. Therefore, quantification of the proportion of apoptotic and mitotic cells within WT and *PrimPol* $^{-/-}$ cells was performed following different doses of UV-C exposure and different

recovery times (figure 5.13). DT40 cells, growing in suspension, requires a cytospinning process prior to any microscopy study, thus dead cells were fixed to the slide at the same time than viable cells. Analysis of apoptosis following 16 hours recovery time indicated a decrease of the proportion of *PrimPol* $^{-/-}$ cells containing a fragmented nucleus compared to WT DT40 cells following UV-C exposure above to 2.5 J/m^2 (figure 5.13A). On average, the apoptosis was decreased by 60% following 2.5 and 5 J/m^2 UV-C irradiation (figure 5.13A and C) and by 40% following 7.5 and 10 J/m^2 UV-C irradiation, in *PrimPol* $^{-/-}$ cells (figure 5.13B). The same trend was observed in a recovery time course experiment performed following 5 J/m^2 irradiation (figure 5.13B); a 40% decrease was recorded at early time points (4 and 8 hours) followed by a 60% reduction of the number of apoptotic cells at later time points (16 and 24 hours) in the absence of PrimPol (figure 5.13B). However, in agreement with the low dose sensitivity previously observed in the survival experiments (figure 5.5A) and flow cytometry analysis (figure 5.11D), a 4-fold increase of apoptosis was also observed in *PrimPol* $^{-/-}$ cells at 48 hours following 1 or 2 J/m^2 UV-C irradiation (figure 5.13D). The absence of PrimPol therefore seems to be correlated with an increase of apoptosis in DT40 cells following low doses of UV-C irradiation (<2 J/m^2) but a decrease of cell death following higher fluences exposure (>2 J/m^2). PrimPol is thus a pro-apoptotic factor following high fluences of UV-C irradiation.

5.2.4. Analysis of γH2AX foci formation in *PrimPol* $^{-/-}$ cells following UV irradiation

Previous experiments showed PrimPol is required for maintaining RF progression on damaged DNA, thus in the absence of the novel primase-polymerase, an increase of RF pausing and/or stalling can result in DNA breaks formation. Therefore, analysis of histone H2A variant X (H2AX) phosphorylation (γH2AX) was next investigated, as this modified form is often considered as a marker for DSBs (Dickey *et al.*, 2009). In early time point (2 hours) following 2 J/m^2 UV-C irradiation, two distinct γH2AX patterns can be observed in both WT and *PrimPol* $^{-/-}$ cells; indeed, a strong homogenous (or pan-nuclear) signal and a more discrete foci pattern can be visualised (figure 5.14A), consistent with previous reports from the literature (Ward and Chen, 2001; de Feraudy *et al.*, 2010). Following 2 hours recovery after a 2 J/m^2 UV-C exposure, 47% of WT cells presented a γH2AX pan-nuclear pattern whereas only 32% of *PrimPol* $^{-/-}$ cells showed this pattern (figure 5.14C). According to the literature, this pan-nuclear γH2AX pattern corresponds to a pre-apoptotic signal (de Feraudy *et al.*, 2010). In both WT and *PrimPol* $^{-/-}$ cells, a 24 hours recovery time was enough to prevent the formation of pan-nuclear γH2AX cells following 2 or 5 J/m^2 UV-C exposure (figure 5.14C, blue bars at 24 hours). Regarding γH2AX foci

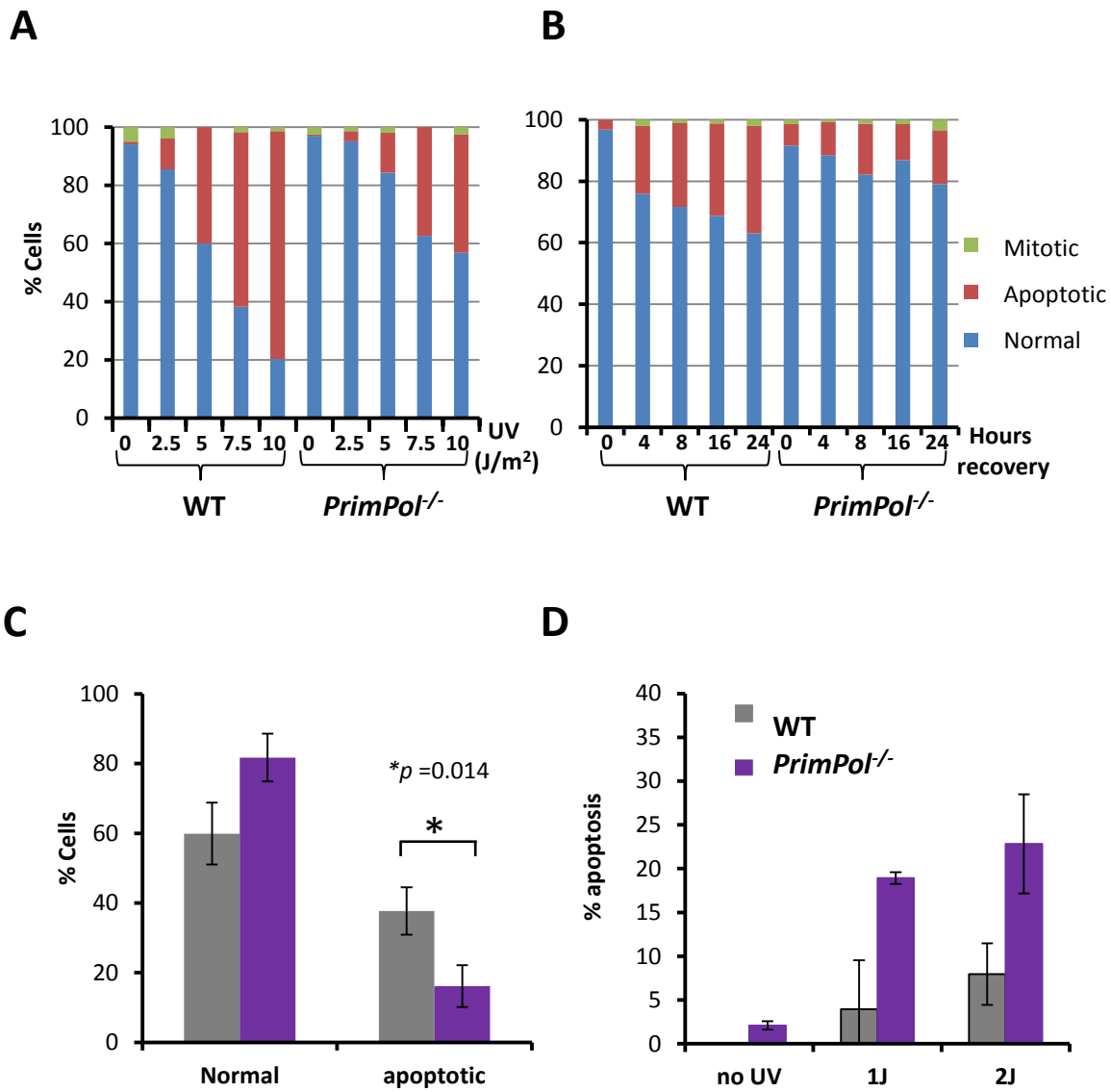

Figure 5.13: Apoptosis assessment following UV-C irradiation.

(**A**) and (**B**) Percentage of mitotic (green), apoptotic (red) or normal (blue) cells was assessed by microscopy and DAPI counting in WT DT40 cells and *PrimPol* $^{-/-}$ cells (clone 2). (**A**) Cells were cyto-spined and fixed 16 hours after UV-C irradiation at different doses. (**B**) Time course of recovery was performed after 5 J/m^2 UV-C irradiation before fixation of the cells and DAPI staining. (**C**) Percentage of apoptotic cells obtained at 16 hours after 5 J/m^2 UV-C irradiation was calculated for three independent samples of WT cells (grey) and *PrimPol* $^{-/-}$ cells (purple); t-test was assessed with to two tails moments (**P*). (**D**) Percentage of apoptotic cells obtained at 48 hours after low doses of UV-C irradiation was calculated for two independent samples of WT cells (grey) and *PrimPol* $^{-/-}$ cells (purple).

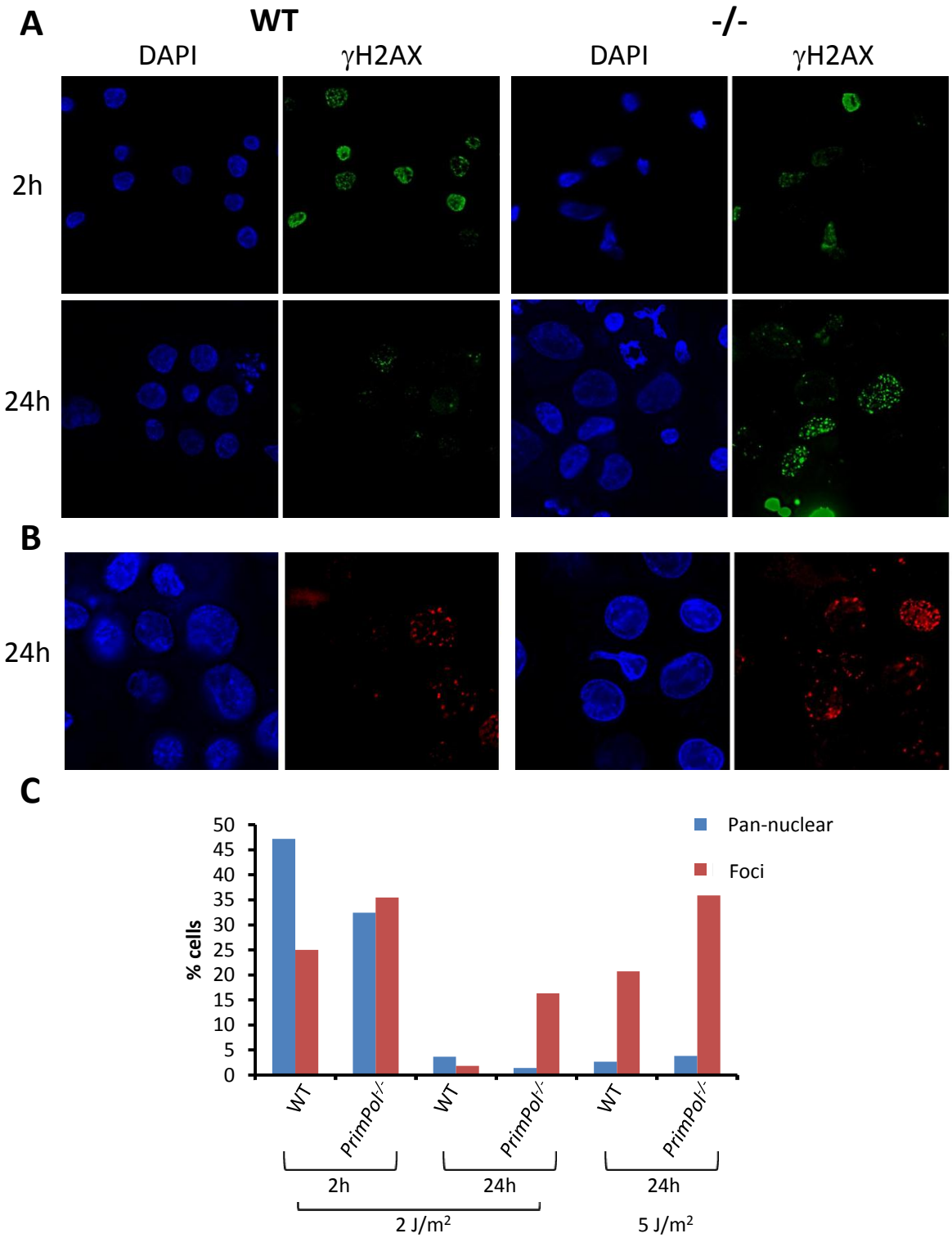

Figure 5.14: γH2AX immunolabelling following UV-C irradiation.

WT and *PrimPol* $^{-/-}$ (-/-) DT40 cells were irradiated with 2 J/m^2 (**A**) or 5 J/m^2 (**B**) UV-C and cyto-spined two hours or twenty-four hours after irradiation. Fixed cells were then immunostained using γH2AX antibodies (green or red) and counterstained with DAPI (blue). (**C**) WT and *PrimPol* $^{-/-}$ cells containing γH2AX pan-nuclear (blue) or focal assembly (red) signals were quantified following different doses of irradiation and different times of recovery (at least 200 cells were scored). Experiment was only performed once.

formation, it has been shown recently that following UV-C irradiation only one half of γH2AX foci corresponded to DSBs (when 53BP1 was also co-localising) and the other half remains unclear (de Feraudy *et al.*, 2010). Nonetheless, at 2 hours after 2 J/m^2 UV-C irradiation, 35% of *PrimPol* $^{-/-}$ cells contained γH2AX foci compared to 25% in WT DT40 cells (figure 5.14C). A similar trend was observed after 24 hours recovery from this dose (2 J/m^2 UV-C), with an increase of the proportion of γH2AX foci containing cells in the absence of the novel primase-polymerase (figure 5.14A, bottom panel). At this time point, the proportion of cells containing γH2AX foci was increased by a factor of 8, from 2% of WT cells to 16% in *PrimPol* $^{-/-}$ cells (figure 5.14C). Following 24 hours recovery after a higher (5 J/m^2) UV-C exposure, absence of PrimPol also appears to be correlated with an increase of γH2AX foci containing cells (figure 5.14B). Indeed, 21% of WT cells versus 36% of *PrimPol* $^{-/-}$ cells contained γH2AX foci (figure 5.14C).

This preliminary analysis, which needs to be repeated and completed (missing 2 hour time point after 5 J/m^2), indicates the absence of PrimPol correlates with a reduction of early apoptosis events (decrease of pan-nuclear signals), but also lead to an increase of γH2AX foci formation and their persistence 24 hours after UV-C exposure. These results, in line with the DNA fibers and the flow cytometry analyses, support an involvement of PrimPol in maintaining RF progression. Indeed in *PrimPol* $^{-/-}$ cells, the increase of RF stalling observed in figure 5.9 could explain the accumulation of γH2AX foci (figure 5.14). A defect in RF maintaining would also generate a delay during S-phase progression (figure 5.12), and lead to an accumulation of cells with an uncompleted 4N content at 24 hours post UV-C irradiation (figure 5.12, wide 4N peak), unable to go through mitosis due to the persistence of the checkpoint activation as suggested by the persistence of γH2AX foci at 24 hours post UV-C irradiation (figure 5.14C).

5.2.5. Analysis of human PrimPol cellular localisation following UV-C irradiation in DT40 *PrimPol* $^{-/-}$ cells

Consistent with a role for PrimPol in the tolerance of UV-C induced DNA damage, *PrimPol* $^{-/-}$ cells presented a defect in RF progression (figure 5.9) accompanied with a decrease in overall DNA synthesis (figure 5.8) and a delay in S-phase completion (figure 5.11 and 5.12) after UV-C irradiation. It would then be expected that following UV-C irradiation, PrimPol would localise to sites of DNA damage, as other TLS polymerases do (Kannouche *et al.*, 2001 and 2003; Tissier *et al.*, 2004; Ogi *et al.*, 2005). It was then decided to investigate PrimPol's localisation following UV-C irradiation. Human PrimPol complementation strain was used for immunuorescence

analysis by monitoring the sub-cellular localisation of human PrimPol protein at different time points following UV-C irradiation. In unperturbed conditions, previous analysis described in Chapter 4, showed human PrimPol localises within the nucleus and the cytoplasm of DT40 cells. At early time point after 5 J/m^2 UV-C irradiation, human PrimPol protein was in the nucleus but also accumulated strongly in a well-defined peri-nuclear area (figure 5.15, 1 hour). At later times post-irradiation, when most of the cells appeared to be in G2 phase of the cell cycle (figure 5.15, large nuclei cells at 8 hours) or in abnormally large G2 cells (figure 5.15, 24 hours, very large nuclei cells), human PrimPol staining was evenly spread throughout the nucleus and the cytoplasm. However, when the cells were fixed 2 or 4 hours following 5 J/m^2 UV-C irradiation, human PrimPol protein was found to accumulate specifically into nuclear foci, some of which co-localising with γH2AX foci (figure 5.16). Previous flow cytometry time course analysis suggested the majority of cells are in S-phase at 2 or 4 hours following 5 J/m^2 UV-C (Figure 5.11C), which would be consistent with these human PrimPol protein foci being observed within these small nuclei S-phase cells (figure 5.16). These data suggested then a potential recruitment of human PrimPol to UV-C damaged DNA sites during S-phase, in accordance with data obtained in human cells and PrimPol protein forming triton-resistant foci following UV-C irradiation (Sean Rudd, Aidan Doherty, personal communication; appendix A), 4NQO and MMS treatments (figure 3.15).

To sum up our current understanding of PrimPol involvement following replication stress (UV-C and 4NQO), the novel primase-polymerase is needed for the maintaining of RF progression following UV-C irradiation (figure 5.9). Otherwise an increase in RF stalling/ pausing is observed along with a decrease of overall replication rate (figure 5.8) and a delay in S-phase progression following high fluences (figures 5.11 and 5.12). PrimPol appears to be involved during on-going RF progression and not in PRR processes (figure 5.10). Nonetheless, 24 hours following UV-C irradiation, cells accumulate in G2 phase (4N content) with an increased proportion of DNA damage (figure 5.14), potentially preventing the entry in mitosis (figure 5.3B). All these phenotypes are consistent with a role for PrimPol in DNA damage tolerance, however the mechanism remains unclear. Whilst primases have been implicated in damage tolerance via re-priming downstream of blocking lesions, which could be possible for PrimPol here, further studies in the Doherty lab have shown PrimPol is capable of TLS of UV photoproducts *in vitro*, extending from CPDs and completely bypassing UV (6-4)PPs. However, *PrimPol* $^{-/-}$ avian cells are more sensitive to low dose of UV-C irradiation (<2 J/m^2) and even appear protected from apoptosis event following higher UV-C fluences (figures 5.5 and 5.13).

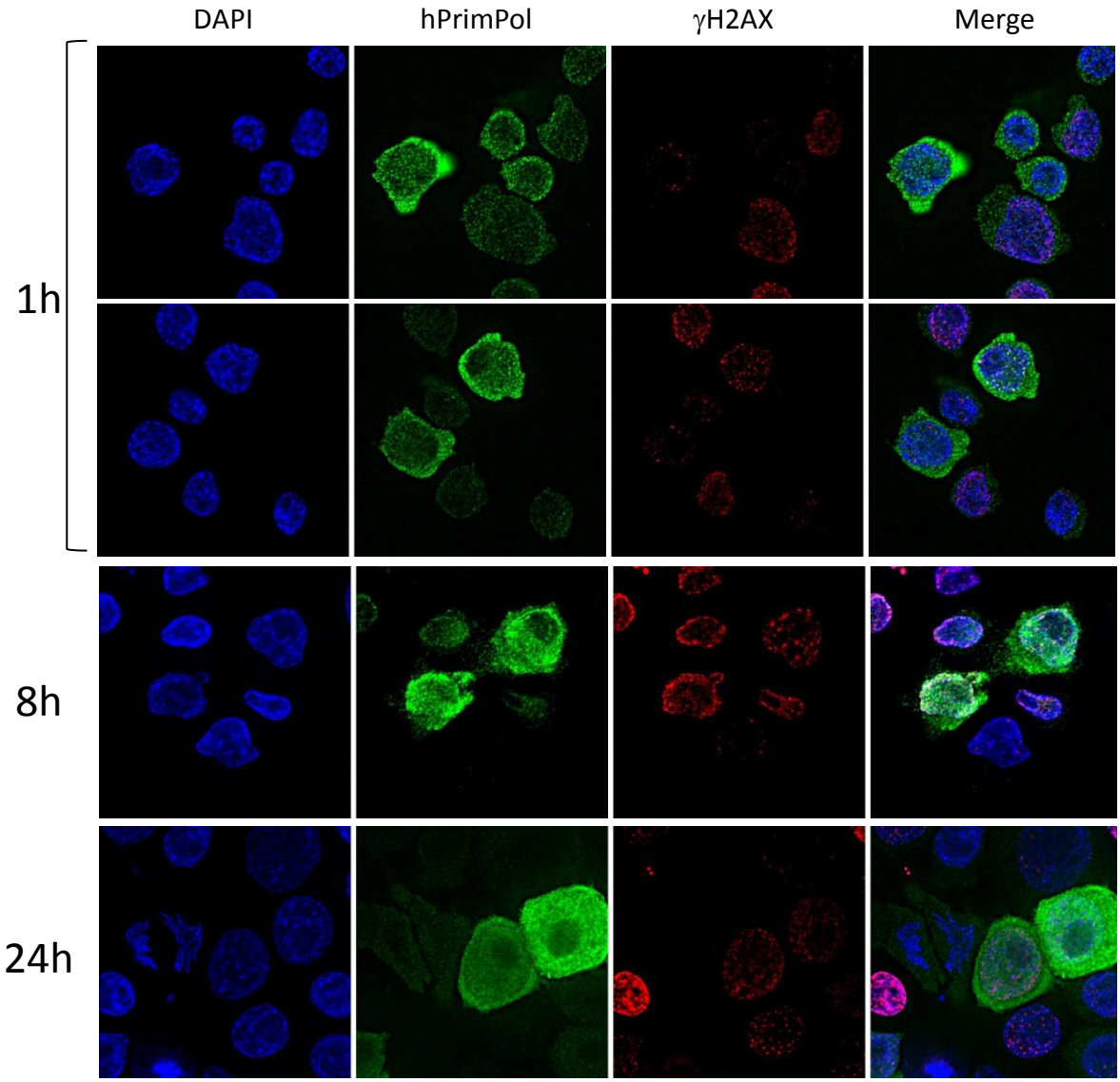

Figure 5.15: Human PrimPol cellular localisation following UV-C irradiation.

PrimPol $^{-/-}$ DT40 cells expressing human PrimPol protein were irradiated with 5 J/m^2 UV-C and cyto-spined at different time points after irradiation (indicated on the left side). Fixed cells were then immunostained using human PrimPol (green) and γH2AX (red) antibodies and counterstained with DAPI (blue).

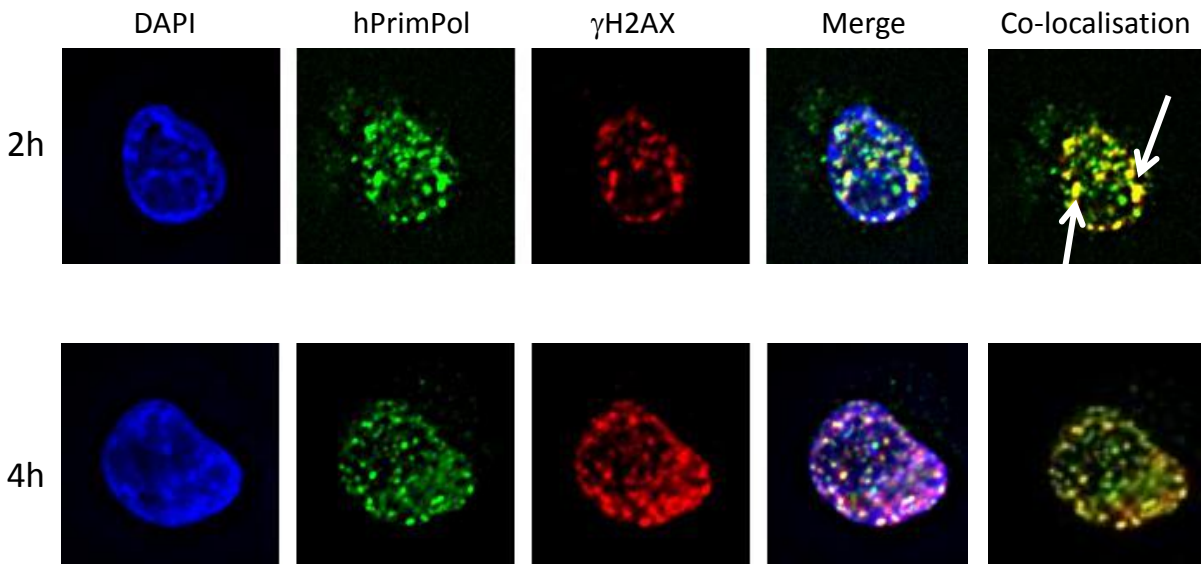

Figure 5.16: Human PrimPol foci formation following 5 J/m² UV-C irradiation.

PrimPol $^{-/-}$ cells expressing human PrimPol protein were irradiated with 5 J/m² UV-C and cyto-spined 2 hours (top pannel) or 4 hours (bottom pannel) after irradiation. Immunostaining with human PrimPol (green) and γH2AX (red) antibodies allow appreciation of the degree of co-localisation (yellow) of hPrimPol with the DNA double-strand break marker. White arrows indicate examples of co-localisation.

To further understand this peculiar feature of *PrimPol* $^{-/-}$ cells, the intra-S checkpoint response was investigated.

5.3. Influence of Chk1 inhibition in *PrimPol* $^{-/-}$ cells

5.3.1. Absence of PrimPol protects from UV-C cytotoxicity when Chk1 is inhibited

UV-C radiation induces the formation of major helix distorting DNA lesions, such as CPDs and (6-4)PPs, which can block replisome progression if not repaired prior to S-phase (Batista *et al.*, 2009; Rastogi *et al.*, 2010). Encounter of the replisome with a UV photoproduct can cause uncoupling of the MCM helicase complex and the replicative polymerase activities, resulting in the generation of long stretches of RPA-coated ssDNA (Byun *et al.*, 2005). As a consequence, the intra-S checkpoint response becomes activated via the ATR kinase, generating a cascade of phosphorylation events (Byun *et al.*, 2005; Kaufman WK, 2010). One of the main goals of the activation of the intra-S checkpoint is to slow down DNA replication progression and to prevent mitosis entry in order to provide more time for the cell to fix their damaged DNA and therefore prevent aneuploid daughter cells (Barkley *et al.*, 2007; Kaufmann, 2010). Chk1 is the main downstream effector kinase of ATR and in addition to being essential for the intra-S checkpoint response, Chk1 has also been shown to be essential for both DNA replication (Maya-Mendoza *et al.*, 2007; Takai *et al.*, 2000) and mitosis progression in unperturbed conditions (Matsuyama *et al.,* 2011).

PrimPol $^{-/-}$ cells present an abnormal response to UV-C radiation, exemplified by low UV-C doses (<2 J/m^2) proving more cytotoxic compared to WT DT40 cells than higher UV-C doses. This prompted the investigation of the role of the intra-S checkpoint in *PrimPol* $^{-/-}$ cells by inhibiting the kinase activity of Chk1. The chemical drug UCN-01 was used, also named 7-hydroxystaurosporine, this allosteric inhibitor of Chk1 prevents the binding of ATP into the kinase pocket in a specific manner (Zhao *et al.*, 2002), thus blocking Chk1's phosphorylation of its downstream targets. Although Chk1 is essential in mammalian cells, intriguingly Chk1 has been successfully deleted from DT40 cells (Zachos *et al.*, 2003). WT and *PrimPol* $^{-/-}$ DT40 cells were grown in the presence of varying concentrations (10, 30, 300 nM) of UCN-01 and the cell viability was analysed. Consistent with Chk1's essential roles in unchallenged cells, treatment of WT cells with 300 nM UCN-01 was highly cytotoxic (figure 5.17A). However, *PrimPol* $^{-/-}$ cells were less sensitive to the cytotoxic effect of the drug as a 15-20% increase in cell viability was observed in the presence of 10 or 30 nM UCN-01 in the absence of PrimPol compared to the WT DT40 population (figure 5.17A). Furthermore, in the presence of 300 nM UCN-01, a 45%

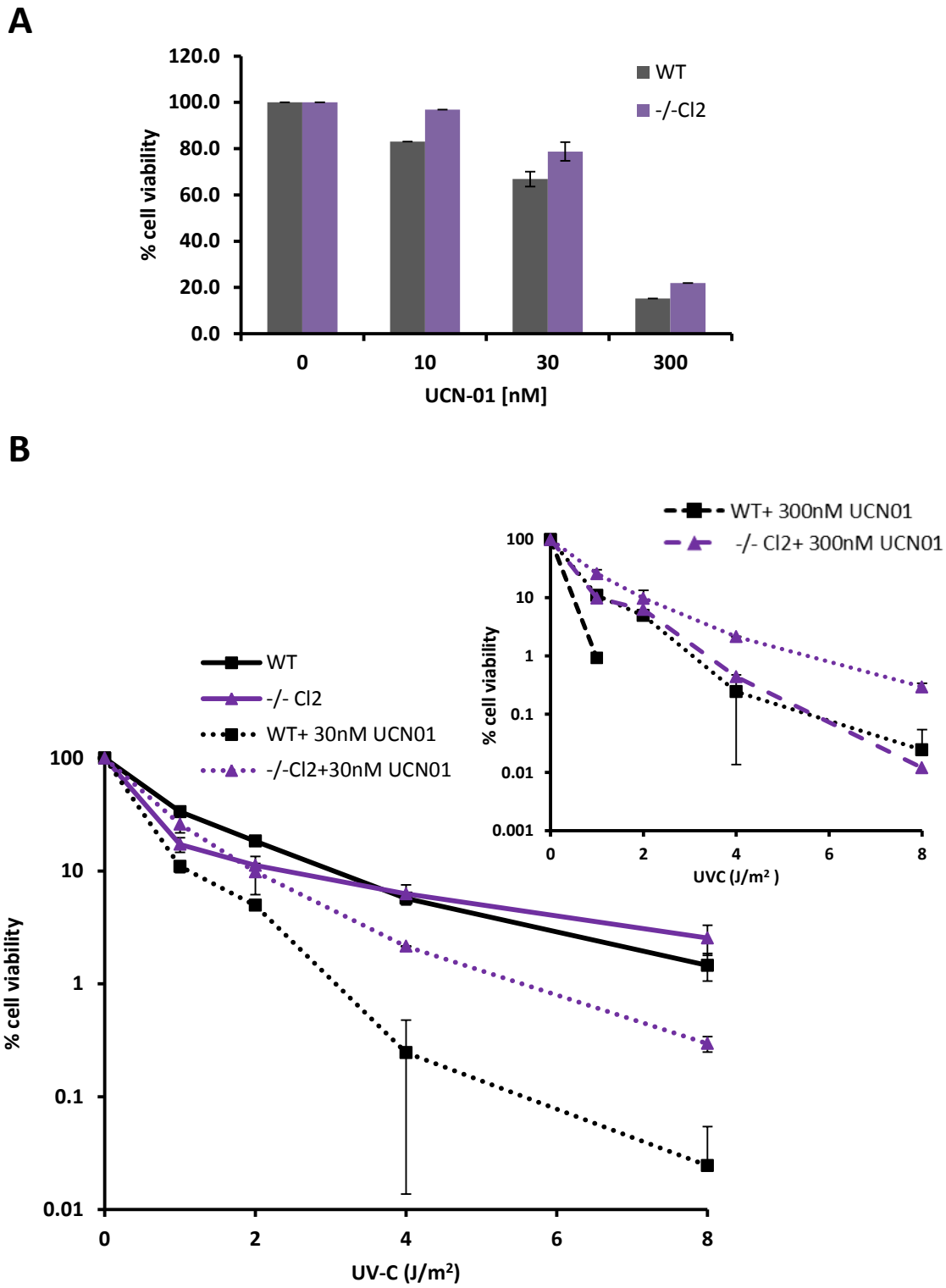

Figure 5.17: Influence of ChK1 inhibitor on cell viability.

(**A**) Cell viability was assessed using CellTiter-Blue technology 48 hours after chronic treatment with ChK1 inhibitor UCN-01. Error bars denote standard deviation of 2 independent experiments. (**B**) WT (black squares) or *PrimPol* $^{-/-}$ (purple triangles) cells were irradiated with UV-C and allowed to recover for 48 hours in normal media (plain lines) or containing 30 nM UCN-01 (dash lines) or 300 nM (right plot, interrupted lines) before performing CellTiter-Blue viability assay. Error bars denote standard deviation of 2 independent experiments.

increase in cell viability was observed in *PrimPol* $^{-/-}$ cells compared to WT DT40 cells. This data suggests the absence of PrimPol protects cells from the cytotoxic effects of Chk1 inhibition and further supports a role for PrimPol during unperturbed S phase as previously demonstrated in Chapter 4.

5.3.1.1. Cell viability assessment in *PrimPol* $^{-/-}$ cells following UV-C irradiation and Chk1 inhibition by UCN-01

PrimPol $^{-/-}$ cells show abnormal response to UV-C with regards to cytotoxcity as the cells are more sensitive to low dose UV-C exposure compared to WT cells than following a high dose exposure. Therefore, *PrimPol* $^{-/-}$ cells were exposed to low doses (1 and 2 J/m^2) and higher fluences (4 and 8 J/m^2) UV-C irradiation and the cell viability was measured in the presence of differences concentrations of UCN-01 (figure 5.17B). First, cells were UV-C irradiated and left to recover for 48 hours in the presence of 30 nM UCN-01 before CellTiter-Blue reagent was added and fluorescence measured (figure 5.17B, left graph). In WT DT40 cells, addition of the drug generated a 3-fold decrease of cell viability after low doses UV-C irradiation and stronger decrease, 25-fold and 60-fold following 4 and 8 J/m^2 UV-C irradiations respectively (figure 5.17B, left graph). On the other hand, in *PrimPol* $^{-/-}$ cells, addition of 30 nM UCN-01 generated a slight increase, from 17 to 26 % cell viability following 1 J/m^2 UV-C and had no effect after 2 J/m^2 UV-C irradiations (figure 5.17B, left graph). Following higher fluences exposure, presence of the drug in the absence of PrimPol generated a mild decrease of cell viability, with 3-fold and 9-fold difference observed after 4 and 8 J/m^2 UV-C irradiations (figure 5.17B, left graph). Therefore, in the presence of a low concentration of Chk1 inhibitor and following UV-C irradiation, the absence of PrimPol had a protective effect on cell survival, as *PrimPol* $^{-/-}$ cells were 10-fold more resistant to UV-C irradiation than WT DT40 cells (figure 5.17B, left graph). This protective effect was even more pronounced in the presence of a high (300 nM) concentration of UCN-01, as WT DT40 irradiated cells with fluences above 1 J/m^2 UV-C presented too low cell viability to be measured (figure 5.17B, right graph, black broken line). However *PrimPol* $^{-/-}$ cells exposed to 300 nM UCN-01 were able to survive to UV-C exposures in a similar manner than WT irradiated cells exposed to 30 nM UCN-01 as the purple broken line and black dotted lines in figure 5.17B (right graph) were almost superimposable. To conclude, the absence of PrimPol protects cells from UV-C cytotoxicity when Chk1 activity is inhibited.

In order to determine whether this phenotype observed was specific to PrimPol protein, and also to compare the influence of Chk1 inhibition towards another known TLS

polymerase, experiments were repeated using the human complementation strain and avian *Polη* $^{-/-}$ cell line. This time the cells were left to recover for 96 hours in the presence of 30 nM UCN-01 following UV-C irradiation and the survival curves obtained were compared to the cell viability assay performed at 144 hours without UCN-01 (figure 5.18A and B). Once again, the presence of Chk1 inhibitor renders *PrimPol* $^{-/-}$ cells less sensitive to UV-C irradiation in comparison with WT DT40 cells (figure 5.18B, black and purple lines). As observed previously when cell viability was assessed at 48 hours, in the presence of 30 nM of Chk1 inhibitor, *PrimPol* $^{-/-}$ cells were almost 10 times less sensitive to high fluences UV-C irradiations (>2 J/m^2) than WT DT40 cells (figure 5.17, purple and black lines). This phenomenon appeared specific to the absence of the novel primase-polymerase, as presence of human PrimPol protein was able to almost fully restore the UV-C sensitivity observed in WT DT40 cells with the presence of 30 nM UCN-01 (figure 5.18B, orange and black lines). To understand whether this phenomenon was specific to PrimPol or whether similar response could be observed from another TLS polymerase KO cell line, cell viability assay in the presence of 30 nM UCN-01 following UV-C irradiation was also tested in *Polη* $^{-/-}$ cell line (figure 5.18, blue lines). Interestingly, the opposite effect was observed as the cell viability of Pol η deficient cells were only affected by the presence of Chk1 inhibitor following low doses of UV-C irradiation (<2 J/m^2). Following 1 J/m^2, a decrease from 10% to 1.8% viable cells was observed in the presence of UCN-01, and following 2 J/m^2, a 25-fold decrease of cell viability was observed in the presence of the drug (figure 5.18A and B, blue lines). Following higher UV-C exposures (>2 J/m^2), the presence of 30 nM UCN-01 in *Polη* $^{-/-}$ cells affected the cell viability by a 3-fold decrease (figure 5.18A and B, blue lines), in a similar manner than in WT DT40 cells (figure 5.18A and B, black lines). These results confirm the protective effect observed by the absence of PrimPol following UV-C irradiation and inhibition of Chk1 pathway by UCN-01, was specific to the novel primase-polymerase and not to the deletion of another TLS polymerase like Pol η.

5.3.1.2. Apoptosis response in *PrimPol* $^{-/-}$ cells following UV-C irradiation and Chk1 inhibition by UCN-01

To confirm these survival experiments did not reflect an artefact of CellTiter-Blue measurements, the apoptosis response was also analysed by DAPI staining following low doses of UV-C irradiations and 48 hours recovery in the presence of different doses of UCN-01 (figure 5.19). In WT DT40 cells, irradiation with 1 J/m^2 UV-C was accompanied with a strong increase of apoptosis response following UCN-01 addition, in a dose response manner (figure 5.19).

A

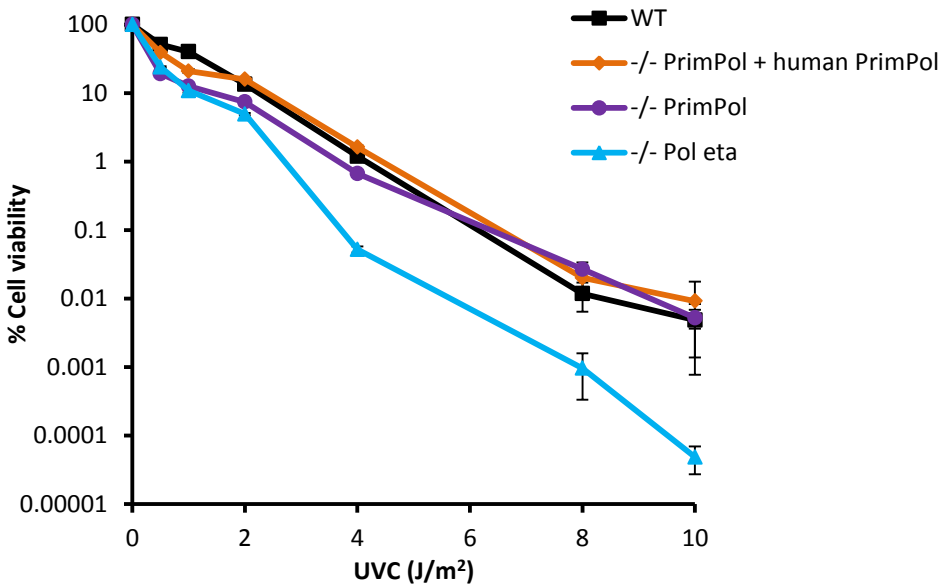

B

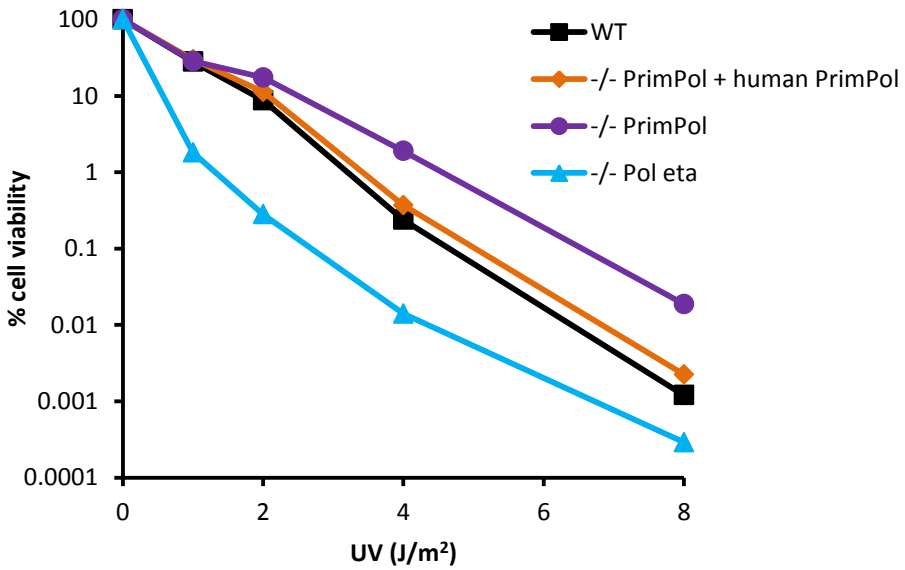

Figure 5.18: Influence of ChK1 inhibitor on cell survival after UV-C irradiation.

Figure 5.12B is presented again here to allow comparison of cell viability after UV-C irradiation without (**A**) or with 30 nM UCN-01 (**B**). CellTiter-Blue was added 144 hours after irradiation (**A**) whereas in the presence of UCN-01, at 96 hours (**B**).

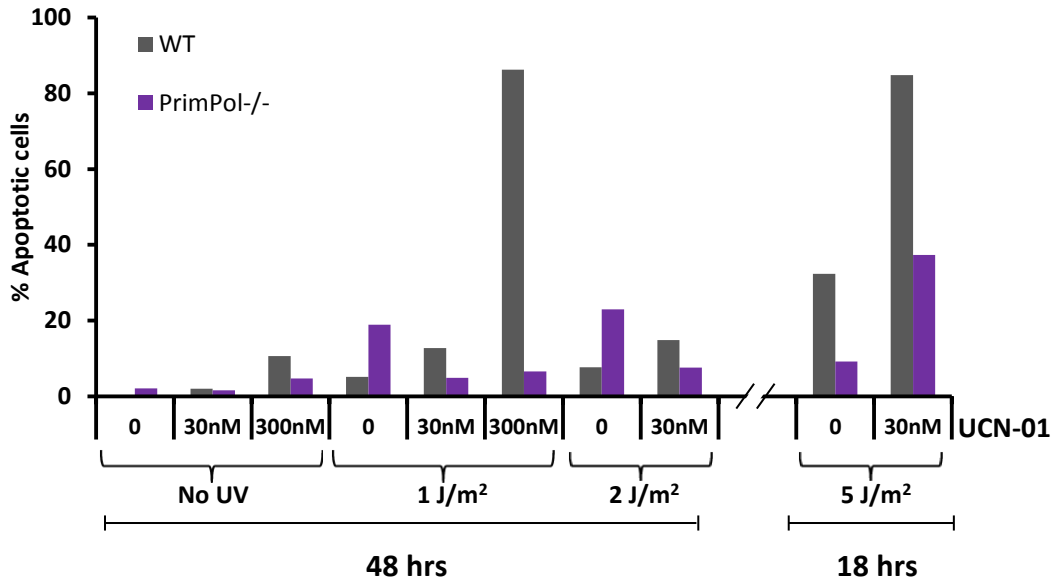

Figure 5.19: Influence of ChK1 inhibitor on apoptosis after UV-C irradiation.

WT (grey) and *PrimPol* $^{-/-}$ (purple) cells were irradiated with different doses of UV-C and cells were kept in media supplemented or not with UCN-01 (30 or 300 nM) for 48 or 18 hours (indicated below the chart). Percentage of apoptotic cells was assessed by microscopy with DAPI staining.

Indeed apoptosis increased from 5% in the absence of the drug to 13% when 30 nM UCN-01 was added and 90% of WT cells were apoptotic following addition of 300 nM UCN-01 after 1 J/m^2 UV-C irradiation (figure 5.19, grey bars). In contrast, the proportion of *PrimPol* $^{-/-}$ apoptotic cells diminished by a factor 4 following addition of Chk1 inhibitor after 1 J/m^2 UV-C irradiation; indeed, the percentage of apoptotic cells diminished from 20% (no UCN-01) to ~5% following the addition of 30 or 300 nM UCN-01 (figure 5.19, purple bars). A similar trend was also observed following 2 J/m^2 UV-C irradiation and addition of 30 nM UCN-01, with a 2-fold increase of apoptosis response in WT cells and a 3-fold decrease in *PrimPol* $^{-/-}$ cells (figure 5.19). Following higher fluences UV-C irradiation and in the presence of UCN-01, apoptosis assessment by DAPI staining was not possible at 48 hours time point due to the high toxicity of the treatment and the low number of viable cells. However, following 5 J/m^2 irradiation and 18 hours recovery with 30 nM UCN-01, the proportion of apoptotic cells was again strongly decreased in the absence on PrimPol, with only 37% of apoptotic cells recorded compared to 85% in WT cells (figure 5.19). These data, along with the survival experiments, confirmed the absence of PrimPol in DT40 cells can partially compensate the cytotoxicity effect of the inhibition of Chk1 response by UCN-01 drug, especially following UV-C irradiation.

5.3.2. Absence of PrimPol reduces aberrant DNA synthesis caused by Chk1 activity inhibition

The sensitivity observed in *PrimPol* $^{-/-}$ cells in response to low dose of UV irradiation seemed to be closely correlated to the checkpoint response and Chk1 activity, as the KO cells became less sensitive to 1 J/m^2 UV-C irradiation after inhibition of Chk1 activity by UCN-01 (figure 5.17B). To understand whether the cytotoxicity fluctuation observed after different UV-C treatments was linked to PrimPol involvement in DNA replication, overall DNA synthesis was analysed in the presence of different doses of UCN-01. Previous studies in the literature report addition of Chk1 inhibitor UCN-01 in human cells is accompanied with an increase of DNA replication initiation mediated by CDK activity (Syljuasen *et al.*, 2005). Moreover, similar results were observed in DT40 cells by analysing spread DNA fibers (Maya-Mendoza *et al.*, 2007). WT DT40 cells treated with 300 nM UCN-01 for 1.5 hours presented a decrease in the fork to fork distance, confirming the role of Chk1 in controlling active origin density by preventing new origin firing (Maya-Mendoza *et al.*, 2007). Consistent with these reports, thymidine incorporation assay performed either after mock or 4 J/m^2 UV-C irradiation (figure 5.20A), indicated the presence of UCN-01 (at 30 or 300 nM) induces an increase in DNA incorporation

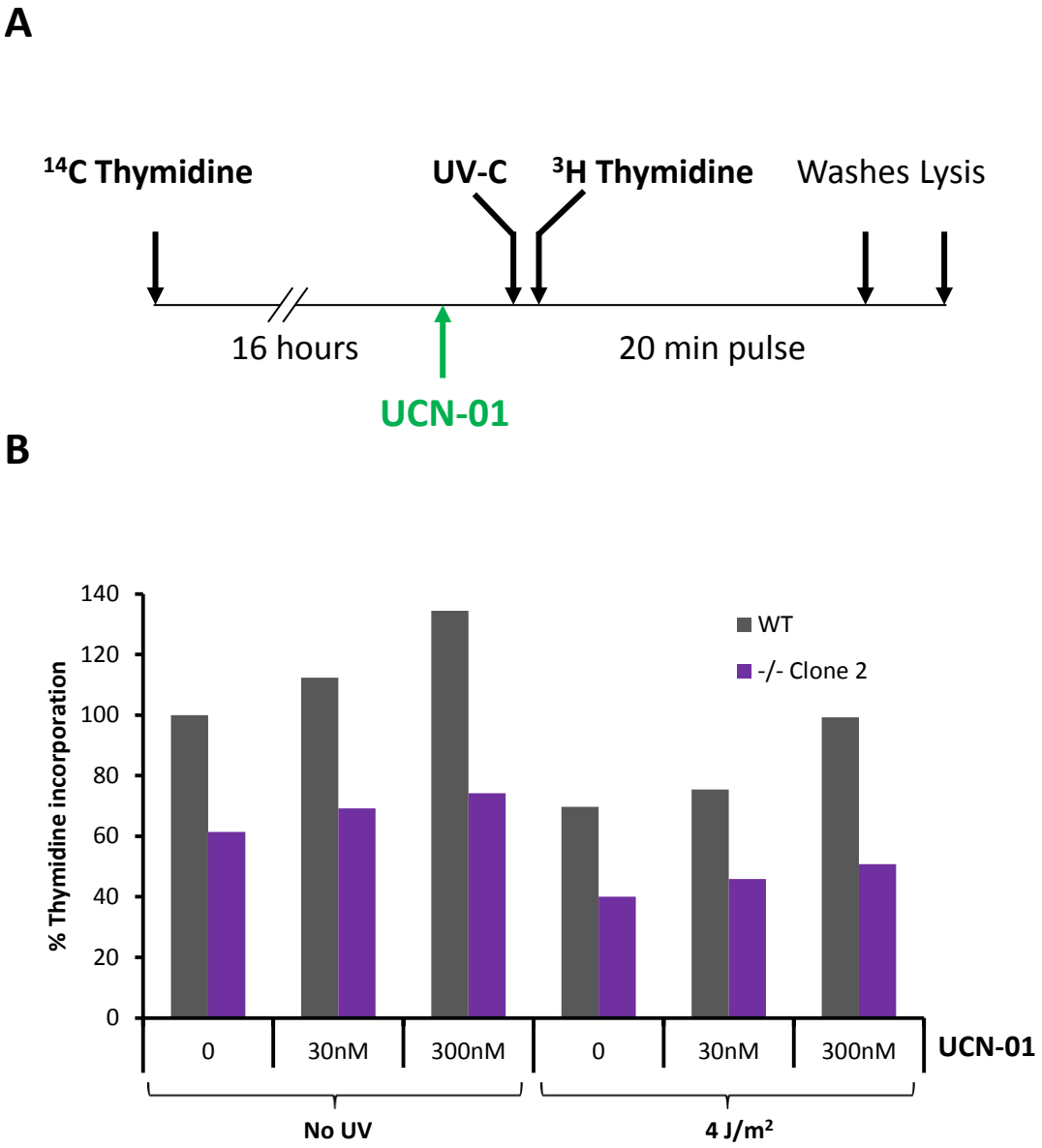

Figure 5.20: Influence of ChK1 inhibition on DNA synthesis rate in *PrimPol* $^{-/-}$ cells.

(**A**) Schematic depicting the labelling process of the thymidine uptake experiment. (**B**) DNA replication rate was performed in presence or absence of UCN-01 (either 30 nM or 300 nM) after 4 J/m^2 UV-C treatment or mock-irradiation (no UV). UCN-01 was added when necessary 1 hour before incorporation of the thymidine, and kept during the time of the radioactive pulse with tritium thymidine (^{3}H Thymidine). Experiment was performed once.

rate, in both WT and *PrimPol* $^{-/-}$ cells (figure 5.20B). Indeed, in WT cells a ~10% increase was seen following the addition of 30 nM UCN-01 and ~35% increase after addition of 300 nM of the drug, independently of the presence of DNA damaged (figure 5.20B, grey bars). However, in the absence of PrimPol, despite a similar incorporation rate increase following addition of 30 nM UCN-01 (~12%), addition of 300 nM UCN-01 was only accompanied with a ~20% increase of thymidine incorporation (figure 5.20B, purple bars). Therefore, when Chk1 activity was severely impaired with 300 nM UCN-01, the absence of PrimPol alone was enough to reduce thymidine incorporation by almost 50%, following or not UV-C treatments (figure 5.20B, black and purple bars at 300 nM). Indeed, a decrease from 135% in WT cells to 74% in KO cells was observed after mock UV treatment, and from 100% to 50% following 4 J/m^2 UV-C irradiations (figure 5.20B, 300 nM). Therefore, the absence of PrimPol was able to compensate for the increase in DNA synthesis observed following the inhibition of Chk1 activity by UCN-01. However, these results corresponded to one experiment only thus several repeats are needed to have a more accurate characterisation of this trend.

5.3.3. Absence of PrimPol partially prevents the premature mitosis entry caused by Chk1 inhibition

As briefly mentioned before, Chk1's activity has been implicated in the regulation of mitotic entry and S-phase progression, both as part of the DNA damage checkpoint response and during normal growth conditions (Kramer *et al.*, 2004; Enomoto *et al.*, 2009). In the first case, intra-S checkpoint activation via ATR induces Chk1 phosphorylation and inactivation of CDC25 A, B, C phosphatases (Sørensen *et al.*, 2003; Sanchez *et al.*, 1997; Schmitt *et al.*, 2006). Therefore, Chk1 participates in CDK1 inactivation by preventing de-phosphorylation of this cyclin dependent kinase, and thus physically blocking the ATP binding within its catalytic site (Sørensen and Syljuasen, 2012). Indeed, it has been shown CDC25A and B dephosphorylates CDK1 (on residues threonine 14 and tyrosine 15) leading to mitosis entry due to an activation of CDK1-cyclin complex (Timofeev *et al.*, 2010; Atherton-Fessler *et al.,* 1994). Inhibition of Chk1 activity by UCN-01 should therefore induce an early mitosis entry, which would reduce the G2/M block observed previously at 16 hours after UV-C irradiation (figures 5.11 and 5.12). To test this hypothesis, WT and *PrimPol* $^{-/-}$ cells were irradiated at 2 J/m^2 or 5 J/m^2 UV-C and left to recover for 16 hours before adding different doses of UCN-01 for 2 hours; a control experiment was also performed with 30 nM UCN-01 added straight after UV-C irradiations and thus left for 18 hours before collection. The percentage of G2 phase cells was then assessed by

PI staining and flow cytometry (figure 5.21) and not with a BrdU/PI double staining as previously performed (figure 5.11 and 5.12). Following 2 J/m^2 UV-C irradiation and no UCN-01 treatment, an enrichment in G2 phase was observed as expected, with ~35% of WT or *PrimPol* $^{-/-}$ cells being in G2 compared to ~10% in non-irradiated populations (figure 5.21A). In WT cells, percentage of G2 phase cells decreased with UCN-01 treatments, but to a lesser extent in *PrimPol* $^{-/-}$ cells (figure 5.21A). However, following increased concentrations of Chk1 inhibitor (300 nM for 2 hours or 30 nM for 18 hours) and exposure to 2 J/m^2 UV-C radiation, no differences were observed between both WT and KO populations (figure 5.21A). Following a higher dose of 5 J/m^2 UV-C irradiation, a stronger G2 arrest was observed in *PrimPol* $^{-/-}$ cells, with 60% of cells being in G2 compared to 35% in the WT DT40 population in the absence of UCN-01 (figure 5.21B, no UCN-01). Nonetheless, in the absence of PrimPol, addition of UCN-01 for 2 hours at 10, 30 and 300 nM induced a dose-dependent decrease of the proportion of G2 phase cells, from 60% (no UCN-01) to 40%, 30% and 20 % respectively (figure 5.21B). On the other hand, WT DT40 cells seemed only sensitive to 300 nM of UCN-01 for 2 hours or 30 nM for 18 hours (figure 5.21B). Nonetheless, a 2-fold or 4-fold increase of *PrimPol* $^{-/-}$ G2 phase cells was observed compared to the WT population following a 300 nM UCN-01 treatment for 2 hours or a 30 nM UCN-01 treatment for 18 hours respectively, following 5 J/m^2 UV-C irradiation (figure 5.21B, 5 J/m^2, 300 nM and 30 nM for 18 hours). To conclude, these experiments indicate that following intra-S checkpoint impairment due to Chk1 inhibition by UCN-01, the absence of PrimPol induces a delay in mitosis entry following UV-C irradiation, thus an increase of the proportion of G2 phase cells. Therefore, the lack of PrimPol compensates partially Chk1 inhibition by UCN-01. However, different responses were observed between low and high dose of UV-C irradiations denoting specific mechanisms are taking place depending on the level of the checkpoint activation.

5.3.4. Chk1 phosphorylation status in *PrimPol* $^{-/-}$ cells

The difference in UV-C sensitivity reported in the absence of PrimPol after low or high fluences has been confirmed to be an intricate phenotype closely linked to the checkpoint response and Chk1 activity in particular. After low dose of UV-C irradiation (below to 2 J/m^2) KO cells are more sensitive to WT cells when the checkpoint response is proficient, but become less sensitive to the irradiation treatment when Chk1 activity is inhibited by UCN-01 drug (figure 5.17B). This phenotype is even amplified after high UV-C fluences exposure and Chk1 inhibition, as the KO cells are less sensitive than WT cells exposed to similar UV-C and UCN-01

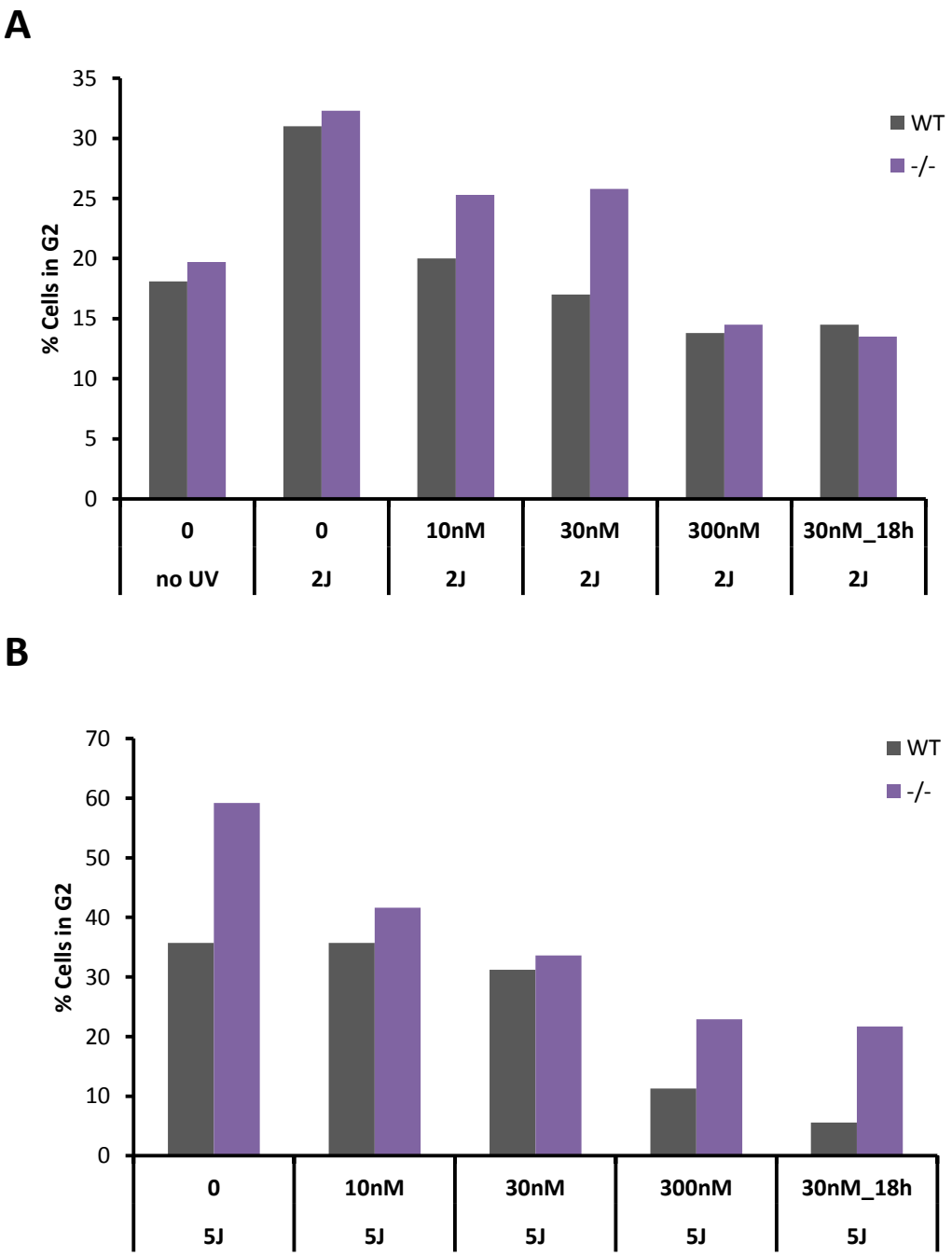

Figure 5.21: Influence of ChK1 inhibition on mitosis entry following UV-C irradiation.

WT (grey) and *PrimPol* $^{-/-}$ (purple) cells were irradiated at 2 J/m^2 (**A**) or 5 J/m^2 (**B**)UV-C and allowed to recover for either 16 hours in normal media followed by 2 hours treatment with different concentrations of UCN-01 drug (10 nM, 30 nM or 300 nM), or for 18 hours in media containing either no drug (0) or 30 nM UCN-01 (30 nM_18h). FACS analysis was performed on PI stained cells and percentage of G2 cells was assessed using FACS CANTO software.

treatments. The absence of PrimPol appears thus to compensate for the loss of a checkpoint response after Chk1 inhibition, by slowing down DNA replication (figure 5.20B) and inducing a delay in mitosis entry (figure 5.21). When the intra-S checkpoint response is activated in response to DNA damage, ATR activates ChK1 by phosphorylating its serine 345 (Zhao *et al.*, 2001). By using an antibody recognising only this phosphorylated form, Chk1 activation can be followed by Western blot analysis (figure 5.22). Indeed, the 50 kDa band appeared only after UV-C irradiation in both WT and KO cells, however the quantification of the signal was more difficult to assess (figure 5.22). In the first set of samples analysed after UV-C treatments, the phosphorylation species appeared more abundant after 4 and 8 J/m^2 UV-C irradiation in the KO cells (figure 5.22A) than WT DT40, respectively 6 times and 3 times more, after quantification with Image J software and normalisation with β-actin signal. However, with two other sets of samples, prepared in similar conditions, it was more difficult to conclude whether a similar trend was reproduced or not (figure 5.22B and C). It appears following 4 J/m^2 UV-C irradiation, more phospho-Chk1 were observed in *PrimPol* $^{-/-}$ cells however the difference was too small to be significant (figure 5.22B and C) and supplemental samples should be analysed in the future to provide sufficient evidence regarding this matter. Moreover, addition of UCN-01 inhibitor at 30 nM for 2 hours did not affect the phosphorylation status of Chk1 in WT DT40 cells, as previously reported in the literature (Syljuasen *et al.*, 2005), but neither in *PrimPol* $^{-/-}$ cells (figure 5.22C). The only significant distinction observed between both cell lines regarding Chk1 phosphorylation profile was the appearance of an extra species above 100 kDa when PrimPol was absent from the cells (figure 5.22B and C, red arrow). This species was present in every set of samples prepared (data not shown) and was always specific to the absence of PrimPol (stronger exposure blots). The significance of this 100 kDa species is unknown in the literature, and no previous reports have ever shown the presence of such a doublet to my knowledge. This phenomenon seems to be PrimPol dependent, but might not be Chk1 related if the antibody is not entirely specific. Also, more complex post-translational modifications could be speculated, resulting in this higher MW species detected by the phospho-specific antibody. To confirm the absence of PrimPol is specifically responsible for the high MW doublet of phospho-Chk1 species, samples from RNAi depleted human cells or from mouse and human PrimPol KO cells recently generated, should be tested as well. Nonetheless, in human cells, following PrimPol RNAi depletion and UV-C irradiation, over-activated phospho-Chk1 (on serine 345) was observed in normal MRC-5 cells and the phosphorylated status was persistent in XP-V cells 24 hours following 2 J/m^2 UV-C irradiation (Sean Rudd, Aidan Doherty, personal communication; appendix A).

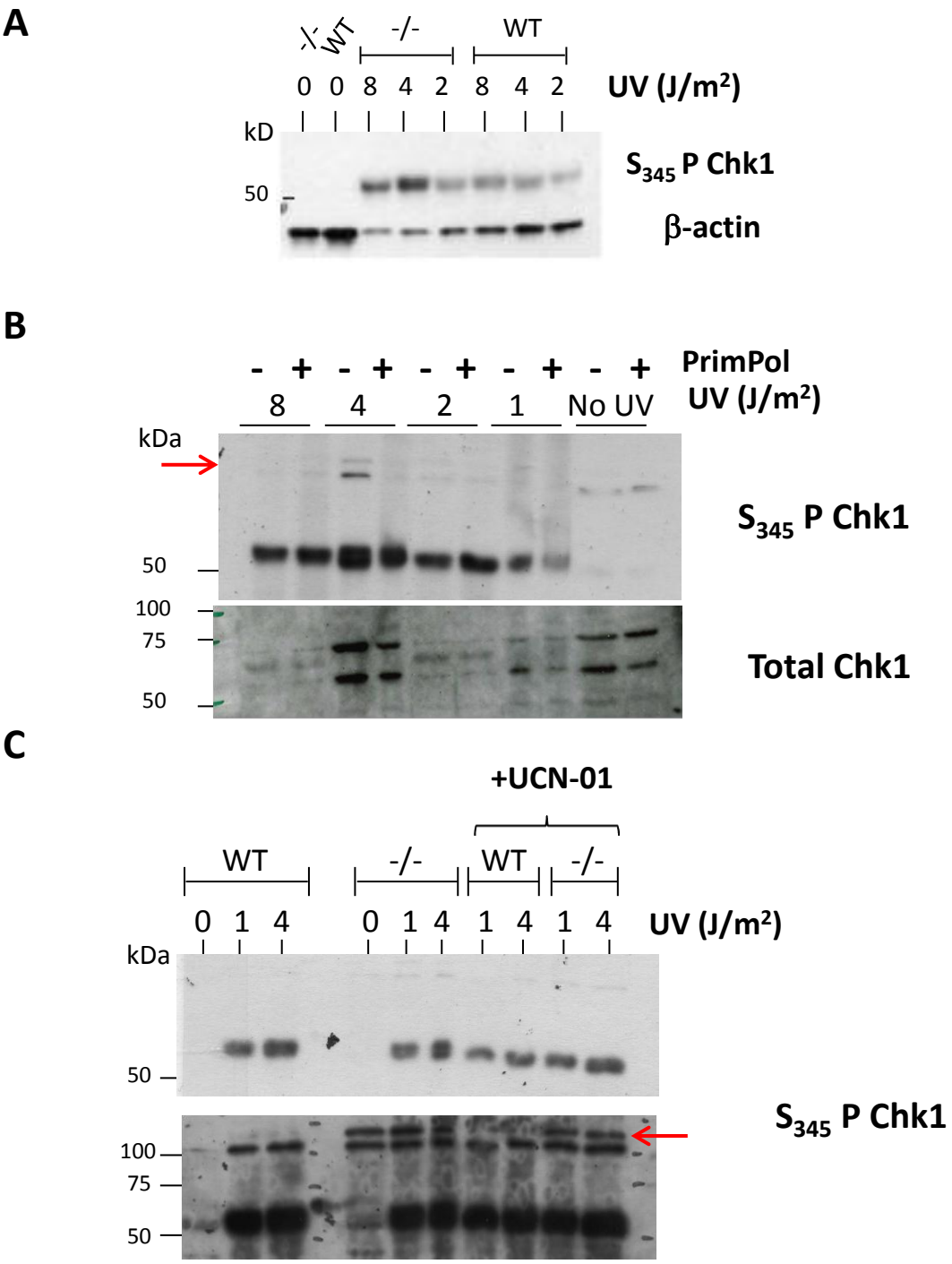

Figure 5.22: ChK1 phosphorylation status in *PrimPol* $^{-/-}$ cells following UV-C irradiation.

Western blot analysis of protein samples extracted after 1 hour (**A** and **B**) or 2 hours (**C**) following different UV-C treatments, using Chk1 total or Ser 345 phospho specific antibodies, and β-actin antibody as loading control. (**B**) Samples prepared from WT cells correspond to the PrimPol status "+", while the ones from the KO cells, "-". (**C**) When indicated, UCN-01 at 30 nM was added for 2 hours following the UV-C treatment. Two different exposures of the same blot are presented, a short exposure on the top and a longer one on the bottom. Red arrow indicates the position of an unknown phospho-Chk1 species.

5.4. Discussion

5.4.1. Summary

Work detailed in this Chapter has established a number of key points regarding PrimPol cellular functions. Following cell viability assay, *PrimPol* $^{-/-}$ cells appeared more sensitive to replication stress (UV light and 4NQO treatments) but not sensitive to ionising radiation. Also the absence of PrimPol was associated with an increase in RF stalling and a decrease in DNA replication rate following UV-C irradiation. A specific recruitment of human PrimPol protein to the sites of DNA damage during S-phase was also suggested as co-localisation with γH2AX foci was observed following UV-C exposure. Together these data establish PrimPol as a novel DNA damage tolerance factor. Interestingly, a counterintuitive UV-C dose-dependent response was observed in *PrimPol* $^{-/-}$ cells and suggested a pro-apoptotic role for PrimPol in response to >4 J/m^2 UV-C irradiation. This prompted further analysis of cell cycle progression and γH2AX signal following low and high UV-C exposures which led towards an investigation of the intra-S checkpoint response. Following UV-C irradiation and inhibition of Chk1 kinase activity by UCN-01, the pro-apoptotic role of PrimPol was further emphasized at both low and high UV-C exposure, and possibly uncovered a novel relationship between DNA damage tolerance and the essential kinase Chk1.

5.4.2. PrimPol's involvement in DNA damage tolerance mechanisms

Following the preliminary characterisation of *PrimPol* $^{-/-}$ cells during unperturbed growth conditions, a small defect in DNA synthesis being visible, analysis of cell viability was then investigated following replicative stress. Survival experiments were first tested using methylcellulose support but proved inapplicable due to the formation of two types of colonies in the absence of PrimPol (figures 5.1 and 5.2). Cell viability assay using CellTiter-Blue technology was then used instead. This type of assay does not reflect directly the ability of cells to survive to genotoxic agent treatments and thus is not always appreciated by the scientific community. However, cell viability assays allow assessment of a percentage of viable cells at a given time in a very accurate and reproducible manner, increasing the sensitivity of the detection. In *PrimPol* $^{-/-}$ DT40 cells, sensitivity towards replicative stress, UV-C and 4NQO, but not following DNA strand breaks induced by ionizing radiation, further supported PrimPol damage tolerance role previously hypothesised in Chapter 4 during unperturbed S-phase. RF progression, analysed by DNA replication rate (figure 5.8) and DNA spreading (figure 5.9) were

both significantly affected by the absence of PrimPol following UV-C irradiation. Moreover human PrimPol protein overexpressed in avian *PrimPol* null background accumulated into foci partially co-localising with γH2AX signal following UV-C irradiation. Together, these data led to the model depicted in figure 5.23. Following endogenously arising impediments, as previously discussed in section 4.5.4 and in by Sergei Mirkin's review (Mirkin and Mirkin, 2007), or following exposure to exogenous damaging agents like UV light or 4NQO for example, bulky lesions can arise and block replicative polymerase progression. In the absence of PrimPol, an increased number of stalled RF are unable to overcome the damaged DNA and thus can potentially collapse, increasing genomic instability (DSBs formation for example). However, presence of PrimPol maintains the level of damage tolerance operating directly at the stalled fork. Two mechanisms can then be envisaged, either the bypass of the bulky lesion by PrimPol TLS capability or the re-start of DNA replication downstream of the lesion via PrimPol primase activity. In this second case, post-replicative mechanisms can allow in a later time the filling of the ssDNA gaps left behind. In both cases, PrimPol's contribution to DNA damage tolerance, whether via re-priming or TLS activity, allows completion of the genome duplication and also the process of DNA lesions by NER by creating a dsDNA environment, thus promoting the removal of the damaged DNA and diminishing genomic instability.

Distinction between the recruitment of PrimPol for a bypass at the fork or for re-priming activity downstream the lesion remains undetermined. TLS activity of PrimPol, characterized *in vitro* on CPD and (6-4)PPs containing template (appendix A), now needs to be address by *in vivo* assay. Plasmid assay containing both CPDs and (6-4)PPs have already been employed in previous studies to characterize other TLS polymerases from the Y-family (Ziv *et al.*, 2012). Similar investigations remain to be done with *PrimPol* $^{-/-}$ DT40 cells to address an eventual mutagenesis signature for both types of UV photoproducts. Previous studies by the Prakash laboratory have described *in vivo* bypass of (6-4)PPs in human and mouse cells are predominantly error-free mechanisms involving Pol ζ enzyme (Yoon *et al.*, 2010). However, in DT40 cells it has been noticed the most common mis-insertion corresponds to the incorporation of a thymidine opposite the first thymidine of the (6-4)PPs, although it happens at a small frequency (Szuts *et al.*, 2008; Hirota *et al.*, 2010). This mutagenesis event is also observed following PrimPol primer extension assay performed *in vitro* with the human recombinant protein following the bypass of this highly distorting lesion (appendix A). An accurate quantification of PrimPol involvement during TLS bypass events of CPD and (6-4)PPs *in vivo* could also be assessed following Zvi Livneh methodology (Ziv *et al.*, 2012). Regarding the study of PrimPol involvement during re-priming events, only a few examples in the

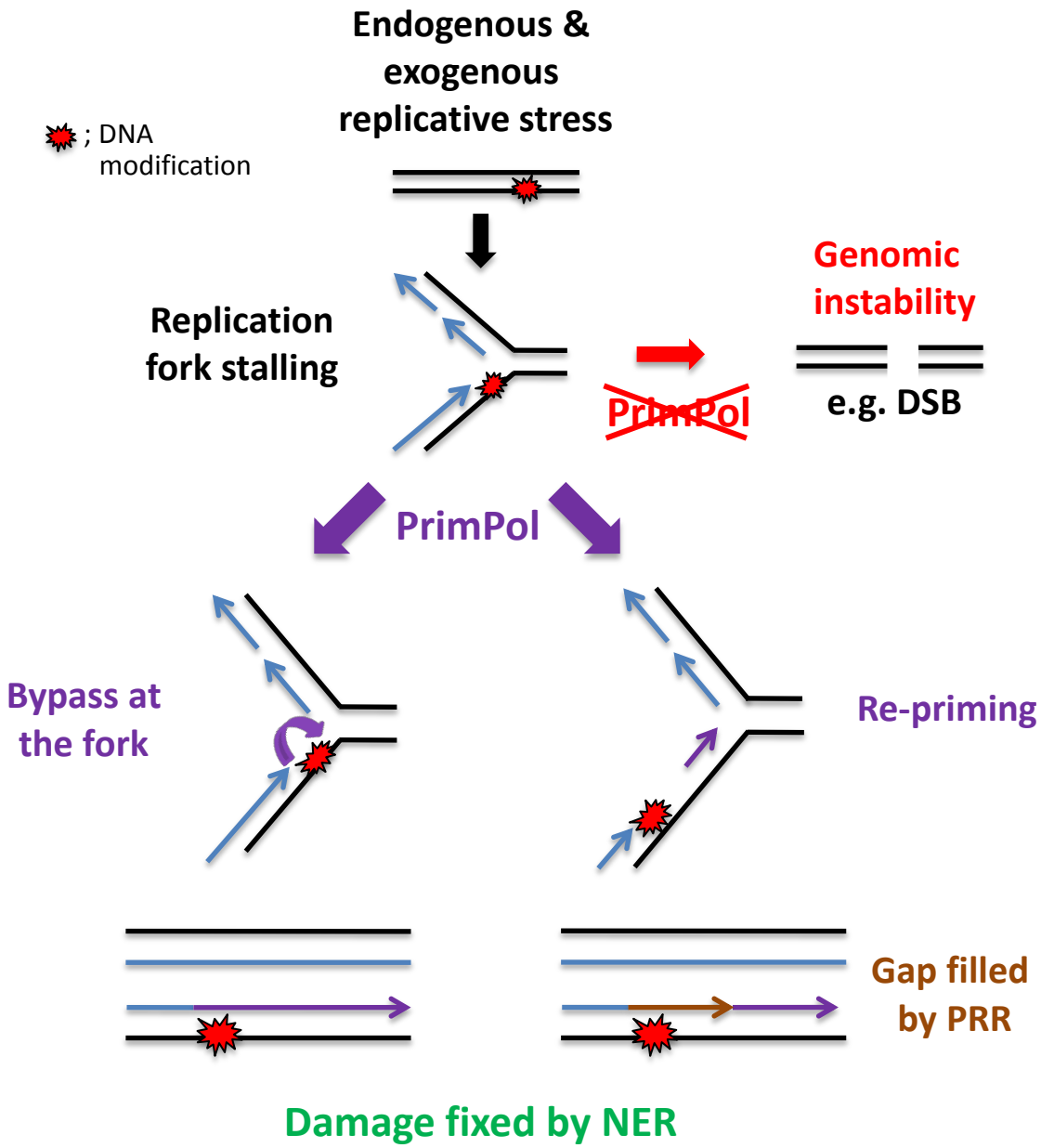

Figure 5.23: Model of PrimPol's involvement in DNA damage tolerance mechanisms.

Following endogenous or exogenous (UV light, 4NQO) replication stress creating bulky lesions blocking replicative polymerases, RF can stall and collapse in the absence of PrimPol (red) which could lead to genomic instability (DSBs formation for example). However, in the presence of PrimPol (purple), damage tolerance operating directly at the stalled RF can either allow the bypass of the bulky lesion by PrimPol TLS capability or re-start DNA replication downstream of the lesion via PrimPol primase activity. In this later case, post replicative mechanisms can allow the filling of the gap (brown). Double-stranded DNA containing the lesion can then be processed by NER to allow the removal of the damaged DNA (green).

literature can be studied to understand a potential place for PrimPol in this mechanism. Indeed, as PrimPol is absent from yeast, electronic microscopy analyses demonstrating the presence of ssDNA gaps following UV-C irradiation in *S. cerevisiae* can thus not be attributed to PrimPol's activity (Lopes *et al.*, 2006). In prokaryotes, re-priming activity described by Heller and Marians were performed using the replisome machinery and DnaG primases (Heller and Marians, 2006). Furthermore, lagging strand DNA synthesis by Pol α-Prim is discontinuous and therefore tolerates DNA damage, as demonstrated in vitro (Svoboda and Vos, 1995). This inherent property of the replisome machinery would also suggest no other damage tolerance specialised primase are needed in eukaryotic cells as Pol α-prim could also allow re-priming activity during the leading strand synthesis. With the discovery of a novel eukaryotic primase PrimPol, this question needs now to be specifically addressed. Preliminary data obtained here during PRR experiments support the fact PrimPol is not the primase required for the formation of ssDNA gaps following UV-C irradiation. However, contribution of PrimPol in this process cannot either be completely ruled out as the UV dose (4 J/m^2) and time window (90 minutes) experimented here might mask an eventual recruitment of PrimPol in other conditions. Moreover, the sensitivity of this assay has been adapted originally to visualise the involvement of the TLS polymerase responsible for filling those post-replicative gaps, and not the primase needed to create them. If Polα-prim is responsible for creating these gaps during the replication of the lagging strand and PrimPol is only needed for re-priming during the leading strand synthesis, sensitivity of this assay might again be too low to visualise this defect in the absence of this novel factor. Indeed ssDNA gaps were observed following UV-C irradiation in yeast every 3 kb on the leading strand whereas on the lagging strand, every 400 bp (Lopes *et al.*, 2006) thus leading to a ratio of primed DNA synthesis of 7.5:1 in favour of the lagging strand (Van *et al.*, 2010). Moreover, DNA spreading experiments, performed on UV damaged template (figure 5.9), do not permit to discriminate between a direct by-pass of the DNA lesion or re-priming activity of PrimPol downstream the UV photoproduct due the low resolution (3-4 kb) of the DNA fibre technique. Indeed if the gap created by the re-priming event is less than 3 kb long it will not be distinguishable from the direct bypass of a DNA lesion by TLS activity as it will be part of the same DNA fibre. Similar findings have previously been described by Helleday's laboratory, with a DNA fibre resolution being close to 2 kb (Elvers *et al.*, 2011).

To further understand the role of PrimPol during RF progression on damaged DNA, one key feature remains to be determined and concerns PrimPol's recruitment to the site of damage. Recent studies in DT40 cells have highlighted a temporal recruitment of TLS factors (Edmunds *et al.*, 2008). In this study, the C-ter of Rev1 is demonstrated to be required for TLS

bypass at the fork, whereas ubiquitylated PCNA is needed for PRR and appears dispensable for efficient RF progression (Edmunds *et al.*, 2008). According to this study and the characterisation of *PrimPol* $^{-/-}$ DT40 cells performed in this Chapter, it is thus possible to speculate PrimPol and Rev1 to be involved in the same pathway allowing a direct bypass of DNA lesions at the fork or "on the fly" mechanism. Epistatic studies should thus be performed to allow direct comparison of cell viability and RF progression following UV-C irradiation in *PrimPol* $^{-/-}$, *Rev1* $^{-/-}$, PCNA K164R and double mutants PrimPol/Rev1 and PrimPol/PCNAK164R DT40 cells. Also, immunofluorescence experiments looking at the presence of ssDNA (following BrdU incorporation and non-denaturing conditions) or the persistence of (6-4)PPs or CPDs at early and late time points following UV-C irradiation in *PrimPol* $^{-/-}$ cells could be performed to confirm the temporal recruitment of PrimPol, as previously described in other cases of TLS polymerase (Despras *et al.*, 2010; Temviriyanukul *et al.*, 2012). Further epistatic studies in combination with Y-family polymerase deficient cells could also be performed to explain the better survival of Pol η/Pol ζ double KO cells compared to individual depletion strains observed in response to UV-C irradiation (Hirota *et al.*, 2010). Indeed, the authors speculate an unknown TLS mechanism can allow the bypass on its own of UV-C damaged DNA in the absence of both Pol η and Pol ζ, whereas single depletion of each of these Y-family polymerases is more detrimental for the cells (Hirota *et al.*, 2010).

5.4.3. Counterintuitive apoptosis response in the absence of PrimPol

5.4.3.1. Sensitivity of *PrimPol* $^{-/-}$ cells towards low doses UV-C irradiation

Cell viability analysis performed with *PrimPol* $^{-/-}$ cells following UV-C exposure has revealed a counterintuitive dose-response phenotype as the cells were more sensitive to a low dose UV-C treatment (< 4 J/m^2) than a higher dose compared to WT DT40 cells (figures 5.3 and 5.5). This phenotype was further confirmed by the analysis of apoptosis response by DAPI counting, indicating an increase of apoptotic cells at 48 hours post 2 J/m^2 and a decrease in apoptosis following 5 J/m^2 in the absence of PrimPol (figure 5.13). Also, analysis of cell cycle progression following UV-C irradiation indicated an increase of sub-G1 population in the absence of PrimPol following 2 J/m^2 and an abnormal 4N peak observed at 24 hours post UV-C exposure (figure 5.11). Following 5 J/m^2 UV-C irradiation, a further delay in S-phase progression was also noticed (figure 5.12). Analysis of γH2AX patterns indicated persistence in γH2AX foci formation at 24 hours post-irradiation in *PrimPol* $^{-/-}$ cells following both low and high doses UV-C

irradiation (figure 5.14). In line with this, abnormally large cells were observed in in *PrimPol* $^{-/-}$ cells following 5 J/m^2 (figure 5.3A) supporting a strong G2/M cell cycle arrest when PrimPol was absent. This checkpoint response was also noticed when cell viability analyses were performed at early time point (48 hours) post UV-C or 4NQO, masking the sensitivity of the KO cells towards these cytotoxic agents (figures 5.5A and 5.6A).

In the literature, low dose UV-C is reported to activate the intra-S checkpoint resulting in the inhibition of replication initiation (Kaufmann *et al.*, 1980 and 1985). Activation of Chk1 by ATR in response to ssDNA at stalled RF leads to a decrease of chromatin bound CDC45 in result of CDK2 and CDC7 inhibition by Chk1 (Petermann *et al.*, 2010). As a result, the interaction of CDC45 and MCM helicase complex is compromised inhibiting origin firing mechanism (reviewed in Kaufmann, 2010). Thus, in *PrimPol* $^{-/-}$ cells, following low dose of UV-C irradiation, the intra-S checkpoint induces a decrease in origin firing and the absence of PrimPol leads to a further DNA synthesis decrease, as observed by the reduced thymidine incorporation rate (figure 5.8). However, *PrimPol* $^{-/-}$ cells still progress through S-phase with no significant delay, but this resulting in an abnormal 4N DNA content peak observed at 16 hours post 2 J/m^2 UV-C irradiation, which persisted until at least 24 hours post-irradiation (4N DNA content, figure 5.12C). Also, an increased proportion of *PrimPol* $^{-/-}$ cells at this time point contained DNA damage, as suggested by γH2AX foci (16% versus 2% in WT cells) (figure 5.14C). The question remains whether these *PrimPol* $^{-/-}$ cells stay arrested in G2 phase for a longer time than WT cells to repair this DNA damage, or progress through mitosis without repair thus leading to a higher risk of mitotic catastrophes and cell death to happen. Both hypotheses could then explain the decrease of cell viability observed in *PrimPol* $^{-/-}$ cells at 48 hours post low dose UV-C irradiation, although a prolonged cell cycle arrest could not explain the increase of *PrimPol* $^{-/-}$ apoptotic cells measured at 48 hours. However, the second hypothesis implicates a G2/M checkpoint blind phenomenon, as mitosis entry would be permitted on damaged/incompletely replicated DNA. In order to discriminate between both hypotheses, time course analysis of apoptosis following a low dose exposure should be undertaken to understand whether the apoptosis response is triggered before or after mitotic events. Moreover, analysis of chromosome stability via chromosome spreads could also indicate whether the absence of PrimPol is accompanied with an increase of mitotic catastrophes. Analysis of cell cycle by PI/BrdU double staining by flow cytometry following 2 J/m^2 UV-C at later time point (48 hours) have been undertaken but proved difficult due to the high cytotoxicity observed at this late time point (data not shown). Nonetheless, analysis of G2 (CENP-F) and mitosis (phosho-histone H3) markers by Western blot or flow cytometry should

be feasible and determine whether an increased proportion of *PrimPol* $^{-/-}$ cells is present in G2 phase between 24 and 48 hours. Thorough analysis of CDC25A, B and CDK1 phosphorylation status would also bring some insight whether the absence of PrimPol results in modifications of the G2/M checkpoint response.

5.4.3.2. Replication-dependent apoptosis phenomenon - PrimPol pro-apoptotic role following high UV-C doses exposure

In contrast to low UV-C doses*, PrimPol* $^{-/-}$ cells were not sensitive to higher UV-C doses and actually protected from apoptosis. Given PrimPol's role during DNA replication, there is a well-documented link between DNA replication and apoptosis. Previous study using DNA polymerases inhibitor aphidicolin on UV damaged cells observed a decrease of apoptosis following DNA synthesis inhibition by this drug (Batista *et al.*, 2006). The authors concluded it was the actual replication of UV damaged DNA that triggered the commitment for suicidal mechanisms, in a transcription independent manner. A similar study, using aphidicolin on docetaxel treated cells, also obtained similar conclusions (Zhang *et al.*, 2010). Similarly, decrease of apoptosis has been observed in confluent cells either NER deficient (XPC and TTD/XPD but not XPA) treated with UV-C (Carvalho *et al.*, 2003) or in Pol β deficient mice treated with MMS (Ochs *et al.*, 2002). These studies strongly support that S-phase progression is an important criterion for the triggering of apoptosis, independently of the repair capacity of the cells. Therefore, the apoptosis decrease observed in *PrimPol* $^{-/-}$ cells irradiated with high UV-C fluences could then be a direct consequence of the delay in S-phase progression (figure 5.12D) caused by the absence of PrimPol-dependent damage tolerance. Further, high fluence exposures cause an increased number of photoproducts leading to a stronger activation of the intra-S checkpoint, thus resulting in inhibition of both DNA replication initiation and elongation (Guo *et al.*, 2002; Seiler *et al.,* 2007; reviewed in Kaufman, 2010). Therefore, absence of PrimPol following specifically high UV-C doses, would further delay DNA replication elongation reinforcing the intra-S checkpoint response and thus further decreases apoptosis response. This pro-apoptotic role of a DNA damage tolerance factor is not unprecedented as Pol η has also been demonstrated to be pro-apoptotic following HU treatments (de Feraudy *et al.*, 2007). Indeed, XP-V cells treated with HU, which reduces the available pool of dNTPs and causes extensive RF stalling, presented a diminution of apoptosis. The authors concluded that this decrease of apoptosis was due to a cell cycle delay in S-phase (due to the absence of the

TLS polymerase), resulting in a slower rate of XPV cells to reach the G1/S boundary responsible for this HU-induced apoptosis response (de Feraudy *et al.*, 2007).

5.4.4. DNA damage tolerance, p53 status and apoptosis, study in XPV cells

The guardian of the genome p53 is an important player in the apoptosis response (Jiang *et al.*, 2010; Timares *et al.*, 2008) (figure 5.24). The lack of p53 function within DT40 cells could further contribute to the apoptosis response observed here in *PrimPol* $^{-/-}$ cells. Indeed, p53 status of XP-V cells has been demonstrated to influence cell survival after UV-C irradiation. For instance, the immortalisation method (via SV40 or HPV16 E6/E7) used conferred a different p53 status to the XP-V cells, and this directly affected the cytotoxicity observed after UV-C irradiation in the presence or absence caffeine. XPV primary fibroblasts are already sensitised by caffeine to UV-C irradiation, but the SV40 immortalisation process, conferring a non-functional p53 status to XP30RO cells, increases the sensitivity of the cells to UV-C irradiation in the presence of the drug (Arlett *et al.*, 1975; Cleaver *et al.*, 1999). In contrast, HPV16 E6&E7 transformed XP-V cells lacking p53 protein, are more sensitive to the UV-C irradiation but not prone to caffeine sensitisation (Cleaver *et al.*, 1999). Interestingly, caffeine sensitisation has been linked to DNA replication progression via Chk1 maintenance of RF stability, but is not yet fully understood (Despras *et al.*, 2010). Further experiments in p53 proficient cells should be undertaken to understand whether this apoptosis response observed here is specific to PrimPol and independent of the p53 status of the cells. Also analysis of the levels of the pro and anti-apoptotic proteins Bax and Bcl2 respectively should be investigated following UV-C exposure in the absence of PrimPol.

5.4.5. Correlation of apoptosis response in *PrimPol* $^{-/-}$ cells and tc-NER deficient cells

The counterintuitive phenotype obtained in *PrimPol* $^{-/-}$ cells between low and high doses of UV-C irradiation is not unprecedented in the literature, as tc-NER deficient cells also present a UV dose dependent induced apoptosis. Indeed, a common feature of tc-NER deficient cells is their increased sensitivity to low doses UV irradiation (Queille *et al.*, 2001). This cytotoxicity is believed to be due to lesions left unrepaired in active genes blocking the RNA polymerase complex which in turn triggers p53 dependent or independent apoptosis response (Ljungman *et al.*, 1996; McKay and Ljungman, 1999; Tornaletti, 2009). However tc-NER deficient cells are

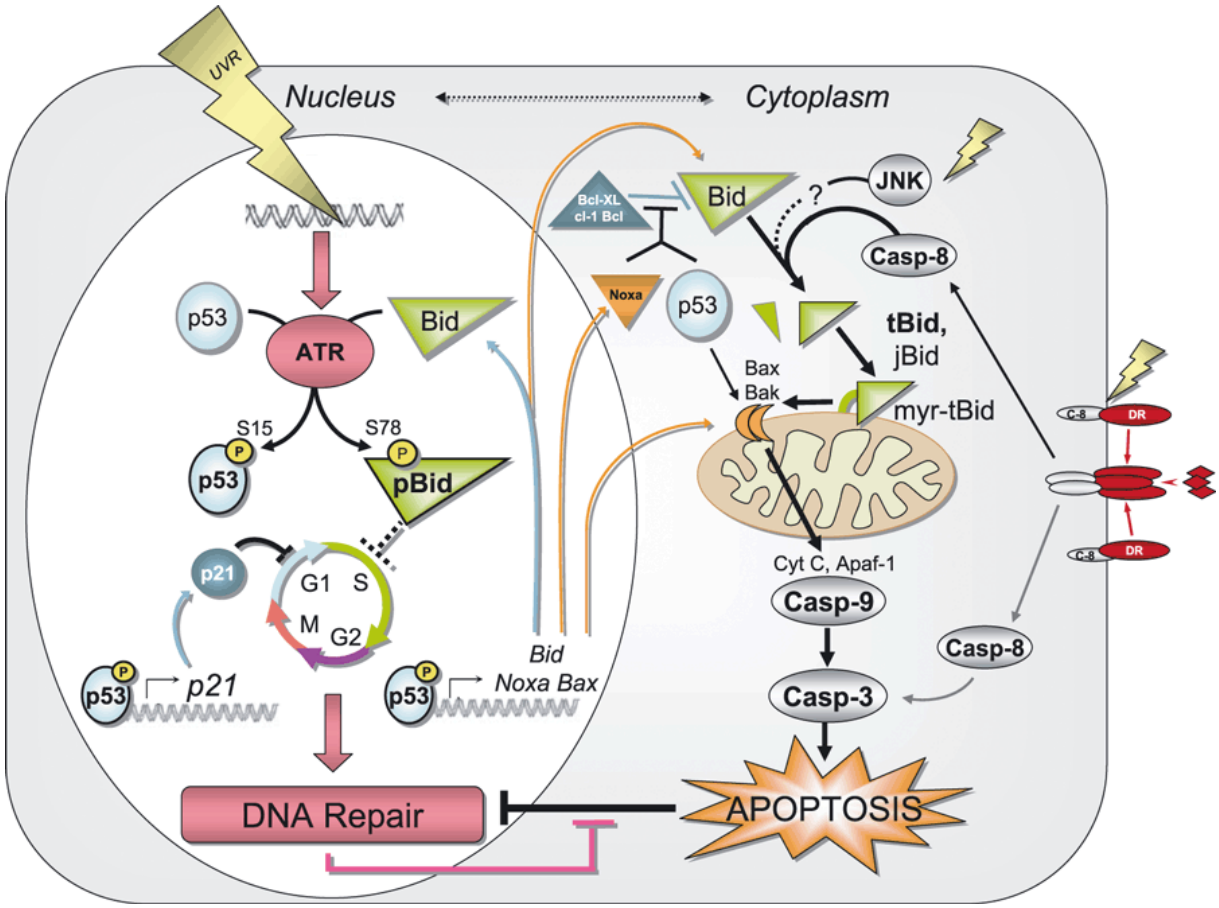

Figure 5.24: Relationship between UV damage response and apoptosis mechanisms.

In the nucleus, following UV light exposure and ATR activation at the site of stalled RF, p53, Bid (BH3 interacting-domain death agonist) and Chk1 gets phosphorylated (yellow P). Phospho-p53 transactivates the p21 gene, contributing to a cell cycle arrest in G1/S and activation of DNA repair mechanisms (pink box). Activated p53 also induces expression of Bid family member genes (Noxa, Bax) triggering apoptosis response in the cytoplasm via the caspase (cysteine protease) cascade. Briefly, activated JNK (c-Jun N-terminal kinases) and caspase 8 (Casp-8) contribute to the cleavage of Bid which can thus translocates to mitochondrial membrane inducing its disruption (via Bax and Bak). By consequence, mitochondria release their pro-apoptotic content like cytochrome c (Cyt C) notably, leading to the activation of the caspase cascade via caspases 9 and 3 (Casp-9 or 3) and the apoptosis response (orange star). Following high dose of UV exposure, death receptors (DR) like Fas (part of the Tumor Necrosis Factor, TNF) can aggregate and trigger activation of caspases 8 and 3 independently of mitochondrial pathway. DNA repair and apoptosis response are thus closely related and inhibit each other. (Cartoon was taken from Timares *et al*., 2008).

also more resistant to apoptosis after higher fluences than tc-NER proficient cells. Apoptosis response is not thus directly proportional to transcription or translation blockage mechanisms (Queille *et al.*, 2001; Mc Kay *et al.*, 2002). However it was noticed S-phase progression was required for the cells to trigger apoptotic pathway (as previously discussed earlier in 5.4.3.2), and perturbation of G1-S transition increased the apoptosis response in all NER defective cell lines tested (Mc Kay *et al.*, 2002). Taken together it is possible to speculate following low UV fluences, S-phase progression is not significantly impaired allowing apoptosis processes to take place in response to RNA polymerase complex stalling at CPD and (6-4)PPs in tc-NER deficient cells. After higher UV doses exposure, intra-S checkpoint activation inducing inhibition of DNA replication elongation results thus in a decrease of apoptosis. Moreover, stalling of RNA polymerase at DNA photoproducts in tc-NER deficient cells could also constitute a further physical blockage for the replisome progression reducing ever more DNA synthesis and the triggering of apoptosis. Having also observed an increased proportion of apoptotic cells following low doses of UV-C irradiation in *PrimPol* $^{-/-}$ cells, RNA synthesis response after UV-C exposure should be investigated in the absence of PrimPol. Indeed, PrimPol being also a DNA dependent RNA polymerase, a potential role during TLS transcription mechanism, preventing RNA polymerase complex from stalling at DNA photoproducts, can thus be speculated. This mechanism possibly introducing mutations in mRNAs, has been less studied than TLS by DNA polymerases due to the efficiency of tc-NER pathway (Cohen and Walker, 2011). Epistatic studies could then be performed in tc-NER deficient strains to evaluate the influence of the absence of PrimPol, in term of cell viability and apoptosis response. Also, the damage tolerance role of PrimPol (via TLS or re-priming, as described previously section 5.4.1), could also interfere with global NER repair pathway, by allowing the bypass of the DNA photoproducts and generating a dsDNA context allowing the removal of the lesion (figure 5.23). Therefore, the absence of PrimPol could result in an increase of unrepair lesions by NER potentially blocking the transcription machinery. It is therefore possible to speculate a link between PrimPol's role (by direct or indirect ways) within the transcription of active genes, as previously described in Chapter 4 during unperturbed S-phase.

5.4.6. Damage tolerance and intra-S checkpoint response, an intricate relationship

Following the counterintuitive cytotoxicity observed following low and high dose UV-C irradiation in *PrimPol* $^{-/-}$ cells, a preliminary study of intra-S checkpoint response was initiated using Chk1 inhibitor UCN-01. Unexpectedly, the absence of PrimPol was able to partially

compensate inhibition of Chk1 as *PrimPol* $^{-/-}$ cells were less sensitive to the cytotoxicity effect of UCN-01 drug, in the presence and absence of UV-C irradiation (figure 5.17, 5.18, 5.19). Moreover, the absence of PrimPol was able to partially compensate the increase of DNA synthesis (figure 5.20) and early mitosis entry (figure 5.21) generated by Chk1 inhibition by UCN-01. Those experiments should be repeated by using Chk1 RNAi depletion instead of UCN-01 to ensure these phenotypes are specific to Chk1 inhibition. However, a recent study shown Chk1 has also an important role as a platform to maintain RF progression (Speroni *et al.*, 2012), thus RNAi depleted cells, or *Chk1* $^{-/-}$ DT40 cells should be complemented with kinase-dead enzyme to specifically investigate inhibition of Chk1 downstream effectors. Previous study of Chk1 inhibition by UCN-01 has demonstrated the increase of DNA synthesis rate was due to an increase binding of CDC45 to chromatin (Syljuasen *et al.*, 2005), thus CDC45 non-extractable protein levels should be quantified in *PrimPol* $^{-/-}$ cells in the presence and absence of UCN-01 to confirm whether the absence of PrimPol influence directly or not origin firing. DNA combing analysis in *PrimPol* $^{-/-}$ cells could also answer this and inform whether a feed-back mechanism of origin firing can compensate the defect in RF progression during perturbed and unperturbed S-phase. To verify whether the early mitotic entry is CDC25A-dependent as suggested by the literature (Xiao *et al.*, 2003), protein levels of CDC25A should be investigated in *PrimPol* $^{-/-}$ cells with the presence and absence of UCN-01.

One particularly intriguing result obtained following Chk1 inhibition by UCN-01 was the increase of cell viability observed in *PrimPol* $^{-/-}$ cells following low doses UV-C irradiation in the presence of 30 nM UCN-01 compared to irradiated *PrimPol* $^{-/-}$ cells with no UCN-01 (figure 5.17B, purple lines at 1 J/m^2). Inhibition of Chk1 was thus beneficial for *PrimPol* $^{-/-}$ cells as less apoptosis was observed at 48 hours post low dose UV-C irradiation (figure 5.19, 1 and 2 J/m^2). Further experiments need then to be done to address whether addition of UCN-01 following low dose UV-C (< 2J/m^2) improve cell viability of *PrimPol* $^{-/-}$ cells by releasing them from a potentially prolonged G2 cell cycle arrest or by directly compensating DNA replication default observed in the absence of PrimPol cells and leading to an abnormal 4N DNA content (figure 5.12C). A thorough analysis of apoptosis response at early time points following low dose UV-C exposure in the presence and absence of UCN-01 could also reveal whether an early increase of replication-induced apoptosis occurred as expected from the inhibition of Chk1. Indeed an early increase of apoptosis due to UCN-01 could then be masked by a release from a G2 arrest in a second time. Analysis of chromosome spreading and quantification of phospho-histone H3 would then help to follow whether mitosis events are perturbed in the absence of PrimPol and Chk1 inhibition.

To further understand how the absence of PrimPol can compensate the UV-C induced cytotoxicity linked to Chk1 inhibition, it is possible to speculate the absence of PrimPol could directly perturbate intra-S checkpoint activation. Indeed, previous studies from the Cimprich laboratory have determined the importance of primed ssDNA for ATR activation (MacDougall et al., 2007; Paulsen and Cimprich, 2007; Cimprich and Cortez, 2008). Recent findings suggest ATR activation is performed in two phases, an initial activation followed by an amplification of the signal, with TopBP1 being a key element in both mechanisms (Lin et al., 2012b; Yan and Michael, 2009b). PrimPol could then be involved in one of these mechanisms. TopBP1 has been shown in Xenopus to be needed for the recruitment of Pol α-prim and the 9-1-1 complex at stalled RFs (Yan and Michael, 2009a). If PrimPol is involved in RF restart (e.g on the leading strand), it could then be involved in providing primed ssDNA, thus influencing the checkpoint response. It has been previously observed PrimPol RNAi depletion in MRC-5 cells and XP-V cells lead to an over-activation/persistence of Chk1 phosphorylation following 2 J/m^2 (appendix). These data confirm thus PrimPol is not directly needed for ATR activation, but could be involved in a process amplifying ATR activation in order to optimise the checkpoint response and a quick repair of the damaged DNA. In the absence of PrimPol, a slower checkpoint response would then take place leading to a persistence of Chk1 phosphorylation. Further analysis are thus needed to confirm if PrimPol could be involved with TopBP1 for amplification of ATR signal, which could reinforce the link between damage tolerance (RF restart) and checkpoint activation.

Further, a recent paper investigated the link between intra-S checkpoint and the caspase-3-dependent apoptosis response (Myers et al., 2009). According to their model, in the absence of Chk1 activation, RPA foci accumulation could trigger a direct caspase-3-dependent apoptotic response. Once again data presented in this Chapter support a pro-apoptotic role of PrimPol due to its role within RF progression maintenance, which could be directly related to this caspase-3-dependent apoptosis response.

CHAPTER VI

Purification of recombinant human PrimPol protein

6.1. Expression of human PrimPol using a baculovirus insect cell system

6.1.1. Overview of expression studies of recombinant human PrimPol

One of the main goals of studying this novel eukaryotic primase-polymerase PrimPol, was to achieve high scale purification of the recombinant protein for biochemical and crystallography studies. Human PrimPol cDNA (from IMAGE clone) was cloned into pEt28 vector (table 2.7) and the construct was inserted in various bacterial expression strains (e.g. B834s (De3), BL21 (De3)) (Andy Green and Aidan Doherty, unpublished data). Unfortunately, the yields of expression of recombinant histidine (His) tagged PrimPol (His-PrimPol) protein were very low. It was also tried to use an optimised version of the cDNA, taking into account *E. coli* codon usage bias methodology (Genscript), but this approach was unsuccessful as the protein remained mainly insoluble (Andy Green, Aidan Doherty, personal communication). As the polypeptide predicted size was above 50 kDa (64 kDa according to ExPASy ProtParam tool; appendix B) it was recommended (Gräslund *et al*., 2008) to use baculovirus system, which provides a more suitable eukaryotic translation environment (e.g. more appropriate tRNAs, molecular chaperones, etc) and also allowing possible post-translational modifications of the protein. In this way the folding of the polypeptide can be improved, potentially increasing the solubility of the recombinant protein (Ghosh *et al.*, 2002). Baculovirus expression vector system (BEVS) exploits the fact that baculovirus can infect insect cells but also mammalian hepatocytes in culture (Ghosh *et al.*, 2002). The genome of the virus (double-stranded and circular) is engineered to integrate the heterologous cDNA of the protein of interest. Infection of insect cells with the recombinant baculovirus shuttle vector (or bacmid) leads to the expression of the ectopic protein within an eukaryotic system in a large quantity.

6.1.2. Expression of human PrimPol using baculovirus expression system

PrimPol cDNA was first cloned into a pFastBac-HT vector in order to express the protein with a N-terminal HIS tag, under the control of a strong polyhedrin promoter according to the Bac to Bac system (Invitrogen). Transposition reaction with Tn7 elements allowed then incorporation of recombinant PrimPol within the bacmid genome (bMON14272, containing an *Autographa californica* multiple nuclear polyhedrosis virus (AcMNPV) genome), as described in figure 6.1 (steps 1 and 2). Following extraction of the recombinant bacmid from *E. coli* DH10Bac cells (figure 6.1, step 3), insect cells *Spodoptera frugiperda* clonal isolate 9 (Sf-9) were transfected in order to obtain a recombinant baculovirus stock P1 (figure 6.1, step 4). Several amplification

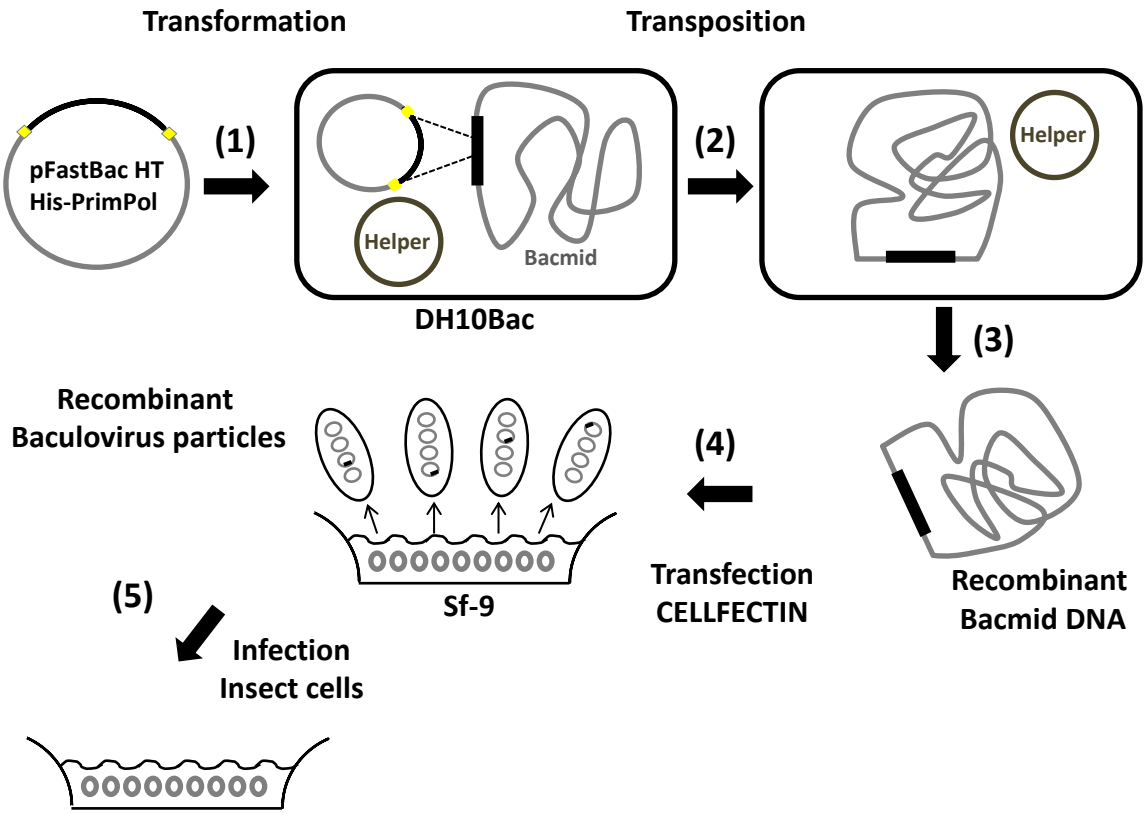

Figure 6.1: Overview of baculovirus expression system.

(**1**) Transformation of *E.coli* DH10Bac cells with pFastBac HT vector containing human PrimPol, cloned inbetween Tn7 transposon sites (yellow squares). Bacterial cells contain a helper plasmid encoding transposase enzyme thus allowing integration of His-PrimPol inside the bacmid genome (black rectangle) (**2**). Recombinant bacmid DNA is extracted from DH10bac cells (**3**) and then transfected into insect cells Sf-9 with CELLFECTIN reagent (**4**). Recombinant baculovirus stock P1 is then re-amplify by infecting fresh Sf-9 cells (**5**) and the process is repeated several time until a decent viral titer is obtained. Cartoon adapted from Invitrogen Bac-to-Bac manual.

rounds were repeated by infecting Sf-9 cells with the previous baculovirus stock until the concentration of the virus reached 10^7 pfu/ml (figure 6.1, step 5). All the steps described here, from the cloning to the generation of P1 baculovirus stock, were performed by a former colleague, Andy Green.

At this stage, different virus concentrations were tested to optimise the infection protocol on a small scale of Sf-9 cells (figure 6.2). A crude purification of PrimPol protein was then performed to determine the optimal conditions of infection (figure 6.2). A 66 kDa protein species, corresponding to His-PrimPol was clearly visible in the elution fractions, and more strongly present in the first fractions, as expected. The last eluted samples contained even purer PrimPol as most of the protein contaminants, species binding the nickel resin non-specifically, were previously eluted. Infection with an intermediate concentration of baculovirus provided the best yield (figure 6.2B). Increasing the amount of virus by a factor 2.5 was probably toxic for the cells as less PrimPol protein was expressed (figure 6.2C). An increase of protein degradation seemed unlikely as the amount of smaller species (< 66 kDa) were similar between both samples obtained following infections with 200 and 500 μl of virus (figure 6.2B and C).

6.1.3. Purification of PrimPol expressed in insect cells using a baculovirus system

Large scale purification was undertaken using the baculovirus infection conditions previously determined (figure 6.3). Once the cells lysed (in triton containing buffer) and the protein recovered from centrifugation, affinity and ion exchange chromatography columns, connected to a low pressure pumping system (ÄKTA Prime, Amersham Pharmacia), was used to accelerate and optimize the purification process (figure 6.3). Following immobilized metal ion affinity chromatography (IMAC), recombinant His-PrimPol protein was recovered from the nickel resin (Ni-NTA) by increasing imidazole concentration in the elution buffer (figure 6.3A). Even the first eluted fraction, obtained with 5% of buffer B, which contained 300 mM imidazole, presented a high proportion of full length PrimPol protein compared to the amount of contaminant or degradation species (figure 6.3A). However, when subsequent purification steps (e.g. ion exchange chromatography) were undertaken on the PrimPol containing IMAC fractions, a vast proportion of the protein was subject to degradation despite keeping the samples on ice and in the presence of protease inhibitors (figure 6.3B, species < 60 kDa). It has been difficult to address if the major degradation species (lanes 3 and 4, underneath full length

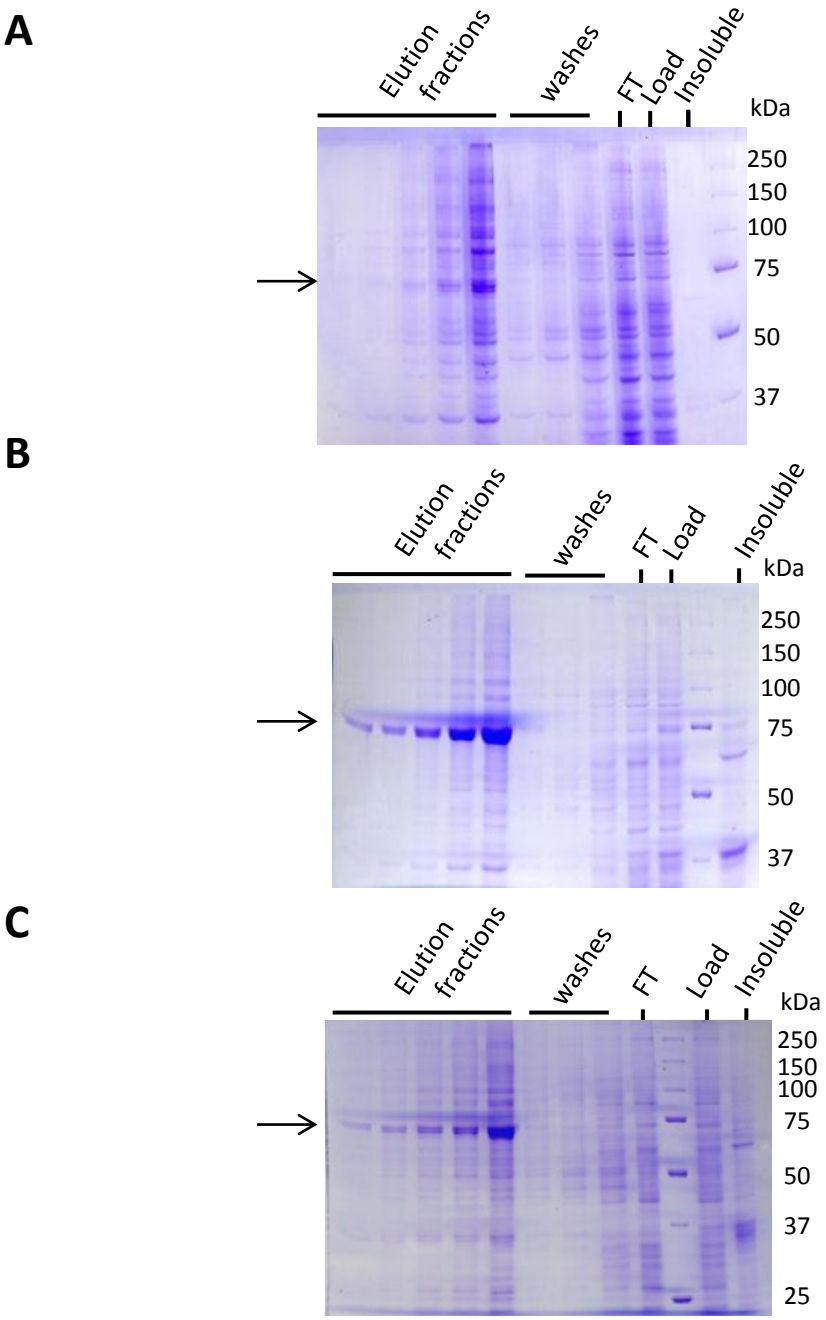

Figure 6.2: Small scale purification of PrimPol recombinant protein in Sf-9 cells using baculovirus system.

Small amount of Sf-9 cells (15 ml) were infected for 96 hours (virus P4) before freezing the cell pellets in liquid nitrogen and stored them at -80°C. Affinity purification using small batch of Ni-NTA resin was performed collecting small aliquot of sample at each step of the process. Coomassie staining of SDS-PAGE analyses are represented here following 3 independent infections with either (**A**) 50 µl (**B**) 200 µl (**C**) or 500 µl of virus P4. "Insoluble" samples corresponded to the pellet obtained following lysis of the cells; "load" fraction corresponded to the cell lysat before binding to the resin. Flow through (FT) represented the fraction of cells which did not bind to the resin. Washes were performed with increased concentrations of imidazole (10 mM, 20 mM and 30 mM from right to left). Five successive elution fractions (from right to left) were performed in lysis buffer supplemented with 300 mM imidazole. Black arrows indicate His-PrimPol protein full length size.

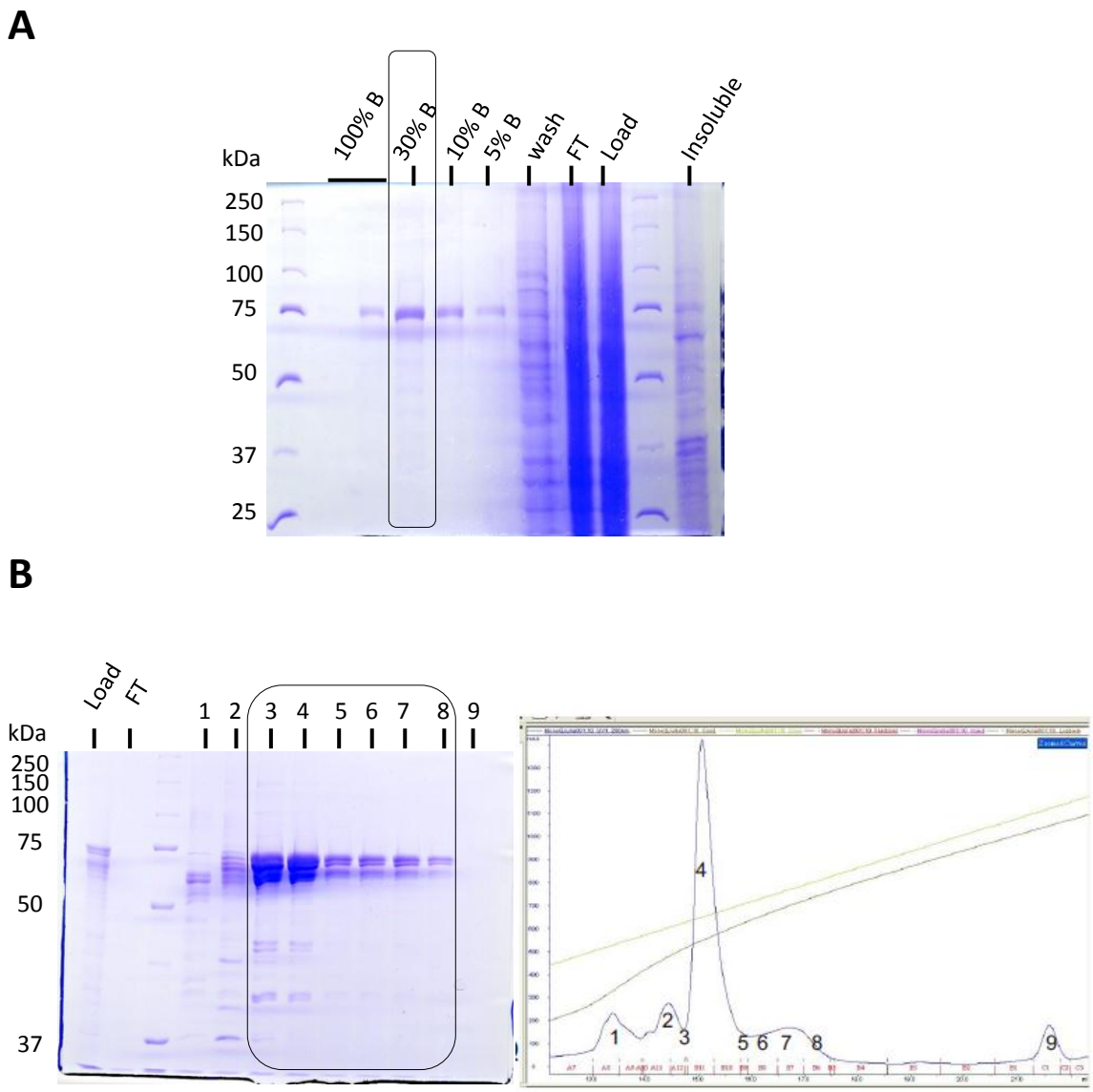

Figure 6.3: PrimPol protein purification in Sf-9 cells using baculovirus system.

Large scale (900 ml) of Sf-9 cells were infected for 96 hours (virus P4) before IMAC purification with Ni-NTA resin was performed on the same day of the cell harvest. (**A**) Coomassie staining of SDS-PAGE analysis allowed visualisation of the protein samples collected at different stages of the IMAC purification. Following the binding of the cell extract onto the resin, flow through (FT) was collected and the resin washed with lysis buffer containing 30 mM imidazole. Elutions with increasing concentration of B buffer (containing 300 mM imidazole) were performed (5% to 100% B). Fraction collected with 30% B (black box) was then used for anion exchange chromatography (**B**) using mono-Q column and ÄKTA purifier (Amersham Pharmacia). Coomassie staining of SDS-PAGE analysis (left panel) was performed to visualise the different fractions collected by the purifier according to optical absorbance fluctuations readings (UV light at 280 nm, blue curve, right panel). Numbers of the fractions (1-9) are indicated under the corresponding peaks of the chart.

PrimPol) resulted from overnight storage at ~4°C, inbetween both chromatography steps, (comparison load sample and 30% IMAC elution) or from the concentration of the protein sample into a low-salt buffer required for ion exchange chromatography (figure 6.3A and B). Moreover, stability of PrimPol baculovirus stocks has posed a real problem in term of reproducibility of Sf-9 infection protocols, and despite the fact fresh stocks of virus were routinely made, this original high yield of PrimPol protein (figure 6.2B) was never achieved again (data not shown). Problems experienced during the purification process (figure 6.3B, high levels of degradation) and during infection of Sf-9 cells (due to the variability of the virus stocks) led us to search for another, more reproducible, expression system.

6.1.4. PrimPol phosphorylation sites identified in recombinant PrimPol

As discussed previously, one advantage of using baculovirus technology is the expression of recombinant protein in eukaryotic system, allowing post-translational modifications to occur *in vivo* before purifying the protein. Notably, recombinant PrimPol protein prepared from baculovirus preparations was observed to migrate as a doublet on SDS-PAGE (figure 6.3B, lanes 5 for example). A similar doublet was previously observed by Western blot analysis with endogenous PrimPol protein from human cell extracts and also with human PrimPol overexpressed in DT40 cells (figures 4.11 and 6.11C). We speculated then that a fraction of PrimPol may be phosphorylated in Sf-9 cells thus resulting in a higher migrating species on SDS-PAGE. To test this hypothesis, recombinant PrimPol protein purified from baculovirus was treated with lambda (λ) phosphatase to see if the potential modification is sensitive to this enzyme (figure 6.4A; experiment performed by Andy Green). The disappearance of the higher species of the doublet, after 15 minutes incubation at 30°C with the enzyme (figure 6.4A), indicated that PrimPol had been phosphorylated *in vivo* by endogenous insect kinases. To confirm this hypothesis and determine the sites of phosphorylation, a sample of each species of the doublet (figure 6.4B) was sent for mass spectrometry analysis (Dr Mark Skehel, CR-UK) and four serine sites were found phosphorylated in the higher species only (figure 6.4C, underlined in red). Following on this analysis, samples prepared from streptavidin pull-down performed with stable Hek293 cell line overexpressing human PrimPol were also send to mass spectrometry and only serine residues 499 and 501 (figure 6.4C, circled in red) were shown to be phosphorylated (Sean Rudd, Aidan Doherty, personal communication). It is therefore possible to speculate that the phosphorylation observed on serine residues 33 and 255 were due to Sf-9 specific kinases. Nonetheless, mutagenesis of S_{499} and S_{501} into alanine residues (AA

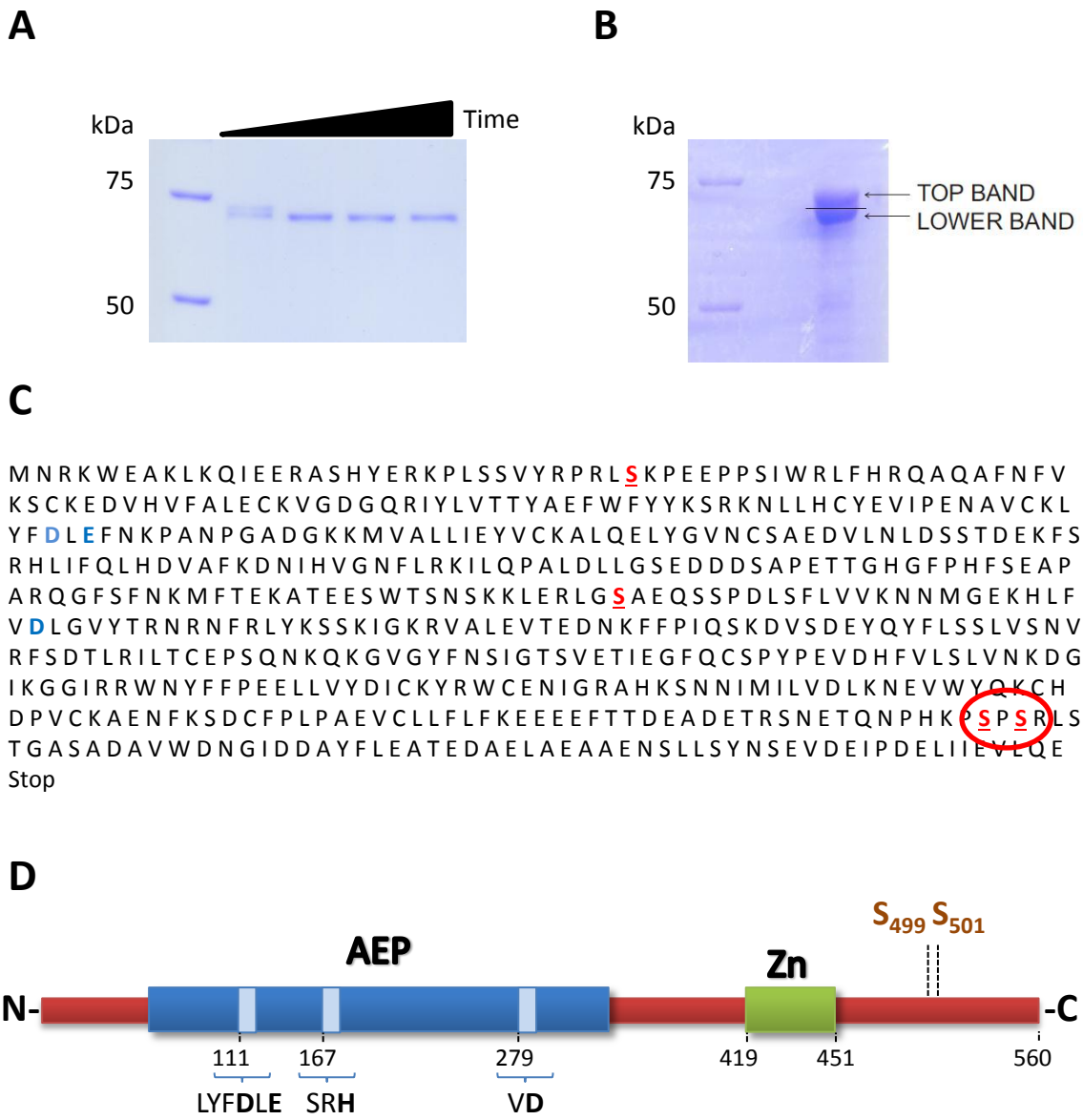

Figure 6.4: Human PrimPol phosphorylated sites in Sf-9 and human cells.

(**A**) λ phosphatase treatments were performed at 30°C with 2 µg of PrimPol protein and 5 µl of enzyme for 0, 15, 60 and 120 minutes before analysing the samples by SDS-PAGE. (experiment performed by A. Green). (**B**) Human His-PrimPol protein expressed by baculovirus system in Sf9 cells and purified by Ni-NTA IMAC, and anion exchange mono Q columns, was run on SDS-PAGE (8% acrylamide) to separate both species of the doublet and sent each band to Dr Mark Skehel (CR-UK) for mass spectrometry analysis. (**C**) Human PrimPol's amino acid sequence contents 4 phosphorylation sites found in the mass spectrometry analysis : serine residues 33, 255, 499 and 501 (underlined in red). S_{499} and S_{501} (circled in red) were also found phosphorylated in Hek293 cells stably expressing human PrimPol. Acidic residues part of the catalytic triad are also indicated (blue). (**D**) Cartoon of human PrimPol protein detailing the positions (amino acid number underneath) of the conserved domains of the protein; motif I, II and III (light blue) are characteristic of AEP domain (dark blue). Consensus sequences are indicated below with the conserved residues (bold) of the catalytic triad (motifs I and III) and nucleotides binding (motif II). Zinc finger domain (green) and the phosphorylation sites (brown) found in both Sf-9 and human cells are also indicated.

phospho-null mutant) or into glutamic acid (EE, phospho mimic mutant) has been performed in Flag-strep PrimPol construct to generate two phosphorylation mutant human cell lines (Laura Bailey, Aidan Doherty, personal communication). Over-expressing PrimPol AA mutant ran as a single species on Western blotting analysis, whereas EE mutant was similar to WT protein extract, confirming the higher band of the doublet corresponded to phosphorylated state of PrimPol (Laura Bailey, Aidan Doherty, personal communication). Further localisation studies are underway with these two cell lines to investigate if the phosphorylation state can influence the cellular distribution of the protein (Laura Bailey, Aidan Doherty, personal communication).

6.2. Expression of human PrimPol using *E. coli* SHuffle system

6.2.1. Overview of *E. coli* SHuffle protein expression system

Several bacterial strains, specifically engineered to improve expression of low solubility protein, (e.g. Rosetta Gami 2, BL21 codon plus) have been tested by former members of the laboratory and SHuffle strain (NEB) provided the most promising results (Tamsyn Cromwell, Aidan Doherty, personal communication). SHuffle strain has been obtained by modifying BL21 *E. coli* cells in order to introduce a deletion of two reductase genes glutaredoxin (*gor*) and thioredoxin reductase (*trxB*); mutation of the peroxidase *ahpC* (alkyl hydroperoxide peroxidase subunit C) to a disulphide reductase is then needed to restore the viability of the cells (Ritz *et al.*, 2001). These modifications of the redox state and the expression of a disulphide bond isomerase (DsbC) allow the formation of stable disulphide bonds within the cytoplasm of these SHuffle cells, as depicted in figure 6.5A (Lobstein *et al.*, 2012). This combination enhances the formation of disulphide bonds within the recombinant proteins improving their correct folding, hence their solubility. Moreover, DsbC has also been shown to act as a chaperone protein independently of its role in disulphide bonds formation (Lobstein *et al.*, 2012). The strain is recommended to be grown at 30°C, slowing down the expression process of the recombinant protein and potentially preventing them for degradation.

6.2.2. Optimisation of purification protocols in *E. coli* SHuffle cells

A small scale expression trial was first performed to determine the optimum conditions of induction of recombinant His-PrimPol (figure 6.6). *E. coli* SHuffle cells, transformed with pEt28-

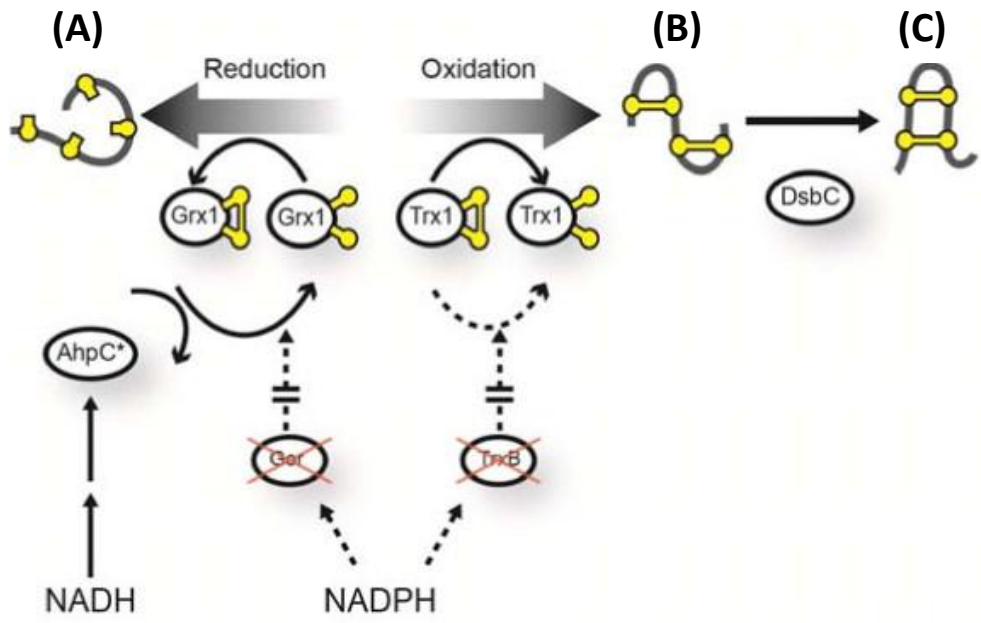

Figure 6.5: Modification of the redox state in *E. coli* SHuffle cells.

Cartoon explaining the modifications engineered in *E.coli* cells to change the redox state of SHuffle cell's cytoplasm. Cysteine residues (yellow balls) are depicted as reduced (ball) or oxidized (ball with stick). Despite the deletion of glutaredoxin reductase gene (*Gor*) Glutaredoxin 1 (Grx1) remains reduced due to the mutation of the peroxidase AhpC into a disulfide reductase (AhpC*). However, Thioredoxin-1 (Trx1) remains oxidised due to the deletion of Trx1 reductase gene *TrxB*. Protein expressed in SHuffle cells can then be reduced by Grx1 (**A**) or oxidised by Trx1 (**B**). Presence of disulphide bond isomerase (DsbC) allows then the correct folding of the mis-oxidised protein (**C**). Cartoon adapted from Lobstein *et al*., 2012.

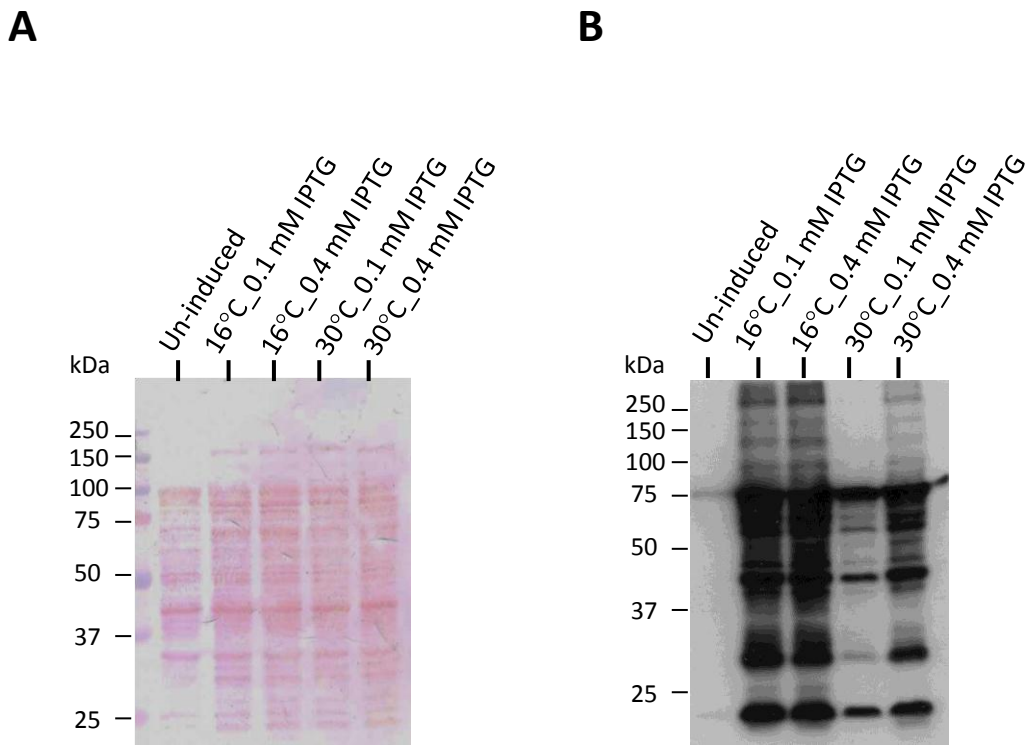

Figure 6.6: Small scale expression of human PrimPol in *E. coli* SHuffle cells.

10 ml of E. *coli* SHuffle cells, transformed with pET28-PrimPol plasmid, were grown at 30°C until optical absorbance at 600 nm reached 0.4. Cultures were then induced with different concentrations of IPTG (0.1 or 0.4 mM final) and incubated for either 3 hours at 30°C or overnight at 16°C before freezing the cell pellets. Cell were then lysed, sonicated and loaded onto 10% SDS poly-acrylamide gel before Western blot analysis. Visualisation of total proteins was achieved by Ponceau staining of the membrane (**A**) and anti-His antibody was used to detect recombinant His-PrimPol protein specifically (**B**).

PrimPol (table 2.7) were grown at 30°C until the culture reach exponential growth (OD_{600} ≈0.4) before different conditions of IPTG induction were tested (figure 6.6). Cultures induced overnight at 16°C resulted in a better yield than cells grown for 3 hours at 30°C as indicated by the Western blot quantification (figure 6.6B). In this case, both IPTG concentrations tested, 0.1 and 0.4 mM, did not make any difference on the amount of total protein produced (figure 6.6B). The process was then scaled up and purification protocols optimised to obtain a large amount of active, non-degraded PrimPol protein, in a preparation deprived of protein contaminants. A 3L culture of SHuffle *E. coli* cells transformed with pET28-PrimPol, was grown in media containing 100 μM zinc sulphate as the metal ion has been previously shown to improve the stability of zinc-finger containing proteins (Berg *et al.*, 1990). After overnight IPTG induction at 16°C, proteins were lysed in a buffer containing NP40 and lysozyme as it was noticed SHuffle cell's walls can be particularly difficult to break down. His-PrimPol was recovered from protein lysate by IMAC purification using Ni-NTA resin (figure 6.7A). Following protein binding step and flow through collection, the resin was washed thoroughly with lysis buffer then with 5% elution buffer B which contained 300 mM imidazole (figure 6.7A). Elution of the remaining full length PrimPol protein was achieved by flushing the Ni-NTA resin with 100% B buffer (figure 6.7A). However, this fraction also contained higher MW species which needed to be removed by further chromatography purification steps (figure 6.7A). An anion exchange Q-Sepharose column was then used to further purify the protein preparation, as PrimPol theoretical isoelectric point is 5.6 according to Expasy protein parameter tool (appendix B), therefore it should be negatively charged at pH 7.5 and able to bind to the positively charged solid support of the Q-Sepharose column. Indeed, after dilution of the sample (100% B elution IMAC) in a low salt buffer, both PrimPol and the higher MW species were still able to bind to the column but the majority of the contaminant was eluted in lower salt concentration fractions (figure 6.7B). However, a small portion of unwanted protein was still present in the first PrimPol containing elution fraction (figure 6.7B, fractions in the box). It was then decided for the subsequent purifications of PrimPol by ion exchange columns, to perform a step elution process where contaminant species were eluted with 20% of B buffer containing 1 M NaCl (data not shown). Otherwise, a heparin-Sepharose column, a pseudo affinity column that mimics DNA's phosphate charged surface, allowed the separation of the DNA binding protein PrimPol from its non-specific contaminants, which did not bind to the column (figure 6.7C).

A final purification step was achieved using size-exclusion chromatography, which allows separation of proteins according to their size and shape. This step is essential to achieve

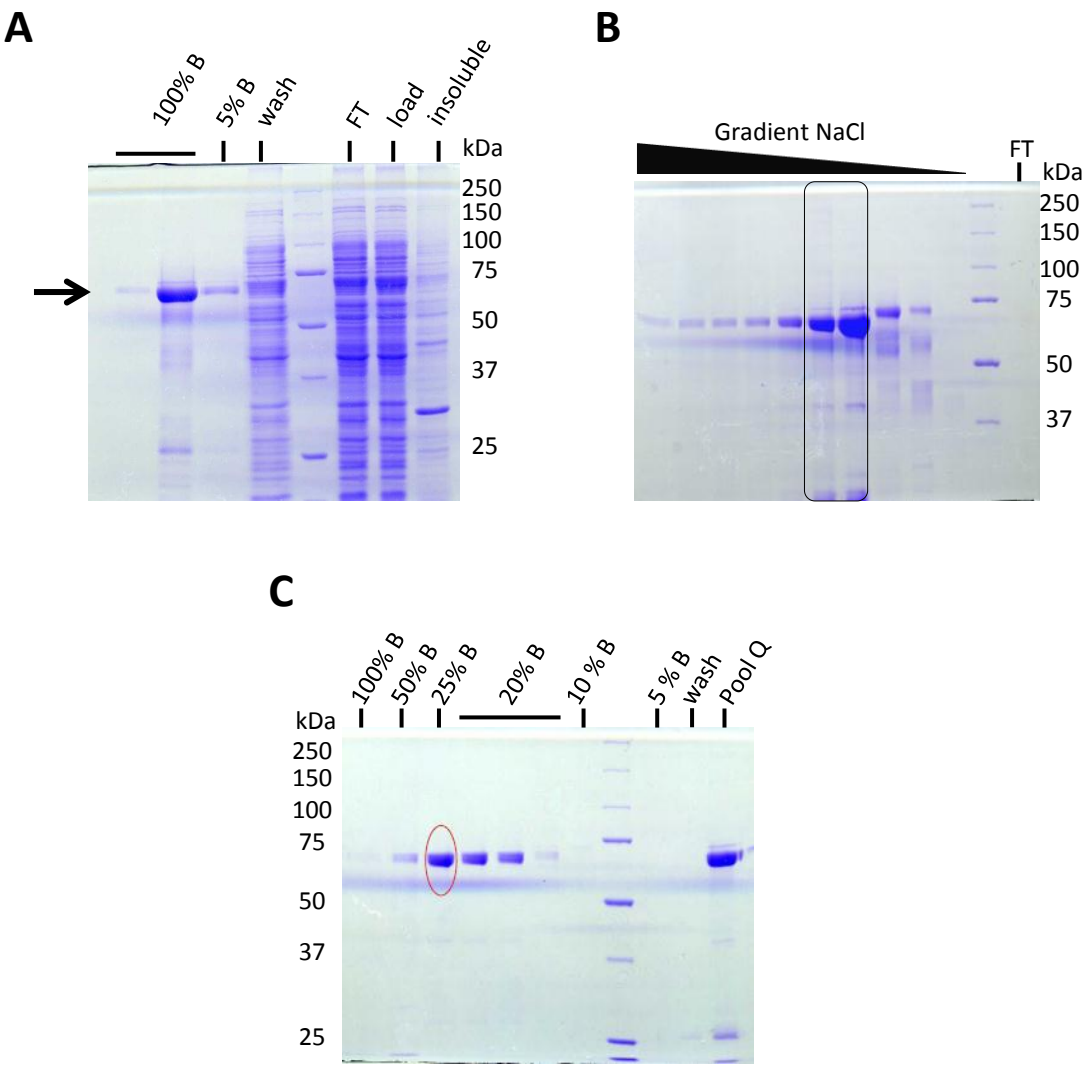

Figure 6.7: Human PrimPol protein purification using in E. *coli* SHuffle cells.

3L of E. *coli* SHuffle cells transformed with pET28-PrimPol were induced at 16˚C for 18 hours with 0.4 mM IPTG before freezing the cells pellet. Coomassie staining of 10% SDS-polyacrylamide gels was performed following the successive purification steps. (**A**) Total protein sample issue of the cell pellet lysis was loaded onto Ni-NTA resin (Load) and the flow through (FT) collected. An aliquot of non-induced and insoluble samples were also loaded onto the gel to check the level of expression and solubility of recombinant human PrimPol. Nickel resin was then washed with lysis buffer (containing 30 mM imidazole) and eluted with 5 or 100% B buffer containing 300 mM imidazole. PrimPol containing fraction (100% B) was then diluted in a buffer with no salt and loaded onto a Q-sepharose column (**B**). Salt gradient (0 to 1M NaCl) was performed to elute the proteins bound to the resin. PrimPol containing fractions (black box) were pooled, diluted with no salt and loaded onto heparin resin (**C**). Step elution with different percentages of B buffer containing 1 M NaCl (10-100% B) allowed separation of contaminants and recombinant human PrimPol (red circle).

very high purity of the protein and eliminate any aggregated species before performing any crystallography studies. Also this chromatography technique allows determination of potential aggregate states of the protein in solution. For example, a dimer will elute at a volume corresponding to twice the MW of monomeric polypeptide. Recombinant human His-PrimPol protein, previously purified by IMAC and heparin-Sepharose affinity columns, was loaded onto a Superdex S200 column and eluted onto 3 ml fractions submitted to UV_{280} absorbance before collection (figure 6.8A). Two main peaks (numbered 1 and 6 on figure 6.8A) each followed by a shoulder (fractions 2 for peak 1, and fractions 7 to 9 for peak 6, figure 6.8A) were registered on the UV absorbance chart. SDS-PAGE analysis of these eluted fractions revealed the presence of a single species (fractions 1 to 6) corresponding to WT full length His-PrimPol protein, and to potentially degradation fragments (fractions 7 to 10) (figure 6.8B). The major peak (number 6) corresponded to the volume of elution of around 60 kDa, thus human PrimPol monomeric size, according to a pre-calibration of the S200 column (Nigel Brissett, Aidan Doherty personal communication). Therefore, peak 1 and its shoulder fractions (pooled and named fraction 2, figure 6.8A) could correspond to aggregation or dimerisation state of PrimPol. After a closer look to the SDS-PAGE analysis, fractions 1 and 2 appeared to migrate slightly lower than the following fractions, suggesting a very small difference in the size of those species (figure 6.8B). This could reflect post-translational modifications of PrimPol within *E. coli* SHuffle cells. To verify this hypothesis, another SDS-PAGE analysis should be performed with a lower acrylamide percentage or using Phos-tag™ technology, which specifically retard the migration of phosphorylated protein to allow their visualisation (Kinoshita *et al.*, 2006). Fractions 7 to 10 (figure 6.8B) contained mainly degradation products of PrimPol and therefore were trapped for a longer time inside the porous matrix of the Sephadex column, resulting in a late elution compared to bigger polypeptides unable to penetrate inside the matrix and eluted earlier (figure 6.8A). Fractions 1 to 5 (figure 6.8) were pooled together, concentrated to 1.1 ml at 1.2 mg/ml and small volumes aliquots were kept in -80°C following snap freezing step in liquid nitrogen until performing *in vitro* activity assays (see following section). Elution fractions composing the main peak number 6, (figure 6.8), were pooled and concentrated to 200 µl at 8.8 mg/ml and utilised for crystallography trails, which have so far proven unsuccessful (data not shown). One of the main reasons for the crystallography attempt failure was the stability of PrimPol protein, which aggregates when kept at 4°C (data not shown).

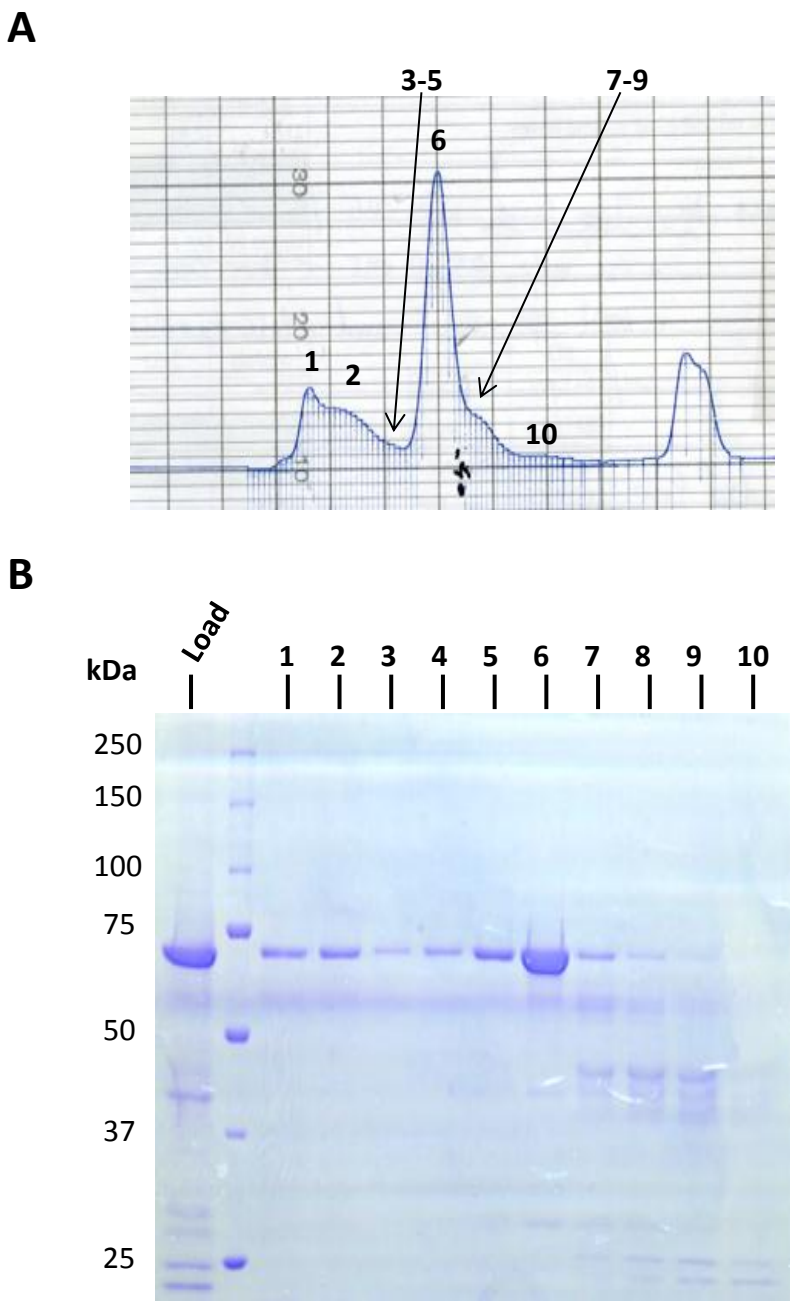

Figure 6.8: Human PrimPol protein elution profile on size exclusion column.

(**A**) Chart record showing the UV absorbance (280 nm) of the different PrimPol protein fractions (vertical blue lines) eluted according to their size from a Superdex S200 column. Fractions composing individual peaks (1, 2, 6 and 10) were pooled and analysed by SDS-PAGE (**B**). Individual fractions preceding (3, 4 and 5) and following (7, 8 and 9) the major peak (number 6) were analysed separately to prevent any potential contamination of the major PrimPol species. The sample loaded onto the column (load) corresponded to His-PrimPol protein purified from IMAC, ion exchange and heparin chromatography columns.

6.2.3. Human PrimPol recombinant protein is an active DNA polymerase

Preliminary characterisations of PrimPol protein, purified from *E. coli* BL21 and baculovirus preparations, previously demonstrated polymerase and primase activities of the enzyme (Andy Green, Aidan Doherty, personal communication). To confirm the protein purified from the *E. coli* SHuffle cells was also an active polymerase, a fluorescent primer extension assay was performed (figure 6.9). To ensure the specificity of the assay, a PrimPol catalytic null mutant was also generated and purified in similar conditions than the WT protein (figure 6.9A). Based on previous structural and mutagenesis site studies of AEPs, residues essential for the catalysis, those responsible for the binding of the divalent metal ions, can be predicted (Iiyer *et al*., 2005; Lipps *et al*., 2003 and 2004). Thus, aspartic acid D_{114} and glutamic acid E_{116} of the motif I of AEP domain of human PrimPol were chosen and mutated to alanine residues by conventional mutagenesis PCR (figure 6.4C and D). Full length WT and catalytic null (referred as AxA mutant) recombinant His-tagged PrimPol proteins were both recovered from *E. coli* SHuffle cell lysates and purified in similar conditions as described in section 6.2.2. Both purification preparations, resulting in similar levels of purity as observed by SDS-PAGE and Coomassie staining (figure 6.9A), were then subjected to fluorescent primer extension assay (figure 6.9B). In the presence of dNTPs and magnesium within the reaction buffer, WT PrimPol was able to fully extend the labelled primer, but the majority of the reaction products were intermediates suggesting the low processivity of PrimPol as a DNA polymerase (figure 6.9B, WT line). Nonetheless, this activity was intrinsic to PrimPol as mutation of the catalytic sites abolished DNA synthesis (figure 6.9B, AxA line). Use of the AxA mutant also allows confirmation of the absence of any contaminant polymerase enzymes that could have potentially been co-purified with PrimPol. This assay allowed us to confirm PrimPol was a DNA-dependent DNA polymerase, and residues D_{114} and E_{116} were essential for the activity of the protein, by presumably allowing the binding of magnesium ions to catalyse the reaction.

Further PrimPol *in vitro* activity studies have been undertaken by another colleague (Jozwiakowski Stanislaw) using the protein stock purified by size exclusion chromatography described in 6.2.2, and allowed the characterisation of PrimPol TLS activity to bypass UV-C photoproducts (appendix A).

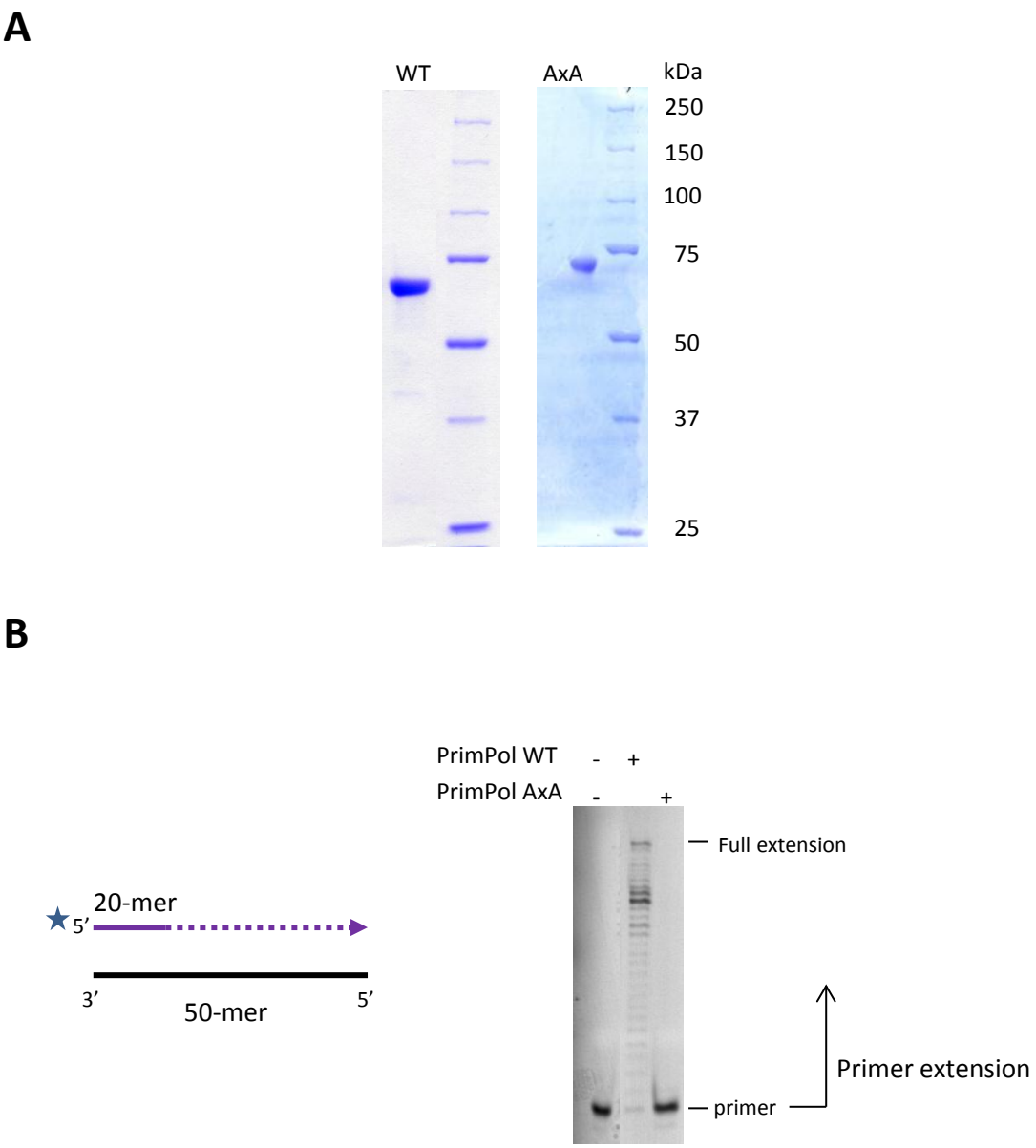

Figure 6.9: Primer extension assay.

(**A**) Visualisation of PrimPol wild type (WT) or catalytic mutant (AxA) proteins by SDS-PAGE and Coomassie staining at the end of the purification process (left and right gels respectively). (**B**) Primer extension assay performed with 100 nM of WT or catalytic mutant AxA PrimPol proteins (purity of the stocks verified in (**A**)) on a 50-mer DNA template with a 20-mer fluorescently labelled primer (star symbol on the 5' end of the primer) as depicted by the cartoon (left panel). Reaction was performed at 37°C for 30 minutes before to be quenched and resolved by DNA-PAGE and the fluorescence detected with a Fuji scanner (right panel). Size of the initial primer and the fully replicated template are indicated on the side of the gel.

6.2.4. Purification of truncated forms of human PrimPol protein

Despite the significant yield of recombinant PrimPol protein recovered from *E. coli* cultures, around 1.5 mg of protein per litre of SHuffle cells, and an optimised protocol of purification allowing the enrichment of human PrimPol protein alone, further optimisation processes need to be performed before crystallography studies can be efficiently and successfully performed. It was first decided to purify truncation forms of the protein e.g. catalytic domain alone, expecting that these smaller domains would be more stable and potentially more soluble too, enabling the protein to be more suitable for future crystallisation studies. The design of truncated forms of PrimPol was guided using *in silico* prediction of the secondary structure of PrimPol, obtained with PSIPRED server (Jones, 1999), to prevent any disruption of conserved domain or folded structures (e.g. α-helix or β-sheet) (Nigel Brisett and Aidan Doherty, personal communication). It was first decided to remove any putative mitochondrial localisation signal (MLS) usually present in the N-ter of the protein, thus deleting the first 60 amino acids of human PrimPol (figure 6.9B, ΔNter). Indeed the probability of this part of the polypeptide sequence to contain a MLS was significant (0.6) according to Mitoprot prediction website (Claros *et al.*, 1996). A protocol adapted from the inverted PCR method was used to generate the construct directly from pET28a-PrimPol WT full length plasmid (primers described in table 2.5 and constructs in table 2.7). The predicted size of this N-ter truncation was 60 kDa (ExPASy), corresponding to the lower band obtained on SDS-PAGE analysis following IMAC purification and Coomassie staining (figure 6.10B, black arrow). Purification of ΔNter PrimPol resulted in the binding and elution of two species, the PrimPol specific band at ~60 kDa but also a ~70 kDa non-specific species (figure 6.10B). Both species were purified at the same level (same intensity of the Coomassie staining), whereas IMAC performed on WT full length His-PrimPol cultures resulted predominantly in the purification of full length (66 kDa) PrimPol species (figure 6.10A, 100% B). This difference in the purification of the contaminant species could be explained by a lower expression level of soluble ΔNter PrimPol, thus allowing an increased binding of non-histidine tagged proteins to the nickel resin. Indeed, deletion of the first 60 amino acids of PrimPol resulted in an increase of insoluble PrimPol protein (figure 6.10B, insoluble lane).

C-ter deletions were also undertaken to study the expression level and the stability of a shorter PrimPol polypeptide. Indeed, the C-ter region of the protein is not highly conserved in all species and is also predicted to be less ordered (Aidan Doherty, personal communication). To generate this construct, a stop codon was introduced by mutagenesis PCR

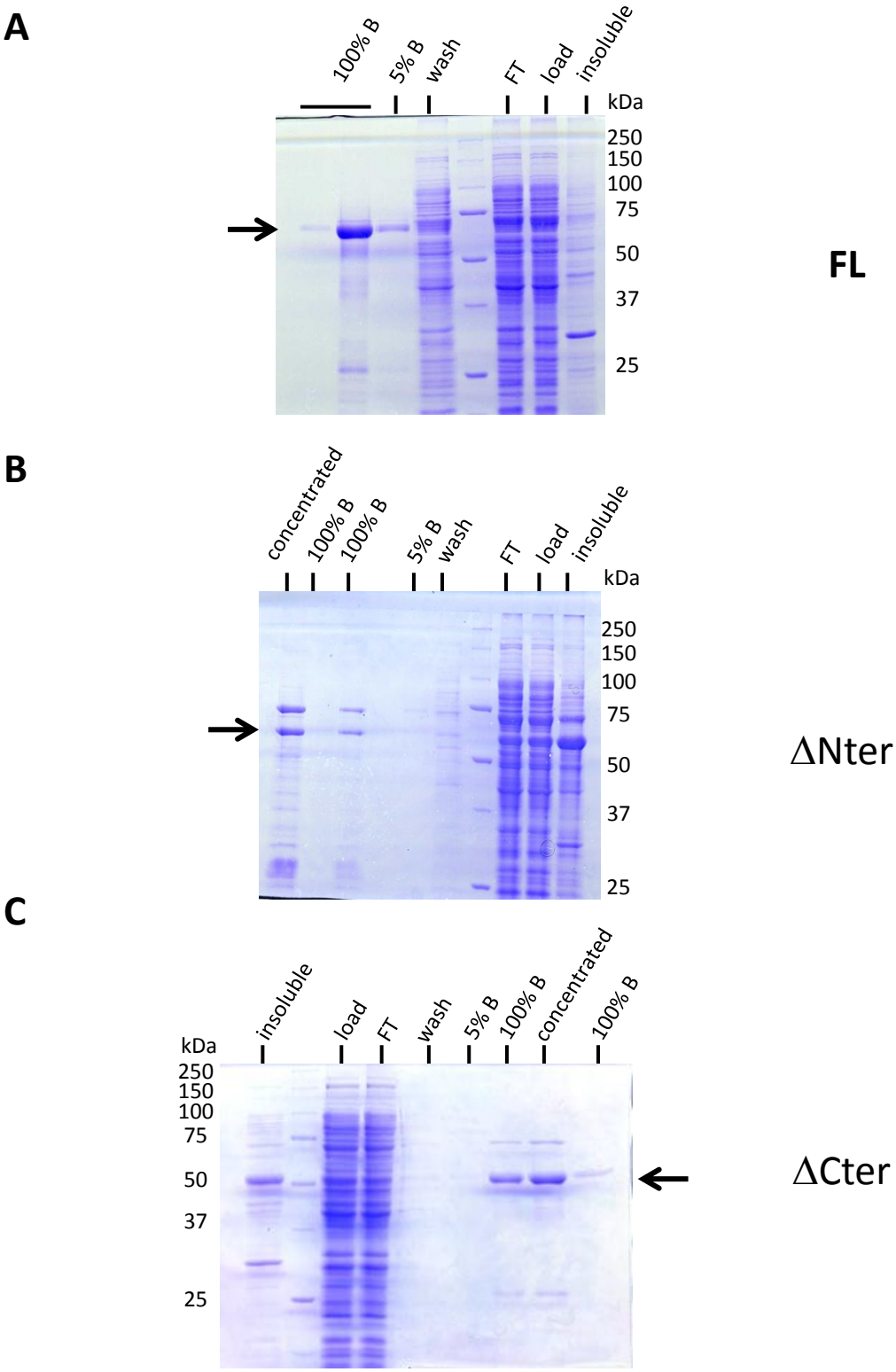

Figure 6.10: PrimPol truncation purifications in *E. coli* SHuffle cells.

Expression and IMAC purifications of PrimPol wild type full length protein (560 amino acids) (**A**), PrimPol deleted of the first 60 amino acids (**B**), and PrimPol truncated of its C terminal domain (stop codon at the position 464) (**C**). All three cultures were grown and purified in similar conditions to allow comparison of the different yields obtained depending on the variation of the size of PrimPol protein.

using pET28-PrimPol WT full length as template (primers described in table 2.5 and construct in table 2.7). By using this method a deletion of 96 amino acids was performed resulting in a polypeptide with a predicted size of 58.7 kDa (figure 6.10C, black arrow). By comparison with the ΔNter construct purification, less contaminant proteins were collected at the end of the IMAC purification, indicating a higher level of expression of this peptide (figure 6.10B and C). However, the solubility of this C-ter truncated form was not improved compared to full length PrimPol (figure 6.10A and C, insoluble fractions), resulting in a poorer yield (figure 6.10A and C, 100% B).

Both truncations, N-ter and C-ter part of PrimPol individually, did not improve the overall expression level of human PrimPol recombinant protein, but further investigations need to be performed to eventually characterise the core domain of the protein, stable enough to allow crystallography studies. Following on this work, two stable domains corresponding at the N-ter catalytic (AEP) domain and the C-ter (zinc-finger) domain have been purified separately and are currently submitted to crystallisation study (Benjamin Keen, Aidan Doherty, personal communication).

6.3. Generation and purification of PrimPol polyclonal antibody

Optimisation of production and purification of recombinant human PrimPol protein has also permitted us to improve the antibodies available for immunoaffinity detection of endogenous human PrimPol protein for cellular biology studies. First, previous immune serum generated by our collaborator Luis Blanco's laboratory has been affinity purified using recombinant PrimPol protein from baculovirus (section 6.1) immobilised onto PVDF membrane or from *E. coli* SHuffle cells (section 6.2.2) cross-linked into an AminoLink column (figure 6.11A and B respectively). As a result, endogenous PrimPol protein from Hela cell extracts has been detected by Western blot analysis only when affinity purified serum was used (figure 6.11A, lanes 2 and 3). Discrimination of the different levels of PrimPol expression inbetween different cell lines was then possible, and a higher expression in U2OS than Hela cells was visible (figure 6.11A, lanes 3 and 5).

Secondly, another polyclonal rabbit antibody was commercially generated by sending 1 milligram of purified human PrimPol (as described in section 6.2.2) to the production service of Eurogentec Company. This antibody was also affinity purified using recombinant human PrimPol from *E. coli* SHuffle cells, immobilised onto PVDF membrane (figure 6.11C). This newly

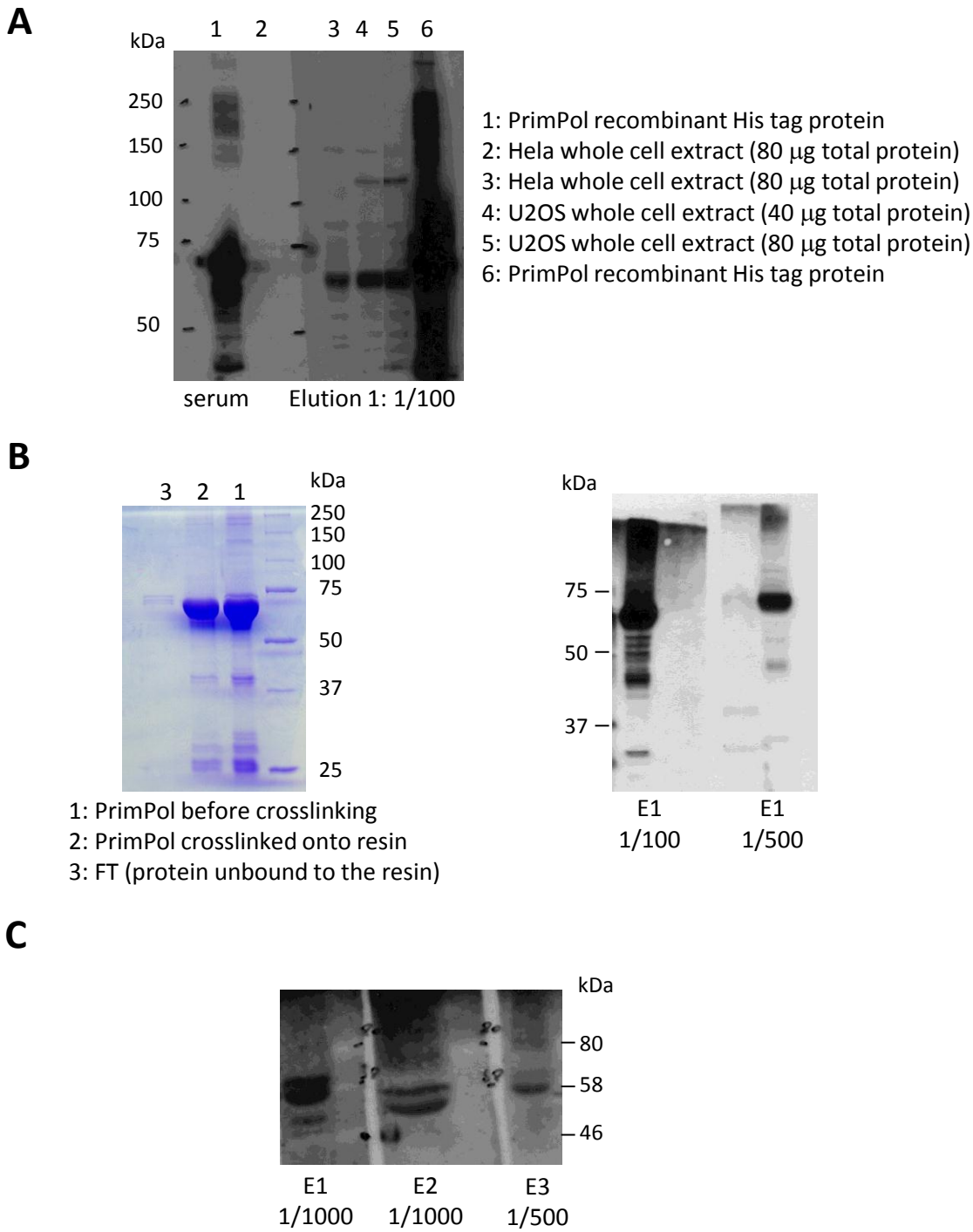

Figure 6.11: Different purification methods of human PrimPol antibodies.

(**A**) Western blot analyses, using un-purified antibody serum sent by our collaborator L. Blanco (lanes 1 & 2) or affinity purified antibody (lanes 3 to 6), allow detection of endogenous PrimPol. (**B**) AminoLink resin was also used to purify L. Blanco's lab serum, by crosslinking recombinant PrimPol protein (left panel, lane 1) to the resin (left panel, lane 2). Serum bound to the resin was then eluted and different dilutions (E1 1/100 and 1/500) tested by Western blot analysis using cell extracts from human conditional DT40 cells (right panel). (**C**) Eurogentec new PrimPol antibody was affinity purified (immunoblot) and three different elutions (E1, E2, E3) were tested by Western blot analysis using human conditional DT40 cells extracts.

purified PrimPol antibody was slightly more specific than the previous antibody (Blanco's laboratory), allowing higher dilutions of the antibody before usage (figure 6.11B and C, compared E1 dilutions in both Western blot analyses). Indeed, Blanco's antibody has been prepared from insoluble purification of PrimPol in *E. coli*, which could result in a lower antigenicity due to incorrect folding of the protein as the antibody was generated directly from urea denatured protein. This new batch of PrimPol antibody was then used for immunofluorescence detection of over-expressed protein (examples in Chapters 3 and 4) but also of endogenous PrimPol (Sean Rudd, Aidan Doherty, personal communication; appendix A). It was also successfully used for immunoprecipitation experiments (Sean Rudd, Aidan Doherty, personal communication) to identify potential cellular partner proteins.

6.4. Summary and discussion

Purification of recombinant His-PrimPol protein, initiated with the baculovirus expression system, has proven more complicated than originally anticipated. Indeed, the poor stability of the virus did not allow reproducibility between infections and even a large scale purification process did not generate enough protein for crystallographic studies. However, this eukaryotic expression system made it possible to analyse post-translation modifications. Several phosphorylation sites have been identified by mass spectrometry and two of these were subsequently confirmed in PrimPol isolated from human cells. As a second strategy, we switched to a bacterial expression system, *E. coli* SHuffle technology, which allowed optimisation of a reproducible purification process, generating significant yield of human recombinant His-PrimPol protein (~1.5 mg/L). This strain is engineered to enhance disulphide bonds within the cytoplasm of cells, thus indicating the correct folding of human PrimPol is an important criterion to improve the solubility of the protein. The purification process was optimised to generate a pure and active preparation of FL recombinant human His-PrimPol, able to extend fluorescently labelled primer. However, the recombinant protein remained still quite unstable and was subject to degradation and precipitation, preventing crystallisation study. Truncation analyses have been undertaken but need to be pursue along with thorough stability studies. A better understanding of the behaviour of the polypeptide in solution will increase the crystallographic potential of PrimPol protein. Also, other expression vectors could be tried, like pET-SUMO vector technology (LifeSensors) which can improve the folding and the solubility of the recombinant protein by expressing SUMO in fusion with the protein of interest. A better understanding of PrimPol interacting partners could be used to generate a co-expression system for PrimPol and its partners, to potentially improve the solubility and the stability of this complex. Indeed, it has been seen previously reported in the literature that proteins co-expressed with their partners can be less prone to proteasome degradation, like Id3 and bHLH for example (Bounpheng *et al.*, 1999). Several strategies for co-expression system are now available and commonly used, with multiple or single expression vectors approaches, in *E. coli,* baculovirus or mammalian cells (Kerrigan *et al.*, 2011).

CHAPTER VII

Conclusions and future studies

The work presented in this thesis provides one of the first cellular characterisations of *CCDC111* gene, a newly discovered eukaryotic AEP member. Indeed, at the beginning of this thesis only *in vitro* characterisations of *CCDC111* gene had been performed by Doherty and co-worker Blanco laboratories, and confirmed the human recombinant protein was capable of both polymerase and primase activities, thus renaming the gene *PrimPol*. Work in this thesis establishes a role for this novel enzyme in DNA damage tolerance mechanisms within both chromosomal and mitochondrial DNA replication in vertebrates.

Investigation of sub-cellular localisation of PrimPol was first undertaken in human cells (Chapter 3). A predominantly cytoplasmic localisation was observed by immunofluorescence and sub-cellular fractionation studies, and further investigations confirmed the presence of PrimPol within mitochondria (Sean Rudd and Aidan Doherty, unpublished data; appendix A). Subsequent studies in Chapter 3 established a role for PrimPol in maintenance of the mitochondrial genome. An increased of mtDNA copy number was observed by Q-PCR and Southern blot analyses following either PrimPol RNAi depletion in human cells or *PrimPol* KO in avian DT40 cells. Moreover, chloramphenicol survival assays in *PrimPol* $^{-/-}$ implicated PrimPol in an error-prone mtDNA synthesis mechanism, which is consistent with a role for PrimPol in DNA damage tolerance possibly by TLS, as detailed further in the cell nucleus. It is thus currently believed PrimPol plays a critical role during replication of this small genome that is constantly exposed to high levels of endogenous damages (e.g. ROS) due to its close proximity to the OXPHOS pathway.

In parallel to the study performed in human cells, KO of *PrimPol* gene was undertaken in a DT40 B-lymphocyte cell line (Chapter 4) and two viable *PrimPol* $^{-/-}$ clones were obtained, thus demonstrating PrimPol is not an essential gene. Nonetheless, a minor proliferative defect and perturbation of the cell cycle profile was observed, and analysis of spread DNA fibres indicated reduced RF speed in the absence of PrimPol, thus also establishing a role for PrimPol in unchallenged chromosomal DNA replication. Subsequently, in Chapter 5, analysis of cell viability following various DNA damaging treatments revealed the absence of PrimPol renders DT40 cells more sensitive to replicative stress, such as UV light and 4NQO, but not DNA strand breaks induced by ionising radiation. DNA fiber analysis of UV-C irradiated *PrimPol* $^{-/-}$ cells indicated PrimPol was involved in maintaining RF progression on UV-damaged DNA. Sedimentation velocity assays of nascent DNA in UV-C irradiated *PrimPol* $^{-/-}$ DT40 cells also demonstrated PrimPol was not involved in PRR, suggesting a recruitment of PrimPol directly to the stalled fork during on-going DNA replication. It remains to be established whether

PrimPol's ability to bypass UV photoproducts by TLS or its primase activity are relevant for this DNA damage tolerance function. Chapter 5 also detailed a peculiar UV-C dose response in *PrimPol* $^{-/-}$ cells, as cells appeared protected from cytotoxicity induced by high UV-C fluences by comparison to WT DT40 cells. This phenomenon was surprisingly enhanced following the inhibition of Chk1 kinase activity by UCN-01. Absence of PrimPol seemed to compensate abnormal DNA synthesis and prevent premature mitosis entry caused by Chk1 inhibition. Finally, in Chapter 6, optimisation of the purification process of recombinant human PrimPol protein is described. Generation of a large amount of pure protein allowed production of a new PrimPol antibody and its purification. Despite the absence of crystallographic data so far, this initial work provided a starting point for truncation studies and also for characterisation of PrimPol's *in vitro* activity (appendix A).

One of the main questions arising from this work regards whether PrimPol utilises TLS polymerase activity to bypass UV photoproducts or AEP priming capacity to restart DNA synthesis downstream of the DNA lesion, or perhaps both. Indeed, PrimPol is capable of both activities *in vitro*, thus complicating our understanding on its involvement on maintaining RF progression on UV-C damaged DNA templates. A possible way of investigating this matter would be by studying the importance of PrimPol's domains and motifs in template and substrate recognition, such as the UL52-like zinc-finger domain, as previous studies in other primases have demonstrated the importance of zinc-finger motifs in primase function (Mendelman *et al.*, 1994; Lao-Sirieix *et al.*, 2005b). Future crystallographic studies in pair with analysis of *in vitro* activity of mutated or truncated versions of PrimPol should bring more insight on this matter.

Secondly, PrimPol's involvement in both nuclear and mitochondrial DNA maintenance, during unperturbed conditions and following DNA damaging treatments, a remaining question concerns the shuttling of the protein between both cellular compartments. Several hypotheses can be speculated to explain whether different forms of the protein are present in each cellular compartment or guide PrimPol transport from one compartment to the other. Thus post-translational modifications, like cleavage of a potential peptide signal, phosphorylation, ubiquitylation or SUMOylation events could be responsible for the distinction between nuclear or mitochondrial PrimPol. Indeed, current unpublished data in the Doherty lab has demonstrated PrimPol is phosphorylated, ubiquitylated, and SUMOylated (Laura Bailey, Violetta Soura, Sean Rudd, Aidan Doherty, unpublished data), and cellular localisation analysis of phospho-mimic or phospho-null (EE or AA mutants respectively) are currently under

investigation in the laboratory. Moreover, complementation studies performed in *PrimPol* $^{-/-}$ DT40 cells, as performed with WT PrimPol in Chapter 4, could be carried out with different PrimPol mutants (mutations of lysine residues preventing the protein's ubiquitylation and/or SUMOylation) or truncated forms, which could contribute to a better understanding of PrimPol cellular trafficking.

Regarding PrimPol recruitment to nuclear or mitochondrial DNA molecules, little is known about the specific actors involved in this process. Data provided in this thesis supports a role of PrimPol directly in maintaining RF progression during unperturbed conditions (Chapter 4) and following exposure to UV-C radiation (Chapter 5). Several protein candidates could then participate in PrimPol's recruitment, like PCNA, Rev1, RPA and also Chk1. Epistatic studies in DT40 cells could thus bring insights to this key question. Further, live cell imaging in *PrimPol* $^{-/-}$ DT40 cells complemented with GFP-PrimPol constructs could also allow visualisation of PrimPol recruitment. This technique could also contribute to determine more precisely the temporal recruitment of PrimPol, whether this novel factor is needed all along S-phase progression or more specifically at the end of replication, in the presence or absence of DNA damaging treatments. *In situ* analysis of chromosome fragile sites (by fluorescence in situ hybridization or FISH) could also contribute to a better characterisation of PrimPol role during chromosomal replication.

Finally, work provided during this thesis shed light on a pro-apoptotic role of PrimPol following high-dose UV-C irradiation and also after inhibition of Chk1 kinase activity by UCN-01. PrimPol could then be directly involved in a pathway triggering apoptosis (Myers *et al.*, 2009), mirroring for example the direct contribution of Pol α in triggering ATR activation during the intra-S checkpoint response. Indeed, the presence of PrimPol appeared closely linked to the replication-dependent apoptosis phenomenon (discussed section 5.4.3.2). Moreover, the apoptosis response being closely related to mitochondrial processes (figure 5.24), with the release of cytochrome c triggering the caspase cascade, the question remains whether PrimPol's involvement in mtDNA maintenance could also influence this apoptosis response. PrimPol being implicated in both chromosomal and mitochondrial DNA maintenance, the pro-apoptotic role of PrimPol following high dose of UV-C could be via mitochondrial dependent or independent processes. According to the preliminary data provided during the study of Chk1 inhibition by UCN-01, the absence of PrimPol appeared to compensate abnormal DNA replication and to prevent premature mitosis entry induced by Chk1 inhibition; to verify this, levels of CDC45 and CDC25A on chromatin should be analysed in the absence of PrimPol. In

this case, chromosomal role of PrimPol would thus directly influence the apoptosis response. Moreover, cell viability assays performed following DNA damaging treatments did not appear biased by PrimPol's role on mtDNA maintenance. Following on this study and to complete our understanding on the influence of PrimPol's mitochondrial role following replicative stress, mtDNA copy number variation following UV-C irradiation is currently under investigation in our laboratory (Laura Bailey, Aidan Doherty, personal communication).

Regarding the nuclear role of PrimPol and the analysis of the checkpoint response following UV-C irradiation, one point remains inconclusive concerning the level of activation of Chk1 in *PrimPol* $^{-/-}$ DT40 cells. In human cells following PrimPol RNAi depletion and UV-C irradiation, Chk1 appeared over-activated in normal cells and persistent in XP-V cells (appendix A), indicative of a DNA damage tolerance defect (Bomgarden *et al*., 2006; Despras *et al*., 2010). However, given the unusual phenotypes observed in DT40 cells following Chk1 inhibition, absence of PrimPol could also be linked to an inefficient activation of the intra-S checkpoint, leading to a delay of the repair mechanisms, thus to a prolonged activation of Chk1. Further investigations regarding RF restart in a TopBP1-dependent manner (Yan and Michael, 2009b) in the presence or absence of PrimPol are then needed. Moreover, during unperturbed DNA replication conditions, absence of PrimPol was accompanied with a RF speed decrease without perturbing the overall S-phase length, similarly to what observed in *Chk1* $^{-/-}$ cells (Petermann et al, 2006). This prompts the question whether dormant origins could also be activated in the absence of PrimPol to prevent a delay in S-phase completion. DNA combing analysis should then be performed to understand these mechanisms taking place in the absence of PrimPol, with or without UCN-01 treatment to follow the role of Chk1 in this process. Indeed, it remains unclear whether this phenomenon is only due to PrimPol's ability to bypass or re-start RF at naturally occurring damaged DNA or to an indirect consequence of perturbing a Chk1-related mechanism. Investigating this intricate relationship between PrimPol and Chk1 could then provide a novel perspective to understand how DNA damage tolerance and checkpoint responses are interlinked.

To conclude, this thesis provides one of the first cellular characterisations of the novel eukaryotic primase-polymerase PrimPol in human and avian DT40 cells. Despite the numerous outstanding questions, this work I have performed has established the involvement of PrimPol in both mtDNA maintenance and chromosomal DNA replication, and reveals a close link of this novel AEP to the intra-S checkpoint response. Together, this thesis has established PrimPol as a novel factor in DNA damage tolerance in vertebrate cells, and further investigation are needed

to determine whether PrimPol accomplishes this role *in vivo* by direct TLS or RF restart mechanisms.

References

Allan C, Burel JM, Moore J, Blackburn C, Linkert M, Loynton S, Macdonald D, Moore WJ, Neves C, Patterson A, Porter M, Tarkowska A, Loranger B, Avondo J, Lagerstedt I, Lianas L, Leo S, Hands K, Hay RT, Patwardhan A, Best C, Kleywegt GJ, Zanetti G, Swedlow JR.(2012) OMERO: flexible, model-driven data management for experimental biology. Nat Methods 9(3):245-53.

Alexeyev MF, Venediktova N, Pastukh V, Shokolenko I, Bonilla G, Wilson GL. (2008) Selective elimination of mutant mitochondrial genomes as therapeutic strategy for the treatment of NARP and MILS syndromes. Gene Ther 15:516–523.

Anderson JP, Angerer B, Loeb LA. (2005) Incorporation of reporter-labeled nucleotides by DNA polymerases. Biotechniques 38(2):257-64.

Aparicio OM, Weinstein DM, Bell SP. (1997) Components and dynamics of DNA replication complexes in S. cerevisiae: redistribution of MCM proteins and Cdc45p during S-phase. Cell 91(1):59-69.

Arakawa H, Buerstedde JM. (2006) Dt40 gene disruptions: a how-to for the design and the construction of targeting vectors. Subcell Biochem. 40:1-9.

Aravind L, Leipe DD, Koonin EV. (1998) Toprim—a conserved catalytic domain in type IA and II topoisomerases, DnaG-type primases, OLD family nucleases and RecR proteins. Nucleic Acids Res. 26, 4205–4213.

Aravind L, Koonin EV. (2001) Prokaryotic homologs of the eukaryotic DNA-end-binding protein Ku, novel domains in the Ku protein and prediction of a prokaryotic double-strand break repair system. Genome Res. 11(8):1365-74.

Arezi B, and Kuchta RD. (2000). Eukaryotic DNA primase. Trends in Biochemical Sciences, 25(11), 572–576.

Arlett CF, Harcourt SA, Broughton BC. (1975) The influence of caffeine on cell survival in excision-proficient and excision-deficient xeroderma pigmentosum and normal cell strains following ultraviolet light. Mutat. Res. *33:* 341-346.

Ashley N, Harris D, Poulton J. (2005) Detection of mitochondrial DNA depletion in living human cells using PicoGreen staining. Exp Cell Res. 303(2):432-46.

Atherton-Fessler S, Liu F, Gabrielli B, Lee M S, Peng C Y, Piwnica-Worms H. (1994). Cell cycle regulation of the p34cdc2 inhibitory kinases. Mol.Biol.Cell 5, 989-1001.

Augustin MA, Huber R and Kaiser JT. (2001) Crystal structure of a DNA-dependent RNA polymerase (DNA primase). Nature Struct. Biol., 8, 57–61.

Avkin S, Livneh Z. (2002) Efficiency, specificity and DNA polymerase-dependence of translesion replication across the oxidative DNA lesion 8-oxoguanine in human cells. Mutat Res 510:81–90.

Baranovskiy AG, Lada AG, Siebler HM, Zhang Y, Pavlov YI, Tahirov TH. (2012) DNA polymerase δ and ζ switch by sharing accessory subunits of DNA polymerase δ. J Biol Chem. 287(21):17281-7.

Barkley LR, Ohmori H, Vaziri C. (2007) Integrating S-phase checkpoint signaling with trans-lesion synthesis of bulky DNA adducts. Cell Biochem Biophys. 47(3):392-408.

Batista LFZ, Chiganças V, Brumatti G, Amarante-Mendes GP, Menck CFM. (2006) Involvement of DNA replication in ultraviolet-induced apoptosis of mammalian cells. Apoptosis, 11(7), 1139-1148.

Batista LF, Kaina B, Meneghini R, Menck CF. (2009) How DNA lesions are turned into powerful killing structures: insights from UV-induced apoptosis. Mutat Res. 681(2-3):197-208.

Beattie TR, Bell SD. (2011) The role of the DNA sliding clamp in Okazaki fragment maturation in archaea and eukaryotes. Biochem Soc Trans. 39(1):70-6.

Bebenek K, Tissier A, Frank EG, McDonald JP, Prasad R, Wilson SH, Woodgate R, Kunkel TA. (2001) 5'-Deoxyribose phosphate lyase activity of human DNA polymerase iota in vitro. Science 291(5511):2156-9.

Beck H, Nähse V, Larsen MS, Groth P, Clancy T, Lees M, Jørgensen M, Helleday T, Syljuåsen RG and Sørensen CS. (2010) Regulators of cyclin-dependent kinases are crucial for maintaining genome integrity in S-phase. J. Cell. Biol. 188, 629–638.

Bell SP and Stillman B. (1992) ATP-dependent recognition of eukaryotic origins of DNA replication by a multi protein complex. Nature 357,128–1348

Bemark M, Khamlichi AA, Davies SL, Neuberger MS. (2000) Disruption of mouse polymerase zeta (Rev3) leads to embryonic lethality and impairs blastocyst development in vitro. Curr Biol 10:1213–1216.

Benne R, Sloof P. (1987) Evolution of the mitochondrial protein synthetic machinery. Biosystems 21(1):51-68.

Berg JM. (1990) Zinc fingers and other metal-binding domains. Elements for interactions between macromolecules. J Biol Chem. 265(12):6513-6.

Berg JM, Tymoczko JL, Stryer L. (2002) Biochemistry 5th edition; New York: W H Freeman; 2002.ISBN-10: 0-7167-3051-0.

Bermudez VP, Lindsey-Boltz L A, Cesare A J, Maniwa Y, Griffith JD, Hurwitz J and Sancar A. (2003) Loading of the human 9-1-1 checkpoint complex onto DNA by the checkpoint clamp loader hRad17–replication factor C complex in vitro. Proc. Natl. Acad.Sci. U.S.A. 100, 1633–1638

Bessman MJ, Kornberg A, Lehman IR, Simms ES. (1956) Enzymic synthesis of deoxyribonucleic acid. Biochim Biophys Acta. 21(1):197-8.

Bétous R, Rey L, Wang G, Pillaire MJ, Puget N, Selves J, Biard DS, Shin-ya K, Vasquez KM, Cazaux C, Hoffmann JS. (2009) Role of TLS DNA polymerases eta and kappa in processing naturally occurring structured DNA in human cells. Mol Carcinog. 48(4):369-78.

Bienko M, Green CM, Crosetto N, Rudolf F, Zapart G, Coull B, Kannouche P, Wider G, Peter M, Lehmann AR, Hofmann K, Dikic I. (2005) Ubiquitin-binding domains in Y-family polymerases regulate translesion synthesis. Science 310(5755):1821-4.

Biertümpfel C, Zhao Y, Kondo Y, Ramón-Maiques S, Gregory M, Lee JY, Masutani C, Lehmann AR, Hanaoka F, Yang W. (2010) Structure and mechanism of human DNA polymerase η. Nature 465, 1044–1048.

Bocquier AA, Liu L, Cann IK, Komori K, Kohda D, Ishino Y. (2001) Archaeal primase: bridging the gap between RNA and DNA polymerases. Curr Biol. 11(6):452-6.

Bogenhagen D, Clayton DA. (1977) Mouse L-cell mitochondrial DNA molecules are selected randomly for replication throughout the cell cycle. Cell 7 1, 719-727.

Bogenhagen DF, Clayton DA. (2003a) The mitochondrial DNA replication bubble has not burst.Trends Biochem. Sci. 28:357–60

Bogenhagen DF, Clayton DA. (2003b) The mitochondrial DNA replication bubble has not burst. Trends Biochem. Sci. 28:404–5

Bomgarden RD, Lupardus PJ, Soni DV, Yee M-C, Ford JM, Cimprich KA. (2006) Opposing effects of the UV lesion repair protein XPA and UV bypass polymerase eta on ATR checkpoint signaling. EMBO J., 25(11), 2605–2614.

Bookout AL, Mangelsdorf DJ. (2003) Quantitative real-time PCR protocol for analysis of nuclear receptor signaling pathways. Nucl Recept Signal 1:e012.

Boudsocq F, Kokoska RJ, Plosky BS, Vaisman A, Ling H, Kunkel TA, Yang W, Woodgate R. (2004) Investigating the role of the little finger domain of Y-family DNA polymerases in low fidelity synthesis and translesion replication. J Biol Chem. 279(31):32932-40.

Bounpheng MA, Dimas JJ, Dodds SG, Christy BA. (1999) Degradation of Id proteins by the ubiquitin-proteasome pathway. FASEB J. 13(15):2257-64.

Brill SJ, Stillman B. (1989) Yeast replication factor-A functions in the unwinding of the SV40 origin of DNA replication. Nature 342(6245):92-5.

Brissett NC, Pitcher RS, Juarez R, Picher AJ, Green AJ, Dafforn TR, Fox GC, Blanco L, Doherty, AJ. (2007) Structure of a NHEJ polymerase-mediated DNA synaptic complex. Science, 318(5849):456-9.

Brissett NC, Martin MJ, Pitcher RS, Bianchi J, Juarez R, Green AJ, Fox GC, Blanco L, Doherty AJ (2011). Structure of a Preternary Complex Involving a Prokaryotic NHEJ DNA Polymerase. Molecular Cell, 41(2), 221–231.

Brown EJ, Baltimore D. (2000) ATR disruption leads to chromosomal fragmentation and early embryonic lethality. Genes Dev. 14, 397–402.

Brun J, Chiu RK, Wouters BG, Gray DA. (2010) Regulation of PCNA polyubiquitination in human cells. BMC Res Notes. 3:85.

Buerstedde JM, Takeda S. (1991) Increased ratio of targeted to random integration after transfection of chicken B cell lines. Cell 67(1):179-88.

Burgers PM. (1991) Saccharomyces cerevisiae replication factor C. II. Formation and activity of complexes with the proliferating cell nuclear antigen and with DNA polymerases delta and epsilon. J Biol Chem. 266(33):22698-706.

Burgers PM, Koonin EV, Bruford E, Blanco L, Burtis KC, Christman MF, Copeland WC, Friedberg EC, Hanaoka F, Hinkle DC, Lawrence CW, Nakanishi M, Ohmori H, Prakash L, Prakash S, Reynaud CA, Sugino A, Todo T, Wang Z, Weill JC, Woodgate R. (2001) Eukaryotic DNA polymerases: proposal for a revised nomenclature. J Biol Chem. 276(47):43487-90.

Byun TS, Pacek M, Yee MC, Walter JC, Cimprich KA. (2005) Functional uncoupling of MCM helicase and DNA polymerase activities activates the ATR-dependent checkpoint. Genes Dev. 19, 1040-1052.

Caldecott KW. (2008) Single-strand break repair and genetic disease. Nat Rev Genet. 9(8):619-31.

Cadet J, Douki T, Gasparutto D, Ravanat JL. (2003) Oxidative damage to DNA: formation, measurement and biochemical features. Mutat Res. 531(1-2):5-23.

Carrodeguas JA, Theis K, Bogenhagen DF, Kisker C. (2001) Crystal structure and deletion analysis show that the accessory subunit of mammalian DNA polymerase gamma, Pol gamma B, functions as a homodimer. Mol Cell. 7(1):43-54.

Carvalho H, da Costa RM, Chiganças V, Weinlich R, Brumatti G, Amarante-Mendes GP, Sarasin A, Menck CF. (2003) Effect of cell confluence on ultraviolet light apoptotic responses in repair deficient cells. Mutat Res 544:159–166

Chagin VO, Stear JH, Cardoso MC. (2010) Organization of DNA replication Cold Spring Harbor perspectives in biology, 2(4), a000737.

Chang DJ, Lupardus PJ, Cimprich KA. (2006) Monoubiquitination of proliferating cell nuclear antigen induced by stalled replication requires uncoupling of DNA polymerase and mini-chromosome maintenance helicase activities. J Biol Chem. 281(43):32081-8.

Chastain PD 2nd, Heffernan TP, Nevis KR, Lin L, Kaufmann WK, Kaufman DG, Cordeiro-Stone M. (2006) Checkpoint regulation of replication dynamics in UV-irradiated human cells. Cell Cycle 5(18):2160-7.

Chen Y, Carrington-Lawrence SD, Bai P, Weller SK. (2005). Mutations in the putative zinc-binding motif of UL52 demonstrate a complex interdependence between the UL5 and UL52 subunits of the human herpes simplex virus type 1 helicase/primase complex. Journal of Virology, 79(14):9088-96.

Chen J, Kadlubar FF, Chen JZ. (2007) DNA supercoiling suppresses real-time PCR: a new approach to the quantification of mitochondrial DNA damage and repair. Nucleic Acids Research, 35(4), 1377-1388.

Chiu RK, Brun J, Ramaekers C, Theys J, Weng L, Lambin P, Gray DA, Wouters BG. (2006) Lysine 63-polyubiquitination guards against translesion synthesis-induced mutations. PLOS Genetics, 2(7):e116.

Chu Z, Li J, Eshaghi M, Karuturi RK, Lin K, Liu J. (2007) Adaptive expression responses in the Pol-gamma null strain of S. pombe depleted of mitochondrial genome. BMC Genomics 8:323.

Cimprich KA, Cortez D. (2008) ATR: an essential regulator of genome integrity. Nat Rev Mol Cell Biol. 9(8):616-27.

Claros MG, Vincens P. (1996) Computational method to predict mitochondrially imported proteins and their targeting sequences. Eur. J. Biochem. 241, 770-786.

Clay Montier LL, Deng JJ, Bai Y. (2009) Number matters: control of mammalian mitochondrial DNA copy number. J Genet Genomics. 36(3):125-31.

Cleaver JE, Kaufmann WK, Kapp LN, Park SD. (1983) Replicon size and excision repair as factors in the inhibition and recovery of DNA synthesis from ultraviolet damage. Biochim Biophys Acta. 739(2):207-15.

Clayton DA. (1982) Replication of animal mitochondrial DNA. Cell 28(4):693-705.

Cleaver JE, Afzal V, Feeney L, McDowell M, Sadinski W, Volpe JP, Busch DB, Coleman DM, Ziffer DW, Yu Y, Nagasawa H, Little JB. (1999) Increased ultraviolet sensitivity and chromosomal instability related to P53 function in the xeroderma pigmentosum variant Cancer Research, 59(5), 1102-8.

Cline SD. (2012) Mitochondrial DNA damage and its consequences for mitochondrial gene expression. Biochim Biophys Acta. 1819(9-10):979-91.

Cobb JA, Bjergbaek L, Shimada K, Frei C, Gasser SM. (2003) DNA polymerase stabilization at stalled replication forks requires Mec1 and the RecQ helicase Sgs1. EMBO J. 22(16):4325-36.

Cohen SE, Walker GC. (2011) New discoveries linking transcription to DNA repair and damage tolerance pathways. Transcription. 2(1):37-40.

Collins NS, Bhattacharyya S, Lahue RS. (2007) Rev1 enhances CAG.CTG repeat stability in Saccharomyces cerevisiae. DNA Repair (Amst) 6(1):38-44.

Coon HG, Ho C. (1977) Transformation of cultured cells to chloramphenicol resistance by purified mammalian mitochondrial DNA. Brookhaven Symp Biol. (29):166-77.

Cooper HM, Spelbrink JN. (2008) The human SIRT3 protein deacetylase is exclusively mitochondrial. Biochem J. 411(2):279-85.

Cordonnier AM, Fuchs RP. (1999) Replication of damaged DNA: molecular defect in xeroderma pigmentosum variant cells. Mutat Res. 435(2):111-9.

Corpet F. (1988) Multiple sequence alignment with hierarchical clustering. Nucl. Acids Res. 16 (22), 10881-10890

Courcelle J, Donaldson JR, Chow KH, Courcelle CT. (2003) DNA damage-induced replication fork regression and processing in Escherichia coli. Science 299(5609):1064-7.

Dai Y, Grant S. (2010) New insights into checkpoint kinase 1 in the DNA damage response signaling network. Clin Cancer Res. 16(2):376-83.

Davies AA, Huttner D, Daigaku Y, Chen S, Ulrich HD. (2008) Activation of ubiquitin-dependent DNA damage bypass is mediated by replication protein a. Mol Cell. 29(5):625-36.

Debatisse M, Le Tallec B, Letessier A, Dutrillaux B, Brison O. (2012) Common fragile sites: mechanisms of instability revisited. Trends in genetics, 28(1), 22-32.

de Feraudy S, Limoli CL, Giedzinski E, Karentz D, Marti TM, Feeney L, Cleaver JE. (2007) Pol η is required for DNA replication during nucleotide deprivation by hydroxyurea. Oncogene 26, 5713–5721.

de Feraudy S, Revet I, Bezrookove von V, Feeney L, Cleaver JE. (2010) A minority of foci or pan-nuclear apoptotic staining of H2AX in the S phase after UV damage contain DNA double-strand breaks. Proceedings of the National Academy of Sciences, 107(15), 6870-6875.

Della M, Palmbos PL, Tseng HM, Tonkin LM, Daley JM, Topper LM, Pitcher RS, Tomkinson AE, Wilson TE, Doherty AJ. (2004) Mycobacterial Ku and ligase proteins constitute a two-component NHEJ repair machine. Science 306(5696):683-5.

Despras E, Daboussi F, Hyrien O, Marheineke K, Kannouche PL. (2010) ATR/Chk1 pathway is essential for resumption of DNA synthesis and cell survival in UV-irradiated XP variant cells. Hum Mol Genet. 19(9):1690-701.

Dickey JS, Redon CE, Nakamura AJ, Baird BJ, Sedelnikova OA, Bonner WM. (2009) H2AX: functional roles and potential applications. Chromosoma. 118(6):683-92.

DiNardo S, Voelkel K, Sternglanz R. (1984) DNA topoisomerase II mutant of Saccharomyces cerevisiae: topoisomerase II is required for segregation of daughter molecules at the termination of DNA replication. Proc Natl Acad Sci U S A. 81(9):2616-20.

Di Re M, Sembongi H, He J, Reyes A, Yasukawa T, Martinsson P, Bailey LJ, Goffart S, Boyd-Kirkup JD, Wong TS, Fersht AR, Spelbrink JN, Holt IJ. (2009) The accessory subunit of mitochondrial DNA polymerase gamma determines the DNA content of mitochondrial nucleoids in human cultured cells. Nucleic Acids Res. 37(17):5701-13.

Doherty AJ, Jackson SP, Weller GR. (2001) Identification of bacterial homologues of the Ku DNA repair proteins. FEBS Lett. 500(3):186-8.

Dornreiter I, Erdile LF, Gilbert IU, von Winkler D, Kelly TJ, Fanning E. (1992) Interaction of DNA polymerase alpha-primase with cellular replication protein A and SV40 T antigen. EMBO J. 11(2):769-76.

Drouin R, Therrien JP. (1997) UVB-induced cyclobutane pyrimidine dimer frequency correlates with skin cancer mutational hotspots in p53. Photochem Photobiol. 66(5):719-26.

Dua R, Levy DL, Campbell JL. (1999) Analysis of the essential functions of the C-terminal protein/protein interaction domain of Saccharomyces cerevisiae pol epsilon and its unexpected ability to support growth in the absence of the DNA polymerase domain. J Biol Chem. 274(32):22283-8.

Dumstorf CA, Clark AB, Lin Q, Kissling GE, Yuan T, Kucherlapati R, McGregor WG, Kunkel TA. (2006) Participation of mouse DNA polymerase iota in strand-biased mutagenic bypass of UV photoproducts and suppression of skin cancer. Proc. Natl. Acad. Sci. U.S.A. 103 18083–18088.

Durkin SG, Glover TW. (2007) Chromosome fragile sites. Annu Rev Genet. 41:169-92.

Duxin JP, Dao B, Martinsson P, Rajala N, Guittat L, Campbell JL, Spelbrink JN, Stewart SA. (2009) Human Dna2 is a nuclear and mitochondrial DNA maintenance protein Molecular and Cellular Biology, 29(15), 4274-82.

Echols H, Goodman MF. (1991) Fidelity mechanisms in DNA replication. Annu. Rev. Biochem. 60: 477-511.

Edmunds CE, Simpson LJ, Sale JE (2008). PCNA Ubiquitination and REV1 Define Temporally Distinct Mechanisms for Controlling Translesion Synthesis in the Avian Cell Line DT40. Molecular cell 30(4), 519-529.

Ekstrand MI, Falkenberg M, Rantanen A, Park CB, Gaspari M, Hultenby K, Rustin P, Gustafsson CM, Larsson NG. (2004) Mitochondrial transcription factor A regulates mtDNA copy number in mammals. Hum. Mol. Genet. 13, 935–944.

Elvers I, Johansson F, Groth P, Erixon K, Helleday T. (2011) UV stalled replication forks restart by re-priming in human fibroblasts. Nucleic Acids Research, 39(16):7049-57.

Enomoto M, Goto H, Tomono Y, Kasahara K, Tsujimura K, Kiyono T, Inagaki M. (2009) Novel positive feedback loop between Cdk1 and Chk1 in the nucleus during G2/M transition. J. Biol. Chem. 284, 34223-34230.

Errico A, Cosentino C, Rivera T, Losada A, Schwob E, Hunt T, Costanzo V. (2009) Tipin/Tim1/And1 protein complex promotes Pol alpha chromatin binding and sister chromatid cohesion. EMBO J. 28(23):3681-92.

Esposito G, Godindagger I, Klein U, Yaspo ML, Cumano A, Rajewsky K. (2000) Disruption of the Rev3l-encoded catalytic subunit of polymerase zeta in mice results in early embryonic lethality. Curr Biol. 10(19):1221-4.

Fachinetti D, Bermejo R, Cocito A, Minardi S, Katou Y, Kanoh Y, Shirahige K, Azvolinsky A, Zakian VA, Foiani M. (2010) Replication termination at eukaryotic chromosomes is mediated by Top2 and occurs at genomic loci containing pausing elements. Mol Cell. 39(4):595-605.

Falkenberg M, Larsson NG, Gustafsson CM. (2007) DNA replication and transcription in mammalian mitochondria. Annu Rev Biochem. 76:679-99.

Feng W, D'Urso G. (2001) Schizosaccharomyces pombe cells lacking the amino-terminal catalytic domains of DNA polymerase epsilon are viable but require the DNA damage checkpoint control. Mol Cell Biol. 21(14):4495-504.

Filipowicz W. (2005) RNAi: the nuts and bolts of the RISC machine. Cell 122(1):17-20.

Foiani M, Marini F, Gamba D, Lucchini G, Plevani P. (1994) The B subunit of the DNA polymerase alpha-primase complex in Saccharomyces cerevisiae executes an essential function at the initial stage of DNA replication. Mol Cell Biol. 14(2):923-33.

Foiani M, Lucchini G, Plevani P. (1997) The DNA polymerase alpha-primase complex couples DNA replication, cell-cycle progression and DNA-damage response. Trends Biochem Sci. 22(11):424-7.

Fousteri M, Vermeulen W, van Zeeland AA, Mullenders LH. (2006) Cockayne syndrome A and B proteins differentially regulate recruitment of chromatin remodeling and repair factors to stalled RNA polymerase II in vivo. Mol Cell. 23(4):471-82.

Franklin R, Gosling RG. (1953) Molecular configuration in sodium thymonucleate. Nature; 171(4356):740-1.

Frick DN, Kumar S, Richardson CC. (1999) Interaction of ribonucleoside triphosphates with the gene 4 primase of bacteriophage T7. J Biol Chem. 274(50):35899-907.

Frick DN and Richardson CC (2001). DNA primases Annual review of biochemistry, 70, 39-80.

Friedberg EC. (2003) DNA damage and repair. Nature. 421(6921):436-40.

Friedel AM, Pike BL, Gasser SM. (2009) ATR/Mec1: coordinating fork stability and repair. Curr Opin Cell Biol. 21(2):237-44.

Friedman KL, Brewer BJ. (1995) Analysis of replication intermediates by two-dimensional agarose gel electrophoresis. Methods Enzymol. 262:613-27.

Frum RA, Khondker ZS, Kaufman DG. (2009) Temporal differences in DNA replication during the S phase using single fiber analysis of normal human fibroblasts and glioblastoma T98G cells. Cell Cycle 8:3133–3148.

Furnari B, Rhind N, Russell P. (1997) Cdc25 mitotic inducer targeted by chk1 DNA damage checkpoint kinase. Science 277:1495-1497.

Fusté JM, Wanrooij S, Jemt E, Granycome CE, Cluett TJ, Shi Y, Atanassova N, Holt IJ, Gustafsson CM, Falkenberg M. (2010) Mitochondrial RNA polymerase is needed for activation of the origin of light-strand DNA replication. Molecular cell, 37(1), 67– 78.

Galiegue-Zouitina S, Bailleul B, Ginot YM, Perly B, Vigny P, Loucheux-Lefebvre MH. (1986) N-2 guanyl and N-6 adenyl arylation of chicken erythrocyte DNA by the ultimate carcinogen of 4-nitroquinoline 1-oxide. Cancer Res, 46, 1858-1863.

Garg P, Stith CM, Sabouri N, Johansson E and Burgers PM. (2004) Idling by DNA polymerase delta maintains a ligatable nick during lagging-strand DNA replication. Genes Dev. 18, 2764-2773.

Garg P, Burgers PM. (2005) DNA polymerases that propagate the eukaryotic DNA replication fork. Crit Rev Biochem Mol Biol. 40(2):115-28.

Gasteiger E, Hoogland C, Gattiker A, Duvaud S, Wilkins MR, Appel RD, Bairoch A. (2005) Protein identification and analysis tools on the ExPASy server. The Proteomics Protocols Handbook In The Proteomics Protocols Handbook, pp. 571-607.

Ge XQ, Jackson DA, Blow JJ. (2007) Dormant origins licensed by excess Mcm2–7 are required for human cells to survive replicative stress. Genes Dev. 21, 3331–3341.

Geuskens M, Hardt N, Pedrali-Noy G, Spadari S. (1981) An autoradiographic demonstration of nuclear DNA replication by DNA polymerase alpha and of mitochondrial DNA synthesis by DNA polymerase gamma. Nucleic Acids Res. 9(7):1599-613.

Ghosh S, Parvez MK, Banerjee K, Sarin SK, Hasnain SE. (2002) Baculovirus as mammalian cell expression vector for gene therapy: an emerging strategy. Mol Ther. 6(1):5-11.

Giles RE, Blanc H, Cann HM, Wallace DC. (1980) Maternal inheritance of human mitochondrial DNA. Proc Natl Acad Sci U S A. 77(11):6715-9.

Gilljam KM, Müller R, Liabakk NB, Otterlei M. (2012) Nucleotide excision repair is associated with the replisome and its efficiency depends on a direct interaction between XPA and PCNA. PLoS One. 7(11):e49199.

Goldar A, Marsolier-Kergoat MC, Hyrien O. (2009) Universal temporal profile of replication origin activation in eukaryotes. PLoS One. 4(6):e5899.

Gohler T, Sabbioneda S, Green CM, and Lehmann AR (2011). ATR-mediated phosphorylation of DNA polymerase is needed for efficient recovery from UV damage. The Journal of Cell Biology, 192(2), 219-227.

Gräslund S, Nordlund P, Weigelt J, Hallberg BM, Bray J, Gileadi O, Knapp S, Oppermann U, Arrowsmith C, Hui R, Ming J, dhe-Paganon S, Park HW, Savchenko A, Yee A, Edwards A, Vincentelli R, Cambillau C, Kim R, Kim SH, Rao Z, Shi Y, Terwilliger TC, Kim CY, Hung LW, Waldo GS, Peleg Y, Albeck S, Unger T, Dym O, Prilusky J, Sussman JL, Stevens RC, Lesley SA, Wilson IA, Joachimiak A, Collart F, Dementieva I, Donnelly MI, Eschenfeldt WH, Kim Y, Stols L, Wu R, Zhou M, Burley SK, Emtage JS, Sauder JM, Thompson D, Bain K, Luz J, Gheyi T, Zhang F, Atwell S, Almo SC, Bonanno JB, Fiser A, Swaminathan S, Studier FW, Chance MR, Sali A, Acton TB, Xiao R, Zhao L, Ma LC, Hunt JF, Tong L, Cunningham K, Inouye M, Anderson S, Janjua H, Shastry R, Ho CK, Wang D, Wang H, Jiang M, Montelione GT, Stuart DI, Owens RJ, Daenke S, Schütz A, Heinemann U, Yokoyama S, Büssow K, Gunsalus KC. (2008) Protein production and purification. Nat Methods. 5(2):135-46.

Graziewicz MA, Bienstock RJ, Copeland WC. (2007) The DNA polymerase gamma Y955C disease variant associated with PEO and parkinsonism mediates the incorporation and translesion synthesis opposite 7,8-dihydro-8-oxo-2'-deoxyguanosine. Hum Mol Genet. 16(22):2729-39.

Guo N, Faller DV, Vaziri C. (2002) Carcinogen-induced S-phase arrest is Chk1 mediated and caffeine sensitive. Cell Growth Differ. 13(2):77-86.

Guo C, Fischhaber PL, Luk-Paszyc MJ, Masuda Y, Zhou J, Kamiya K, Kisker C, Friedberg EC. (2003) Mouse Rev1 protein interacts with multiple DNA polymerases involved in translesion DNA synthesis. EMBO J. 22(24):6621-30.

Guo C, Kosarek-Stancel JN, Tang TS, Friedberg EC. (2009) Y-family DNA polymerases in mammalian cells. Cell Mol Life Sci. 66(14):2363-81.

Hada M, Georgakilas AG. (2008) Formation of clustered DNA damage after high-LET irradiation: a review. J Radiat Res. 49(3):203-10.

Hanna M, Ball LG, Tong AH, Boone C, Xiao W. (2007) Pol32 is required for Pol zeta-dependent translesion synthesis and prevents double-strand breaks at the replication fork. Mutat Res 625:164–176

Hance N, Ekstrand MI, Trifunovic A. (2005) Mitochondrial DNA polymerase gamma is essential for mammalian embryogenesis. Human Molecular Genetics, 14(13), 1775-1783.

Haracska L, Johnson RE, Unk I, Phillips B, Hurwitz J, Prakash L, Prakash S. (2001a) Physical and functional interactions of human DNA polymerase ! with PCNA. Molecular and Cellular Biology, 21(21), 7199-206.

Haracska L, Johnson RE, Unk I, Phillips B, Hurwitz J, Prakash L, Prakash S. (2001b) Targeting of human DNA polymerase iota to the replication machinery via interaction with PCNA. Proc Natl Acad Sci U S A. 98(25), 14256-61.

Haracska L, Unk I, Johnson RE, Phillips BB, Hurwitz J, Prakash L, Prakash S. (2002a) Stimulation of DNA synthesis activity of human DNA polymerase kappa by PCNA. Mol Cell Biol. 22(3):784-91.

Haracska L, Prakash L, Prakash S. (2002b) Role of human DNA polymerase kappa as an extender in translesion synthesis. Proc Natl Acad Sci U S A. 99(25):16000-5.

Hayashi J, Ohta S, Kikuchi A, Takemitsu M, Goto Y, Nonaka I. (1991) Introduction of disease-related mitochondrial DNA deletions into HeLa cells lacking mitochondrial DNA results in mitochondrial dysfunction. Proc Natl Acad Sci U S A. 88(23):10614-8.

Heffernan TP, Unsal-Kaçmaz K, Heinloth AN, Simpson DA, Paules RS, Sancar A, Cordeiro-Stone M, Kaufmann WK. (2007) Cdc7-Dbf4 and the human S checkpoint response to UVC. J Biol Chem. 282(13):9458-68.
Hégarat N, Smith E, Nayak G, Takeda S, Eyers PA, Hochegger H. (2011) Aurora A and Aurora B jointly coordinate chromosome segregation and anaphase microtubule dynamics. J Cell Biol. 195(7):1103-13.

Heichinger C, Penkett CJ, Bahler J, Nurse P. (2006) Genome-wide characterization of fission yeast DNA replication origins. Embo J 25: 5171–5179.

Heller RC, Marians KJ. (2006) Replication fork reactivation downstream of a blocked nascent leading strand. Nature 439(7076):557-62.

Hendel A, Krijger PH, Diamant N, Goren Z, Langerak P, Kim J, Reissner T, Lee KY, Geacintov NE, Carell T, Myung K, Tateishi S, D'Andrea A, Jacobs H, Livneh Z. (2011) PCNA ubiquitilation is important, but not essential for translesion DNA synthesis in mammalian cells. PLoS Genet. 7(9):e1002262.

Herrick J. (2011) Genetic variation and DNA replication timing, or why is there late replicating DNA? Evolution 65(11):3031-47.

Hirota K, Sonoda E, Kawamoto T, Motegi A, Masutani C, Hanaoka F, Szüts D, Iwai S, Sale JE, Lehmann A, Takeda S. (2010) Simultaneous Disruption of Two DNA Polymerases, Polη and Polζ, in Avian DT40 Cells Unmasks the Role of Polη in Cellular Response to Various DNA Lesions. (J. E. Haber, Ed.) PLoS Genetics, 6(10), e1001151.

Hochegger H, Takeda S, Hunt T. (2008) Cyclin-dependent kinases and cell-cycle transitions: does one fit all? Nat Rev Mol Cell Biol. 9(11):910-6.

Hoege C, Pfander B, Moldovan GL, Pyrowolakis G, Jentsch S. (2002) RAD6-dependent DNA repair is linked to modification of PCNA by ubiquitin and SUMO. Nature 419(6903):135-41.

Hoeijmakers JH. (2001) Genome maintenance mechanisms for preventing cancer. Nature 411(6835):366-74.

Holt IJ, Lorimer HE, Jacobs HT. (2000) Coupled leading- and lagging-strand synthesis of mammalian mitochondrial DNA. Cell. 100(5):515-24.

Holt IJ, Jacobs HT. (2003) Response: The mitochondrial DNA replication bubble has not burst. Trends Biochem. Sci. 28, 355–356.

Holt IJ, He J, Mao CC, Boyd-Kirkup JD, Martinsson P, Sembongi H, Reyes A, Spelbrink JN. (2007) Mammalian mitochondrial nucleoids: organizing an independently minded genome. Mitochondrion 7:311-321.

Holt IJ. (2010) Zen and the art of mitochondrial DNA maintenance. Trends Genet. 26(3):103-9.

Holt IJ, Reyes A. (2012) Human mitochondrial DNA replication. Cold Spring Harb Perspect Biol. 4(12).

Huang TT, Nijman SM, Mirchandani KD, Galardy PJ, Cohn MA, Haas W, Gygi SP, Ploegh HL, Bernards R, D'Andrea AD. (2006) Regulation of monoubiquitilated PCNA by DUB autocleavage. Nat Cell Biol. 8(4):339-47.

Hübscher U, Kuenzle CC, Spadari S. (1979) Functional roles of DNA polymerases beta and gamma. Proc Natl Acad Sci U S A. 76(5):2316-20.

Hughes P, Tratner I, Ducoux M, Piard K, and Baldacci G. (1999) Isolation and identification of the third subunit of mammalian DNA polymerase delta by PCNA-affinity chromatography of mouse FM3A cell extracts. Nucleic Acids Res. 27, 2108–2114.

Hunter SE, Jung D, Di Giulio RT, Meyer JN. (2010) The QPCR assay for analysis of mitochondrial DNA damage, repair, and relative copy number Methods (San Diego, Calif.), 51(4), 444-51.

Iiizumi S, Nomura Y, SoS, Uegaki K, Aoki K, Shibahara K, Adachi N, Koyama H. (2006) Simple one-week method to construct gene targeting vectors: application to production of human knockout cell lines. BioTechniques 41:311-316.

Ingman, M. and Gyllensten, U. (2006) mtDB: Human Mitochondrial Genome Database, a resource for population genetics and medical sciences. Nucleic Acids Res 34, D749-D751.
Ishino Y, Komori K, Cann IK, Koga Y. (1998) A novel DNA polymerase family found in Archaea. J Bacteriol. 180(8):2232-6.

Ito N, Nureki O, Shirouzu M, Yokoyama S, Hanaoka F. (2003) Crystal structure of the Pyrococcus horikoshii DNA primase-UTP complex: implications for the mechanism of primer synthesis. Genes Cells 8(12):913-23.

Iyer LM, Koonin EV, Leipe DD, Aravind L. (2005) Origin and evolution of the archaeo-eukaryotic primase superfamily and related palm-domain proteins: structural insights and new members. Nucleic Acids Res. 33(12):3875-96.

Jackson DA, Pombo A. (1998) Replicon clusters are stable units of chromosome structure: evidence that nuclear organization contributes to the efficient activation and propagation of S-phase in human cells. J Cell Biol. 140(6):1285-95.

Jansen JG, Langerak P, Tsaalbi-Shtylik A, van den Berk P, Jacobs H, de Wind N. (2006) Strand-biased defect in C/G transversions in hypermutating immunoglobulin genes in Rev1-deficient mice. J Exp Med. 2006 Feb 20;203(2):319-23.

Jansen JG, Tsaalbi-Shtylik A, Hendriks G, Gali H, Hendel A, Johansson F, Erixon K, Livneh Z, Mullenders LH, Haracska L, de Wind N. (2009) Separate domains of Rev1 mediate two modes of DNA damage bypass in mammalian cells. Mol Cell Biol. 29(11):3113-23.

Jazin EE, Cavelier L, Eriksson I, Oreland L, Gyllensten U. (1996) Human brain contains high levels of heteroplasmy in the noncoding regions of mitochondrial DNA. Proc. Natl. Acad. Sci. USA 93: 12382–12387.

Jenuth JP, Peterson AC, Shoubridge EA. (1997) Tissue-specific selection for different mtDNA genotypes in heteroplasmic mice. Nat. Genet. 16: 93–95.

Ji K, Kogame T, Choi K, Wang X, Lee J, Taniguchi Y, Takeda S. (2009) A Novel Approach Using DNA-Repair–Deficient Chicken DT40 Cell Lines for Screening and Characterizing the Genotoxicity of Environmental Contaminants. Environ Health Perspect. 117(11): 1737–1744.

Jiang L, Sheikh MS, Huang Y. (2010) Decision Making by p53: Life versus Death. Mol Cell Pharmacol. 2(2):69-77.

Johnson RE, Prakash S, Prakash L. (1999a) Efficient bypass of a thymine-thymine dimer by yeast DNA polymerase, Pol eta. Science 283(5404):1001-4.

Johnson RE, Kondratick CM, Prakash S, Prakash L. (1999b) hRAD30 mutations in the variant form of xeroderma pigmentosum. Science 285(5425):263-5.

Johnson RE, Prakash S, Prakash L. (2000) The human DINB1 gene encodes the DNA polymerase Pol theta. Proc Natl Acad Sci U S A. 97(8):3838-43.

Johnson RE, Haracska L, Prakash L, Prakash S. (2006) Role of hoogsteen edge hydrogen bonding at template purines in nucleotide incorporation by human DNA polymerase iota. Mol Cell Biol. 26(17):6435-41.

Johnson N, Shapiro GI. (2010) Cyclin-dependent kinases (cdks) and the DNA damage response: rationale for cdk inhibitor-chemotherapy combinations as an anticancer strategy for solid tumors. Expert Opin Ther Targets. 14(11):1199-212.

Johnson RE, Prakash L, Prakash S. (2012) Pol31 and Pol32 subunits of yeast DNA polymerase δ are also essential subunits of DNA polymerase ζ. Proc Natl Acad Sci U S A. 109(31):12455-60.

Jones DT. (1999) Protein secondary structure prediction based on position-specific scoring matrices. J. Mol. Biol. 292: 195-202.

Jozwiakowski SK, Connolly BA. (2010) A Modified Family-B Archaeal DNA
Polymerase with Reverse Transcriptase Activity. ChemBioChem, 12(1), 35–37.

Kaguni LS. (2004) DNA polymerase gamma, the mitochondrial replicase. Annu Rev Biochem. 73:293-320.

Kang YH, Galal WC, Farina A, Tappin I, Hurwitz J. (2012) Properties of the human Cdc45/Mcm2-7/GINS helicase complex and its action with DNA polymerase epsilon in rolling circle DNA synthesis. Proc Natl Acad Sci U S A. 109(16):6042-7.

Kano C, Hanaoka F, Wang JY. (2012) Analysis of mice deficient in both REV1 catalytic activity and POLH reveals an unexpected role for POLH in the generation of C to G and G to C transversions during Ig gene hypermutation. Int Immunol. 24(3):169-74.

Kannouche P, Broughton BC, Volker M, Hanaoka F, Mullenders LH, Lehmann AR. (2001) Domain structure, localization, and function of DNA polymerase eta, defective in xeroderma pigmentosum variant cells. Genes Dev. 15(2):158-72.

Kannouche P, Fernández de Henestrosa AR, Coull B, Vidal AE, Gray C, Zicha D, Woodgate R, Lehmann AR. (2003) Localization of DNA polymerases eta and iota to the replication machinery is tightly co-ordinated in human cells. EMBO J. 22(5):1223-33.

Kannouche PL, Wing J, Lehmann AR. (2004) Interaction of human DNA polymerase eta with monoubiquitilated PCNA: a possible mechanism for the polymerase switch in response to DNA damage. Mol Cell. 14(4):491-500.

Kao HI and Bambara RA. (2003) The protein components and mechanism of eukaryotic Okazaki fragment maturation.Crit. Rev. Biochem. Mol. Biol. 38: 433–452.

Kasamatsu H, Robberson DL, Vinograd J. (1971) A novel closed-circular mitochondrial DNA with properties of a replicating intermediate. Proc Natl Acad Sci U S A. 68(9):2252-7.

Kasiviswanathan R, Gustafson MA, Copeland WC, Meyer JN. (2012) Human mitochondrial DNA polymerase γ exhibits potential for bypass and mutagenesis at UV-induced cyclobutane thymine dimers. J Biol Chem. 287(12):9222-9.

Kaufmann WK, Cleaver JE, Painter RB. (1980) Ultraviolet radiation inhibits replicon initiation in S phase human cells. Biochim. Biophys. Acta, 608, 191-195.

Kaufmann WK, Cleaver JE. (1981) Mechanisms of inhibition of DNA replication by ultraviolet light in normal human and xeroderma pigmentosum fibroblasts. J Mol Biol. 149(2):171-87.

Kaufmann WK, Boyer JC, Smith BA, Cordeiro-Stone M. (1985) DNA repair and replication in human fibroblasts treated with (+/-)-r-7,t-8-dihydroxy-t-9,10-epoxy-7,8,9,10-tetrahydrobenzo[a]pyrene. Biochim. Biophys. Acta 824,146-151.

Kaufmann WK. (2010) The human intra-S checkpoint response to UVC-induced DNA damage. Carcinogenesis. 31(5):751-65.

Kawamoto T, Araki K, Sonoda E,Yamashita YM, Harada K, Kikuchi K, Masutani C, Hanaoka F, Nozaki K, Hashimoto N, Takeda S. (2005) Dual roles for DNA polymerase eta in homologous DNA recombination and translesion DNA synthesis. Molecular Cell, Vol. 20, 793–799.

Keck JL, Berger JM. (2001) Primus inter pares (first among equals). Nature Structural Biology, 8(1), 2–4.

Kelly RD, Mahmud A, McKenzie M, Trounce IA, St John JC. (2012) Mitochondrial DNA copy number is regulated in a tissue specific manner by DNA methylation of the nuclear-encoded DNA polymerase gamma A. Nucleic Acids Res. 40(20):10124-38.

Kemp MG, Akan Z, Yilmaz S, Grillo M, Smith-Roe SL, Kang TH, Cordeiro-Stone M, Kaufmann WK, Abraham RT, Sancar A, Unsal-Kaçmaz K. (2010) Tipin-replication protein A interaction mediates Chk1 phosphorylation by ATR in response to genotoxic stress. J Biol Chem. 285(22):16562-71.

Kent WJ, Sugnet CW, Furey TS, Roskin KM, Pringle TH, Zahler AM, Haussler D. The human genome browser at UCSC. Genome Res. 2002 Jun;12(6):996-1006.

Kerrigan JJ, Xie Q, Ames RS, Lu Q. (2011) Production of protein complexes via co-expression. Protein Expr Purif. 75(1):1-14.

Kilkenny ML, De Piccoli G, Perera RL, Labib K, Pellegrini L. (2012) A conserved motif in the C-terminal tail of DNA polymerase α tethers primase to the eukaryotic replisome. J Biol Chem. 287(28):23740-7.

Kinoshita E, Kinoshita-Kikuta E, Takiyama K, Koike T. (2006) Phosphate-binding tag, a new tool to visualize phosphorylated proteins. Mol Cell Proteomics. 5(4):749-57.

Kirk BW, Kuchta RD. (1999a) Arg304 of human DNA primase is a key contributor to catalysis and NTP binding: primase and the family X polymerases share significant sequence homology. Biochemistry. 38(24):7727-36.

Kirk BW, Kuchta RD. (1999b) Human DNA primase: anion inhibition, manganese stimulation, and their effects on in vitro start-site selection. Biochemistry. 38(31):10126-34.

Kirouac KN, Ling H. (2011) Unique active site promotes error-free replication opposite an 8-oxo-guanine lesion by human DNA polymerase iota. Proc Natl Acad Sci U S A.;108(8):3210-5.

Koonin EV, Wolf YI, Kondrashov AS, Aravind L. (2000) Bacterial homologs of the small subunit of eukaryotic DNA primase. J Mol Microbiol Biotechnol. 2(4):509-12.

Kornberg A, Baker TA. (1992) DNA Replication. 2 ed. W. H. Freeman and Co., San Francisco.

Korhonen JA, Pham XH, Pellegrini M, Falkenberg M. (2004) Reconstitution of a minimal CDK replisome in vitro. EMBO J. 23(12):2423-9.

Kosarek JN, Woodruff RV, Rivera-Begeman A, Guo C, D'Souza S, Koonin EV, Walker GC, Friedberg EC. (2008) Comparative analysis of in vivo interactions between Rev1 protein and other Y-family DNA polymerases in animals and yeasts. DNA Repair (Amst) 7, 439-451.

Kramer A, Mailand N, Lukas C, Syljuasen RG, Wilkinson CJ, Nigg EA, Bartek J, Lukas J. (2004). Centrosome-associated Chk1 prevents premature activation of cyclin-B-Cdk1 kinase. Nat. Cell Biol. 6, 884-891.

Krijger PH, Lee KY, Wit N, van den Berk PC, Wu X, Roest HP, Maas A, Ding H, Hoeijmakers JH, Myung K, Jacobs H. (2011) HLTF and SHPRH are not essential for PCNA polyubiquitination, survival and somatic hypermutation: existence of an alternative E3 ligase. DNA Repair (Amst). 10(4):438-44.

Krishna TS, Kong XP, Gary S, Burgers PM, Kuriyan J. (1994) Crystal structure of the eukaryotic DNA polymerase processivity factor PCNA. Cell 79(7):1233-43.

Kroon AM. (1965) Protein synthesis in mitochondria. 3. On the effects of inhibitors on the incorporation of amino acids into protein by intact mitochondria and digitonin fractions. Biochim Biophys Acta. 108(2):275-84.

Krude T, Jackman M, Pines J, Laskey RA. (1997) Cyclin/Cdk-dependent initiation of DNA replication in a human cell-free system. Cell 88,109–119.

Kuchta RD, Stengel G. (2010) Mechanism and evolution of DNA primases. Biochim Biophys Acta. 1804(5):1180-9.

Kuida K, Zheng TS, Na S, Kuan CY, Yang D, Karasuyama H, Rakic P, Flavell RA. (1996) Decreased apoptosis in the brain and premature lethality in CPP32-deficient mice. Nature 384:368–372.

Kumagai A, Dunphy WG. (2000) Claspin, a novel protein required for the activation of Chk1 during a DNA replication checkpoint response in Xenopus egg extracts,Mol. Cell 6 839–849.

Kumagai A, Kim SM and Dunphy WG. (2004) Claspin and the activated form of ATR–ATRIP collaborate in the activation of Chk1. J. Biol. Chem. 279, 49599–49608.

Kumagai A, Shevchenko A, Shevchenko A, Dunphy WG. (2010) Treslin collaborates with TopBP1 in triggering the initiation of DNA replication. Cell 140(3):349-59.

Kunkel TA, Mosbaugh DW. (1989) Exonucleolytic proofreading by a mammalian DNA polymerase. Biochemistry. 28(3):988-95.

Kutik S, Stroud DA, Wiedemann N, Pfanner N. (2009) Evolution of mitochondrial protein biogenesis. Biochim Biophys Acta. 1790(6):409-15.

Lagerwerf S, Vrouwe MG, Overmeer RM, Fousteri MI, Mullenders LH. (2011) DNA damage response and transcription. DNA Repair (Amst). 10(7):743-50.

Lao-Sirieix SH, Bell SD. (2004) The heterodimeric primase of the hyperthermophilic archaeon Sulfolobus solfataricus possesses DNA and RNA primase, polymerase and 3'-terminal nucleotidyl transferase activities. J Mol Biol. 344(5):1251-63.

Lao-Sirieix SH, Pellegrini L, Bell SD. (2005a) The promiscuous primase. Trends Genet. 21(10):568-72.

Lao-Sirieix SH, Nookala RK, Roversi P, Bell SD, Pellegrini L. (2005b) Structure of the heterodimeric core primase. Nat Struct Mol Biol. 12(12):1137-44.

Lange SS, Takata K, Wood RD (2011). DNA polymerases and cancer. Nature Reviews Cancer, 11(2), 96-110.

Lange SS, Wittschieben JP, Wood RD. (2012) DNA polymerase zeta is required for proliferation of normal mammalian cells Nucleic Acids Research, 40(10), 4473-82.

Larkin MA, Blackshields G, Brown NP, Chenna R, McGettigan PA, McWilliam H, Valentin F, Wallace IM, Wilm A, Lopez R, Thompson JD, Gibson TJ, Higgins DG. (2007) Clustal W and Clustal X version 2.0. Bioinformatics. 23(21):2947-8.

Larsen NB, Rasmussen M, Rasmussen LJ. (2005) Nuclear and mitochondrial DNA repair: similar pathways? Mitochondrion. 5(2):89-108.

Larsson NG. (2010) Somatic Mitochondrial DNA Mutations in Mammalian Aging. Annu. Rev. Biochem. 79:14.1–14.24.

Lazzaro F, Novarina D, Amara F, Watt DL, Stone JE, Costanzo V, Burgers PM, Kunkel TA, Plevani P, Muzi-Falconi M. (2012) RNase H and postreplication repair protect cells from ribonucleotides incorporated in DNA. Mol Cell. 45(1):99-110.

Lee HC, Yin PH, Lu CY, Chi CW, Wei YH (2000). Increase of mitochondria and mitochondrial DNA in response to oxidative stress in human cells. Biochem J. 348(Pt 2): 425–432.

Lee JH, Paull TT. (2004) Direct activation of the ATM protein kinase by the Mre11/Rad50/Nbs1 complex. Science 304(5667):93-6.

Lehmann AR. (1972) Postreplication repair of DNA in ultraviolet-irradiated mammalian cells. J Mol Biol. 66(3):319-37.

Lehmann AR, Kirk-Bell S, Arlett CF, Paterson MC, Lohman PH, de Weerd-Kastelein EA, Bootsma D. (1975) Xeroderma pigmentosum cells with normal levels of excision repair have a defect in DNA synthesis after UV-irradiation. Proc Natl Acad Sci U S A. 72(1):219-23.

Lehmann AR. (2003) DNA repair-deficient diseases, xeroderma pigmentosum, Cockayne syndrome and trichothiodystrophy. Biochimie 85(11):1101-11.

Lehmann AR. (2006) Translesion synthesis in mammalian cells. Exp Cell Res. 312(14):2673-6.

Lehmann AR. (2011) DNA polymerases and repair synthesis in NER in human cells. DNA Repair (Amst). 10(7):730-3.

Lehmann AR, McGibbon D, Stefanini M. (2011) Xeroderma pigmentosum. Orphanet J Rare Dis. 6:70.

Lei M, Kawasaki Y, Young MR, Kihara M, Sugino A, Tye BK. (1997) Mcm2 is a target of regulation by Cdc7-Dbf4 during the initiation of DNA synthesis. GenesDev.11, 3365–3374.

Lemontt JF. (1971) Mutants of yeast defective in mutation induced by ultraviolet light. Genetics. 68:21–33.

Levitt M. (1978) How many base-pairs per turn does DNA have in solution and in chromatin? Some theoretical calculations. Proc. Natl. Acad. Sci. USA Vol. 75, No. 2, pp. 640-644, Biochemistry.

Li X, Heyer WD. (2008) Homologous recombination in DNA repair and DNA damage tolerance. Cell Res. 18(1):99-113.

Lin JR, Zeman MK, Chen JY, Yee MC, Cimprich KA. (2011) SHPRH and HLTF act in a damage-specific manner to coordinate different forms of postreplication repair and prevent mutagenesis. Mol Cell. 42(2):237-49.

Lin CS, Lee HT, Lee SY, Shen YA, Wang LS, Chen YJ, Wei YH. (2012a) High mitochondrial DNA copy number and bioenergetic function are associated with tumor invasion of esophageal squamous cell carcinoma cell lines. Int J Mol Sci. 13(9):11228-46.

Lin SJ, Wardlaw CP, Morishita T, Miyabe I, Chahwan C, Caspari T, Schmidt U, Carr AM, Garcia V. (2012b) The Rad4(TopBP1) ATR-activation domain functions in G1/S phase in a chromatin-dependent manner. PLoS Genet. 8(6):e1002801.

Lindahl T. (1993) Instability and decay of the primary structure of DNA. Nature 362 pp. 709–715.

Lipps G, Röther S, Hart C, Krauss G. (2003) A novel type of replicative enzyme harbouring ATPase, primase and DNA polymerase activity. EMBO J. 22,2516–2525.

Lipps G, Weinzierl AO, von Scheven G, Buchen C, Cramer P. (2004) Structure of a bifunctional DNA primase-polymerase. Nat Struct Mol Biol. 11(2):157-62.

Liu L, Komori K, Ishino S, Bocquier AA, Cann IK, Kohda D, Ishino Y. (2001) The archaeal DNA primase: biochemical characterization of the p41-p46 complex from Pyrococcus furiosus. J Biol Chem. 276(48):45484-90.

Liu P, Barkley LR, Day T, Bi X, Slater DM, Alexandrow MG, Nasheuer HP, Vaziri C. (2006) The Chk1-mediated S-phase checkpoint targets initiation factor Cdc45 via a Cdc25A/Cdk2-independent mechanism. J Biol Chem. 281(41):30631-44.

Liu P, Demple B (2010). DNA repair in mammalian mitochondria: Much more than we thought Environmental and molecular mutagenesis, 51(5), 417-26.

Livneh Z, Ziv O, Shachar S. (2010) Multiple two-polymerase mechanisms in mammalian translesion DNA synthesis. Cell Cycle.9(4):729-35.

Ljungman M, Zhang F. (1996) Blockage of RNA polymerase as a possible trigger for u.v. light-induced apoptosis. Oncogene 13, 823–831.

Lobstein J, Emrich CA, Jeans C, Faulkner M, Riggs P, Berkmen M. (2012) SHuffle, a novel Escherichia coli protein expression strain capable of correctly folding disulfide bonded proteins in its cytoplasm. Microb Cell Fact. 11(1):56.

Lodish H, Berk A, Zipursky SL, Matsudaira P, Baltimore D, Darnell J. (2000) Molecular Cell Biology, 4th edition; Freeman, W. H. & Co. N. Y.

Lone S, Townson SA, Uljon SN, Johnson RE, Brahma A, Nair DT, Prakash S, Prakash L, Aggarwal AK. (2007) Human DNA polymerase kappa encircles DNA: implications for mismatch extension and lesion bypass. Mol Cell. 25(4):601-14.

Lopes M, Foiani M, Sogo JM. (2006) Multiple mechanisms control chromosome integrity after replication fork uncoupling and restart at irreparable UV lesions. Mol Cell. 21(1):15-27.

López-Contreras AJ, Fernandez-Capetillo O. (2010) The ATR barrier to replication-born DNA damage. DNA Repair (Amst). 9(12):1249-55.

Lopez-Contreras AJ, Fernandez-Capetillo O. (2012). Signalling DNA Damage, Protein Phosphorylation in Human Health, Dr. Cai Huang (Ed.), ISBN: 978-953-51-0737-8.

Lord CJ, Ashworth A. (2012) The DNA damage response and cancer therapy. Nature 481(7381):287-94.

Lutzmann M, Maiorano D, Méchali M. (2006) A Cdt1-geminin complex licenses chromatin for DNA replication and prevents rereplication during S-phase in Xenopus. EMBO J. 25(24):5764-74.

Lutzmann M, Méchali M. (2008) MCM9 binds Cdt1 and is required for the assembly of prereplication complexes. Mol Cell. 31(2):190-200.

MacDougall CA, Byun TS, Van C, Yee MC, Cimprich KA. (2007) The structural determinants of checkpoint activation. Genes Dev 21(8): 898–903.

Maga G, Villani G, Tillement V, Stucki M, Locatelli GA, Frouin I, Spadari S, Hübscher U. (2001) Okazaki fragment processing: modulation of the strand displacement activity of DNA polymerase delta by the concerted action of replication protein A, proliferating cell nuclear antigen, and flap endonuclease-1. Proc Natl Acad Sci U S A. 98(25):14298-303.

Maher VM, Ouellette LM, Curren RD, McCormick JJ. (1976) Frequency of ultraviolet light-induced mutations is higher in xeroderma pigmentosum variant cells than in normal human cells. Nature 261(5561):593-5.

Majka J, Burgers PM. (2004) The PCNA-RFC families of DNA clamps and clamp loaders. Prog Nucleic Acid Res Mol Biol. 78:227-60.

Majka J, Chung BY, Burgers PM. (2004) Requirement for ATP by the DNA damage checkpoint clamp loader. J Biol Chem. 279(20):20921-6.

Malakhova L, Bezlepkin VG, Antipova V, Ushakova T, Fomenko L, Sirota N, Gaziev AI (2005). The increase in mitochondrial DNA copy number in the tissues of gamma-irradiated mice Cellular molecular biology letters, 10(4), 721-32.

Maor-Shoshani A, Ben-Ari V, Livneh Z. (2003) Lesion bypass DNA polymerases replicate across non-DNA segments. Proc Natl Acad Sci U S A. 100(25):14760-5.

Mancini M, Anderson BO, Caldwell E, Sedghinasab M, Paty PB, Hockenbery DM. (1997) Mitochondrial proliferation and paradoxical membrane depolarization during terminal differentiation and apoptosis in a human colon carcinoma cell line. The Journal of Cell Biology, 138(2), 449-69.

Masai H, Matsumoto S, You Z, Yoshizawa-Sugata N, Oda M. (2010) Eukaryotic chromosome DNA replication: where, when, and how? Annu. Rev. Biochem. 79, 89–130.

Masumoto H, Sugino A, and Araki H. (2000) Dpb11 controls the association between DNA polymerases alpha and epsilon and the autonomously replicating sequence region of budding yeast. Mol Cell Biol 20:2809–2817.

Masutani C, Kusumoto R, Yamada A, Dohmae N, Yokoi M, Yuasa M, Araki M, Iwai S, Takio K, Hanaoka F. (1999) The XPV (xeroderma pigmentosum variant) gene encodes human DNA polymerase eta, Nature 399 700–704.

Matsuyama M, Goto H, Kasahara K, Kawakami Y, Nakanishi M, Kiyono T, Goshima N, Inagaki M. (2011) Nuclear Chk1 prevents premature mitotic entry. J Cell Sci 124: 2113–9.

Maya-Mendoza A, Petermann E, Gillespie DA, Caldecott KW, Jackson DA. (2007) Chk1 regulates the density of active replication origins during the vertebrate S phase. EMBO J. 26: 2719–31.

Mechali M. (2010). Eukaryotic DNA replication origins: many choices for appropriate answers. Nat. Rev. Mol. Cell Biol. 11, 728–738.

Mendelman LV, Beauchamp BB, Richardson CC. (1994) Requirement for a zinc motif for template recognition by the bacteriophage T7 primase. EMBO J. 13(16):3909-16.

McKay BC, Ljungman M. (1999) Role for p53 in the recovery of transcription and protection against apoptosis induced by ultraviolet light. Neoplasia. 1(3):276-84.

McKay BC, Becerril C, Spronck JC, Ljungman M. (2002) Ultraviolet light-induced apoptosis is associated with S-phase in primary human fibroblasts. DNA Repair (Amst). 1(10):811-20.

Milenkovic D, Matic S, Kühl I, Ruzzenente B, Freyer C, Jemt E, Park CB, Falkenberg M, Larsson NG. (2013) TWINKLE is an essential mitochondrial helicase required for synthesis of nascent D-loop strands and complete mtDNA replication. Hum Mol Genet.

Minca EC, Kowalski D. (2011) Replication fork stalling by bulky DNA damage: localization at active origins and checkpoint modulation. Nucleic Acids Res. 39(7):2610-23.

Mirkin EV, Mirkin SM. (2007) Replication Fork Stalling at Natural Impediments. Microbiology and Molecular Biology Reviews, 71(1), 13-35.

Moldovan GL, Pfander B, Jentsch S. (2007) PCNA, the maestro of the replication fork. Cell 129(4):665-79.

Mordes DA, Cortez D. (2008) Activation of ATR and related PIKKs. Cell Cycle 7, 2809–2812.

Morrison A, Araki H, Clark AB, Hamatake RK, Sugino A. (1990) A third essential DNA polymerase in S. cerevisiae. Cell 62:1143–1151.
Mouret S, Baudouin C, Charveron M, Favier A, Cadet J, Douki T. (2006) Cyclobutane pyrimidine dimers are predominant DNA lesions in whole human skin exposed to UVA radiation. Proc Natl Acad Sci U S A. 103(37):13765-70.

Moyer SE, Lewis PW, Botchan MR. (2006) Isolation of the Cdc45/Mcm2-7/GINS (CMG) complex, a candidate for the eukaryotic DNA replication fork helicase. Proc Natl Acad Sci USA 103: 10236–10241.

Mozzherin DJ, Tan CK, Downey KM, Fisher PA. (1999) Architecture of the
active DNA polymerase delta-proliferating cell nuclear antigen template-primer complex.
J. Biol. Chem. 274, 19862–19867.

Muzi-Falconi M, Giannattasio M, Foiani M, Plevani P. (2003) The DNA polymerase alpha-primase complex: multiple functions and interactions. Scientific World Journal. 3:21-33.

Myers K, Gagou ME, Zuazua-Villar P, Rodriguez R, Meuth M. (2009) ATR and Chk1 suppress a caspase-3-dependent apoptotic response following DNA replication stress. PLoS Genet. 5(1):e1000324.

Nair DT, Johnson RE, Prakash L, Prakash S, Aggarwal AK. (2005) Rev1 employs a novel mechanism of DNA synthesis using a protein template. Science 309, 2219–2222.

Nakamura K, Kogame T, Oshiumi H, Shinohara A, Sumitomo Y, Agama K, Pommier Y, Tsutsui KM, Tsutsui K, Hartsuiker E, Ogi T, Takeda S, Taniguchi Y. (2010) Collaborative action of Brca1 and CtIP in elimination of covalent modifications from double-strand breaks to facilitate subsequent break repair. PLoS Genet. 6(1):e1000828.

Nam EA, Cortez D. (2011) ATR signalling: more than meeting at the fork. Biochem J. 436(3):527-36.

Nasheuer HP, Moore A, Wahl AF, Wang TS. (1991) Cell cycle-dependent phosphorylation of human DNA polymerase alpha. J Biol Chem. 266(12):7893-903.

Nass MM, Nass S. (1963) Intramitochondrial fibers with DNA characteristics. I. Fixation and electron staining reactions. J Cell Biol. 19:593-611.

Nelson JR, Lawrence CW, Hinkle DC. (1996) Deoxycytidyl transferase activity of yeast REV1 protein. Nature 382(6593):729-31.

Nelson JR, Gibbs PE, Nowicka AM, Hinkle DC, Lawrence CW. (2000) Evidence for a second function for Saccharomyces cerevisiae Rev1p. Mol Microbiol. 37(3):549-54.

Nethanel T, Reisfeld S, Dinter-Gottlieb G, Kaufmann G. (1988) An Okazaki Piece of Simian Virus 40 May Be Synthesized by Ligation of Shorter Precursor Chains. J. Virol. 6:2867–73

Nick McElhinny SA, Gordenin DA, Stith CM, Burgers PM, Kunkel TA. (2008) Division of labor at the eukaryotic replication fork. Mol Cell. 30(2):137-44.

Nick McElhinny SA, Kumar D, Clark AB, Watt DL, Watts BE, Lundström EB, Johansson E, Chabes A, Kunkel TA. (2010) Genome instability due to ribonucleotide incorporation into DNA. Nat Chem Biol. 6(10):774-81.

Nikolaishvili-Feinberg N, Jenkins GS, Nevis KR, Staus DP, Scarlett CO, Unsal-Kaçmaz K, Kaufmann WK, Cordeiro-Stone M. (2008) Ubiquitylation of proliferating cell nuclear antigen and recruitment of human DNA polymerase η. Biochemistry. 47(13):4141-50.

Noguchi E, Noguchi C, McDonald WH, Yates JR 3rd, Russell P. (2004) Swi1 and Swi3 are components of a replication fork protection complex in fission yeast. Mol Cell Biol. 24(19):8342-55.

Ochs K, Lips J, Profittlich S, Kaina B. (2002) Deficiency in DNA Polymerase β Provokes Replication-dependent Apoptosis via DNA Breakage, Bcl-2 Decline and Caspase-3/9 Activation. Cancer Res. 62:1524-1530.

Ogawa T, Okazaki T (1980). Discontinuous DNA replication Annual review of biochemistry, 49, 421-57.

Ogi T, Shinkai Y, Tanaka K, Ohmori H. (2002) Polkappa protects mammalian cells against the lethal and mutagenic effects of benzo[a]pyrene. Proc Natl Acad Sci U S A. 99(24):15548-53.

Ogi T, Kannouche P, Lehmann AR. (2005) Localisation of human Y-family DNA polymerase kappa: relationship to PCNA foci. J Cell Sci. 118(Pt 1):129-36.

Ogi T, Lehmann AR. (2006) The Y-family DNA polymerase kappa (pol kappa) functions in mammalian nucleotide-excision repair. Nat Cell Biol. 8(6):640-2.

Ogi T, Limsirichaikul S, Overmeer RM, Volker M, Takenaka K, Cloney R, Nakazawa Y, Niimi A, Miki Y, Jaspers NG, Mullenders LH, Yamashita S, Fousteri MI, Lehmann AR. (2010) Three DNA polymerases, recruited by different mechanisms, carry out NER repair synthesis in human cells. Mol Cell. 37(5):714-27.

Ohashi E, Bebenek K, Matsuda T, Feaver WJ, Gerlach VL, Friedberg EC, Ohmori H, Kunkel TA. (2000) Fidelity and processivity of DNA synthesis by DNA polymerase kappa, the product of the human DINB1 gene. J Biol Chem. 275(50):39678-84.

Ohmori H, Friedberg EC, Fuchs RP, Goodman MF, Hanaoka F, Hinkle D, Kunkel TA, Lawrence CW, Livneh Z, Nohmi T, Prakash L, Prakash S, Todo T, Walker GC, Wang Z, Woodgate R. (2001) The Y-family of DNA polymerases. Mol Cell. 8(1):7-8.

Ohta S, Tatsumi Y, Fujita M, Tsurimoto T and Obuse C. (2003) The ORC1 cycle in human cells :II. Dynamic changes in the human ORC complex during the cell cycle .J.Biol.Chem. 278,41535–41540

Ollis DL, Brick P, Hamlin R, Xuong NG, Steitz TA. (1985) Structure of large fragment of Escherichia coli DNA polymerase I complexed with dTMP. Nature 313(6005):762-6.

Pacek M, Walter JC. (2004) A requirement for MCM7 and Cdc45 in chromosome unwinding during eukaryotic DNA replication. EMBOJ. 23,3667–3676.

Pagliacci MC, Spinozzi F, Migliorati G, Fumi G, Smacchia M, Grignani F, Riccardi C, Nicoletti I. (1993) Genistein inhibits tumour cell growth in vitro but enhances mitochondrial reduction of tetrazolium salts : a further pitfall in the use of the MTT assay for evaluating cell growth and survival. Eur J Cancer. 29A(11):1573-7.

Papouli E, Chen S, Davies AA, Huttner D, Krejci L, Sung P, Ulrich HD. (2005) Crosstalk between SUMO and ubiquitin on PCNA is mediated by recruitment of the helicase Srs2p. Mol. Cell 19, 123–133.

Patel PK, Arcangioli B, Baker SP, Bensimon A, Rhind N. (2006) DNA replication origins fire stochastically in fission yeast. Mol Biol Cell. 17(1):308-16.

Paulsen RD, Cimprich KA. (2007) The ATR pathway: fine-tuning the fork. DNA Repair (Amst). 6(7):953-66.

Pavlov YI, Shcherbakova PV. (2010) DNA polymerases at the eukaryotic fork-20 years later. Mutat Res. 685(1-2):45-53.

Petermann E, Maya-Mendoza A, Zachos G, Gillespie DAF, Jackson DA, Caldecott KW. (2006) Chk1 Requirement for High Global Rates of Replication Fork Progression during Normal Vertebrate S-phase. Molecular and Cellular Biology, 26(8), 3319-3326.

Petermann E, Helleday T, Caldecott KW. (2008) Claspin Promotes Normal Replication Fork Rates in Human Cells. Mol Biol Cell. 19(6): 2373–2378.

Petermann E, Woodcock M, Helleday T. (2010) Chk1 promotes replication fork progression by controlling replication initiation. Proc Natl Acad Sci U S A. 107(37):16090-5.

Petta TB, Nakajima S, Zlatanou A, Despras E, Couve-Privat S, Ishchenko A, Sarasin A, Yasui A, Kannouche P. (2008) Human DNA polymerase iota protects cells against oxidative stress. EMBO J. 27(21):2883-95.

Pfander B, Moldovan GL, Sacher M, Hoege C, Jentsch S. (2005) SUMO modified PCNA recruits Srs2 to prevent recombination during S-phase. Nature 436, 428–433.

Pinz KG, Bogenhagen DF. (2000) Characterization of a catalytically slow AP lyase activity in DNA polymerase gamma and other family A DNA polymerases. J Biol Chem. 275(17):12509-14.

Pitcher RS, Tonkin LM, Green AJ, Doherty AJ. (2005) Domain structure of a NHEJ DNA repair ligase from Mycobacterium tuberculosis. J Mol Biol. 351(3):531-44.

Pitcher RS, Brissett NC, Picher AJ, Andrade P, Juarez R, Thompson D, Fox GC, Blanco L, Doherty AJ. (2007a) Structure and function of a mycobacterial NHEJ DNA repair polymerase. J Mol Biol. 366(2):391-405.

Pitcher RS, Brissett NC, Doherty AJ. (2007b) Nonhomologous end-joining in bacteria: a microbial perspective. Annu Rev Microbiol. 61:259-82.

Plevani P, Foiani M, Valsasnini P, Badaracco G, Cheriathundam E, Chang LMS. (1985) Polypeptide structure of DNA primase from a yeast DNA polymerase-primase complex. J. Biol. Chem. 260,7102—7107.

Pohjoismäki JL, Wanrooij S, Hyvärinen AK, Goffart S, Holt IJ, Spelbrink JN, Jacobs HT. (2006) Alterations to the expression level of mitochondrial transcription factor A, TFAM, modify the mode of mitochondrial DNA replication in cultured human cells. Nucleic Acids Research, 34(20), 5815-28.

Pohjoismäki JL, Holmes JB, Wood SR, Yang MY, Yasukawa T, Reyes A, Bailey LJ, Cluett TJ, Goffart S, Willcox S, Rigby RE, Jackson AP, Spelbrink JN, Griffith JD, Crouch RJ, Jacobs HT, Holt IJ. (2010) Mammalian mitochondrial DNA replication intermediates are essentially duplex but contain extensive tracts of RNA/DNA hybrid. J Mol Biol. 397(5):1144-55.

Prakash S, Johnson RE, Prakash L. (2005) Eukaryotic translesion synthesis DNA polymerases: specificity of structure and function. Annu Rev Biochem. 74:317-53.
Prelich G, Tan CK, Kostura M, Mathews MB, So AG, Downey KM, Stillman B. (1987) Functional identity of proliferating cell nuclear antigen and a DNA polymerase-delta auxiliary protein. Nature 326(6112):517-20.

Pursell ZF, Isoz I, Lundström EB, Johansson E, Kunkel TA. (2007) Yeast DNA polymerase epsilon participates in leading-strand DNA replication. Science 317(5834):127-30.

Qimron U, Lee SJ, Hamdan SM, Richardson CC. (2006) Primer initiation and extension by T7 DNA primase. EMBO J. 25 2198–2208.

Queille S, Drougard C, Sarasin A, Daya-Grosjean L. (2001) Effects of XPD mutations on ultraviolet-induced apoptosis in relation to skin cancer-proneness in repair-deficient syndromes. J Invest Dermatol. 117(5):1162-70.

Rampakakis E, Gkogkas C, Di Paola D, Zannis-Hadjopoulos M. (2010) Replication initiation and DNA topology: the twisted life of the origin. Journal of Cellular Biochemistry 110:35–43.

Rastogi RP, Richa, Kumar A, Tyagi MB, Sinha RP. (2010) Molecular Mechanisms of Ultraviolet Radiation-Induced DNA Damage and Repair. J Nucleic Acids. 2010:592980.

Reijns MA, Rabe B, Rigby RE, Mill P, Astell KR, Lettice LA, Boyle S, Leitch A, Keighren M, Kilanowski F, Devenney PS, Sexton D, Grimes G, Holt IJ, Hill RE, Taylor MS, Lawson KA, Dorin JR, Jackson AP. (2012) Enzymatic removal of ribonucleotides from DNA is essential for mammalian genome integrity and development. Cell 149(5):1008-22.

Remus D, Beuron F, Tolun G, Griffith JD, Morris EP, Diffley JF. (2009) Concerted loading of Mcm2-7 double hexamers around DNA during DNA replication origin licensing. Cell 139(4):719-30.

Rey L, Sidorova JM, Puget N, Boudsocq F, Biard DS, Monnat RJ Jr, Cazaux C, Hoffmann JS. (2009) Human DNA polymerase eta is required for common fragile site stability during unperturbed DNA replication. Mol Cell Biol. 29(12):3344-54.

Reyes A, Yasukawa T, Holt IJ. (2007) Analysis of replicating mitochondrial DNA by two-dimensional agarose gel electrophoresis. Methods Mol Biol. 372:219-32.

Ritz D, Lim J, Reynolds CM, Poole LB, Beckwith J. (2001) Conversion of a peroxiredoxin into a disulfide reductase by a triplet repeat expansion. Science 294(5540):158-60.

Ross AL, Simpson LJ, Sale JE. (2005) Vertebrate DNA damage tolerance requires the C-terminus but not BRCT or transferase domains of REV1. Nucleic Acids Res 33, 1280-1289

Ross AL, Sale JE. (2006) The catalytic activity of REV1 is employed during immunoglobulin gene diversification in DT40. Mol Immunol. 2006 Apr;43(10):1587-94.

Roth V. 2006 <http://www.doubling-time.com/compute.php>

Rothwell PJ, Waksman G. (2005) Structure and Mechanism of DNA Polymerases. Advances in Protein Chemistry00653233 (Vol. 71, pp. 401–440). Elsevier.

Rupp WD, Howard-Flanders P. (1968) Discontinuities in the DNA synthesized in an excision-defective strain of Escherichia coli following ultraviolet irradiation, J. Mol. Biol. 31 291–304.

Rupp WD, Wilde CE, 3rd, Reno DL, Howard-Flanders P. (1971) Exchanges between DNA strands in ultraviolet-irradiated Escherichia coli. J Mol Biol. 61(1):25-44.

Sakabe K, Okazaki R. (1966) A unique property of the replicating region of chromosomal DNA. Biochim Biophys Acta. 129(3):651-4.

Sale JE. (2012) Competition, collaboration and coordination - determining how cells bypass DNA damage. Journal of Cell Science, 125(7), 1633-1643.

Sale JE, Lehmann AR, Woodgate R. (2012) Y-family DNA polymerases and their role in tolerance of cellular DNA damage. Nature Reviews Molecular Cell Biology, 13(3), 141-152.

Sambrook J, Russell DW. (2006) SDS-Polyacrylamide Gel Electrophoresis of Proteins. CSH Protoc. (4). pii: pdb.prot4540.

Sampath D, Shi Z, Plunkett W. (2002) Inhibition of cyclin-dependent kinase 2 by the Chk1-Cdc25A pathway during the S-phase checkpoint activated by fludarabine: dysregulation by 7-hydroxystaurosporine. Mol Pharmacol. 62(3):680-8.

Sánchez A, Sharma S, Rozenzhak S, Roguev A, Krogan NJ, Chabes A, Russell P. (2012) Replication fork collapse and genome instability in a deoxycytidylate deaminase mutant. Mol Cell Biol. 32(21):4445-54.

Sanchez Y, Wong C, Thoma RS, Richman R, Wu Z, Piwnica-Worms H, Elledge SJ. (1997) Conservation of the Chk1 checkpoint pathway in mammals: linkage of DNA damage to Cdk regulation through Cdc25. Science 277:1497–1501.

Santamaría D, Viguera E, Martínez-Robles ML, Hyrien O, Hernández P, Krimer DB, Schvartzman JB. (2000) Bi-directional replication and random termination. Nucleic Acids Res. 28(10): 2099–2107.

Santocanale C, Foiani M, Lucchini G, and Plevani P. (1993) The isolated 48,000 dalton subunit of yeast DNA primase is sufficient for RNA primer synthesis. J. Biol. Chem. 268, 1343—1348.

Santos JH, Meyer JN, Mandavilli BS, van Houten B. (2006) Quantitative PCR-based measurement of nuclear and mitochondrial DNA damage and repair in mammalian cells. Methods in molecular biology (Clifton, N.J.), 314, 183-99.

Sarkies P, Reams C, Simpson LJ, Sale JE. (2010) Epigenetic instability due to defective replication of structured DNA. Mol Cell. 40(5):703-13.

Sayers EW, Barrett T, Benson DA, Bolton E, Bryant SH, Canese K, Chetvernin V, Church DM, Dicuccio M, Federhen S, Feolo M, Fingerman IM, Geer LY, Helmberg W, Kapustin Y, Krasnov S, Landsman D, Lipman DJ, Lu Z, Madden TL, Madej T, Maglott DR, Marchler-Bauer A, Miller V, Karsch-Mizrachi I, Ostell J, Panchenko A, Phan L, Pruitt KD, Schuler GD, Sequeira E, Sherry ST, Shumway M, Sirotkin K, Slotta D, Souvorov A, Starchenko G, Tatusova TA, Wagner L, Wang Y, Wilbur WJ, Yaschenko E, Ye J. (2011) Database resources of the National Center for Biotechnology Information. Nucl. Acids Res. 39(Database issue): D38–D51.

Schmitt E, Boutros R, Froment C, Monsarrat B, Ducommun B, Dozier C. (2006) CHK1 phosphorylates CDC25B during the cell cycle in the absence of DNA damage. J. Cell Sci. 119:4269–4275.

Schmutz V, Janel-Bintz R, Wagner J, Biard D, Shiomi N, Fuchs RP, Cordonnier AM. (2010) Role of the ubiquitin-binding domain of Polη in Rad18-independent translesion DNA synthesis in human cell extracts. Nucleic Acids Res. 38(19):6456-65

Schwab RA, Niedzwiedz W. (2011) Visualization of DNA Replication in the Vertebrate Model System DT40 using the DNA Fiber Technique. J. Vis. Exp. (56), e3255.

Scorah J, Dong MQ, Yates JR 3rd, Scott M, Gillespie D, McGowan CH. (2008) A conserved proliferating cell nuclear antigen-interacting protein sequence in Chk1 is required for checkpoint function. J Biol Chem. 283(25):17250-9.

Seiler JA, Conti C, Syed A, Aladjem MI, Pommier Y. (2007) The intra-S-phase checkpoint affects both DNA replication initiation and elongation: single-cell and -DNA fiber analyses Molecular and Cellular Biology, 27(16), 5806-18.

Shachar S, Ziv O, Avkin S, Adar S, Wittschieben J, Reissner T, Chaney S, Friedberg EC, Wang Z, Carell T, Geacintov N, Livneh Z. (2009) Two-polymerase mechanisms dictate error-free and error-prone translesion DNA synthesis in mammals. EMBO J 28:383-93.

Sheaff RJ, Kuchta RD. (1993) Mechanism of calf thymus DNA primase: slow initiation, rapid polymerization, and intelligent termination. Biochemistry. 32(12):3027-37.

Simpson LJ, Sale JE. (2006) Colony survival assay. Subcell Biochem.40:387-91.

Smith KD, Fu MA, Brown EJ. (2009) Tim-Tipin dysfunction creates an indispensible reliance on the ATR-Chk1 pathway for continued DNA synthesis. J Cell Biol. 187(1):15-23.

Smits VA, Reaper PM, Jackson SP. (2006) Rapid PIKK-dependent release of Chk1 from chromatin promotes the DNA-damage checkpoint response, Curr. Biol.16 150–159.

Snyderwine EG, Bohr VA. Gene- and strand-specific damage and repair in Chinese hamster ovary cells treated with 4-nitroquinoline 1-oxide. Cancer Res. 52:4183–4189.

Sobolewski I, Polska K, Zylicz-Stachula A, Jeżewska-Frąckowiak J, Rak J, Skowron P. (2011) Enzymatic synthesis of long double-stranded DNA labeled with haloderivatives of nucleobases in a precisely pre-determined sequence. BMC Biochem. 12:47.

Solignac M, Monnerot M, Mounolou JC. (1983) Mitochondrial DNA heteroplasmy in Drosophila mauritiana. Proc. Natl. Acad. Sci. USA 80: 6942–6946.

Sonoda E, Okada T, Zhao GY, Tateishi S, Araki K, Yamaizumi M, Yagi T, Verkaik NS, van Gent DC, Takata M, Takeda S. (2003) Multiple roles of Rev3, the catalytic subunit of polzeta in maintaining genome stability in vertebrates. EMBO J. 22(12):3188-97.

Sørensen CS, Syljuåsen RG, Falck J, Schroeder T, Ronnstrand L, Khanna KK, Zhou BB, Bartek J, Lukas J. (2003) Chk1 regulates the S phase checkpoint by coupling the physiological turnover and ionizing radiation-induced accelerated proteolysis of Cdc25A. Cancer Cell. 3:247–258.

Sørensen CS, Syljuåsen RG (2012). Safeguarding genome integrity: the checkpoint kinases ATR, CHK1 and WEE1 restrain CDK activity during normal DNA replication. Nucleic Acids Research, 40(2), 477-486.

Spelbrink JN, Li FY, Tiranti V, Nikali K, Yuan QP, Tariq M, Wanrooij S, Garrido N, Comi G, Morandi L, Santoro L, Toscano A, Fabrizi GM, Somer H, Croxen R, Beeson D, Poulton J, Suomalainen A, Jacobs HT, Zeviani M, Larsson C. (2001) Human mitochondrial DNA deletions associated with mutations in the gene encoding Twinkle, a phage T7 gene 4-like protein localized in mitochondria. Nat Genet. 28(3):223-31.

Speroni J, Federico MB, Mansilla SF, Soria G, Gottifredi V. Kinase-independent function of checkpoint kinase 1 (Chk1) in the replication of damaged DNA. Proc Natl Acad Sci U S A. 2012 May 8;109(19):7344-9.

Spiga MG, D'Urso G. (2004) Identification and cloning of two putative subunits of DNA polymerase epsilon in fission yeast. Nucleic Acids Res. 2004 Sep 23;32(16):4945-53.

Steitz TA. (1999) DNA polymerases: structural diversity and common mechanisms. J Biol Chem. 274(25):17395-8.

Stefanini M, Botta E, Lanzafame M, Orioli D. (2010) Trichothiodystrophy: from basic mechanisms to clinical implications. DNA Repair (Amst).;9(1):2-10.

Stelter P, Ulrich HD. (2003) Control of spontaneous and damage-induced mutagenesis by SUMO and ubiquitin conjugation. Nature 425(6954):188-91.

Stillman B. (1994) Smart machines at the DNA replication fork. Cell 78(5):725-8.

Stukenberg PT, Turner J, O'Donnell M. (1994) An explanation for lagging strand replication: polymerase hopping among DNA sliding clamps. Cell 78(5):877-87.

Sullivan M, Morgan DO. (2007) Finishing mitosis, one step at a time. Nat Rev Mol Cell Biol. 8(11):894-903.

Sundin O, Varshavsky A. (1981) Arrest of segregation leads to accumulation of highly intertwined catenated dimers: Dissection of the final stages of SV40 DNA replication. Cell 25, 659.

Sutovsky P, Moreno RD, Ramalho-Santos J, Dominko T, Simerly C, Schatten G. (1999) Ubiquitin tag for sperm mitochondria. Nature 402(6760):371-2.

Suzuki M, Savoysky E, Izuta S, Tatebe M, Okajima T, Yoshida S. (1993) RNA priming coupled with DNA synthesis on natural template by calf thymus DNA polymerase alpha-primase. Biochemistry. 32(47):12782-92.

Svoboda DL, Vos JM. (1995) Differential replication of a single, UV-induced lesion in the leading or lagging strand by a human cell extract: fork uncoupling or gap formation. Proc Natl Acad Sci U S A. 92(26):11975-9.

Swamynathan SK, Varma BR, Weber KT, Guntaka RV. (2002) Targeted disruption of one allele of the Y-box protein gene, Chk-YB-1b, in DT40 cells results in major defects in cell cycle. Biochemical and Biophysical Research Communications 296(2):451-7.

Syljuåsen RG, Sørensen CS, Hansen LT, Fugger K, Lundin C, Johansson F, Helleday T, Sehested M, Lukas J, Bartek J. (2005) Inhibition of Human Chk1 Causes Increased Initiation of DNA Replication, Phosphorylation of ATR Targets, and DNA Breakage. Molecular and Cellular Biology, 25(9), 3553-3562.

Szüts D, Marcus AP, Himoto M, Iwai S, Sale JE. (2008) REV1 restrains DNA polymerase zeta to ensure frame fidelity during translesion synthesis of UV photoproducts in vivo. Nucleic Acids Res. 36(21):6767-80.

Takai H, Tominaga K, Motoyama N, Minamishima YA, Nagahama H, Tsukiyama T, Ikeda K, Nakayama K, Nakanishi M, Nakayama K. (2000) Aberrant cell cycle checkpoint function and early embryonic death in Chk1(-/-) mice. Genes Dev. 14(12):1439-47.

Takao N, Kato H, Mori R, Morrison C, Sonada E, Sun X, Shimizu H, Yoshioka K, Takeda S, Yamamoto K. (1999) Disruption of ATM in p53-null cells causes multiple functional abnormalities in cellular response to ionizing radiation. Oncogene 18(50):7002-9.

Takeda DY, Dutta A. (2005) DNA replication and progression through S phase. Oncogene 24(17):2827-43.

Tang Y, Schon EA, Wilichowski E, Vazquez-Memije ME, Davidson E, King MP. (2000) Rearrangements of human mitochondrial DNA (mtDNA): new insights into the regulation of mtDNA copy number and gene expression. Mol Biol Cell. 11(4):1471-85.

Temviriyanukul P, van Hees-Stuivenberg S, Delbos F, Jacobs H, de Wind N, Jansen JG. (2012) Temporally distinct translesion synthesis pathways for ultraviolet light-induced photoproducts in the mammalian genome. DNA Repair (Amst). 11(6):550-8.

Tercero JA, Diffley JF. (2001) Regulation of DNA replication fork progression through damaged DNA by the Mec1/Rad53 checkpoint. Nature 412 553–557.

Thakker DR, Yagi H, Lu AY, Levin W, Conney AH. (1976) Metabolism of benzo[a]pyrene: conversion of (+/-)-trans-7,8-dihydroxy-7,8-dihydrobenzo[a]pyrene to highly mutagenic 7,8-diol-9,10-epoxides. Proc Natl Acad Sci U S A. 73(10):3381-5.

Thomas DC, Roberts JD, Sabatino RD, Myers TW, Tan CK, Downey KM, So AG, Bambara RA, Kunkel TA. (1991) Fidelity of mammalian DNA replication and replicative DNA polymerases. Biochemistry. 30(51):11751-9.
Thomson AM, Gillespie PJ, Blow JJ. (2010) Replication factory activation can be decoupled from the replication timing program by modulating Cdk levels. J. Cell Biol. 188, 209–221.

Timares L, Katiyar SK, Elmets CA. (2008) DNA damage, apoptosis and langerhans cells--Activators of UV-induced immune tolerance. Photochem Photobiol. 84(2):422-36.

Timofeev O, Cizmecioglu O, Settele F, Kempf T, Hoffmann I. (2010) Cdc25 phosphatases are required for timely assembly of CDK1-cyclin B at the G2/M transition. J Biol Chem 285: 16978–16990.

Tissier A, Frank EG, McDonald JP, Iwai S, Hanaoka F, Woodgate R. (2000) Misinsertion and bypass of thymine-thymine dimers by human DNA polymerase iota. EMBO J. 19(19):5259-66.

Tissier A, Kannouche P, Reck MP, Lehmann AR, Fuchs RP, Cordonnier A. (2004) Co-localization in replication foci and interaction of human Y-family members, DNA polymerase pol eta and REVl protein. DNA Repair (Amst). 3(11):1503-14.

Tornaletti S. (2009) DNA repair in mammalian cells: Transcription-coupled DNA repair: directing your effort where it's most needed. Cell Mol Life Sci. 66(6):1010-20.

Trenz K, Errico A, Costanzo V. (2008) Plx1 is required for chromosomal DNA replication under stressful conditions. EMBO J. 27, 876–885.

Tsakraklides V, Bell SP. (2010) Dynamics of pre-replicative complex assembly. J Biol Chem. 285(13):9437-43.

Tsurimoto T, Stillman B. (1991) Replication factors required for SV40 DNA replication in vitro. I. DNA structure-specific recognition of a primer-template junction by eukaryotic DNA polymerases and their accessory proteins. J Biol Chem. 266(3):1950-60.

Tuppen HA, Blakely EL, Turnbull DM, Taylor RW. (2010) Mitochondrial DNA mutations and human disease. Biochim Biophys Acta. 1797(2):113-28.

Turner JJ, Ewald JC, Skotheim JM. (2012) Cell Size Control in Yeast. Current Biology 22, R350–R359.

Tyynismaa H, Sembongi H, Bokori-Brown M, Granycome C, Ashley N, Poulton J, Jalanko A, Spelbrink JN, Holt IJ, Suomalainen A. (2004) Twinkle helicase is essential for mtDNA maintenance and regulates mtDNA copy number. Hum Mol Genet. 13(24):3219-27.

Ulrich HD. (2011) Timing and spacing of ubiquitin-dependent DNA damage bypass. FEBS Lett. 585(18):2861-7.

Um M, Yamauchi J, Kato S, Manley JL. (2001) Heterozygous Disruption of the TATA-Binding Protein Gene in DT40 Cells Causes Reduced cdc25B Phosphatase Expression and Delayed Mitosis. Mol Cell Biol. 21(7): 2435–2448.

Unsal-Kaçmaz K, Chastain PD, Qu PP, Minoo P, Cordeiro-Stone M, Sancar A, Kaufmann WK. (2007) The human Tim/Tipin complex coordinates an Intra-S checkpoint response to UV that slows replication fork displacement. Mol Cell Biol. 27(8):3131-42.

Vaithiyalingam S, Warren EM, Eichman BF, Chazin WJ. (2010) Insights into eukaryotic DNA priming from the structure and functional interactions of the 4Fe-4S cluster domain of human DNA primase. Proc Natl Acad Sci U S A. 107(31):13684-9.

Van C, Yan S, Michael WM, Waga S, Cimprich KA. (2010) Continued primer synthesis at stalled replication forks contributes to checkpoint activation. J Cell Biol. 189(2):233-46.

Waga S, Stillman B. (1994) Anatomy of a DNA replication fork revealed by reconstitution of SV40 DNA replication in vitro. Nature 369(6477):207-12.

Waga S, Stillman B. (1998) The DNA replication fork in eukaryotic cells. Annu. Rev. Biochem. 67, 721–751.

Walter J, Newport J. (2000) Initiation of Eukaryotic DNA Replication: Origin Unwinding and Sequential Chromatin Association of Cdc45, RPA, and DNA Polymerase a. Mol Cell. 5(4):617-27.

Walworth N, Davey S, Beach D. (1993) Fission yeast chk1 protein kinase links the rad checkpoint pathway to cdc2. Nature 363:368-371.

Wanrooij S, Goffart S, Pohjoismäki JL, Yasukawa T, Spelbrink JN. (2007) Expression of catalytic mutants of the mtDNA helicase Twinkle and polymerase POLG causes distinct replication stalling phenotypes. Nucleic Acids Res. 353238-3251.

Wanrooij S, Fusté JM, Farge G, Shi Y, Gustafsson CM, Falkenberg M. (2008) Human mitochondrial RNA polymerase primes lagging-strand DNA synthesis in vitro. Proc Natl Acad Sci U S A. 105(32):11122-7.

Wanrooij S, Falkenberg M. (2010) The human mitochondrial replication fork in health and disease. Biochim. Biophys. Acta 1797:1378-1388.

Ward IM, Chen J. (2001) Histone H2AX is phosphorylated in an ATR-dependent manner in response to replicational stress. J Biol Chem. 276(51):47759-62.

Washington MT, Johnson RE, Prakash S, Prakash L. (1999) Fidelity and processivity of Saccharomyces cerevisiae DNA polymerase eta. J Biol Chem. 274(52):36835-8.

Washington MT, Johnson RE, Prakash L, Prakash S. (2002) Human DINB1-encoded DNA polymerase kappa is a promiscuous extender of mispaired primer termini. Proc Natl Acad Sci U S A. 99(4):1910-4.

Watson JD, Crick FHC. (1953) A Structure for Deoxyribose Nucleic Acid. *Nature* 171, 737-738.

Weinert T, Hartwell L. (1989) Control of G2 delay by the rad9 gene of Saccharomyces cerevisiae. J Cell Sci Suppl. 12:145-8.

Weller GR, Doherty AJ. (2001) A family of DNA repair ligases in bacteria? FEBS Lett. 505(2):340-2.

Weller GR, Kysela B, Roy R, Tonkin LM, Scanlan E, Della M, Devine SK, Day JP, Wilkinson A, d'Adda di Fagagna F, Devine KM, Bowater RP, Jeggo PA, Jackson SP, Doherty AJ. (2002) Identification of a DNA nonhomologous end-joining complex in bacteria. Science 297(5587):1686-9.

Wilkins MHF, Stokes AR, Wilson HR. (1953) Molecular Structure of Nucleic Acids: Molecular Structure of Deoxypentose Nucleic Acids. Nature 171, 738-740.

Wilson RC, Jackson MA, Pata JD. (2012) Y-Family Polymerase Conformation Is a Major Determinant of Fidelity and Translesion Specificity. Structure. pii: S0969-2126(12)00420-0.

Wittschieben J, Shivji MK, Lalani E, Jacobs MA, Marini F, Gearhart PJ, Rosewell I, Stamp G, Wood RD. (2000) Disruption of the developmentally regulated Rev3l gene causes embryonic lethality. Curr Biol. 10(19):1217-20.

Wojtaszek J, Liu J, D'Souza S, Wang S, Xue Y, Walker GC, Zhou P. (2012a) Multifaceted recognition of vertebrate Rev1 by translesion polymerases ζ and κ. J Biol Chem. 287(31):26400-8.

Wojtaszek J, Lee CJ, D'Souza S, Minesinger B, Kim H, D'Andrea AD, Walker GC, Zhou P. (2012b) Structural basis of Rev1-mediated assembly of a quaternary vertebrate translesion polymerase complex consisting of Rev1, heterodimeric polymerase (Pol) ζ, and Pol κ. J Biol Chem. 287(40):33836-46.

Wold MS. (1997) Replication protein A: a heterotrimeric, single-stranded DNA-binding protein required for eukaryotic DNA metabolism. Annu Rev Biochem. 66:61-92.

Wong TW, Clayton DA. (1985) Isolation and characterization of a DNA primase from human mitochondria. J Biol Chem. 260(21):11530-5.

Wong TW, Clayton DA. (1986) DNA primase of human mitochondria is associated with structural RNA that is essential for enzymatic activity. Cell 45(6):817-25.

Xiao Z, Chen Z, Gunasekera AH, Sowin TJ, Rosenberg SH, Fesik S, Zhang H. (2003) Chk1 mediates S and G2 arrests through Cdc25A degradation in response to DNA-damaging agents. J Biol Chem. 278(24):21767-73.

Xu B, Clayton DA. (1996). RNA-DNA hybrid formation at the human mitochondrial heavy-strand origin ceases at replication start sites: An implication for RNA-DNA hybrids serving as primers. The EMBO Journal, 15, 3135–3143.

Xu S, Zhong M, Zhang L, Wang Y, Zhou Z, Hao Y, Zhang W, Yang X, Wei A, Pei L, Yu Z. (2009). Overexpression of Tfam protects mitochondria against beta-amyloid-induced oxidative damage in SH-SY5Y cells The FEBS journal, 276(14):3800-9.

Xu Y, Baltimore D. (1996) Dual roles of ATM in the cellular response to radiation and in cell growth control. Genes Dev. 10(19):2401-10.

Yabuki M, Ordinario EC, Cummings WJ, Fujii MM, Maizels N. (2009) E2A acts in cis in G1 phase of cell cycle to promote Ig gene diversification. J Immunol. 182:408–415.

Yamaguchi M, Hendrickson EA, DePamphilis ML. (1985) DNA primase-DNA polymerase alpha from simian cells: sequence specificity of initiation sites on simian virus 40 DNA. Mol Cell Biol. 5(5):1170-83.

Yamazoe M, Sonoda E, Hochegger H, Takeda, S (2004). Reverse genetic studies of the DNA damage response in the chicken B lymphocyte line DT40. DNA Repair, 3(8-9), 1175-1185.

Yan S, Michael WM. (2009a) TopBP1 and DNA polymerase-alpha directly recruit the 9-1-1 complex to stalled DNA replication forks. J Cell Biol. 184(6):793-804.

Yan S, Michael WM. (2009b) TopBP1 and DNA polymerase alpha-mediated recruitment of the 9-1-1 complex to stalled replication forks: implications for a replication restart-based mechanism for ATR checkpoint activation. Cell Cycle. 8(18):2877-84.

Yang XH, Zou L. (2006) Recruitment of ATR–ATRIP, Rad17, and 9-1-1 complexes toDNA damage. Methods Enzymol. 409 (2006) 118–131.

Yang XH, Shiotani B, Classon M, Zou L. (2008) Chk1 and Claspin potentiate PCNA ubiquitilation. Genes Dev. 22(9):1147-52.

Yasukawa T, Reyes A, Cluett TJ, Yang MY, Bowmaker M, Jacobs HT, Holt IJ. (2006) Replication of vertebrate mitochondrial DNA entails transient ribonucleotide incorporation throughout the lagging strand. EMBO J. 25(22):5358-71.

Yeeles JT, Marians KJ. (2011) The Escherichia coli replisome is inherently DNA damage tolerant. Science 334(6053):235-8.

Yoon JH, Prakash L, Prakash S. (2010) Error-free replicative bypass of (6-4) photoproducts by DNA polymerase zeta in mouse and human cells. Genes Dev. 24(2):123-8.

Yoon JH, Prakash S, Prakash L. (2012) Requirement of Rad18 protein for replication through DNA lesions in mouse and human cells. Proc Natl Acad Sci U S A. 109(20):7799-804.

Yoshida Y, Izumi H, Ise T, Uramoto H, Torigoe T, Ishiguchi H, Murakami T, Tanabe M, Nakayama Y, Itoh H, Kasai H, Kohno K. (2002) Human mitochondrial transcription factor A binds preferentially to oxidatively damaged DNA. Biochem. Biophys. Res. Commun. 295, 945–951.

Yoshida Y, Izumi H, Torigoe T, Ishiguchi H, Itoh H, Kang D, Kohno K. (2003) p53 Physically interacts with mitochondrial transcription factor A and differentially regulates binding to damaged DNA. Cancer Res. 63, 3729–3734.

Youle RJ, Narendra DP. (2011) Mechanisms of mitophagy. Nat Rev Mol Cell Biol. 12(1):9-14.

Zachos G, Rainey MD, Gillespie DA. (2003) Chk1-deficient tumour cells are viable but exhibit multiple checkpoint and survival defects. EMBO J. 22(3):713-23.

Zeng X, Winter DB, Kasmer C, Kraemer KH, Lehmann AR, Gearhart PJ. (2001) DNA polymerase eta is an A-T mutator in somatic hypermutation of immunoglobulin variable genes. Nat Immunol. 2(6):537-41.

Zerbe LK, Kuchta RD. (2002) The p58 subunit of human DNA primase is important for primer initiation, elongation, and counting. Biochemistry. 41(15):4891-900.

Zhang Y, Wu X, Rechkoblit O, Geacintov NE, Taylor JS, Wang Z. (2002) Response of human REV1 to different DNA damage: preferential dCMP insertion opposite the lesion. Nucleic Acids Res. 30, 1630–1638.
Zhang F, Zhang T, Qu Y, Jiang T, Cao YX, Li C, Fan L, Mei QB. (2010) Replication-dependent γ-H2AX formation is involved in docetaxel-induced apoptosis in NSCLC A549 cells. Oncol Rep. 24(5):1297-305.

Zhao H, Piwnica-Worms H. (2001) ATR-mediated checkpoint pathways regulate phosphorylation and activation of human Chk1. Mol Cell Biol. 21(13):4129-39.

Zhao B, Bower MJ, McDevitt PJ, Zhao H, Davis ST, Johanson KO, Green SM, Concha NO, Zhou BB. (2002). Structural basis for Chk1 inhibition by UCN-01. The Journal of biological chemistry, 277(48), 46609-15.

Zhou JQ, He H, Tan CK, Downey KM, So AG. (1997). The small subunit is required for functional interaction of DNA polymerase delta with the proliferating cell nuclear antigen. Nucleic Acids Res. 25, 1094–1099.

Zhou BB, Anderson HJ, Roberge M. (2003) Targeting DNA checkpoint kinases in cancer therapy. Cancer Biol Ther. 2(4 Suppl 1):S16-22.

Zhu Z, Zheng T, Lee CG, Homer RJ, Elias JA. (2002) Tetracycline-controlled transcriptional regulation systems: advances and application in transgenic animal modeling. Semin Cell Dev Biol. 13(2):121-8.

Zhu H, Nandakumar J, Aniukwu J, Wang LK, Glickman MS, Lima CD, Shuman S. (2006) Atomic structure and nonhomologous end-joining function of the polymerase component of bacterial DNA ligase D. Proc Natl Acad Sci U S A. 103(6):1711-6.

Zimmermann W, Chen SM, Bolden A, Weissbach A. (1980) Mitochondrial DNA replication does not involve DNA polymerase alpha. J Biol Chem. 255(24):11847-52.

Ziv O, Geacintov N, Nakajima S, Yasui A, Livneh Z. (2009) DNA polymerase zeta cooperates with polymerases kappa and iota in translesion DNA synthesis across pyrimidine photodimers in cells from XPV patients. Proc Natl Acad Sci U S A. 106(28):11552-7.

Ziv O, Diamant N, Shachar S, Hendel A, Livneh Z. (2012) Quantitative measurement of translesion DNA synthesis in mammalian cells. Methods Mol Biol. 920:529-42.

Appendix A

PrimPol, a eukaryotic translesion synthesis DNA polymerase bypassing UV photoproducts

Julie Bianchi[1§], Sean G. Rudd[1§], Stanislaw K. Jozwiakowski[1], Laura J. Bailey[1], Elaine Taylor [2], Andrew J. Green[1], Violetta Soura[1], Howard D. Lindsay[2], Aidan J. Doherty[1]

[1] Genome Damage and Stability Centre, University of Sussex, Brighton BN1 9RQ, UK. [2] Lancaster Medical School, Faculty of Health and Medicine, Lancaster University, Lancaster, LA1 4YQ, UK.

[§] Contributed equally to this work

*Corresponding author: Email: ajd21@sussex.ac.uk

SUMMARY

Ultraviolet (UV) light exposure is a major environmental source of DNA damage in human cells. UV irradiation of DNA produces photoproducts, modified nucleobases, that significantly alter the helical structure of DNA. These lesions act as potent obstacles to DNA replication and must be repaired or bypassed to avoid genomic instability and cell death. Here, we show that higher eukaryotic cells contain an additional nuclear DNA polymerase, primase-polymerase (PrimPol), that is capable of bypassing UV lesions. PrimPol localizes onto chromatin during nuclear replication. PrimPol-deficient ($PrimPol^{-/-}$) cells are sensitive to UV and 4NQO (UV mimetic agent) and these genotoxins enhance chromatin association. Human PrimPol can bypass UV photoproducts, including the highly distorting 6-4 lesion, a feat not previously demonstrated for any mammalian polymerase. $PrimPol^{-/-}$ cells have pronounced fork stalling/slowing after UV damage and reduced DNA synthesis, supporting a role for this polymerase in bypassing UV photoproducts during replication. Finally, depletion of PrimPol in xeroderma pigmentosum variant (XP-V) cells, an inherited syndrome caused by deficiency in a major UV lesion bypass polymerase (Pol η), caused a synergistic sensitivity to UV damage. Together, these findings demonstrate that PrimPol, is a nuclear DNA damage tolerance polymerase that assists in the replication of highly distorting UV lesions and defines a distinct lesion bypass pathway that maintains genome stability in higher eukaryotes. This study also establishes that eukaryotic primases, assumed to only operate in priming DNA replication, are *bona fida* DNA polymerases involved in additional roles in nuclear DNA metabolism.

INTRODUCTION

Replication of the ~6 billion nucleotides constituting the human genome is a herculean task that our cells face every cell cycle. A finely tuned replisome machinery, containing highly accurate and processive DNA polymerases, is tasked with performing this complex process. However, DNA is routinely exposed to various environmental insults and endogenous cellular processes that damage its structure and, if not corrected prior to DNA replication, these lesions can result in physical blockage of the replicative polymerases[1-4]. To avoid replication stalling, cells have evolved specialized mechanisms to allow DNA lesion tolerance. One of these is an error-free bypass pathway that likely involves template switching[4] and the other employs trans lesion synthesis (TLS) DNA polymerases capable of directly synthesizing across templates containing blocking lesions[1-3]. However, these enzymes have low fidelity on undamaged DNA and so their deployment must be highly regulated. In human cells, TLS is predominantly carried out by the Y family (eta, η; iota, ι; kappa, κ & REV1) and B family (zeta, ζ) DNA polymerases[1-3].

Ultraviolet light (UV) is one of the most common sources of DNA damage in terrestrial organisms[5]. The resulting photoproducts are potent causes of replication stalling in cells and have therefore been adopted as model lesions for studying the cellular mechanisms of lesion bypass and tolerance[1,5,6]. UV irradiation results in the formation of major DNA lesions, particularly crosslinks between adjacent pyrimidine bases[5]. The two most common modifications generated by UV are cyclobutane pyrimidine dimers (CPDs) and pyrimidine-pyrimidone (6-4) photoproducts. Both lesions distort the DNA helix and profoundly block replication[6]. Pol η is highly specialized in bypassing CPDs[7,8], which it does in a largely error-free manner[7]. Loss of functional Pol η results in the variant form of xeroderma pigmentosum (XP-V)[7,8], an inherited skin disorder characterised by sunlight-induced pigment changes and a high incidence of skin cancers[8], due to inefficient bypass of CPDs[7]. In the case of 6-4 photoproducts, no single polymerase has been shown to efficiently catalyze TLS past these lesions. Instead, it has been proposed that two polymerases co-operate to facilitate TLS. The first polymerase, suggested to be Pol η or ι, catalyses the initial insertion step, which is mutagenic, and Pol ζ carries out the subsequent extension step, before the replicative polymerases resume[9].

We recently identified a novel primase-polymerase in human cells, called PrimPol (CCDC111 or FLJ33167)[10]. PrimPol is a member of the archaeo-eukaryotic primase (AEP) superfamily[11]. The only other higher eukaryotic member of the AEP superfamily is the DNA primase (Pri1; small catalytic subunit) associated with Pol α, responsible for the initiation of DNA synthesis by producing RNA primers[12]. In prokaryotes and archaea,

AEPs have been shown to be a more versatile group of polymerases involved in a variety of cellular processes, including DNA break repair [13-15]. More akin to its ancestral orthologues, human PrimPol is capable of synthesizing both RNA and DNA primers and extend primers in a DNA template dependent manner[10]. In mammalian cells, PrimPol localizes to mitochondria where it required for maintenance of the mitochondrial genome[10].

Here, we report that PrimPol is present in the nucleus of mammalian cells, where it re-localises and associates with chromatin following UV damage. Human PrimPol catalyzes TLS opposite UV photoproducts *in vitro*, most notably error-prone bypass of 6-4 photoproducts. Additionally, we present evidence for PrimPol-dependent TLS *in vivo* and show that PrimPol protects XP-V cells, that are deficient in the major UV-tolerance pathway (Pol η), from UV damage. We establish that this novel polymerase functions in an alternate TLS damage bypass pathway in mammalian cells that is required for the bypass of UV-induced DNA photoproducts.

RESULTS

Nuclear localisation of human PrimPol

We considered whether PrimPol, shown to play an important role in mitochondrial (mt) DNA metabolism[10], also has additional roles within the nucleus. RNA interference (RNAi) depletion of PrimPol causes a significant proliferative defect in human cultured cells (Figure 1a). We speculated whether this was due to the loss of PrimPol's contribution to mtDNA metabolism. PrimPol protein levels were identical in an osteosarcoma 143B cell line depleted of mtDNA (143B ρ^0) (Figure S1) and these cells showed a similar decrease in proliferation after depleting PrimPol (Figure 1a). As the mitochondria in these cells contain no DNA, and thus do not require proteins involved in its maintenance, this provided evidence for a possible role for PrimPol independent of mtDNA. Immunofluorescent (IF) detection of endogenous PrimPol in 143B cells showed it was predominantly located in the cytoplasm/mitochondria (Figure 1b) however, a small proportion of PrimPol was also detected in nuclei (Figure 1b). This nuclear staining pattern was specific to the PrimPol protein as RNAi-mediated depletion significantly reduced IF detection (Figure 1b). Furthermore, the localisation of PrimPol to nuclei was much more apparent when the protein was stably over-expressed in human cells (Figure 1c). The confirmation of an mtDNA-independent function for PrimPol, taken together with the nuclear localisation, provided compelling evidence for a possible role for PrimPol in nuclear DNA metabolism.

To investigate this further, we analysed PrimPol's association with chromatin during nuclear DNA replication. Human MRC5 fibroblasts were separated into detergent soluble and insoluble fractions, the latter enriching for chromatin and proteins associated with chromatin. Following a prolonged aphidicolin treatment, which stalls cells in early S-phase, a marked increase in insoluble PrimPol was observed (Figure 1d). In contrast, removal of aphidicolin, allowing progression of cells into S-phase, resulted in a decrease of insoluble PrimPol close to the level observed in asynchronous cells (Figure 1d). These data imply that chromatin association of PrimPol occurs during replication stress, but in an unperturbed S-phase it may be below the detection threshold. To examine this S-phase phenomena in more detail, we examined PrimPol's localization on chromatin during a synchronous round of DNA replication in *Xenopus* cell-free egg extracts. We observed that PrimPol became bound to chromatin during an unperturbed S-phase, but that this binding was abolished when replication was inhibited prior to initiation by geminin or the CDK inhibitor, roscovitine (Figure 1e). Blocking DNA replication during the elongation stage with aphidicolin, resulted in increased PrimPol chromatin binding (Figure 1e). This chromatin binding was completely dependent on DNA replication as it could be abrogated by prior treatment with geminin (Figure 1e). Together, these data indicate that

PrimPol is loaded onto chromatin in an S-phase-dependent manner and that this replication-dependent chromatin association is even more readily apparent when replication forks are stalled with aphidicolin.

PrimPol deficient avian cells are sensitive to DNA damaging agents

To investigate the cellular roles of PrimPol, we disrupted the *PrimPol* gene in avian DT40 cells (*G. gallus)* as these have been widely used to study other novel polymerases[16] and we obtained two *PrimPol* $^{-/-}$ knock-out clones (Figure S2). *PrimPol* $^{-/-}$ cells showed minor cell-cycle defects, having a slightly longer doubling time and a higher proportion of cells in G2 phase (Figure S3). To determine if PrimPol had any roles related to DNA repair or lesion bypass, we treated *PrimPol* $^{-/-}$ cells with a range of DNA damaging agents. *PrimPol* $^{-/-}$ cells were sensitive to low-doses of UV-C radiation, comparable to Pol η deficient cells (Figure 2a, left panel). A more pronounced sensitivity was observed following treatment with the UV mimetic 4-nitroquinoline 1-oxide (4NQO) with cell viability decreasing ~30-fold after chronic exposure to a low concentration (Figure 2a, centre panel). However, *PrimPol* $^{-/-}$ cells were not sensitive to all DNA damaging agents. For example, no sensitivity was observed following treatment with ionizing radiation (IR) (Figure 2a, right panel). Both UV-C and 4NQO sensitivities could be partially rescued by expression of human PrimPol (Figure 2a), confirming that the observed cell viability defects were due to the absence of PrimPol protein in these cells.

Localisation of PrimPol onto chromatin following UV damage

We next investigated PrimPol's cellular localization following UV irradiation. HEK-293 cells stably expressing PrimPol were exposed to UV-C radiation and, prior to IF staining, were pre-extracted with a detergent buffer, leaving only those proteins bound to cellular structures (e.g. chromatin). In mock-irradiated cells, this treatment resulted in almost no detectable PrimPol (Figure 2b). However, following UV-C irradiation PrimPol was visible as focal accumulations in nuclei (Figure 2b and c), numbering approximately between 50 and several hundred per cell, and these foci were dependent upon the UV-C dose administered (Figure 2d). PrimPol did not assemble into foci following treatment with all DNA damaging agents, as no foci were observed following exposure to ionizing radiation (Figure 2a) which induces DNA breaks. The accumulation of sub-nuclear detergent-resistant foci suggests that PrimPol is tightly associated with chromatin. To confirm this, cells stably expressing PrimPol were separated into detergent-soluble and insoluble (chromatin enriched) fractions following UV-C irradiation. A substantial increase in insoluble PrimPol was observed following UV-C irradiation (Figure 2e), which was almost completely solubilized by DNase treatment (Figure 2e), confirming that insoluble PrimPol was chromatin bound. Endogenous PrimPol in human fibroblasts also becomes insoluble following UV-C irradiation (Figure 2f). Together, these data demonstrate PrimPol becomes tightly associated with chromatin following UV damage.

PrimPol catalyzes TLS bypass of UV photoproducts

UV-dependent chromatin association has been reported for TLS polymerases [17-20]. Therefore, given the UV-dependent chromatin association of PrimPol, together with the damage sensitivity of *PrimPol*$^{-/-}$ cells, we next queried if PrimPol functions in UV TLS bypass. To address this, we assayed PrimPol's capacity to perform TLS bypass of UV T-T photoproducts (CPD and 6-4). Human PrimPol was capable of DNA-dependent DNA synthesis (Figure 4a) and this was intrinsic to PrimPol as mutation of active site residues (DxE) abolished catalytic activity (Figure S4). PrimPol was incapable of reading-through a templated cis-syn thymine-thymine (T-T) CPD, stalling prior to the lesion (Figure 3a). As PrimPol could not insert nucleotides opposite a T-T CPD, we asked whether PrimPol could extend from nucleotides already present opposite the lesion. It has been demonstrated *in vitro* that replicative polymerases, particularly when aided by PCNA, are capable of inserting two deoxyadenosines (AA) opposite a T-T CPD before stalling[21-23] and we therefore tested PrimPol's ability to extend a primer in this context. We observed PrimPol-dependant extension from a primer containing a 3' terminal AA annealed with the T-T CPD, with an efficiency comparable to that of the undamaged template (Figure 3b). We confirmed this primer terminus annealed to a CPD is a block for replicative polymerases (Figure S4), demonstrating PrimPol is capable of TLS, functioning as an extender in CPD bypass. Next, we examined PrimPol's ability to bypass the major helix-distorting 6-4 lesion that blocks replication as evident by the inability of replicative polymerases (Figure S4) to extend past this damage. Strikingly, we observed that PrimPol could efficiently read through a templated T-T 6-4 photoproduct (Figure 3c). Single incorporation experiments revealed that PrimPol bypass of a T-T 6-4 photoproduct was error-prone, incorporating T opposite the 3'-terminal T and C or G opposite the 5'-terminal T of the DNA lesion (Figure 3d). Since it was previously reported that T:T mismatched primers are a strong blockage for replicative DNA polymerases[24], we tested if PrimPol can extend a primer with a 3' terminal T:T mismatch annealed to a non-damaged template. We observed that PrimPol was unable to extend the primer with a T:T mismatch (Figure 3e). In contrast, when this TT primer was annealed with a template containing a 6-4 photoproduct, we observed efficient extension of the mismatched primer implicating a distinctive mechanism and a high level of specialization of PrimPol for bypass 6-4 photoproducts. Together, these data establish that PrimPol can function in TLS of UV photoproducts, playing a role in extension from CPDs and bypassing 6-4 photoproducts. To our knowledge, this is the first demonstration of a human DNA polymerase that can efficiently bypass the highly distorting 6-4 photoproduct without the assistance of other polymerases.

PrimPol facilitates the replication of UV-damaged DNA *in vivo*

In cells, TLS occurs either at replication forks or in a post-replication manner[3] and therefore the absence of a particular TLS polymerase will lead to a defect in one or both of these processes[25-28]. To determine the cellular timing of PrimPol-mediated TLS, we first assessed the ability of *PrimPol* $^{-/-}$ cells to perform TLS post-replicatively using a velocity sedimentation assay (Figure 4a). When replication forks stall at UV lesions, re-priming and DNA synthesis can occur down-stream of the lesion leaving a single stranded gap that is later filled by a TLS polymerase in a process called post-replication repair[1,3,4,6]. A post-replication repair defect was observed in Pol η $^{-/-}$ cells (Figure 4b, red arrow) consistent with previous reports[25,26] however, no defect was observed in *PrimPol* $^{-/-}$ cells (Figure 4b). These data establish that PrimPol is not required for TLS at post-replication gaps and also suggests that PrimPol may not initiate DNA synthesis downstream of the lesion, which was a possibility given the *in vitro* DNA/RNA priming activities associated with this enzyme[10].

We next looked for evidence that PrimPol-dependent TLS occurs at the replication forks, using the DNA fiber technique[29]. This assay allows analysis of the progression of individual replication forks by *in vivo* labeling of newly replicated DNA. We applied this technique to DT40 *PrimPol* $^{-/-}$ cells that had been UV irradiated between CldU and IdU labeling periods, and calculated the ratios between the two labels (Figure 4c). In mock irradiated cells, this ratio was close to 1 (data not shown) and, following UV irradiation, this ratio increased significantly due to the shortening of the second track indicating an impediment in replication fork progression. Compared to wild-type cells, PrimPol $^{-/-}$ cells showed a substantial increase in the spread and mean of CldU:IdU ratios (Figure 4d and e), indicating a marked increase in delay or blockage of replication fork progression after UV-C irradiation. In line with this, a 15-20% reduction of thymidine incorporation was observed in PrimPol $^{-/-}$ cells compared to wild-type cells, following varying UV-C doses (Figure 4f), indicating decreased DNA synthesis. Together, these results demonstrate that PrimPol is required for replication of UV damaged DNA *in vivo* and this is consistent with PrimPol's demonstrated ability to perform TLS bypass of UV photoproducts.

PrimPol operates in a UV lesion TLS pathway that is independent of Polη

The capacity of PrimPol to bypass the particularly toxic and helix-distorting 6-4 UV photoproducts, and extend from a CPD *in vitro*, suggested that it may operate in a novel TLS pathway that is complementary to the established Pol η-dependent lesion bypass pathway. To test this hypothesis, we exploited human XP-V (XP30RO) fibroblast cells that lack a functional Pol η and queried if these cells have an increased reliance upon PrimPol to protect them from the lethal effects of UV irradiation. XP-V cells were only mildly sensitive to UV-C irradiation[30] (Figure 5a) and PrimPol depleted (RNAi) fibroblasts (MRC5) also did not exhibit major UV-C sensitivity (Figure 5a). However, PrimPol

depletion in XP-V cells rendered them synergistically sensitive to UV-C irradiation, decreasing the surviving fraction by up to 4-fold. This establishes that PrimPol operates in a lesion tolerance pathway that is non-epistatic with Pol η pathway and that this PrimPol-dependent TLS pathway protects XP-V cells from UV cytotoxicity, as would be expected based on the complementary UV lesion bypass activities (CPD versus 6-4) associated with these two distinct TLS polymerases.

Although major UV-C sensitivity was not observed in PrimPol depleted human cells, we predicted that these cells should display molecular signatures of impaired TLS. For example, failure of the replisome to bypass a UV lesion would result in uncoupling of leading and lagging strand synthesis producing long tracts of RPA coated single stranded DNA, which in turn activates the intra-S checkpoint[31]. Notably, in UV-C irradiated PrimPol depleted cells, we observed a significant increase in the proportion of cells with RPA foci and phosphorylated Chk1 (Ser345), compared to mock RNAi treated cells (Figure 5b and c). Both of these markers confirm that an activated damage response has occurred and that PrimPol is required for the appropriate cellular response to UV damage. As TLS of UV lesions is already substantially impaired in XP-V cells, following UV-C irradiation no further increase in RPA foci or in the initial level of phosphorylated Chk1 was observed in PrimPol depleted XP-V cells (Figure 5b and c). However, elevated levels of Chk1 phosphorylation were persistent in these cells 24 hours after UV-C irradiation with a dose of 2 J/m^2 (Figure 5c), suggesting sustained replication problems occur in the absence of both Pol η and PrimPol. Together, these data demonstrate the requirement for PrimPol in the normal cellular response to UV-C radiation in human cells and establishes that this polymerase functions in a novel TLS pathway that operates independently of, and complementary to, Pol η in the cellular response of mammalian cells to UV damage (Figure 6).

Concluding remarks

In mammalian cells, seven TLS polymerases have so far been described, which mediate cellular tolerance to DNA lesions that would otherwise act as major barriers to DNA replication in the nucleus. Here, we present evidence for a new player, the novel primase-polymerase PrimPol. Previously, we reported that this enzyme functions in mtDNA maintenance[10]. However, we now demonstrate that PrimPol is also a nuclear enzyme that performs TLS bypass of UV photoproducts and is required for maintaining timely replisome progression on UV-damaged DNA templates.

In archaea and eukaryotes, AEP primases are essential enzymes that synthesize RNA primers at the initiation of DNA replication[12]. It has therefore been widely assumed that AEPs are DNA-dependent RNA polymerases specializing in primer synthesis. However, this assignment was first called into question with the discovery that AEPs also exist in bacteria[32,33], which deploy a distinct DnaG primase for replication. Notably, prokaryotic and archaeal AEPs can also synthesise DNA[13-15] an bacterial AEP orthologues are required for DNA break repair in prokaryotes[13,34]. Thus, most AEPs should be reclassified as members of the DNA polymerase superfamily[35] and this reassignment would suggest that they are likely to play other pivotal roles in DNA maintenance. This study extends this paradigm into eukaryotes with the demonstration that AEPs can perform TLS across DNA lesions, with PrimPol providing the first example of a human DNA polymerase that can efficiently bypass UV 6-4 photoproducts. This striking lesion bypass activity is most likely attributable to the relatively open and malleable active site characteristic of AEPs that, like Y family polymerases, can accommodate major helix distorting DNA lesions that replicative polymerases cannot. This inherent adaptability of the catalytic centre of AEPs, including PrimPol, to accept a diverse range of DNA substrates (e.g. DNA breaks and lesions) has made these polymerases ideal for roles in DNA repair and lesion tolerance.

Our current understanding of the bypass of UV photoproducts by TLS pathways in mammalian cells, centered around the Y family polymerases and Pol ζ, needs to be revised to now include PrimPol (Figure 6). It has been established that the more abundant, but less toxic, CPD photoproducts are efficiently bypassed by Pol η in an error-free manner, whilst in XP-V cells it has been proposed that Pol ι and κ possibly function as inserters and Pol ζ as an extender, in an error-prone back-up mechanism[36]. Our *in vitro* data suggest that PrimPol can function in an error-free alternate pathway, relying on other polymerases to perform the initial TLS opposite the lesion, allowing PrimPol to carry out the subsequent extension step. In addition to Pol η error-free incorporating two A's opposite a T-T CPD, it has been demonstrated *in vitro* that replicative polymerases are also capable of catalyzing this before stalling[21-23]. Although

CPD photoproducts are efficiently bypassed by Pol η, it is less well established how the much more distorting and toxic 6-4 lesions are bypassed in cells. A two polymerase model involved Pol η or ι inserting nucleotides opposite the lesion and Pol ζ extending, which is thought to occur in both an error-prone and error-free manner has been proposed[9,37]. We have shown that PrimPol is capable of complete bypass of a 6-4 photoproduct in an error-prone manner *in vitro*, suggesting PrimPol could offer an alternative to the two-step pathway but possibly could also function in either an insertion or extension step with other polymerases. TLS of T-T 6-4 photoproducts *in vivo* has been reported to be largely error-free, however the most frequent mis-insertion was shown to be incorporation of a T opposite the 3' T of the lesion[37-39], which is consistent with PrimPol-dependent TLS *in vitro*.

The contribution of PrimPol to UV photoproduct bypass *in vivo* has yet to be fully determined. However, our current analysis of PrimPol deficient cells places it at the replication fork, maintaining fork progression on UV damaged DNA, presumably through its TLS activity but it appears to dispensable for post-replication repair. A similar phenotype has been observed for vertebrate REV1[26], which has been proposed to act as a platform for TLS recruitment[40]. It will therefore be interesting to determine if REV1 contributes to PrimPol-dependent TLS pathway *in vivo*. Consistent with a role for PrimPol in TLS, PrimPol depleted human fibroblasts have increased RPA foci and phosphorylated Chk1 following UV irradiation, compared to mock RNAi cells. Despite these results, depletion or complete absence of PrimPol did not greatly sensitize cells to UV cytotoxicity. This is not surprising given that mammalian cells deploy an extremely proficient nucleotide excision repair (NER), which can rapidly remove 6-4 photoproducts and related lesions, as well as utilizing its collection of alterative TLS polymerases to tolerate various DNA lesions. In human cells, UV sensitivity was observed only in the absence of functional Pol η, in XP-V cells. This establishes that PrimPol operates in an alternate DNA damage tolerance pathway to Pol η and therefore deficiency of one polymerase can be compensated by the presence of the other, at least in regard to UV cytotoxicity. As XP-V patients have a higher rate of UV induced mutations that contribute to skin carcinogenesis, an important question is whether PrimPol protects, via its error-free bypass (CPD), or promotes, via its error-prone bypass (6-4 photoproduct), skin carcinogenesis in these patients. We are currently investigating if mutations affecting *PrimPol* gene are associated with human diseases (e.g. cancer predisposition) as reported for other TLS polymerases[2]. As PrimPol also operates in the mitochondria of mammalian cells (TLS has not been identified previously in this organelle) it is likely to provide an important damage tolerance pathway to allow bypass of lesions, including photoproducts, that would otherwise block mtDNA replication[23].

Although this current study focuses on PrimPol's function in TLS bypass of UV-induced DNA damage, it is likely that PrimPol is also required for tolerating other replication blocking lesions in the nucleus and mitochondria. Proliferative defects in the absence of PrimPol, together with PrimPol's presence on chromatin[41] (Figure 1), point to roles in unperturbed S-phase, which is not unprecedented for TLS polymerases[42]. In addition, increased chromatin association of PrimPol was observed following aphidicolin treatment in both Xenopus and human cells, suggesting PrimPol responds to replication fork stalling in the absence of DNA lesions. These intriguing features of PrimPol are currently the subjects of further investigations.

METHODS SUMMARY

Cell culture. Human 143B and HEK-293 Flp-In™ T-REx™ cells were cultured in DMEM supplemented with 10 % fetal calf serum (FCS), ρ^0 (mtDNA null) cells were supplemented with 50 μg/ml uridine (Sigma), and SV40-transformed MRC5 and XP30RO cells were cultured in MEM supplemented with 15 % FCS. All cells were grown in 1 % L-glutamine and 1 % PenStrep.

RNAi depletion. Transfection of 10 nM PrimPol siRNA was performed using Lipofectamine 2000 (with 143B cells) or Lipofectamine RNAiMAX (Invitrogen) according to manufacturer recommendations. Incucyte phase contrast live cell microscope (Essen Biosciences) was used to generate growth curves.

Immunofluorescent analysis. In house PrimPol antibody was diluted 1:200 as well as anti-RPA2 (Cell Signalling), and Mitotracker Deep Red used at 250 nM (Invitrogen). If necessary prior to fixation cells were pre-extracted with a wash of 0.5 % Triton X-100 in PBS.

Cellular fractionation. Cellular fractionation protocol was adapted as described[43,44], more details are provided in supplementary methods.

***Xenopus* egg extract.** Demembranated sperm nuclei and interphase Xenopus egg extracts were prepared as described[45,46], more details are available in supplementary methods.

DT40 cell viability. Avian PrimPol gene was disrupted with histidinol and puromycin targeted cassettes following procedure previously described[47]. Human PrimPol cDNA was sub-cloned into TET inducible vector (adapted from Clontech) containing luciferase gene reporter for clone selection. Cell viability assay was performed using CellTiter-Blue (Promega) following manufacturer's instructions.

Fluorescent primer extension. All the primer extension assays were performed at 37ºC as described previously[48] and primers sequences are in supplementary methods.

DNA fiber spreading and post replication repair. Both techniques were performed as previously described[26]. Post Replication Repair protocol was adapted to measure total DNA replication rate following UV-C, by pre-labeling cells with ^{14}C thymidine over two doubling time to normalize the amount of total DNA.

Clonogenic survivals. MRC5 and XP30RO cells were either mock or PrimPol siRNAi (10 nM) transfected Lipofectamine RNAiMAX, both at seeding and 24 hours after. At 72 hours dilutions of the transfected cells were plated in triplicate on 10 cm dishes. The next day the media was removed and cells were washed with PBS and then UV-C irradiated. After irradiation media was replaced and colonies allowed to grow over 10 days, before fixing with 100% ethanol and staining with methylene blue to allow counting.

REFERENCES

1. Sale, J. E., Lehmann, A. R., & Woodgate, R. Y-family DNA polymerases and their role in tolerance of cellular DNA damage. *Nature Reviews Molecular Cell Biology*, **13**, 141–152 (2012).
2. Loeb, L. A., & Monnat, R. J. DNA polymerases and human disease. *Nature Reviews Genetics*, **9**, 594–604, (2008).
3. Sale, J. E. Competition, collaboration and coordination - determining how cells bypass DNA damage. *Journal of Cell Science*, **125**, 1633–1643, (2012).
4. Chang, D. J., & Cimprich, K. A. DNA damage tolerance: when it's OK to make mistakes. *Nature Chemical Biology*, **5**, 82–90, (2009).
5. Rastogi, R. P., Richa, Kumar, A., Tyagi, M. B., & Sinha, R. P. Molecular Mechanisms of Ultraviolet Radiation-Induced DNA Damage and Repair. *Journal of Nucleic Acids*, **2010,** 1–32, (2010).
6. Rupp, W. D., & Howard-Flanders, P. Discontinuities in the DNA synthesized in an excision-defective strain of Escherichia coli following ultraviolet irradiation. *Journal of Molecular Biology*, **31**, 291–304, (1968)
7. Masutani, C., Kusumoto, R., Yamada, A., Dohmae, N., Yokoi, M., Yuasa, M., Araki, M., Iawi, S., Takio, K. and Hanaoka, F. The XPV (xeroderma pigmentosum variant) gene encodes human DNA polymerase eta. *Nature*, **399**, 700–704, (1999).
8. Johnson, R. E., Kondratick, C. M., Prakash, S., & Prakash, L. hRAD30 mutations in the variant form of xeroderma pigmentosum. *Science*, **285**, 263–265, (1999).
9. Johnson, R. E., Washington, M. T., Haracska, L., Prakash, S., & Prakash, L. Eukaryotic polymerases iota and zeta act sequentially to bypass DNA lesions. *Nature*, **406**, 1015–1019, (2000).
10. Garcia-Gómez, S., Reyes, A., Bianchi, J., Martinez, M., Rudd, S. G., Choncrón, S., Méndez, J., Holt, I. J., Doherty, A. J. & Blanco, L. PrimPol, an Archaic Primase/Polymerase Operating in Human Mitochondria. Submitted.
11. Iyer, L. M., Koonin, E. V., Leipe, D. D., & Aravind, L. Origin and evolution of the archaeo-eukaryotic primase superfamily and related palm-domain proteins: structural insights and new members. *Nucleic Acids Research*, **33**, 3875–3896, (2005).
12. Frick, D. N., & Richardson, C. C. DNA primases. *Annual Review of Biochemistry*, **70**, 39–80, (2001).
13. Della, M., Palmbos, P.L., Tseng, H.M., Tonkin, L.M., Daley, J.M., Topper, L.M., Pitcher, R.S., Tomkinson, A.E., Wilson, T.E. & Doherty, A. J. Mycobacterial Ku

and ligase proteins constitute a two-component NHEJ repair machine. *Science,* **306**, 683-685 (2004).

14. Bocquier, A. A., Liu, L., Cann, I. K., Komori, K., Kohda, D., & Ishino, Y. Archaeal primase: bridging the gap between RNA and DNA polymerases. *Current biology,* **11**, 452–456, (2001).
15. Lipps, G., Röther, S., Hart, C., & Krauss, G. A novel type of replicative enzyme harbouring ATPase, primase and DNA polymerase activity. *The EMBO journal*, **22**, 2516–2525, (2003).
16. Hirota, K., Sonoda, E., Kawamoto, T., Motegi, A., Masutani, C., Hanaoka, F., Szüts, D., Iwai, S., Sale, J. E., Lehmann, A. R., Takeda, S. Simultaneous Disruption of Two DNA Polymerases, Polη and Polζ, in Avian DT40 Cells Unmasks the Role of Polη in Cellular Response to Various DNA Lesions. *PLoS Genetics*, **6**, e1001151, (2001).
17. Kannouche, P., Broughton, B. C., Volker, M., Hanaoka, F., Mullenders, L. H. F., Lehmann, A. R. Domain structure, localization, and function of DNA polymerase eta, defective in xeroderma pigmentosum variant cells. *Genes & Development*, **15**, 158–172, (2001).
18. Kannouche, P., Fernández de Henestrosa, A. R., Coull, B., Vidal, A. E., Gray, C., Zicha, D., Woodgate, R., Lehmann, A. R. Localization of DNA polymerases eta and iota to the replication machinery is tightly co-ordinated in human cells. *The EMBO journal*, **22**, 1223–1233, (2003).
19. Tissier, A., Kannouche, P., Reck, M, P., Lehmann, A. R., Fuchs, R. P. P., & Cordonnier, A. Co-localization in replication foci and interaction of human Y-family members, DNA polymerase pol eta and REVI protein. *DNA repair*, **3**, 1503–1514, (2004).
20. Ogi, T., Kannouche, P., & Lehmann, A. R. Localisation of human Y-family DNA polymerase kappa: relationship to PCNA foci. *Journal of Cell Science*, **118**, 129–136, (2005).
21. O' Day, C. L., Burgers, P. M., & Taylor, J. S. PCNA-induced DNA synthesis past cis-syn and trans-syn-I thymine dimers by calf thymus DNA polymerase delta in vitro. *Nucleic acids research*, **20**, 5403–5406, (1992).
22. Narita, T., Tsurimoto, T., Yamamoto, J., Nishihara, K., Ogawa, K., Ohashi, E., Evans, T., Iwai, S., Takeda, S., Hirota, K. Human replicative DNA polymerase δ can bypass T-T (6-4) ultraviolet photoproducts on template strands. *Genes to Cells*, **15**, 1228–1239, (2010).
23. Kasiviswanathan, R., Gustafson, M. A., Copeland, W. C., & Meyer, J. N. (2011). Human mitochondrial DNA polymerase exhibits potential for bypass and mutagenesis at UV-induced cyclobutane thymine dimers. *The Journal of biological chemistry*, **287**, 9222-9229, (2011).

24. Johnson, S. J. & Beese, L. S. Structures of mismatch replication errors observed in a DNA polymerase. *Cell*, **116**, 803-16, (2004).
25. Lehmann, A. R., Kirk-Bell, S., Arlett, C. F., Paterson, M. C., Lohman, P. H., de Weerd-Kastelein, E. A., Bootsma, D. Xeroderma pigmentosum cells with normal levels of excision repair have a defect in DNA synthesis after UV-irradiation. *Proceedings of the National Academy of Sciences,* **72**, 219-23, (1975).
26. Edmunds, C. E., Simpson, L. J., Sale, J. E. PCNA ubiquitination and REV1 define temporally distinct mechanisms for controlling translesion synthesis in the avian cell line DT40. *Molecular Cell,* **30**, 519-529, (2008).
27. Jansen, J. G., Tsaalbi-Shtylik, A., Hendriks, G., Gali, H., Hendel, A., Johansson, F., Erixon, K., Livneh, Z., Mullenders, L. H. F., Haracska, L., de Wind, N. Separate Domains of Rev1 Mediate Two Modes of DNA Damage Bypass in Mammalian Cells. *Molecular and Cellular Biology*, **29**, 3113–3123, (2009).
28. Jansen, J. G., Tsaalbi-Shtylik, A., Hendriks, G., Verspuy, J., Gali, H., Haracska, L., & de Wind, N. Mammalian polymerase ζ is essential for post-replication repair of UV-induced DNA lesions. *DNA repair*, ***8***, 1444–1451, (2009).
29. Jackson, D. A., Pombo, A. Replicon clusters are stable units of chromosome structure: evidence that nuclear organization contributes to the efficient activation and propagation of S phase in human cells. *Journal of Cell Biology*, **140**, 1285-1295, (1998).
30. Arlett, C. F., Harcourt, S. A., Broughton, B. C. The influence of caffeine on cell survival in excision-proficient and excision-deficient xeroderma pigmentosum and normal human cell strains following ultraviolet-light irradiation. *Mutation Research,* **33**, 341-346, (1975).
31. Jones, R. M., & Petermann, E. (2012). Replication fork dynamics and the DNA damage response. *Biochemical Journal*, **443**, 13–26, (2012).
32. Weller, G.R. & Doherty, A.J. A family of DNA repair ligases in bacteria? *FEBS Letters*, **505***,* 340-342, (2001).
33. Aravind, L. & Koonin, E. V. Prokaryotic homologs of the eukaryotic DNA-end-binding protein Ku, novel domains in the Ku protein and prediction of a prokaryotic double-strand break repair system. *Genome Research,* **11**, 1365-1374, (2001).
34. Brissett, N. C., Pitcher, R. S., Juarez, R., Picher, A. J., Green, A. J., Dafforn, T. R., Fox, G. C., Blanco, L. and Doherty, A. J. Structure of a NHEJ polymerase-mediated DNA synaptic complex. *Science,* **318**, 456-459, (2007).
35. Brissett N. C. & Doherty A. J. Repairing DNA double-strand breaks by the prokaryotic non-homologous end-joining pathway. *Biochemical Society Transaction*, **37**, 539-545, (2009).
36. Ziv, O., Geacintov, N., Nakajima, S., Yasui, A., & Livneh, Z. DNA polymerase zeta cooperates with polymerases kappa and iota in translesion DNA synthesis

across pyrimidine photodimers in cells from XPV patients. *Proceedings of the National Academy of Sciences*, **106**, 11552–11557, (2009).

37. Yoon, J. H., Prakash, L., & Prakash, S. Error-free replicative bypass of (6-4) photoproducts by DNA polymerase in mouse and human cells. *Genes & Development*, **24**, 123–128, (2010).
38. Szuts, D., Marcus, A. P., Himoto, M., Iwai, S., & Sale, J. E. REV1 restrains DNA polymerase to ensure frame fidelity during translesion synthesis of UV photoproducts in vivo. *Nucleic acids research*, **36**, 6767–6780, (2008).
39. Hendel, A., Ziv, O., Gueranger, Q., Geacintov, N., & Livneh, Z. Reduced efficiency and increased mutagenicity of translesion DNA synthesis across a TT cyclobutane pyrimidine dimer, but not a TT 6-4 photoproduct, in human cells lacking DNA polymerase η. *DNA repair*, **7**, 1636–1646, (2008).
40. Guo, C., Fischhaber, P. L., Luk-Paszyc, M. J., Masuda, Y., Zhou, J., Kamiya, K., Kisker, C. & Friedberg, E. C. Mouse Rev1 protein interacts with multiple DNA polymerases involved in translesion DNA synthesis. *The EMBO journal*, **22**, 6621–6630, (2003).
41. Nikolov, M., Stützer, A., Mosch, K., Krasauskas, A., Soeroes, S., Stark, H., Urlaub, H., & Fischle, W. Chromatin affinity purification and quantitative mass spectrometry defining the interactome of histone modification patterns. *Molecular & cellular proteomics,* **10**, M110.005371, (2011).
42. Rey, L., Sidorova, J. M., Puget, N., Boudsocq, F., Biard, D. S. F., Monnat, R. J., Cazaux, C., Hoffmann, J. S. Human DNA Polymerase Is Required for Common Fragile Site Stability during Unperturbed DNA Replication. *Molecular and Cellular Biology*, **29**, 3344–3354, (2009).
43. Kannouche, P. L., Wing, J. & Lehmann, A. R. Interaction of human DNA polymerase eta with monoubiquitinated PCNA: a possible mechanism for the polymerase switch in response to DNA damage. *Molecular cell*, **14**, 491–500, (2004).
44. Zlatanou, A., Despras, E., Braz-Petta, T., Boubakour-Azzouz, I., Pouvelle, C., Stewart, G. S., Nakajima, S., Yasui, A., Ishchenko, A. A., Kannouche, P. L. The hMsh2-hMsh6 Complex Acts in Concert with Monoubiquitinated PCNA and Pol eta in Response to Oxidative DNA Damage in Human Cells. *Molecular cell*, **43**, 649–662, (2011).
45. Murray, M. T., Krohne, G. & Franke, W. W. Different forms of soluble cytoplasmic mRNA binding proteins and particles in Xenopus laevis oocytes and embryos. *Journal of Cell Biology*, **112**, 1-11, (1991).
46. Kubota, Y. & Takisawa, H. Determination of initiation of DNA replication before and after nuclear formation in Xenopus egg cell free extracts. *Journal of Cellular Biology*. **123**, 1321-1331, (1993).

47. Sonoda, E., Sasaki, M. S., Buerstedde, J. M., Bezzubova, O., Shinohara, A., Ogawa, H., Takata, M., Yamaguchi-Iwai, Y., and Takeda, S. Rad51-deficient vertebrate cells accumulate chromosomal breaks prior to cell death. *The EMBO Journal,* **17**, 598-608, (1998).
48. Jozwiakowski, S. K. & Connolly, B. A. A modified family-B archaeal DNA polymerase with reverse transcriptase activity. *Chembiochem*, **12**, 35-7, (2011).

Figure Legends

Figure 1. PrimPol localises to nuclei and associates with chromatin in a replication-dependant manner.

a, Proliferative defect following PrimPol RNAi is independent of PrimPol's mitochondrial role. Wild type 143B cells (ρ^+) and those lacking mtDNA (ρ^0) were treated with PrimPol RNAi and cell density monitored using an Incucyte phase contrast microscope at 3 hourly intervals over 80 hours. Data are representative of 3 independent experiments, and error bars denote standard deviation of triplicate wells in which 9 regions were analysed per sample. **b,** Immunofluorescent detection of PrimPol in the nucleus. 143B cells were either mock or PrimPol RNAi treated and 48 hours after, subjected to immunofluorescent analysis with an anti-PrimPol antibody (green). Cells were counterstained with Mitotracker Deep Red to visualize mitochondria (red) and DAPI to visualize nuclei (blue). **c,** Immunofluorescent detection of over-expressed PrimPol in nuclei. HEK-293 cells induced for PrimPol-HA stable over-expression for 18 hours, were subjected to immunofluorescent analysis with an anti-HA antibody (green), counterstaining with Mitotracker Deep Red (red) and DAPI (blue). **d,** PrimPol becomes insoluble following prolonged aphidicolin treatment, suggesting chromatin binding. MRC5 fibroblasts were either mock (-) or aphidicolin treated (2 μg/ml, ~16 hours) and allowed to recover for the time indicated before being separated into Triton X-100 soluble and insoluble fractions and subjected to Western blot analysis with antibodies indicated. Histone H1 was used to detect chromatin, PCNA and slower migrating mono-ubiquitylated (Ub)-PCNA indicates stalled replication forks. **e,** PrimPol associates with chromatin in a replication-dependant manner. Left panel, human recombinant His tagged PrimPol (hPrimPol at 12 ng/μl) was added to *Xenopus* egg extract supplemented with sperm nuclei. Extracts were treated with geminin 80nM, roscovitine 0.5mM or aphidicolin 100μg/ml and incubated at 21°C. At the indicated times (minutes), chromatin was isolated and associated proteins subjected to Western blot analysis with the antibodies indicated. Right panel, the same experiment was repeated at a 60 minute time point and last lane corresponds to a sample pre-incubated with geminin followed by aphidicolin treatment.

Figure 2. *PrimPol*$^{-/-}$ DT40 cells are sensitive to UV-C and 4NQO, and human PrimPol tightly associates with chromatin following UV damage.

a, *PrimPol*$^{-/-}$ DT40 cells are sensitive to UV-C and "UV-mimetic" 4NQO, but not IR**.** Cell viability was assessed at 48 hours after UV-C or X-ray irradiation by measuring metabolic capacity of cells. Cell viability was measured at 96 hours in 4NQO treated cells, 48 hours after removal of chronic treatment with this drug. Error bars denote standard deviation of three independent experiments. **b,** Human PrimPol assembles into triton-resistant sub-nuclear foci following UV-C irradiation. **b, c, d, e,** using HEK-293

cells stably over-expressing PrimPol-FlagStrep for 18 hours. **b,** Cells were either mock, UV-C (30 J/m^2), or X-Ray (5 Gy) irradiated, allowed to recover for 1 hour (UV) or 30 minutes (IR), and then pre-extracted with a Triton X-100 containing buffer and paraformaldehyde (PFA) fixed. Cells were subjected to immunofluorescent analysis with anti-PrimPol antibody (green) and counterstained with DAPI (blue). **c,** Panel of PrimPol focal nuclei. Cells were UV-C irradiated (10 or 30 J/m^2), allowed to recover for 8 hours, and pre-extracted prior to immunofluorescent staining with anti-PrimPol antibody (green), and counterstaining with DAPI (blue). **d,** The proportion of cells with PrimPol foci is UV-C dose dependant. Cells were UV-C irradiated with the doses indicated, and allowed to recover for 8 hours prior to pre-extraction and immuofluorescent analysis with anti-PrimPol and DAPI. The proportion of cells in which PrimPol was localised into foci was determined, at least 200 cells counted for each dose, error bars indicate standard deviation of 3 independent experiments. **e,** PrimPol associates with chromatin following UV-C irradiation. Cells were either mock or UV-C (30 J/m^2) irradiated, and allowed to recover for 8 hours before being lysed in a Triton X-100 containing buffer. The insoluble pellet was resuspended in a DNase (Benzonase) containing buffer and further separated into soluble and insoluble fractions. The resulting samples were subjected to Western blot analysis with anti-PrimPol and anti-PCNA antibodies. **f,** Endogenous PrimPol becomes insoluble following UV-C irradiation. Human MRC5 fibroblasts were either mock (-) or UV-C (30 J/m^2) irradiated, and following recovery for the time indicated, were separated into Triton X-100 soluble and insoluble fractions. Equivalent amounts of whole cell extract (WCE), Triton soluble and insoluble fractions were analysed by Western blot. Histone H1 serves as a chromatin marker, and mono-ubiquitylated (Ub)-PCNA as a marker of stalled replication forks.

Figure 3. PrimPol can catalyze TLS of UV photoproducts *in vitro*

Substrates for primer extension assays are represented schematically in each figure, location of fluorescent label (Hex), DNA lesion (red), and relevant sequence context indicated. Triangles above gel indicate increasing reaction time (5, 10, 15, 30 minutes) and C refers to no enzyme control, 100 nM PrimPol final concentration was used. Templated base annealed to 3-terminus of the primer is denoted “n”. Further details regarding primer extensions in Supplementary Methods. **a,** PrimPol cannot read-though a templated T-T CPD, stalling prior to the lesion. Left panel is undamaged template and right panel is CPD containing template, lesion is at position n+8 and n+9 of template. **b,** PrimPol can extend from two deoxyadenosines (A-A) annealed opposite a T-T CPD. Left panel is undamaged template and right panel is CPD containing template, lesion is at position n-1 and n-2. **c,** PrimPol can read-through a templated T-T 6-4 photoproduct. Left panel is undamaged template and right panel is 6-4 photoproduct (6-4 PP) containing template, DNA lesion is at n+1 and n+2 positions. **d,** PrimPol bypasses 6-4 photoproducts in an error-prone manner. Primer extensions performed with all or single

dNTP(s) as indicated. Left panel is undamaged template, middle panel is 6-4 PP template with incorporation opposite 3' T of the lesion, right panel is opposite 5' T of the lesion. **e,** PrimPol can extend from a T:T mismatch only when annealed opposite a T-T 6-4 photoproduct. Left panel is undamaged template and right panel is 6-4 photoproduct containing template, DNA lesion at position n and n+1.

Figure 4. PrimPol is required for replication fork progression on UV damaged templates in DT40 cells.

a, Cartoon depicting velocity sedimentation analysis of radio-labeled nascent DNA following exposure of 4 J/m^2 UV-C. **b,** Proficient PRR in *PrimPol*$^{-/-}$ cells. Relative amount of radioactivity in each fraction of the gradient was plotted in order to visualize cell capability to fill post replicative gaps left behind replication forks after exposure of 4 J/m^2 UV-C (red line). The red arrow indicates PRR defect observed in Pol η deficient cells (bottom panel) whereas WT and *PrimPol*$^{-/-}$ cells (respectively higher and middle panel) have no defect. **c**, Cartoon depicting DNA fiber labelling process and the order of incorporation of thymidine analogues CldU (before UV-C exposure) and IdU (after 20 J/m^2 irradiation). **d,** PrimPol is required for replication fork progression on UV damaged templates. CldU and IdU tracks were visualised using immunofluorescent staining and measured using OMERO software. CldU:IdU ratios distribution was assessed for WT DT40 cells (upper panel) and both *PrimPol*$^{-/-}$ clones (middle and lower panels). Data are representative of 2 sets of experiments with at least 100 fibers scored each time. **e,** Average of both experiments mentioned in (b) are represented as a cumulative percentage of forks at each ratio after 20 J/m^2 UV-C irradiation. **f,** Decreased DNA synthesis following UV-C irradiation in *PrimPol*$^{-/-}$ cells. Cells were pulsed labeled for 20 minutes with tritium thymidine following UV-C treatments. Incorporation rate was calculated and normalised against undamaged wild-type cells; ^{14}C thymidine overnight pre-labelling was used for total DNA normalisation.

Figure 5. PrimPol operates in a TLS pathway that is independent of Pol η.

a, PrimPol protects XP-V cells from UV-C cytotoxicity. UV clonogenic survival assays were performed with normal MRC5 fibroblasts and XP30RO cells either mock or PrimPol siRNA treated. Error bars denote standard deviation of three experiments. **b,** Normal MRC5 or XP30RO cells were either mock or PrimPol siRNA treated and mock (-) or UV-C irradiated (10 J/m^2), allowed to recover for 6 hours, before immunofluorescent analysis with an anti-RPA2 antibody. The proportion of cells presenting RPA foci was determined; at least 200 cells were counted for each condition, error bars denote standard deviation of three experiments. Significance was assessed with two-tailed T-test (**P =0.01). **c,** Normal MRC5 or XP30RO cells were either mock or PrimPol siRNA treated and mock (-) or UV-C (2 J/m^2) irradiated and allowed to recover for the time

indicated before cell lysates prepared and subjected to Western blot analysis with antibodies indicated.

Figure 6. Model of UV photoproduct TLS in mammalian cells.

a, Bypass of a CPD lesion in mammalian cells. Pol η readily bypasses CPDs in an error-free manner. One or two-step backup mechanisms are present in XP-V cells (polymerases in orange). PrimPol (green) could provide an alternative error-free mechanism. **b,** Bypass of a 6-4 photoproduct in mammalian cells. PrimPol provides an error-prone one-step bypass mechanism for a 6-4 photoproduct, in addition to the known two-step mechanisms. PrimPol could also function in insertion and extension in combination with other polymerases.

Supplementary information. This information is compiled in an accompanying document.

Acknowledgements

We declare that none of the authors have a financial interest related to this work. AJD laboratory was supported by a project grant from BBSRC and a PhD studentship and centre grant from the MRC. HDL laboratory supported by North West Cancer Research Fund grants CR782 and CR869. We thank Nadia Hegerat, Helfrid Hochegger, Alan Lehmann and Simone Sabbioneda for reagents, technical assistance and discussions. We also thank Shunichi Takeda for kindly providing Pol η DT40 cells and Shigenori Iwai who kindly provided DNA containing 6-4 photoproduct.

Figure 1

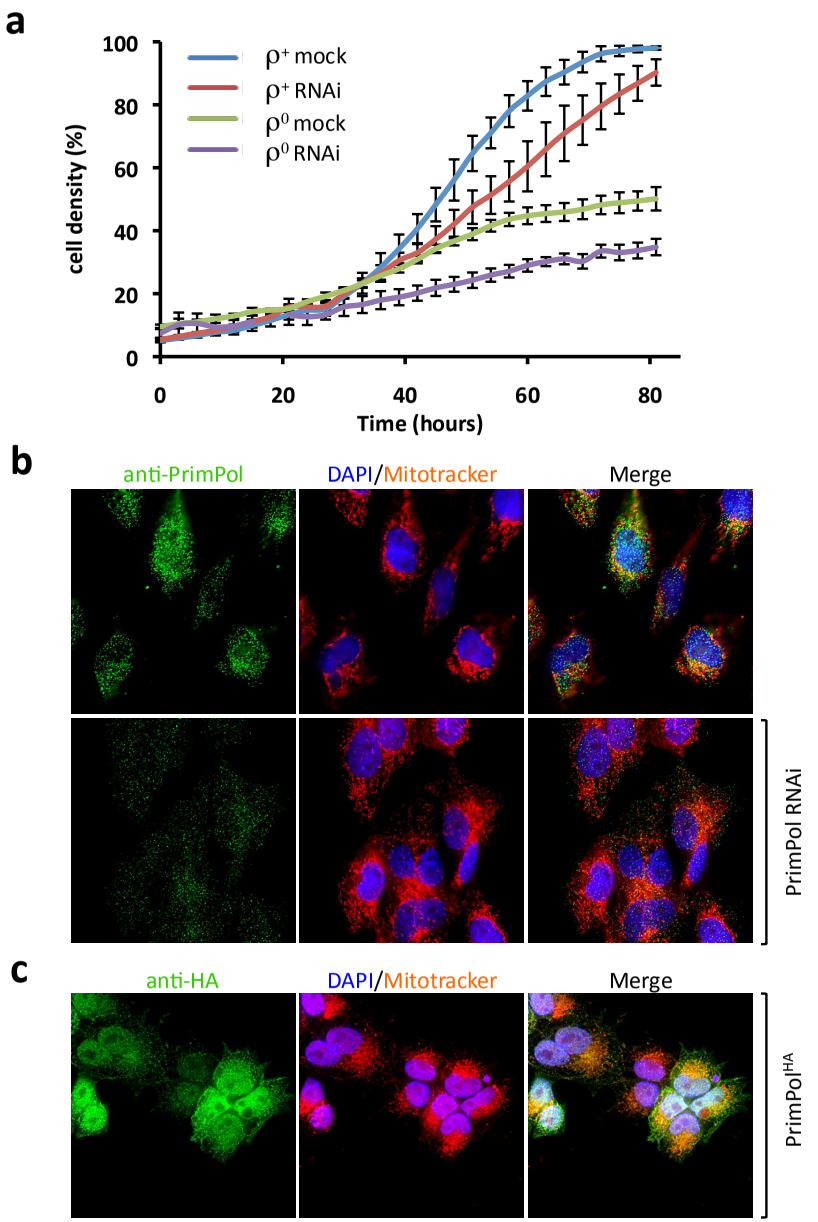
a
100
80
60
40
20
0
cell density (%)
ρ+ mock
ρ+ RNAi
ρ0 mock
ρ0 RNAi
0
20
40
60
80
Time (hours)
b
anti-PrimPol
DAPI/Mitotracker
Merge
PrimPol RNAi
c
anti-HA
DAPI/Mitotracker
Merge
PrimPolHA

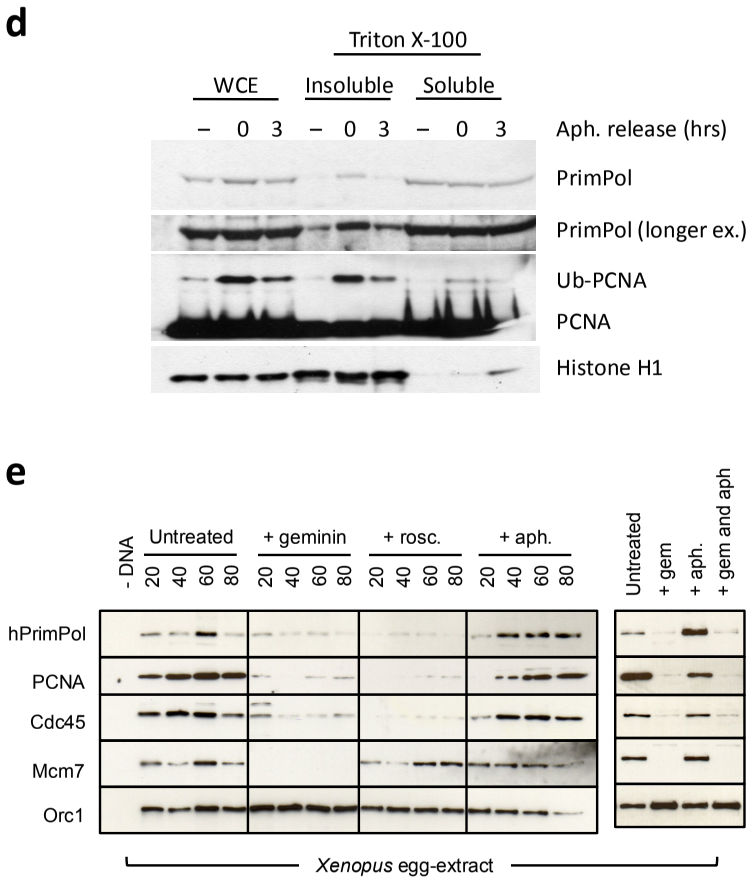
d
Triton X-100
WCE
Insoluble
Soluble
– 0 3 – 0 3 – 0 3
Aph. release (hrs)
PrimPol
PrimPol (longer ex.)
Ub-PCNA
PCNA
Histone H1
e
- DNA
Untreated
+ geminin
+ rosc.
+ aph.
20 40 60 80 20 40 60 80 20 40 60 80 20 40 60 80
Untreated
+ gem
+ aph.
+ gem and aph
hPrimPol
PCNA
Cdc45
Mcm7
Orc1
Xenopus egg-extract

Figure 2

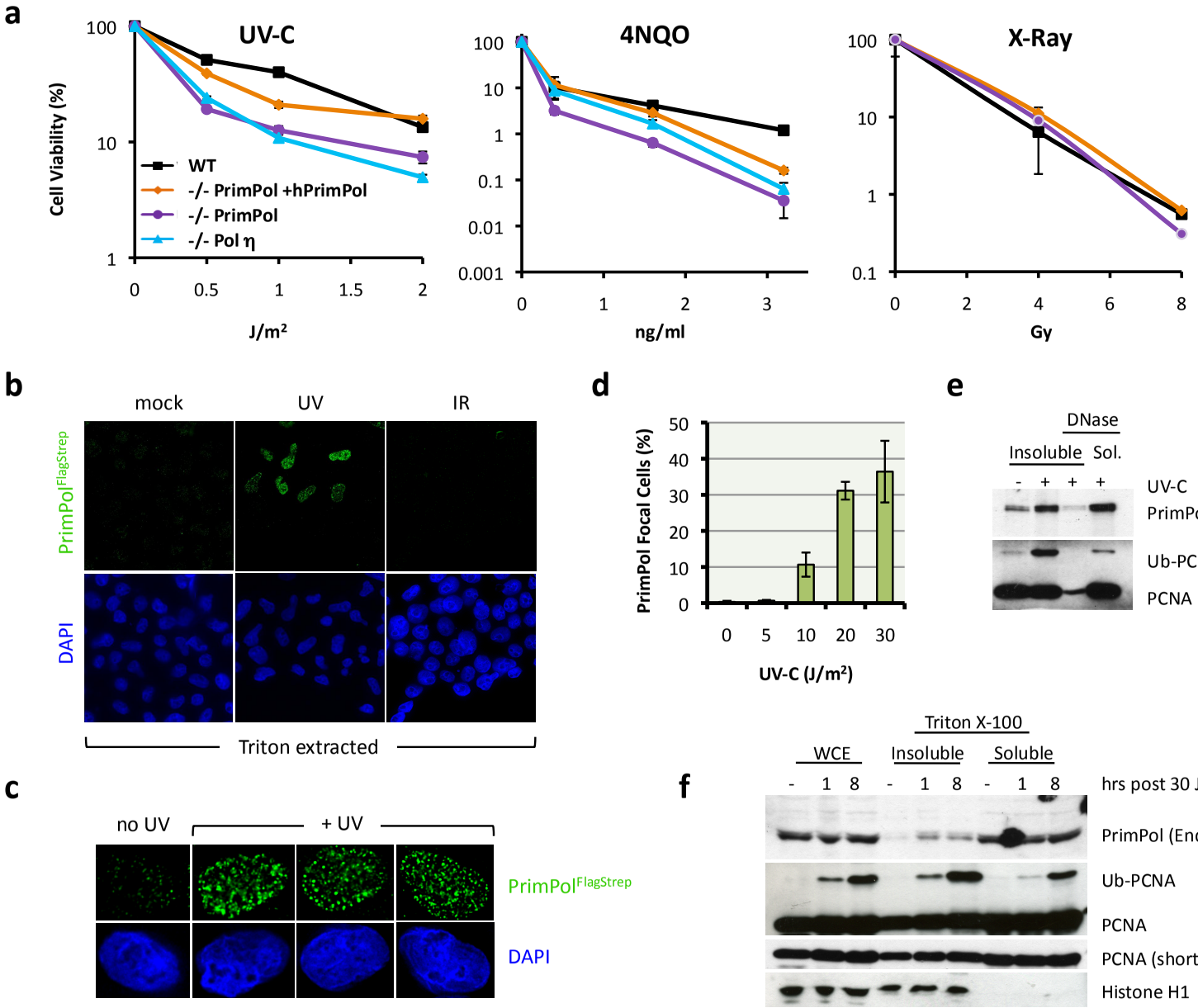
a
UV-C
4NQO
X-Ray
Cell Viability (%)
WT
-/- PrimPol +hPrimPol
-/- PrimPol
-/- Pol η
J/m²
ng/ml
Gy
b
mock
UV
IR
PrimPolFlagStrep
DAPI
Triton extracted
c
no UV
+ UV
PrimPolFlagStrep
DAPI
d
PrimPol Focal Cells (%)
UV-C (J/m²)
e
DNase
Insoluble
Sol.
UV-C
PrimPolFlagStrep
Ub-PCNA
PCNA
f
Triton X-100
WCE
Insoluble
Soluble
hrs post 30 J/m² UV-C
PrimPol (Endogenous)
Ub-PCNA
PCNA
PCNA (short exp.)
Histone H1

Figure 3

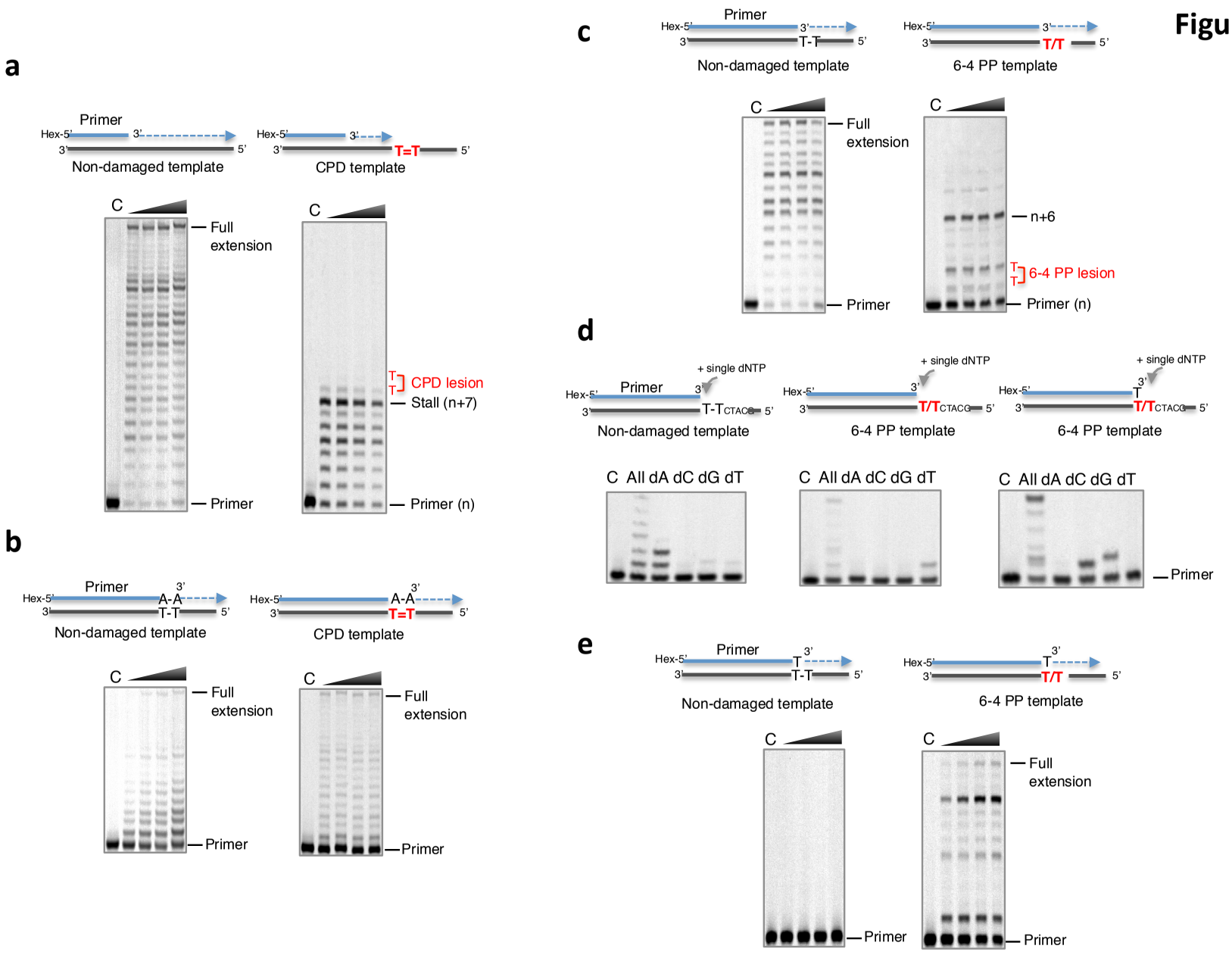
a
Primer
Hex-5'
3'
5'
Non-damaged template
T=T
CPD template
C
Full extension
Primer
CPD lesion
Stall (n+7)
Primer (n)
b
A-A
T-T
c
T-T
T/T
6-4 PP template
n+6
6-4 PP lesion
d
+ single dNTP
T-TCTACG
T/TCTACG
C All dA dC dG dT
e

Figure 4

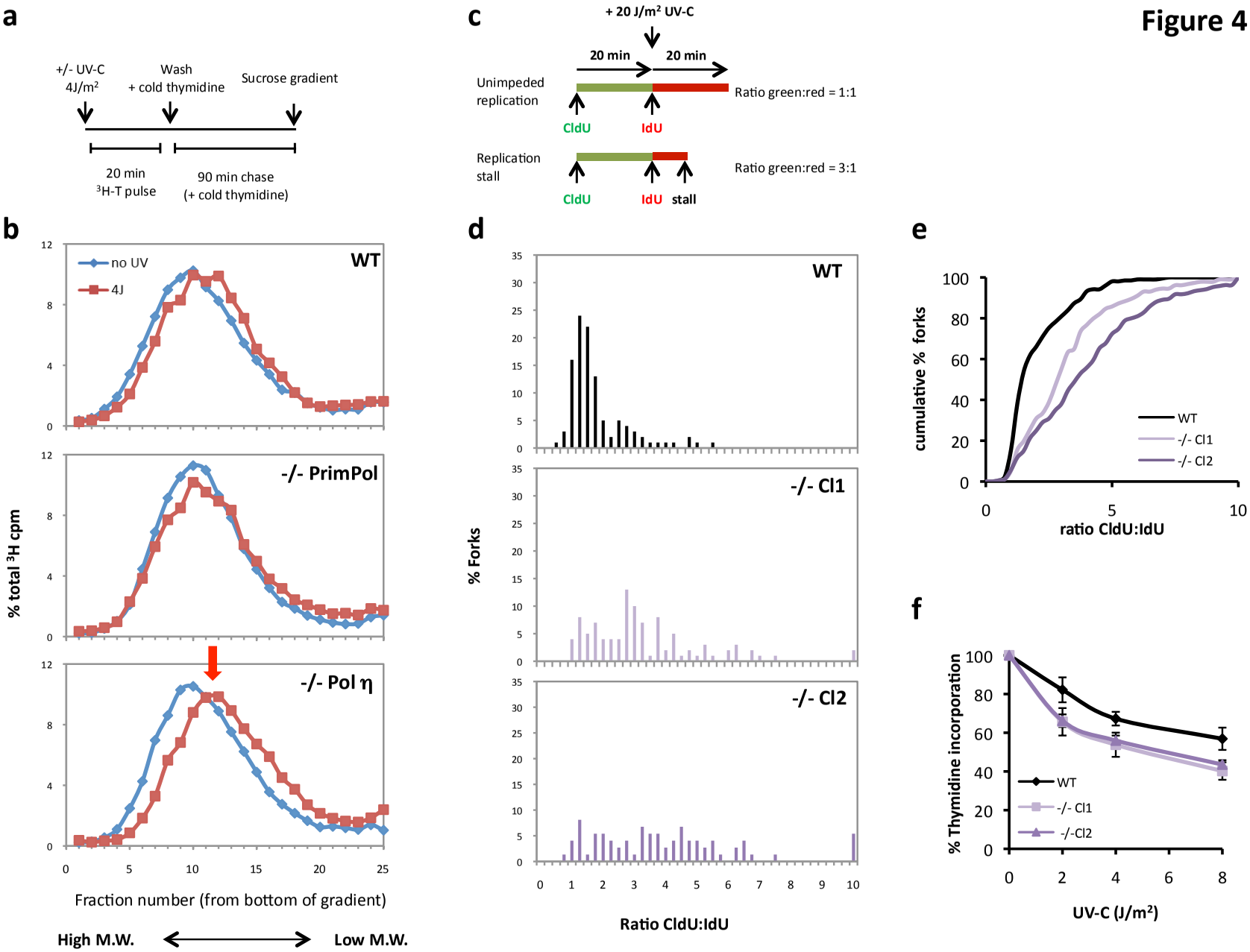
a
+/- UV-C
4J/m²
Wash
+ cold thymidine
Sucrose gradient
20 min
³H-T pulse
90 min chase
(+ cold thymidine)
b
no UV
4J
WT
-/- PrimPol
-/- Pol η
% total ³H cpm
Fraction number (from bottom of gradient)
High M.W.
Low M.W.
c
+ 20 J/m² UV-C
20 min
20 min
Unimpeded replication
Ratio green:red = 1:1
CldU
IdU
Replication stall
Ratio green:red = 3:1
CldU
IdU
stall
d
WT
-/- Cl1
-/- Cl2
% Forks
Ratio CldU:IdU
e
cumulative % forks
WT
-/- Cl1
-/- Cl2
ratio CldU:IdU
f
% Thymidine incorporation
WT
-/- Cl1
-/-Cl2
UV-C (J/m²)

Figure 5

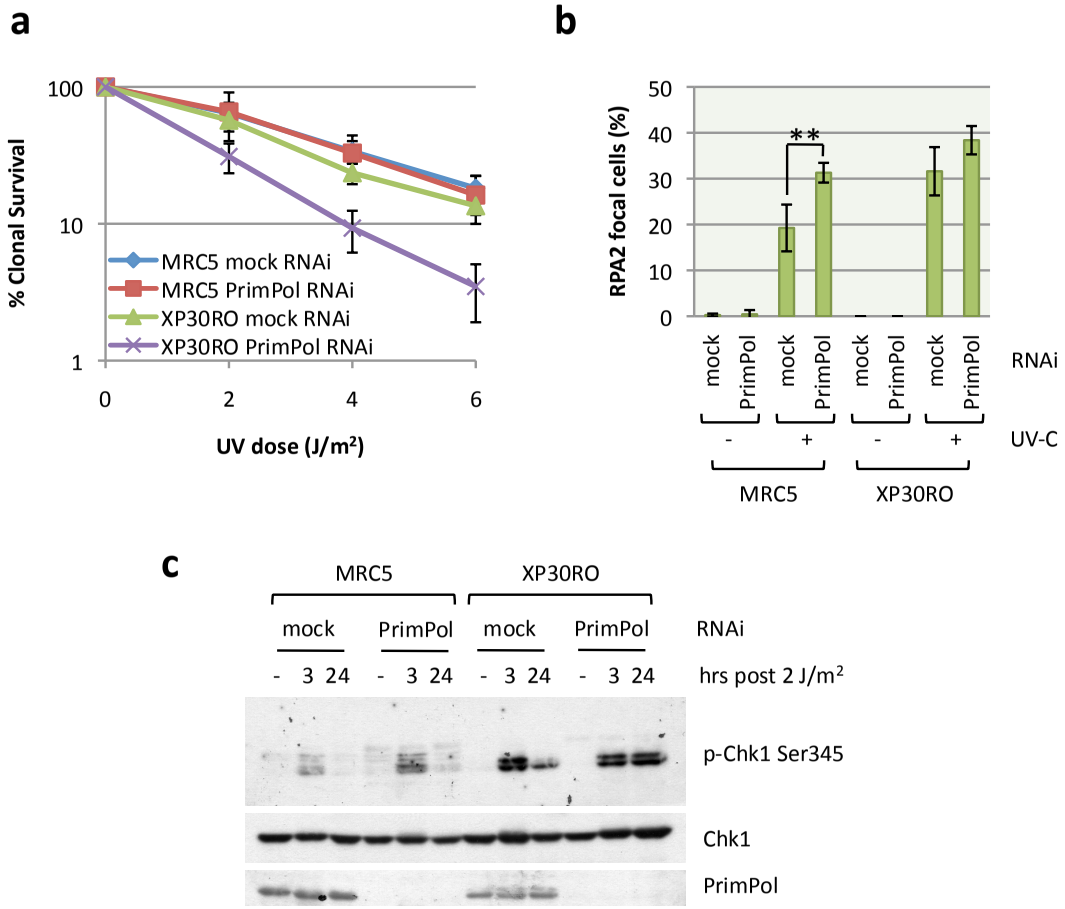
a
100
10
1
% Clonal Survival
0
2
4
6
UV dose (J/m²)
MRC5 mock RNAi
MRC5 PrimPol RNAi
XP30RO mock RNAi
XP30RO PrimPol RNAi
b
50
40
30
20
10
0
RPA2 focal cells (%)
**
mock
PrimPol
mock
PrimPol
mock
PrimPol
mock
PrimPol
RNAi
-
+
-
+
UV-C
MRC5
XP30RO
c
MRC5
XP30RO
mock
PrimPol
mock
PrimPol
RNAi
- 3 24 - 3 24 - 3 24 - 3 24
hrs post 2 J/m²
p-Chk1 Ser345
Chk1
PrimPol

Figure 6

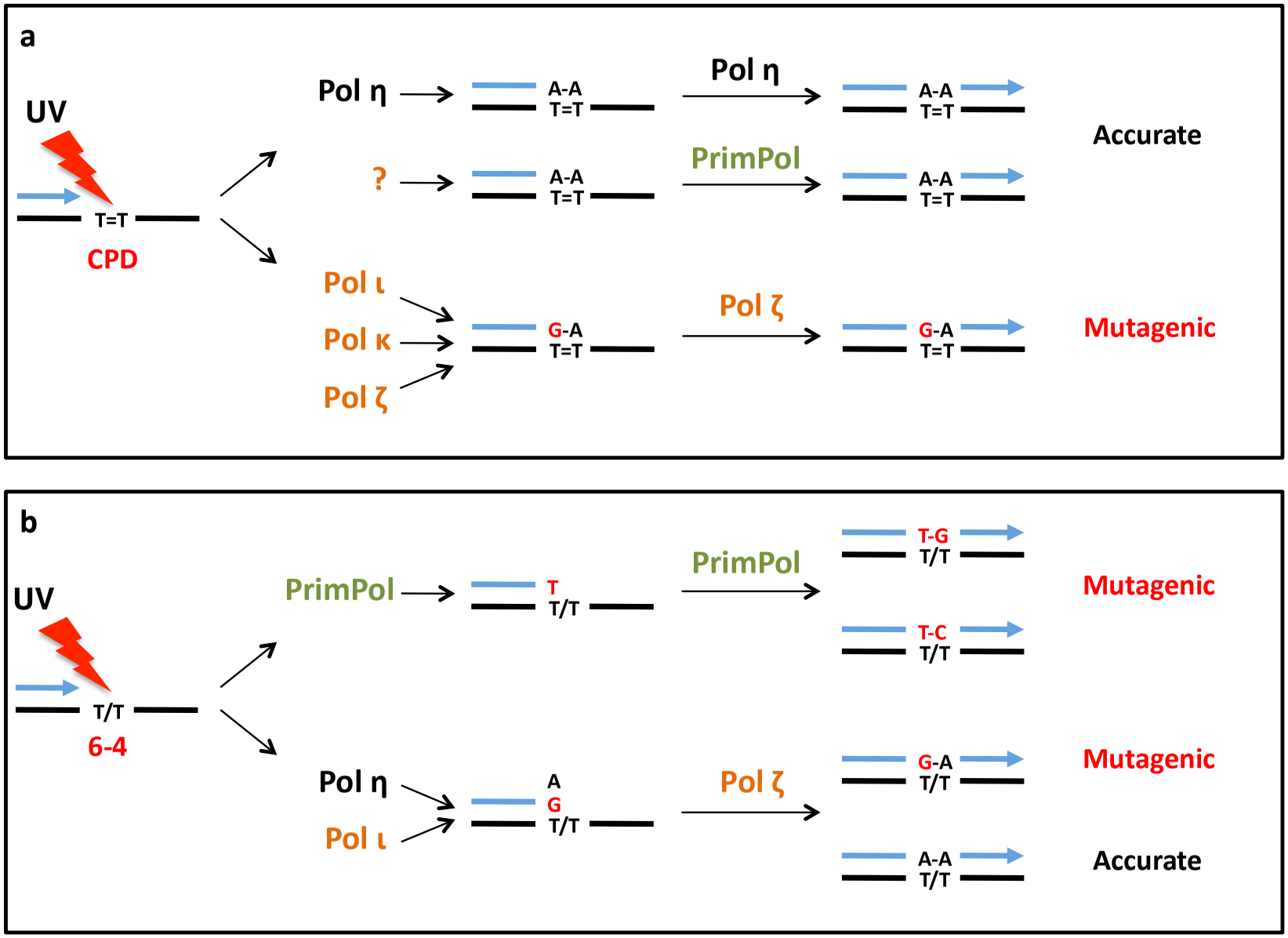
a
UV
T=T
CPD
Pol η
A-A
T=T
Pol η
A-A
T=T
Accurate
?
A-A
T=T
PrimPol
A-A
T=T
Pol ι
Pol κ
Pol ζ
G-A
T=T
Pol ζ
G-A
T=T
Mutagenic
b
UV
T/T
6-4
PrimPol
T
T/T
PrimPol
T-G
T/T
Mutagenic
T-C
T/T
Pol η
Pol ι
A
G
T/T
Pol ζ
G-A
T/T
Mutagenic
A-A
T/T
Accurate

SUPPLEMENTARY METHODS

RNAi depletion.

Sequences of stealth RNAi (Invitrogen) used for transfection were:
5'-GAGGAAACCGUUGUCCUCAGUGUAU-3',
5'-AUACACUGAGGACAACGGUUUCCUC-3'.

Immunofluorescent analysis.

Cells were grown on coverslips, which for HEK-293 Flp-In™ T-REx™ cells were poly-L-lysine coated. Following siRNA transfection and/or DNA damaging agent and recovery time, cells were either fixed directly in 3 % paraformaldehye (in PBS) for 15 minutes or pre-extracted by washing in 0.5 % Triton X-100 in PBS before fixing. Cells were permeabilised with 0.2 % Triton X-100 in PBS for 10 minutes, blocked with 3 % BSA in PBS, and incubated with primary and following wash steps, secondary antibodies. Coverslips were mounted on slides with Prolong Gold anti-fade (Invitrogen). Slides were analysed on a widefield Deltavision microscope for images, and a Nikon E400 for counting.

Antibodies used were anti-PrimPol 1:200 (Gàrcia-Gomez *et al*, submitted), anti-RPA2 1:200 (Cell Signalling). Secondary antibodies were Alexa Fluor 488 goat anti-rabbit 1:2000, and Alexa Fluor 594 goat anti-mouse 1:2000. Cells were incubated with 250 nM Mitotracker Deep Red (final concentration) for 30 minutes prior to fixation.
Immunolabeling of DNA fibers was performed with anti-rat BrdU (abcam) 1:1000, anti-mouse BrdU (Becton Dickinson) 1:500 and secondary Alexa Fluor 488-labeled anti-rat and Alexa Fluor 594-labeled anti-mouse (Invitrogen) both 1:250.

Cellular fractionation.

Cellular fractionation protocol was modified (Kannouche *et al*, 2004). Cell pellet was resuspended in cytoskeletal (CSK) buffer (100 mM NaCl, 300 mM sucrose, 3 mM $MgCl_2$, 10 mM Pipes (pH 6.8), 1 mM EGTA, 0.2 % Triton X-100) supplemented with protease and phosphotase inhibitors (Roche), and incubated on ice for 5 minutes and then spun in a cold centrifuge for 10 minutes at 13,000 rpm. The supernatant was collected as the soluble fraction, and the insoluble pellet was twice PBS washed before resuspended and boiled in Laemmli sample buffer. For further fractionation the insoluble pellet was resuspended in CSK buffer but with 50 mM NaCl and 1 μl/ml Benzonase, at room temperature for 20 minutes with occasional agitation, before centrifugation. The soluble fraction was retained and the insoluble fraction boiled in Lameli sample buffer. Whole cell extracts were prepared by lysing cells in NETN buffer (150 mM NaCl, 50 mM Tris (pH 7.5), 5 mM EDTA, 0.5 % NP-40), and incubated on ice before sonication and determining protein concentration.

Xenopus egg extract.

Demembranated sperm nuclei were prepared by lysolecithin treatment as previously described (Murray, 1991). For preparation of interphase Xenopus egg extracts, unfertilized eggs were dejellied, washed and activated with the calcium ionophore A23187 as previously described (Kubota and Takisawa, 1993). Activated eggs were washed in extraction buffer (XB: 10mM Hepes-KOH, pH 7.7, 100mM KCl, 0.1mM CaCl2, 1mM MgCl2, 50mM sucrose) at 4°C, and then, following removal of excess buffer, crushed by centrifugation at 15,000 x g for 10 minutes. The cytoplasmic layer was supplemented with aprotinin (10μg/ml), cytochalasin B (50μg/ml), creatine phosphate (30mM) and creatine phosphokinase (150μg/ml) then centrifuged at 60,000 x g 10 min, 4°C (Beckman Optima TLA-55) to generate the replication-competent supernatant fraction. Chromatin isolation was carried out using the method of (Errico et al 2007) and recombinant GST-geminin prepared as previously described (Stokes et al 2003). PCNA and MCM7 antibodies were both from AbCam while Cdc45 antibody was a generous gift of Vincenzo Costanzo (CRUK Clare hall) and Orc1 antibody, from Dr Julian Blow (Dundee University).

DT40 Knock out study.

Construction of targeted vectors containing antibiotic resistance cassettes was performed via gateway cloning system (Liizumi et al., 2006) and the primers used summarized in table 1. DT40 cells were electroporated and clones selected as described previously (Sonoda et al., 1998) using histidinol and puromycin (Sigma) respectively at 1mg/ml and 0.5mg/ml. Resistant clones were screened for alleles disruption via Southern blot analysis and RT-PCR using superscript one step kit (Invitrogen), with primers summarized in table 2.

DT40 cells were grown at 39°C in RPMI 1640 medium supplemented with 10–5 M β-mercaptoethanol, penicillin, streptomycin, 10% foetal calf serum and 1% chicken serum (Sigma), and counted manually on haemocytometer with trypan blue (Invitrogen) staining to assess growth defect. Cell cycle analysis was determined by BrdU labelling and flow cytometry analysis as described previously (Hegarat *et al*, 2012).

Purification of recombinant proteins.

Human PrimPol cDNA was sub-cloned into pET28a (Novagen) using NdeI and BamHI restriction sites to generate a 6 Histidine N terminal tagged recombinant protein. Catalytic null mutant AxA (both Asp114 and Glu116 changed to alanines) was obtained by site directed mutagenesis PCR of this construct using forward 5'-AGCTTTATTTTGCTTTGGCATTTAACAAACC-3' and reverse 5'-GGTTTGTTAAATGCCAAAGCAAAATAAAGCT-3' primers. Both proteins were expressed using Bl21 E. coli strain following overnight induction at 16°C by adding 0.4mM IPTG and

purified with Ni^{2+}-NTA (Qiagen) followed by heparin and size-exclusion (GE Healthcare) chromatography columns (protocols adapted from Gàrcia-Gomez *et al*, submitted). Archaeal family-B DNA polymerase from *Thermococcus gorgonarius* (Tgo PolB exo-) used in control primer extension reactions on synthetic substrates containing UV induced DNA lesions was purified as described previously (Evans et al., 2000).

Fluorescent primer template based assays.

The HPLC grade DNA oligomers used to prepare synthetic primer-template substrates were purchased from ATDbio (Southampton, UK). The DNA oligomer containing pyrimidine-pyrimidone (6-4) photoproduct was kindly provided by Professor Shigenori Iwai (Osaka University, Japan). Primers contained a 5' Hex fluorophore label.

All the primer extension assays were performed at 37ºC as described previously (Jozwiakowski and Connolly, 2011). The typical primer extension reaction was performed in 20ul volume containing 10 mM Bis-Tris-Propane-HCl, pH 7,0, 10 mM NaCl, 10 mM $MgCl_2$, 1 mM DTT, 20 nM primer-template substrate, 200 µM dNTP's (Roche) with 100 nM recombinant human PrimPol. The products of the primer-template extension reactions were monitored over time course of 5, 10, 15, 30 minutes. All single incorporation assays were performed in present of single dNTP and reactions were quenched after 30 minutes incubation. Control primer extension (with Tgo-PolB exo-) were performed at 50ºC in 20ul volume containing 20mM Tris-HCl, pH 8,5, 20mM NaCl, 2mM MgSO4, 20nM primer-template substrate, 100µM dNTP's (Roche) with 50nM recombinant Tgo PolB exo-.

Table 1, DT40 KO primers:

Histidinol upstream ARM primer FOR	5'-GGGGACAACTTTGTATAGAAAAGTTGGGCGGCAGCGCGCGGGCCGCGGAGAGG-3'
Histidinol upstream ARM primer REV	5'-GGGGACTGCTTTTTTGTACAAACTTGTATACATTTAAATATCTTTGTGGATC-3'
Histidinol downstream ARM primer FOR	5'-GGGGACAGCTTTCTTGTACAAAGTGGTGAGAGGGGAGCTGAAAGCAGTTT-3'
Histidinol downstream ARM primer REV	5'-GGGGACAACTTTGTATAATAAAGTTGCCATGGGCTCTGTTTAAACAAACAAGC-3'

Puromycin upstream ARM primer FOR	5’-GGGGACAACTTTGTATAGAAAAGTTGTTAAAGGTTTGAGTGATTCTGAATATAGCC-3’
Puromycin upstream ARM primer REV	5’-GGGGACTGCTTTTTTGTACAAACTTGTTACTCCTTGCAGGTTTTCACAAATC-3’
Puromycin downstream ARM primer FOR	5’-GGGGACAGCTTTCTTGTACAAAGTGGAACCAAATACAGTCCATGCTGAAAC-3’
Puromycin downstream ARM primer REV	5’-GGGGACAACTTTGTATAATAAAGTTGGTGGCCAACTAAGACTATGCAAAC-3’

Table 2, Southern blot probe and RT-PCR primers

Southern blot probe, primer FOR	5’-ACGGAGTGCAAGGAGGTAAC-3’
Southern blot probe, primer REV	5’-GACTGGATCGTGGCACTTC-3’
G. gallus PrimPol cDNA, primer FOR	5’-ATGAAGAGAAAATGGGAAGAAAGAGTGAAGAAAGTTG -3’
G. gallus PrimPol cDNA, primer REV	5’-AGCCTTTGGAAGCATCTTCGACT-3’
G.gallus Bora cDNA, primer FOR	5’- ATGGGCGATACAGAAGAAGCCCAAATGCAG-3’
G.gallus Bora cDNA, primer REV	5’-CTCGAGAGGAGAAGGAACTATGAGACTCTTTGTGAAAACTCC-3’

Table 3

Figure	Primer (5’→3’)	Template (5’→3’)
3A	TGTCGTCTGTTCGGTCGTTC	CGCGCAGGGCGCACAACAGCCTTGAAGACCGAACGACCGAACAGACGACA
3A	TGTCGTCTGTTCGGTCGTTC	CGCGCAGGGCGCACAACAGCCT=TGAAGACCGAACGACCGAACAGACGACA
3B	TGTCGTCTGTTCGGTCGTTCGGTCTTCAA	CGCGCAGGGCGCACAACAGCCTTGAAGACCGAACGACCGAACAGACGACA
3B	TGTCGTCTGTTCGGTCGTTCGGTCTTCAA	CGCGCAGGGCGCACAACAGCCT=TGAAGACCGAACGACCGAACAGACGACA
3C	CACTGACTGTATGATG	CTCGTCAGCATCTTCATCATACAGTCAGTG
3C	CACTGACTGTATGATG	CTCGTCAGCATCT/TCATCATACAGTCAGTG
3D	CACTGACTGTATGATG	CTCGTCAGCATCTTCATCATACAGTCAGTG
3D	CACTGACTGTATGATG	CTCGTCAGCATCT/TCATCATACAGTCAGTG
3D	CACTGACTGTATGATGT	CTCGTCAGCATCT/TCATCATACAGTCAGTG
3E	CACTGACTGTATGATGT	CTCGTCAGCATCTTCATCATACAGTCAGTG
3E	CACTGACTGTATGATGT	CTCGTCAGCATCT/TCATCATACAGTCAGTG

Supplementary Figure 1 (S1)

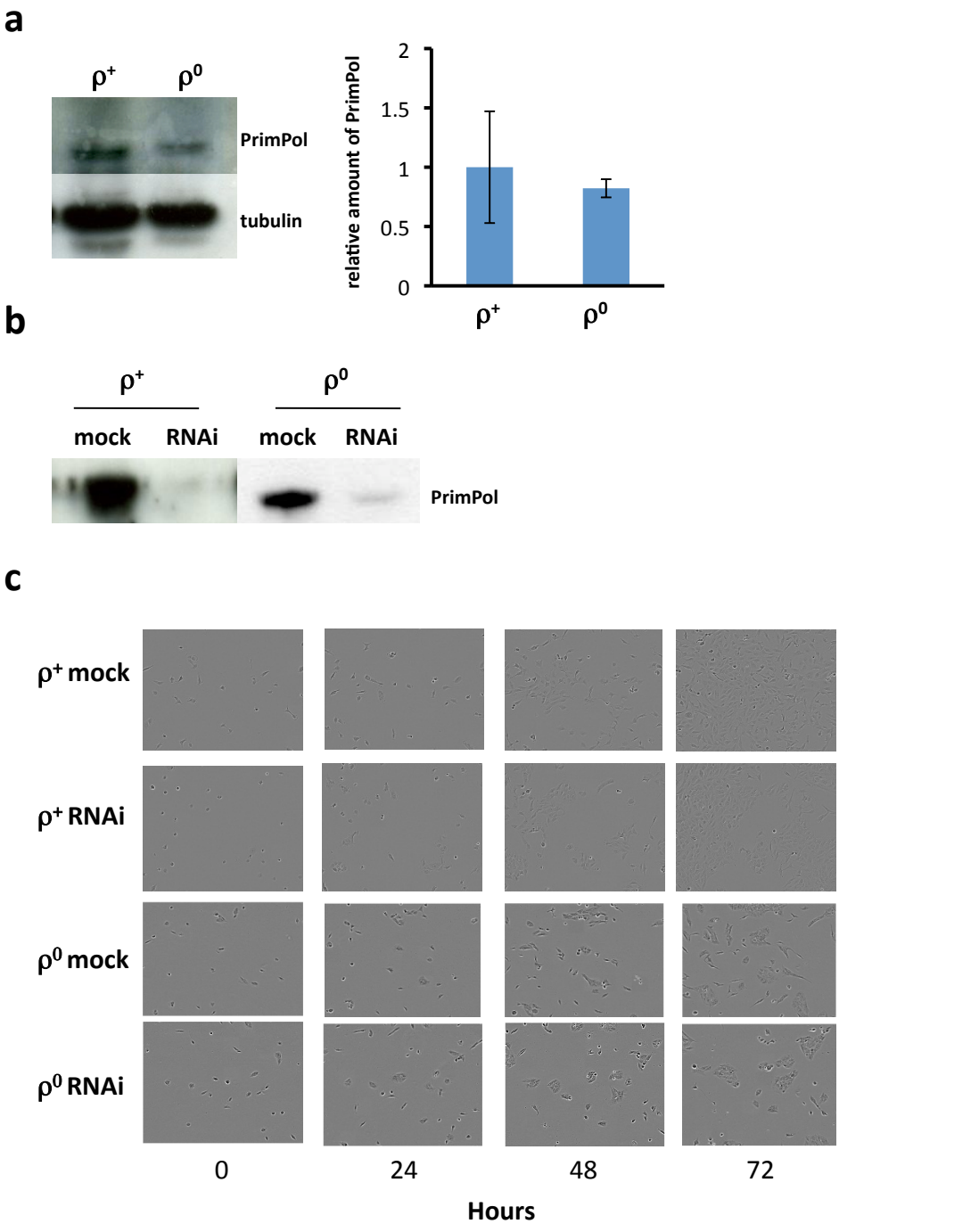

Figure S1l Cells lacking mtDNA have an equal level of PrimPol and show proliferation defects comparable to wild type cells after PrimPol RNAi.
a, PrimPol protein levels are visualised by Western blot analysis of whole cell lysate in wild type (ρ^+) 143B cells and those lacking mtDNA (ρ^0), and then quantified in relation to tubulin levels (right panel). Error bars denote standard deviation of 3 independent extract preparation. **b,** PrimPol depletion was confirmed at 72 hours after RNAi treatment, compared to mock treated cells by Western blot analysis of whole cell lysate. **c,** Representative images taken every 24 hours from Incucyte phase contrast microscope after PrimPol RNAi depletion of wild type (ρ^+) and mtDNA deficient (ρ^0) 143B cells.

Supplementary Figure 2 (S2)

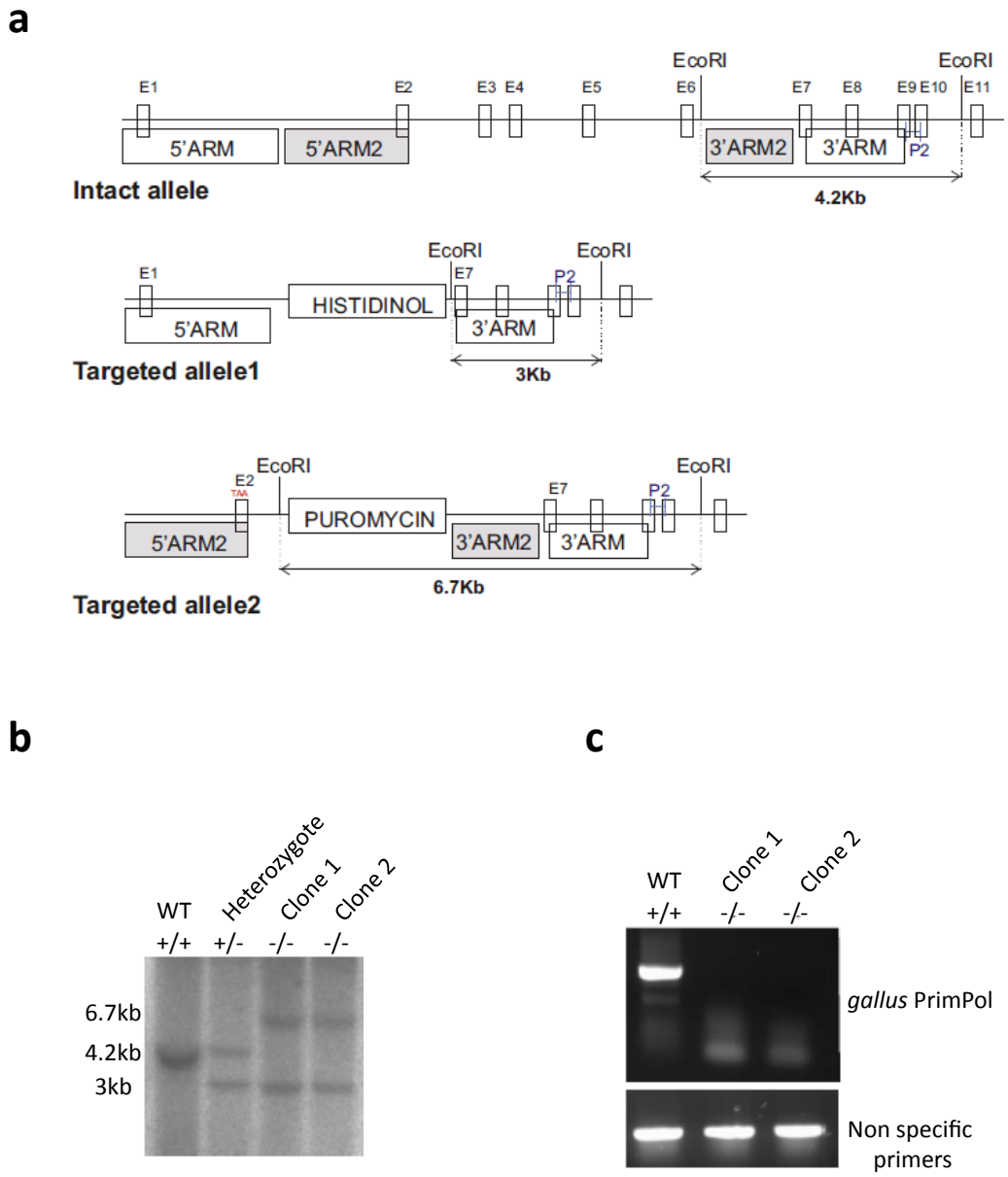

Figure S2| Generation of PrimPol knockout cell lines in avian DT40 cells.
a, Illustration of Southern blot strategy used to disrupt *G. gallus PrimPol* gene; exons (square boxes), EcoRI restriction sites and Southern blot probe (P2) are depicted along with expecting band size (under horizontal arrows) for Southern blot analysis. Both disruption cassettes (histidinol and puromycin) are flanked by two distinct sets of recombination arms (white or grey boxes) in order to specifically target the wild type allele remaining in heterozygotes clones WT/HIS. **b,** Southern blot of genomic DNA of WT DT40 cells (+/+) and clones obtained after *PrimPol G. gallus* gene disruption showing the loss of both wild type alleles in clone 1 and 2 (-/-) or only one allele remaining in the heterozygote clone (+/-). **c,** RT-PCR performed on RNA extracted from WT and both KO clones, using *gallus PrimPol* specific primers (upper gel) or unspecific *G. gallus* primers (lower gel) as PCR control.

Supplementary Figure 3 (S3)

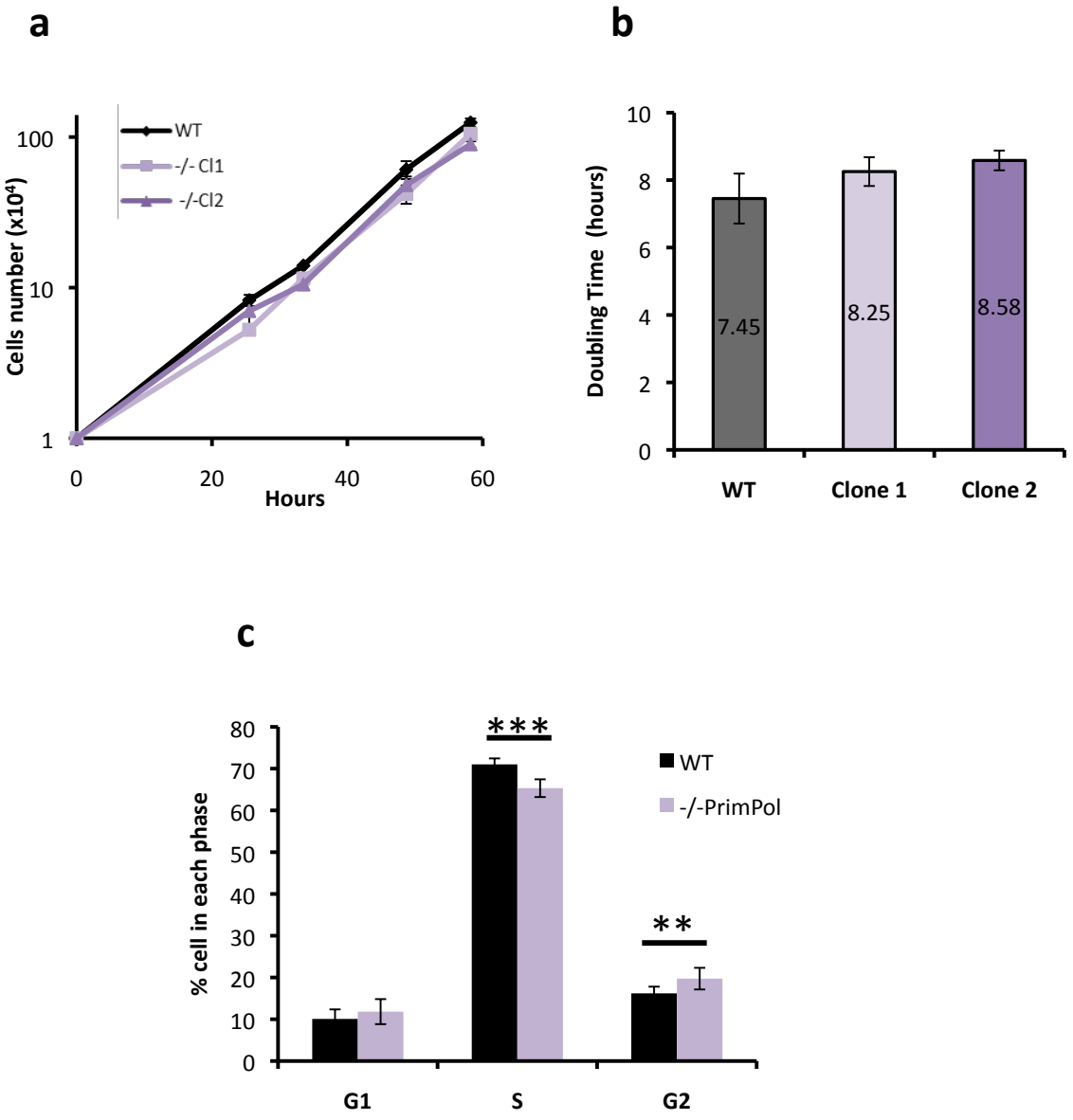

Figure S3| *PrimPol*$^{-/-}$ DT40 cells have minor proliferation and cell-cycle defects.
a, *PrimPol*$^{-/-}$ cells have a minor proliferative defect. Growth curves of DT40 WT (black line) and *PrimPol*$^{-/-}$ (light and dark purple) cells were assessed by counting duplicate cultures of each population over 7 generations (56 hours), using a haemocytometer with trypan blue dye exclusion staining. **b,** *PrimPol*$^{-/-}$ cells have a slightly longer doubling time. Doubling time for each population was determined using an exponential regression algorithm; average of 3 independent experiments is indicated in the middle of each plot and the standard deviation represented by error bars. **c,** Increase proportion of G2 phase *PrimPol*$^{-/-}$ cells. Cell cycle profile of WT DT40 (black) or average of both *PrimPol*$^{-/-}$ clones (purple) was determined using flow cytometry after BrdU incorporation. Error bars denote standard deviation of 5 experiments, and the t test was assessed with two tails moments to determine p values (***P =0.000132, **P =0.0114).

Supplementary Figure 4 (S4)

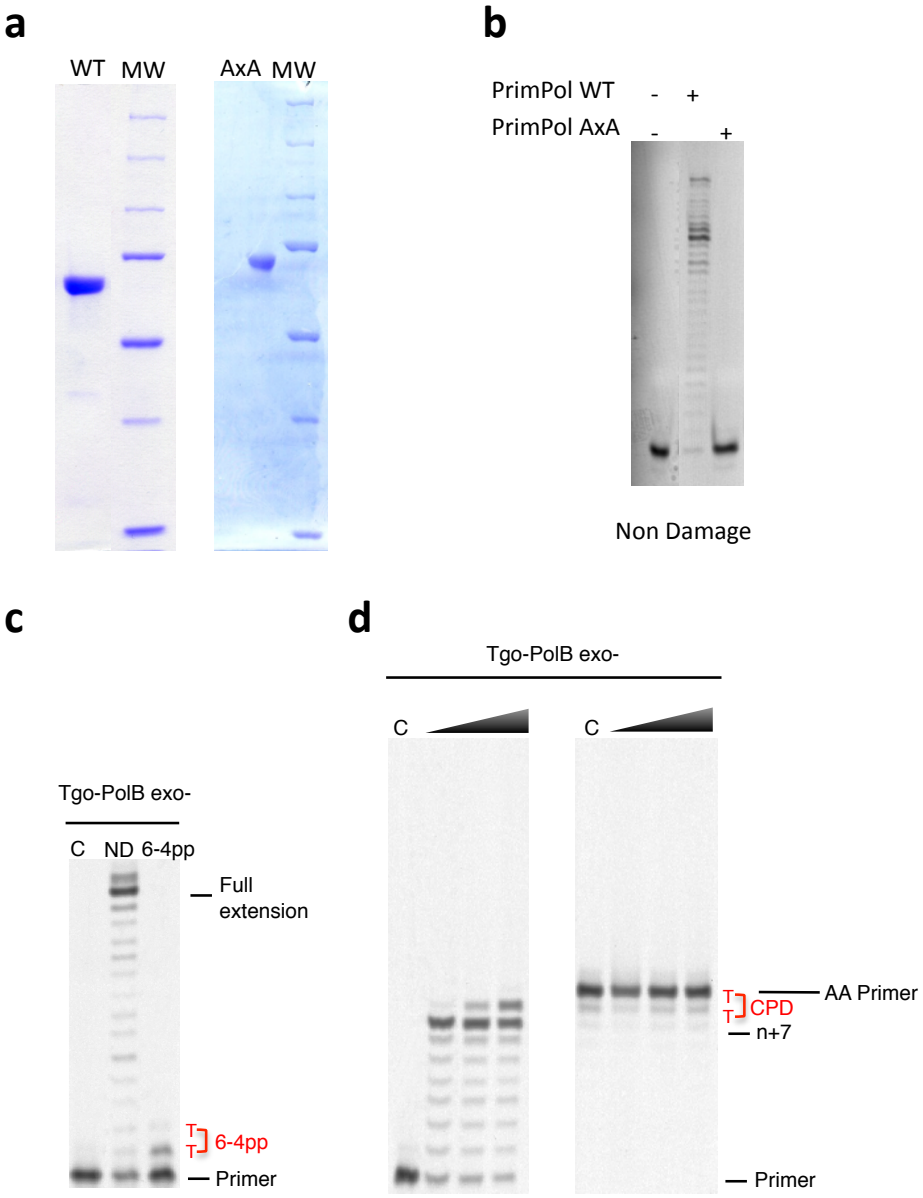

Figure S4| Preparation of recombinant human PrimPol proteins, and primer extension control assays. **a,** SDS PAGE analysis of histidine-tagged human recombinant PrimPol, wild type full length polypeptide (WT) or catalytic null mutant (AxA), after Ni-NTA affinity purification, and heparin chromatography. **b,** DNA polymerase activity is intrinsic to PrimPol protein. Primer extension assay performed on an undamaged DNA template (substrate described in Figure 3a) with wild type and catalytic null (AxA) recombinant human PrimPol (100 nM). **c,** DNA substrate containing 6-4 photoproduct cannot be extended by a replicative polymerase. No enzyme control (C) and Tgo PolB exo- (*Thermococcus gorgonarius* exonuclease dead polymerase B, at 50 nM) were incubated with non-damaged (ND) or 6-4 photoproduct (6-4 PP) containing substrate (as in Figure 3c) for 30 minutes at 50°C. **d,** Substrates containing a CPD lesion cannot be fully replicated by a replicative polymerase. No enzyme control (C) and Tgo PolB exo- were incubated with DNA substrate containing CPD lesion (as described in Figure 3a), Left panel. Tgo PolB exo- can incorporate only the first nucleotide opposite CPD lesion before stalling (n +8). Same experiment was repeated with DNA substrate containing two deoxyadenosines (A-A) annealed opposite a T-T CPD (as in figure 3b) , right panel, blocking replicative polymerase progression. Triangles above gel indicate increasing reaction time (30, 60 and 120 seconds).

Appendix B

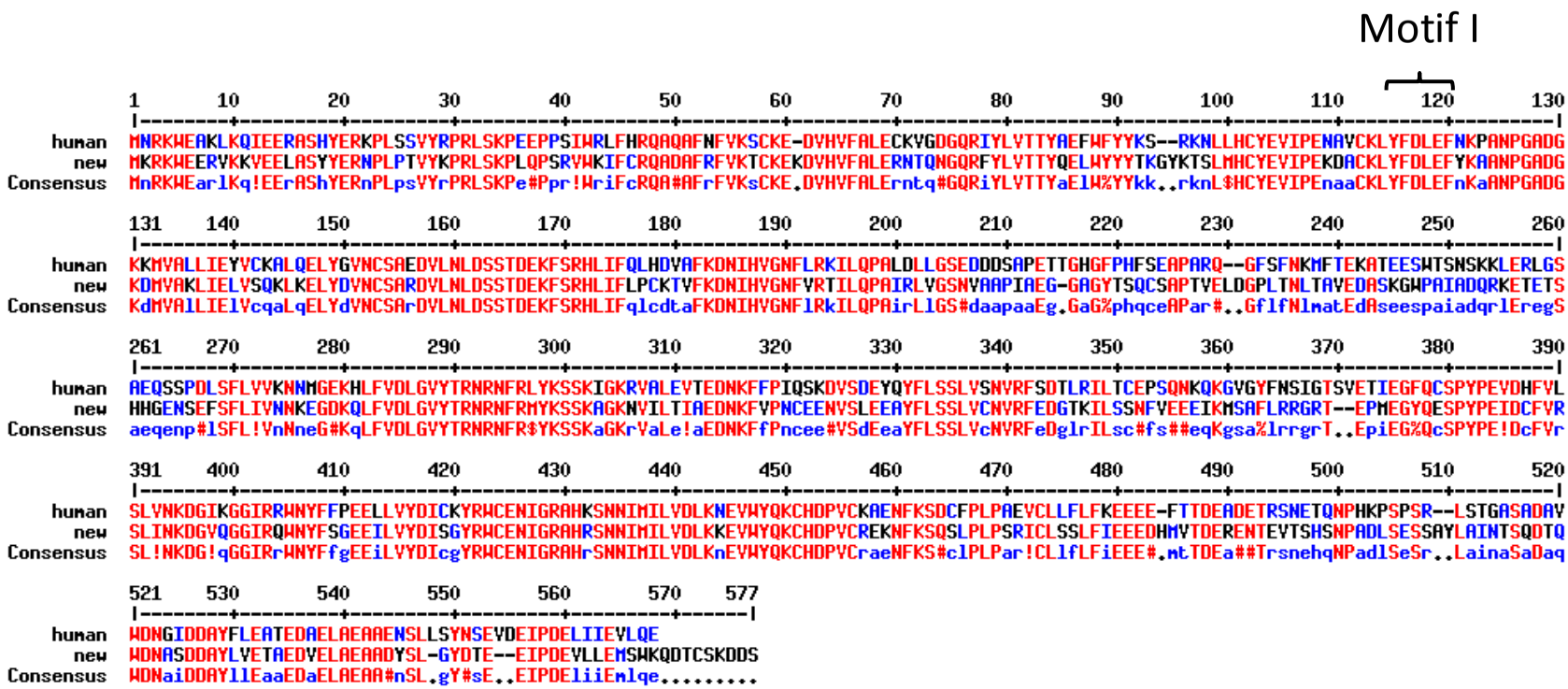

Multiple sequences alignment between human and *G. gallus* PrimPol proteins using an annotated versions of *G. gallus* PrimPol protein sequence (new). Both protein homologues shares approximately 50.8% identity according to Clustaw software.

G. gallus PrimPol ORF and amino acid sequences

```
atgaagagaaaatgggaagaaagagtgaagaaagttgaagaactagcgtcttactatgaa 60
 M  K  R  K  W  E  E  R  V  K  K  V  E  E  L  A  S  Y  Y  E
agaaaccctcttcctacagtttacaaaccaagactgtccaaacccttacagccatcccgt 120
 R  N  P  L  P  T  V  Y  K  P  R  L  S  K  P  L  Q  P  S  R
gtctggaaaatattctgtcgacaggctgatgctttcagatttgtgaaaacctgcaaggag 180
 V  W  K  I  F  C  R  Q  A  D  A  F  R  F  V  K  T  C  K  E
gatgttcatgtatttgccttggaaaggaacacacaaaatggacagaggttttaccttgtg 240
 D  V  H  V  F  A  L  E  R  N  T  Q  N  G  Q  R  F  Y  L  V
actacatatcaagagctttggtattattacaccaaaggttataaaacaagtcttatgcat 300
 T  T  Y  Q  E  L  W  Y  Y  Y  T  K  G  Y  K  T  S  L  M  H
tgctatgaagtaattcctgaaaaagatgcttgcaaactttattttgatttggagttctac 360
 C  Y  E  V  I  P  E  K  D  A  C  K  L  Y  F  D  L  E  F  Y
aaagcagcaaatcctggtgctgatggcaaggatatggttgcaaagctaattgagcttgtc 420
 K  A  A  N  P  G  A  D  G  K  D  M  V  A  K  L  I  E  L  V
agccagaagttaaaagaactgtatgatgttaactgctcagccagagatgtcttgaattta 480
 S  Q  K  L  K  E  L  Y  D  V  N  C  S  A  R  D  V  L  N  L
gattccagtactgatgaaaaatttagtcggcacttaatattcctaccctgcaagactgta 540
 D  S  S  T  D  E  K  F  S  R  H  L  I  F  L  P  C  K  T  V
tttaaggataacattcacgtcggtaactttgtgagaaccattttgcagcctgccataagg 600
 F  K  D  N  I  H  V  G  N  F  V  R  T  I  L  Q  P  A  I  R
ttagtggggagtaacgtcgctgctcccattgcagaaggaggagcaggatatacgtcccag 660
 L  V  G  S  N  V  A  A  P  I  A  E  G  G  A  G  Y  T  S  Q
tgttctgcaccaacagttgagttagatggtcctcttacaaacctcacagcagtcgaagat 720
 C  S  A  P  T  V  E  L  D  G  P  L  T  N  L  T  A  V  E  D
gcttccaaaggctggccagccattgctgaccaaagaaaggaaacagaaacatcacaccat 780
 A  S  K  G  W  P  A  I  A  D  Q  R  K  E  T  E  T  S  H  H
ggagaaaactctgaattttcttttctaatagtaaataacaaagaaggagacaagcaactt 840
 G  E  N  S  E  F  S  F  L  I  V  N  N  K  E  G  D  K  Q  L
tttgtggatctaggagtttacacaaggaacagaaatttccggatgtataagtcatcaaaa 900
 F  V  D  L  G  V  Y  T  R  N  R  N  F  R  M  Y  K  S  S  K
gcaggaaaaaacgtgatcctgacaatagcagaggataataagtttgtccccaactgtgaa 960
 A  G  K  N  V  I  L  T  I  A  E  D  N  K  F  V  P  N  C  E
gagaacgtttctttggaagaagcgtattttctttcctctttggtctgcaatgttagattt 1020
 E  N  V  S  L  E  E  A  Y  F  L  S  S  L  V  C  N  V  R  F
gaagatggcacaaaaattctatcatctaactttgtagaagaggagataaagatgtccgct 1080
 E  D  G  T  K  I  L  S  S  N  F  V  E  E  E  I  K  M  S  A
tttttaagaagtaaaaccaccagaagcaccagaggtactgcaagcctattctgctccata 1140
 F  L  R  S  K  T  T  R  S  T  R  G  T  A  S  L  F  C  S  I
ggagcccatggaaggctatcaggagtcaccgtatccagagatgattgttttgttcgttct 1200
 G  A  H  G  R  L  S  G  V  T  V  S  R  D  D  C  F  V  R  S
ttgattaataaagacggagtgcaaggaggtaacaactgtgccattatttacagaaattca 1260
 L  I  N  K  D  G  V  Q  G  G  N  N  C  A  I  I  Y  R  N  S
gcaacagtatttataaacaagttttccttttcagggataaggcaatggaattatttctca 1320
 A  T  V  F  I  N  K  F  S  F  S  G  I  R  Q  W  N  Y  F  S
ggggaagaaatacttgtttatgacatttctggttaccgttggtgtgaaaatattggaaga 1380
 G  E  E  I  L  V  Y  D  I  S  G  Y  R  W  C  E  N  I  G  R
gcccacagaagtaacaacatcatgattctggtagatctaaagaaggaagtctggtatcag 1440
 A  H  R  S  N  N  I  M  I  L  V  D  L  K  K  E  V  W  Y  Q
aagtgccacgatccagtctgcagggaaaaaaacttcaaatcacaaagtcttccattgcct 1500
 K  C  H  D  P  V  C  R  E  K  N  F  K  S  Q  S  L  P  L  P
tctaggatatgtttgtcttctcttttcatagaggaggaagatcatatggtaacagatgaa 1560
 S  R  I  C  L  S  S  L  F  I  E  E  E  D  H  M  V  T  D  E
cgtgagaacacagaagtaacatcacactccaaccctgcagatttgtcagaaagctcagcc 1620
 R  E  N  T  E  V  T  S  H  S  N  P  A  D  L  S  E  S  S  A
tatctagcaataaacacatctcaagacactcagtgggacaatgcaagtgatgatgcctat 1680
 Y  L  A  I  N  T  S  Q  D  T  Q  W  D  N  A  S  D  D  A  Y
ttggtagaaactgctgaagatgtggagctggcagaagctgcagattatagtctgggttac 1740
 L  V  E  T  A  E  D  V  E  L  A  E  A  A  D  Y  S  L  G  Y
```

```
gacacagaagaaattcctgatgaagttcttttggaaatgtcatggaaacaagacacttgc 1800
 D  T  E  E  I  P  D  E  V  L  L  E  M  S  W  K  Q  D  T  C
agcaaagacgacagctaaccatggacttggctagcaaacagactagtagcaacaaagctt 1860
 S  K  D  D  S  -  P  W  T  W  L  A  N  R  L  V  A  T  K  L
gctttaatactgcatgggtatcacatgccttctgtgaaagatactgcgatgtagttcaaa 1920
 A  L  I  L  H  G  Y  H  M  P  S  V  K  D  T  A  M  -  F  K
agcactcttctagagctgatagacaaagtgagtaactgctaaaaacaagcaaccttgaga 1980
 S  T  L  L  E  L  I  D  K  V  S  N  C  -  K  Q  A  T  L  R
acagattaaatgggtataaagagatcacaggggctgaagaagactgggctggaaactctt 2040
 T  D  -  M  G  I  K  R  S  Q  G  L  K  K  T  G  L  E  T  L
catgaaggctgcttcaagacatttagcactttgaaggcttattgtcatgcaatttctatt 2100
 H  E  G  C  F  K  T  F  S  T  L  K  A  Y  C  H  A  I  S  I
ttcttagctgtttgctcaacttctactgataagccaaatactgtatttcttcacttccag 2160
 F  L  A  V  C  S  T  S  T  D  K  P  N  T  V  F  L  H  F  Q
atatggaagaacactatttatttctgatacagagttaataataaagagatttgtctgtca 2220
 I  W  K  N  T  I  Y  F  -  Y  R  V  N  N  K  E  I  C  L  S
ctggttcatccaaa
 L  V  H  P
```

Nucleotides sequence (lower case) of *G. gallus* PrimPol ORF and the corresponding amino acid sequences (upper case). The nucleotides sequence was re-annotated from the *G. gallus* genome (UCSC genome browser).

G. gallus PrimPol protein

MKRKWEERVKKVEELASYYERNPLPTVYKPRLSKPLQPSRVWKIFC
RQADAFRFVKTCKEDVHVFALERNTQNGQRFYLVTTYQELWYYYTK
GYKTSL**M**HCYEVIPEKDACKLYFDLEFYKAANPGADGKD**M**VAKLIEL
VSQKLKELYDVNCSARDVLNLDSSTDEKFSRHLIFLPCKTVFKDNIH
VGNFVRTILQPAIRLVGSNVAAPIAEGGAGYTSQCSAPTVELDGPLT
NLTAVEDASKGWPAIADQRKETETSHHGENSEFSFLIVNNKEGDKQ
LFVDLGVYTRNRNFR**M**YKSSKAGKNVILTIAEDNKFVPNCEENVSLE
EAYFLSSLVCNVRFEDGTKILSSNFVEEEIK**M**SAFLRSKTTRSTRGT
ASLFCSIGAHGRLSGVTVSRDDCFVRSLINKDGVQGGNNCAIIYRNS
ATVFINKFSFSGIRQWNYFSGEEILVYDISGYRWCENIGRAHRSNNI
MILVDLKKEVWYQKCHDPVCREKNFKSQSLPLPSRICLSSLFIEEED
H**M**VTDERENTEVTSHSNPADLSESSAYLAINTSQDTQWDNASDDAY
LVETAEDVELAEAADYSLGYDTEEIPDEVLLE**M**SWKQDTCSKDDS

Number of amino acids: 609

Molecular weight: 69397.0

Theoretical pI: 5.28

MW and isoelectric point (pI) are provided according to Expasy tools.

Human PrimPol ORF and amino acid sequences

```
atgaatagaaaatgggaagcaaaactgaagcaaattgaagaacgagcatctcattatgag
 M  N  R  K  W  E  A  K  L  K  Q  I  E  E  R  A  S  H  Y  E
aggaaaccgttgtcctcagtgtatagaccaagattgtccaagccagaagaaccaccctcc
 R  K  P  L  S  S  V  Y  R  P  R  L  S  K  P  E  E  P  P  S
atctggagactatttcatcgacaagctcaagcttttaattttgttaaaagctgtaaagaa
 I  W  R  L  F  H  R  Q  A  Q  A  F  N  F  V  K  S  C  K  E
gacgttcatgtatttgctttggaatgcaaagtaggagatggacaacgtatttaccttgtg
 D  V  H  V  F  A  L  E  C  K  V  G  D  G  Q  R  I  Y  L  V
acaacctatgctgaattttggttttactataaatccagaaaaaatctcttacactgctat
 T  T  Y  A  E  F  W  F  Y  Y  K  S  R  K  N  L  L  H  C  Y
gaagttattcctgaaaatgctgtgtgcaagctttattttgatttggaatttaacaaacct
 E  V  I  P  E  N  A  V  C  K  L  Y  F  D  L  E  F  N  K  P
gccaacccaggagctgatgggaaaaagatggttgcattactcattgagtatgtgtgtaaa
 A  N  P  G  A  D  G  K  K  M  V  A  L  L  I  E  Y  V  C  K
gcacttcaagagttatacggtgttaattgctcagctgaagatgttttgaacttggattct
 A  L  Q  E  L  Y  G  V  N  C  S  A  E  D  V  L  N  L  D  S
agcactgatgaaaaattcagccggcatttaatatttcagctccatgatgtggcatttaaa
 S  T  D  E  K  F  S  R  H  L  I  F  Q  L  H  D  V  A  F  K
gataatattcatgttggtaatttttgagaaaaattttgcagcctgctcttgacttgctt
 D  N  I  H  V  G  N  F  L  R  K  I  L  Q  P  A  L  D  L  L
ggcagtgaagatgatgatagcgctccagagacaacaggccatggatttccccatttttca
 G  S  E  D  D  D  S  A  P  E  T  T  G  H  G  F  P  H  F  S
gaagcacctgcaagacaaggattttctttcaataaaatgttcacagaaaaggctacagag
 E  A  P  A  R  Q  G  F  S  F  N  K  M  F  T  E  K  A  T  E
gaaagctggacatcgaattcaaagaaactggagaggctggggtcagctgagcaaagcagt
 E  S  W  T  S  N  S  K  K  L  E  R  L  G  S  A  E  Q  S  S
cctgacctttcatttctagttgtgaagaataacatgggagagaagcatctttttgtagat
 P  D  L  S  F  L  V  V  K  N  N  M  G  E  K  H  L  F  V  D
ctcggagtttatacaagaaatagaaactttcggctatataaatcatcaaaaattggaaag
 L  G  V  Y  T  R  N  R  N  F  R  L  Y  K  S  S  K  I  G  K
cgtgtggctttggaggttactgaagataacaaatttttttcctatacagtcaaaagatgtt
 R  V  A  L  E  V  T  E  D  N  K  F  F  P  I  Q  S  K  D  V
tctgacgaatatcaatattttctctcttctttggtcagcaatgtcaggttctcagatact
 S  D  E  Y  Q  Y  F  L  S  S  L  V  S  N  V  R  F  S  D  T
ttacgaattcttacatgtgagccatctcagaataaacaaaaaggagttggatattttaac
 L  R  I  L  T  C  E  P  S  Q  N  K  Q  K  G  V  G  Y  F  N
agtatcggcacttcagtagaaaccattgaaggttttcagtgttctccctatcctgaagtt
 S  I  G  T  S  V  E  T  I  E  G  F  Q  C  S  P  Y  P  E  V
gatcattttgttctttctttggtgaataaagatggcattaaaggaggaattcggcgttgg
 D  H  F  V  L  S  L  V  N  K  D  G  I  K  G  G  I  R  R  W
aactactttttcccagaagaattactggtttatgatatttgtaaatatcggtggtgtgaa
 N  Y  F  F  P  E  E  L  L  V  Y  D  I  C  K  Y  R  W  C  E
aacattggaagagcccataagagtaataatataatgattctggttgatctgaaaaatgaa
 N  I  G  R  A  H  K  S  N  N  I  M  I  L  V  D  L  K  N  E
gtttggtatcaaaaatgtcatgaccctgtatgtaaagcagaaaacttcaaatctgactgt
 V  W  Y  Q  K  C  H  D  P  V  C  K  A  E  N  F  K  S  D  C
ttcccattacctgctgaagtatgtctcctgtttctttttcaaagaggaagaagagtttaca
 F  P  L  P  A  E  V  C  L  L  F  L  F  K  E  E  E  E  F  T
acagatgaagcagatgaaactaggagcaatgaaacccagaatcctcataaaccatcacct
 T  D  E  A  D  E  T  R  S  N  E  T  Q  N  P  H  K  P  S  P
agcaggctgtcaacaggtgcatctgctgatgctgtctgggataatggcattgatgatgct
 S  R  L  S  T  G  A  S  A  D  A  V  W  D  N  G  I  D  D  A
tatttttagaagctactgaagatgctgaattagctgaagctgcagagaacagtcttctc
 Y  F  L  E  A  T  E  D  A  E  L  A  E  A  A  E  N  S  L  L
agttataacagtgaagtggatgaaattcctgatgaactaattatagaagtattacaagag
```

S Y N S E V D E I P D E L I I E V L Q E
taa

Human His-PrimPol protein

H H H H H H S S G L V P R G S H **M** N R K W E A K L K Q I E E R A S H Y E R K P L S S V Y R
P R L S K P E E P P S I W R L F H R Q A Q A F N F V K S C K E D V H V F A L E C K V G D G Q
R I Y L V T T Y A E F W F Y Y K S R K N L L H C Y E V I P E N A V C K L Y F D L E F N K P A N
P G A D G K K **M** V A L L I E Y V C K A L Q E L Y G V N C S A E D V L N L D S S T D E K F S R
H L I F Q L H D V A F K D N I H V G N F L R K I L Q P A L D L L G S E D D D S A P E T T G H G
F P H F S E A P A R Q G F S F N K **M** F T E K A T E E S W T S N S K K L E R L G S A E Q S S P
D L S F L V V K N N **M** G E K H L F V D L G V Y T R N R N F R L Y K S S K I G K R V A L E V T E
D N K F F P I Q S K D V S D E Y Q Y F L S S L V S N V R F S D T L R I L T C E P S Q N K Q K G
V G Y F N S I G T S V E T I E G F Q C S P Y P E V D H F V L S L V N K D G I K G G I R R W N Y
F F P E E L L V Y D I C K Y R W C E N I G R A H K S N N I **M** I L V D L K N E V W Y Q K C H D P
V C K A E N F K S D C F P L P A E V C L L F L F K E E E E F T T D E A D E T R S N E T Q N P H
K P S P S R L S T G A S A D A V W D N G I D D A Y F L E A T E D A E L A E A A E N S L L S Y
N S E V D E I P D E L I I E V L Q E **Stop**

Number of amino acids: 590

Molecular weight: 67885.4

Theoretical pI: 5.62

MW and isoelectric point (pI) are provided according to Expasy tools.